MAX-PLANCK-INSTITUT FÜR KOHLENFORSCHUNG

technische universität dortmund

New Horizons in Dirhodium(II) Catalysis: From the Development of Heterochiral-at-Metal Catalysts to Studies of the Innate Role of Amidate Ligands

Dissertation

zur Erlangung des akademischen Grades

Doktor der Naturwissenschaften

(Dr. rer. nat.)

vorgelegt von

Matthias Peeters

an der

Fakultät für Chemie und Chemische Biologie

der Technischen Universität Dortmund

Mülheim an der Ruhr

September 2025

Eidesstattliche Versicherung (Affidavit)

Peeters, Matthias
Name, Vorname
(Surname, first name)

237644
Matrikel-Nr.
(Enrolment number)

Belehrung:

Wer vorsätzlich gegen eine die Täuschung über Prüfungsleistungen betreffende Regelung einer Hochschulprüfungsordnung verstößt, handelt ordnungswidrig. Die Ordnungswidrigkeit kann mit einer Geldbuße von bis zu 50.000,00 € geahndet werden. Zuständige Verwaltungsbehörde für die Verfolgung und Ahndung von Ordnungswidrigkeiten ist der Kanzler/die Kanzlerin der Technischen Universität Dortmund. Im Falle eines mehrfachen oder sonstigen schwerwiegenden Täuschungsversuches kann der Prüfling zudem exmatrikuliert werden, § 63 Abs. 5 Hochschulgesetz NRW.

Die Abgabe einer falschen Versicherung an Eides statt ist strafbar.

Wer vorsätzlich eine falsche Versicherung an Eides statt abgibt, kann mit einer Freiheitsstrafe bis zu drei Jahren oder mit Geldstrafe bestraft werden, § 156 StGB. Die fahrlässige Abgabe einer falschen Versicherung an Eides statt kann mit einer Freiheitsstrafe bis zu einem Jahr oder Geldstrafe bestraft werden, § 161 StGB.

Die oben stehende Belehrung habe ich zur Kenntnis genommen:

Official notification:

Any person who intentionally breaches any regulation of university examination regulations relating to deception in examination performance is acting improperly. This offence can be punished with a fine of up to EUR 50,000.00. The competent administrative authority for the pursuit and prosecution of offences of this type is the chancellor of the TU Dortmund University. In the case of multiple or other serious attempts at deception, the candidate can also be unenrolled, Section 63, paragraph 5 of the Universities Act of North Rhine-Westphalia.

The submission of a false affidavit is punishable.

Any person who intentionally submits a false affidavit can be punished with a prison sentence of up to three years or a fine, Section 156 of the Criminal Code. The negligent submission of a false affidavit can be punished with a prison sentence of up to one year or a fine, Section 161 of the Criminal Code.

I have taken note of the above official notification.

Mülheim an der Ruhr
Ort, Datum
(Place, date)

Unterschrift
(Signature)

Titel der Dissertation:
(Title of the thesis):

New Horizons in Dirhodium(II) Catalysis:
From the Development of Heterochiral-at-Metal Catalysts to Studies of the Innate role of
Amidate Ligands

Ich versichere hiermit an Eides statt, dass ich die vorliegende Dissertation mit dem Titel selbstständig und ohne unzulässige fremde Hilfe angefertigt habe. Ich habe keine anderen als die angegebenen Quellen und Hilfsmittel benutzt sowie wörtliche und sinngemäße Zitate kenntlich gemacht.
Die Arbeit hat in gegenwärtiger oder in einer anderen Fassung weder der TU Dortmund noch einer anderen Hochschule im Zusammenhang mit einer staatlichen oder akademischen Prüfung vorgelegen.

I hereby swear that I have completed the present dissertation independently and without inadmissible external support. I have not used any sources or tools other than those indicated and have identified literal and analogous quotations.

The thesis in its current version or another version has not been presented to the TU Dortmund University or another university in connection with a state or academic examination.*

*Please be aware that solely the German version of the affidavit ("Eidesstattliche Versicherung") for the PhD thesis is the official and legally binding version.

Ort, Datum
(Place, date)

Unterschrift
(Signature)

1. Berichterstatter: Prof. Dr. Alois Fürstner

2. Berichterstatter: Prof. Dr. Norbert Krause

Die vorliegende Arbeit entstand unter der Anleitung von Prof. Dr. Alois Fürstner in der Zeit von Dezember 2021 bis August 2025 am Max-Planck-Institut für Kohlenforschung in Mülheim an der Ruhr. Teile dieser Arbeit wurden bereits veröffentlicht:

Peeters, M.; Decaens, J.; Fürstner, A.: Taming of Furfurylidenes by Chiral Bismuth-Rhodium Paddlewheel Catalysts. Preparation and Functionalization of Optically Active 1,1-Disubstituted (Trifluoromethyl)cyclopropanes*, Angewandte Chemie International Edition* **2023**, 62, e202311598.

Peeters, M.; Baldinelli, L.; Leutzsch, M.; Caló, F.P.; Auer, A.A.; Bistoni, G.; Fürstner, A.: *In Situ* Observation of Elusive Dirhodium Carbenes and Studies on the Innate Role of Carboxamidate Ligands in Dirhodium Paddlewheel Complexes: A Combined Experimental and Computational Approach, *Journal of the American Chemical Society*, **2024**, 146, 38, 26466-26477.

Peeters, M.; Baldinelli, L.; Lerda, S.; Bistoni, G.; Fürstner, A.: Dirhodium Complexes Heterochiral-at-the-Metal Centers: An Alternative Type of Paddlewheel Catalyst for Asymmetric Synthesis, *Journal of the American Chemical Society*, **2025**, 147, 15, 12418-12424.

Die Arbeiten erfolgten zum Teil in Zusammenarbeit mit Prof. Dr. Alexander Auer, Prof. Dr. Giovanni Bistoni, Dr. Jonathan Decaens und Dr. Markus Leutzsch. Die von diesen Mitarbeitern alleinverantwortlich erzielten Ergebnisse wurden als solche an entsprechender Stelle gekennzeichnet.

Acknowledgements

First and foremost, I would like to thank my Doktorvater, Prof. Dr. Alois Fürstner, for the opportunity to conduct my doctoral studies in his group, for the many fruitful discussions and for giving me plenty of freedom in my research. I learned a lot over the past four years for which I am entirely grateful.

I would like to thank Prof. Dr. Krause for the co-examination of this thesis.

Special thanks goes to our laboratory technicians, Saskia Schulthoff, Christian Wille and Christopher Rustemeier, for maintaining the lab and the working space in exquisite conditions. Particularly, I would like to thank Chris for his contributions to my research, but also for his friendship. It was a pleasure to share so many nice adventures with you over the past years and I am sure many more will follow in the future! I also would like to thank our former technician, Karin Radkowski, who made me feel welcome in the group from the very beginning and provided invaluable mentoring advice in the first stressful weeks of the PhD. I would also like to express my gratitude to our secretary, Andrea Bosserhoff, for the excellent administrative support during my time at the KOFO.

Of course, I have to acknowledge all the service departments of the KOFO for their excellent service. Within particular, I would like to thank Roswitha Leichtweiss and Sandra Klimmek for their excellent HPLC service. Additionally, I would like to thank Dr. Markus Leutzsch not only for his excellent NMR service, but also for the many fruitful discussions and for his numerous contributions to my research, which really influenced my PhD work significantly.

Thank you to Anne Zimmer, Noah Richter, Paul Moths and Eduardo Garcia for the fast and excellent revisions of this thesis. I also want to thank all the current and former members of the Fürstner group for the nice working atmosphere and all the engaging chemistry discussions. Special thanks goes to Dr. Peter Chapple, Dr. Fabio P. Caló, Dr. Anne Zimmer, Dr. Mingxu Cui. Additionally, I am grateful to Dr. Eduardo Garcia and Dr. Rakan Saeb for the many engaging chemistry discussions, both within and outside the institute.

Last but not least, I would like to express my gratitude to my parents and my grandma for their unconditional support. Bedankt voor jullie steun en voor er altijd voor mij te zijn!

Überblick

Cyclopropane sind weit verbreitete Bausteine in der medizinischen Chemie, der Agrochemie und kommen in einer Vielzahl an Naturstoffen vor. Die asymmetrische Synthese bestimmter Cyclopropan-Motive stellt eine Herausforderung dar und ist daher ein zentrales Thema in der asymmetrischen Katalyse. Eines dieser anspruchsvollen Motive sind 1,1-disubstituierte (trifluormethylierte) Cyclopropane, da sie Bioisostere von *tert*-Butyl-Gruppen mit verbesserter metabolischer Stabilität darstellen und schwer in optisch aktiver Form herzustellen sind. In dieser Arbeit wird eine neuartige Methodik beschrieben, bei der eine luft- und lagerstabile Carbenquelle (**58**) in einer asymmetrischen Cyclopropanierung unter Verwendung eines chiralen [BiRh]-Schaufelrad-Komplexes (**47**) eingesetzt wird. Dadurch wurde eine Vielzahl von 2-Furyl-Cyclopropanen mit ausgezeichneter Enantioselektivität erhalten. Durch oxidative Spaltung der Furan-Einheit konnten die entsprechenden Carbonsäuren zugänglich gemacht werden, welche ihrerseits wertvolle Bausteine darstellen und sich unter Stereoretention leicht derivatisieren lassen.

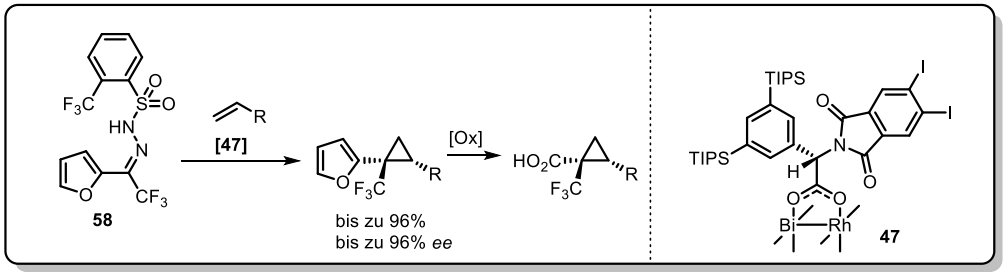

Darüber hinaus wurde ein neuartiger chiraler Dirhodium-Katalysator entwickelt, der sich konzeptionell von traditionellen Dirhodium-Komplexen dadurch unterscheidet, dass seine Chiralität nicht aus der Ligandensphäre, sondern direkt von den Metallzentren selbst stammt. Dieser heterochiral-am-Metall-Katalysator (**134**) wurde erfolgreich in der asymmetrischen Cyclopropanierung von α-stannylierten Diazoestern eingesetzt und lieferte die entsprechenden Cyclopropane mit hoher *cis*-Diastereoselektivität und exzellenten Enantiomerenüberschüssen. Darüber hinaus zeigte dieser Katalysator seine Überlegenheit in der asymmetrischen Cyclopropanierung von α-trifluormethylierten Diazoestern, wobei die Cyclopropane mit hoher *trans*-Diastereoselektivität und ebenfalls hervorragendem *ee* erhalten wurden. DFT-Studien zeigten, dass der Amidat-Ligand des Katalysators entscheidend für das außergewöhnliche Maß an Stereoinduktion in diesen Transformationen ist, da er die selektive Carbenbildung an der [O_3N]-Seite des Katalysators ermöglicht und über eine Wasserstoffbrückenbindung mit der entsprechenden Carbonylfunktion des Carben-Zwischenprodukts interagiert.

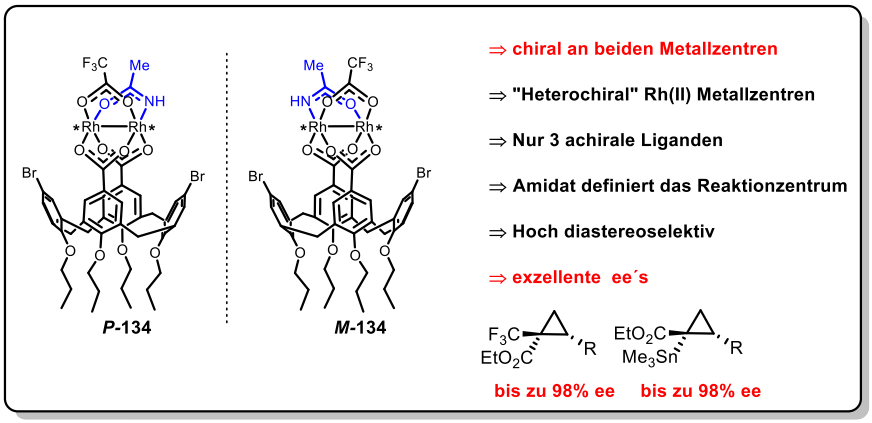

Grundlegende Studien wurden zur intrinsischen Rolle von Amidat-Liganden hinsichtlich der Reaktivität und Selektivität verschiedener heteroleptischer Dirhodium-Schaufelrad-Komplexe in der Katalyse durchgeführt. Bemerkenswerterweise ist der Einfluss des Amidat-Liganden stark von der Art der katalytischen Transformation, an der er beteiligt ist, abhängig. In der durchgeführten Fallstudie konnte die weit verbreitete Annahme widerlegt werden, dass die Carbenbildung den geschwindigkeitsbestimmenden Schritt im katalytischen Zyklus einer Cyclopropanierungsreaktion darstellt. Umfangreiche DFT-Studien zeigten, dass im Fall einer intramolekularen Cyclopropanierung mit einem heteroleptischen Amidat-Komplex (**101**) die Cyclopropanierung selbst und nicht die Carbenbildung den geschwindigkeitslimitierenden Schritt ausmacht.

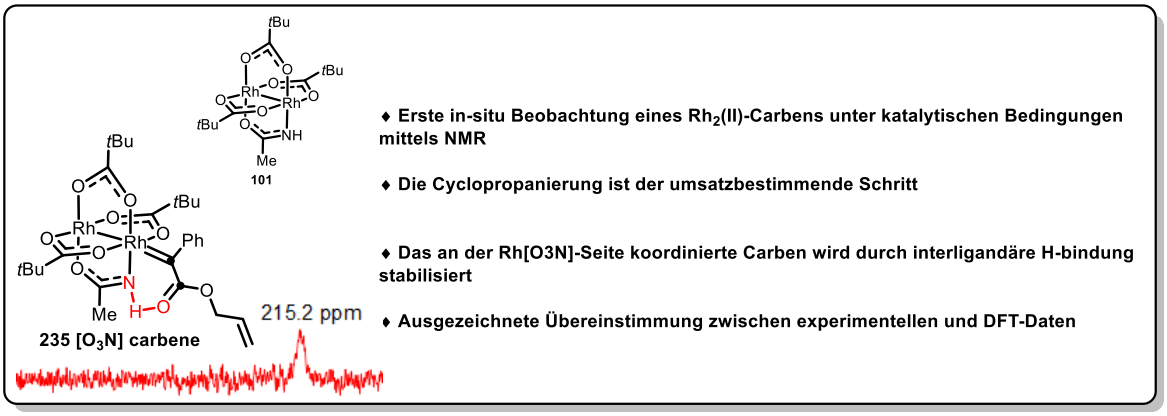

Dies wurde durch den Nachweis des Carben-Zwischenprodukts unter echten katalytischen Bedingungen mittels in situ-^{13}C-NMR-Spektroskopie bestätigt. Die Beobachtung eines derart reaktiven Intermediats unter katalytischen Bedingungen war bislang beispiellos. Mit Komplex **101** konnte nur ein Signal bei 215.2 ppm detektiert werden, das dem an der [O_3N]-Koordinationsgesicht gebundenen Carben (**235**) entspricht, da dieses thermodynamisch stabiler ist als das alternative Isomer.

Abstract

Cyclopropanes are prevalent building blocks in medicinal chemistry, agrochemistry and occur in a wide array of natural products. The synthesis of certain cyclopropane motifs in stereoselective manner is challenging and therefore remains a focus point in asymmetric catalysis. One such challenging motif are 1,1-disubstituted (trifluoromethyl)cyclopropanes**,** as they represent bioisosteres of *tert*-butyl groups of improved metabolic stability and are difficult to synthesize in optically active form. Herein, a novel methodology is described which engages a bench-stable carbene source (**58**) in the asymmetric cyclopropanation catalyzed by a chiral [BiRh]-paddlewheel complex (**47**) affording a variety of 2-furyl cyclopropanes with excellent enantioselectivity. Oxidative cleavage of the furan moiety gave access to the corresponding carboxylic acids, which in turn are precious building blocks and can be easily derivatized in a stereoretentive manner.

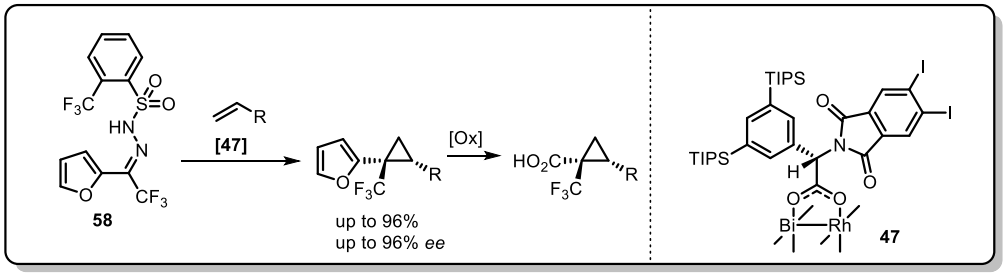

Additionally, a novel chiral dirhodium catalyst was developed, which conceptually stands out from the traditional dirhodium complexes in the sense that it bears its chirality on the metal centers themselves and not on the ligand sphere. This heterochiral-at-metal catalyst (**134**) was successfully employed in the asymmetric cyclopropanation of α-stannylated diazoesters furnishing the corresponding cyclopropanes with high *cis*-diastereoselectivity and excellent ee. Furthermore, this catalyst showed its superiority in the asymmetric cyclopropanation reaction of α-trifluoromethylated diazoesters, furnishing the cyclopropanes with high *trans*-diastereoselectivity and excellent *ee*. DFT studies have shown that the amidate ligand of the catalyst is key for the high levels of stereoinduction achieved in these transformations as it ensures selective carbene formation at the [O_3N]-face of the catalyst and engages in interligand hydrogen-bonding with the corresponding carbonyl moiety of the carbene.

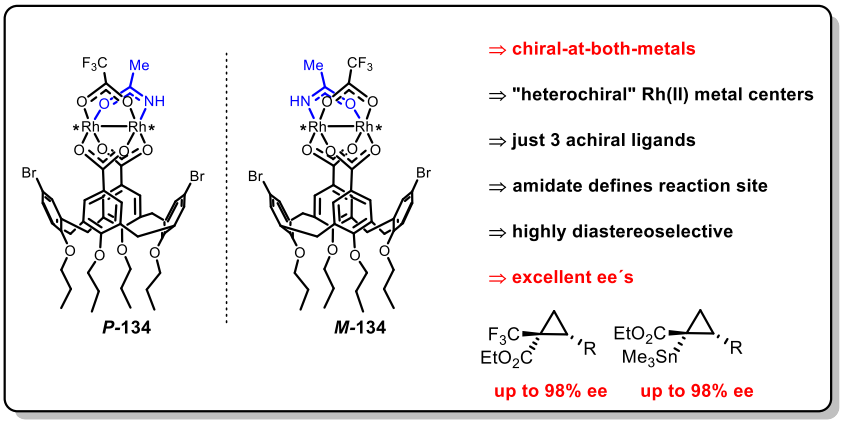

More fundamental studies were performed on the innate role of amidate ligands on the reactivity and selectivity of a variety of heteroleptic dirhodium paddlewheel complexes in catalysis. Notably, the effect of the amidate ligand differs strongly depending on the kind of catalytic transformation in which it is involved. In the performed case study, the general widely held belief that carbene formation is the rate-determining step in the catalytic cycle of a cyclopropanation reaction could be debunked. Extensive DFT studies showed that in the case of an intramolecular cyclopropanation reaction with heteroleptic amidate complex (**101**) the rate-determining step is the cyclopropanation rather than carbene formation.

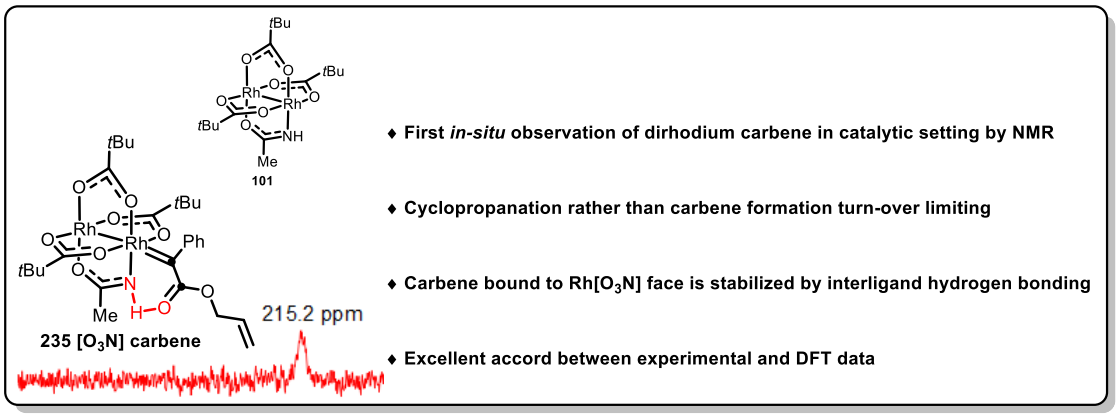

This was verified by detection of the carbene intermediate under truly catalytic settings via *in situ* ^{13}C NMR spectroscopy. So far, the observation of such reactive intermediates under catalytic conditions was unprecedented. With complex **101**, only one resonance at 215.2 ppm was observed, corresponding to the $[O_3N]$-bound carbene (**235**), as it is the thermodynamically more stable one of the two possible isomers.

“Nothing in life is to be feared, it is only to be understood. Now is the time to understand more, so that we may fear less."

Marie Skłodowska Curie

Table of Contents

1. General Introduction

1.1. Asymmetric Catalysis

Chirality plays a crucial role for life, as most of the essential biological building blocks (amino acids, nucleic acids and saccharides) are inherently dissymmetric. A wide range of biological and physical functions are generated through precise molecular recognition that requires matching of chirality. Therefore, the structural difference between enantiomers often has significant impact on the mode of action within the human body. Such effects are particularly seen when administering drug molecules, as the pharmacological activities of one enantiomer with respect to the other can differ significantly.[2] The most infamous example of such drastic differences in pharmacological properties is thalidomide, which was administered in racemic form to pregnant women in the 1960s to treat morning sickness. The *R* enantiomer of the drug had the desirable sedative properties, while the *S* enantiomer was teratogenic and induced fetal malformations.[3-4] Remarkably, until the early 1990s, the vast majority of chiral drugs were supplied as racemates, despite the known risks of administering drugs in racemic form. This was mainly due to the lack of practical methods for the synthesis of optically pure molecules.[5] It was only until 1992 when the FDA introduced strict guidelines for the commercialization of racemic drugs that the focus shifted towards the synthesis of optically pure molecules and the development of useful synthetic methods.[6] Discovery of truly efficient methods was challenging and initially relied on chiral pool approaches in which enantiopure starting materials from natural sources were employed.[7] Further, methods to separate racemates[8] have also been employed, however, the maximum theoretical yield is limited to 50% as only one of the two enantiomers is desired, unless it is possible to convert the opposite enantiomer into the desired one by dynamic kinetic resolution.[9] Alternatively, chiral auxiliary reagents provide access to optically pure compounds, although the use of these reagents incur a cost of at least 2 additional steps in a synthetic sequence.[10] Much more versatile and often more economical are catalytic, asymmetric processes, in which the chiral information is transferred via a catalyst. The development of novel catalytic systems that can be applied in a wide variety of synthetic transformations rendering compounds in a highly optically pure manner has been at the forefront of organic and organometallic chemistry in the past decades and has found its way into industrial applications.[11] The importance of the field is reflected by the three Nobel prizes in chemistry that were awarded to chemists who contributed to asymmetric catalysis: Cornforth in 1975 for his pioneering studies in enzymatic catalysis and Prelog for his studies on stereochemistry,[12] Knowles, Noyori and Sharpless for their contributions to asymmetric transition-metal catalysis,[13] and to MacMillan and List for their contributions to asymmetric organocatalysis.[14]

1.2. Metal Carbenes

In general, metal carbenes are usually classified in two main types: Fischer and Schrock carbenes (Figure 1).[15-17] The difference between the two lies both in the electronic and structural properties of the carbenes. Fischer carbenes are electrophilic in nature and have long carbon-metal bonds, often with the metal center in a formally low oxidation state. Schrock carbenes on the other hand are nucleophilic in nature and present rather short carbon double bonds to metals, which are usually in a formally high oxidation state.[18-19]

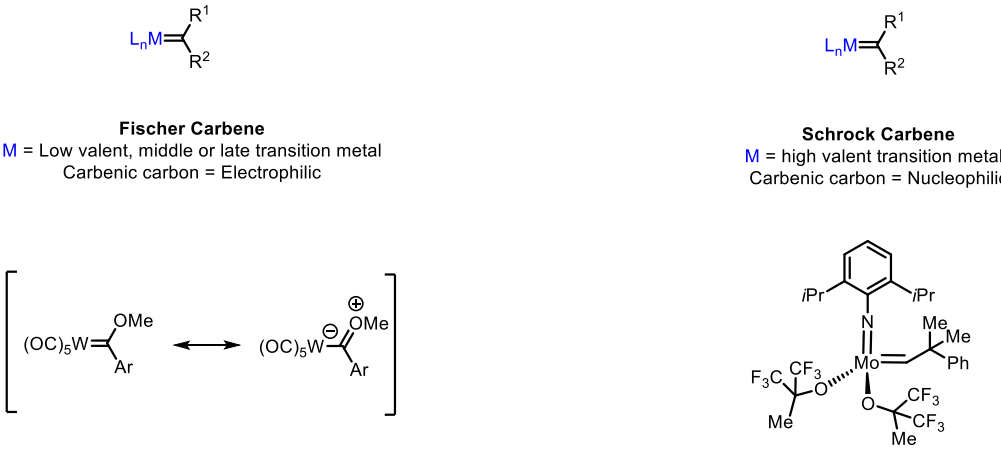

Figure 1-General classification of Fischer and Schrock type carbenes with a representative example of each type.

The difference in the inherent reactivity between these two types of carbenes can be rationalized by the corresponding bonding models (Figure 2).[19] Fischer-type carbenes are best described using an electronic structure model involving a singlet carbene. In this case, the carbene carbon donates via σ-donation from the filled sp^2-orbital into an empty d-orbital of the metal, together with weak π-backdonation of a filled d-orbital of the metal to an empty p-orbital of the carbenic carbon. This dual interaction results in a partial positive charge on the carbon atom, endowing the carbene with electrophilic character.

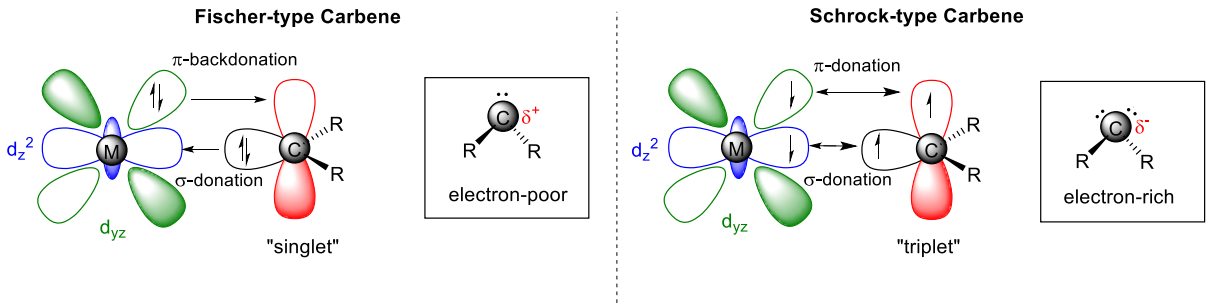

Figure 2-Bonding models for Fischer- and Schrock-type metal carbenes.

In contrast, Schrock-type carbenes are better understood through a model where both the metal and the carbene are in a triplet electronic configuration. The bonding in these systems is negatively polarized toward the carbon atom, due to its higher electronegativity compared to the metal. As a result, the carbon center in Schrock carbenes tends to have nucleophilic character.

Given that the central focus of this thesis lies in the chemistry of dirhodium carbenes, their structure, bonding, and reactivity will be discussed in greater detail in the following chapter.

1.3. Rhodium Carbenes

Dirhodium tetraacetate (**1**) was first prepared and characterized in the mid-1960s[20] and was shown in the early 1970s to effectively decompose ethyl diazoacetate.[21] Over the past 60 years, a wide variety of dirhodium paddlewheel complexes have been developed and these complexes are widely regarded as some of the most effective catalysts for asymmetric carbene transformations. A dirhodium paddlewheel complex typically comprises four equatorial μ_2-ligands and two labile axial ligands. The equatorial ligands are kinetically inert as can be seen by the rather forcing conditions that are necessary if one wishes to replace such equatorial ligands; in contrast, the axial ligands are kinetically labile, due to the *trans*-effect of the Rh–Rh bond. This axial site lability is a key factor underlying the catalytic efficiency of these complexes.

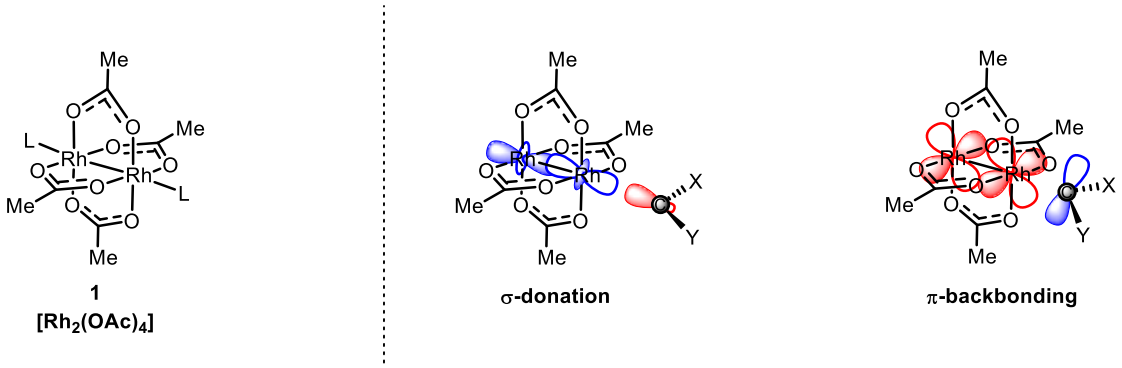

Figure 3-Left: structure of $[Rh_2(OAc)_4]$ in neutral axial ligands (L) are displayed. Right: Frontier orbital interactions between dirhodium tetraacetate and the carbene species. The orbitals in red are occupied; the orbitals in blue are unoccupied.

The exceptional reactivity of dirhodium carbenes is attributed to their unique three-center, four-electron (3c/4e) bonding framework, which significantly enhances their electrophilic character. Therefore, dirhodium carbenes are commonly regarded as "superelectrophilic" intermediates, distinguishing them from less reactive Fischer-type carbene analogs that

usually involve 2c/2e bonds.[22] Frontier orbital analysis of the electronic structure of dirhodium carbenes show that the HOMOs and the LUMOs of the axially free dirhodium(II) complex and a singlet carbene fragment are perfectly matching in terms of symmetry; the HOMO of the carbene fragment (a filled sp^2 C orbital) has σ-symmetry with respect to the Rh–Rh axis, enabling it to donate electron density into the σ^*_{Rh-Rh} orbital (LUMO) (Figure 3). Additionally, the filled π^*_{Rh-Rh} orbital (HOMO) can back-donate electron density into an empty p π orbital (LUMO) of the carbenic carbon. This π-backbonding results in a low-lying LUMO that is polarized toward the carbene carbon. The low energy of this LUMO, associated with the three-center, four-electron bonding interaction, makes it more accessible to nucleophiles than the LUMO of a conventional two-center, two-electron bond.[22]

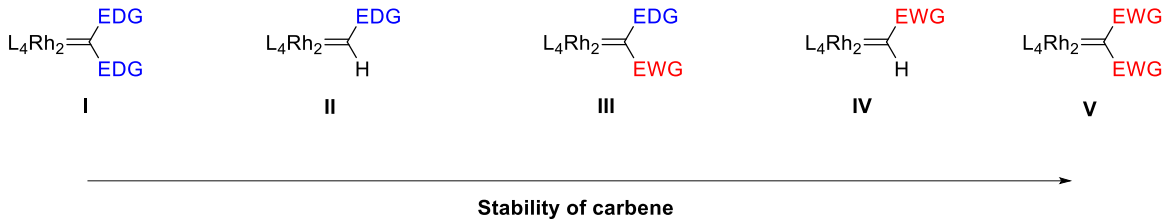

Figure 4-Classification of dirhodium carbenes according to their electronic properties. EWG = CO_2R, COR, NO_2, $PO(OR)_2$, CF_3, SO_2R; EDG = alkyl, (Het)aryl, alkenyl, alkynyl.

In general, dirhodium carbenes can be divided into five classes, **I-V**, based on their stability/reactivity (Figure 4). Typically, electron withdrawing groups destabilize the carbene intermediate, whereas electron donating groups stabilize the reactive intermediate, hence their subdivision in donor/donor (**I**), donor (**II**), donor/acceptor (**III**), acceptor (**IV**) and acceptor/acceptor (**V**) compounds.[23] Due to the highly reactive nature of these carbenes, usually these intermediates are fleeting, making them extremely difficult to characterize. However, over the last decade a few carbene intermediates of type **I** and **III** have been successfully characterized.[24-26] Particularly, Fürstner and coworkers were able to obtain X-ray crystallographic data of these intermediates. Notably, the Rh–C bond length of **2** determined by single-crystal X-ray analysis is 2.061 Å.[24] This comparatively long bond length suggests a bond order of less than two and thus indicates only slight π-backbonding from the dirhodium(II) core to the carbene, which explains the super-electrophilic character of the carbene carbon.

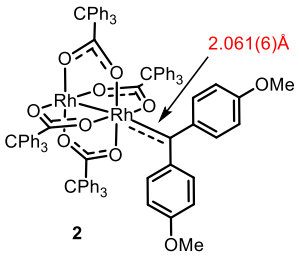

Figure 5-Carbene intermediate **2** with the Rh–C bond length displayed as characterized by XRD.

1.4. The Prevalence of Cyclopropanes in Industry and Natural Products

Cyclopropanes are the smallest carbocyclic motifs and exhibit rather unique physical and chemical properties.[27] They display an extremely high ring strain (27.5 kcal·mol^{-1}), largely owing to its 60° C–C bond angles.[28] The bare cyclopropane has led to a variety of theoretical postulations to describe its reactivity. Arguably, the most widely accepted model to describe its inherent properties is the Walsh model.[29] In essence, this theory explains the unusual bonding and reactivity of cyclopropane by showing that its C–C bonds have significant π-character, resulting from the overlap of bent sp^3 orbitals, therefore leading to a hybridization close to sp^2. It is for that reason that the chemical properties of a cyclopropyl ring resemble those of olefins.[30]

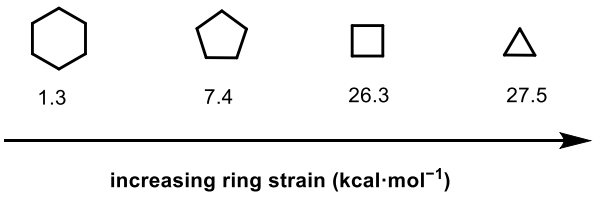

Figure 6-Ring strain of unsubstituted cycloalkanes (from cyclopropane to cyclohexane).

Cyclopropanes play an important role in medicinal chemistry due to their unique structural properties. Acting as bioisosteres for alkyl groups, cyclopropane rings can help lock a drug molecule in a favorable conformation, thereby improving both its chemical stability and biological activity.[31] Compared to alkanes like ethane, cyclopropanes have stronger and shorter C–H bonds (≈106 kcal·mol^{-1} vs. ≈101 kcal·mol^{-1}), which makes hydrogen abstraction less favorable and slows down oxidative metabolism.[32] Beyond enhanced metabolic resistance, introducing a cyclopropane unit into a drug candidate can also lead to increased potency, better bioavailability, improved brain penetration, and higher solubility in aqueous media.[32] A few examples of well-known drug molecules on the market containing cyclopropane motif(s) are montekulast, drospirenone, efavirenz and saxagliptin.[33]

Montekulast functions as a leukotriene receptor antagonist and is commonly used for treatment of asthma and allergic rhinitis.[34] Drospirenone is a progestin and antiandrogen medication, which is used in birth control pills to prevent pregnancy and in menopausal hormone therapy.[35] Efavirenz is an antiretroviral medication and is frequently prescribed to treat HIV/AIDS.[36] Saxagliptin is an oral hypoglycemic of the dipeptidyl peptidase-4 inhibitor class and often described to treat type 2 diabetes.[37]

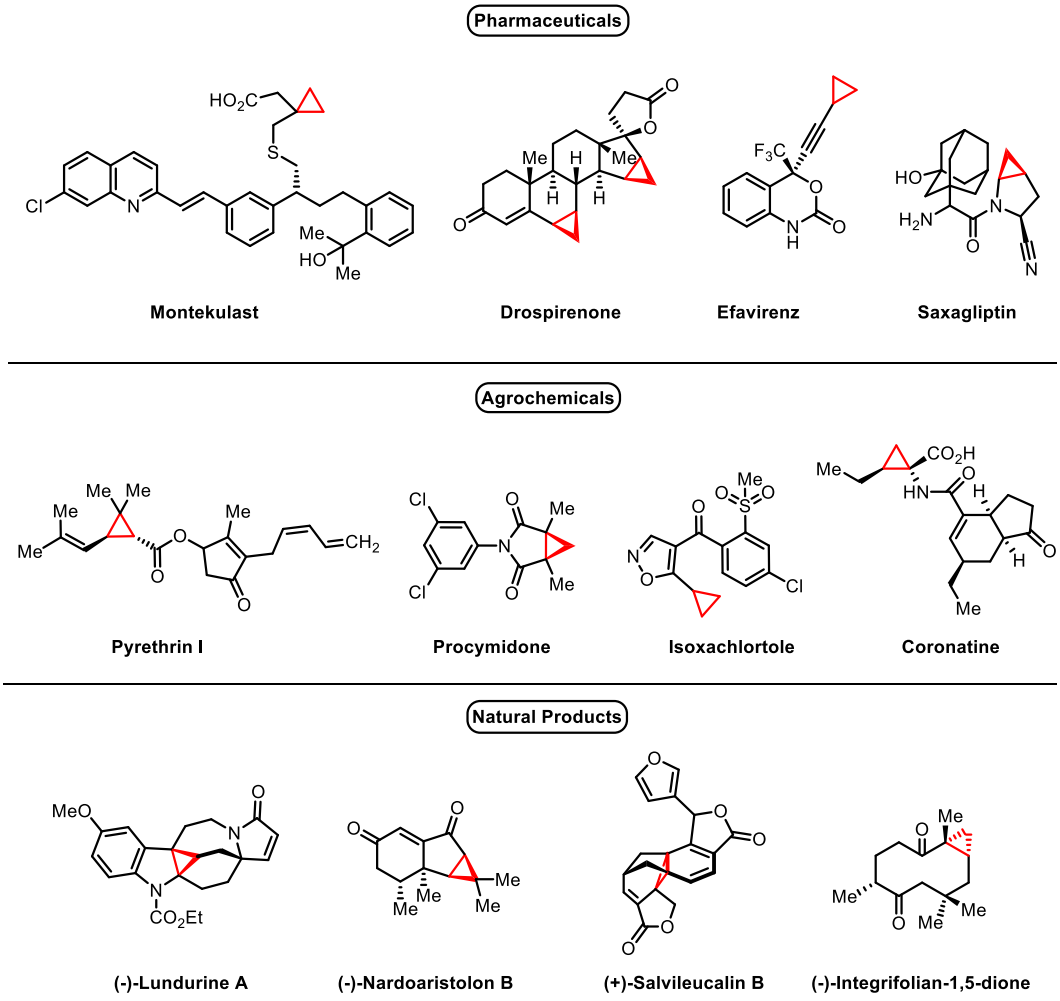

Figure 7-Examples of pharmaceuticals, agrochemicals and natural products containing one or more cyclopropane rings.

In addition to their prominent role in medicinal chemistry, cyclopropanes certainly have found their applications in agrochemistry. Synthetic pyrethroids[38] such as allethrin I, along with naturally occurring pyrethrins like pyrethrin I, are widely used insecticides whose structures are based on chrysanthemic acid, a monoterpenic cyclopropane.[39] Cyclopropanes are also found in fungicides (e.g. procymidone), herbicides (e.g. isoxachlortole) and even in plant growth regulators (e.g. coronatine).[40] Cyclopropanes can also be found in a broad variety of natural products that have been isolated over the past decades and that were subject to copious

amounts of total syntheses.[41-42] A variety of methods were used to construct the cyclopropyl motif. For example, (–)-Lundurine A was synthesized by Qin and coworkers via a late-stage intramolecular Simmons–Smith cyclopropanation.[43] For (+)-Salvileucalin B, Reisman and coworkers constructed the central tricyclo[3.2.1.0]octane core via an intramolecular carbene cyclopropanation of an arene, using a diazo-based precursor.[44] Echavarren and coworkers employed a gold-catalyzed oxidative cyclization as the key step in their synthesis of (−)-nardoaristolone B.[45] Just recently, Fürstner and coworkers reported the total synthesis of (−)-Integrifolian-1,5-dione in which the cyclopropane motif was formed via a rhodium(II)-catalyzed [2+1]cycloaddition involving an α-stannylated diazo precursor.[46]

1.5. Rhodium(II)-Catalyzed Cyclopropanation Reactions

Due to the unique structural and electronic characteristics of cyclopropanes, there are plenty of applications in which these motifs are used (*vide supra*). Therefore, the construction of cyclopropanes has remained a key focus in organic synthesis, particularly in asymmetric fashion. Broadly, two principal strategies are employed for cyclopropane formation: the first relies on the formal [2+1] cycloaddition of carbenes to alkenes, while the second involves a 1,3-cyclization process driven by an entropically favored, irreversible ring closure.[47] Particularly, [2+1]-cycloaddition reactions between a carbene and an olefin, catalyzed by transition metals, are an attractive option to construct the cyclopropane ring in a stereoselective fashion. Since the initial report by Nozaki, Noyori and coworkers in 1966,[48] who reported the first asymmetric copper catalyzed cyclopropanation reaction of ethyl diazoacetate (**3**) with styrene (Scheme 1), many other catalytic systems based on Cu,[49-52] Ru,[49, 51, 53] Pd[49, 51, 54] and Rh[49, 51-52, 55] have been developed over the last decades.

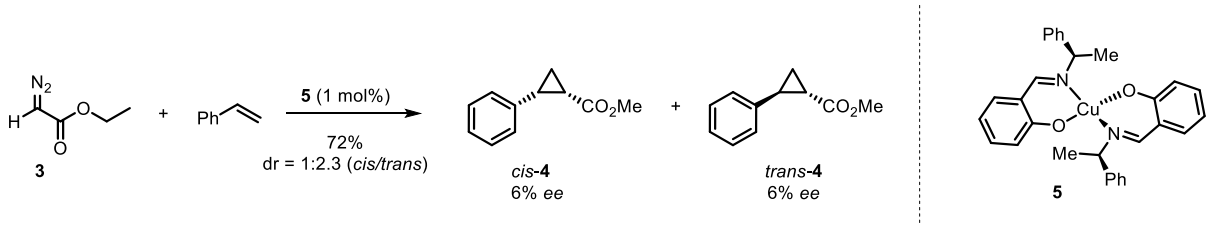

Scheme 1-First example of [2+1]-cycloaddition using a transition metal catalyst reported by Nozaki, Noyori and coworkers.[48]

Arguably, the most reactive of all are dirhodium(II) catalysts which have emerged as highly successful catalysts for asymmetric cyclopropanations. Moreover, these catalysts are air and moisture stable, making them easy to handle. The most commonly used equatorial ligands are carboxylates, that are μ_2-coordinated to the rhodium core. Besides carboxylate ligands a variety of complexes bearing amidate and phosphate ligands have been reported.[56-57]

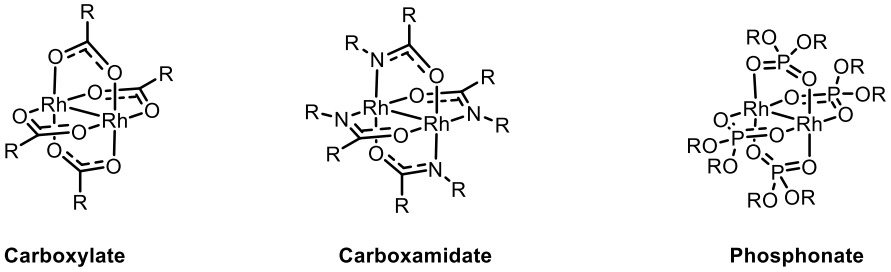

Figure 8-General structures of dirhodium(II) complexes bearing different types of μ_2-ligands.

1.5.1. Mechanism

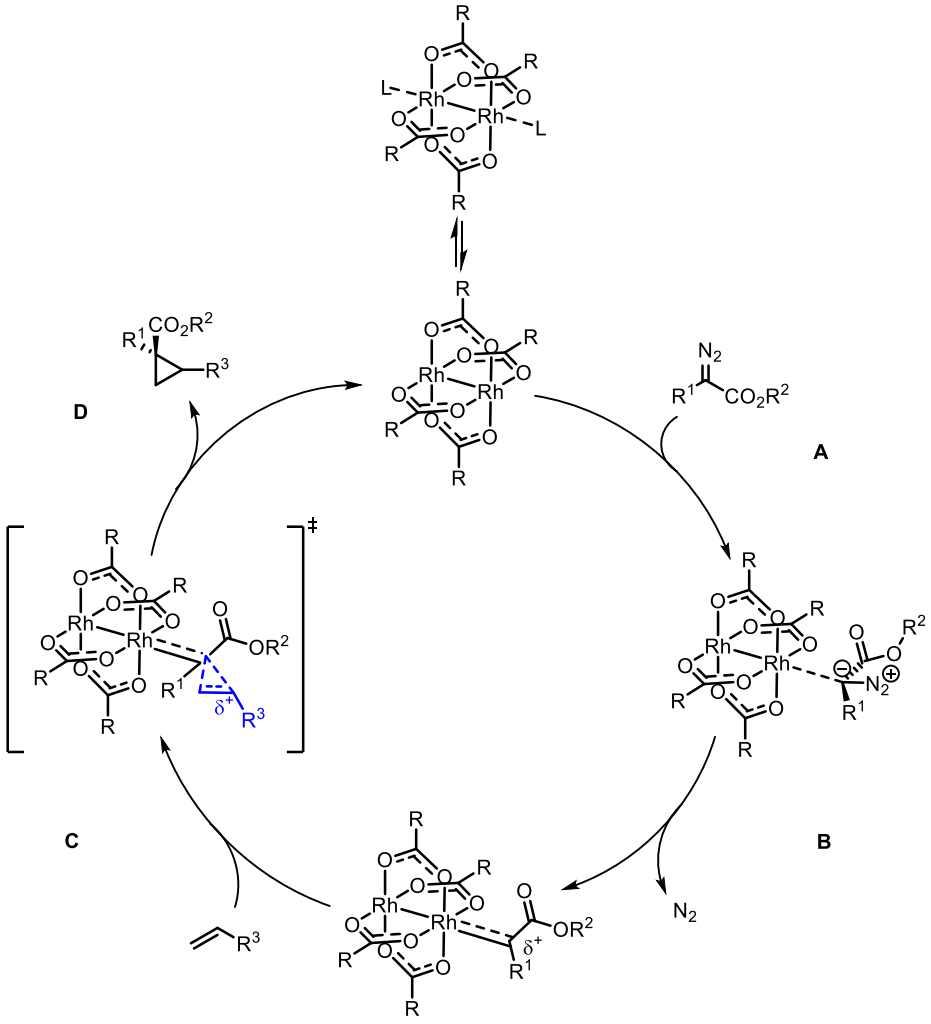

Scheme 2-General mechanism of a dirhodium(II) catalyzed cyclopropanation.

The mechanism of a dirhodium-catalyzed cyclopropanation is relatively well understood, thanks to the various mechanistic,[58-62] theoretical[60, 63-64] and spectroscopic studies[65] that have been performed in the last two decades. It is generally agreed that the reaction proceeds through two fundamental steps: the decomposition of the diazo compound to the

corresponding metal carbene, followed by the nucleophilic attack on this highly reactive "superelectrophilic" species. Before the first step of the reaction can occur, at least one of the axial ligands of the dirhodium(II) catalyst must dissociate to create an open coordination site for the diazo compound to bind to (Scheme 2, **A**).[66] Therefore, it is quintessential that in this type of transformations solvents are avoided that can block the axial position through coordination (e.g. MeCN) or react with the metal carbene intermediate (e.g. THF, dioxane). Carbene formation then proceeds in two stages, with DFT calculations suggesting that nitrogen extrusion (Scheme 2, **B**) is the rate-determining step of the reaction.[63] As the reaction proceeds, the reactive carbene intermediate undergoes a [2+1] cycloaddition with an olefin to form the cyclopropane (Scheme 2, **C**, **D**). The associated transition state is described as concerted but asynchronous.[60, 63]

1.5.2. State of the Art of Asymmetric Cyclopropanations

In general, achieving enantioselectivity in a cyclopropanation reaction is a result of the chiral ligand environment around the carbene, which dictates the stereocontrol during the enantio-discriminating [2+1]-cycloaddition event. The chiral ligand environment directs the attack of the alkene to one of the prochiral faces of the carbene intermediate and limits the spatial freedom of the carbene itself. The shape of the chiral pocket around the rhodium center is influenced by the three-dimensional structure of the ligands. The orientation of these chiral ligands in the dirhodium complexes can in theory adopt four different conformations due to the free rotation around the carboxylate C–C bond. If the direction in which the more sterically demanding substituent points (i.e. the structural element that forms the chiral pocket) is defined as the α-face, the possible arrangements are α,α,α,α; α,β,α,β; α,α,β,β; and α,α,α,β (Figure 9).[67]

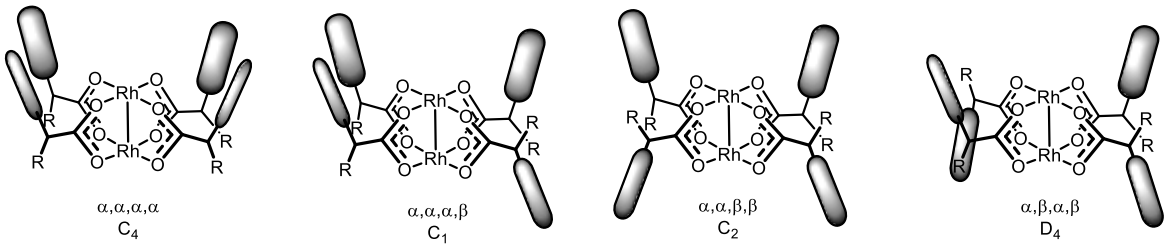

Figure 9-Schematic representations of the four different conformers of chiral ligands around the Rh(II) paddlewheel. The Paddles represent the sterically more demanding part of the ligand.

Originally, Davies and co-workers proposed that only catalysts with α,β,α,β or α,α,β,β symmetry would provide high levels of asymmetric induction.[55] Although no crystal structure of [Rh_2(*S*-DOSP)$_4$] has been published to date, Davies and co-workers proposed an α,β,α,β

arrangement of the ligands based on symmetry considerations (Figure 10).[68] Hashimoto and coworkers, postulated an α,α,β,β arrangement for their [Rh_2(*S*-PTTL)$_4$], which also induces high enantioselectivities.[69] However, Fox and coworkers refuted this postulate based on single X-ray diffraction analysis of the precatalyst [Rh_2(*S*-PTTL)$_4$], indicating that the phthalimide ligands adopt an α,α,α,α arrangement. This conformation is often referred to as a "chiral crown", where the phthalimide moieties encircle one axial site, and the bulky *tert*-butyl groups sterically hinder access to the opposite face of the complex.[70-71]

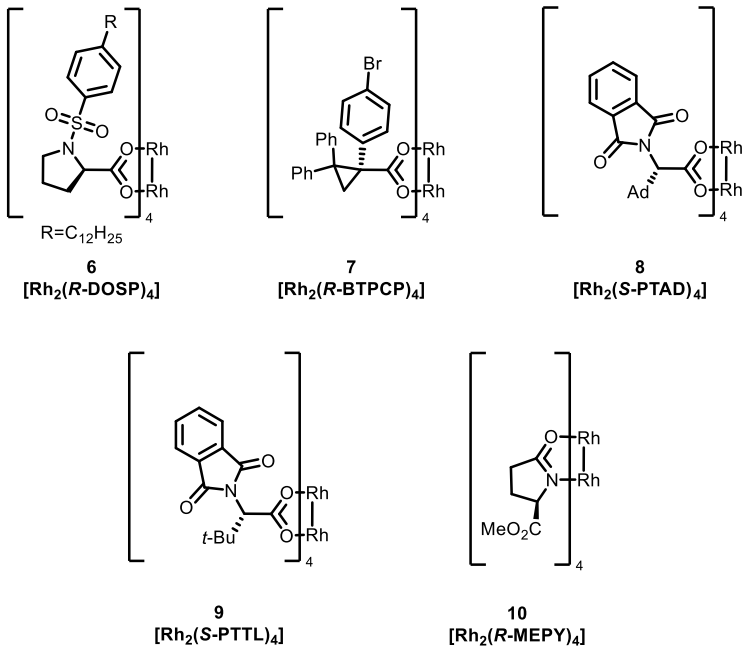

Figure 10-Examples of established dirhodium(II) complexes with chiral ligands.

The exact arrangement adopted during formation of the carbene intermediate and concomitant [2+1]-cycloaddition was uncertain, and as a result, the precise mode of enantioinduction remained unclear. However, pioneering work of Fürstner and coworkers,[26] in which a single-crystal structure of a carbene intermediate with [Rh_2(*S*-PTTL)$_4$] was obtained, showed that the four chiral phthalimide ligands are indeed arranged in an α,α,α,α conformation (Figure 11). Additional spectroscopic data showed that this conformation is retained in solution. These findings enabled the possibility to draw essential conclusions about the stereochemical course of an ensuing cyclopropanation reaction. The nucleophile preferentially approaches from the side of the aryl substituent. One of the four phthalimide ligands shields the back face (Re face) of the aryl group, such that only the front face (Si face) of the carbene remains accessible for attack by the olefin. As a result, cyclopropanations with donor–acceptor carbenes catalyzed by [Rh_2(*S*-PTTL)$_4$] proceed with high enantioselectivity in a predictable fashion.[26]

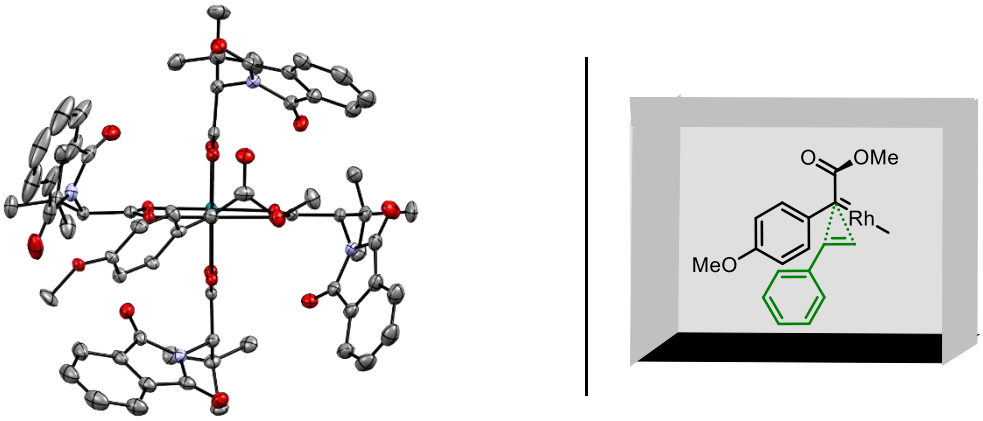

Figure 11-Left: X-ray structure of dirhodium(II) carbene with complex **9** (hydrogen atoms have been omitted for clarity). Right: Graphical representation of the favored styrene approach to the carbene intermediate of complex **9**.

1.6. Heteroleptic Dirhodium(II) Complexes

Homoleptic dirhodium(II) complexes represent the predominant class of catalysts in dirhodium(II) based carbene transfer chemistry. These complexes are typically synthesized through complete ligand exchange, starting from readily available precursors such as $[Rh_2(OAc)_4]$, using an excess of the desired ligand to achieve full substitution at the equatorial positions.[72] In contrast, heteroleptic dirhodium(II) complexes, which contain two or more distinct equatorial ligands, remain significantly less studied, with relatively few examples reported in the literature.[73] Most of these complexes are also prepared from $[Rh_2(OAc)_4]$ (**1**) under conditions similar to those used for the homoleptic analogues typically by reacting **1** with the selected ligand in high boiling solvents at reflux temperature. Cases have been reported in which the introduction of a second, structurally distinct equatorial ligand has led to notable advantages. These include the ability to fine-tune properties of catalysts, the opportunity for interesting ligand interactions that lead to catalytic improvements, and ways to heterogenise complexes.[73-74]

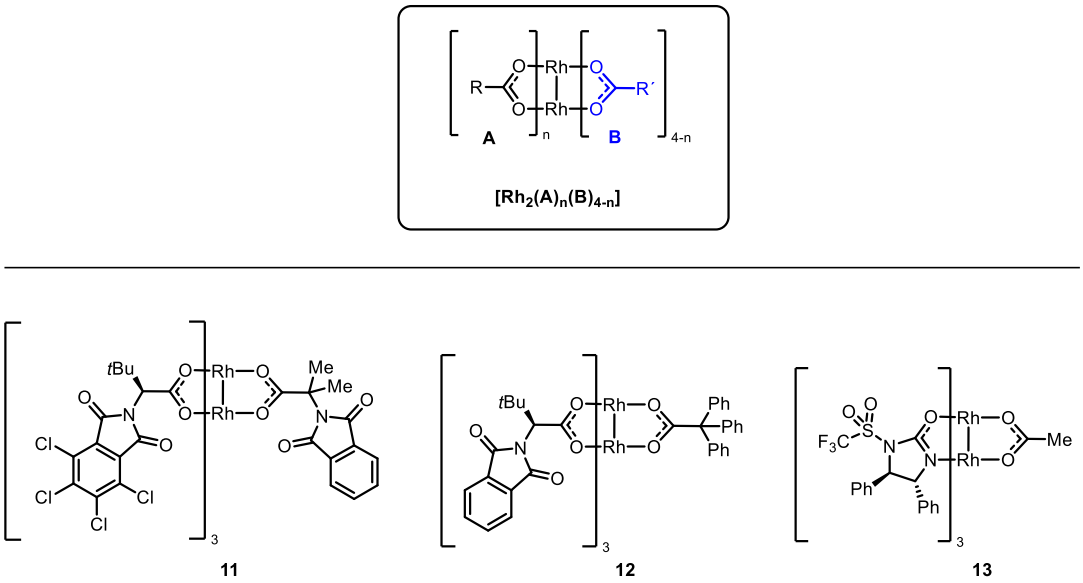

Figure 12-Top: general structure of a heteroleptic dirhodium(II) complex (consisting of carboxylate ligands). Bottom: examples of chiral heteroleptic dirhodium(II) complexes.

An example of such a complex was reported by Charette and coworkers,[75] who described a heteroleptic dirhodium complex composed of one achiral *N*-phthalimido-2-aminoisobutyrate (PTAiB) ligand and three chiral *N*-tetrachlorophthaloyl-*tert*-leucinate (TCPTTL) ligands. The application of this complex (**11**) in the cyclopropanation of **14** resulted in a modest improvement in enantioselectivity (Scheme 3, A). A more drastic improvement in stereoselectivity was seen with complex **12** reported by Fox and coworkers.[76] This heteroleptic catalyst proved especially effective in minimizing side reactions resulting from β-hydride shifts, which commonly affect carbene transformations involving α-alkyl diazoacetates (Scheme 3, B). In the cyclopropanation of styrene with ethyl-α-diazobutanoate (**16**), this heteroleptic complex delivered superior diastereo- and enantioselectivity compared to the homoleptic reference catalyst Rh_2(*S*-PTTL)$_4$.

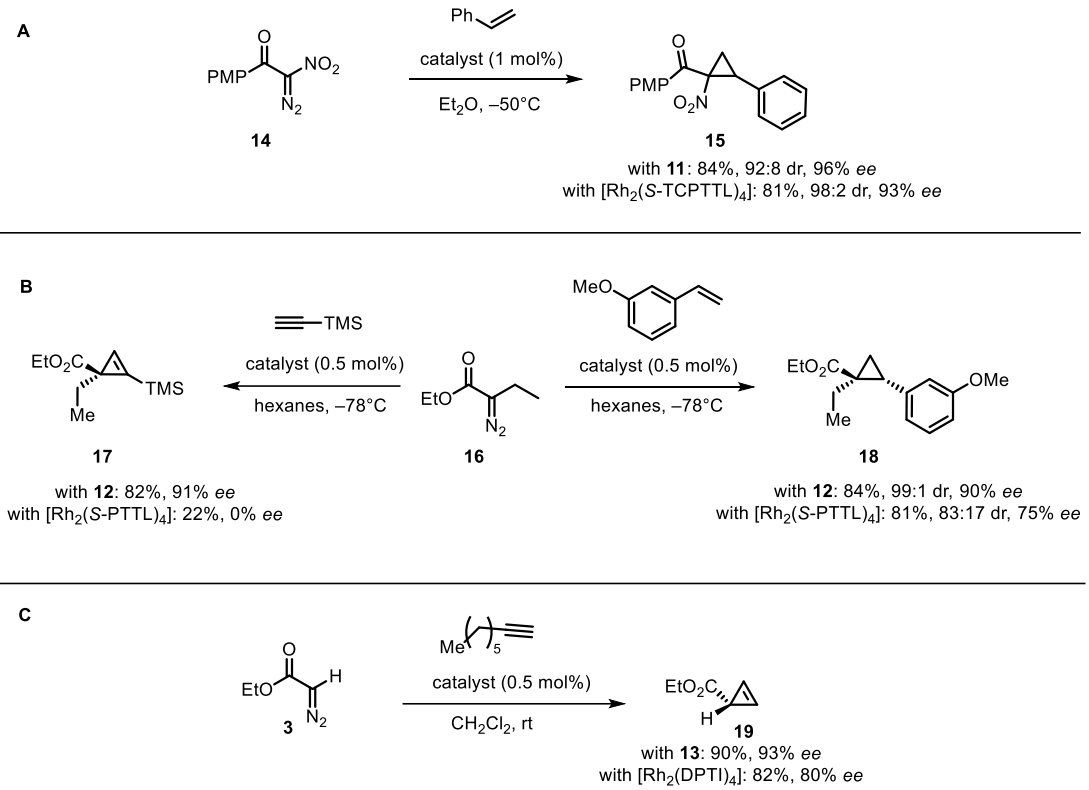

Scheme 3-Examples of [2+1] cycloadditions using chiral heteroleptic dirhodium(II) complexes.

The superiority of this complex was even more pronounced when employed in the cyclopropenation of diazo compound **16** with TMS-acetylene, as it yielded the desired cyclopropene in excellent yield and enantiopurity — in contrast to its homoleptic analogue Rh_2(*S*-PTTL)$_4$, which failed to induce any stereoselectivity in the transformation.[77] In addition to purely carboxylate-based complexes, Corey and coworkers reported the mixed carboxylate/carboxamidate dirhodium(II) complex $Rh_2(DPTI)_3(OAc)$ (**13**), featuring one acetate and three *R*,*R*-diphenyl-*N*-triflylimidazolidinone (DPTI) ligands.[78] This heteroleptic catalyst enabled a highly efficient and enantioselective synthesis of cyclopropenes from ethyl diazoacetate (**3**) and terminal alkynes, outperforming its homoleptic analogue $Rh_2(DPTI)_4$ (Scheme 3, C). Notably, the complex exhibited excellent chemoselectivity, reacting exclusively with terminal alkynes in the presence of alkenes.[79]

More recently, Fürstner and coworkers disclosed a heteroleptic dirhodium(II) complex bearing one acetamidate and three chiral triphenylcyclopropyl carboxylate ligands.[80] Given their relevance to the presented work (*infra in hoc*), the synthesis and reactivity of this complex are discussed in detail in Subchapter 1.7.

1.7. Heteroleptic Amidate-TPCP Dirhodium(II) Complexes

The Fürstner group reported in 2021 a heteroleptic complex comprising one acetamidate ligand and three chiral triphenylcyclopropyl carboxylate ligands, which was highly effective in the cyclopropanation reaction of α-stannylated diazoesters.[80] Moreover, the resulting α-stannylated cyclopropanes can undergo stereoretentive Stille-Migita cross-coupling reactions, allowing the synthesis of a broad space of cyclopropane motifs in highly asymmetric fashion.

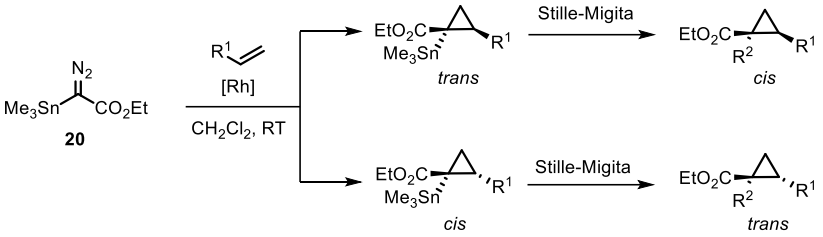

Figure 13-Conceptual outline of the [2+1] cycloaddition of a stannylated diazoester and their corresponding downstream functionalization by Stille-Migita cross-coupling reaction.

1.7.1. First Generation Amidate-TPCP Dirhodium(II) Catalysts

The first generation of amidate–TPCP dirhodium(II) catalysts was discovered serendipitously during asymmetric cyclopropanation reactions of terminal alkenes with stannylated, silylated, and germylated α-diazo esters.[80] An unexpected trace impurity present in a batch of $[Rh_2(R\text{-TPCP})_4]$ (**21**) was found to be uniquely effective, delivering both *cis*- and *trans*-cyclopropanes with high enantiomeric excess. Thorough HPLC analysis of the "contaminated" sample revealed the active species to be $[Rh_2(acam)(R\text{-TPCP})_3]$ (**25**), a heteroleptic complex containing a single acetamidate ligand. In contrast, a purified batch of $[Rh_2(R\text{-TPCP})_4]$ (**21**) was completely inactive under identical conditions, producing no detectable cyclopropane product, thereby highlighting the superior catalytic performance of the heteroleptic species **25**.

The synthesis of heteroleptic complex **25** was achieved by a two-step sequence starting from $[Rh_2(OTfa)_4]$. Three-fold ligand exchange with *R*-TPCP acid (**23**) furnished complex **24**. Complex **24** was then transformed to the desired amidate complex (**25**) either via treatment with $n\text{Bu}_4\text{NOH}$ in acetonitrile (22% yield) or through thermal ligand exchange with acetamide in refluxing chlorobenzene (31% yield) (Scheme 4). A structurally related *N*-methylated analogue of **26** was also prepared by a similar route. Notably, the introduction of an *N*-methyl group resulted in a significant reduction in enantioselectivity, highlighting the importance of the protic acetamidate ligand for the stereochemical outcome of the cyclopropanation. This

observation suggested potential hydrogen-bond interactions with the carbene intermediate and implied that the reaction predominantly, if not exclusively takes place on the Rh[O_3N] site of the catalyst.

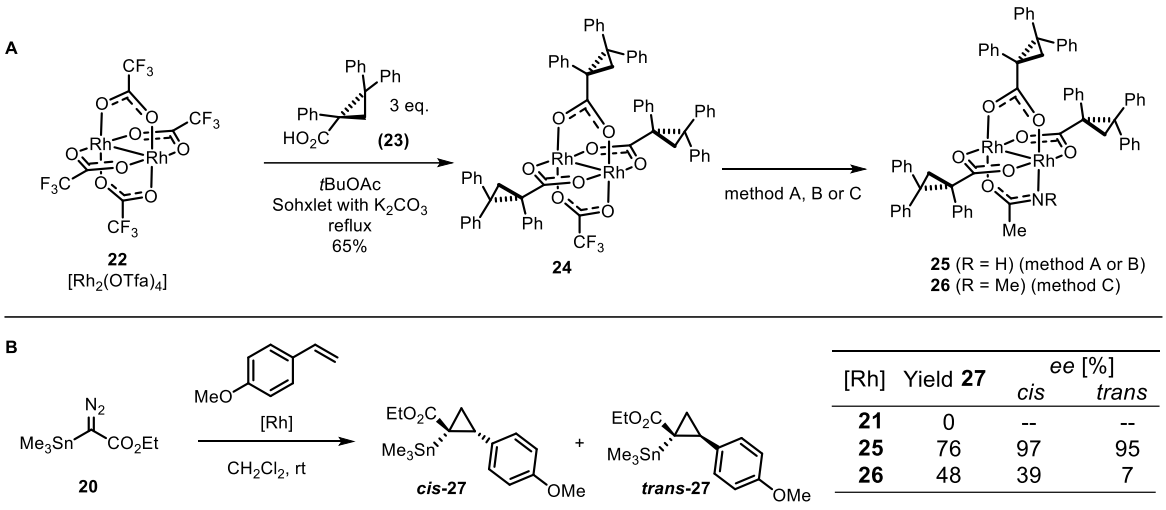

[Rh]	Yield **27**	*ee* [%] *cis*	*ee* [%] *trans*
21	0	--	--
25	76	97	95
26	48	39	7

Scheme 4-A: Preparation of heteroleptic complex amidate-TPCP complex (method A: nBu_4NOH, MeCN, 22%; method B: acetamide, chlorobenzene, Soxhlet with K_2CO_3, reflux, 31%; method C: molten *N*-methylacetamide, 90 °C, 6 h, 3%) B: cyclopropanation of α-stannylated diazo ester with *p*-methoxystyrene catalyzed by complexes **21**, **25** and **26**.

DFT calculations confirmed that the –NH group engages in interligand hydrogen-bonding with the carbonyl moiety of the stannylated carbene, therefore restricting the carbene´s conformational freedom. Furthermore, detailed computational analysis of all four possible transition states revealed that the approach of the olefin via quadrants **B** or **D** incurs a significant enthalpic penalty. This is attributed to the disruption of the established hydrogen-bonding array, rendering these transition states energetically unfavorable. These findings provided a compelling rationale for the excellent enantioselectivities observed experimentally.[81]

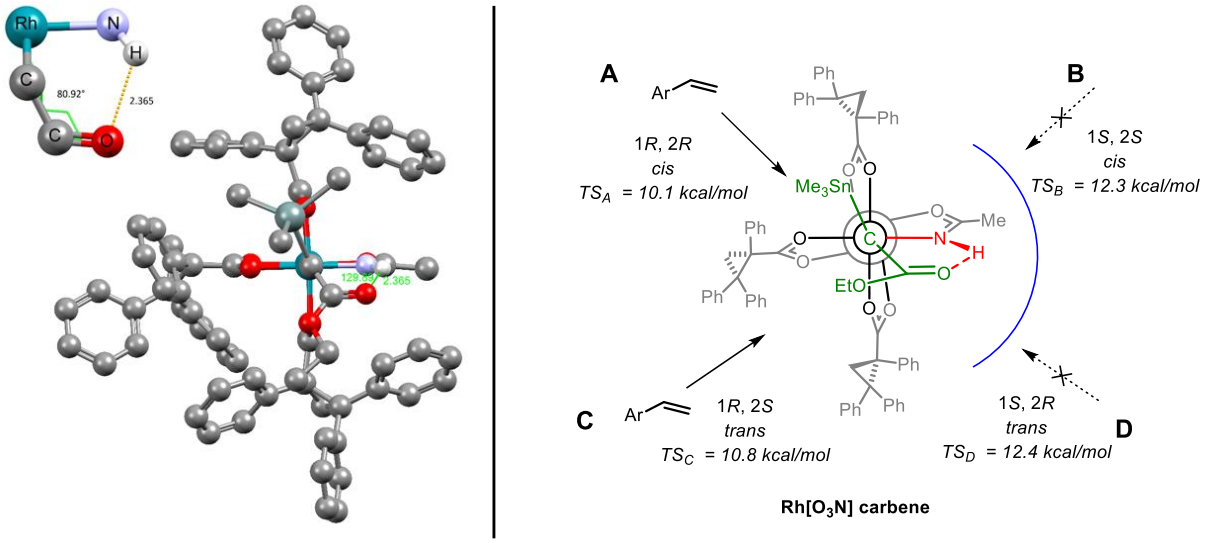

Figure 14-Left: computed structure of stannylated carbene intermediate with complex **25** calculated at the B3LYP-D3/def2-svp level of theory. Right: Schematic overview for the four possible olefin trajectories, displaying the transition states energies calculated for the cyclopropanation with *p*-methoxystyrene.

Following the successful development of a method for the asymmetric cyclopropanation of terminal olefins, which provided a broad set of optically active cyclopropylstannanes, the authors showcased the possibility for functionalization through Stille–Migita cross coupling. Productive conditions were identified using a slightly altered catalytic system reported by the Biscoe group,[82] consisting of $Pd(dba)_2$, JackiePhos, CuCl, and KF in tetrahydrofuran at 60 °C (Scheme 5). Under these conditions, the cross-coupled product was obtained with "retention" of configuration at the quaternary carbon center. This transformation constitutes the first case of quaternary stereocenter formation via a Stille–Migita reaction and underscores the potential of this approach in stereospecific carbon–carbon bond construction.

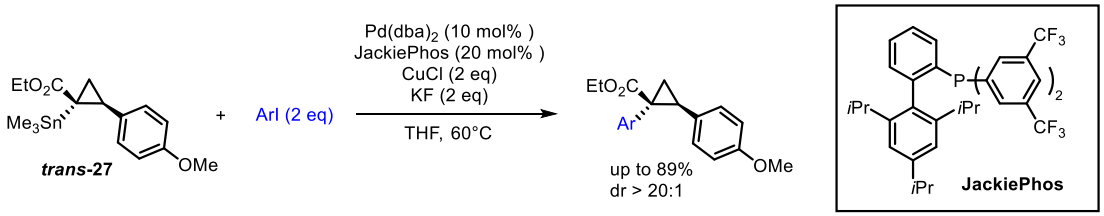

Scheme 5-General conditions for stereoretentive Stille-Migata conditions of cyclopropylstannanes.

1.7.2. Second Generation Amidate-TPCP Dirhodium(II) Catalysts

Despite its excellent enantioselectivity, the lack of diastereoselectivity of catalyst **25** constituted a major drawback. From the steric bulk map generated from a computed carbene intermediate derived from **25** (Figure 15), it can be seen that there is little to no steric bulk in the periphery of the carbene intermediate; Therefore, the energetic difference in transition states A and C (*vide supra*) is rather small (0.7 kcal·mol^{-1}). These insights prompted the conclusion to block one of the remaining two transition states (TS_A or TS_C) by chemically altering the ligand scaffold in order to achieve increased diastereoselectivity. Based on the structural information obtained by DFT calculations, the authors envisioned that a substituent on the *para*-position of the α-phenyl ring of the ligand might induce enough steric hindrance in quadrant A. This should make it less feasible for the olefin to approach via this trajectory, resulting in a *trans*-diastereoselective transformation. In a similar fashion, it was hypothesized that placing steric bulk on the *meta*-position of the α-phenyl ring of the ligand could result in a *cis*-diastereoselective transformation.

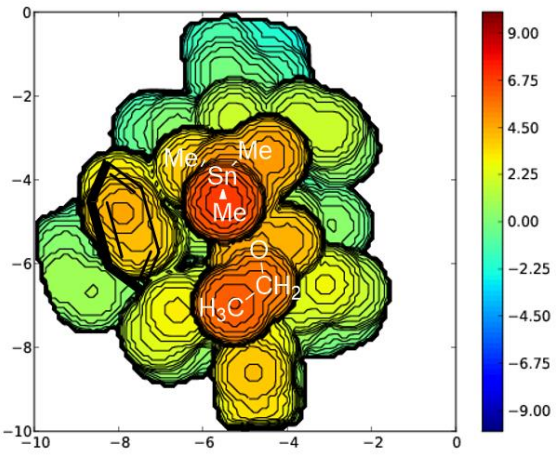

Figure 15-Topographic steric bulk map of dirhodium stannylated carbene intermediate with complex **25** generated with SambVca.[1]

The most effective catalysts for achieving either *cis*- or *trans*-selectivity are shown below. These complexes were accessed via an improved synthetic route toward amidate–TPCP dirhodium(II) catalysts. In this approach, $[Rh_2(acam)_4]$ (**28**) was treated with a slight excess of the corresponding *R*-TPCP acid (or its derivatives) under reflux conditions, leading to the desired threefold ligand exchange and formation of the heteroleptic complexes in a single step.

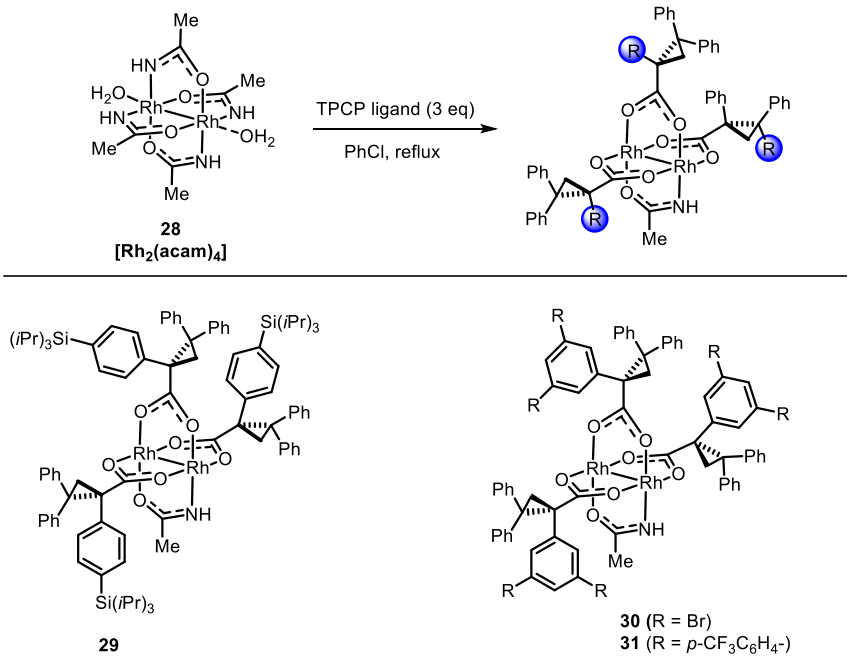

Scheme 6-General synthesis of amidate-TPCP Rh(II)-catalysts (top) and the most effective 2nd generation catalysts (bottom).

Cyclopropanation of *p*-methoxystyrene using catalyst **29** afforded the *trans*-isomer with excellent stereoselectivity. Alternatively, when complex **30** was employed under otherwise identical conditions, the corresponding *cis*-isomer was obtained as the major product, with a moderate diastereomeric ratio of 5:1 but with high enantiomeric purity. The ability to access both diastereomers of the stannylated cyclopropane in their optically enriched forms illustrates a rare example of diastereodivergent asymmetric catalysis.[83-89]

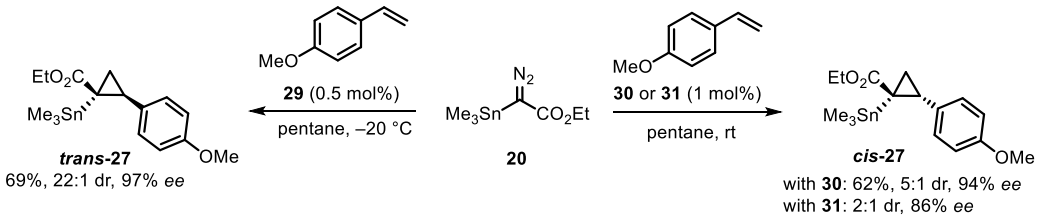

Scheme 7-Diastereodivergent enantioselective cyclopropanation reaction of stannylated diazo ester **20** with complexes **29**, **30** or **31**.

A plausible explanation for the reduced level of *cis*-selectivity relative to the *trans*-selectivity may be derived from a structural comparison between the X-ray structures of **32**, which has similar substitution pattern to **31**, and the X-ray crystal structure of the first-generation analogue **25** (Figure 16). Overlaying the two structures reveals that one of the three substituted TPCP ligands in complex **32** is rotated by approximately 180° around the C–C bond between the cyclopropane ring and the carboxylate group ligating the two rhodium atoms. This

conformational difference significantly alters the topology of the chiral environment as can be seen from the steric bulk map, thereby influencing substrate approach. Therefore, it would be highly desirable to find new catalytic systems that enable high *cis*-diastereoselectivity while maintaining the excellent enantioselectivity. The high levels of *trans*-selectivity can be best visualized by steric bulk map as the upper left olefin trajectory is now clearly blocked by the steric bulk of the ligand sphere.

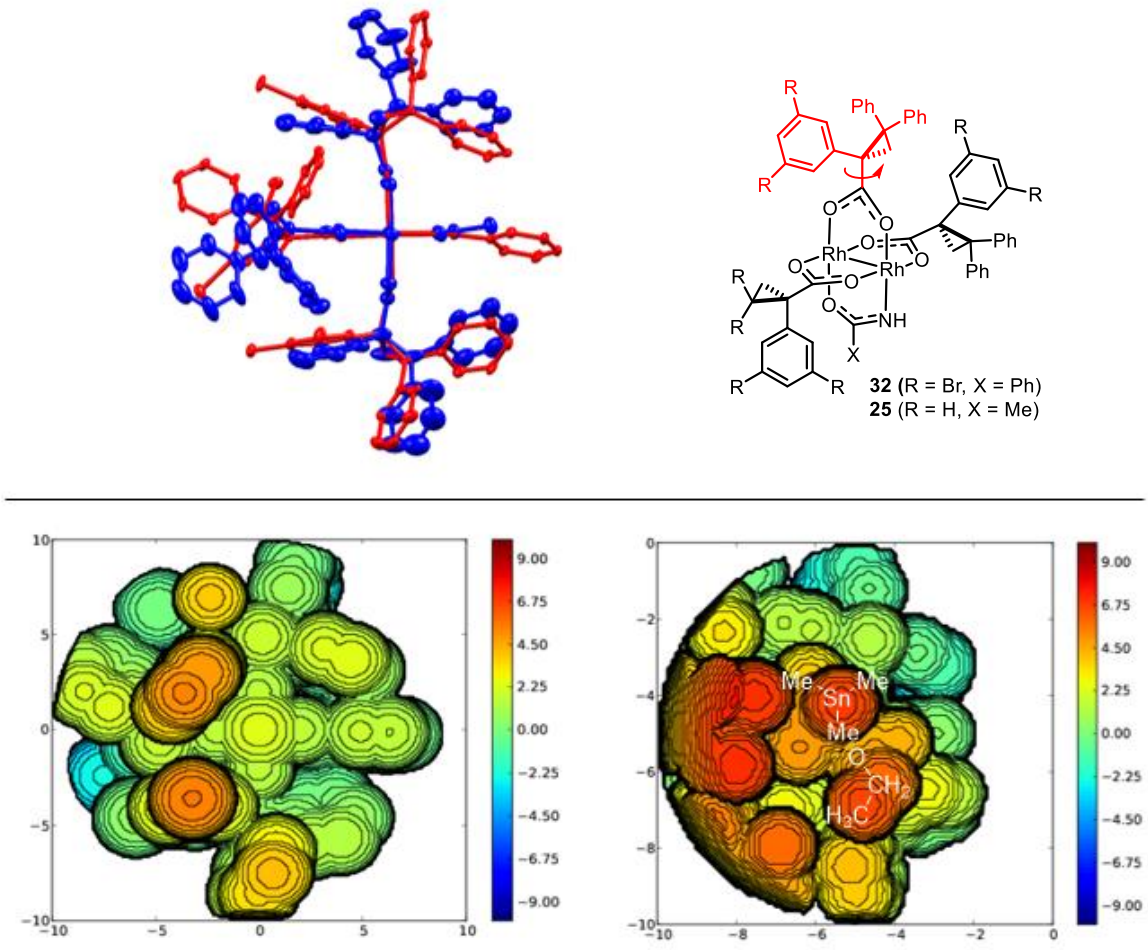

Figure 16-Top: overlay of the X-ray structures of the 1st generation complex **25** (blue) and the only moderate *cis*-selective catalyst **32** (red) in a Newman-type projection (the graphical representation can be found on the right). Bottom: topographic steric bulk maps created with SambVca[1] for *cis*-selective catalyst **31** (left) *trans*-selective catalyst **29** (right).

1.8. Heterobimetallic Bismuth-Rhodium(II) Complexes

The first bismuth-rhodium paddlewheel complex was reported by Dikarev and co-workers[90] in 2005. They obtained [BiRh(OTfa)$_4$] (**34**) by heating a sealed ampoule containing a stoichiometric mixture of [Bi$_2$(OTfa)$_4$] and[Rh$_2$(OTfa)$_4$] in the solid state. In 2012, the same group reported a more practical synthesis of **34** in solution, which was based on a one-pot reaction of **33** and [Rh$_2$(OTfa)$_4$], using freshly-ground bismuth metal as a reducing reagent (Scheme 8).[91] Initial studies by Davies and Dikarev showed that these heterobimetallic complexes could serve as catalysts for metal carbenoid transformations, albeit at a significantly slower rate than their homobimetallic analogues.[92]

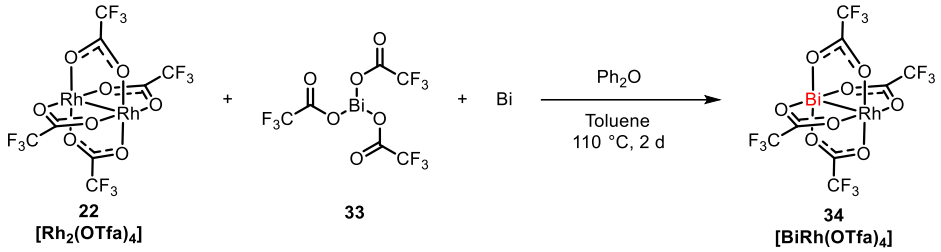

Scheme 8-Preparation of [BiRh(OTfa)$_4$} in solution according to the procedure of Dikarev and coworkers.

These initial findings were nuanced by Fürstner and co-workers who could show that bismuth-rhodium analogues exhibit complementary reactivity showing great potential for small molecule and solvent activation chemistry.[93] An example of such unprecedented reactivity is the cyclopropanation of very electron-deficient polychlorinated alkene **35** catalyzed by [BiRh(esp)$_2$] (Scheme 9), which cannot be achieved with any other dirhodium paddlewheel complex. This reactivity can be ascribed to the enhanced electrophilicity of the carbene intermediate as a result of weaker π-backbonding interactions between the carbene and the bismuth-rhodium complex compared to dirhodium carbene complexes.[93]

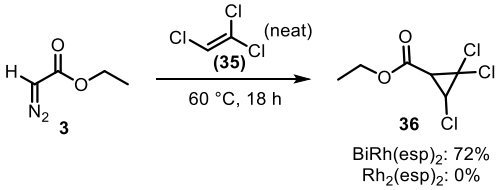

Scheme 9-Direct comparison of the reactivity of EDA with trichloroethylene catalyzed by [BiRh(esp)$_2$] and [Rh$_2$(esp)$_2$].

The groups of Davies[94] and Fürstner[95] reported independently the first asymmetric variant of such bismuth-rhodium complexes, which both performed well in the asymmetric cyclopropanation and C–H insertion reactions of donor-acceptor diazo compounds. The chiral

μ_2-carboxylates are typically installed via a four-fold ligand exchange reaction from [BiRh(OTfa)$_4$] (**34**) affording the corresponding chiral bismuth-rhodium complexes.

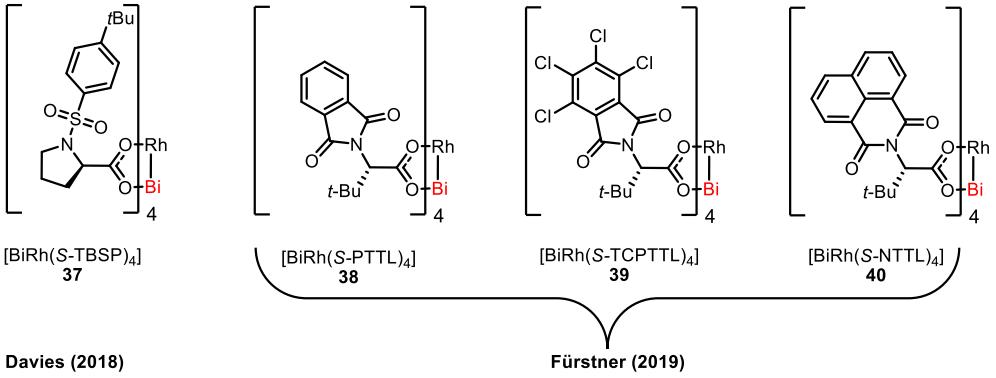

Scheme 10-Overview of the first chiral bismuth-rhodium complexes.

[BiRh(*S*-TBSP)$_4$] (**37**) was described by Davies and co-workers to induce slightly higher levels of asymmetric induction in cyclopropanation reactions in comparison with its dirhodium(II) analogue [Rh$_2$(*S*-TBSP)$_4$], however significantly longer reaction times were necessary. Fürstner and coworkers reported significantly higher *ee´*s with [BiRh(*S*-PTTL)$_4$] (**38**) when compared to Hashimoto´s [Rh$_2$(*S*-PTTL)$_4$] (**9**)[96-97] in the cyclopropanation reaction of diazo compound **41** with styrene (Scheme 11). Detailed spectroscopic studies had previously shown that [Rh$_2$(*S*-PTTL)$_4$] adopts an α,α,α,α-conformation (see section 1.5) in which all *N*-phthalimido groups of the carboxylate ligands are oriented to the same side in both solid state and in solution.[26] The formal replacement of a Rh(II) atom in complex **9** with a Bi(II) atom imparts a conical shape to the ligand sphere (**38**), due to bismuth's larger van der Waals radius. Hence, the more tightened chiral calyx at the Rh(II)-site leads to better enantioinduction. Furthermore, Bi(II) does not decompose the diazo ester, effectively suppressing any racemic background reaction.[95] Indeed, a **38**·EtOAc adduct in the solid state adopts a C$_4$ symmetric "all up" conformer in which the phthalimido ligands point towards the reactive rhodium center. Additionally, the co-crystallized EtOAc is bound to rhodium, leaving the bismuth center unligated, indicating its poor Lewis acidity.

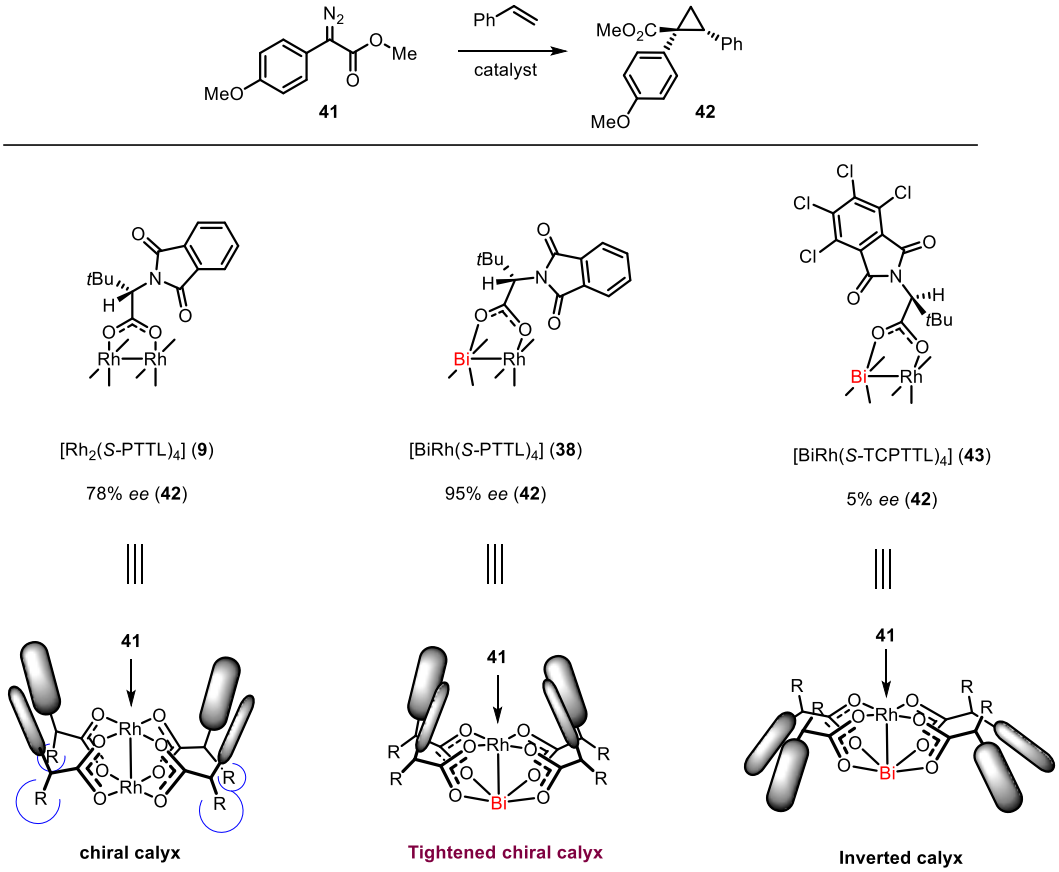

Scheme 11-Results of cyclopropanation reaction of **41** with complexes **9, 38 and 43.** The ´paddles´ in the schematic drawing represent the phthalimido groups and R= *t*Bu.

Interestingly, cyclopropane **42** was afforded in nearly racemic fashion when complex **43** was used as the catalyst. X-ray analysis revealed that [BiRh(*S*-TCPTTL)$_4$] (**43**) features an inverted calix in which the chiral environment envelopes the unreactive Bi(II)-site.

Even though the *ee* was drastically improved in many cases by using heterobimetallic [BiRh(*S*-PTTL)$_4$] (**38**), limitations were encountered with less electron-rich donor-acceptor diazo derivatives. Fürstner and co-workers reported an improved catalyst design based on London-dispersion interactions, stabilizing the shape and directionality of the calyx.[98] In this design, the *tert*-leucine derived ligands were replaced by phenylglycine derivatives carrying TIPS-groups at the *meta*-positions of the aromatic ring, rendering complexes **44-45** (Scheme 12). Computational analysis unambiguously showed that the TIPS-groups induce enough intramolecular contacts to entail stabilization via dispersion interactions. Additionally, complex **45** benefitted from installing *tert*-butyl groups on the phthalimido moiety of the ligand as it stabilizes the conformer by an additional 1.7 kcal·mol^{-1} with respect to **44**, leading to a notably more confined chiral calyx. These complexes performed well in [2+1]-cycloadditions of both electron-rich and electron-deficient aryl diazoesters. Excellent results

were also obtained with donor-acceptor α-diazo ketones and donor-donor diazo derivatives. Strikingly, the reactivity of these complexes is remarkably high; the authors report complete conversion of the diazo compound at −10 °C within 10 min at catalyst loadings as low as 0.25 mol%, indicating favorable interactions with the incoming substrate.

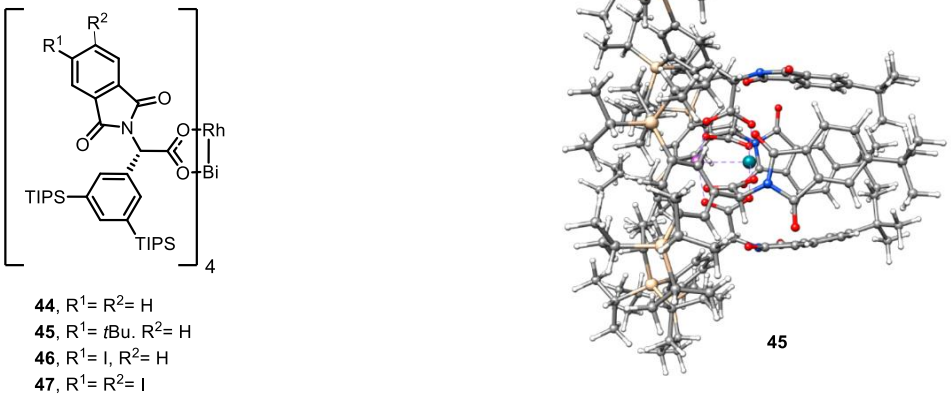

Scheme 12-Left: phenylglycine derived bismuth-rhodium paddlewheel complexes (**44-45**) empowered by London-dispersion. Right: side view of structure **45**, computed at the PBE/def2-SVP level of theory with D3(Bj) dispersion correction.

The authors also demonstrated that the applicability of complexes **44-47** could be extended to C–H insertion reactions (Scheme 13).[99] The confined ligand sphere around the donor-acceptor carbene results in the stereoselective insertions, resulting in enantioenriched products **48-54**. Even gaseous ethane could be used as a substrate, resulting in the corresponding product (**54**). The wide scope and excellent levels of stereoselectivity makes this asymmetric approach complementary to the outcome of traditional asymmetric ester alkylation, allylation, benzylation, propargylation and aldol reactions.

[2+1]-cycloadditions:

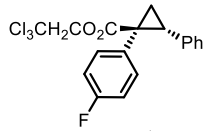

48[b]
90%, 83% *ee*
99%, 98% *ee*

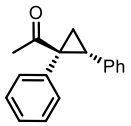

49[b]
25%, 78% *ee*
68%, 91% *ee*

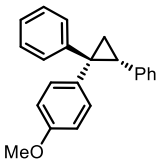

50[d]
68%, 99% *ee*

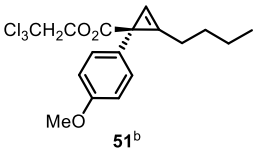

51[b]
54%, 96% *ee*
82%, >99% *ee*

C-H insertions:

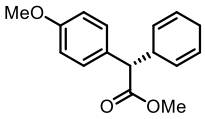

52[b]
61%, 97% *ee*
78%, 99% *ee*

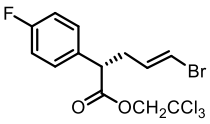

53[c]
80%, 96% *ee*

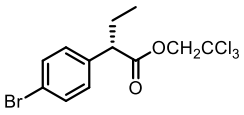

54[e]
80%, 94% *ee*

Scheme 13-Selected examples of [2+1]-cycloadditions and C–H insertion reactions. a) Color code: black: **45**, red **38**. b) in pentane at –10°C. c) in C_6F_6 at rt. d) at rt in pentane. e) at 25 atm in C_6F_6 at rt.

2. Further Exploration of the Reactivity of Chiral Bismuth-Rhodium Paddlewheel Catalysts

2.1 Introduction and Motivation

As discussed in section 1.8, chiral heterobimetallic bismuth-rhodium complexes (**44-47**) empowered by London-dispersion rank amongst the most effective and selective catalysts known to date for [2+1]-cycloadditions. Additionally, they also have an outstanding performance in a wide variety of C–H insertion reactions. With such well-performing catalysts at hand, we were interested in exploring further reactivity with rather unconventional diazo derivatives or surrogates thereof to get novel cyclopropane motifs.

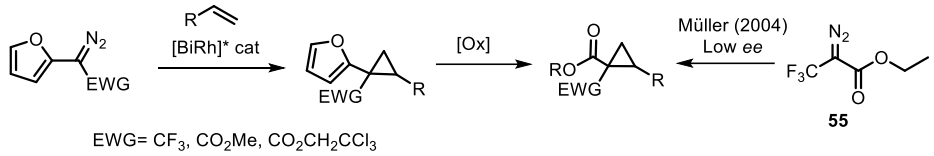

Scheme 14-Approach to 2-furyl substituted cyclopropanes, 1,1-EWG substituted cyclopropanes and derivatives thereof.

Particularly, 2-furyl diazo derivatives came to our attention as suitable candidates for the following reasons: i) cyclopropane motifs bearing a 2-furyl moiety are rarely reported to date, there are no reports of asymmetric versions; ii) oxidative cleavage of the 2-furyl substituted cyclopropane would give access to a carboxylic acid, therefore allowing the preparation of 1,1-EWG substituted cyclopropanes in asymmetric fashion. Especially 1-(trifluoromethyl)cyclopropane-1-carboxylic acid derivatives were of interest, as these compounds cannot be obtained with any decent level of optical purity by direct asymmetric cyclopropanation of alkenes with ethyl-3-trifluoro-2-diazopropionate.[100]

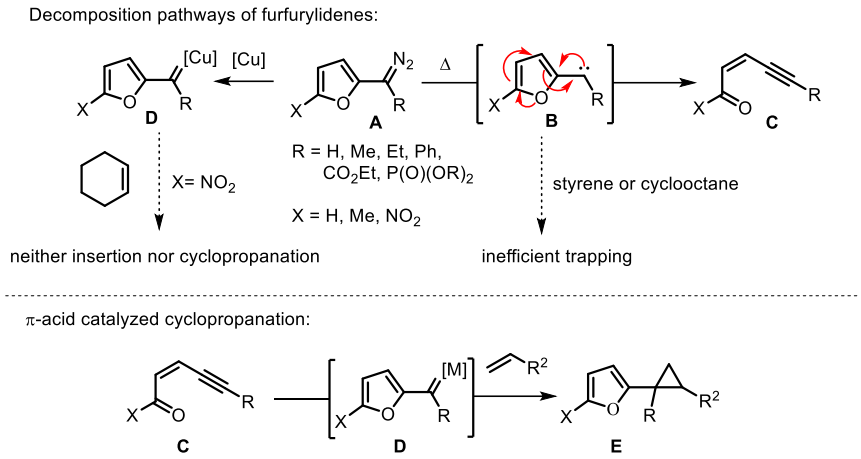

Scheme 15-Incongruent prior art: top: decomposition pathways of furfurylidenes described by Hoffman and co-workers.[101] Bottom: π-acid catalyzed cyclopropanation.

Early studies reported by Hofmann and co-workers[101-102] showed that this transformation could be particularly challenging as thermolysis of 1-diazo-1-(2-furyl)-alkanes **A** resulted in instant electrocyclic ring opening of the transient furfurylidenes **B**, forming enynal derivatives of type **C** (Scheme 15). Attempts to intercept such intermediate **B** in neat cyclooctane or styrene resulted in very low yields. Efforts to perform such reaction via a copper mediated pathway failed to afford any cyclopropane or C-H insertion product. This stands in partial contrast to numerous reports[103-105] that imply intervention of furyl metal carbenes **D**, generated *in-situ* by π-acid-catalyzed cycloisomerisation of compounds of type **C**, which can be seen as the microscopic reverse of the decomposition pathway proposed by Hofmann. The incongruent prior art might imply that free furfurylidenes are fleeting intermediates, whereas furyl metal carbenes are discrete species under certain settings.

2.2. Results and Discussion

This project was conducted in collaboration with Dr. Jonathan Decaens. The initial discovery and part of the optimization related to the synthesis of 2-(1-(trifluoromethyl)cyclopropyl)furans were carried out by him. To provide a comprehensive and coherent overview of the research, these contributions have been incorporated into this thesis with permission of the author.

2.2.1 Initial Results

The synthesis of diazo compound **59** commenced from trifluoromethyl hydrazone **57**, which was readily prepared by condensation of trifluoromethyl ketone **56** with tosylhydrazine. It was envisioned that Bamford-Stevens rearrangement of **57** would lend access to diazo compound **59**. However, attempts to obtain diazo compound **59** resulted in either decomposition or no conversion of the corresponding trifluoromethyl hydrazone **57** (Scheme 16). Directly

subjecting **57** to catalysis in the presence of a base resulted in no conversion. As hydrazone **57** is not very reactive, it was envisioned that enhancing the acidity of the hydrazone moiety might lead to increased reactivity. Triftosylhydrazones have shown to be significantly more reactive than tosylhydrazones, allowing the Bamford-Stevens rearrangement to occur under mild conditions.[106] Although isolation of **59** failed, trifluoromethyl hydrazone **58** was successfully converted to afford cyclopropane **60** with excellent levels of enantioselectivity albeit in a moderate 36% yield.

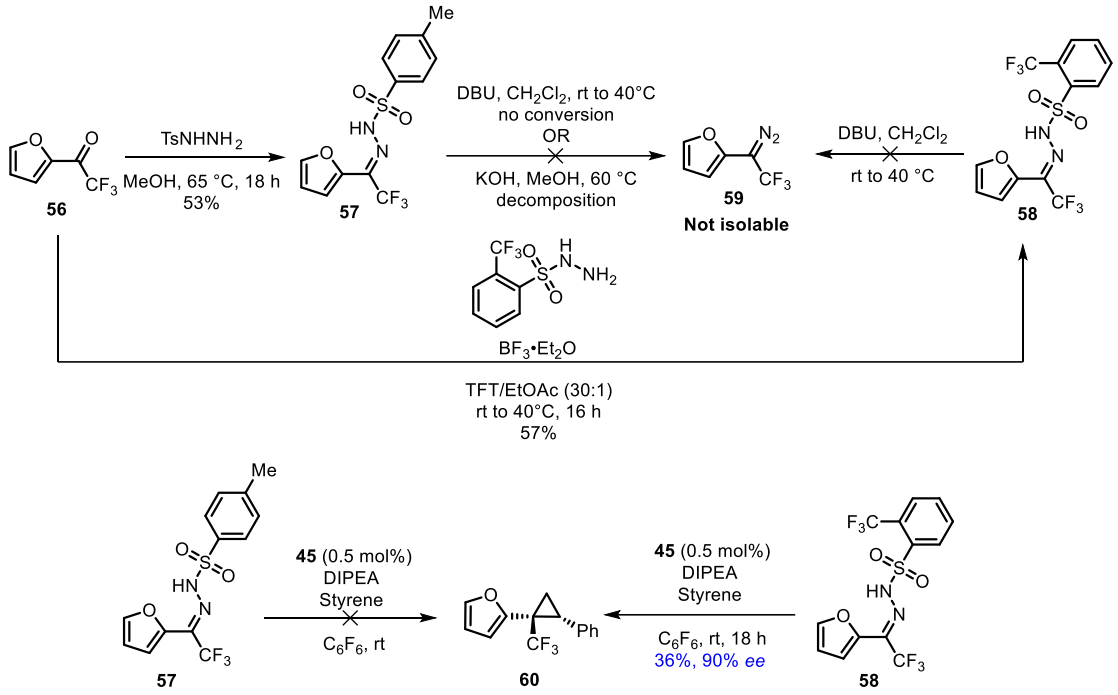

Scheme 16-Initial attempts towards diazo compound **59** and cyclopropane **60**.

In a similar fashion, it was attempted to perform the cyclopropanation with methylester hydrazone **61** which afforded the desired cyclopropane **63** in 62% yield with a moderate 64% *ee* (Table 1). Using a more bulky trichloroethyl ester (**62**) resorted in an increase of the *ee* to 75%. TLC analysis indicated in both reactions full consumption of the starting material, however the formation of a yellow side product could be observed. It was envisioned that lowering the temperature might result in an increase of the enantioselectivity and suppress byproduct formation, which presumably was ascribed to the electrocyclic ring opening of the furfurylidenic moiety described by Hoffman.[101] Although, the *ee* did increase to 86% upon lowering the temperature to –20 °C (entry 3), still significant amounts of byproduct were formed. Lowering the temperature to –40 °C (entry 4) did not result in full consumption of **62**, moreover the yield of cyclopropane **64** did not improve. Due to the unsatisfactorily low yield of cyclopropane **64**, subsequent efforts were directed toward the most promising trifluoromethylated cyclopropane analogue **60**.

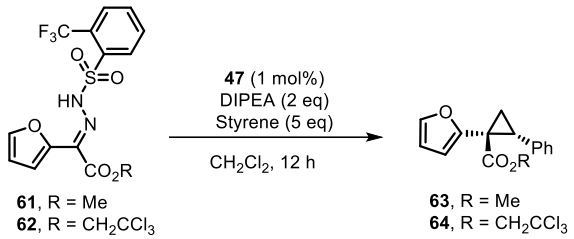

#	R	T [°C]	Yield % [^{1}H NMR]	*ee* %
1	Me	rt	62	64
2	CH_2CCl_3	rt	60	75
3	CH_2CCl_3	–20	[26]	86
4[a]	CH_2CCl_3	–40	[22]	88

Table 1-Cyclopropanation with hydrazone esters (**61-62**). The yields in brackets refer to NMR yields, determined with 1,3,5-trimethoxybenzene as internal standard. a) stirred for 48 h.

2.2.2 Catalyst Screening and Optimization

As described above, cyclopropane **60** was formed directly from hydrazone **58** when Hünig base was added dropwise over a course of 30 min in the presence of [BiRh] catalyst **45** and styrene, resulting in a moderate yield of 36% and 90% *ee* (Table 2). Fast addition of the base (entry 3) and changing the order of addition of the reagents (entry 2) resulted in drastically lower yields, indicating that slow base addition is crucial for a gentle release of the diazo compound **59**. Performing the reaction in pentane (entry 4) led only to traces of cyclopropane due to the poor solubility of **58** in pentane. The yield could be drastically improved when dichloromethane was used as the solvent. Remarkably, cooling the reaction to –10 °C (entry 7), led to complete inhibition of the reaction, most likely the Bamford-Stevens rearrangement does not occur at such low temperatures. In fact, increasing the temperature to 40 °C (entry 8) led to almost quantitative isolation of cyclopropane **60** with only a minor loss of enantioselectivity. Testing the iodo and diiodo substituted bismuth-rhodium catalysts **46** and **47** in refluxing dichloromethane led to a slight increase of the *ee*, however the yield dropped by nearly 10%, to 75% and 74%, respectively. Running the reaction at room temperature with the diiodo-substituted catalyst **47** (entry 11) afforded the cyclopropane in 84% and 92% *ee*. Performing the reaction in dichloroethane (entry 12) and toluene (entry 13) did not have any effect on the enantioselectivity, however the yields were drastically lowered. Room temperature proved to be the optimal condition for this transformation, as performing the reaction at 10 °C resulted in a marked decrease in yield, as illustrated in entry 14.

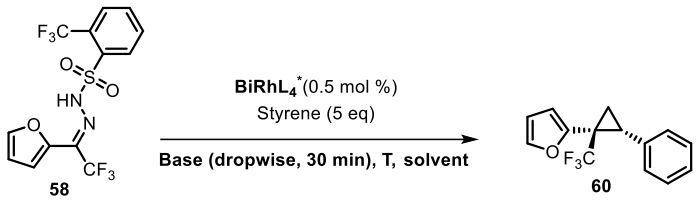

#	Catalyst	Base	T [°C]	Solvent	Yield % [^{1}H NMR]	*ee* %
1	**45**	DIPEA	rt	C_6F_6	36	90
2[a]	**45**	DIPEA	rt	C_6F_6	[15]	n.d.
3[b]	**45**	DIPEA	rt	C_6F_6	[16]	n.d.
4	**45**	DIPEA	rt	Pentane	[<5]	n.d.
5	**45**	DIPEA	rt	CH_2Cl_2	59 [60]	89
6	**45**	DBU	rt	CH_2Cl_2	52	89
7	**45**	DIPEA	–10	CH_2Cl_2	0	n.d.
8	**46**	DIPEA	40	CH_2Cl_2	95	88
9	**47**	DIPEA	40	CH_2Cl_2	75	90
10	**47**	DIPEA	40	CH_2Cl_2	74	91
11	**47**	DIPEA	rt	CH_2Cl_2	84	92
12	**47**	DIPEA	rt	DCE	46	92
13	**47**	DIPEA	rt	Toluene	52	92
14	**47**	DIPEA	10	CH_2Cl_2	[60]	93

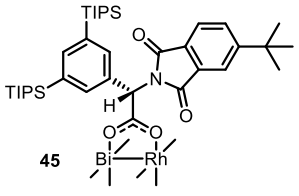

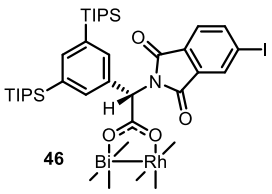

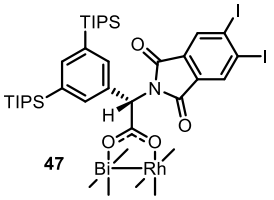

Table 2-Optimization of the conditions for the cyclopropanation of **58**. All screening reactions were performed on a 0.1 mmol scale. Yields in brackets are determined via crude ^{1}H NMR analysis with triphenylmethane as internal standard. All other yields are isolated yields. [a] DIPEA was added to **58** in C_6F_6, stirred for 10 min, followed by addition of catalyst and styrene in C_6F_6. [b] DIPEA was added in one shot to a solution of catalyst, styrene and hydrazone **58**.

2.2.3 Scope

2.2.3.1 Initial Scope

With the optimized conditions at hand, the scope of cyclopropanation of diazo surrogate **58** with various olefins was investigated (Scheme 17). Reacting electron-rich styrene derivatives afforded the corresponding cyclopropanes (**65-67**) in excellent enantioselectivity and with good yields. Even a heteroaromatic olefinic substrate as 2-vinylthiophene resulted in cyclopropane **68** in high optical purity. However, when *p*-bromostyrene was employed, the yield of cyclopropane **69** decreased significantly, with only 65% observed in the crude reaction mixture. Given that *p*-bromostyrene contains only a mildly deactivating bromo-substituent, there was concern that more strongly deactivated olefins might afford minimal amounts of the corresponding cyclopropanes. Consequently, efforts were directed toward improving the yield using *p*-bromostyrene as the model [2+1] cycloaddition partner.

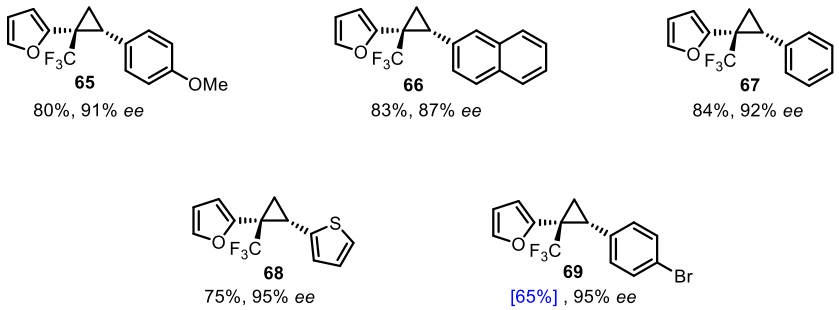

Scheme 17-1,1-Disubstituted (trifluoromethyl)cyclopropane derivatives formed by [BiRh] catalyzed [2+1] cycloaddition using triftosylhydrazone **58** as the carbene source. All reactions were carried out on a 0.1 mmol scale with complex **47** (0.5 mol%) and DIPEA (2 eq) in CH_2Cl_2 at ambient temperature using 5 equivalents of the respective alkene. Yield in brackets is ^{1}H-NMR yield determined with 1,3,5-trimethoxybenzene as internal standard.

2.2.3.2 Further Reaction Optimization

Further optimization of the cyclopropanation reaction was carried out using *p*-bromostyrene as the model alkene (Table 3). Increasing the catalyst loading resulted in a higher yield of cyclopropane **69** (entry 2). The most significant improvement was observed upon doubling the amount of alkene from five to ten equivalents, affording an 82% (^{1}H NMR) yield (Entry 3). A slower addition of Hünig's base over five hours instead of 30 minutes (entry 4) also led to enhanced product formation. In contrast, raising the reaction temperature (entry 5) caused a substantial decrease in yield, with only 39% cyclopropane detected (^{1}H NMR). Since, certain individual factors (addition time, amount of alkene, catalyst loading) had a beneficial impact on the yield of cyclopropane **69**, it was investigated if synergistic effects existed between those individual reaction parameters. Unfortunately, no enhancing effects were observed, as a combination of these parameters (entry 6) did not surpass the yield obtained in entry 3. Under

the optimized conditions, cyclopropane **69** was isolated in 73% yield with an excellent 95% enantiomeric excess (entry 7).

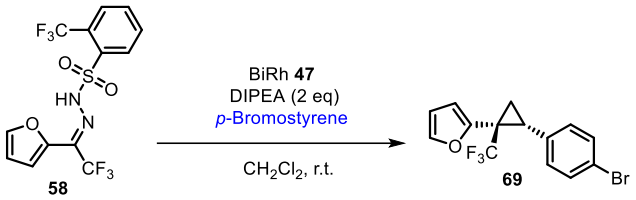

#	Eq Alkene	Catalyst loading [mol%]	Addition time base [h]	T [°C]	Yield % [^{1}H NMR]	*ee* %
1	5	0.5	0.5	rt	[65]	n.d.
2	5	1	0.5	rt	[75]	n.d.
3	10	0.5	0.5	rt	[82]	94
4	5	0.5	5	rt	[78]	n.d.
5	5	0.5	0.5	40	[39]	91
6	10	1	1	rt	[83]	94
7	10	0.5	0.5	rt	73	95

Table 3-Further optimization with *p*-bromostyrene as model alkene. Screening reactions were performed on a 15 mg scale. Yields in brackets are determined via crude ^{1}H NMR analysis with 1,3,5-trimethoxybenzene as internal standard. Entry 7 was performed on a 0.1 mmol scale + isolated yield.

2.2.3.3 Scope

Under the further optimized conditions the scope was expanded (Scheme 18). Usage of variously substituted styrene derivatives resulted in the corresponding cyclopropanes (**70-73**) with excellent enantioselectivity, largely independent of whether they carry electron-donating or -withdrawing substituents at the *para*-position of the phenyl ring. Placing the substituents in *ortho*- or *meta*-position resulted in slightly lower enantioinduction, affording cyclopropanes (**73-74**) in 89% and 81% *ee*, respectively. Also, a more complex tricyclic motif **75** could be obtained with indene as the corresponding alkene with an enantiomeric excess of 91%. In addition to 2-vinylthiophene (*vide supra*), *N*-Boc-2-vinylpyrrole could be employed affording **76** with good levels of asymmetric induction. It is important to note that all of these products were obtained virtually as single diastereomers (dr > 20:1(*trans*)). In contrast, the reaction with α-methylstyrene is hardly discriminative, resulting in **79** with a dr of 1.6:1. The

relative configuration of several products was rigorously assigned via ^{1}H-^{1}H and ^{1}H-^{19}F NOESY experiments.

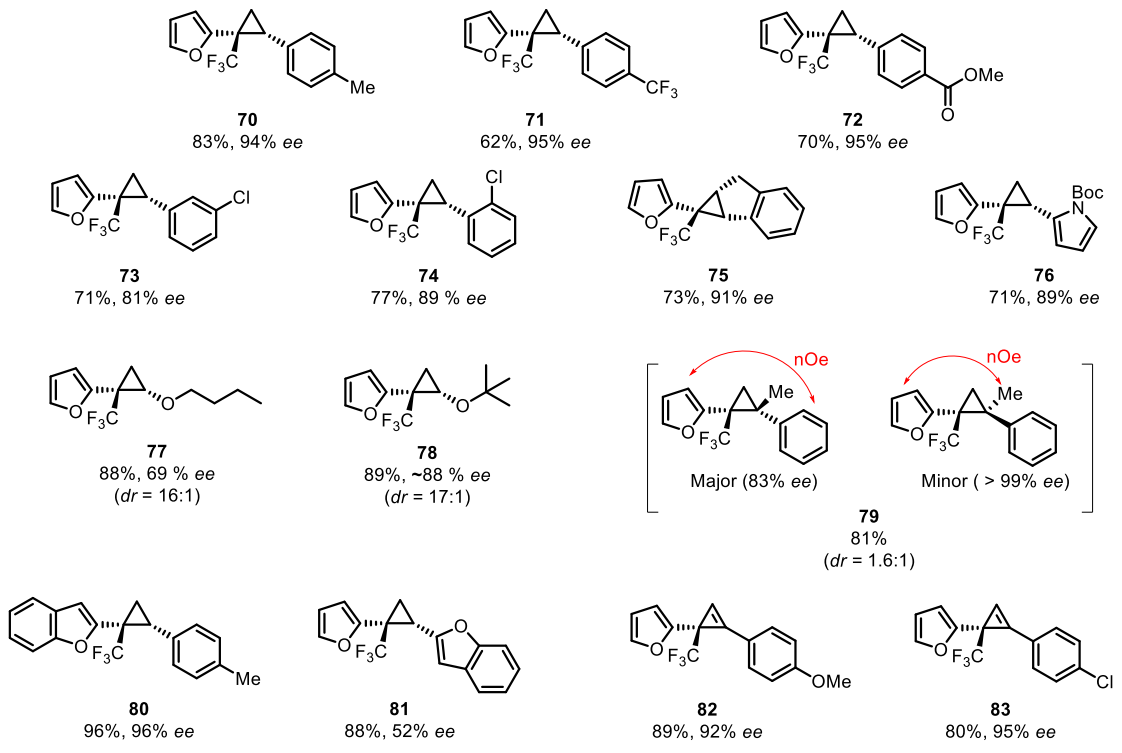

Scheme 18-Scope of cyclopropanes/cyclopropenes formed by a [BiRh] catalyzed [2+1] cycloaddition using *N*-triftosylhydrazone as the carbene source. All reactions were carried out on a 0.1 mmol scale with complex **47** (0.5 mol%) and DIPEA (2 eq) in CH_2Cl_2 at ambient temperature using 10 equivalents of the respective alkene/alkyne.

In addition to styrene derivatives, the scope could be expanded to electron-rich vinyl ethers, leading to appreciable results (**77-78**). However, 2-vinylbenzofuran afforded product **81** in high yield, but with significantly lower levels of enantioinduction. A control experiment was carried out in which the benzofuran moiety was incorporated in the *N*-triftosylhydrazone reagent and reacted with *p*-methylstyrene, gratifyingly leading to product **80** in excellent yield and *ee*. The methodology could also be expanded to cyclopropenations as terminal arylalkynes reacted swiftly in [2+1]-cycloadditions leading to compounds **82-83** in high optical purity. It is important to mention that not all olefins resulted in satisfying results; *E*-configured β-methylstyrene, vinyl MIDA-boronate and ordinary alkenes such as 1-hexene, allyltrimethylsilane and vinyltrimethxlsiloxane failed to react.

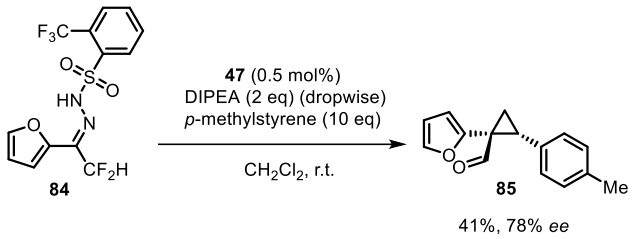

Scheme 19-Cyclopropanation of difluoro hydrazone **84**, resulting in an aldehyde **85**.

A surprising result was obtained when difluoromethyl hydrazone **84** was subjected to catalysis. Instead of the anticipated difluoromethyl-substituted cyclopropane, 1-(2-furyl)cyclopropane-1-carbaldehyde **85** was isolated in 41% yield and 78% *ee* (Scheme 19). This result shows that, in addition to the [2+1] cycloaddition, a defluorination event occurred. It remains unclear whether this defluorination took place during catalysis or upon work-up. Given the moderate enantioselectivity observed, further investigation into this side reaction was not pursued.

2.2.3.4 Investigation into the Cyclopropanation of other Heterocyclic Hydrazones

Since furyl and benzofuryl hydrazones could be successfully transformed into cyclopropanes with high levels of asymmetric induction (*vide supra*), it was of interest to investigate other heterocyclic hydrazones comprising oxazolic, thiazolic and benzoxazolic motifs. Access to the corresponding cyclopropanes would not only add additional value to the developed methodology by means of the vast interest into these heterocyclic motifs in pharmaceutical industry,[107-111] but would open up the pathway to other functionalities (e.g. a thiazole can be conveniently transformed under oxidative conditions to an aldehyde[112]). The corresponding hydrazones **86-88** were synthesized in analogous manner to **58**.

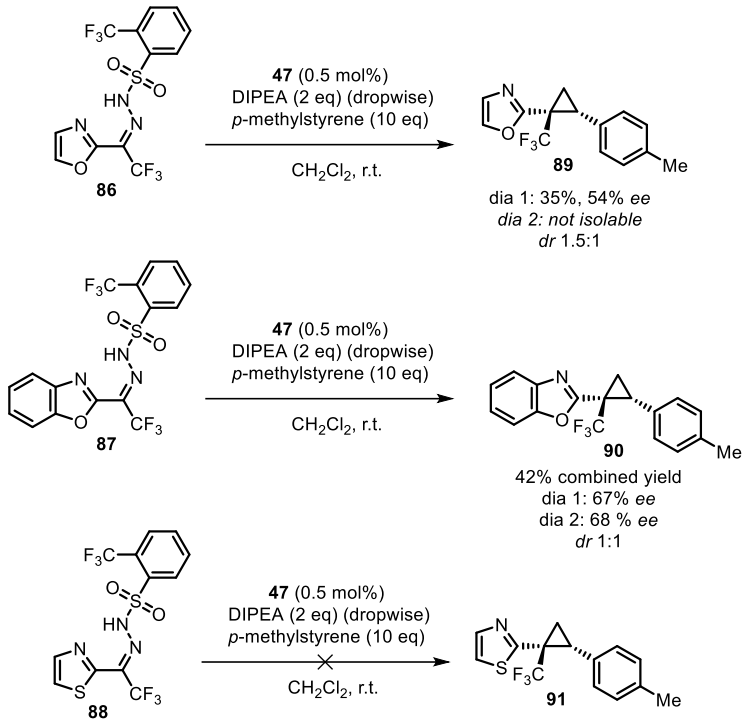

Scheme 20-Attempted cyclopropanation reaction of heterocyclic hydrazones **86-88**.

Subjecting hydrazone **86** to the standard catalytic conditions led to oxazole-substituted cyclopropane **89** in a dr of 1.5:1 (Scheme 20). Only one diastereomer could be isolated which had only 54% *ee*. Benzoxazole-substituted cyclopropane **90** could be isolated as a diastereomeric mixture (dr = 1:1), both diastereomers showed only moderate levels of enantioinduction. Attempts to perform the cyclopropanation with thiazole-containing hydrazone **88** did not result in any observable amounts of cyclopropane **91**.

2.2.4 Post-Functionalisation of 1-(Trifluoromethyl)-1-(2-furyl)cyclopropanes

2.2.4.1 Scalability and Performance of Bismuth-Rhodium Catalysts at Reduced Loadings

To demonstrate the applicability of the developed methodology, a gram-scale experiment was performed in which the catalyst loading was reduced to 0.05 mol% (one order of magnitude lower than the 0.5 mol% used in the reactions performed to explore the scope) leading to cyclopropane **70** without any noticeable loss of yield nor stereoselectivity (Scheme 21); this illustrates once more the high stability and reactivity of the bismuth-rhodium catalysts, which aligns well with earlier reported findings.[98]

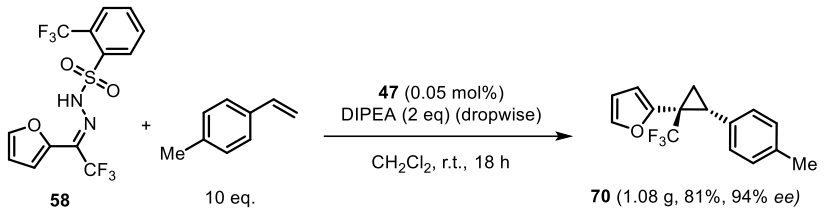

Scheme 21-Gram-scale preparation of cyclopropane **70** under a reduced catalyst loading of 0.05 mol%.

2.2.4.2 Oxidative Cleavage of Furan and Further Downstream Modifications

As outlined in section 2.1 of this chapter, we envisioned an oxidative cleavage of the furan moiety to access 1-(trifluoromethyl)cyclopropane-1-carboxylic acid derivatives, which are otherwise challenging to synthesize with high optical purity.[100] Gratifyingly, treatment of **70** with a catalytic amount of $RuCl_3$ and a stoichiometric amount of $NaIO_4$ in a biphasic solvent mixture (heptane/EtOAc/H_2O) resulted in selective cleavage of the furan while leaving the benzene moiety untouched to give acid **92** as a pure isomer in 65% yield (Table 4, entry 1). HPLC analysis on a chiral stationary phase comparing the enantioenriched product to the corresponding racemate confirmed retention of configuration. However, detailed evaluation of the crude reaction mixture revealed a diastereomeric ratio of 6:1, indicating that partial epimerization had occurred under the oxidative cleavage conditions, as the starting cyclopropane **70** initially displayed a dr >20:1. Efforts to suppress epimerization — such as buffering the reaction medium or modifying the biphasic solvent system — were unsuccessful (entries 2–4). Similarly, lowering the reaction temperature to ambient levels resulted in incomplete conversion of the starting material (entry 5).

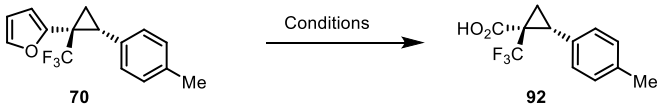

#	Reaction conditions	Yield % [^{1}H NMR]	Comments
1	$RuCl_3$ (2x 2.5 mol%), $NaIO_4$ (2 x 5 eq), Heptane/EtOAc/H_2O, 30 °C, 17 h	65	Full conversion of sm, epimerization (dr = 6:1)
2	$RuCl_3$ (10 mol%), $NaIO_4$ (15 eq), CCl_4/MeCN/H_2O, Buffered with $NaHCO_3$ (20 eq), rt, 17 h	n.d.	Full conversion of sm, epimerization (dr = 2.5:1)

3	$RuCl_3$ (10 mol%), $NaIO_4$ (15 eq),Heptane/ EtOAc/pH 7 buffer, rt, 17 h	[40]	Full conversion of sm, messy reaction profile
4	$RuCl_3$ (2.5 mol%), $NaIO_4$ (5 eq), Heptane/EtOAc/H_2O, rt, Buffered with $NaHCO_3$ (20 eq), rt, 17 h	n.d.	No full conversion, epimerization (dr = 1.6:1)
5	$RuCl_3$ (5 mol%), $NaIO_4$ (5 eq), Heptane/EtOAc/H_2O, rt, 17h	n.d.	Mostly sm left
6	O_3, CH_2Cl_2: MeOH (3:1), –78 °C, 10 min	25	Full consumption of sm, messy reaction profile
7	$KMnO_4$ (4 eq), H_2O:MeCN (3:1), reflux, 5 h	n.d.	Mostly sm left

Table 4-Optimization of oxidative cleavage of cyclopropylfuran **70** to the carboxylic acid. Reported yields are isolated yield of pure isomer. Yields in brackets are determined via ^1H NMR analysis of the crude reaction mixture with triphenylmethane as internal standard.

Alternative oxidative methods were also explored without success; ozonolysis of furan **70** led to a significantly reduced yield and a complex mixture of side products, indicating a lack of selectivity (entry 6). Potassium permanganate oxidation (entry 7) resulted in only partial conversion, even when the reaction mixture was heated to reflux temperature.

Under the described conditions of entry 1, cyclopropanes **67** and **71** were also converted successfully in the corresponding carboxylic acid with 79% and 72% yield, respectively. Unfortunately, under these conditions the oxidative cleavage of cyclopropane **79** did not lead to any isolable amounts of the related carboxylic acid.

For further downstream functionalization, acid **92** was coupled with glycine methyl ester to give modified peptidic building block **93** in 72% yield as a crystalline solid (Scheme 22). Suitable crystals for X-ray diffraction were grown by slow evaporation of a solution of **93** in dichloromethane, which revealed the absolute configuration of the product (Figure 17). The absolute stereochemistry of all other compounds shown in the schemes above were assigned by analogy.

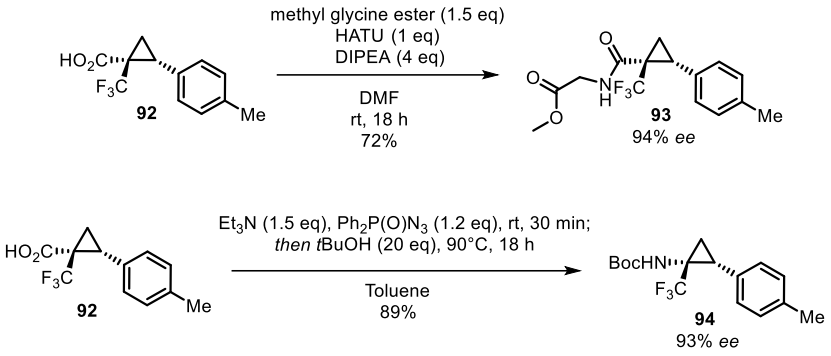

Scheme 22-Further downstream functionalization of acid **92**.

Acid **92** also successfully underwent a Curtius rearrangement to give *N*-Boc protected amine **94** in 89% yield (Scheme 15). It is important to note that the above-described transformations were stereoretentive as well.

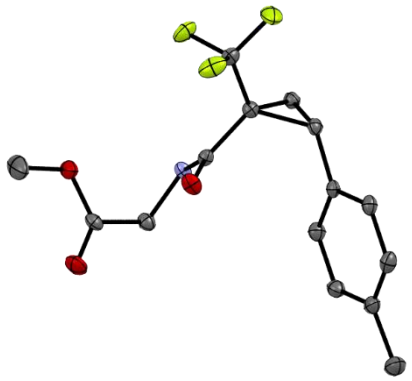

Figure 17-X-ray structure of cyclopropane **93**. For clarity, all hydrogen atoms were omitted.

2.2.4.5 Failed Derivatizations of Cyclopropane 70

It was envisioned that furan **70** could be converted into dihydropyran **96** via an Achmatowicz rearrangement. The synthetic route commenced with the lithiation of the furan, followed by the addition of excess DMF, which afforded furfural **95** in 86% yield (Scheme 23). In contrast, Vilsmeier-Haack conditions only provided the product in low yield. Reduction of **95** with $LiAlH_4$ led to near quantitative conversion to the corresponding alcohol, to which *m*-CPBA was added to induce the desired rearrangement. However, this step failed to yield the target dihydropyran **96**.

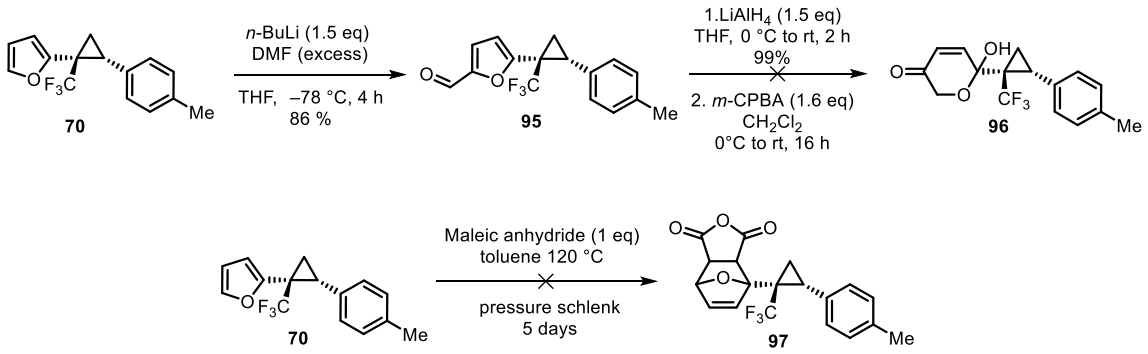

Scheme 23-Failed Achmatowicz rearrangement and Diels-Alder reaction of cyclopropane **70**.

Additionally, a Diels-Alder reaction was attempted using maleic anhydride as the dienophile. No conversion of the starting material was observed at room temperature, nor after extended heating in toluene over several days. These results suggest either poor reactivity of substrate **70** or that the retro-Diels-Alder reaction is favored under these conditions.

2.3. Conclusion

In conclusion, the usage of bismuth-rhodium catalysts **45-47** has enabled the synthesis of novel cyclopropane motifs with high stereoselectivity, therefore expanding the applicability of these bismuth-rhodium catalysts paddlewheel catalysts. A hydrazone relay approach, utilizing *N*-triftosylhydrazone **58** — a stable, crystalline diazo surrogate — successfully provided access to 2-(1-(trifluoromethyl)cyclopropyl)furan derivatives. By dropwise addition of base to *N*-triftosylhydrazone **58**, in the presence of the [BiRh] catalyst and olefin, furfurylidenes were effectively tamed, leading to the desired cyclopropane product without substantial byproduct formation. Optimization of the cyclopropanation conditions revealed that the reaction can be simply performed at ambient temperature with diiodo-substituted catalyst **47** to afford cyclopropane **60** in 84% yield and 92% *ee*.

The versatility of this methodology was demonstrated by the successful synthesis of a diverse range of cyclopropanes (**65-81**). Notably, the approach was not limited to olefins; alkynes also underwent efficient [2+1]-cycloaddition, yielding the corresponding cyclopropenes (**82–83**).

Oxidative cleavage of the furan moiety gave access to 1-(trifluoromethyl)cyclopropane-1-carboxylic acid derivatives in a highly asymmetric fashion, which could not be made by any other method with high optical purity so far. Moreover, the acid **92** serves as a building block for further downstream functionalization such as peptide-couplings and Curtius rearrangement to give access to cyclopropanes **93** and **94**, both in a stereoretentive manner.

3. Advances in the Synthesis of Heteroleptic Dirhodium Paddlewheel Complexes

3.1. Introduction and Motivation

As discussed in section 1.6, most heteroleptic complexes are prepared via thermal ligand exchange procedures at reflux temperatures, with the exception of complexes ***cis*-98** and ***trans*-98** described by Corey and co-workers[78] (Scheme 24). In this pioneering study, the authors observed that exposure of $[Rh_2(OAc)_4]$ to excess trifluoroacetic acid at ambient temperature led to *cis*-$[Rh_2(OTfa)_2(OAc)_2]$, while *trans*-$[Rh_2(OTfa)_2(OAc)_2]$ was prepared from $[Rh_2(OTfa)_4]$ by exposure to a stoichiometric amount of tetrabutylammonium acetate.

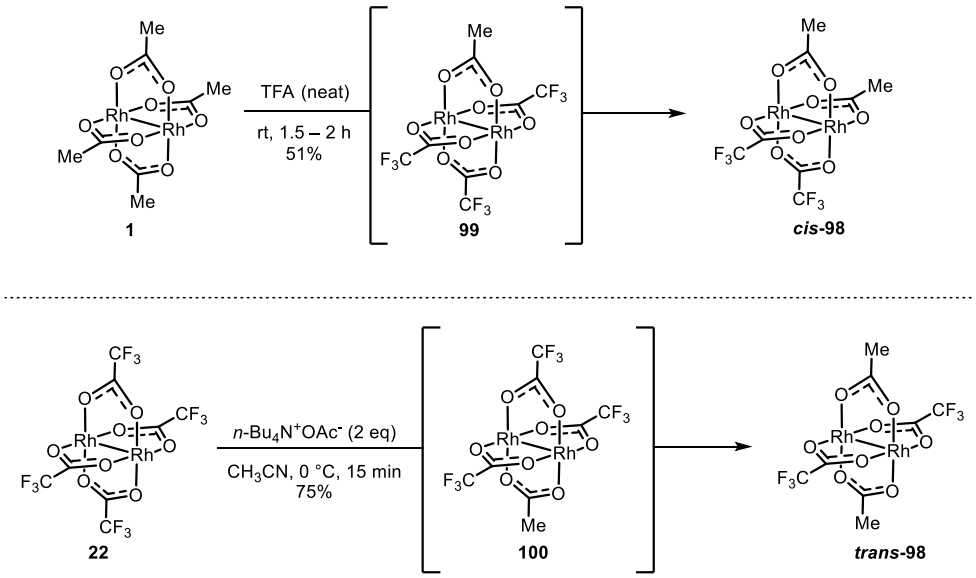

Scheme 24-Preparation of *trans*- and *cis*-$[Rh_2(OTfa)_2(OAc)_2]$ by Corey and co-workers.

The authors attributed the formation of the *cis* isomer to the more tightly bound acetate bridge *trans* to the electronegative trifluoroacetate group in $[Rh_2(OTfa)(OAc)_3]$ (**99**), making it more difficult to displace. Conversely, the formation of the *trans* isomer was ascribed to the relatively facile displacement of the trifluoroacetate ligand *trans* to acetate in $[Rh_2(OTfa)_3(OAc)]$ (**100**), driven by the replacement of the more stabilized trifluoroacetate ion with the less stabilized acetate ion. These findings clearly show the impact of the *trans*-effect in which the coordination strength of the bridging ligands dictates the selectivity of the ligand replacement processes. Hence, a rational choice of precursor complexes constitutes a strategy for the controlled synthesis of advanced heteroleptic dirhodium species.

Recently, the Fürstner group has shown the preparation of heteroleptic dirhodium-amidate-trifluoroacetate complexes in which the trifluoroacetate ligands can be selectively replaced by other less acidic carboxylate ligands via a base-promoted ligand exchange reaction, and therefore can serve as "dummy"-ligands.[113-114] This approach enabled the synthesis of heteroleptic amidate complexes that are difficult or impossible to access via other methods. The preparation of complex **101** serves as an illustrative example; thermal ligand exchange of $[Rh_2(acam)_4{\cdot}2H_2O]$ in the presence of three equivalents pivalic acid resulted in only 16% of **101** (Scheme 25A), with significant amounts of $[Rh_2(OPiv)_4]$ (**102**) formed as a byproduct. Alternatively, complex **101** is obtained in 32% yield via base-promoted ligand exchange from complex **103** (Scheme 25B). Complex **103** is prepared by reaction of $[Rh_2(acam)_4{\cdot}2H_2O]$ with neat trifluoroacetic acid in 72% yield, in which it is important to stop the reaction after 7 min.

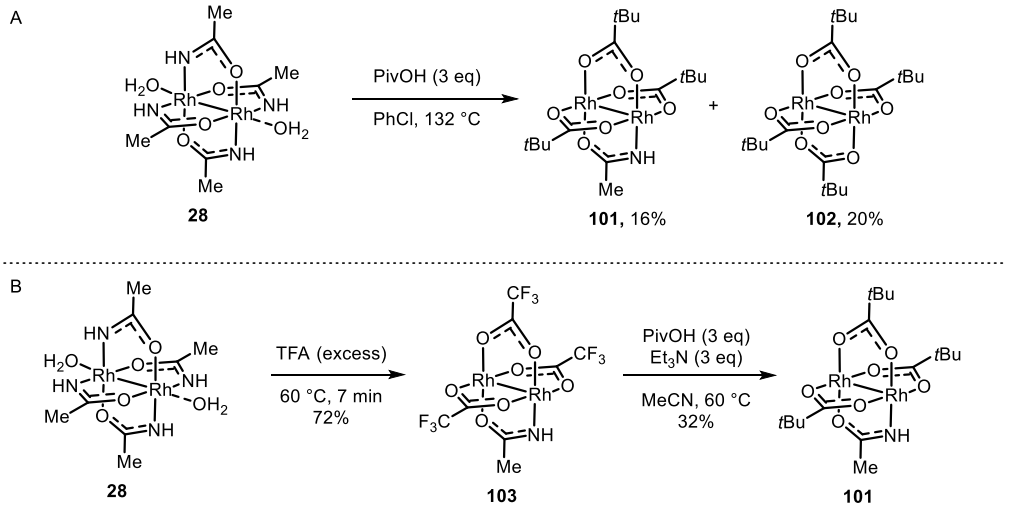

Scheme 25- A: thermal ligand exchange reaction forming complex **101** from $[Rh_2(acam)_4{\cdot}2H_2O]$. B: preparation of complex **101** from $[Rh_2(acam)_4{\cdot}2H_2O]$ via intermediate complex **103.**

In particular, complex **103** can serve as great precursor to obtain a wide variety of other heteroleptic dirhodium-amidate complexes. Building on this intermediate, it was envisioned that combining base-promoted ligand exchange as a mild and selective method with the "*trans* effect" described by Corey and co-workers could lead to more complex heteroleptic dirhodium complexes bearing three or more different ligands.

3.2. Results and Discussion

In this chapter, some results of the doctoral thesis of F. Caló have been incorporated to provide a comprehensive and coherent overview of the research related to this project. These initial contributions have been incorporated into this thesis with permission of the author.

In order to investigate the selective ligand exchange starting from the heteroleptic dirhodium amidate-trifluoroacetate complex **103**, it had to be synthesized first. Described in the doctoral thesis of F. Caló,[113] it was found that complex **103** could be isolated in good yields by reacting $[Rh_2(acam)_4{\cdot}2H_2O]$ with excess trifluoroacetic acid, in which the reaction temperature and duration were of crucial importance for the reaction outcome (Scheme 26). Performing the reaction at reflux temperature and longer reaction time resulted in a significant decrease of the desired [3,1]-complex (**103**) due to significant formation of $[Rh_2(OTfa)_4]$. At room temperature the main product formed is the [2,2]-complex (*cis*/*trans* mixture) even after extended exposure to TFA for up to 180 minutes.

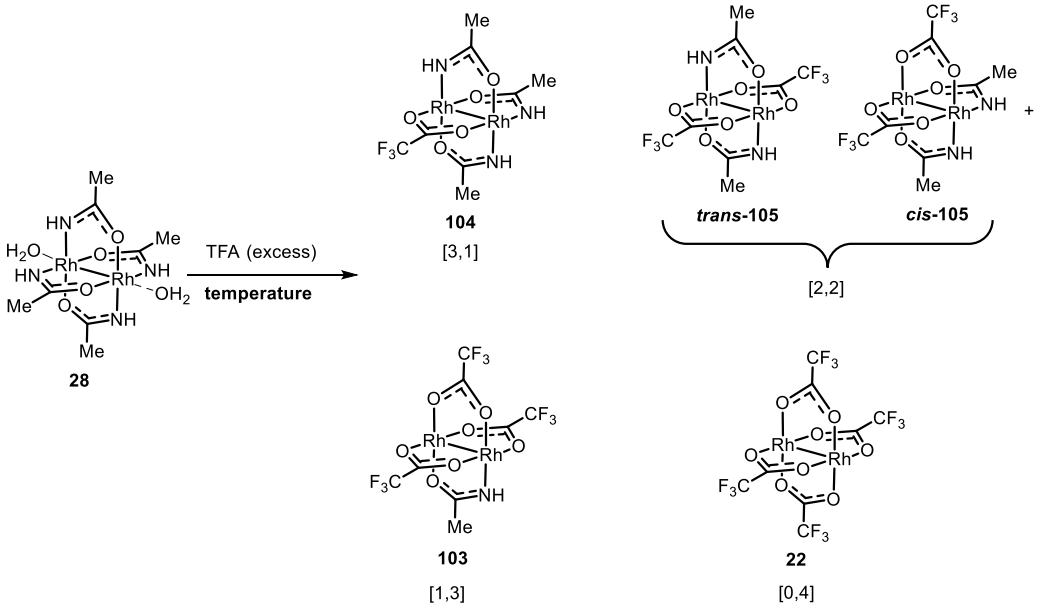

#	T [°C]	t [min]	%[2,2]	%[1,3]	%[0,4]
1	rt	180	45	24	0
2	72	15	0	43	47
3	60	7	19	72	4

Scheme 26-Initial results from the doctoral thesis F. Caló for the preparation of complex **103**. The reported yields are isolated yields. Complex **104** could not be isolated.

Based on these results it was attempted to synthesize [1,3]-complex (**103**) according to entry 3. However, despite numerous attempts, the yields fluctuated significantly and the previously reported 72% yield was never reached. The brevity of the reaction time — only 7 minutes — as well as the lack of detailed information concerning the exact stoichiometry of trifluoroacetic acid, likely contributed to the variability in outcomes. These inconsistencies underscore the need for a more systematic and comprehensive investigation, aimed at developing a robust and reproducible protocol for the preparation of complex **103**.

3.2.1. Kinetic Studies of the Ligand Exchange Process with Trifluoroacetic Acid

In order to get a better understanding of the ligand exchange process of rhodium-amidate complexes with trifluoroacetic acid, kinetic analyses using reverse phase HPLC were performed. Using the same conditions as described in entry 3 (Scheme 26), a superstoichiometric amount of trifluoroacetic acid was added to $[Rh_2(acam)_4{\cdot}2H_2O]$ at 60 °C and the reaction was monitored via HPLC in short time intervals for a period of time in which the product composition was carefully analyzed (Figure 18).

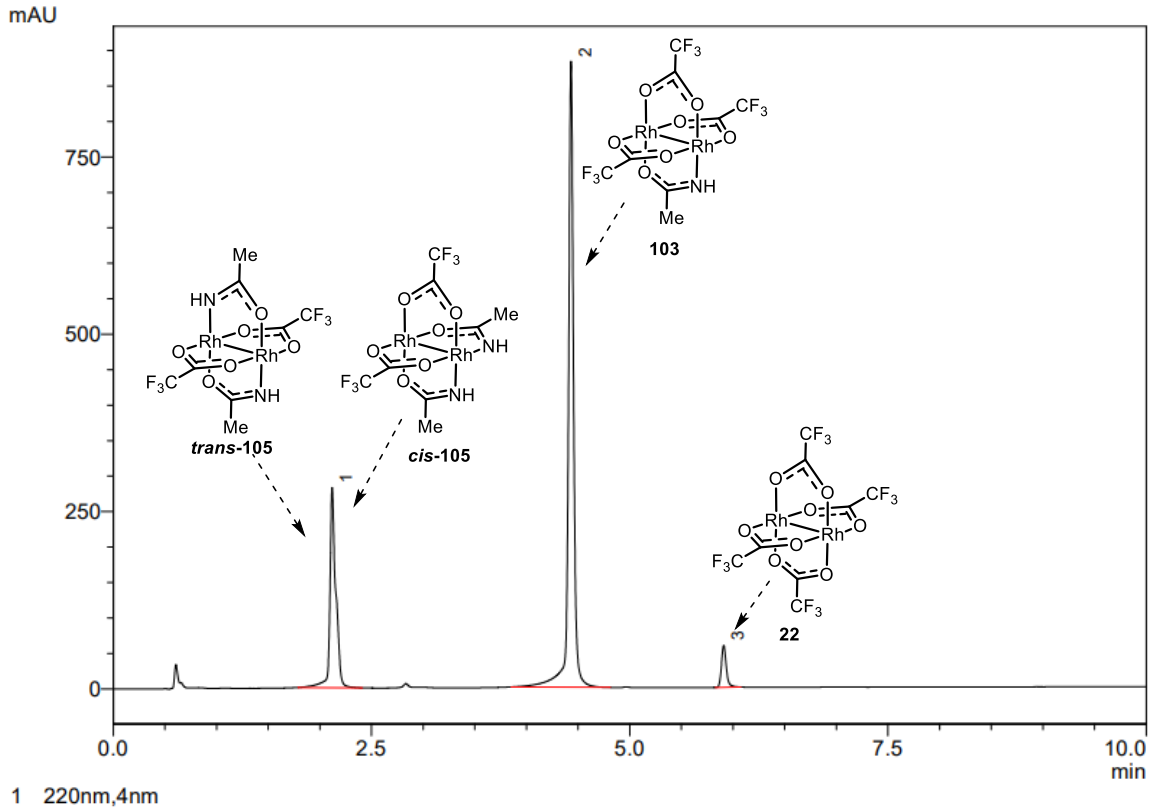

Figure 18-HPLC chromatogram recorded after 10 min reaction time of $[Rh_2(acam)_4{\cdot}2H_2O]$ and TFA at 60 °C showing the relative production composition of complexes **105**, **103** and **22**.

The analysis of all product compositions obtained in a time interval of 20 min resulted in a kinetic reaction profile (Figure 19) of which the following conclusions can be derived: Exposure of the amidate complex **28** to trifluoroacetic acid immediately leads to the formation of complex **105** (*cis*/*trans* mixture), indicating that the mono-fold ligand exchange product **104** is a fleeting intermediate under these reaction conditions. The desired [1,3]-complex **103** forms progressively over the course of 15 min. Beyond this point, product formation begins to level off, ultimately reaching a maximum yield of 82% at a reaction time of 20 min. These observations provide a clear rationale for the significant variability in yield reported when the reaction was stopped prematurely — around the 7-minute mark — as initially described. In contrast, the formation of the fully substituted [$Rh_2(OTfa)_4$] complex proceeds at a markedly slower rate, with only 11% formed after 20 min.

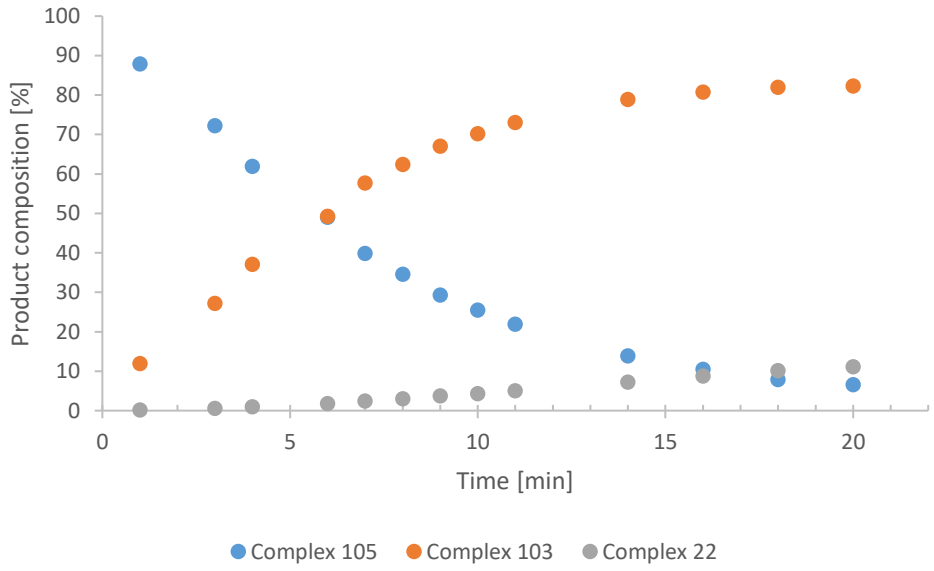

Figure 19-Reaction profile of the ligand exchange reaction of [$Rh_2(acam)_4{\cdot}2H_2O$] with TFA at 60 °C monitored via HPLC.

Monitoring the reaction at reflux temperature (72 °C) resulted in a reaction profile in which the formation of the desired complex **103** is significantly faster, reaching its maximum at around 8 min reaction time, after which it starts to decrease due to the faster formation of [$Rh_2(OTfa)_4$] (**22**) (Figure 20).

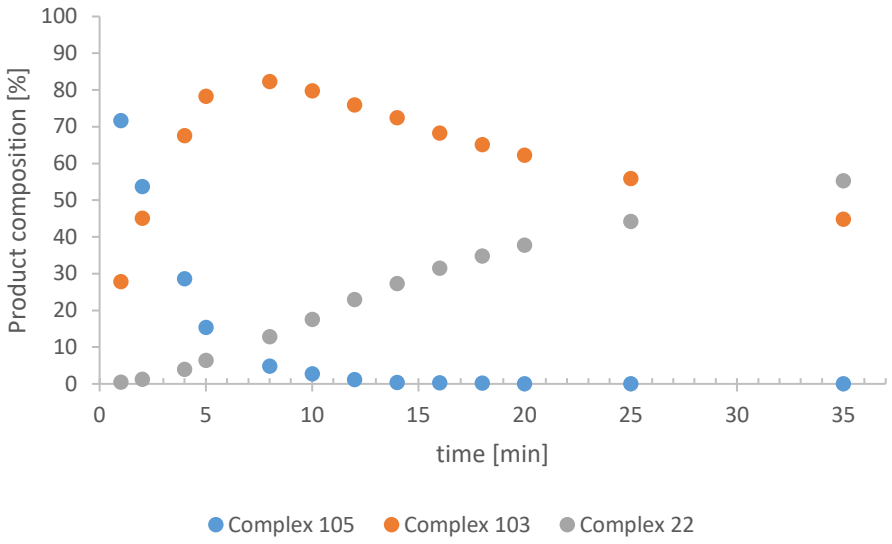

Figure 20-Reaction profile of the ligand exchange reaction of $[Rh_2(acam)_4 \cdot 2H_2O]$ with TFA at 72 °C monitored via HPLC.

The reaction was repeated several times and stopped after 20 min (±3 min) at 60 °C, which resulted in a reproducible 79% yield of **103**, even when scaled up to 400 mg. Following a similar approach, the ligand exchange with trifluoroacetic acid was optimized for $[Rh_2(bnam)_4]$ **112** (see Appendix 1 for the kinetic profile). Performing the reaction at 60 °C for 30 min yielded the [1,3]-complex (**106**) in an isolated yield of 75%.

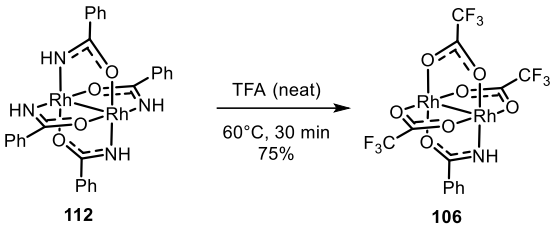

Scheme 27-Optimized conditions for the ligand exchange of $[Rh_2(bnam)_4]$ with trifluoroacetic acid, yielding complex **106**.

3.2.2. *trans*-Selective Ligand Exchange Reactions of Dirhodium Amidate-Trifluoroacetate Complexes

With a high-yielding and robust protocol established for the synthesis of [1,3]-amidate–trifluoroacetate complexes, the attention was turned to the possibility of selectively replacing the trifluoroacetate ligand positioned *trans* to the amidate. This approach exploits the *trans*-effect, wherein the strong σ-donating amidate ligand enhances the lability of the opposing trifluoroacetate ligand by weakening its coordination to the rhodium center, thereby facilitating its selective substitution.

Pivalic acid was chosen as the reaction partner of choice to investigate the *trans*-selective ligand replacement of complex **103** (Table 5). Initial experiments using trimethylamine as a base — previously effective in multi-fold ligand exchange reactions involving the amidate complex **103**[114] — yielded only 17% of the desired *trans*-isomer **107** (entry 1). Given this low efficiency, a comprehensive base screening was undertaken, focusing primarily on non-nucleophilic bases. Pyridine-derived bases such as DMAP and 2,6-di-*tert*-butylpyridine showed no significant activity in promoting ligand exchange at room temperature (entry 2-3). In contrast, the use of Hünig's base or potassium carbonate led to a notable improvement in product formation (entry 4-5). DBU, a slightly stronger non-nucleophilic base, gave the highest isolated yield of the *trans*-isomer **107**, reaching 60% (entry 6). Conversely, LiHMDS primarily induced decomposition of the metal complex (entry 7). Attempts to improve *trans*-selectivity by lowering the reaction temperature to 0 °C using Hünig's base (entry 8) proved ineffective, as the *trans:cis* ratio remained unchanged at 6:1, consistent with the values observed in entries 4 and 5.

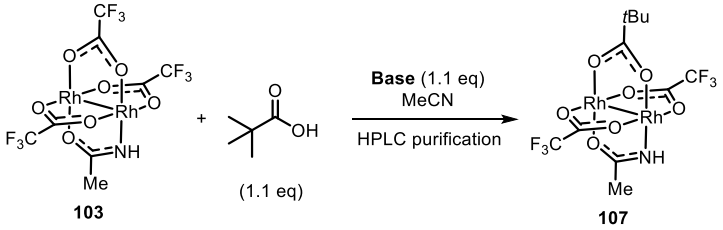

#	Base	T [°C]	t [h]	Yield [%]
1	Et_3N	r.t.	4	17
2	DMAP	r.t.	4	n.d.
3	2,6-*t*Bu_2-pyridine	r.t.	4	n.d.
4	DIPEA	r.t.	4	45
5	K_2CO_3	r.t.	4	49
6	DBU	r.t.	4	60
7	LiHMDS	r.t.	8	n.d.
8	DIPEA	0	16	45

Table 5-Base screening of the *trans*-selective ligand exchange of amidate complex **103** with pivalic acid. The reactions were performed on a 20 mg scale.

With DBU identified as the optimal base, subsequent efforts focused on evaluating the influence of solvent on the ligand exchange process (Table 6). Running the reaction in acetonitrile, the initial solvent of choice, proved most effective, yielding 57% of the *trans*-product. While THF facilitated complete conversion, the isolated yield was slightly reduced. In contrast, less polar solvents such as methyl *tert*-butyl ether and a 1:1 mixture of dichloromethane and THF led to incomplete ligand exchange and diminished yields.

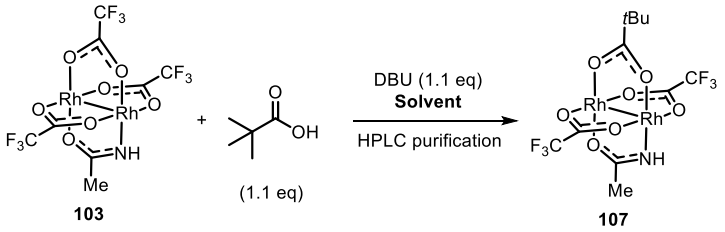

#	Solvent	T [°C]	t [h]	Yield [%]
1	MeCN	r.t.	5	57
2	THF	r.t.	5	51
3	MTBE	r.t.	5	34
4	THF/CH_2Cl_2 (1:1)	r.t.	5	n.d.

Table 6-Solvent screening of the *trans*-selective ligand exchange of amidate complex **103** with pivalic acid. The reactions were performed on a 20 mg scale.

With the optimized conditions at hand the reaction was performed on >100 mg scale, affording the desired *trans*-complex **107** in 55% isolated yield. Single crystals suitable for X-ray diffraction were obtained, which showed a dimer of complex **107** bridged at the oxygen atoms of the amidate ligands with the neighboring rhodium atoms. The dimeric structure, unambiguously confirmed the *trans*-configuration of the complex **107** (Figure 21).

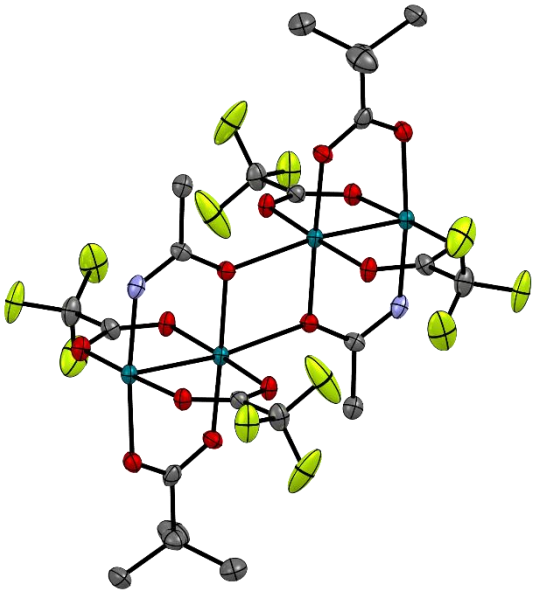

Figure 21-X-ray structure of a dimer of **107** displaying the *trans*-configuration of the pivalate to the amidate ligand. The axial ligands and hydrogen atoms are omitted for clarity.

In a similar fashion, using the optimized conditions described for complex **107**, different *trans*-selective ligand exchange reactions were successfully performed leading to complexes **108-111** in moderate yields (Scheme 28). In these reactions, alternative carboxylic acids were incorporated in place of pivalic acid or different [1,3]-amidate-trifluoroacetate complexes were employed in the transformation.

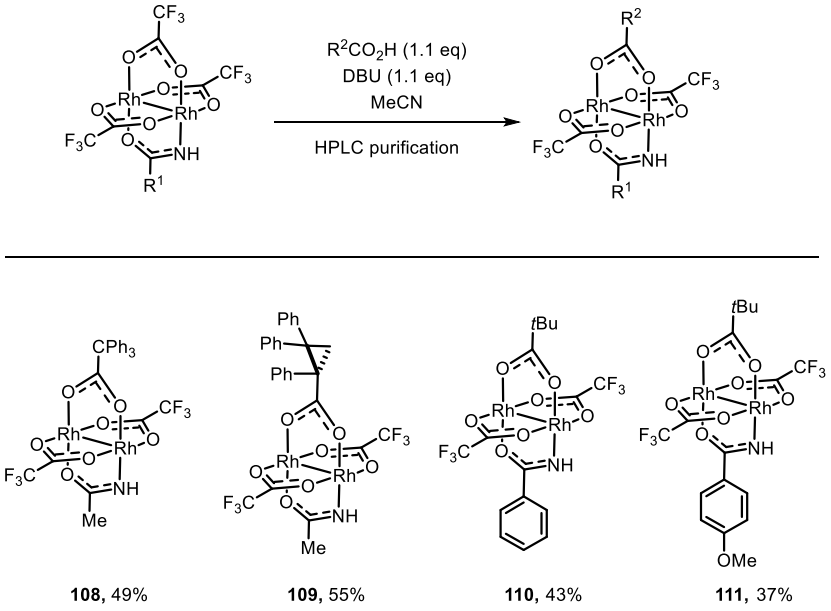

Scheme 28-Synthesis of complexes **108-111** by *trans*-selective ligand replacement of the corresponding [1,3]-amidate-trifluoroacetate dirhodium complexes.

In these cases, the moderate yields can be attributed to the incomplete suppression of multifold ligand exchange, as well as yield losses due to HPLC purification. Nevertheless, it should be emphasized that, to date, no other efficient method exists for the selective replacement of μ_2-coordinated ligands in dirhodium(II) complexes, making this approach the most effective method that is currently available.

3.3. Conclusion

The ligand exchange process of dirhodium-amidate complexes with trifluoroacetic acid was further optimized, demonstrating that HPLC-based kinetic analysis is an excellent tool for the development of a robust and reproducible protocol. This approach enabled the efficient synthesis of the desired [1,3]-dirhodium-amidate–trifluoroacetate complexes **103** and **106** in excellent yields. With the [1,3]-dirhodium complexes at hand, a base-promoted monofold ligand exchange could be performed in which the *trans*-effect of the stronger σ-donating amidate ligand could be leveraged to selectively replace the trifluoroacetate moiety by a less acidic carboxylate. Extensive screening identified DBU as the optimal base and acetonitrile as the most suitable solvent for such base-promoted selective ligand exchange, allowing the synthesis of a variety of heteroleptic dirhodium-amidate complexes (**108-111**). This methodology provides a general platform for the synthesis of heteroleptic dirhodium complexes bearing three or four distinct ligands. The ability to fine-tune the ligand environment in this way opens new avenues for the development of highly selective catalysts — a topic that will be further explored in detail in Chapter 4.

4. Development of Stereoselective Chiral-at-Metal Dirhodium(II) Complexes

4.1. Introduction and Motivation

The vast majority of dirhodium paddlewheel complexes used in asymmetric catalysis comprise chiral carboxylate or carboxamidate ligands.[55, 67, 115-118] To date, only one example exists in the literature that is fundamentally different, as the rhodium atoms themselves are stereogenic whereas the ligands are not (Scheme 29, bottom). This complex exists of two *ortho*-metalated phosphine ligands in a *cisoid* head-to-tail arrangement and was prepared by thermal ligand exchange of arylphosphine ligands with $[Rh_2(OAc)_4]$. Although originally described already in 1984 by Cotton and co-workers,[119-120] it was Lahuerta, Pérez-Prieto and co-workers[121] who succeeded in the separation of the enantiomers by chiral resolution. These enantiopure complexes were successfully employed in the intramolecular cyclopropanation and C-H insertion reactions of diazoketones, however the results were strongly case dependent.[122-127]

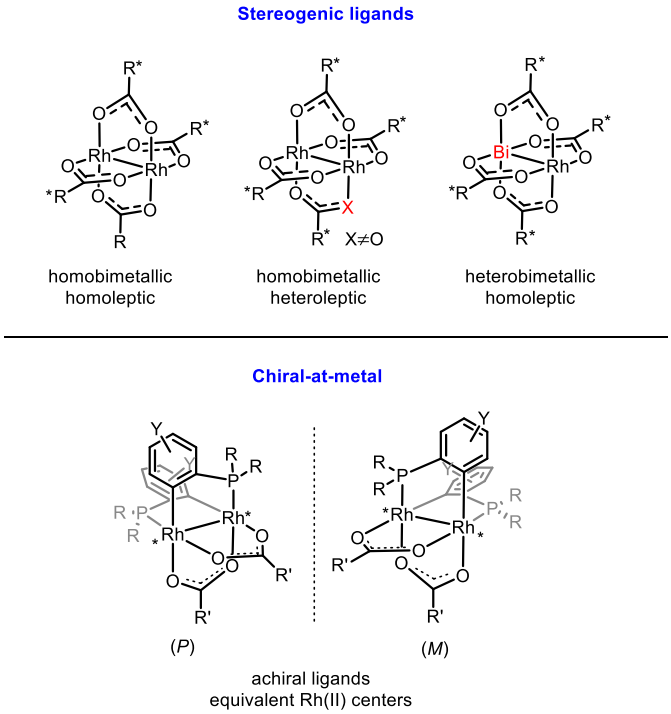

Scheme 29-Top: overview of different classes chiral dirhodium paddlewheel complexes. bottom: chiral-at-metal dirhodium complex described by Lahuerta and Pérez-Prieto.

As discussed in section 1.7, our group recently described a heteroleptic amidate complex for the cyclopropanation of stannylated diazoesters in a highly asymmetric manner.[80-81] Key to its success is the formation of an interligand hydrogen bond between the –NH group of the

amidate and the ester carbonyl of the emerging rhodium carbene. Together with the advances made in selective ligand exchange reactions of dirhodium paddlewheel complexes as described in Chapter 3, it was envisioned to develop a dirhodium complex comprising an amidate ligand in which the rhodium metal centers are stereogenic.

4.2. Results and Discussion

This project was conducted in collaboration with Lorenzo Baldinelli, Sofia Lerda and Prof. Dr. Giovanni Bistoni, who performed the DFT calculations. To provide a comprehensive and coherent overview of the research, these contributions have been incorporated into this thesis with permission of the authors.

4.2.1. Design of Heterochiral-at-Metal Rh(II) Complexes for Asymmetric Catalysis

An initial attempt towards a heterochiral-at-metal dirhodium complex was made by a monofold ligand exchange reaction of complex **103** with pivalic acid, which afforded **113** in 30% (Scheme 30). The introduction of the additional pivalate ligand disrupts the original symmetry of **103**, imparting intrinsic backbone chirality to the resulting species.

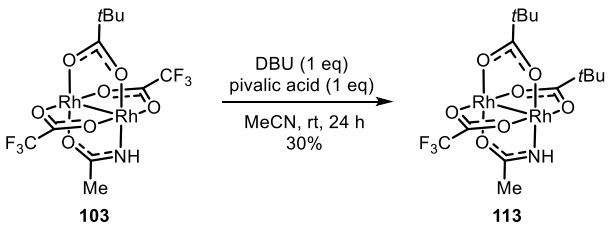

Scheme 30- Synthesis of the heterochiral-at-metal dirhodium paddlewheel complex **113**.

Despite its successful synthesis, this design of the complex is unlikely to be effective in asymmetric catalysis due to insufficient steric hindrance in proximity to the reactive site. The steric bulk introduced by the pivalate moiety is likely insufficient and spatially distant from the catalytic center, limiting its ability to induce stereocontrol. To address this limitation, two alternative catalyst designs were proposed that offer more strategically positioned steric elements to enhance stereoselectivity in the target transformation (*vide infra*).

Formamidinate based design

In this design, the complex features one amidate ligand and two formamidinate ligands coordinated in a *cisoid* arrangement. The formamidinate ligands position their *N*-substituents in close proximity to the reactive metal center, analogous to the spatial arrangement of the

arylphosphine ligands in the homochiral-at-metal complexes reported by Lahuerta and Pérez-Prieto. Furthermore, the amidate ligand is envisioned to play a dual role: directing the site of carbene formation and engaging in hydrogen bonding interactions that restrict the conformational flexibility of the carbene intermediate. This conformational constraint is expected to enhance stereocontrol during the catalytic transformation.

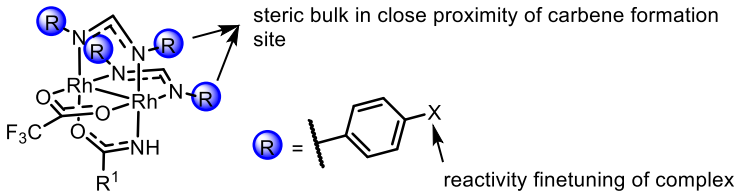

Figure 22-Design of heterochiral-at-metal catalyst for asymmetric catalysis based on formamidinate ligands.

Cisoid chelating carboxylate design

This design incorporates an amidate ligand and a chelating carboxylate ligand, both coordinated in a *cisoid* fashion on the dirhodium scaffold. By judicious selection of a suitably bulky tethered carboxylate ligand that is capable of sterically hindering potential nucleophilic approach pathways, and in combination with hydrogen-bonding interactions between the amidate and the carbene intermediate, this catalyst architecture is expected to impart a high degree of stereocontrol on the target transformation.

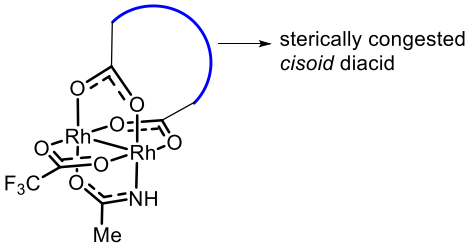

Figure 23-Design of heterochiral-at-metal catalyst for asymmetric catalysis based on a bulky *cisoid* chelating diacid.

4.2.3. Towards Formamidinate Chiral-at-Metal Dirhodium(II) Complexes

Dirhodium(II) formamidinate complexes, either homoleptic or heteroleptic in nature, have been used in electrocatalysis and material science.[128-131] Interestingly, Piraino and co-workers reported in 1987 a heteroleptic dirhodium paddlewheel complex **116** which was formed by the chemical oxidation of a binuclear rhodium(I) formamidinate complex **115** with AgOTfa.[132] Remarkably, this transformation rendered uniquely the *cis* isomer in which the formamidinate ligands are arranged in a *cisoid* manner. Due to the rather labile trifluoroacetate ligands, it was envisioned that this complex would make a great precursor for our target catalyst if it enables the selective replacement with an amidate salt.

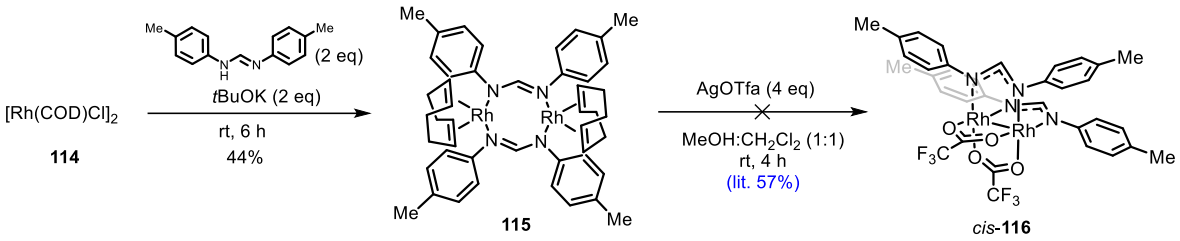

Scheme 31-Failed synthetic route towards Rh(II) formamidinate complex **116**, originally described by Piraino and co-workers.

The synthesis commenced by preparing **116** according to the protocol described by Piraino; however the chemical oxidation step failed in our hands in several attempts (Scheme 30). Therefore it was decided to alter the synthetic route and go via a homoleptic formamidinate dirhodium(II) complex (**117**) which was subjected to a ligand exchange reaction with trifluoroacetic acid to render *cis*-[2,2]-complex **118** (Scheme 32).

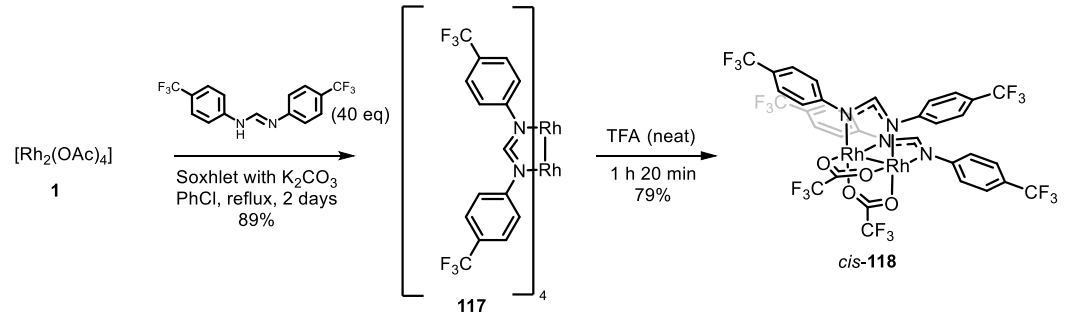

Scheme 32-Preparation of *cis*-**118** from commercially available $[Rh_2(OAc)_4]$.

Gratifyingly, the homoleptic formamidinate complex **117** was obtained in excellent yield. Subsequent ligand exchange reaction with trifluoroacetic acid afforded the desired complex **118**, also in excellent yield. To confirm the presence of the *cis*-configuration of **118**, single crystals were grown for X-ray diffraction analysis. The resulting data indicated a *cisoid* arrangement of the formamidinate ligands. However, due to significant crystal twinning, the structural data did not meet the quality standards required for publication.

Replacement of one of the trifluoroacetate ligands in complex **118** with an amidate ligand was expected to decrease the catalytic activity of the complex, as the amidate is a stronger σ-donor, thereby reducing the electrophilicity of the metal center.[133] Furthermore, previous attempts at late-stage incorporation of amidate ligands into similar complexes have proven challenging. For these reasons, it was deemed necessary to first evaluate the catalytic reactivity of **118** prior to amidate introduction.

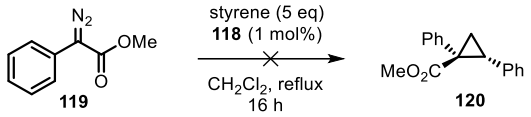

Scheme 33-Attempted cyclopropanation of diazo compound **119** catalyzed by complex **118**.

The catalytic reactivity of complex **118** was tested in the cyclopropanation reaction of diazoester **119** (Scheme 33). However, even after heating the reaction mixture to reflux temperature for 16 h, no characteristic cyclopropane signals were observed by ^{1}H NMR spectroscopy when analyzing the crude residue, indicating the poor reactivity of the complex. Given this poor catalytic performance, further efforts toward the synthesis of the targeted chiral-at-metal amidate-containing complex were not pursued.

4.2.4 *Cisoid* Chelating Carboxylate Chiral-at-Metal Dirhodium(II) Complexes

4.2.4.1. Rh(II) Complexes Featuring an Esp/O-Esp Ligand

A well-established dirhodium paddlewheel complex that features tethered carboxylate ligands is [Rh_2(esp)$_2$], which was originally reported by Du Bois and coworkers in 2004.[134] This catalyst contains two α,α,α′,α′-tetramethyl-1,3-benzenedipropionate ligands, commonly referred to as "esp ligands", and has been employed *inter alia* in oxidative C–H activation of sulfamate, sulfamide, carbamate, urea, and guanidine substrates through nitrene insertion.[134-135] Given the commercial availability of the parent Esp ligand (**120**) and its established *cisoid* coordination mode to the dirhodium core, it was attempted to form complex **121** from the [1,3]-complex **103** by a base-promoted ligand exchange (Scheme 34). Gratifyingly, **121** was obtained in 55% yield. Since this complex is heterochiral at the metal centers, it was attempted to separate the enantiomers by HPLC on a chiral stationary phase. However, after screening a wide variety of chiral stationary phases and eluents, no separation could be achieved.

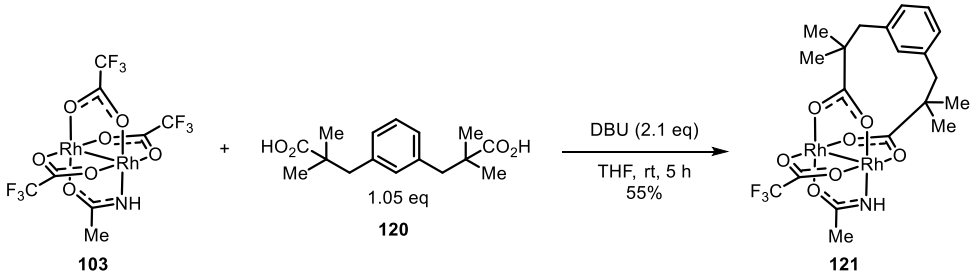

Scheme 34-Synthesis of heterochiral-at-metal complex **121** via base-promoted ligand exchange from [1,3]-complex **103**.

In an effort to modify the polarity of the chelating ligand, an ether variant of the esp ligand was employed. This ligand, which can be conveniently synthesized from resorcinol following

literature procedures,[136] will herein be referred to as "O-Esp" for simplicity. A small library of these tethered ligand complexes was made in which different substituents were installed on the 2,4-position of the aryl ring (Scheme 35).

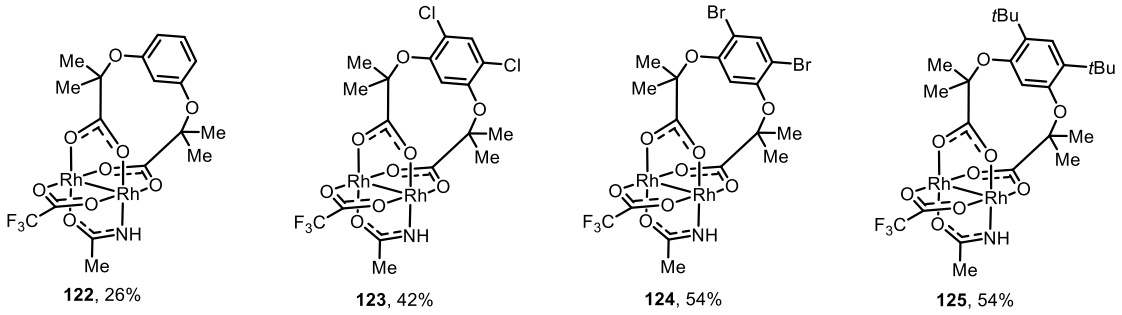

Scheme 35-Overview of different O-esp ligated complexes **122-125** in which the 2,4-positions of the aryl ring are varied.

Interestingly, a trend was observed in which the isolated yields of the corresponding O-Esp complexes increased with the steric bulk of the aryl substituents. A plausible explanation for this phenomenon is that increased steric hindrance at the 2,4-positions forces the carboxylic acid termini of the ligand closer together, inducing a more bent (less linear) conformation of the diacid. This conformational constraint likely reduces the propensity for undesired oligomerization during complex formation, thereby enhancing the isolated yields.

With complexes **122-125** at hand, efforts were made to separate the corresponding enantiomers by preparative chiral HPLC. Pleasingly, separation conditions were found for complex **122**. However upon concentration of the collected enantiomeric fractions, the complex seemingly decomposed, as could be observed by HPLC analysis (Figure 24). After thorough analysis, it was found that the decomposition of the isolated enantiomers could be prevented by the addition of water to the enantiomeric fractions before concentration (Figure 25). In a similar manner, the enantiomers of complexes **123** and **124** could be obtained. No suitable separation conditions were found for complex **125**.

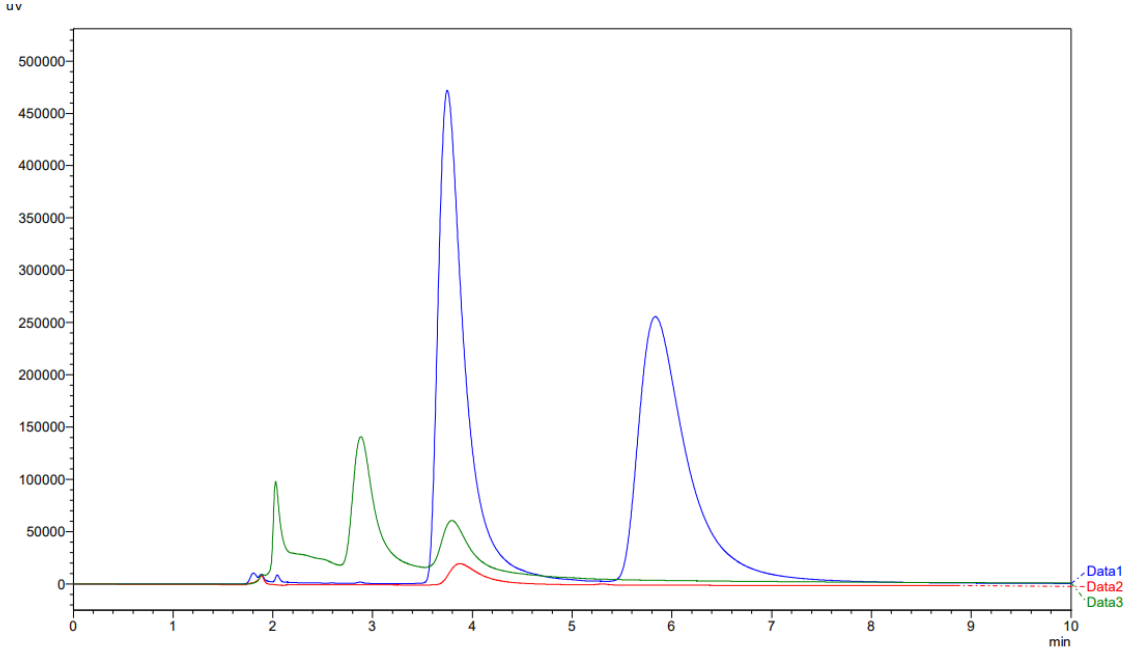

Figure 24- HPLC chromatograms of complex **122**; the original racemic sample (blue), the separated 1st enantiomer before concentration of the fraction (red), the separated 1st enantiomer after concentration of the fraction (green).

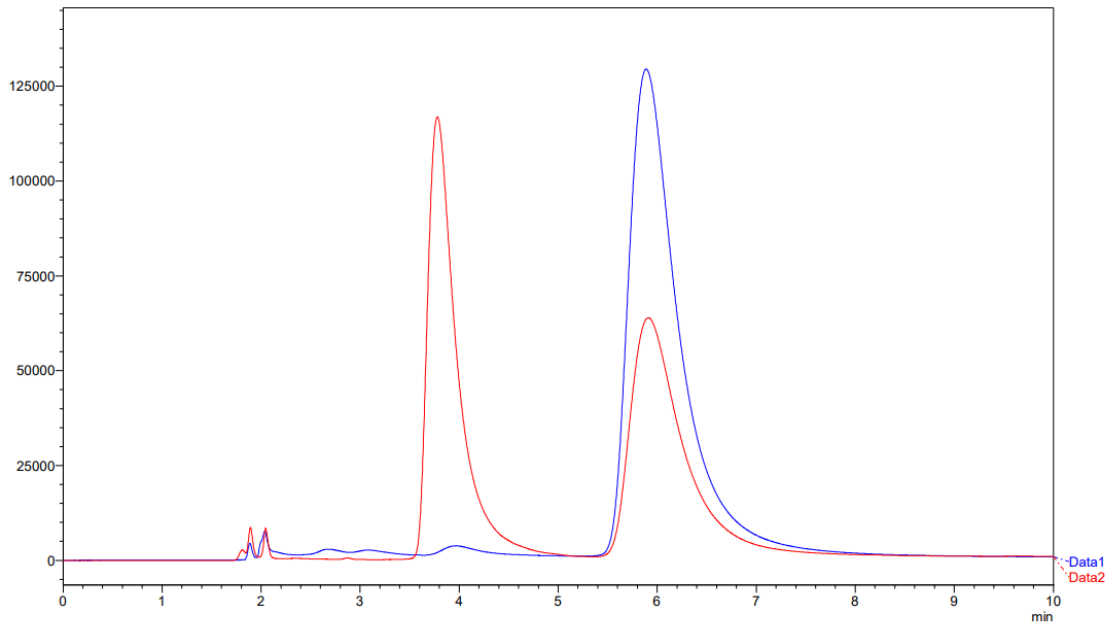

Figure 25- HPLC chromatograms of complex **122**; the original racemic sample (red), the separated 2nd enantiomer after concentration of the fraction when water was added (blue).

Surprisingly, the measured optical rotation values of both enantiomers of **122** were 113.9 and 52.5, respectively ($[\alpha]_D^{20}$, c= 0.05, $CHCl_3$). Due to the intensely colored solution of complex **122** in chloroform, the optical rotation could not be measured at higher concentration than 0.05 g/100mL. With such low dilution factor, it made us wonder whether the optical rotation values can be correctly interpreted at such low concentrations. As a test, DBU, which does not

contain any chiral element, was measured at concentrations of 1.0 and 0.1 g/100mL. The corresponding optical rotation values were 0 and 11.5, respectively. This shows that the optical rotation values measured at our polarimeter are not representative at very low concentrations and therefore cannot be relied on.

Indirect evidence was gained by exchanging the trifluoroacetate ligand of racemic complex **125** with an enantiopure ligand. Both *N*-tosyl-(*L*)-proline and (*R*)-Mosher´s acid could be successfully coupled to the rhodium scaffold in good yields and resulted in a 1:1 ratio of diastereomers according to ^{1}H NMR spectroscopy (Scheme 36). In the case of *N*-tosyl-(*L*)-proline, the diastereomers could be separated by preparative HPLC on an achiral stationary phase. Both the spectroscopic and the chromatographic evidence obtained for these complexes indicate that complex **125** is inherently racemic, thus does contain stereogenic metal centers.

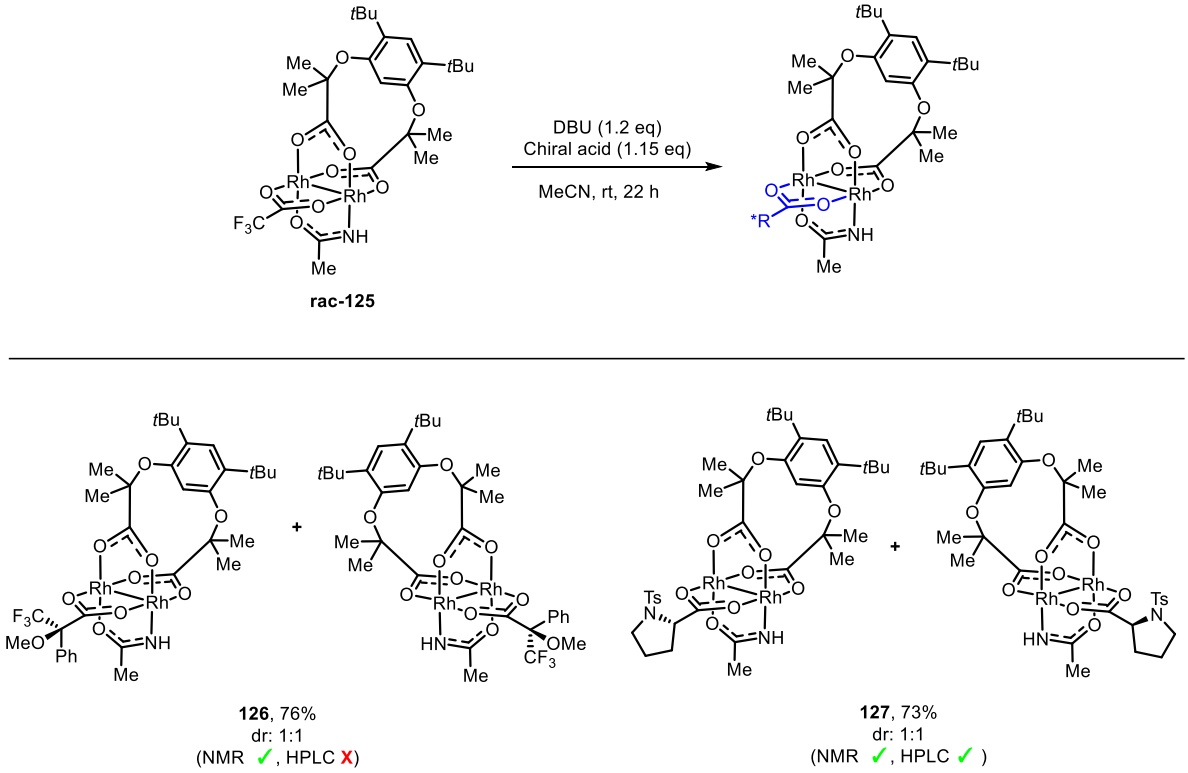

Scheme 36-Synthesis of diastereomeric complexes **126** and **127** by selective trifluoroacetate ligand replacement with a chiral acetate ligand of complex **125**.

It was noticed that the heterochiral-at-metal complexes **122-125** exhibited limited stability in deuterated acetonitrile over several days. Similar instability issues have previously been observed for dirhodium paddlewheel complexes bearing a trifluoroacetate ligand in our group.[113] With the aim of improving solution stability to enable single-crystal growth for X-ray diffraction analysis, it was hypothesized that substituting the labile trifluoroacetate ligand with a more strongly coordinating acetate would enhance the robustness.

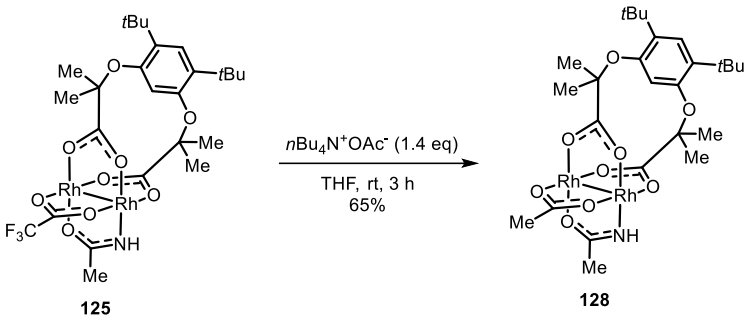

Scheme 37-Ligand exchange reaction of complex **125** with tetrabutylammoniumacetate yielding complex **128**.

This ligand exchange was successfully carried out, affording the corresponding acetate-substituted complex **128** in 65% yield (Scheme 37). As anticipated, the resulting complex displayed significantly improved stability in acetonitrile, remaining intact for several weeks. Despite this increased stability, multiple attempts to obtain single crystals of suitable quality for X-ray diffraction analysis were unsuccessful.

O-Esp Ligated Heterochiral-at-Metal Complexes in Catalysis

The catalytic activity of one of the enantiomers of complex **122** was tested in the cyclopropanation of diazo methylester **119** (Scheme 38). Reaction monitoring by TLC indicated full consumption of the diazo substrate in less than 10 minutes. The asymmetric induction induced by **122** was rather poor, as the corresponding cyclopropane had only 6% *ee*. From a conceptual point of view the fact that this novel complex achieved some level of stereocontrol could be seen as a success as it indirectly evidenced the inherent chirality of these novel catalysts.

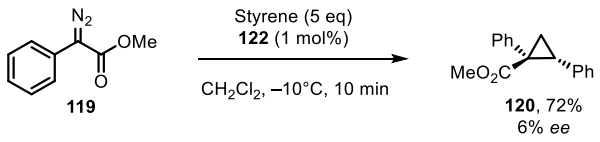

Scheme 38-Cyclopropanation of diazo methylester **119** catalyzed by heterochiral-at-metal complex **122**.

To get a better understanding of why the induced enantioselectivity was so low, the complex was geometrically optimized using the B3LYP-D3/def2-SVP def2/J level of theory. A steric bulk map made of complex **122** showed that the esp ligand does not induce a lot of steric bulk and is located relatively far away from the reactive metal center (Figure 26). Additionally, adding more steric bulk on the aryl ring of the O-Esp ligand would not lead to an increased amount of stereoinduction as the 2,4-substituents point away from the reactive center.

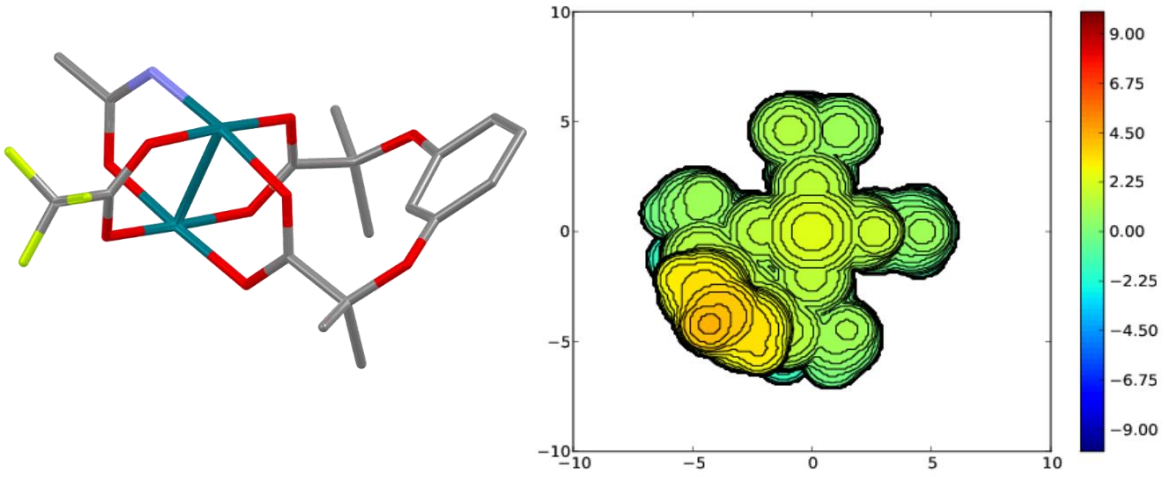

Figure 26- Left: computed structure of complex **122** (hydrogens have been omitted for clarity). Right: topological steric bulk map made from the computed structure of **122**.

4.2.4.2. Rh(II) Complexes Featuring a Calix[4]arene Ligand

As the asymmetric induction induced by the O-Esp ligated heterochiral-at-metal complexes was poor, other tethered carboxylate ligands were sought which comprised more steric bulk. Interestingly, Maas and co-workers reported the homoleptic dirhodium complex **129** bearing two calix[4]arene carboxylate ligands.[137] XRD data of this complex show that the bromo-substituents on the aryl rings are placed in proximity of the axial coordination sites of the rhodium atoms, where they can steer the catalytic transformation without preventing it from happening (Figure 27). Moreover, the bromo-substituted aryl rings also provide an interesting handle for further fine-tuning, if necessary. Therefore, it was deemed the ideal candidate for the synthesis of a heterochiral-at-metal dirhodium catalyst with the potential of high asymmetric induction.

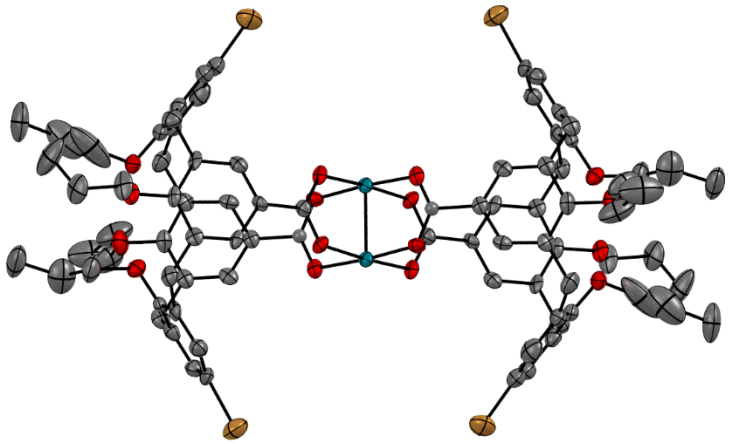

Figure 27-X-ray crystal structure of homoleptic complex **129** (hydrogen atoms were omitted for clarity).[140]

The synthesis of calix[4]arene diacid **133** is well described in the literature and can be easily prepared in gram-scale from commercially available calix[4]arene **130** over four steps in good overall yield (Scheme 39). It is worth mentioning that the twofold lithium-bromine exchange with *n*-BuLi occurs selectively at the opposing aryl groups and not at the vicinal aryl bromide entities. Subsequent treatment of the dilithiated calix[4]arene **132** with gaseous CO_2 gives the desired calix[4]arene diacid **129**.[138]

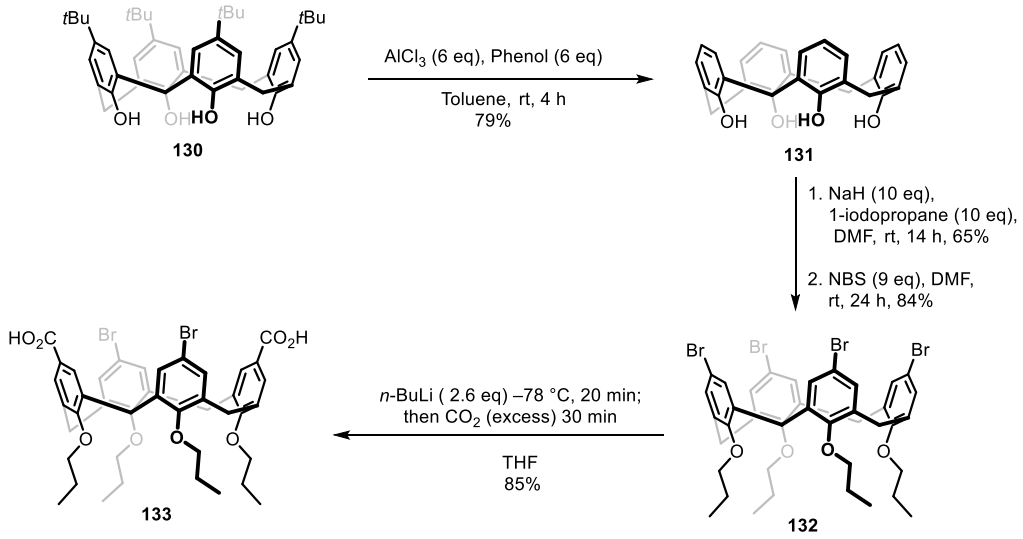

Scheme 39-Synthetic route towards calix[4]arene diacid **133** starting from commercially available calix[4]arene **130**.

Efforts were made to obtain complex **134** by base promoted ligand exchange reaction starting from complex **103**. However, although complex **103** was fully consumed, no desired complex could be isolated. The reason why the base-promoted ligand exchange with calix[4]arene **133** did not succeed, remains unclear. In order to successfully couple calix[4]arene diacid **133** with the dirhodium precursor, a thermal ligand exchange reaction was performed with a Soxhlet apparatus filled with K_2CO_3 to drive the reaction towards the desired complex. Purification of the reaction mixture by simple flash chromatography on silica, afforded the desired racemic complex **134** in 37% yield.

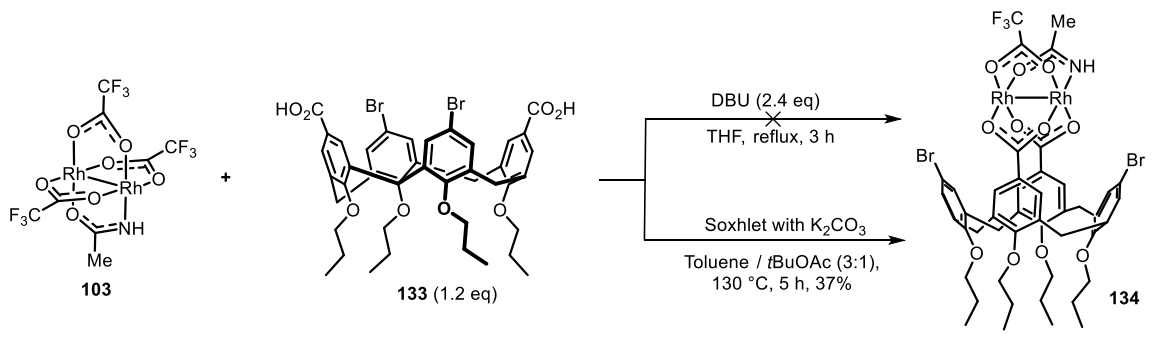

Figure 28- Preparation of racemic heterochiral-at-metal complex **134** by thermal and base-promoted ligand exchange with calix[4]arene diacid **133**.

Gratifyingly, the enantiomers of **133** could be separated by preparative HPLC. Even though the XRD data of complex **129** (*vide supra*) showed that the cone conformation of the calix[4]arene units had remained, a detailed spectroscopic study was performed to further examine the conformation of the calix[4]arene ligand on the dirhodium scaffold. The NOE data suggests that all of the propoxy groups are facing downwards as X6' (X = 4, 5, 6, 7) shows cross correlations to X7 (Figure 29). X6'' instead only shows NOEs to the aromatic signals X2 and X4 (X = 4, 5, 6, 7). Therefore, the cone shape of the calix[4]arene entity was assured.

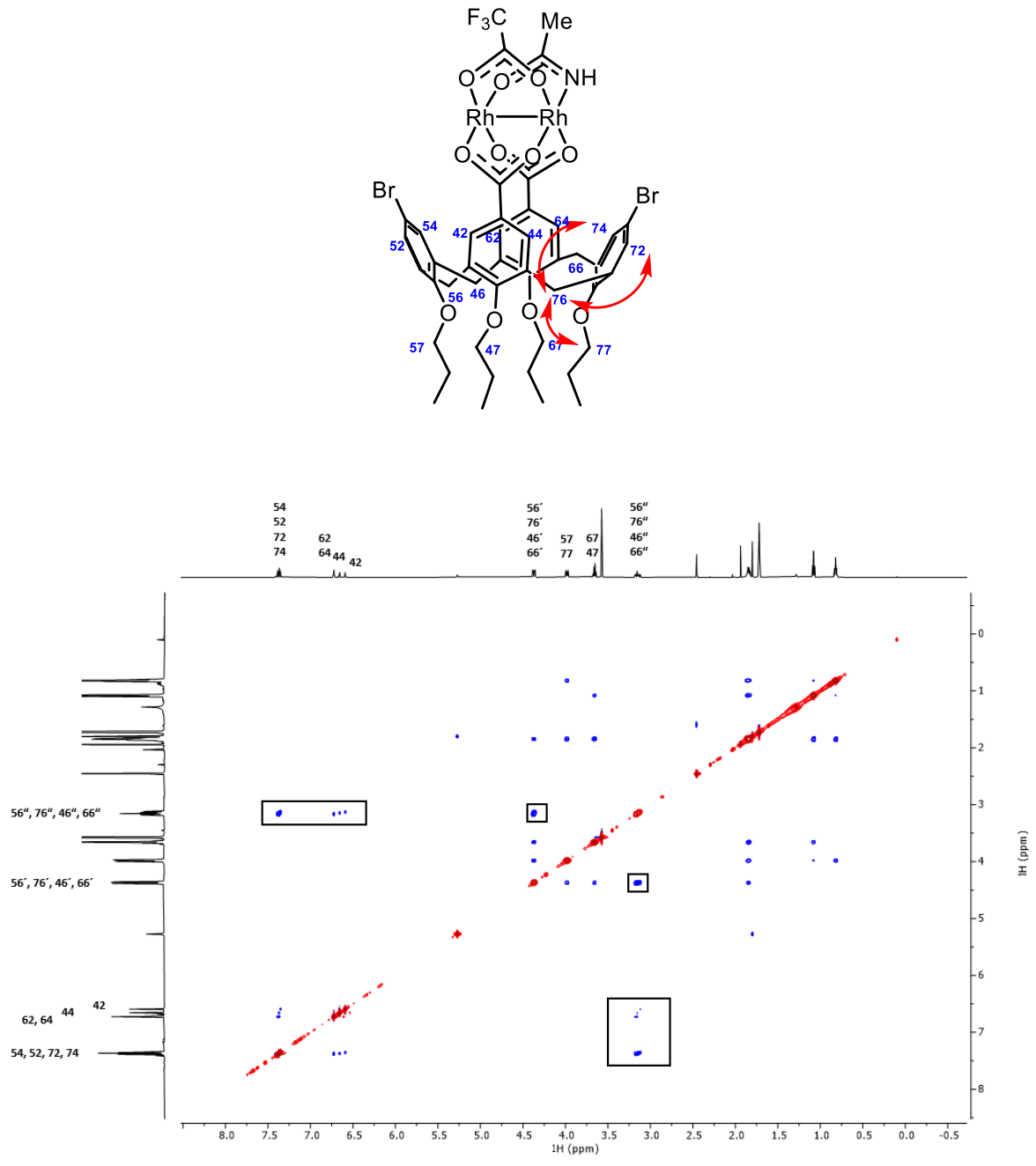

Figure 29-^{1}H–^{1}H NOESY of complex **134** (measured in [D$_8$]-THF) (the areas of interest are highlighted with a black square).

DFT calculations were performed to further investigate the conformational stability of the complex. The complexes bearing a calix[4]arene cone conformer and a 1,3-alternate conformer were calculated at the B3LYPD3(BJ) /def2-SVP level of theory. An energy scan of the dihedral angle responsible for the interconversion from the cone to the 1,3-alternate conformer revealed that the computed energy barrier is prohibitively high, thus guaranteeing its conformational stability.

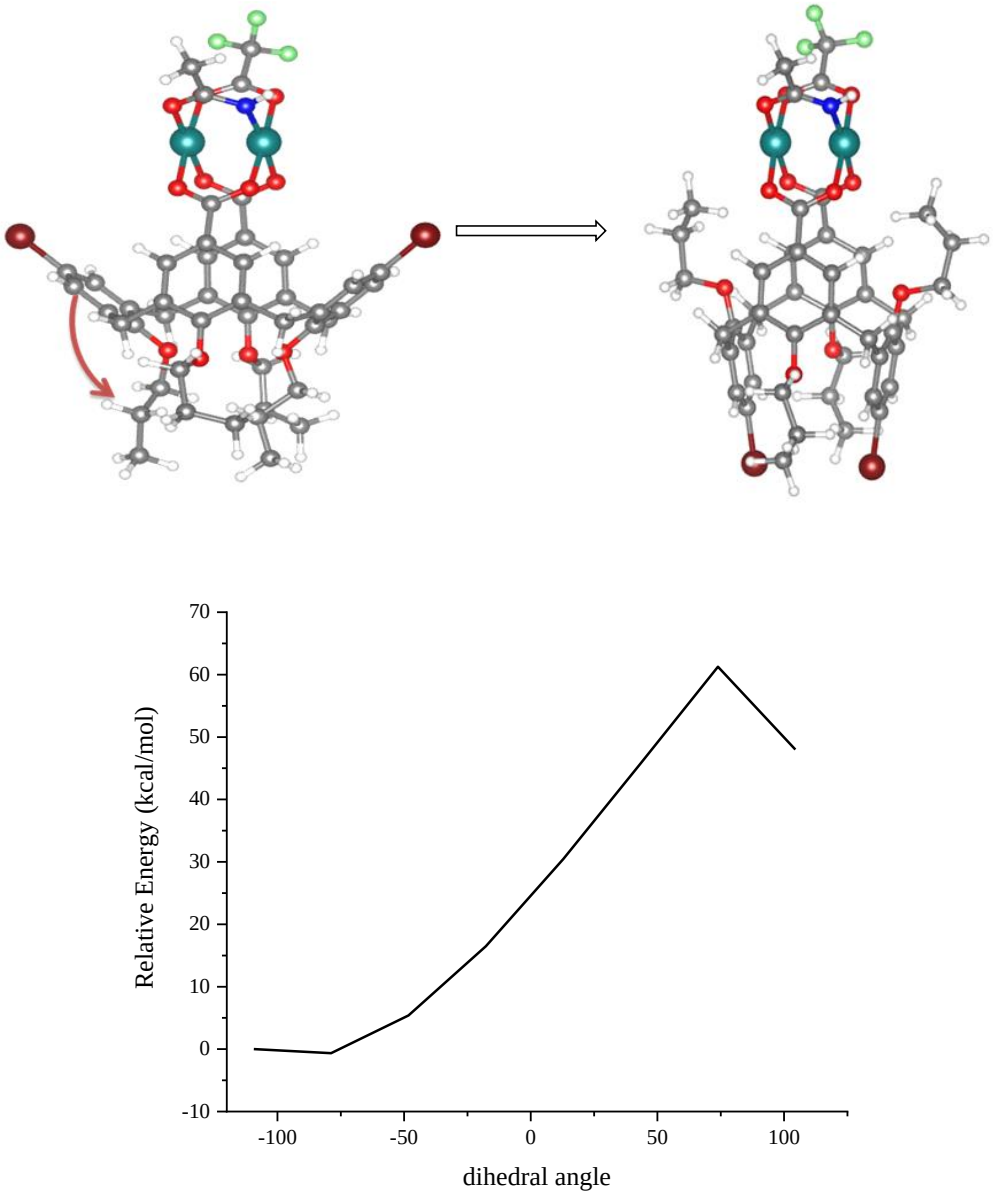

Figure 30-Top: representative computed structures of the cone and 1,3-alternate calix[4]arene conformers of complex **134**. Bottom: energy profile of the dihedral rotation converting from a cone to a 1,3-alternate calix[4]arene conformer.

Extensive efforts to obtain single crystals of either racemic or enantiopure samples of complex **134** suitable for X-ray diffraction (XRD) analysis were unsuccessful, as no data of sufficient

quality could be acquired. Consequently, the absolute configurations of the enantiomers were determined by comparing the experimental circular dichroism (CD) spectra with those obtained from DFT calculations (Figure 31). The computational and experimental CD spectra showed good agreement and the protocol employed for the CD simulations was additionally validated by demonstrating good agreement between the calculated and experimentally measured UV-Vis spectra of complex **134** (see Appendix 2). Hence, the complexes were assigned as helically chiral entities and designated as ***M*-134** and ***P*-134**. The reasoning behind the assigned stereodescriptors will be explained below.

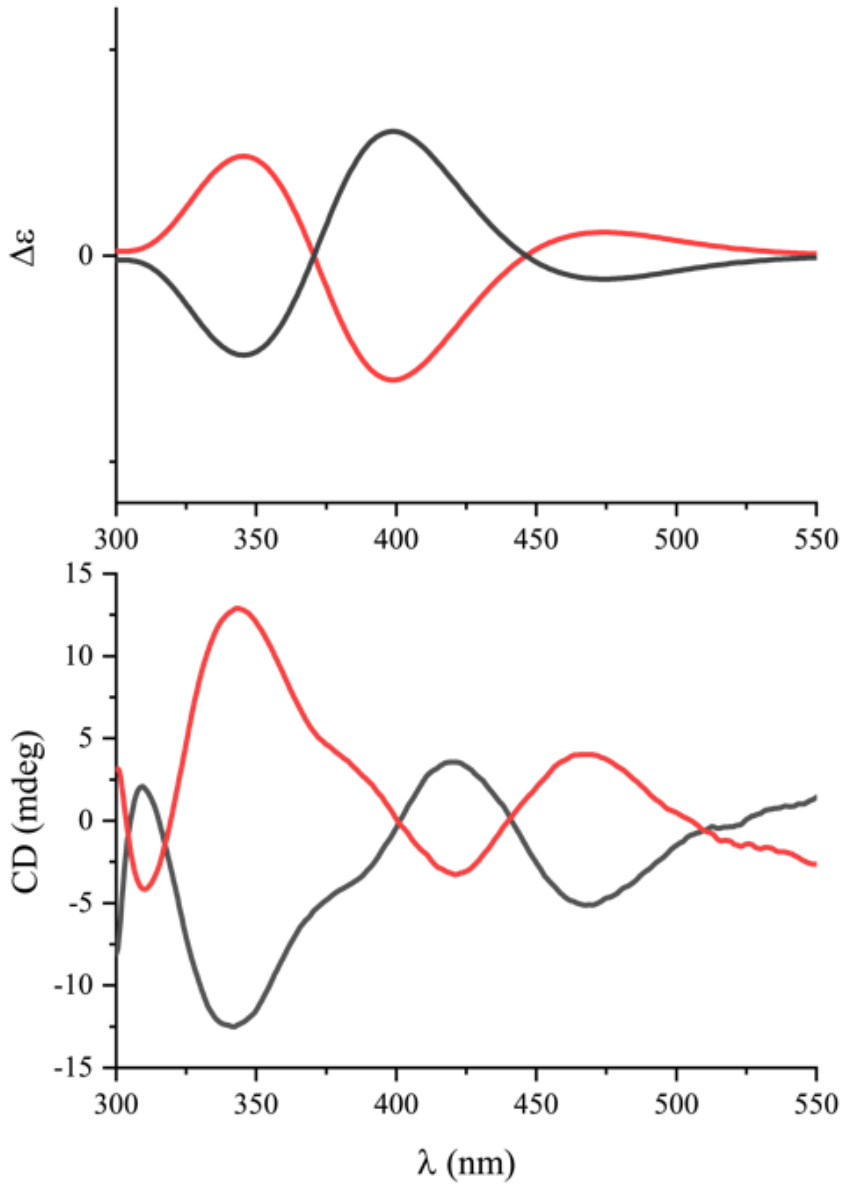

Figure 31-Top: Boltzmann-weighted computed CD spectra of complex **134** (black: ***P*-134**, red: ***M*-134**). Bottom: experimentally recorded CD spectra in methyl *tert*-butyl ether (black: ***P*-134**, red: ***M*-134**).

Nomenclature of Heterochiral-at-Metal Complexes of Type 134

Based on a comprehensive review of the existing literature, no previously reported binuclear complexes have been identified that feature two stereochemically distinct chiral-at-metal centers. To appropriately describe these novel structures, the conventional principles of inorganic stereonomenclature were modified and extended.

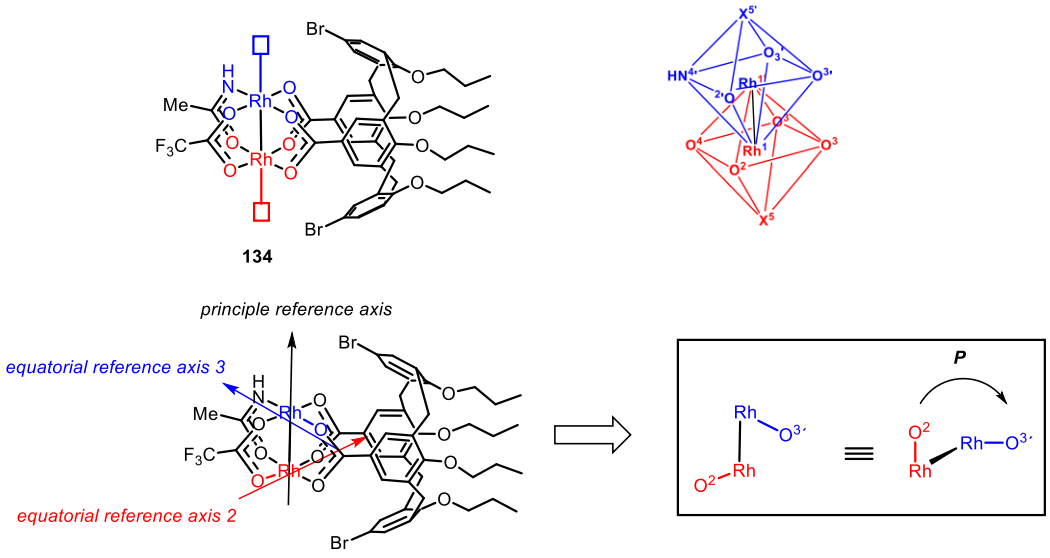

Figure 32-Stereonomenclature analysis of complex **134**. The superscript to the element symbol refers to the ligand priorities within each of the interpenetrating octahedral in which 1 is assigned the highest priority.

Complex **134** can formally be seen as two mutually interpenetrating octahedra, in which the axial coordination sites are occupied by either a solvent molecule or prospective carbene (Figure 32). Hence, if the rules of inorganic stereonomenclature are applied, the Rh–Rh bond can be formally identified as the principal reference axis (the lowest priority, 5, is given to the axially ligated solvent/carbene entity; the highest priority, 1, is assigned to the corresponding distal rhodium atom). In a similar fashion the priority of the other axes can be assigned, allowing the stereodescription of the two chiral-at-metal coordination octahedral as: Rh[O_4]: OC-6-53-A and Rh[O3N]: OC-6- 5‘3‘-C. Since this way of describing catalyst **134** bears a certain complexity and is not intuitive, one can also regard the complex as a helically chiral object similar to how Lahuerta and co-workers descripted their homochiral-at-metal complexes,[121] hence allowing for the assignment of *P* and *M* stereodescriptors. Again the Rh-Rh axis can be assigned as principal axis in which the Rh[O_4] site is the metal center with highest priority. Next, the diagonal axes within the equatorial plane of each Rh-center are defined, which contain the ligand of relative highest priority and, at the same time, are not collinear to each other. In case of complex **134**, the equatorial reference axis at Rh[O_4] passes from O^2 to $O^{3'}$. The equatorial reference axis at Rh[O_4] passes from $O^{3'}$to $HN^{4'}$. With both equatorial reference axes

assigned, one has to look along the Rh-Rh axis with Rh[O_4] as the metal center with the highest priority in front and Rh[O_3N] in the back; a turn from the ligand with highest priority O^2 at Rh[O_4] to the ligand with highest priority $O^{3'}$ at Rh[O_3N], indicates a clockwise turn, thus the depicted enantiomer of complex **134** is *P*-configured.

In cases where the trifluoracetate ligand of the heterochiral-at-metal complex is replaced by an acetate ligand (e.g. complex **135**), the assignment of highest priority ligand at Rh[O_4] becomes more complex. Namely, both O-atoms of the calix[4]arene-based chelate ligand occupy positions of highest priority within the equatorial plane at both chiral-at-metal rhodium centers. However, as they are intrinsically equivalent, there is no obvious point from which to initiate stereochemical assignment. Therefore, the rule of *trans*-maximum-difference was applied.[139-140] In that case, the O^2-O^4 axis gains priority over the O^2-O^3 axis. The other axis at Rh[O_3N] that is non-collinear to the O^2-O^4 axis, is $O^{2'}$–$O^{3'}$. On this basis, the chirality axis of **135** can be assigned as *P*-configured, as the O^2–Rh–Rh–$O^{2'}$ unit describes a clockwise turn.

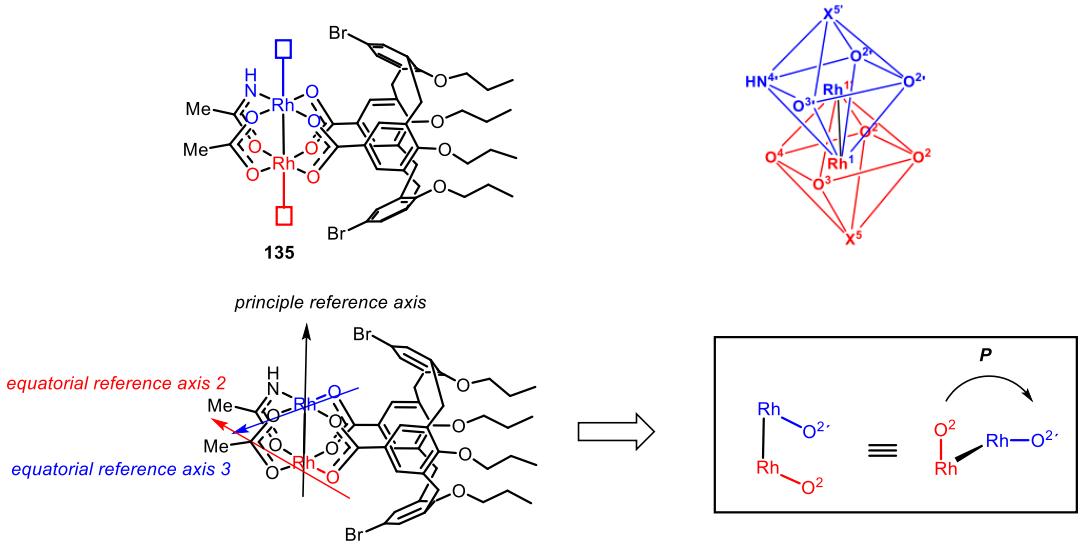

Figure 33-Generalisation of the helical stereonomenclature illustrated for complex **135**.

Initial Cyclopropanation Reactions with Complex 134

With the enantiomerically pure forms of complex **134** in hand, their catalytic performance was evaluated in the cyclopropanation of diazo methyl ester **119**. Using 1 mol% of ***P*-134**, rapid conversion to the corresponding cyclopropane **120** was observed, with an enantiomeric excess of 20%. Given that, in dirhodium catalysis, replacing the methyl ester of the diazo compound with a more sterically congested trichloroethyl ester is known to enhance enantioselectivity,[141] the corresponding diazo trichloroethyl ester **136** was synthesized and subjected to cyclopropanation under otherwise identical conditions, yielding the product with

49% *ee*. While the level of enantioinduction achieved with ***P*-134** was moderate, these results suggested that further tuning of the steric environment of the calix[4]arene scaffold in complex **134** could improve stereocontrol in this transformation.

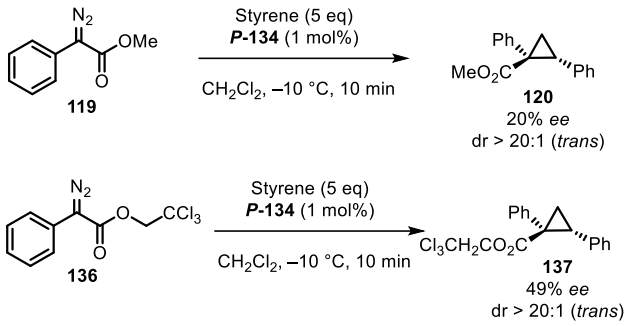

Figure 34-Cyclopropanation reactions of diazo esters **119** and **136** catalyzed by ***P*-134**.

2.5. Further Development of Calix[4]arene Heterochiral-at-Metal Dirhodium Complexes

Initial efforts focused on the late-stage functionalization of complex **134**, based on the rationale that the bromo-substituents on the aryl rings of the calix[4]arene entity could serve as handles for C–C cross-coupling reactions. Notably, only a few late-stage functionalization reactions of homoleptic dirhodium paddlewheel complexes exist.[142-143] However, attempts to perform a two-fold Suzuki–Miyaura cross-coupling under conditions reported by Shibasaki and co-workers[142] were unsuccessful, with no desired product formation observed. Consequently, the strategy was revised to introduce structural modifications to the calix[4]arene ligand prior to coordination with the dirhodium core.

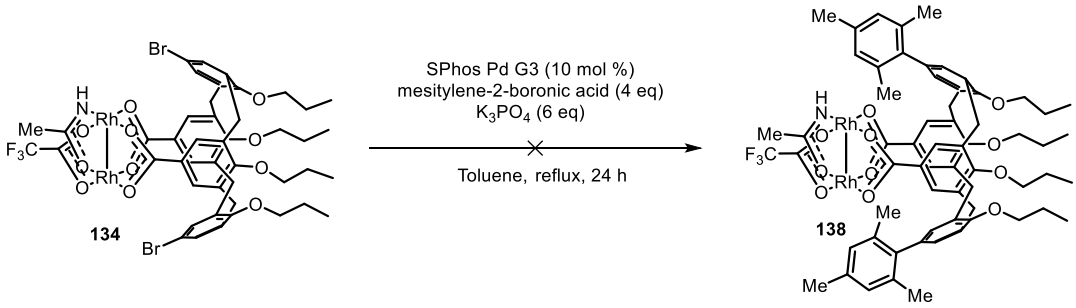

Figure 35-Twofold Suzuki-Miyaura cross-coupling reaction of complex **134** with mesitylene boronic acid.

It was envisioned that tetra-bromo-substituted calix[4]arene **132** could serve as an ideal synthetic handle in our quest for calix[4]arene functionalization. This was pursued via two consecutive twofold lithium-bromine exchange reactions,[138] in which the intermediate aryl-lithiated species were quenched with the electrophile of interest and subsequently with CO_2.

When the initial part of the sequence was performed with TMSCl as the electrophile, clean conversion to **139** was achieved (Table 7). In contrast, attempts to introduce more bulky alkylsilanes (entries 2–3) proved completely non-selective, as NMR spectroscopy revealed a complex mixture of side products. It was considered plausible that the reactive dilithiated intermediate reacts in part with traces of HCl in the chlorosilane, therefore resulting in a mixture of products. Hudrlik and coworkers described that premixing the chlorosilane with Et_3N prior to addition to the calix[4]arene derivative led to cleaner reaction profiles.[144] This approach was met with success: using the supernatant solution of $PhMe_2Cl$ and Et_3N to quench the dilithiated intermediate resulted in clean conversion into **142** (entry 4).

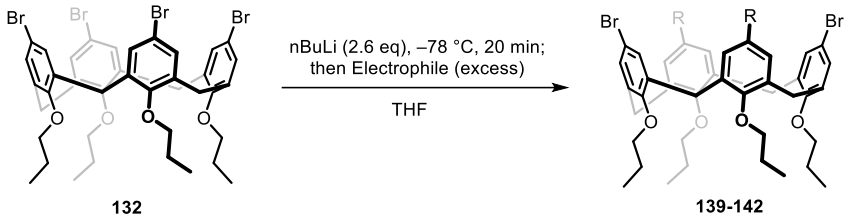

#	Electrophile	Product	Yield %	Comment
1	TMSCl	**139**	90	
2	TIPSCl	**140**	n.d.	Messy reaction profile
3	TBDMSCl	**141**	n.d.	Messy reaction profile
4	$PhMe_2Cl/Et_3N$	**142**	72	

Table 7-Twofold lithium-bromine exchange followed by addition of different chlorosilanes. The reported yields are isolated yields.

C-silylated calix[4]arenes **139** and **142** were successfully converted into the diacid precursors **143** and **144** in moderate yields (Scheme 40).

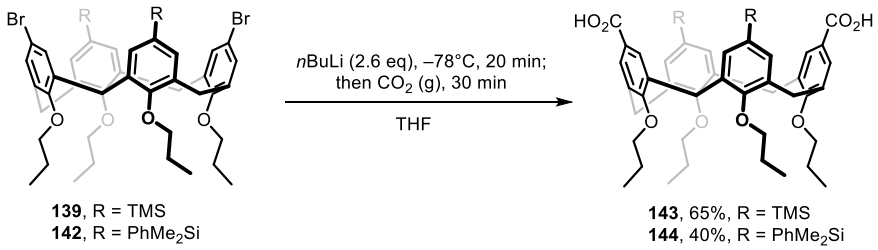

Scheme 40- Synthesis of C-silylated diacid calix[4]arenes **140-141**.

Alternatively, the dilithiated species derived from **132** and *n*-BuLi was quenched with triethyl borate [$B(OEt)_3$] instead of a chlorosilane (Scheme 41). Acidic treatment with HCl furnished the corresponding diboronic acid, which was directly converted into the 1,3-propanediol-

based boronic ester **145**. This ester successfully underwent a Suzuki–Miyaura coupling with *p*-iodotoluene, yielding the desired product **146** in excellent yield. However, the extremely low solubility of **146** prevented further functionalization.

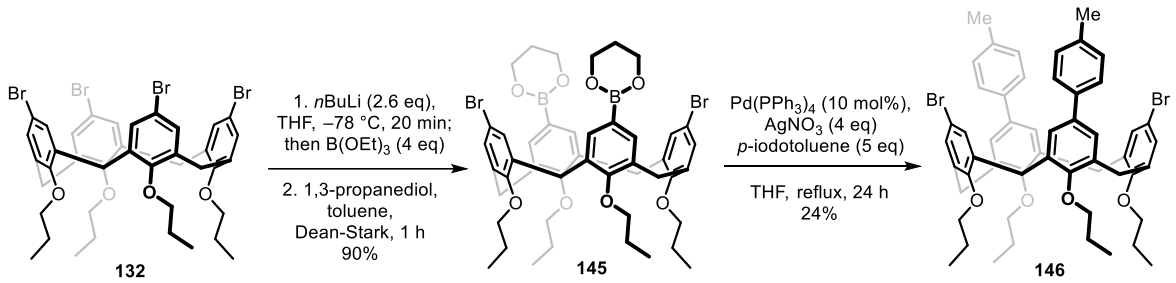

Scheme 41-Initial synthetic approach to functionalize the calix[4]arene scaffold with aryl-substituents.[145]

Therefore, another strategy was sought to be able to get to the desired target **151**. It was envisioned that protection of the diacid functionality of **133** by converting it into a methyl ester, would allow for a C(sp^2)–C(sp^2) coupling reaction, followed by a simple deprotection of the methyl ester to the desired diacid motif. An initial attempt to synthesize methyl ester **147** by deprotonating the carboxylic acid with potassium carbonate followed by methylation using methyl iodide was unsuccessful. However, **147** was successfully obtained in 76% yield via Steglich esterification (Scheme 42). Twofold Suzuki-Miyaura cross coupling with 3,5-dimethylphenylboronic acid and *p*-methylphenylboronic acid yielded **148** and **149** in moderate yields, respectively. Deprotection with KOTMS, followed by subsequent treatment with citric acid afforded the desired functionalized diacids **150** and **151**.

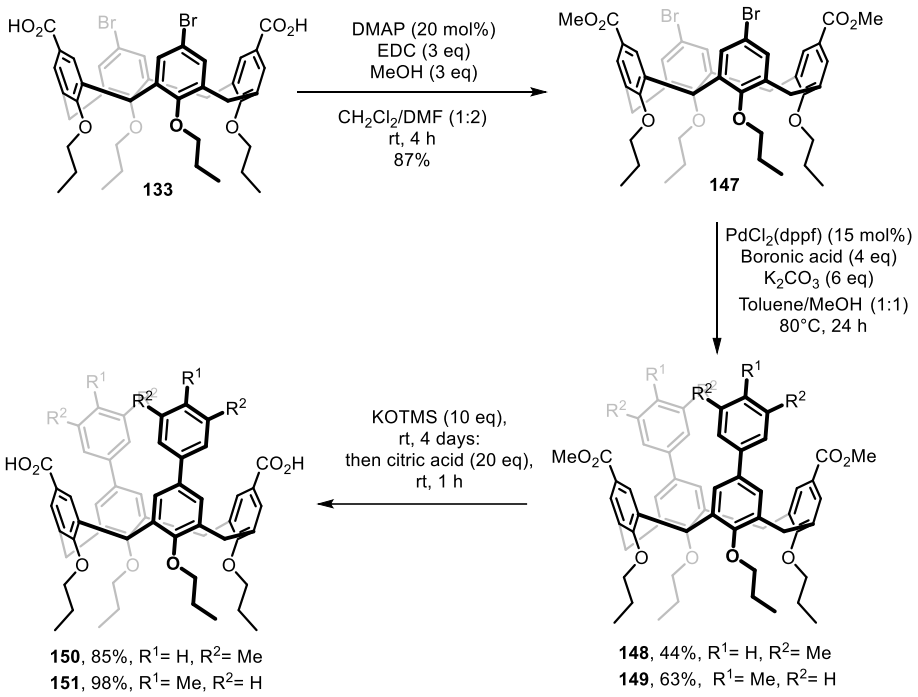

Scheme 42-Synthetic overview of the protection-cross-coupling-deprotection approach to get towards aryl functionalized calix[4]arene diacids **150** and **151**. [Conditions for failed protection reaction: K_2CO_3 (4.4 eq), MeI (5 eq), DMF, rt, 12 h].

Additionally, methyl ester **147** was treated under Buchwald´s aromatic Finkelstein conditions,[146] enabling the efficient substitution of the bromo groups with iodo substituents in excellent yield (Scheme 43). Subsequent deprotection of the ester functionalities yielded the calix[4]arene diacid **153**.

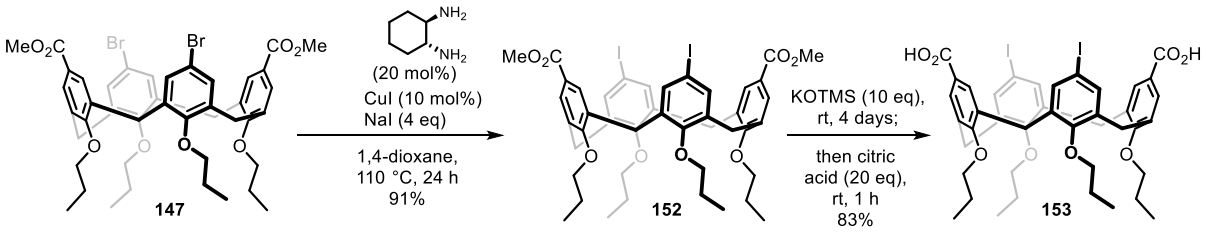

Scheme 43-Synthetic route towards iodo-substituted calix[4]arene diacid **153** enabled via an aromatic Finkelstein reaction.

With a variety of functionalized calix[4]arene diacids at hand, the ligands were successfully installed on the dirhodium scaffold by thermal ligand exchange conditions similar to prototype complex **134** (Scheme 44). The enantiomers of complexes **154-157** were successfully separated by preparative HPLC. Only the enantiomers of **159** could not be successfully separated due to instability issues of the complex. Additionally complex **158** was prepared from its corresponding [1,3]-benzamidate-trifluoroacetate precursor.

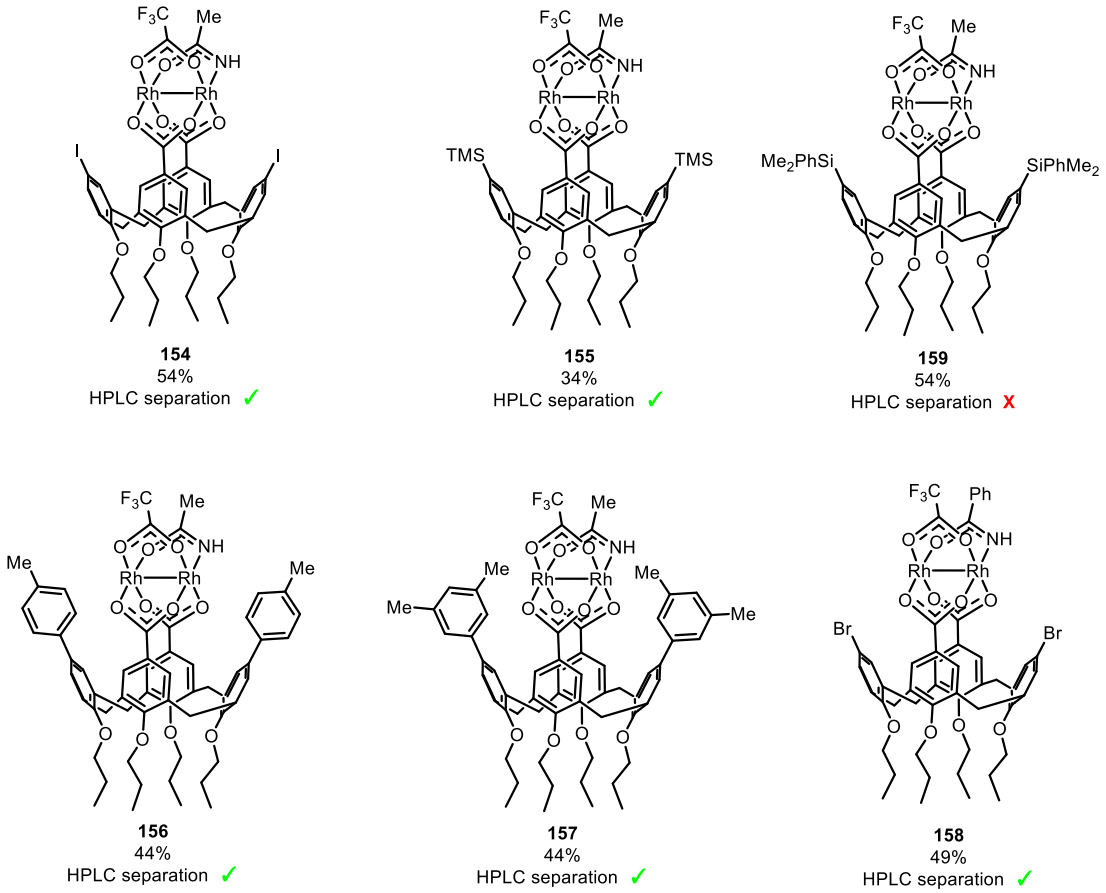

Scheme 44-Synthesized heterochiral-at-metal Rh(II) complexes bearing a calix[4]arene unit. Successful preparative chiral HPLC separation of the corresponding enantiomers is represented by a green check mark, if unsuccessful marked by a red cross.

To test the importance of interligand hydrogen bonding interactions of the amidate ligand with the carbene intermediate on the outcome of the asymmetric cyclopropanation reaction, a complex was synthesized comprising an *N*-methylacetamidate ligand which lacks the ability to engage as a hydrogen bond donor. Homoleptic *N*-methylacetamidate complex **160** was made from commercially available $[Rh_2(OAc)_4]$ by thermal ligand exchange. Subsequent ligand exchange reaction with trifluoroacetic acid resulted in the desired [1,3]-complex **161** in 44% over the two steps (Scheme 45). Thermal ligand exchange with calix[4]arene diacid **133** resulted in 61% yield of the racemic complex **162**, which was successfully separated by preparative HPLC on a chiral stationary phase to afford the enantiomers of the complex.

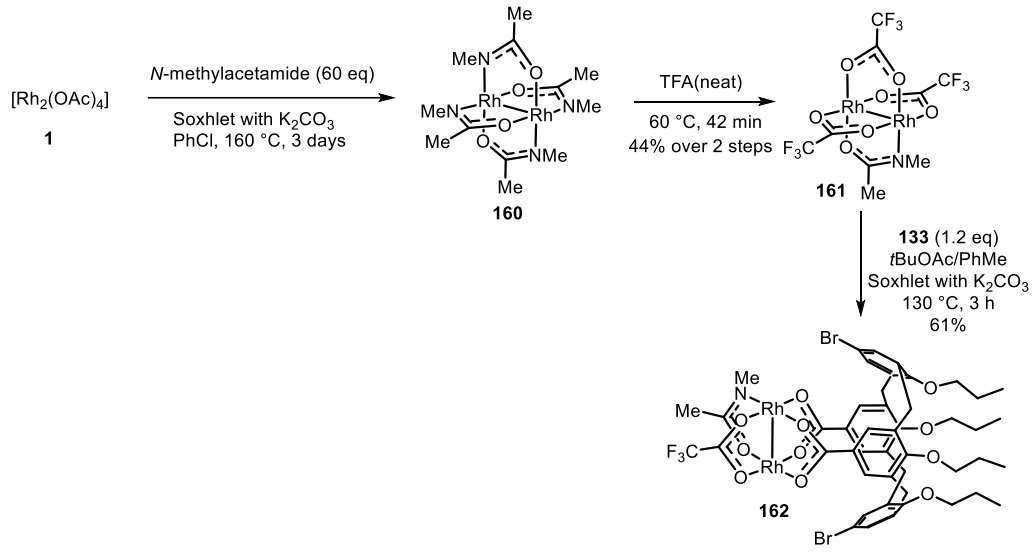

Scheme 45-Synthetic route towards *N*-methylated complex **160** starting from the commercially available $[Rh_2(OAc)_4]$.

Also, a homochiral complex **163** bearing two amidate ligands was synthesized by refluxing $[Rh_2(acam)_4]$ in the presence of **133** in chlorobenzene. A mixture of two isomers was obtained, which could be separated from each other by preparative HPLC separation on an achiral stationary phase which afforded the desired complex in 7% yield (Scheme 46). The enantiomers of complex **163** were obtained by preparative HPLC on a chiral stationary phase.

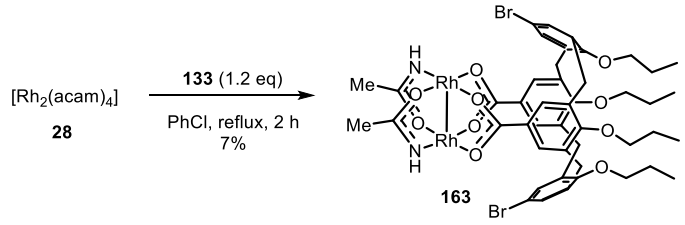

Scheme 46-Synthesis of homochiral-at-metal complex **163** from $[Rh_2(acam)_4]$.

The enantiomers of complexes **154-157**, **162** and **163** were evaluated as catalysts in the cyclopropanation of diazo trichloroethyl ester **136**, with particular focus on their ability to induce enantioselectivity. The iodo-substituted complex ***M*-154** led to a modest improvement in enantiomeric excess compared to the prototype bromo-substituted complex ***M*-134** (Table 8, entry 2). In contrast, all other derivatives in the series (**155-157**) exhibited slightly reduced levels of enantioinduction (entries 3-5). A control experiment using the *N*-methylated acetamide analogue ***P*-162**, which lacks hydrogen-bond donor capability, underscored the significance of hydrogen bonding interactions in the catalytic system, as only 11% *ee* was obtained under otherwise identical conditions (entry 6). The homochiral complex ***P*-163** also afforded low enantioselectivity in the cyclopropanation reaction (entry 7).

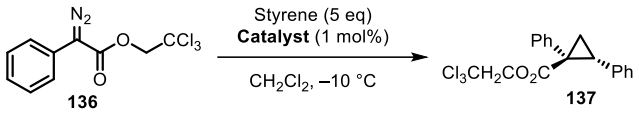

#	Catalyst	T [°C]	solvent	Yield [%]	*ee* [%]
1	***M*-134**	–10	CH_2Cl_2	n.d.	49
2	***M*-154**	–10	CH_2Cl_2	72	52
3	***P*-155**	–10	CH_2Cl_2	71	–36
4	***P*-156**	–10	CH_2Cl_2	77	–43
5	***P*-157**	–10	CH_2Cl_2	76	–41
6 [a]	***P*-162**	–10	CH_2Cl_2	60	–11
7 [a]	***P*-163**	–10	CH_2Cl_2	74	–25
8	***M*-134**	–10	pentane	78	61
9 [b]	***M*-134**	–40	pentane	71	70
10	***M*-154**	–40	pentane	69	73

Table 8-Overview of the level of enantiocontrol induced in the cyclopropanation reaction of diazoester **136** catalyzed by complexes **134**, **154-157**, **162** and **163**. Unless otherwise stated, the reaction were performed on 0.07 mmol (20 mg) scale The stereodescriptor of catalysts **154-157**, **162** and **163** was assigned by comparison of the absolute stereochemistry of cyclopropane **137** with the stereochemistry induced by prototype complex ***M*-134** for which the stereochemistry is known by circular dichroism spectroscopy. a: these catalysts were tentatively assigned as the ***P*** stereodescriptor. b: reaction was performed on 0.1 mmol scale.

Notably, optimization of reaction parameters using the prototype complex ***M*-134** revealed that switching the solvent from dichloromethane to pentane led to a 12% increase in *ee* (entry 8). Further lowering the reaction temperature to –40 °C resulted in a significant enhancement of enantioselectivity, reaching 70% *ee* (entry 9). Under these optimized conditions, application of the iodo-substituted complex ***M*-154** afforded only a marginal additional increase in enantioselectivity (entry 10).

4.2.5.3 Cyclopropanation Reactions with a α-Stannylated Diazoester

Previously developed heteroleptic complexes from our group containing an amidate functionality, which engages in similar noncovalent interactions, have shown high levels of enantioselectivity in the cyclopropanation of α-stannylated diazo compounds (see section 1.7).[80-81] Therefore, we were eager to test the stereoselectivity induced by the heterochiral-at-metal prototype complex **134** in such transformation.

In an initial attempt, the stannylated diazo ester **20** was subjected to cyclopropanation using complex ***P*-134** under the conditions reported by Fürstner and co-workers (Scheme 47).[81] While the reaction proceeded in low yield, the enantio- and diastereoselectivity were remarkably high. Notably, the reaction delivered the ***cis***-diastereomer (assigned by a 2D-NOESY experiment) as the major product with exceptional selectivity, which by far exceeded the 5:1 *cis:trans* ratio of the best *cis*-selective catalyst **31** previously known.

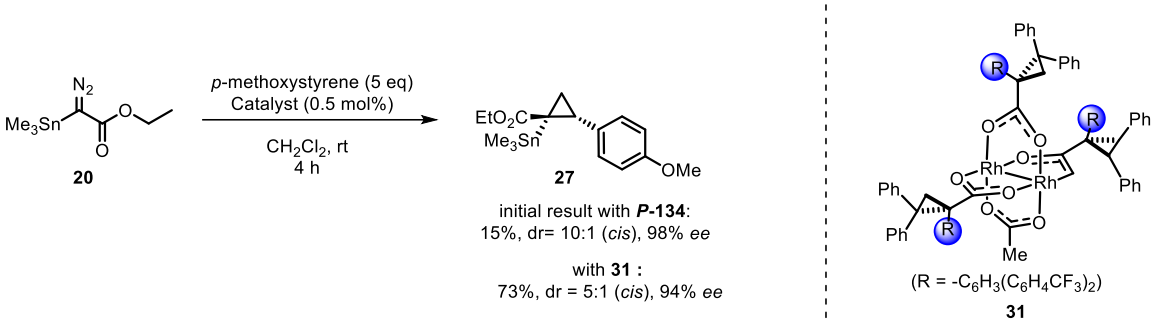

Scheme 47- Initial results of cyclopropanation of α-stannylated diazoester **20** with ***P*-134**. For comparison, the result of the best *cis*-selective catalyst **31** is also included.

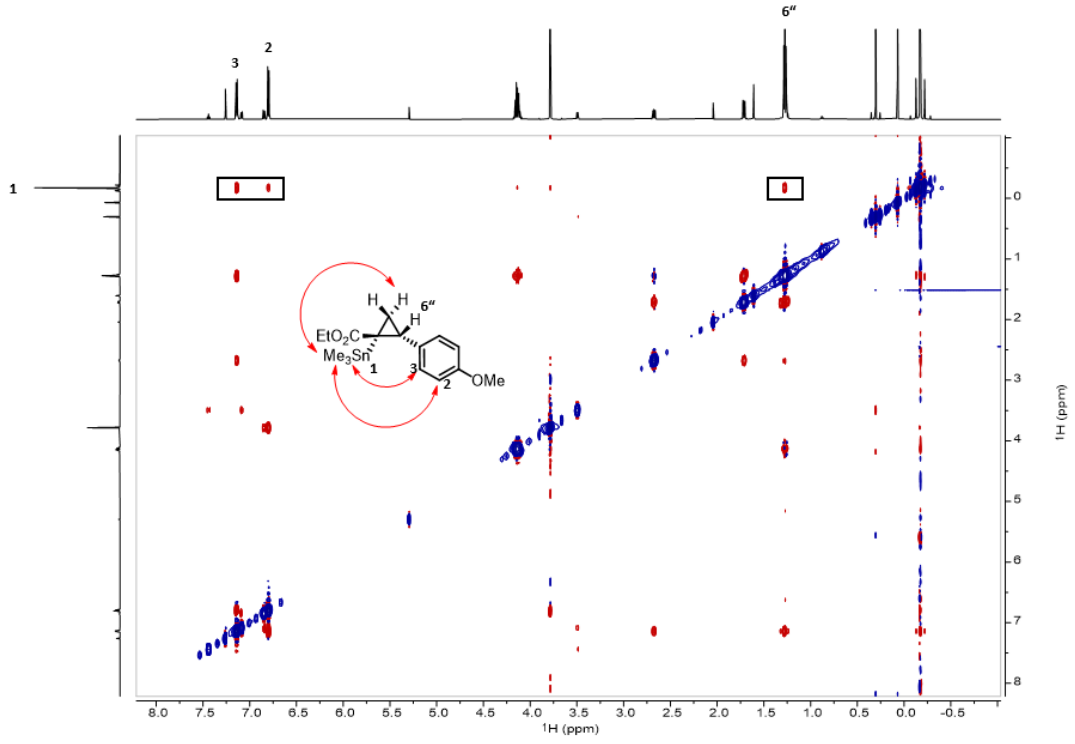

Figure 36-^{1}H–^{1}H NOESY spectrum of cyclopropane **27,** ascribing the cis-configuration of **27**. The designated areas of interest are highlighted with a black box.

Encouraged by this promising result, further efforts were undertaken to improve the yield of the cyclopropane product **27** (Table 9). Increasing the catalyst loading had no measurable impact on conversion (entry 2). Substitution of the labile trifluoroacetate ligand in complex **134** with a standard acetate ligand in racemic complex ***rac*-135** resulted in a decreased diastereomeric ratio and no improvement in yield (entry 3). Interestingly, rapid addition of the diazo compound led to significantly cleaner reactions and improved yields (entry 4). In contrast, lowering the reaction temperature to –20 °C caused a substantial drop in product formation (entry 5).

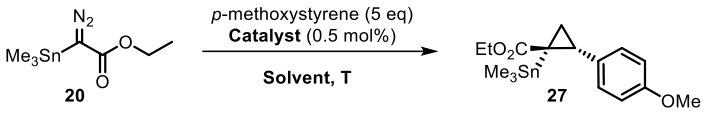

#	Catalyst	Mol% cat	Solvent	T [°C]	Addition time diazo	Yield % [^{1}H NMR]	*cis:trans*	*ee* [%]
1	***P*-134**	0.5	CH_2Cl_2	rt	5 h	15 [37]	10:1	98
2	***P*-134**	1.0	CH_2Cl_2	rt	5 h	[30]	10:1	98
3	***P*-135**	0.5	CH_2Cl_2	rt	5 h	[22]	7:1	n.d.
4	***P*-134**	0.5	pentane	rt	<1 min	[65]	9:1	n.d.
5	***P*-134**	0.5	CH_2Cl_2	–20	<1 min	[15]	10:1	n.d.
6	***P*-154**	0.5	CH_2Cl_2	rt	<1 min	[61]	12:1	89
7 [a]	***P*-134**	0.5	CH_2Cl_2	rt	<1 min	40 [75]	10:1	n.d.
8 [b, d]	***P*-134**	0.5	CH_2Cl_2	rt	<1 min	58 [85]	10:1	98
9 [c]	***P*-162**	0.5	CH_2Cl_2	rt	<1 min	37 [64]	3:1	48

Table 9-Optimization table of the cyclopropanation reaction of stannylated diazo ester **20**. Unless stated otherwise, all the reactions in the screening were performed on a 0.1 mmol scale. Yields in brackets were determined by ^{1}H NMR analysis of the crude material using mesitylene as internal standard. All other yields are isolated yields. [a] Molecular sieves (4Å) were added to the reaction. [b] The reaction was performed with freshly sublimed diazo ester **20** (<48h prior to use). [c] The chosen catalyst was tentatively assigned as ***P*-162**. [d] reaction was performed on a 0.2 mmol scale.

The iodo-substituted complex, which previously showed promising enantioselectivity in reactions with aryl diazo compounds (*vide supra*), was also tested in this system. Although the diastereomeric ratio improved to 12:1 in favor of the *cis*-isomer, the enantiomeric excess decreased by nearly 10% compared to complex ***P*-134** (entry 6). Ultimately, it was discovered that using freshly sublimed diazo compound **20** (within 48 hours of preparation) led to even

cleaner conversion (entry 8). Under these optimized conditions, the cyclopropane product was isolated by flash chromatography as the pure *cis*-isomer in 58% yield and 98% *ee*. A control experiment was performed with catalyst ***P*-162**, which featured a methyl substituent on the acetamidate ligand, therefore lacking hydrogen bond donor capabilities. As expected, the yield, dr and *ee* of cyclopropane **27** all dropped significantly, which indicates that the protic –NH group is quintessential for achieving high levels of stereoselectivity. Additionally, this finding supports the notion that the reaction takes place at the chiral Rh-center ligated to the N-atom.

With the optimized conditions in hand, the scope of the cyclopropanation reaction of stannylated diazo ester **20** with a variety of olefins was explored (Scheme 48). Where available, data obtained using catalyst **31** are included for comparison. Cyclopropanation of an electron-deficient styrene afforded product **164** in good yield and excellent stereoselectivity, demonstrating that the electronic nature of the styrene substrate has minimal impact on stereocontrol in this transformation. Moreover, both *ortho*- and *meta*-substituted styrenes were well tolerated, furnishing products **166-167** efficiently. A direct comparison between cyclopropane **166** obtained using catalyst ***P*-134** and that formed with catalyst **31** revealed slightly improved enantio- and diastereoselectivity in case of ***P*-134**. The superiority of ***P*-134** becomes even more pronounced in the case of substrate **170**; replacement of **31** by ***P*-134** resulted in an increase in yield and dr from 2:1 to >20:1, approaching the detection limits of the minor diastereomer. *tert*-Butyl vinyl ether reacted similarly well to afford **165** with dr >20:1 and 96% *ee*. High levels of stereoselectivity were likewise observed in the cyclopropanation of indene and 2-vinylthiophene, affording **168** and **169**, respectively. Employing allyltrimethylsilane resulted in notably lower levels of diastereoselectivity (dr = 3:1) in comparison with the other formed cyclopropanes, but the enantiomeric excess of **171** remained excellent.

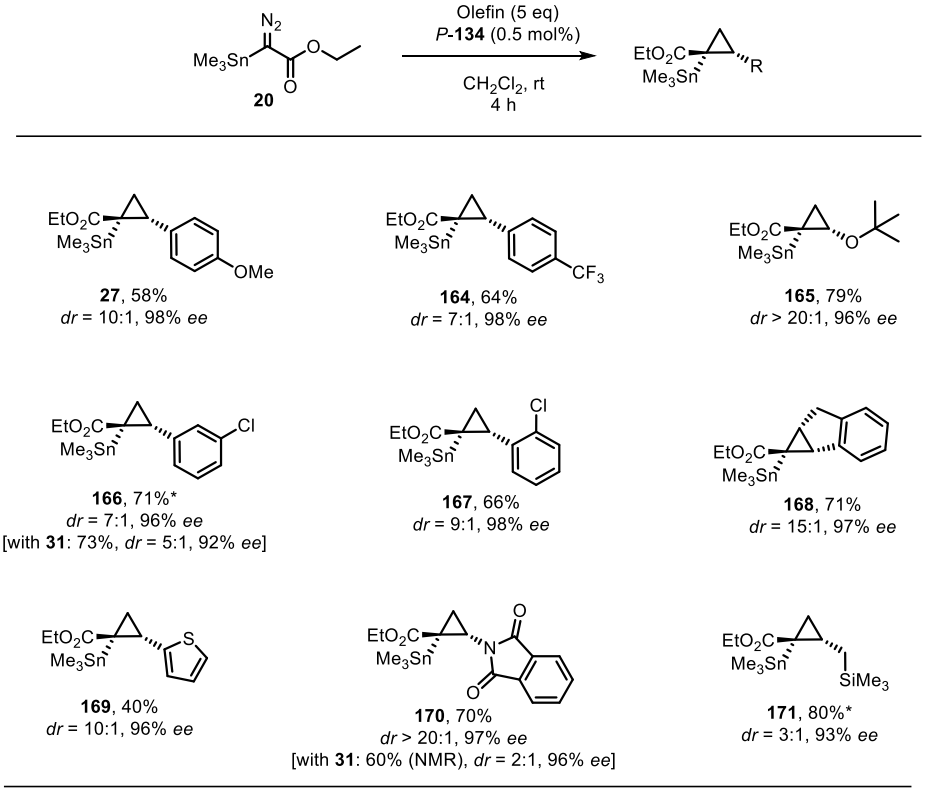

Scheme 48-Scope of the cyclopropanation of stannylated diazoester **20** with ***P*-134** set up on 0.2 mmol scale. Unless stated otherwise, the yields refer to pure *cis*-isomer after flash chromatography, the dr to the crude product (NMR). The compounds indicated with an asterisk (*) are isolated as a mixture of *cis*- and *trans*-isomers.

Computations

Given the novelty of the catalyst and the interesting stereochemistry, a more detailed analysis of the mode of action of ***P*-134** was deemed appropriate. Therefore, efforts were made by DFT calculations to achieve more insight. Interestingly, it was found that in the most stable conformer of the carbene intermediate, the Me_3Sn- group orients itself towards the calix[4]arene unit (Figure 37). Looking at the topographic steric bulk map generated from this carbene intermediate (Figure 38), it is clear that the bromo-substituted calix[4]arene unit displays enough steric bulk, to block the incoming nucleophile approaching from that side. Nucleophile approaches via the quadrants on the right side are energetically less favored, as the hydrogen bond between the –NH group and carbonyl moiety of the carbene would get distorted. The only possible trajectory for the nucleophile to approach would be the upper left side of the carbene. However, to explain the observed stereochemistry displayed by cyclopropane **27**, the carbene would need to reposition itself and twist 180° in order to meet the observed *cis*-isomer of **27**.

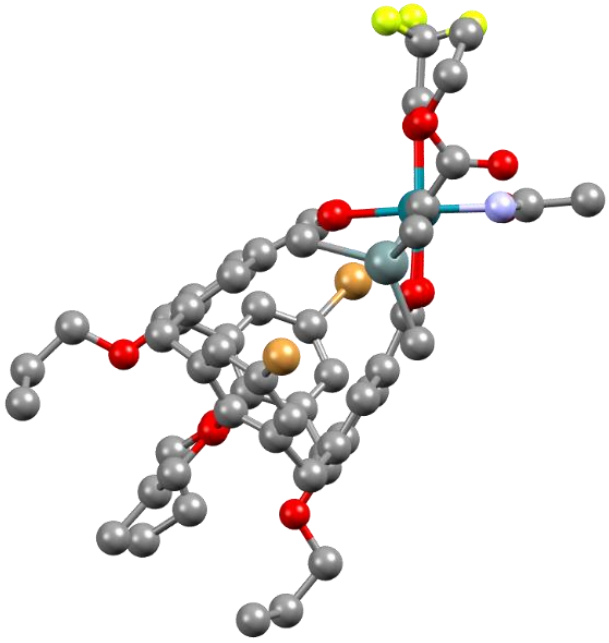

Figure 37-Computed structure of carbene intermediate of complex ***P*-134**, calculated at computed at B3LYP-D3(BJ)/def2-SVP(-f) + RIJCOSX + CPCM(CH_2Cl_2) level of theory.

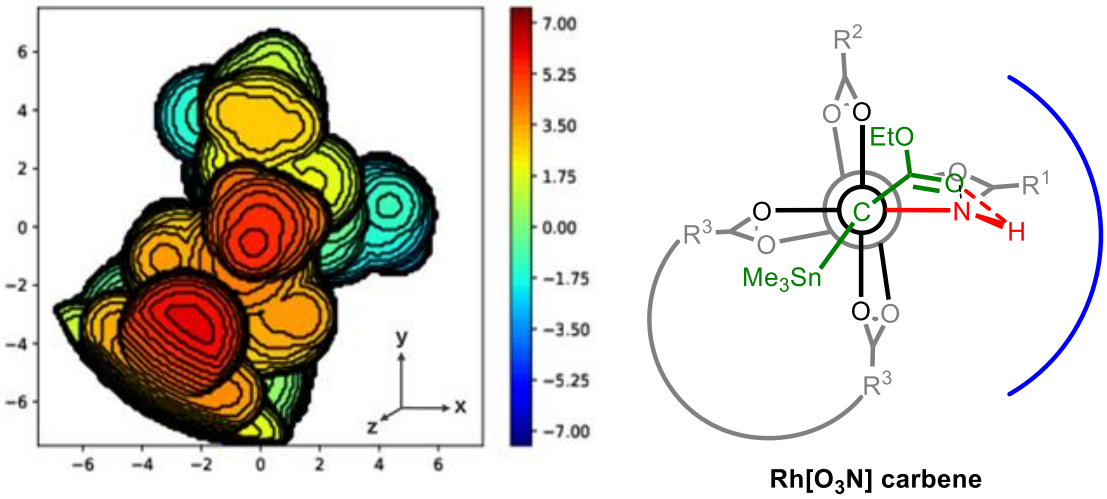

Figure 38- Topological steric bulky map generated with SambVca[1] for computed carbene intermediate (left) and a graphical representation of the carbene intermediate (right).

Therefore, the transition states (TS) of all four nucleophile trajectories were calculated with *p*-methoxystyrene as the nucleophile of choice (Figure 39). As expected, the lowest-lying TS shows *p*-methoxstyrene attacking via the top-back quadrant to the carbene intermediate in which the Me_3Sn- group points "upward" to reside in fairly unencumbered space. This eventually results in the formation of *cis*-(1*R*,2*R*)-configured cyclopropane **27** which is agreement with the experimentally observed stereochemistry. Both TS on the geometrically open quadrants on the right side suffer from high energetic barriers, which originates from a massive distortion of the peripheral hydrogen bond. The large difference of the TS-energies of the two *cis*-channels ($\Delta\Delta G^{\ddagger}$ = 7.42 kcal·mol^{-1}) is perfectly in line with the attained 98% *ee*. In contrast, the relatively small energy difference of the TS energies of the two *trans*-channels ($\Delta\Delta G^{\ddagger}$ = 1.65 kcal·mol^{-1}) would indicate that the *trans*-isomer should be of comparatively low optical purity. This was verified by the observations made in several cases during the optical purity measurements by HPLC (*trans*-**164**: 57% *ee*, *trans*-**166**: 38% *ee*, *trans*-**171**: 4% *ee*), putting extra emphasis on the accuracy of the computational analysis.

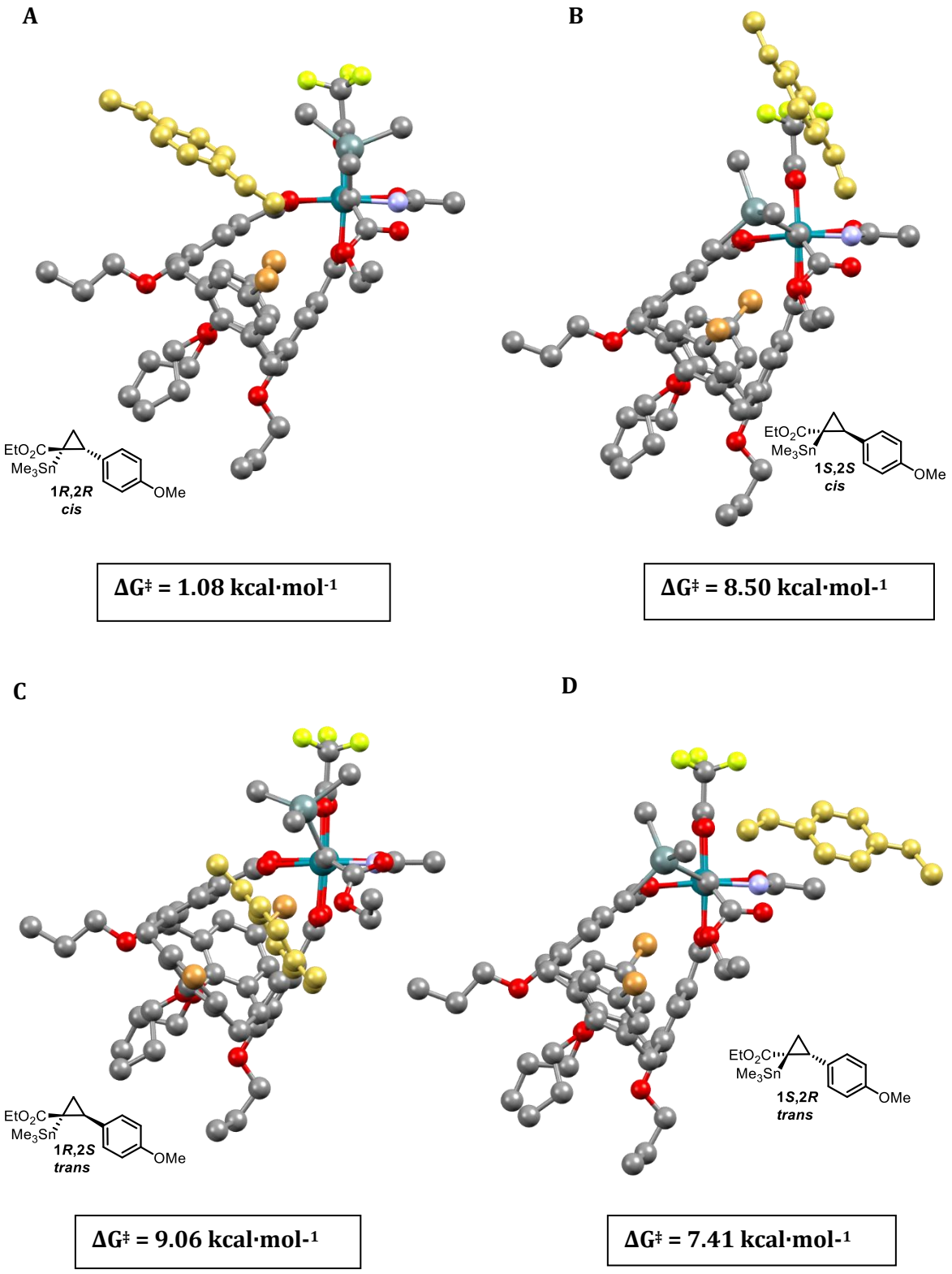

Figure 39-Transition states of the [2+1] cycloaddition of stannylated carbene of ***P*-134** and *p*-methoxystyrene that lead to the four different cyclopropane isomers calculated by DFT.

4.2.5.4. Cyclopropanation Reactions with α-Trifluoromethyl Diazoester

To investigate the range of applicability of the prototype heterochiral-at-metal complex **134**, attention was turned to acceptor/acceptor diazo compounds, with emphasis on α-trifluoromethyl diazo esters. Cyclopropanation with such diazo compounds would render 1,1-disubstituted (trifluoromethyl)cyclopropanes. These motifs are gaining prominence in the pharmaceutical industry due to their function as *tert*-butyl bioisosteres with enhanced metabolic stability.[147-148] As discussed in Chapter 2, no catalyst to date can achieve high levels of asymmetric induction in the direct cyclopropanation of α-trifluoromethyl diazo esters. Only via a hydrazone relay approach with consecutive oxidative cleavage as described in Chapter 2, access could be gained to the desired 1,1-disubstituted (trifluoromethyl)cyclopropane motifs. An overview of the level of stereoinduction induced in the cyclopropanation of diazoester **55** by a wide range of chiral dirhodium paddlewheel catalysts is given in Table 10. [100]

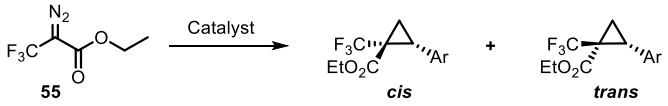

#	Catalyst	Olefin	Yield %	*cis*: *trans*	*ee* (*cis*) %	*ee* (*trans*) %
1	$[Rh_2((S)\text{-PTPA})_4]$	styrene	64	43:57	16	24
2	$[Rh_2((S)\text{-TBSP})_4]$	styrene	44	60:40	18	24
3	$[Rh_2((S)\text{-DOSP})_4]$	styrene	58	44:56	18	50
4	$[Rh_2((S)\text{-NTTL})_4]$	styrene	50	45:55	14	22
5	$[Rh_2((S)\text{-Campha})_4]$	styrene	72	52:48	8	32
6	$[Rh_2((S)\text{-MPMT})_4]$	styrene	50	40:60	2	0
7 [a]	$[Rh_2((S)\text{-MEPY})_4]$	styrene	43	40:60	4	0
8 [a]	$[Rh_2((S)\text{-MEOX})_4]$	styrene	24	30:70	0	0
9[a]	$[Rh_2((S)\text{-BNAZ})_4]$	styrene	36	46:54	4	50
10[a]	$[Rh_2((S)\text{-PHOX})_4]$	styrene	36	43:57	8	42
11[b,c]	$[Rh_2(acam)(S\text{-TPCP})_3]$	*p*-(OMe)styrene	80	61:39	10	5

Table 10- Overview of tested chiral Rh(II) complexes in the cyclopropanation of diazo compound **55** (In entry 1-10 the data are taken from the publication of Muller and co-workers).[100] Except stated otherwise, the reactions were set up at room temperature in CH_2Cl_2 with 5 mol% of catalyst. The yields refer to isolated yields. [a] Set up in DCE at 80 °C. [b] Set up with 0.5 mol% catalyst. [c] Result taken from the lab notebook of F. Caló (CAF-CA-766). [154]

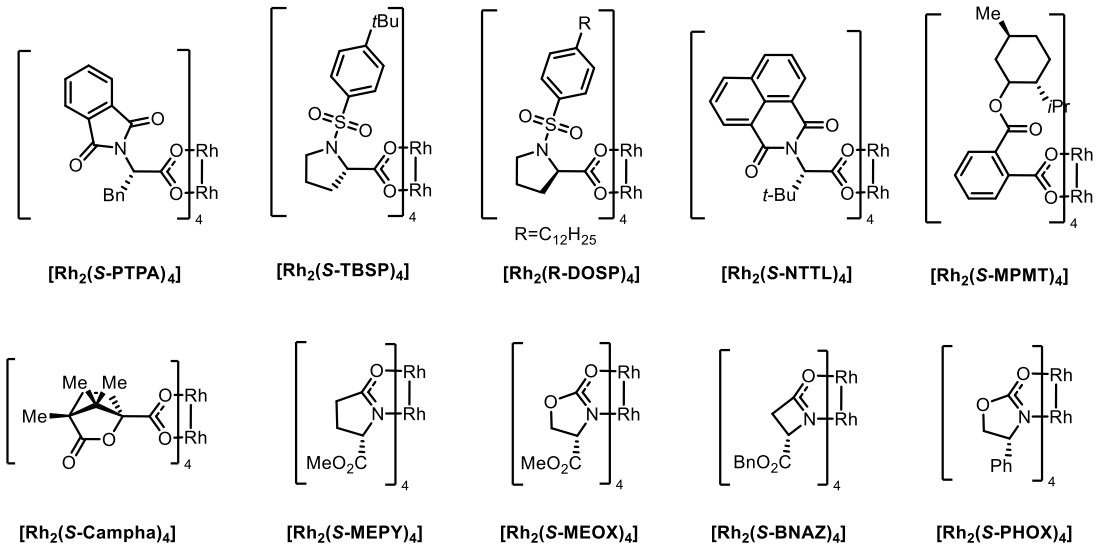

Scheme 49- Graphical overview of the chiral dirhodium complexes used in the screening of cyclopropanation reaction with ethyl 3,3,3-trifluoro-2-diazopropionate and styrene, described by Muller. [100]

In an initial attempt, the trifluoromethylated diazo ester **55** was subjected to cyclopropanation using complex ***P*-134** under the conditions reported by Muller and coworkers.[100] To our delight, cyclopropane **172** was formed in 79% combined yield, displaying a diastereomeric ratio of 4:1 in favor of the *trans*-isomer with 75% *ee* (Scheme 50). The relative configuration of cyclopropane **172** was determined by NMR, using a $^{1}H–^{19}F$ HOESY experiment (Figure 40). The initial result clearly showed the potential of prototype complex ***P*-134** as the enantiomeric excess of the *trans*-isomer was notably higher than best result obtained with $[Rh_2((S)\text{-DOSP})_4]$ or $[Rh_2((S)\text{-BNAZ})_4]$ (Table 10, entries 3 and 9).

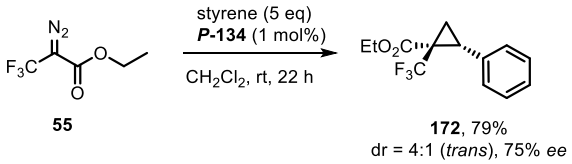

Scheme 50-Initial attempt of the cyclopropanation reaction of trifluoromethylated diazo ester **55** catalyzed by ***P*-134**. The yield refers to the combined yield of both *trans*/*cis* isomers.

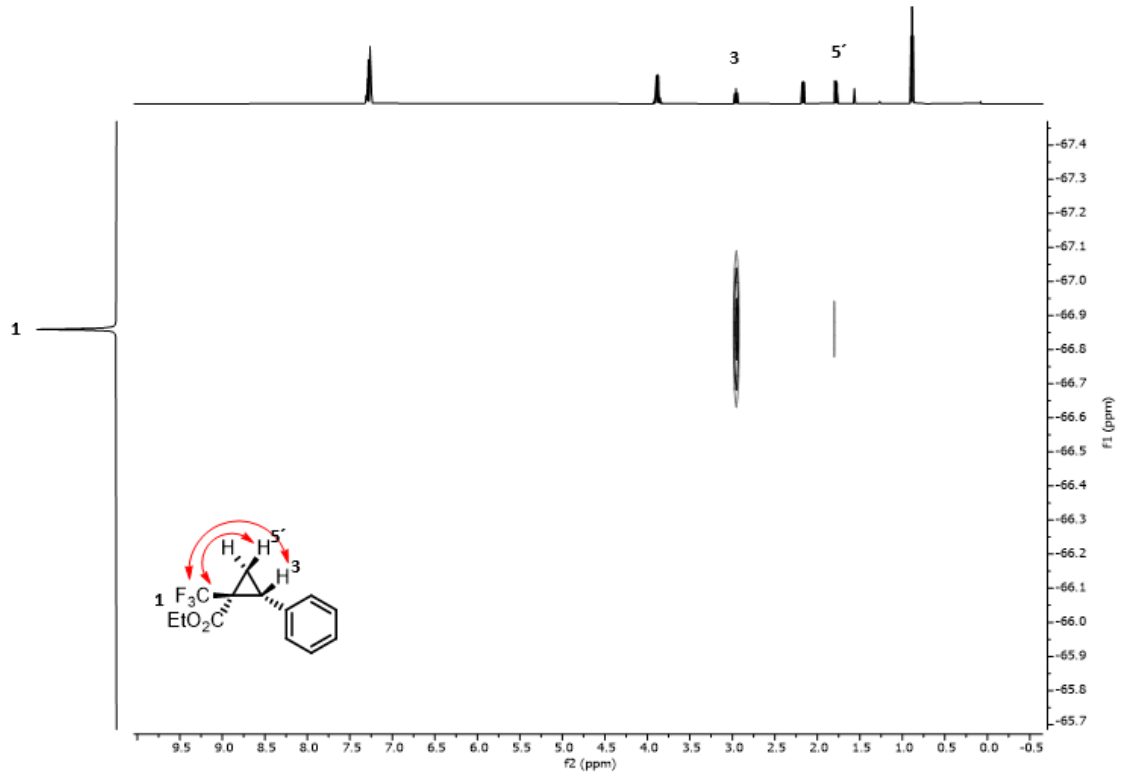

Figure 40-^{1}H–^{19}F HOESY spectrum of cyclopropane **172**, ascribing the *trans*-configuration of the cyclopropane.

Replacing the ethyl ester of diazo compound **55** by a more sterically congested ester was hypothesized to potentially increase the enantiodiscrimination in the cyclopropanation reaction as observed in the cyclopropanation of aryl diazo esters (*vide supra*), thus resulting in higher *ee*. However, synthesizing such diazo compounds proved to be extremely challenging (Scheme 51). Initial attempts to obtain trichloroethyl diazoester **175** by Regitz diazo transfer of **176** failed (**A**), as it led to decomposition of the starting material. Attempts to synthesize the trifluoromethyl pyruvate esters **177-178** (**B**), which would serve as the precursor for the diazo synthesis in the same way as the diazo ethyl ester **55** is made, failed as well. A more exotic approach (**C**) was attempted by synthesizing 2,2,2-trifluorodiazoethane (**179**), followed by treatment with trichloroethyl chloroformiate in the presence of a mild base, which led to a complex mixture of products. As an alternative, hydrated diisopropyl ketoester **183** was successfully synthesized from **182** by treatment with Ruppert´s reagent in the presence of catalytic amounts of cesium fluoride.[149] With the hydrate of **183** at hand, the corresponding diazo compound was synthesized in similar way to how diazo ethyl ester **184** is prepared.[150]

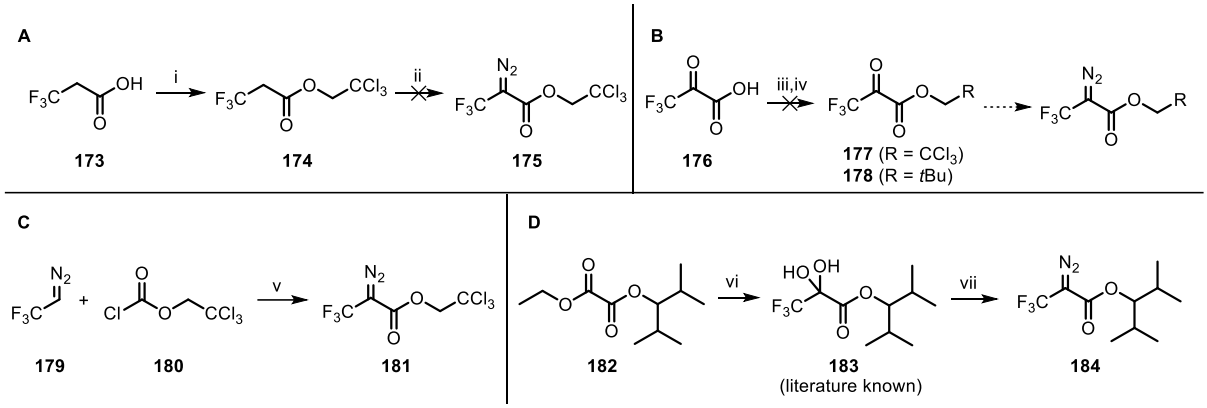

Scheme 51-Synthetic approaches towards more sterically congested trifluoromethylated diazo esters. Reaction conditions: i) trichloroethanol (1.2 eq), EDC (1.15 eq), DMAP (15 mol%), CH_2Cl_2, 16 h, 79% yield. ii) *p*-ABSA (1.25 eq), DBU (1.35 eq), MeCN, rt, 18 h. iii) neopentylalcohol or trichloroethanol (1.2 eq), DCC (1.5 eq), DMAP (15 mol%), CH_2Cl_2/DMF, rt, 18 h. iv) neopentylalcohol (1 eq), H_2SO_4 (5 mol%), Dean-Stark, toluene, reflux, 24 h. v) **179** (1.1 eq), pyridine (1.1 eq), 0°C, 30 min. vi) $TMSCF_3$ (1 eq), CsF (10 mol%), rt, 24 h. vii) $TsNHNH_2$ (1.2 eq), CH_2Cl_2 then POCl3 (1.2 eq), Pyridine, rt, 24 h, then Et_3N (1.2 eq), reflux 2 h.

Although not fully pure, **184** was subjected to a cyclopropanation reaction. The resulting product exhibited a substantially reduced enantiomeric excess (55% *ee*) compared to cyclopropane **172** (Scheme 52), suggesting that increasing the steric bulk of the ester moiety may not be a viable strategy for enhancing enantioselectivity.

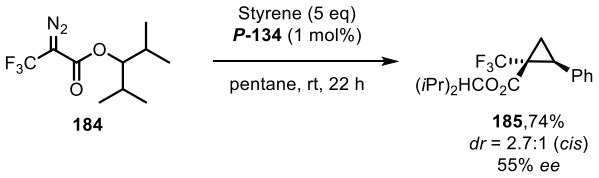

Scheme 52- Cyclopropanation of sterically congested trifluoromethyl diazoester **184** catalyzed by ***P*-134**.

Therefore, attention was turned to further optimize the cyclopropanation reaction with diazo ethyl ester **55**, as this diazo compound is well studied and can be easily synthesized from commercially available trifluoromethyl pyruvate ethyl ester (Table 11).

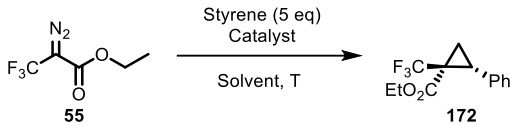

#	Catalyst	Mol% cat	Solvent	T [°C]	Yield % [^{1}H NMR]	*trans*:*cis*	*ee* [%]
1	***P*-134**	1.0	CH_2Cl_2	rt	79 [86]	4:1	75
2	***P*-134**	1.0	CH_2Cl_2	–20	[66]	6:1	78
3	***P*-134**	1.0	TFT	rt	60[69]	4.5:1	78
4	***P*-134**	1.0	DCE	rt	36[56]	4:1	73
5	***P*-134**	1.0	pentane	rt	75[87]	6:1	85
6	***P*-134**	1.0	pentane	–20	77[89]	8.5:1	93
7	***P*-154**	1.0	CH_2Cl_2	rt	59 [78]	4.5:1	73
8	***P*-134**	1.0	pentane	–40	n.d.	11.5:1	95
9	***P*-134**	0.5	pentane	–40	75 [85]	11.5:1	95
10	***P*-162**	0.5	pentane/ CH_2Cl_2	–20	55 [64]	1.5:1	28

Table 11-Optimization table of the cyclopropanation of trifluoromethylated diazo ester **55**. All the reactions in the screening were performed on a 0.16 mmol scale. Yields in brackets were determined by ^{1}H NMR analysis of the crude material using 1,3,5-trimethoxybenzene as internal standard, and refer to combined yield of cis and trans isomer. All other yields are combined (*cis*- and *trans*-isomer) isolated yields.

Lowering the reaction temperature to –20 °C did not lead to a notable improvement in enantioselectivity; however, a significant decrease in yield was observed based on analysis of the crude reaction mixture (entry 2). The influence of the solvent was then examined at room temperature. Using pentane as the reaction medium led to a marked increase in both enantiomeric excess and diastereomeric ratio, reaching 85% *ee* and 6:1 dr, respectively (entry 5). In contrast, solvents such as trifluorotoluene (TFT) and dichloroethane (DCE) produced no substantial enhancement in selectivity. Further cooling of the reaction to −20 °C resulted in a pronounced increase in stereoselectivity, affording the cyclopropane product with 93% *ee* and a dr of 8.5:1 (entries 3-4). Iodo-subsituted catalyst ***P*-154** was also tested, but while it delivered comparable levels of stereoselectivity, the overall yield was notably lower (entry 7). It was tested if the stereoselectivity would further increase by lowering the reaction temperature even more to –40 °C. Pleasingly, under these conditions, the enantiomeric excess increased to 95%, accompanied by a dr of 11.5:1, favoring the *trans*-isomer. Further reduction

of the catalyst loading to 0.5 mol% was not at cost of the reactivity, as the *cis/trans*-cyclopropane mixture could be isolated in 75% combined yield (entry 9).

As a control experiment to reassess whether the hydrogen-bonding interactions provided by the acetamidate ligand are crucial to the stereoselective outcome of this reaction, the *N*-methylated acetamidate complex ***P*-162** was employed (entry 10). As anticipated, the enantiomeric excess dropped to 28% and the diastereomeric ratio to 1.5:1, marginally favoring the *trans*-isomer. This result clearly highlights the detrimental effect of removing the hydrogen-bonding capability of the acetamidate ligand.

With the optimized conditions at hand, the scope of the cyclopropanation reaction of trifluoromethylated diazo ester **55** with a variety of olefins was explored (Scheme 53). The cyclopropanation of styrene was repeated, affording 63% of pure *trans*-isolated product with a dr of 12:1 and 95% *ee*. From cyclopropanes **186** and **188**, it was observed that using a more electron rich styrene resulted in a slight decrease in stereoselectivity. The transformation also tolerated both *ortho*- and *meta*-substituents, as demonstrated by **187** and **189**, respectively. Even more sterically congested styrenes were well tolerated without any loss of stereoselectivity or reactivity (**194**). The best diastereomeric ratio was obtained when employing indene as the corresponding olefin, resulting in **191** with a dr of 50:1 and 97% *ee*. The scope could be further expanded to the usage of dienes as manifested by the respectable levels of stereoselectivity obtained for **192** and **193**. Additionally, vinyl ethers could be employed, resulting in cyclopropane **190** in dr of 5:1 and 92% *ee*. In contrast, when dimethylphenylallylsilane was used, only moderate levels of stereoinduction were observed, affording product **195** with a dr of 2:1 and 68% *ee*. Also, these reactions could be easily scaled to gram scale in which the catalyst loading could be reduced to 0.1 mol%, as demonstrated by cyclopropane **172** which was prepared in >1 g without any noticeable loss of yield nor stereoselectivity (Scheme 53).

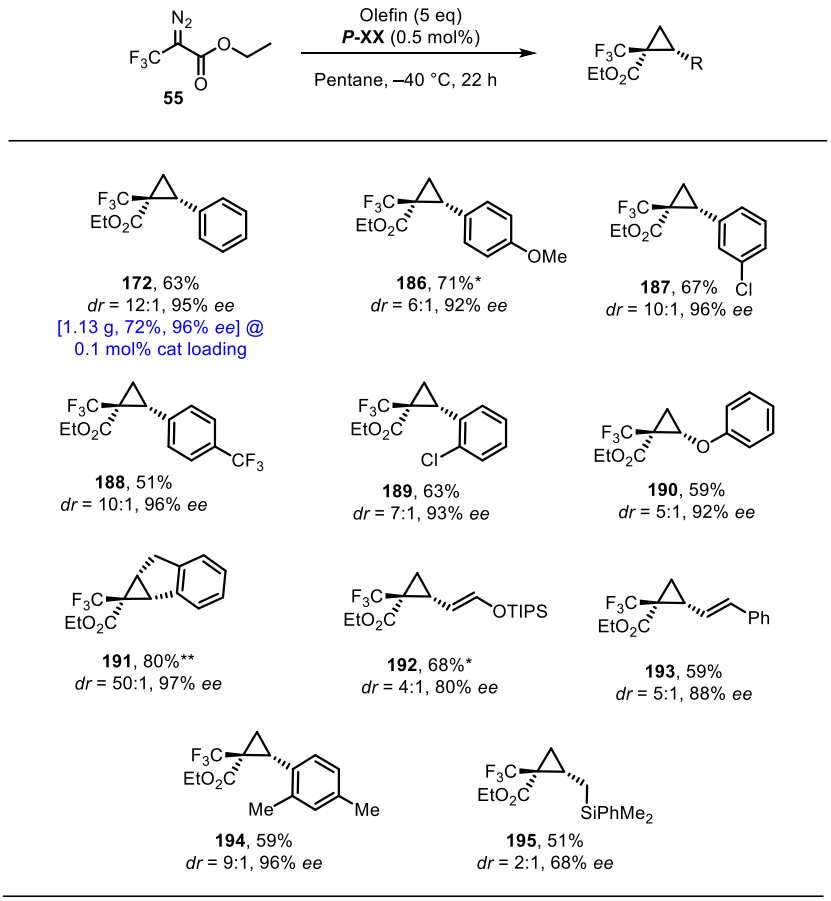

Scheme 53-Scope of the cyclopropanation reaction of trifluoromethyl diazo ester **55** catalyzed by ***P*-134** set up on 0.2 mmol scale. Unless stated otherwise, the yields refer to pure *trans*-isomer after flash chromatography, the dr to the crude product (NMR). The compounds indicated with an asterisk (*) are isolated as a mixture of *cis*- and *trans*-isomers. Compound indicated with ** needed to be purified via preparative achiral HPLC to obtain an analytically pure sample.

Despite these promising results, the methodology exhibits notable limitations. Only olefinic substrates that were sufficiently soluble in pentane at low temperatures could be employed. With the exception of indene, attempts to improve solubility by adding toluene did not lead to complete conversion of the diazo compound. As a result, substrates such as *N*-vinylphthalimide, 2-vinylthiophene, and 2-vinylnaphthalene showed poor reactivity, with negligible levels of product formation. Also, *p*-methoxyphenyl acetylene failed to react, even at 0 °C. Additionally, the presence of a chromophore in the resulting cyclopropane was essential for product isolation at the scale used to ensure visibility of the product containing fractions on TLC during chromatographic separation. Although usage of allyltrimethylsilane and *tert*-butyl vinyl ether led to full consumption of diazo compound **55**, the corresponding cyclopropane products could not be isolated, due to challenges in purification and detection.

Since all cyclopropane products (**172** and **186-195)** were obtained as oils, the absolute configuration of cyclopropane **172** was determined by circular dichroism spectroscopy (Figure 41). Comparison of the experimentally measured CD spectrum with the simulated spectra generated by DFT calculations allowed unambiguous assignment of the cyclopropane as the 1*S*,2*R*-enantiomer.

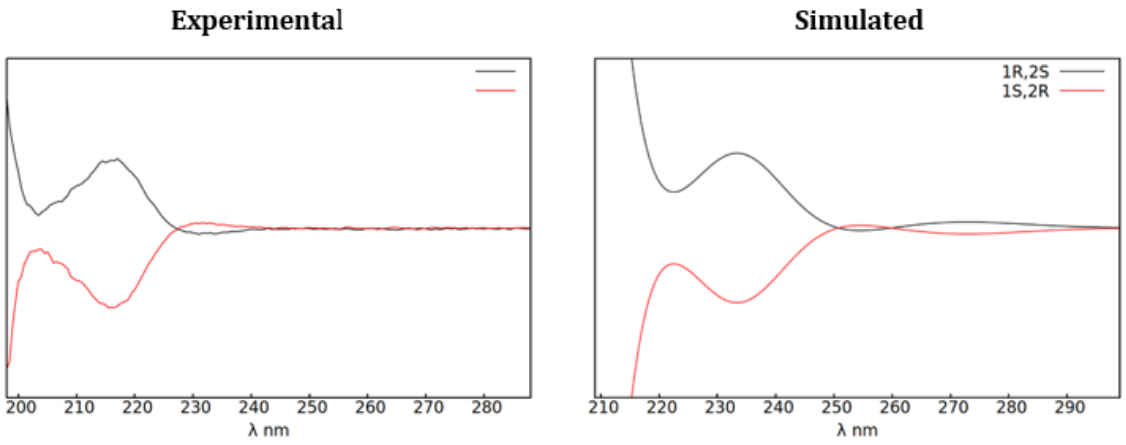

Figure 41-Left: Experimental circular dichroism spectra of the two possible enantiomers of cyclopropane **172**, obtained with ***P*-134** (orange) and ***M*-134** (black). Right: Simulated CD spectra of the enantiomers, computed at the ωB97X/def2-TZVP(-f) + RIJCOSX + CPCM(heptane) level of theory with incorporated shift calibration.

Further confirmation was obtained by deprotecting the ester moiety of cyclopropane **172** to yield the corresponding carboxylic acid **196** with complete stereoretention (Scheme 54)**.** The optical rotation value of **196** matched that of the identical molecule that was obtained by oxidative cleavage of furan **71** described in chapter 2. The absolute configuration was assigned in analogy to the *p*-tolyl analogue **93**.

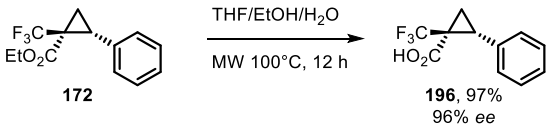

Scheme 54-Stereoretentive deprotection of cyclopropane ester **172** to carboxylic acid **196.**

Computations

To better understand the origin of the observed selectivity, and in particular why the *trans*-isomer is formed in this case as opposed to the *cis*-selectivity observed with catalyst ***P*-134** in the cyclopropanation of stannylated diazo esters, DFT calculations were carried out. Interestingly, the most stable carbene intermediate adopts a geometry similar to that found in the stannylated system, where the trifluoromethyl group is oriented toward the calix[4]arene unit. In this case, however, the intermediate is stabilized not only by the expected hydrogen bonding between the carbonyl group of the carbene and the acetamidate ligand, but also by additional fluorine–bromine interactions (Figure 42). This is showcased by the three most stable conformers of the carbene intermediate, which were found computationally: The most stable conformer **A** engages in both hydrogen bonding and fluorine-bromine interactions. In contrast, conformers **B** and **C** exhibit either hydrogen bonding or fluorine-bromine interactions alone.

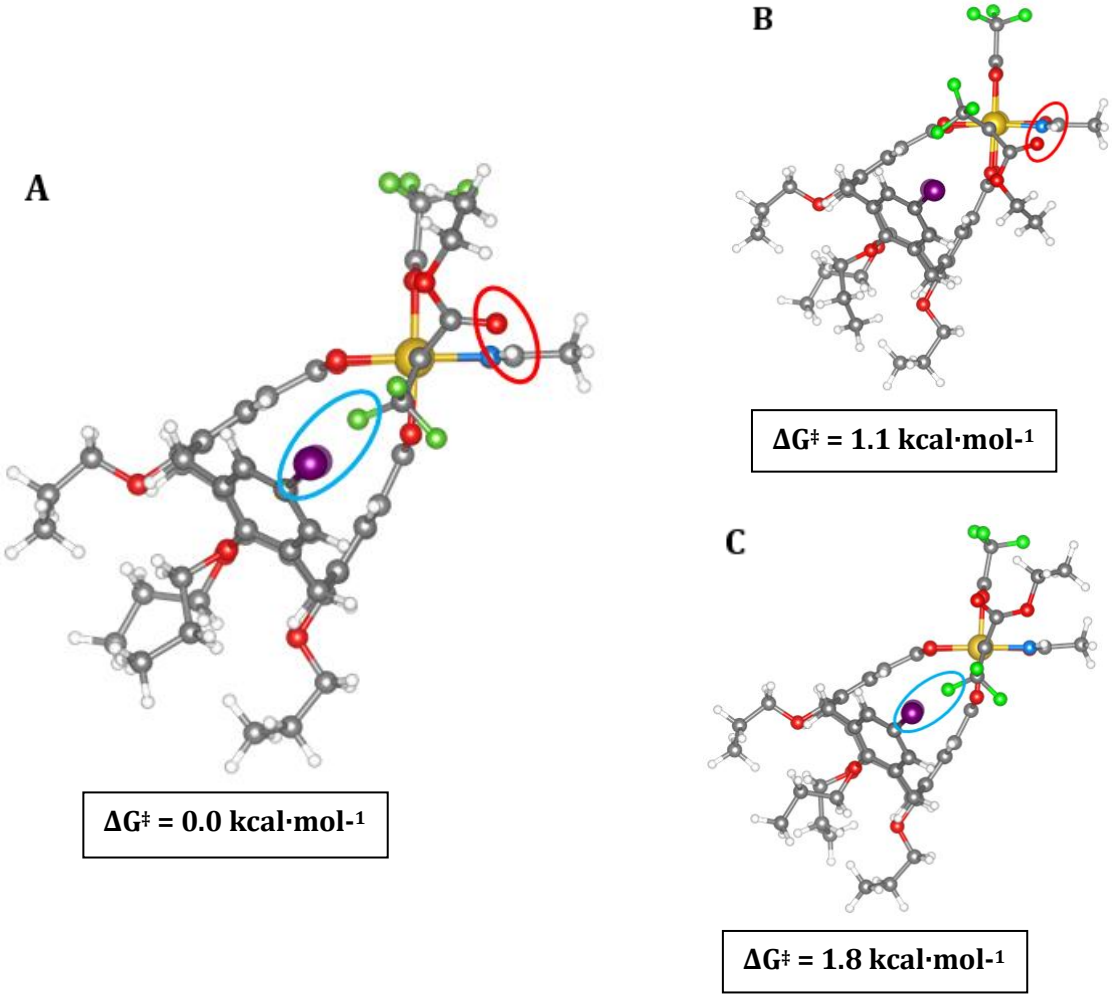

Figure 42- Three most stable conformers of the carbene intermediate. Each conformer is reported with the corresponding free energy relative to the most stable conformer **A**. Initial conformational sampling was performed with GOAT and CREST calculations. The geometries were further refined at the B3LYP-D3BJ/def2-SVP+RIJCOSX+CPCM(pentane) level of theory.

To investigate the nature of the fluorine-bromine interactions, a simplified model system was constructed using phenylbromide and trifluoroethane, with their geometries fixed to mimic the spatial arrangement found in carbene intermediate **A**. Single-point electronic energy calculations were performed for the dimeric assembly, consisting of both components, as well as for each individual molecule (B3LYP-D3BJ/def2-TZVP+RIJCOSX+CPCM(pentane) level of theory). The heterodimer was found to be 0.81 kcal·mol^{-1} lower in energy compared to the sum of the isolated species, suggesting a stabilizing interaction. In contrast, when the same calculations were performed without accounting for dispersive forces, the energy ordering was reversed, and the heterodimer was 1.53 kcal·mol^{-1} higher in energy than the separated molecules. This clearly shows that the dimeric system is stabilized by dispersive interactions rather than electrostatic interactions, hence these observations can be extrapolated to the carbenic system. Additionally, the electrostatic interactions by fluorine-bromine interactions via the σ-hole of the bromine atom were ruled out. The computed electrostatic potential map of the dimeric model revealed that the more electron dense regions of the fluorine atoms are not oriented towards the σ-hole of the bromine atom, which further reinforces the conclusion that the observed stabilization arises primarily from dispersive interactions (Figure 43).

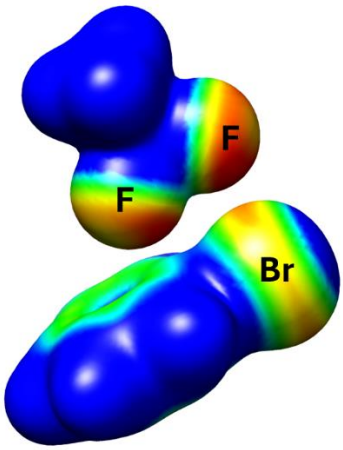

Figure 43-Electrostatic potential map of a dimeric model existing of phenylbromide and trifluoroethane, displayed at an isosurface value of 0.008. The color scale ranges from −0.02 (red, electron-rich regions) to +0.02 (blue, electron-deficient regions).

Interestingly, attempts to locate the transition state for styrene addition to the carbene via the most accessible quadrant A revealed that formation of the 1*S*,2*R*-cyclopropane proceeds without requiring any rearrangement of the carbene intermediate. In contrast, nucleophilic attack from either quadrant B or D would disrupt the hydrogen bond between the amidate ligand and the carbonyl group of the carbene, resulting in destabilization. Approach via quadrant C is also disfavored due to significant steric hindrance imposed by both the

calix[4]arene framework and the carbene itself. Moreover, this trajectory would interfere with the stabilizing dispersive interactions between the fluorine and bromine atoms.

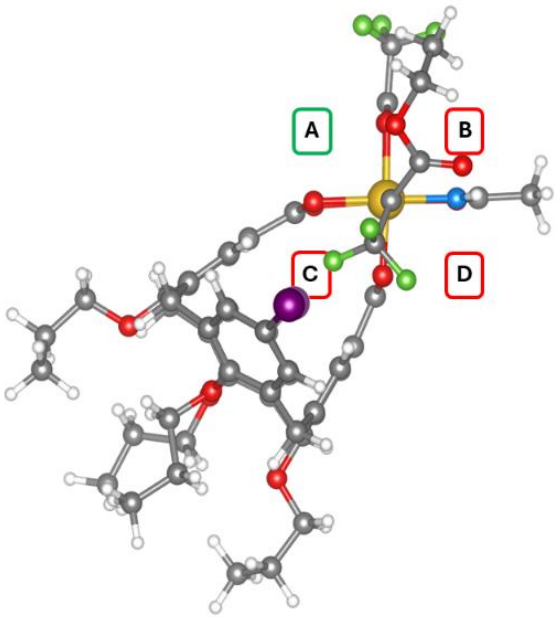

Figure 44- Representation of the most stable carbene intermediate. The four quadrants leading to the four possible stereoisomers are labeled (A-D).

To further examine the proposed barrierless pathway via quadrant A, a potential energy surface was generated through relaxed surface scans (Figure 45). The results revealed a continuous decrease in energy as the distance between styrene and the carbene center decreased from an initial separation of 5.53 Å to the final C–C bond length of 1.51 Å, thus confirming that the approach of styrene in this quadrant proceeds without an energetic barrier.

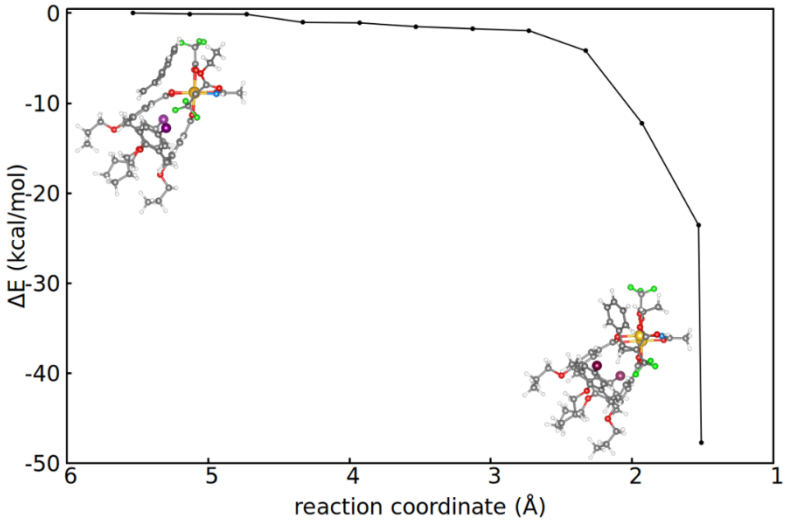

Figure 45-Potential energy surface leading to the 1*S*,2*R*-configured cyclopropane obtained through relaxed surface scans (attack from quadrant A). Electronic energies are reported as relative to the first point of the PES. The relaxed surface scans were performed at the B3LYP-D3BJ/def2-SVP-RIJCOSX-CPCM(pentane), followed by single-point energy refinement using the def2-TZVP level.

The increased reactivity of the trifluoromethylated carbene compared to its stannylated analogue can be understood on intuitive grounds. The trifluoromethyl group exerts a strong inductive electron-withdrawing effect, which lowers the electron density at the carbenic carbon, thereby enhancing the electrophilicity and overall reactivity of the intermediate. To support this interpretation with quantitative data, Mulliken and Löwdin population analyses were performed on the carbenic carbon atoms of both species. The results, summarized in Table 12, show a lower electron density at the carbene center in the trifluoromethylated species, confirming its more pronounced electron deficiency relative to the stannylated counterpart.

	Mulliken	Löwdin
CF_3 carbene	–0.235	0.030
$Sn(CH_3)_3$ carbene	–0.368	–0.087
Δ	0.133	0.117

Table 12-Partial charge at carbenic carbon for the trifluoromethylated carbene and stannylated carbene, calculated via Mulliken and Löwdin population analyses.

4.3. Conclusion

In this chapter, a new type of heteroleptic chiral-at-metal dirhodium paddlewheel complexes is described with inequivalent Rh-centers. Key elements in this design are the amidate ligand and the tethered carboxylate ligand bound in *cisoid* manner to the dirhodium scaffold. In total two different tethered ligands were employed, O-esp and calix[4]arene dicarboxylates, of which the prototype complex of the latter (**134**) showed great potential in the cyclopropanation reactions of the already established aryl diazo esters. Attempts to further improve the prototype catalyst by replacement of the bromo-substituents of the calix[4]arene unit by a variety of other substituents showed less success. Although an acceptable level of asymmetric induction (~70% *ee*) was achieved with ***M*-134**, it clearly does not outcompete the chiral bismuth-rhodium catalysts **45** developed in our group, which are the most selective catalysts described to date.[98]

However, employing prototype complex ***P*-134** in the cyclopropanation reaction of α-stannylated diazoester (**20**) resulted in cyclopropanes (**27, 164-171**) with remarkably high enantioselectivity and *cis*-diastereoselectivity. This obtained diastereoselectivity is complementary to the *trans*-diastereoselectivity obtained in similar transformations with **31**, previously described in our group.[81] By choice of catalyst, each stereoisomer of cyclopropane can be formed with high levels of asymmetric induction, making this an enantioselective diastereoconvergent transformation. Similar to catalyst **31**, extensive DFT studies into the mode of action of prototype complex **134** showed that a hydrogen-bonding interaction between the amidate ligand and the carbonyl moiety of the carbene is key to the success in this transformation.

Additionally, the applicability of the prototype complex ***P*-134** could be extended to the cyclopropanation of acceptor/acceptor diazo compounds, within particular to α-trifluoromethyl diazo ester (**55**), in which the corresponding cyclopropanes (**172, 186-195**) were obtained with excellent enantioselectivity and good *trans*-diastereoselectivity. To date, no other catalytic system is able to achieve such high stereoselectivity with this kind of reagent, thus the level of stereoinduction achieved with ***P*-134** is truly remarkable. DFT studies have shown that in addition to the hydrogen-bonding interactions, the catalytic system also picks up dispersive fluorine-bromine interactions between the CF_3- group of the diazo and the bromo-substituents of the calix[4]arene unit. Owing to this non-covalent interactions the 1*S*,2*R*-configured cyclopropane without any energetic barrier in the [2+1]-cycloaddition event.

5. Studies towards Chiral-at-Metal Bismuth-Rhodium Paddlewheel Complexes

5.1. Introduction and Motivation

In Chapter 4, we described the successful preparation of chiral-at-metal dirhodium complexes, which exhibit notable stereoselectivity and reactivity. Building upon this work, we sought to explore whether the concept of intrinsic backbone chirality could be extended to bismuth-rhodium complexes. If successful, this would not only represent the first example of a bismuth-rhodium complex with intrinsic chirality at the metal center but also the first documented case of a chiral-at-metal heterobimetallic complex in general. Formally, the metal centers become stereogenic when the complex contains at least three different μ_2-bridging ligands of which two identical ligands are coordinated in *cisoid* fashion to the metal backbone. This *cisoid* coordination can be achieved by tethering the ligands together. Notably, the use of carboxamidate ligands is unnecessary in this context, as the introduction of bismuth inherently disrupts the C_2-symmetric element that is typically present in dirhodium paddlewheel complexes. The creation of such complexes would provide new insights into the synthesis, stability, and reactivity of bimetallic species and could open the door to (novel) applications in catalysis.

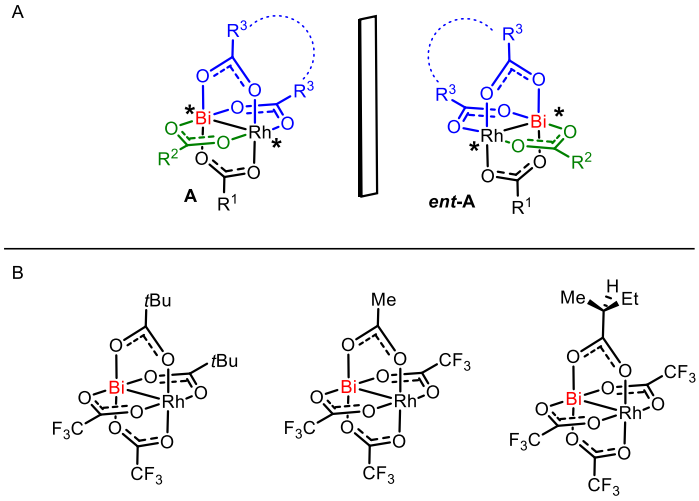

Scheme 55-A: conceptual depiction of chiral-at-metal bismuth-rhodium paddlewheel complexes. B: examples of heteroleptic BiRh(II) complexes.

One of the key aspects into the successful preparation of these complexes would be the ability to control selective ligand replacement. Unlike heteroleptic dirhodium complexes, heteroleptic bismuth-rhodium paddlewheel complexes are extremely rare, with only three known

examples reported by Dikarev and co-workers (Scheme 55, B).[151] This scarcity underscores both the synthetic challenges and the novelty associated with this class of compounds. To address these difficulties, our approach relies on mild and more selective methods — strategies that have already demonstrated their effectiveness in the synthesis of the chiral-at-metal dirhodium analogues, as discussed in Chapter 4.

5.2. Results and Discussion

Our synthetic approach began with [BiRh(OTfa)$_4$], from which two trifluoroacetate ligands were replaced by a chelating diacid coordinated in a *cisoid* fashion. It was then envisioned that selective mono-fold ligand exchange of an additional trifluoroacetate would generate racemic chiral-at-metal BiRh complexes. As with the dirhodium analogues, these racemates could potentially be separated by preparative HPLC on a chiral stationary phase. Following the strategy established for chiral-at-metal dirhodium complexes, we focused primarily on two types of chelating diacids for this purpose.

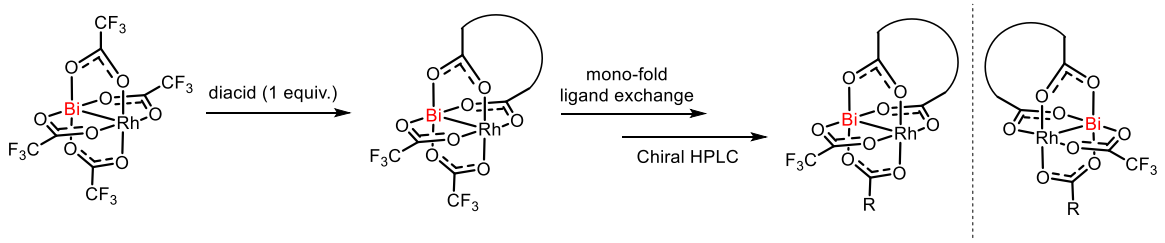

Scheme 56-Synthetic approach towards chiral-at-metal bismuth-rhodium paddlewheel complexes.

5.2.1. Studies towards Chiral-at-Metal Bismuth-Rhodium Complexes with O-Esp Derivatives

It was envisioned that the O-Esp ligand could be installed onto the BiRh-scaffold via base promoted ligand exchange. Gratifyingly, complexes **197-199** were obtained in moderate yields after a simple flash chromatographic separation. Subsequent mono-fold ligand exchange with pivalic acid led to a complex mixture of products which after HPLC separation afforded pure racemic complex **200** and **201** in 26% and 19% yield, respectively (Scheme 57). When complex **199** was subjected to the same reaction conditions, only overreacted product **202** could be isolated. Attempts to perform the mono-fold ligand exchange with other carboxylic acids only led to traces of the desired product as observed via HPLC-MS analysis.

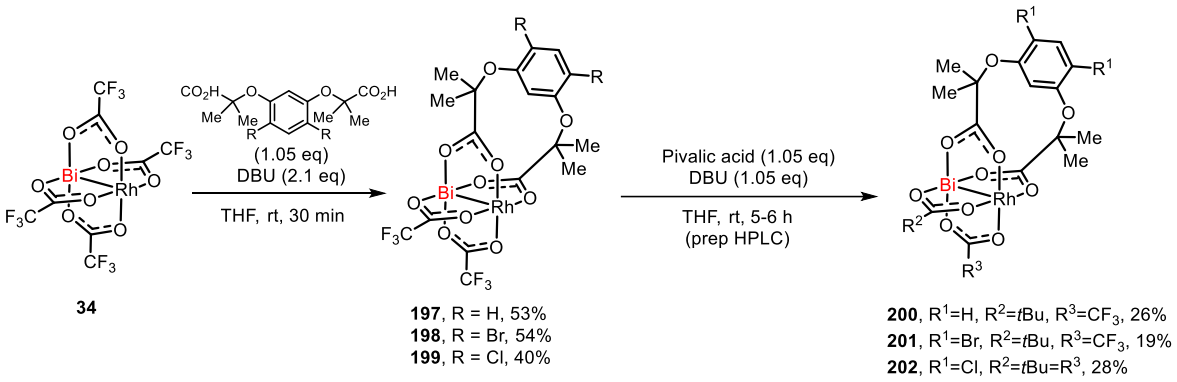

34

197, R = H, 53%
198, R = Br, 54%
199, R = Cl, 40%

200, R^1=H, R^2=*t*Bu, R^3=CF_3, 26%
201, R^1=Br, R^2=*t*Bu, R^3=CF_3, 19%
202, R^1=Cl, R^2=*t*Bu=R^3, 28%

Scheme 57-Preparation of racemic chiral-at-metal BiRh-complexes bearing an O-Esp ligand.

After a thorough HPLC screening on a variety of chiral stationary phases, enantiomeric separation was achieved exclusively for complex **200** (Figure 46A), while no suitable conditions were identified for complex **201**. With the optimized separation conditions at hand, a preparative separation was attempted (Figure 46B). However, upon concentration of the separated enantiopure samples, spectroscopic analysis showed significant decomposition of the isolated enantiomers. This observation indicated that the enantiomers of complex **200** were not sufficiently stable in the mobile phase employed for the separation. To further investigate this hypothesis, one of the enantiomers was reanalyzed after several hours upon standing in solution, confirming significant degradation over time. Attempts to mitigate decomposition — presumably induced by the alcoholic solvent — through the addition of co-solvents such as water or methyl *tert*-butyl ether were unsuccessful.

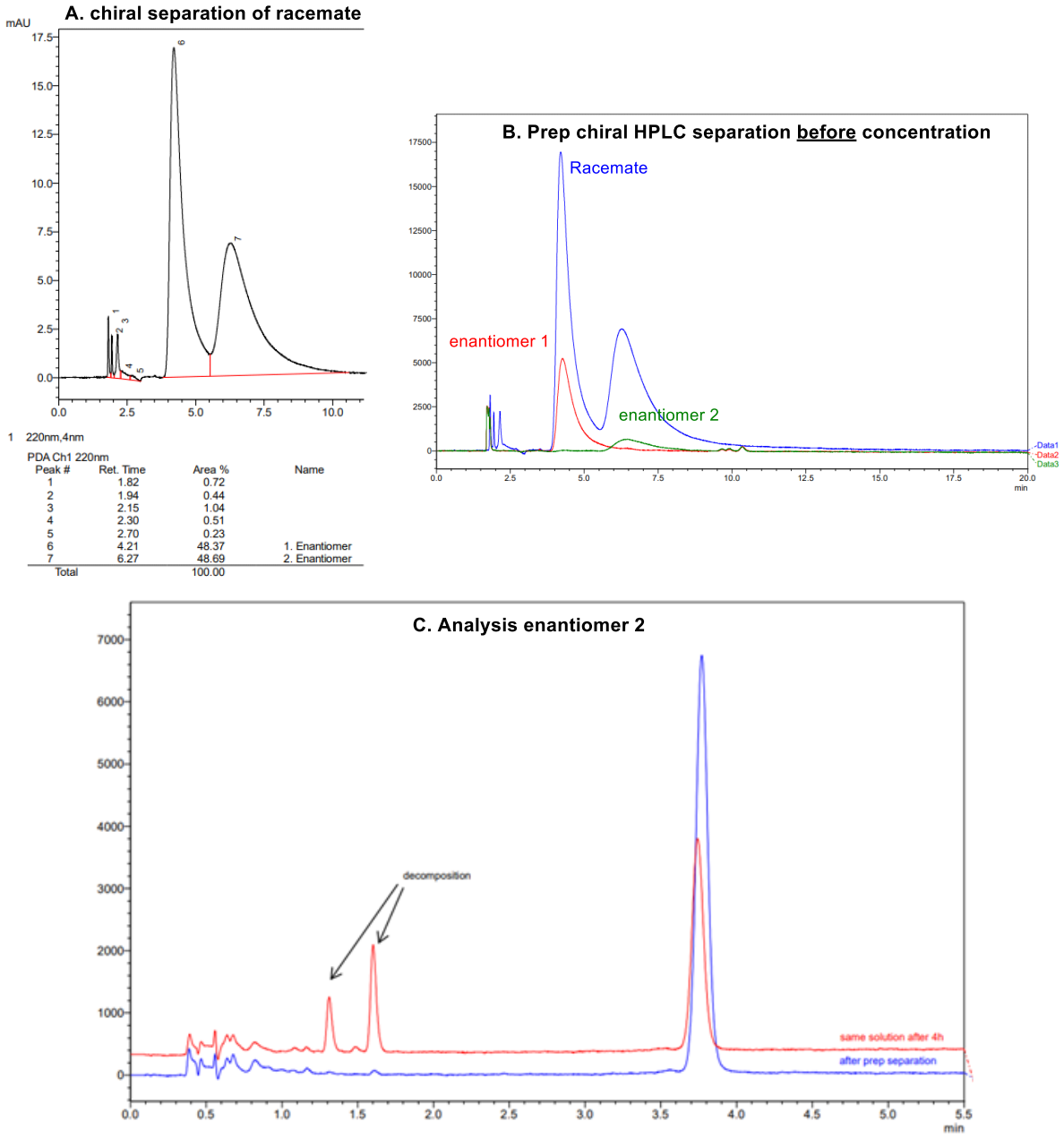

Figure 46-A: HPLC chromatogram of racemic complex **200** on a chiral stationary phase (Chiralpak IG-3 column). B: comparison of the racemate with the separated enantiomers after preparatory HPLC, before concentration of the sample to dryness. C: comparison of the analysis of enantiomer 2 of **200**, directly after the preparatory HPLC separation (blue) and after 4h in solution (red).

5.2.2. Studies towards Chiral-at-Metal Bismuth-Rhodium Complexes with Calix[4]arene Derivatives

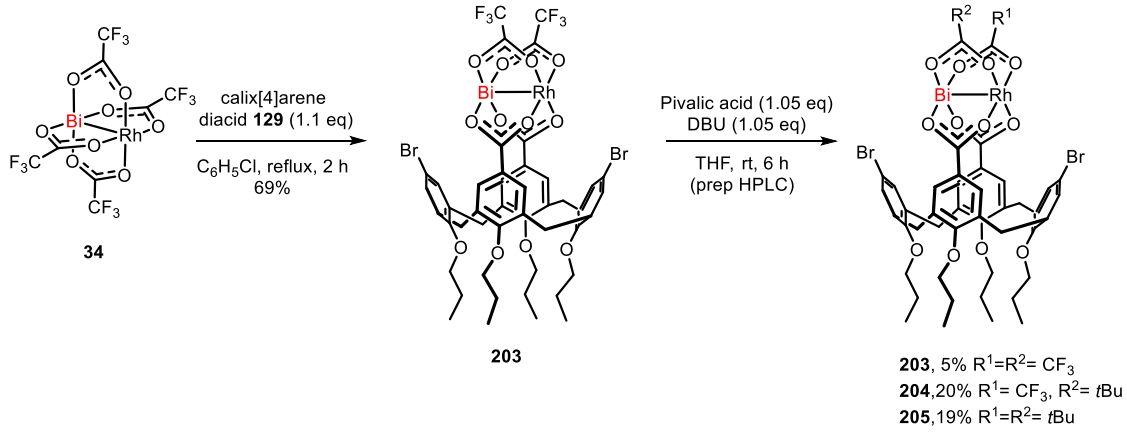

Scheme 58-Preparation of racemic chiral-at-metal BiRh-complex **204** bearing a calix[4]arene ligand.

Complex **203** was prepared from [BiRh(OTfa)$_4$] by thermal ligand exchange with calix[4]arene diacid **129** in a gratifying 69% yield (Scheme 58). Mono-fold ligand exchange with pivalic acid resulted in a complex mixture of products as observed by HPLC analysis. After preparative HPLC separation and isolation of the main species present in the mixture, the starting material **203**, the desired complex **204** and the overreacted product **205** were obtained in 5%, 20% and 19% yield, respectively. So far, no attempts were made to test the separation on a chiral stationary phase of the corresponding enantiomers.

5.3. Conclusion

Even though chiral-at-metal dirhodium paddlewheel complexes showed promising results in catalysis as discussed in Chapter 4, initial attempts towards enantiopure bismuth-rhodium analogues with intrinsic backbone chirality were not successful. In this chapter, it is shown that two distinct chelating acids could be coupled to the [BiRh(OTfa)$_4$] precursor resulting in complexes **197-199** and **204** in moderate to good yields. Subsequent mono-fold ligand exchange with pivalic acid resulted in the desired chiral-at-metal complex in racemic form, albeit in rather poor yields (**200** and **201**). Attempts to resolve the enantiomers via HPLC using a chiral stationary phase were unsuccessful. This failure was attributed either to the unavailability of suitable separation conditions or to the decomposition of the individual enantiomers during isolation. These observations suggest that the bismuth-rhodium complexes possess significantly lower stability compared to their dirhodium counterparts. It remains to be seen if separation conditions can be found for complex **204**, and if so, if the enantiomers pertain a higher stability upon concentration of the samples after preparative HPLC.

6. ^{103}Rh NMR Studies of Axially Ligated Phosphines/ Carbenes to Rh(II) Complexes

6.1. Introduction and Motivation

^{103}Rh NMR spectroscopy is a technique featuring exceptional responsiveness to the chemical environment of a given rhodium complex. It allows for the detection of small changes in the electronic and geometric coordination environment, with a shift range spanning over 12.000 ppm.[152-154] Thus, this technique is an excellent tool to gain insights in the electronic nature of rhodium complexes. The main drawback though is the low gyromagnetic ratio in combination with disproportionally long relaxation times.[155] The relative sensitivity of ^{103}Rh compared to ^{1}H is only $3.1 \cdot 10^{-5}$, thus making the acquisition of such shifts challenging. Until recently, 2D inverse detection techniques based on polarization transfer, predominantly HMQC (Heteronuclear Multiple Quantum Correlation) experiments were the best way to overcome this significant challenge. However, the applicability of such methods is limited to rhodium complexes in which a sensitive nucleus (^{1}H, ^{31}P) is directly coupled to the Rh-center, therefore excluding Rh(II) paddlewheel complexes as they do not fulfill these requirements.[154-156]

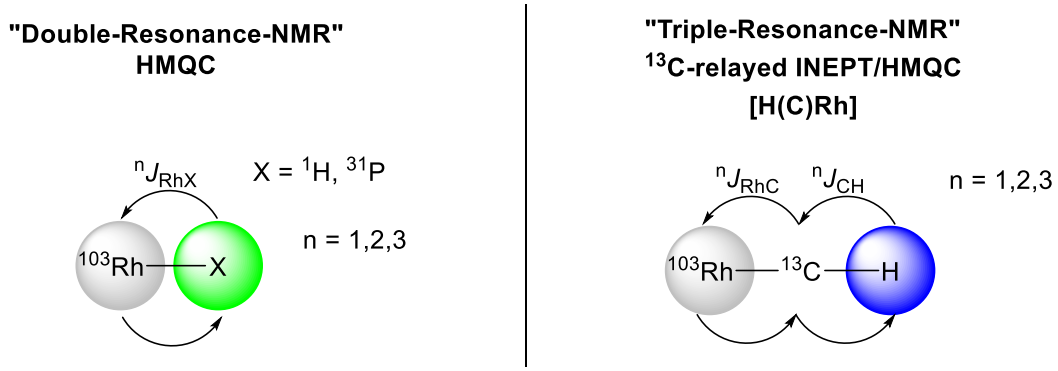

Figure 47-Established indirect detection methods for the determination of ^{103}Rh chemical shifts of rhodium complexes.[157]

However, a triple resonance experiment recently developed by Fürstner, Leutzsch and co-workers[157] overcomes such limitations enabling the rapid detection of the ^{103}Rh chemical shifts of a wide variety of rhodium complexes including dirhodium tetracarboxylate/tetracarboxamidate complexes. In this experiment, initial magnetization transfer from ^{1}H to ^{13}C by INEPT (Intensive Nuclei Enhancement by Polarization Transfer) is used, followed by a HMQC transfer from ^{13}C to ^{103}Rh. After chemical shift evolution at the ^{103}Rh nucleus, the magnetization is subsequently transferred back to ^{13}C and then to ^{1}H.[157] Particularly, the influences of different equatorial ligands of Rh(II) complexes on the ^{103}Rh

chemical shifts were investigated (Figure 48). One of the most remarkable observations is that incorporation of one acetamidate ligand on the dirhodium scaffold (**101**) induces a 1000 ppm shift difference between the two Rh-centers, thus showing how relatively subtle changes in the ligand environment can a have drastic impact on the ^{103}Rh chemical shifts.[114, 157]

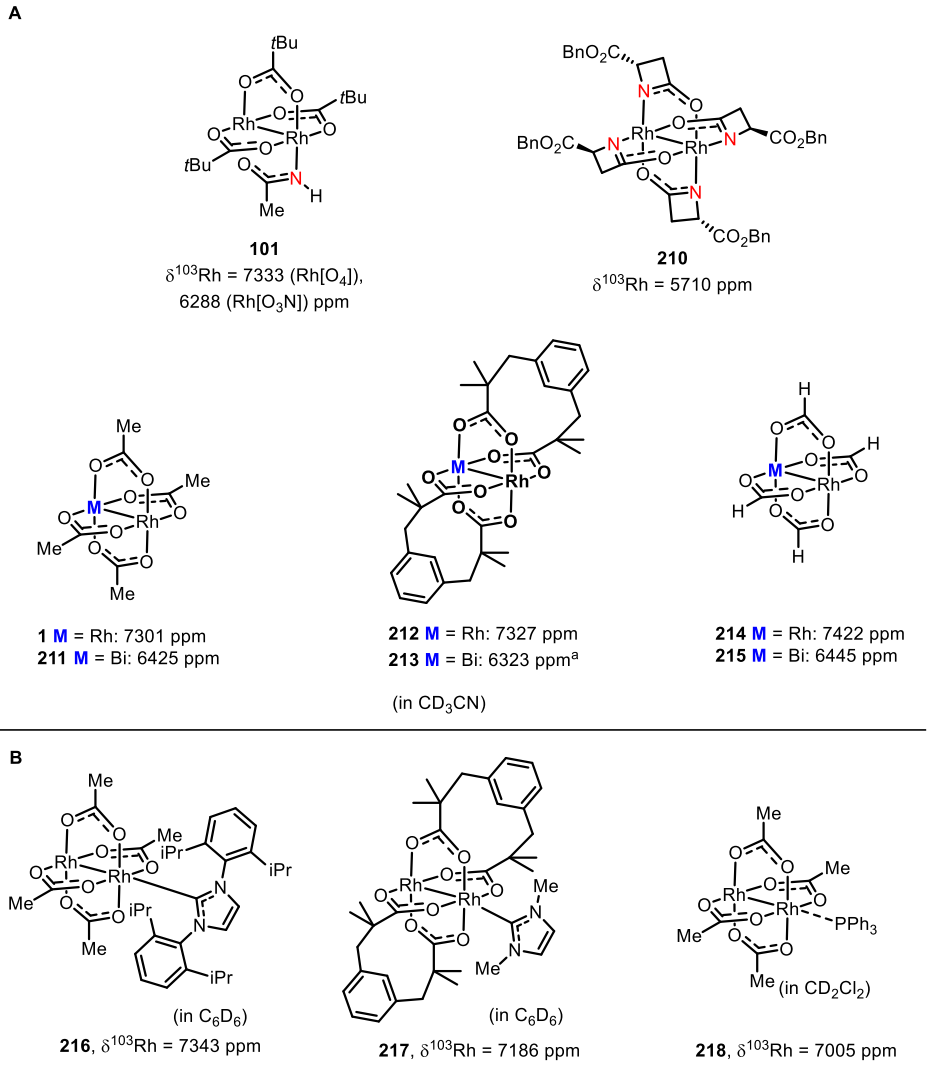

Figure 48-A. Examples of ^{103}Rh chemical shifts of a variety of dirhodium paddlewheel complexes derived by ^{103}Rh triple resonance experiments. B. Examples of ^{103}Rh chemical shift of axially ligated phosphine or NHC adducts.

In parallel, some initial efforts were made to assess the impact of axial coordination on the ^{103}Rh chemical shift in Rh(II) complexes, with particular focus on adducts involving phosphines and *N*-heterocyclic carbenes (NHCs).[113] These adducts have proven to be effective in catalysis, particularly in facilitating 1,2-additions of aryl boronic acids to aldehydes — enabling certain reactivities which cannot be achieved with the bare dirhodium complex alone.[158-166] However, when applying the triple-resonance experiment to these adducts, only a single ^{103}Rh chemical shift was observed, most likely corresponding to the distal metal center that is not bound to the axial ligand. To get a better understanding on how axial ligation changes the overall

electronic nature of the complex and, therefore, also the intrinsic reactivity that comes along with it, it was deemed quintessential to seek options to derive both ^{103}Rh chemical shifts. Additionally, it would be highly interesting to extend the ^{103}Rh NMR measurements to actual reactive carbene intermediates, as it would provide more insight in the electronic nature of such intermediates that are highly relevant in asymmetric catalysis.

6.2. Results and Discussion

The ^{103}Rh NMR measurements described in this chapter were carried out by Dr. Markus Leutzsch.

6.2.1. ^{103}Rh NMR studies of Phosphine/NHC adducts with [Rh$_2$(OAc)$_4$]

NHC adducts of Rh(II) complexes exhibit great stability at ambient conditions, thus making the isolation of such carbene species possible. As the preliminary ^{103}Rh NMR spectroscopic studies of such intermediates (**216-218**) employing the triple resonance sequence only resulted in the observation of one ^{103}Rh signal, it was attempted to see whether lower temperature [H(C)Rh]-measurements would resolve the second Rh signal. Therefore, carbene adducts **219** and **220** were prepared for which a ^{103}Rh chemical shift of 7285 and 7213 ppm were measured, respectively. Changing the per-deuterated solvent from C_6D_6 to [D_8]-toluene allowed to cool the sample to –40 °C, but did not result in the observation of the second Rh signal.

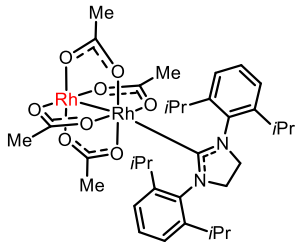

219, δ^{103}Rh = 7285 ppm

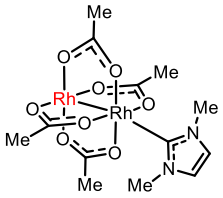

220, δ^{103}Rh = 7213 ppm

Scheme 59-^{103}Rh chemical shifts of dirhodium(II)-NHC complexes **219** and **220** measured in C_6D_6 (298 K, Ξ(^{103}Rh = 3,16 %).

Since triple resonance experiments were not successful in the observation of the second rhodium signal for NHC-adducts **219** and **220**, attention was turned to phosphine adducts. Two phosphine adducts **218** and **221** were prepared. Using a 2D heteronuclear sequence based on the polarization transfer directly from ^{31}P to ^{103}Rh, it was envisioned to increase the chance of acquiring both ^{103}Rh resonances. A costum-made QUAD Systems HPX triple-resonance probe, equipped a ^{31}P and a low-γ X-Channel, was used to perform these experiments. Gratifyingly, both ^{103}Rh chemical shifts were obtained with a ^{103}Rh—^{31}P{^{1}H} HMBC experiment for both adducts (**218, 221**) (Scheme 49A). The chemical shifts could be

assigned by selective ^{103}Rh decoupling in the ^{31}P-NMR of the two resonances (Figure 49B). The larger $J_{^{103}Rh-^{31}P}$ coupling constant (e.g. 95 Hz for **218**) is generally observed for the phosphorus atom directly bound to rhodium, whereas the distal one exhibits a significantly smaller coupling (e.g. 31 Hz for **218**). Furthermore, the obtained ^{103}Rh chemical shift for **218** (δ^{103}Rh = 7001 ppm) of the distal Rh-center via this measurement is in good agreement with the value obtained via triple resonance experiment (*vide supra*, δ^{103}Rh = 7005 ppm). As expected the axially ligated adducts (**218, 221**) result in ^{103}Rh chemical shifts that appear at lower resonances than [$Rh_2(OAc)_4$] (*vide supra*, δ^{103}Rh = 7301 ppm in CD_3CN). Comparison of the obtained data for adducts **218** and **221** shows that in both cases the distal rhodium-center is more deshielded with respect to the adduct-bound Rh center. Additionally, both ^{103}Rh atoms of adduct **221** are more shielded by ca. 150 ppm compared to the triphenylphosphine-adduct, likely because the dimethylphenylphosphine ligand is a stronger electron donating ligand.

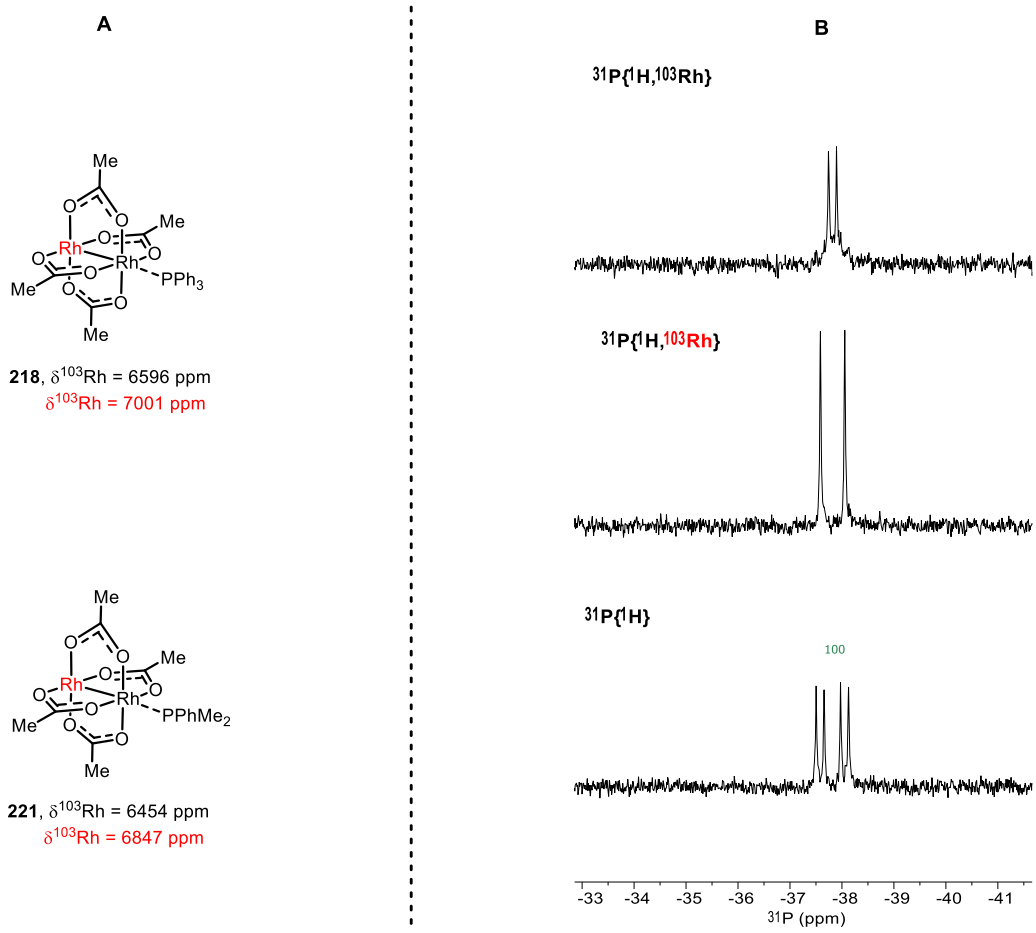

Figure 49-A) ^{103}Rh chemical shifts of dirhodium(II)-NHC complexes **218** and **221** (in CD_2Cl_2) acquired by ^{103}Rh-^{31}P{^{1}H} HMBC optimized to different optimal J_{RhP} values for the magnetization transfer (**221**: 30Hz & 102Hz, **218**: 30Hz & 92Hz). B) Selective ^{103}Rh decoupling in the ^{31}P-NMR of the two resonances of **218**.

6.2.2. ^{103}Rh NMR studies of Phosphine/NHC adducts with [Rh$_2$(formate)$_4$]

Building on the successful use of double resonance NMR spectroscopy to acquire both ^{103}Rh resonances via HMBC experiments, it was deemed valuable to develop a more general approach applicable to both phosphine and NHC adducts. Replacing [Rh$_2$(OAc)$_4$] with [Rh$_2$(formate)$_4$] enables a double resonance NMR measurement that exploits polarization transfer directly from the H-atom of the equatorial ligand coordinated to the dirhodium core, rather than via the axially ligated adduct itself, which would extend its applicability. Similarly to **220**, adduct **222** was prepared from [Rh$_2$(formate)$_4$] and subsequently measured with success via a ^{1}H–^{103}Rh-HMBC experiment to afford both ^{103}Rh chemical shifts (δ^{103}Rh = 6670, 7320 ppm). Also, the dimethylphenylphosphine adduct **223** was successfully measured via this technique, to yield both ^{103}Rh resonances (δ^{103}Rh = 6529, 6963 ppm). Unfortunately, the preparation of a triphenylphosphine adduct resulted in a mixture of species. Phosphorous containing ligands with even weaker donor strength (perfluorated triphenylphosphine, trimethoxyphosphite) failed to bind to [Rh$_2$(formate)$_4$].

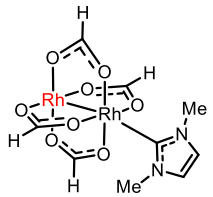

222, δ^{103}Rh = 7320 ppm
δ^{103}Rh = 6670 ppm

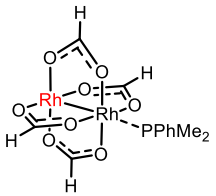

223, δ^{103}Rh = 6529 ppm
δ^{103}Rh = 6963 ppm

Scheme 60-^{103}Rh chemical shifts of dirhodium(II)-adducts **222** (in C_6D_6) and **222** (in CD_2Cl_2) acquired by ^{1}H–^{103}Rh-HMBC experiment.

As expected, the ^{103}Rh chemical shifts of both the phosphine (**222**) and the NHC adduct (**223**) appear at lower resonances than [Rh$_2$(formate)$_4$] itself (*vide supra*, δ^{103}Rh = 7422 ppm in CD_3CN). Intriguingly, a noteworthy observation emerged when comparing the ^{103}Rh chemical shifts of NHC adduct **222** with phosphine adduct **223**. In the NHC adduct, the distal rhodium center appears more shielded than the rhodium bound to the NHC. In contrast, the phosphine adduct exhibits the opposite trend: the distal rhodium nucleus is more deshielded relative to the rhodium center coordinated to the phosphine. Considering the intrinsic electronic properties of these ligand classes, NHCs are generally regarded as strong σ-donors with minimal or negligible capacity for π-back-donation,[167-169] whereas phosphines, although also reasonable σ-donors, often participate in π-backbonding to a greater extent.[170-171] These fundamental differences, however, do not straightforwardly translate to predictable patterns in ^{103}Rh NMR behavior within the dirhodium(II) framework. Therefore, a more in depth study

by computational analysis is necessary to better understand the electronic effects exerted by the corresponding axial ligand on the dirhodium scaffold.

6.2.3. ^{103}Rh NMR Studies of Reactive Carbene Intermediates with [Rh$_2$(formate)$_4$]

As the ^{103}Rh chemical shifts of NHC and phosphine adducts were successfully obtained by a ^{1}H-^{103}Rh-HMBC experiment, the question arose as to whether it was possible to obtain the ^{103}Rh chemical shifts of reactive carbene intermediates, which would provide direct insight into the electronic nature of the Rh(II) paddlewheel complexes exerted by the bound carbene. A donor/donor carbene was identified as an ideal candidate for initial investigations, due to its higher electron density and reduced reactivity relative to donor/acceptor or acceptor/acceptor carbenes. Notably, our research group had previously succeeded in the spectroscopic characterization of such intermediates at low-temperature.[25-26] Following an established protocol,[25] the corresponding diazo compound was reacted with [Rh$_2$(formate)$_4$] at 8 °C to afford carbene intermediate **224**, and the solution was warmed to 10 °C within the NMR magnet. To our delight, a ^{1}H-^{103}Rh-HMBC measurement afforded both ^{103}Rh chemical shifts. Additionally, due to its stability, the carbene chemical shift could also be measured and was assigned at 254.3 ppm, which is in similar range as the value reported for the analogous carbene derived from [Rh$_2$(esp)$_2$] (δ^{13}C = 253.5 ppm).[25] Attempts to obtain the ^{103}Rh chemical shifts of a donor/acceptor carbene intermediate **225** failed, even when the NMR probe was cooled to −78 °C. Most likely the low solubility of [Rh$_2$(formate)$_4$] is the reason for the failure of this experiment, as it was noticed that the majority of the material crashed out when cooling the sample.

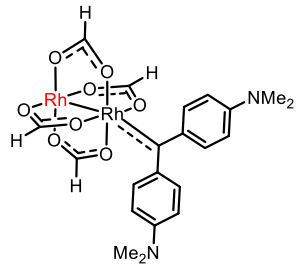

224, δ^{103}Rh = 7305 ppm
δ^{103}Rh = 6425 ppm
δ^{13}C(carbene) = 254.3 ppm

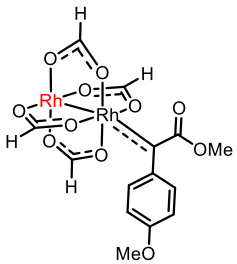

225, failed

Scheme 61-^{103}Rh chemical shifts of reactive dirhodium(II)-carbene intermediates **224** (in C_6D_6) and **225** (in CD_2Cl_2) acquired by ^{1}H-^{103}Rh-HMBC experiment.

As anticipated, the electronic behavior of the carbene intermediate **224** more closely resembles that observed for the NHC adduct **222**, as reflected in the ^{103}Rh NMR data. The

chemical shift of the rhodium center directly coordinated to the carbene is nearly identical to that of the NHC-bound rhodium in adduct **222** (7305 vs. 7320 ppm), indicating a comparable local electronic environment at the binding site. However, a notable difference arises at the distal rhodium nucleus, which appears significantly more shielded than in the corresponding NHC adduct (6425 vs. 6670 ppm). Attempts were also made to obtain the ^{103}Rh resonances of a more reactive donor-acceptor carbene **225**, but did not meet with success.

6.3. Conclusion

This chapter demonstrates that the previously perceived limitation of accessing only one of the ^{103}Rh chemical shifts of NHC or phosphine adducts of Rh(II) complexes (**216-220**) via triple resonance NMR spectroscopy can be overcome. Specifically, it was shown that for phosphine adducts (**218, 221**), a double resonance ^{103}Rh–^{31}P{^{1}H} HMBC experiment provides a viable alternative for acquiring both ^{103}Rh chemical shifts. Additionally, replacing [$Rh_2(OAc)_4$] with [$Rh_2(formate)_4$] enabled the use of a ^{1}H–^{103}Rh HMBC experiment to determine both ^{103}Rh chemical shifts of Rh(II) phosphine/NHC-adducts (**222-223**).

Importantly, this methodology was extended to a reactive donor/donor carbene intermediate **224**, for which the ^{103}Rh chemical shifts could be obtained. The resulting data revealed that the chemical environment at rhodium resembles mostly that of NHC adduct **222**, however the distal rhodium nucleus is more shielded than in the NHC adduct.

To rationalize the influence of different axial ligands on the electronic environment at rhodium, particularly in terms of donor strength, a more systematic understanding is required. Therefore, ongoing computational calculations will be crucial for gaining deeper insight on how the observed chemical shifts can be correlated to the ligand donor properties.

7. A Comparative Study on the Effect of Carboxylate and Carboxamidate Ligands in Heteroleptic Dirhodium(II)-Complexes

7.1. Introduction and Motivation

As briefly discussed in the general introduction, carboxylate and carboxamidate ligands represent the most prominent equatorial ligands of dirhodium(II) paddlewheel complexes. These μ_2-bridging ligands are strongly bound to the dirhodium core, impart high stability and have a significant influence on the selectivity and reactivity in a widespread range of catalytic transformations, of which metal carbene chemistry is the most eminent.[23, 51, 55, 133, 172-176] Although these types of catalysts have been known for several decades and are well-studied, the influence of the ligand sphere on the correlation between reactivity and selectivity is less apparent. In general, there is a widely held belief that dirhodium carboxamidate complexes are less active but more selective than their carboxylate counterparts.[56, 177-181] This assumption is often attributed to the stronger σ-donating ability of carboxamidate ligands, which increases the electron density at the rhodium center and thereby enhances back-donation to the carbene carbon.[55, 182-183] Although this intuitive explanation for the potentially lower reactivity of metal carbenes may be valid in certain cases, one should be cautious about generalizing that carboxamidates enhance selectivity at the expense of reactivity. In fact, the observations reported by Nemoto, Hamada and co-workers[184] illustrate the opposite (Scheme 62).

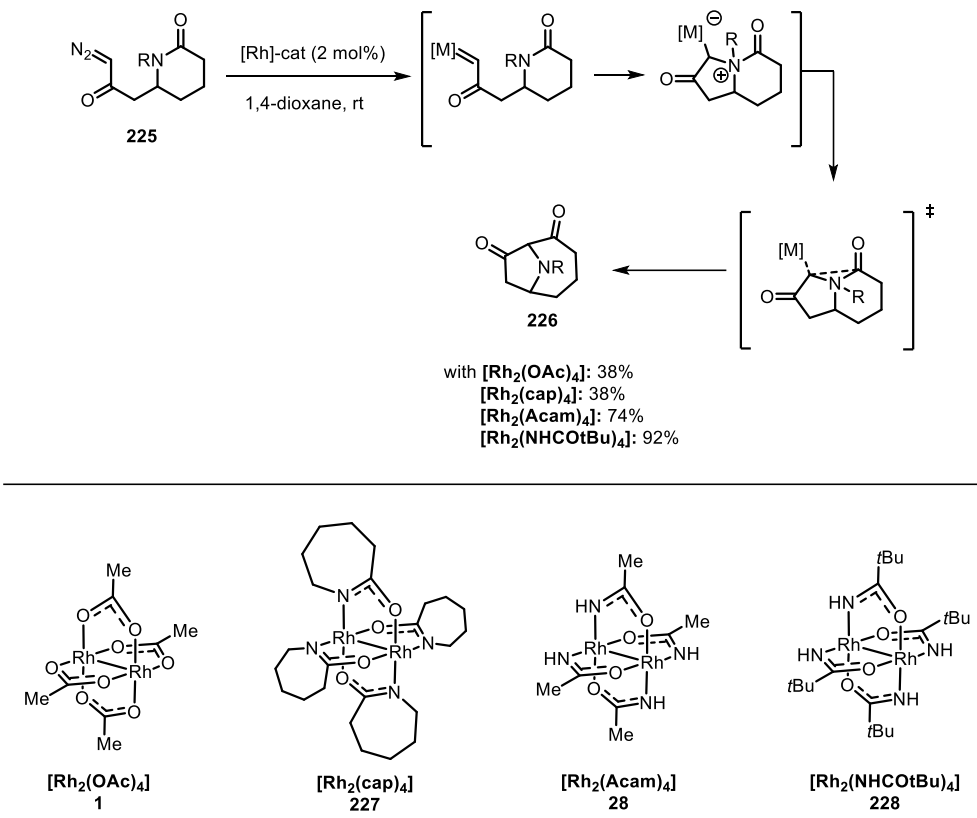

Scheme 62-Comparison of different homoleptic dirhodium complexes on the transformation of diazo ketone **225** to *N*-bridged bicycle **226**.

The formation of nitrogen-bridged bicyclic compound **226** from diazoketone **225** is proposed to proceed via initial nucleophilic attack by the amide nitrogen atom on the rhodium carbene intermediate, generated in situ. This is followed by a Stevens-type [1,2]-acyl shift, culminating in the formation of the final bicyclic product. Catalysts such as $[Rh_2(OAc)_4]$ and the conventional tetracarboxamidate complex $[Rh_2(cap)_4]$ (**227**) exhibited low efficiency under these conditions. In contrast, the use of $[Rh_2(acam)_4]$ or $[Rh_2(NHC(O)tBu)_4]$ (**228**) significantly improved the yield. These observations suggest that the nature of the bridging ligand — specifically whether it is a carboxylate or a carboxamidate — is not solely responsible for catalytic performance. Instead, the structural features of the carboxamidate ligand, particularly the distinction between primary and secondary types, appear to play a crucial role. The possibility of transient hydrogen bonding interactions involving reactive intermediates was proposed as a tentative explanation for the observed selectivity and efficiency.[184-186]

Our group recently also observed that selectivity of dirhodium carboxamidate catalysts does not come at the expense of reactivity. On the contrary, the heteroleptic complex **25**, a uniquely effective and selective catalyst for the cyclopropanation of α-metallated diazoacetates (see section 1.7), appears to contradict the general perception that incorporation of amidate(s) into

dirhodium complexes leads to reduced reactivity. The high stereoselectivity induced by **25** is attributed to the protic –NH moiety which facilitates an intermolecular hydrogen-bonding interaction with the carbene intermediate. This interaction implies that the reaction preferentially occurs at the Rh-center ligated to the N-atom (Rh[O_3N]), which was further confirmed by detailed computational analysis.[81]

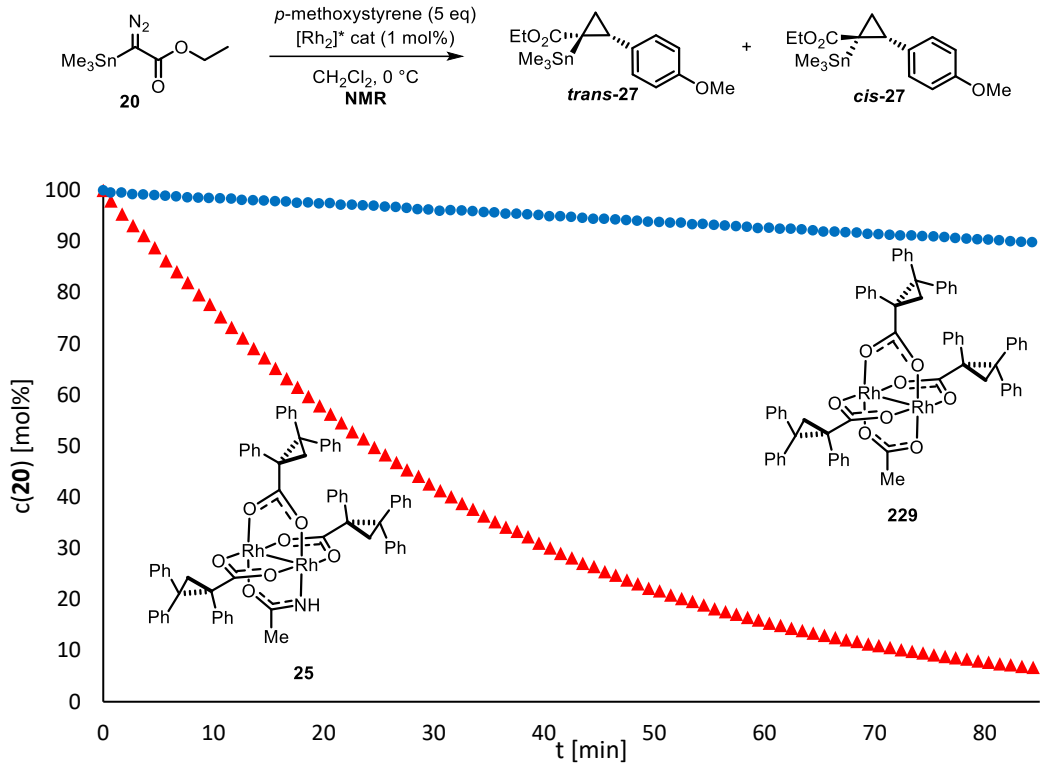

Figure 50-Kinetic profiles showing the consumption of stannylated diazo ester **20** during the cyclopropanation reaction of *p*-methoxystyrene catalyzed by dirhodium complexes **25** (red) and **229** (blue).

Additionally, the comparison of the kinetic data from the cyclopropanation of **20** with complexes **25** and **229** shows that the reaction is significantly faster with **25** than with the analogous acetate-containing complex **229** (Figure 50). These findings clearly demonstrate that the primary amidate ligand enhances both reactivity and selectivity in the described transformation.

While a rationale for the selectivity of complex **25** in the cyclopropanation of **20** could be given, the question as to why the reaction does not occur at the [O_4]-face still remained unanswered. Furthermore, it is not yet fully understood whether the reactive [O_3N]-face can be primarily ascribed to the steric bulk of the triphenylcyclopropyl carboxylate ligands. To address these uncertainties, we aimed to investigate whether altering the steric environment of the catalyst

— specifically by introducing smaller equatorial ligands — would influence the facial selectivity and reactivity.

7.2. Results and Discussion

This project was conducted in collaboration with Lorenzo Baldinelli and Prof. Dr. Giovanni Bistoni, who performed the DFT calculations. To provide a comprehensive and coherent overview of the research, these contributions have been incorporated into this thesis with permission of the authors.

7.2.1 Computational Analysis of [O_3N] versus [O_4]-Stannylated Carbenes

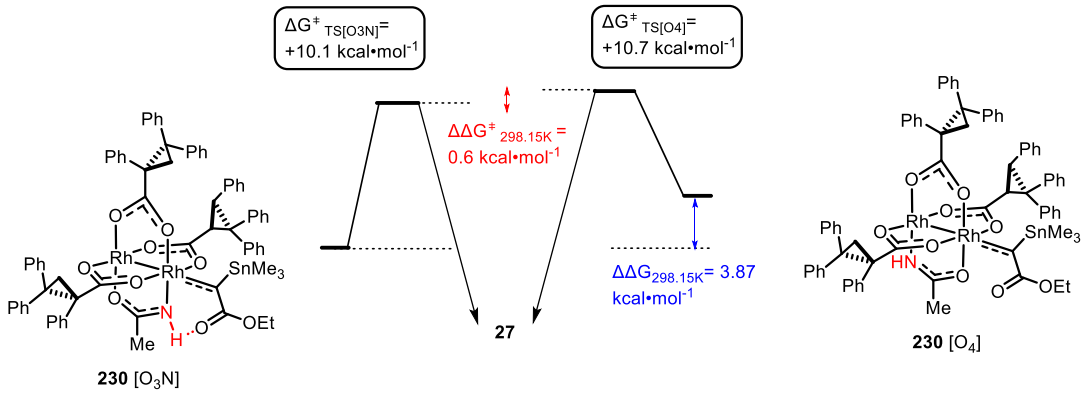

Figure 51-Computed barriers for the cyclopropanation of *p*-methoxystyrene by the isomeric carbenes **230**[O_3N] and **230**[O_4]-bound to the [O_3N]-face and [O_4]-face of complex **25**, respectively.

To understand why the cyclopropanation reaction of stannylated diazo compound **20** predominantly occurs at the [O_3N]-face of complex **25**, the barrier for cyclopropanation with *p*-methoxystyrene of the stannylated carbene intermediates at both the [O_3N] and [O_4]-face were computed (Figure 51). Due to the lack of stabilizing peripheral H-bond interactions at the [O_4]-face, the carbene intermediate **230** was notably less stable (ΔG(**230**[O_3N]-**230**[O_4])$_{298.15K}$= −3.87 kcal·mol^{-1}). Additionally, it was found that the energetic barrier for cyclopropanation was slightly higher than for the carbene intermediate at the [O_3N]-face ($\Delta\Delta G^{\ddagger}_{298.15K}$ = −0.6 kcal·mol^{-1}). These results show that the carbene at the [O_3N]-face is thermodynamically more favored and furthermore profits from a lower energetic barrier for the [2+1]-cycloaddition event which makes it kinetically favored. Together, these computational findings support the experimental observation that the cyclopropanation of **230** predominantly, if not exclusively, occurs at the [O_3N]-face of complex **25**.

7.2.2. Kinetic Studies of Heteroleptic Dirhodium(II) Complexes

Initially, the cyclopropanation reaction with stannylated diazoester **20** was attempted with sterically less encumbered achiral complexes (**100-101, 233-234**) under the same experimental setup as for complex **25**. However, the reaction profile turned out to be messy and the conversion to cyclopropane **27** was rather slow. Hence, these issues prompted a search for a more suitable diazo substrate. Diazo compound **231** which entails an allylic ester was envisioned to be a good candidate for this systematic study as it allows for an intramolecular cyclopropanation event to take place, thus reducing the risk of side product formation to occur.

To compare catalytic performance, the kinetic profiles of the intramolecular cyclopropanation of this new diazo compound were monitored by ^{1}H NMR using both the amidate complex **25** and its acetate analogue **229** (Figure 52). The data clearly indicated that the reaction proceeded significantly faster with complex **25**. To quantify the difference, a variable time normalization analysis according to the method developed by Burés[187] was employed, this revealed that the reaction catalyzed by complex **25** was approximately ten times faster than with its analogue. This observation suggests that the catalytic reaction proceeds largely at the [O_3N]-face of **25** which is in analogy with the observations made for stannylated diazoester **20**. Interestingly, both complexes seemed to induce hardly any enantioselectivity in this transformation as shown from chiral HPLC analysis of the formed products (5% *ee* with complex **25** and 0% *ee* with the acetate-containing counterpart).

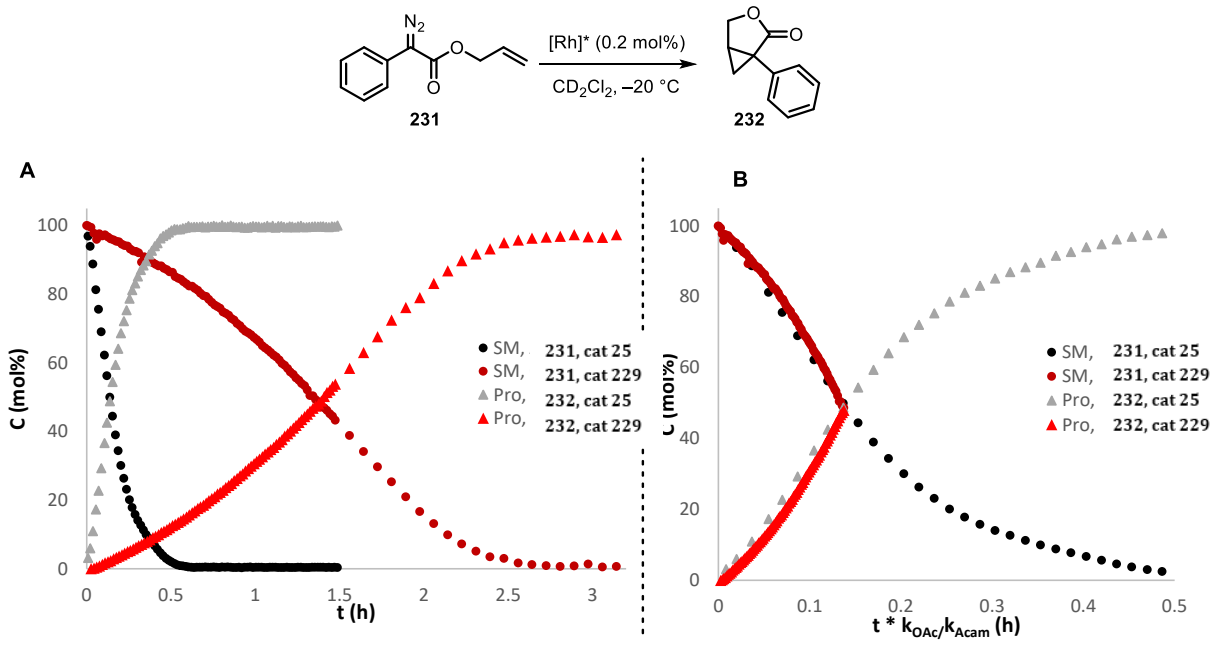

Figure 52-A: kinetic profiles of the cyclopropanation of **231** with complexes **25** and **229**. B: Reaction profiles with time-normalized scales.

When the same reaction was performed with the sterically less encumbered achiral complexes, **100**-**101** and **233-234,** a striking difference in reactivity was observed (Figure 53). Complexes **100** and **234** comprising an acetate or a trifluoroacetate outcompeted complex **101** bearing an acetamidate ligand by factors of 2 and 7, respectively. Additionally, it was observed that complex **233** bearing a trifluoroacetamidate enhanced the reactivity by a factor of 3.5 with respect to reference complex **101**. These findings contrast with the previously described results for the intermolecular cyclopropanation of stannylated diazoester **20**. To reconcile this discrepancy and develop a more coherent mechanistic understanding, further experimental and computational investigations were undertaken (*vide infra*).

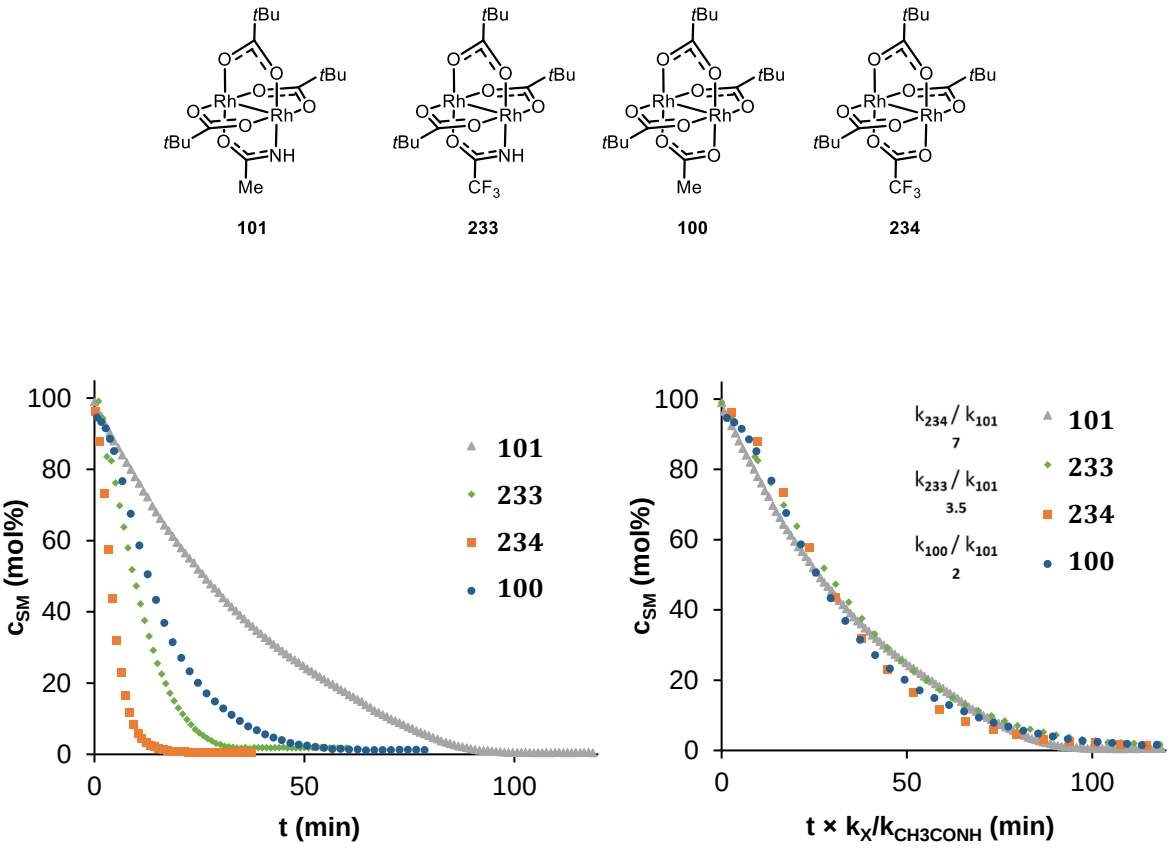

Figure 53-Left: kinetic profiles of the consumption of the diazoester **231** with complexes **100-101, 233-234** monitored by ^{1}H-NMR (reaction conditions: 0.05 mol% catalyst in CD_2Cl_2 at –30 °C). Right: reaction profiles with time normalized scales.

7.2.3. ^{103}Rh NMR of Heteroleptic Dirhodium(II) Complexes

To gain insight in the electronic characteristics of these complexes, ^{103}Rh chemical shifts were recorded for complexes **100-101** and **233-234** using a ^{103}Rh NMR triple resonance sequence (see Chapter 6). These data were used to explore potential qualitative correlations between the spectral data and the observed reactivity trends. Notably, in the amidate containing complexes **101** and **233** the chemical shifts between the two rhodium centers differ by >1000 ppm, of which the Rh[O_3N] is the more shielded one with respect to the neighboring Rh[O_4]. Similar trends had been observed before.[157] Furthermore, trifluoromethylation induces hardly any chemical shift changes at the Rh[O_3N] center, while the adjacent Rh[O_4]-site is clearly affected ($\Delta\delta \approx 86$ ppm). Similarly, complexes **100** and **234** show almost the same chemical shift difference at their respective Rh[O_4] sites ($\Delta\delta \approx 82$ ppm).

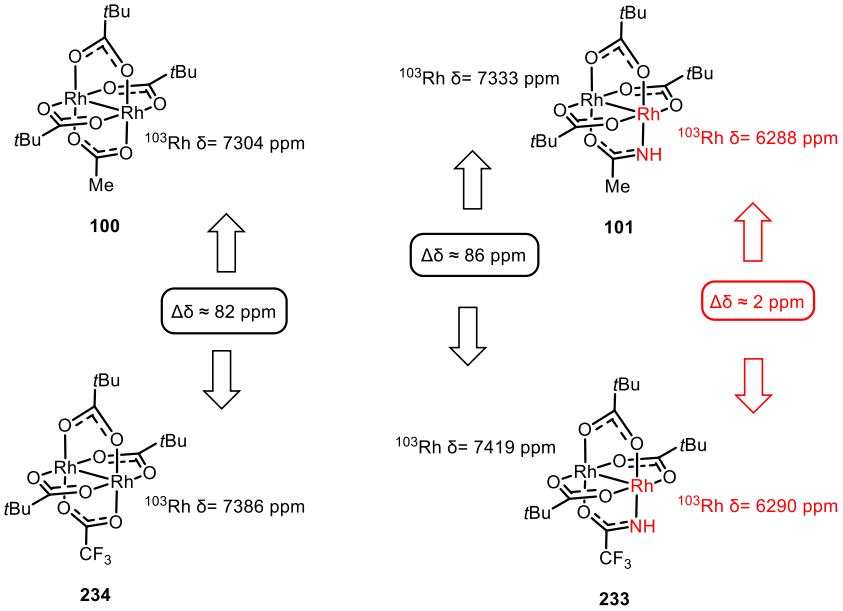

Scheme 63-Comparison of the ^{103}Rh chemical shifts of complexes **100-101** and **233-234** measured in CD_3CN.

As can be seen from Figure 53, the incorporation of trifluoromethylated ligands results in notable higher reaction rates. This observation is in good agreement with the observation of Davies and co-workers who concluded from their computational data that trifluoromethylation of a homoleptic dirhodium(II) complex lowers all barriers.[63] As mentioned above, the analysis of ^{103}Rh NMR chemical shifts reveals that in complex **233**, only the Rh[O_4] experiences notable deshielding relative to the non-fluorinated analogue **101**, while the Rh[O_3N] remains largely unaffected. This suggests that cyclopropanation preferentially occurs at the [O_4]-face in these amidate-containing heteroleptic complexes. On this basis, catalyst **100** — which features two Rh[O_4] sites — would be expected to exhibit higher

reactivity than its amidate-containing counterpart **101**. Similarly, **234** should be more reactive than **233**, a trend that is corroborated by the experimental kinetic data (*vide supra*).

While this interpretation provides a coherent picture, it is important to consider potential indirect effects of trifluoromethylation on the [O_3N]-face. Specifically, the electron-withdrawing nature of the trifluoromethyl group leads to acidification of the amidate –NH moiety, as evidenced by downfield shifts in the corresponding NMR signals (**101**: δ_{NH} = 4.86 ppm; **233**: δ_{NH} = 6.47 ppm). This change may modulate the strength of the interligand hydrogen bond between the protic amidate ligand and the adjacent carbene. Although an influence of this hydrogen-bonding interaction on reactivity is plausible, the extent to which it acts synergistically with the electronic effects imparted onto the rhodium centers remains to be elucidated.

7.2.4. Computational studies

While the ^{103}Rh NMR data provide a plausible rationale for the observed reactivity trends in the sterically less hindered achiral complexes **100-101** and **233-234**, these conclusions appear to be at odds with the reactivity patterns exhibited by the more bulky triphenylcyclopropyl-substituted complexes **25** and **229**: The strong computational and experimental evidence in the intermolecular cyclopropanation of stannylated diazo compounds shows that the reaction occurs at the [O_3N]-face of complex **25**, whereas the intramolecular cyclopropanation of **231** with complex **101** gives strong indications that the reaction takes place at the [O_4]-site. In order to get a better understanding as to why this might be the case, a detailed computational study was performed in which the overall reaction profile was calculated.

The computational protocol employed in this study builds upon methodologies previously validated in mechanistic investigations of related reactions.[81, 188] An initial conformational search for relevant intermediates was conducted using the CREST algorithm at the GFN2-xTB level.[189-190] Geometry optimizations, frequency calculations, and thermal corrections at 298.15 K were performed using the B3LYP-D3(BJ) hybrid functional in conjunction with the def2-SVP basis set.[191-195] Final single-point electronic energies were refined using the B3LYP-D3(BJ)/def2-TZVP(-f) level of theory. Solvent effects were included using the C-PCM implicit solvation model for CH_2Cl_2 as the implicit solvent.[196-197] The resolution-of-identity (RI) approximation was employed in the RIJCOSX framework, utilizing appropriate auxiliary basis sets.[198-199] Transition state (TS) guesses were initially generated via nudged elastic band (NEB) and relaxed coordinate scan techniques.[200-201] These were subsequently refined

through full geometry optimization. All stationary points were characterized through vibrational analysis: true intermediates exhibited no imaginary frequencies, while transition states were confirmed by the presence of a single imaginary mode corresponding to the reaction coordinate.

The computed reaction profile (Figure 54) shows that initial adduct formation of diazo ester **231** to complex **101** is nearly a barrierless process at both faces. Comparison of both TS shows that the reaction is somewhat easier at the [O_4]-face ($\Delta G^{\ddagger}_{TS1\ [O4]}$ = 8.5 kcal·mol^{-1}) than at the [O_3N]-face ($\Delta G^{\ddagger}_{TS1\ [O3N]}$ = 8.8 kcal·mol^{-1}). The carbene intermediate **235** at the [O_3N]-face profits from interligand hydrogen bonding and is therefore 3.1 kcal·mol^{-1} more stable than its [O_4] counterpart. The cyclopropanation step appears to be kinetically more favored for the carbene intermediate at [O_4] ($\Delta G^{\ddagger}_{TS2\ [O4]}$ = 10.5 kcal·mol^{-1}). In order for the *intramolecular* cyclopropanation step to occur at the [O_3N]-site, the hydrogen bond gets severely distorted upon approach of the tethered olefin, and therefore suffers from an enthalpic penalty. This is in contrast to what had been found for the *intermolecular* cyclopropanation of **20** with complex **25**, in which the hydrogen bond persists and plays a crucial role in the stereoselective process, but might explain the low *ee* observed in the *intramolecular* cyclopropanation (*vide supra*). Given the small free energy difference between the transition states associated with cyclopropanation at the **235**[O_4] and **235**[O_3N] sites ($\Delta\Delta G^{\ddagger}_{TS2}$ = 1.2 kcal·mol^{-1}), it is likely that the cyclopropanation will occur to some extent at both inequivalent rhodium sites.

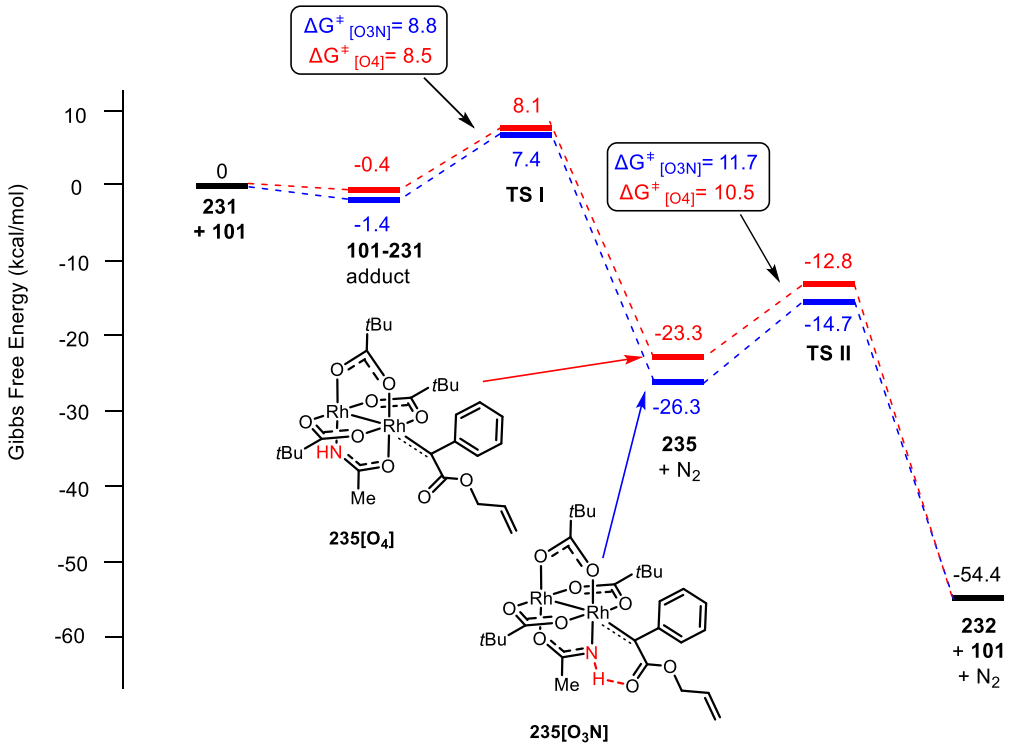

Figure 54-Gibbs free energy profile of the intramolecular cyclopropanation of **231** into **232** catalyzed by complex **101**.

Notably, the rate-determining step is the cyclopropanation event irrespective of whether the reaction occurs at the $[O_3N]$- or $[O_4]$-face. This finding stands in contrast to the widely accepted view that carbene formation constitutes the turnover-limiting step, which is an assumption initially deduced from the computational work from Davies and Autschbach over a decade ago.[92] More recent, kinetic studies by Davies and Blackmond have reinforced this interpretation.[202] Additionally, experimental investigations by Pirrung and co-workers[61, 203] have indicated that the formation of dirhodium carbenes from diazoketones represents the turnover-limiting process, irrespective of the subsequent transformation (e.g., cyclopropanation, C–H insertion, or ylide formation).

Since the initial calculations by Davies and Autschbach no longer represent state-of-the-art computational methodologies, we opted to recalculate the reaction energy profiles with our computational settings which take entropy, solvent, thermal corrections, zero-point energy vibrations, and dispersion corrections into account (Figure 55). Interestingly, under the revised conditions the rate determining step turned out to be the cyclopropanation event and not the carbene formation ($\Delta G^{\ddagger}_{TS2} > \Delta G^{\ddagger}_{TS1}$) as Davies and Autschbach had suggested.[92]

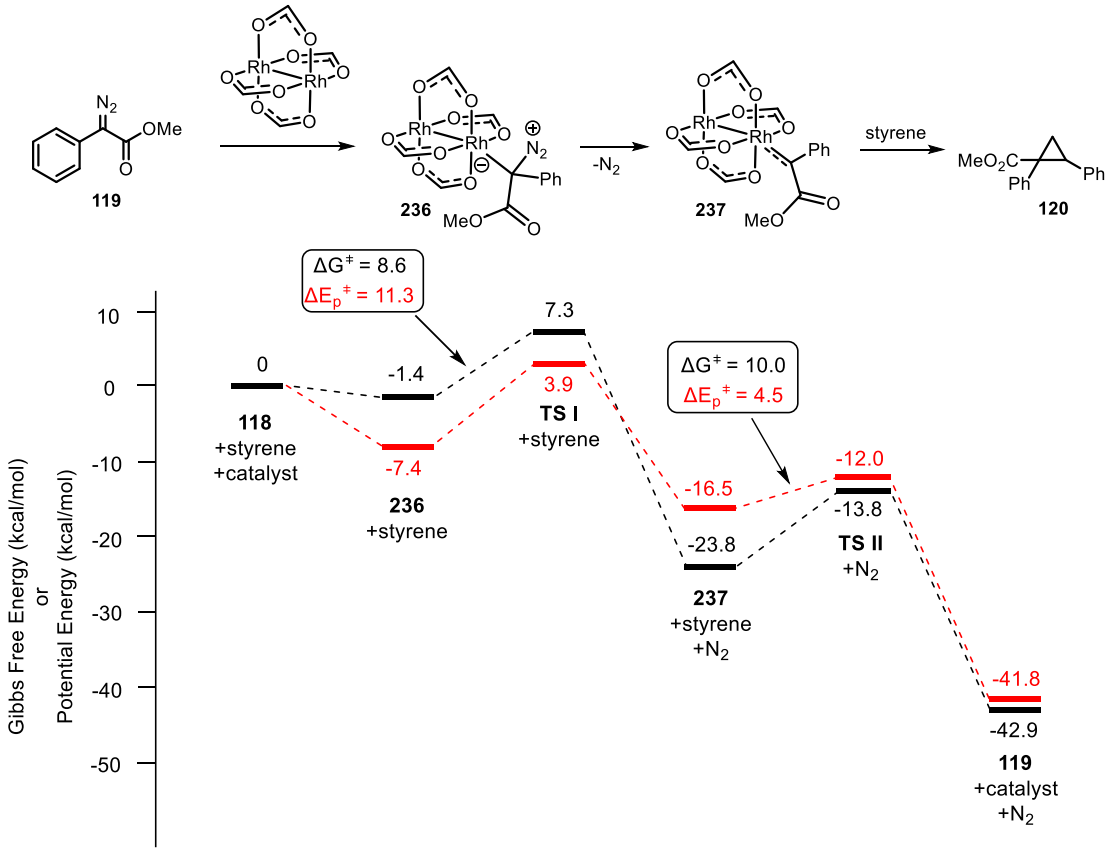

Figure 55- Reaction energy profiles for the cyclopropanation of diazoester **119** with dirhodiumtetraformate from Davies and Autschbach (shown as potential energy surface in red) and our revised calculations (shown as Gibbs-free energy in black).

Additionally, the reaction energy profiles were computed for a model that includes one axially coordinated acetone molecule bound to the complex throughout the catalytic cycle. Acetone was selected — to be consistent with the earlier approach by Davies and Autschbach — as a simple representative of carbonyl-containing reactants or products that may coordinate to the second rhodium center during the catalytic cycle. As expected, the acetone–dirhodium adduct that forms initially appears to be more stable and binds more strongly than the diazo substrate, ultimately contributing to a higher energetic barrier for the carbene formation to take place (Figure 56).

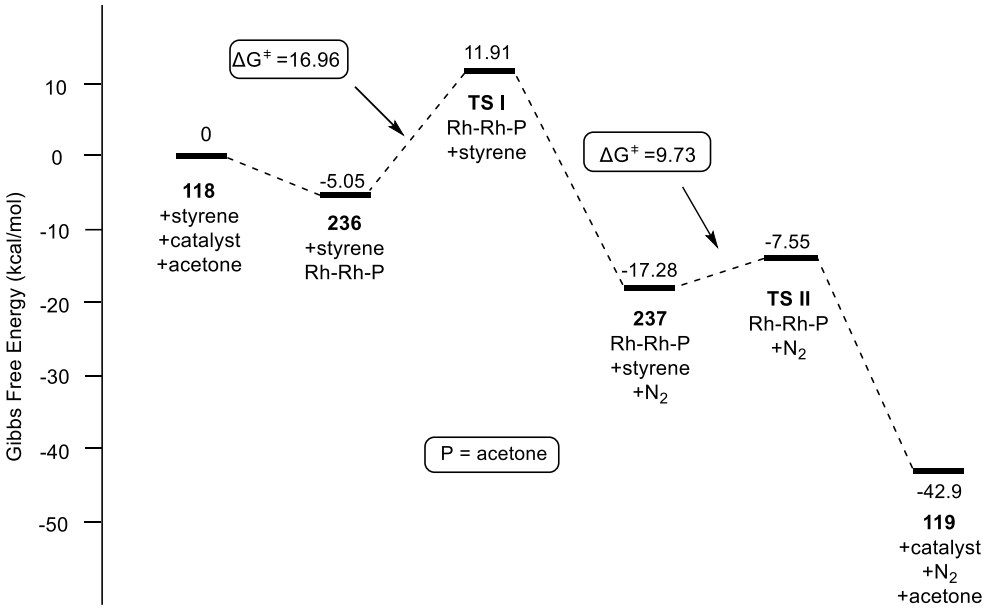

Figure 56-Reaction energy profile for the cyclopropanation of diazoester **119** with $[Rh_2(O_2CH)_4]$ in the presence of acetone.

In this scenario, the turn-over limiting step is the carbene formation which is in agreement with the initial finding of Davies and Autschbach.[92] However, this mechanism is not fully correct, as it did not take into account the possible dissociation of the axial ligand during the course of the reaction. Therefore, we calculated the reaction energy profile in which possible dissociation of the acetone molecule is allowed (Figure 57). In that case, acetone dissociation is energetically preferred prior to carbenoid formation and consequently lowers the TS by 4.6 kcal·mol^{-1}.

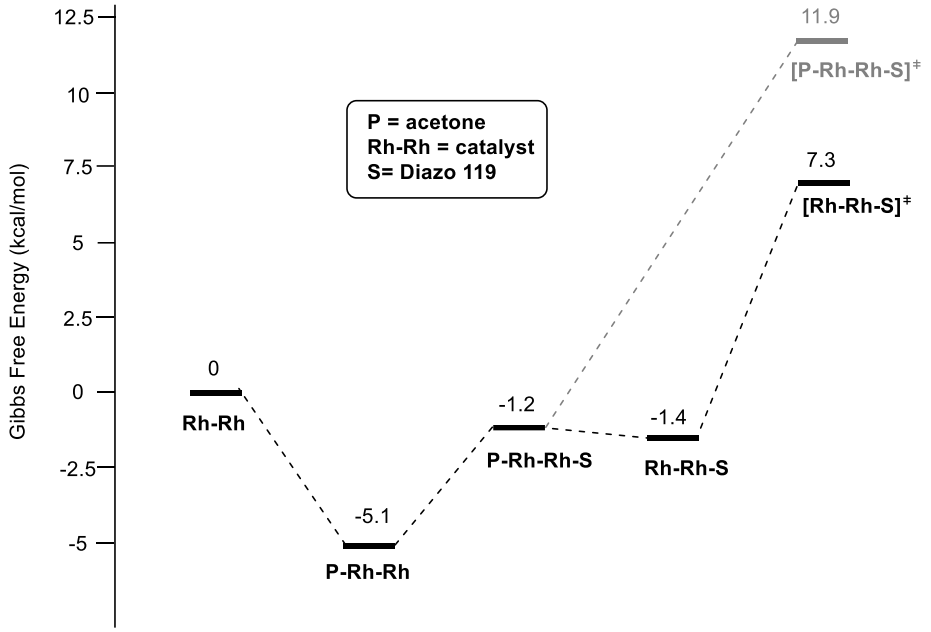

Figure 57- Reaction energy profiles with and without dissociation of the ligated acetone.

Taking the observation into account that carbonyl containing compounds can significantly influence the reaction energy profile and hence the rate-determining step, it seemed possible that lactone **232**, which accumulates as the intramolecular reaction proceeds, might gain a role of an axial ligand and impact the reaction profile. If so, the turn-over limiting step might change with increasing conversion. In order to rule out such changes, the reaction pathways at both [O_3N]- and [O_4]-faces were calculated (Figure 58).

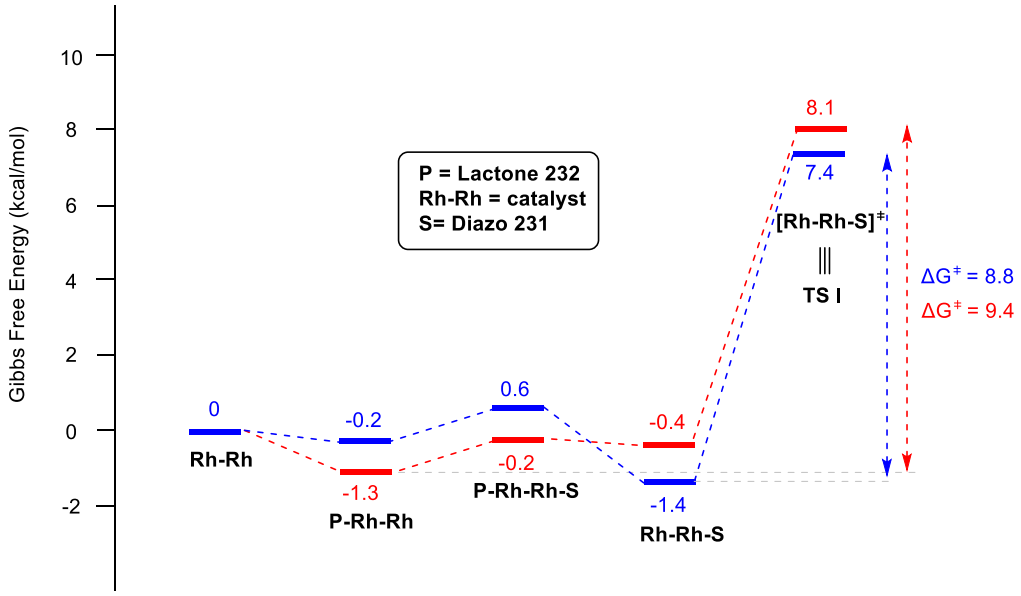

Figure 58-Reaction energy profiles calculated at the [O_3N] face (Blue) and [O_4]-face (red) of catalyst **101** taking into account binding of lactone **232** at the distal Rh center of the catalyst.

Lactone **232** binds indeed to the dirhodium complex on either the $[O_3N]$- or $[O_4]$-face , but does not cause a significant energetic change. Therefore, the cyclopropanation event rather than carbene formation remains the rate-determining step.

Although it is clear that the reaction profile can change significantly due to the presence of additives (*vide supra*), this effect can be neglected in the context of the present study. The primary objective was to investigate the intrinsic properties imparted by the different equatorial ligands. Accordingly, rigorous precautions were implemented during kinetic measurements to prevent the coordination of any external ligands that could compete with the diazo substrate for the axial binding sites. This approach ensured that the observed reactivity accurately reflects the inherent behavior of the catalyst system, avoiding potential misinterpretations arising from extraneous ligand interference.

7.2.5. Hunting Down Reactive Carbene Intermediates in Catalytic Transformations

As can be seen from Figure 52, DFT calculations indicate that in the intramolecular cyclopropanation of **231** to give lactone **232** catalyzed by complex **101**, the cyclopropanation event is the turn-over limiting step. This would mean that the carbene intermediate might be in the catalyst resting state and could build up in detectable concentration. In this case, it could possibly be characterized by *in situ* spectroscopic techniques. It is worth emphasizing that due to the highly reactive character that these superelectrophilic dirhodium carbenes impart, the direct detection of such species had been defied for decades. It was not until 2013 that Davies, Berry and co-workers reported the first spectroscopic characterization of a donor-acceptor carbene formed by diazo decomposition with a stoichiometric amount of dirhodium complex.[65] Fürstner and co-workers managed shortly thereafter to characterize a variety of different dirhodium carbenes by crystallography and spectroscopy, again under stoichiometric conditions.[24-26, 204]

Detection of a carbene intermediate under truly catalytic settings poses an even greater challenge as the carbene remains a highly reactive fleeting intermediate. As observed in the kinetic experiments the cyclopropanation reaction occurs rapidly even at low temperatures.

Interestingly, during the kinetic experiments (Figure 51), it was observed by ^{1}H NMR that the *tert*-butyl groups experience a change in their chemical shift upon mixing of the diazoester **231** with catalytic amounts of complex **101**. To study this effect in a more detailed manner, the reaction was set up again at –40 °C with 0.5 mol% of catalyst loading in CD_2Cl_2, in which the region where the *tert*-butyl groups occur were carefully monitored over time (Figure 59).

Directly upon mixing of the sample, in the first acquired ^{1}H NMR spectrum, the *tert*-butyl groups show slightly broadened singlets at δ_H = 0.97 and 0.88 ppm. Over time, these signals lost intensity and, once fully disappeared (when the diazoester was fully consumed), the corresponding *tert*-butyl signals of the bare catalyst appeared again and gained intensity over time. Most likely, the observed putative carbene intermediate is the one bound to the $[O_3N]$-face of the catalyst, as it is thermodynamically more stable and exhibits a higher energetic barrier for cyclopropanation compared to its $[O_4]$-counterpart, making it the longer-lived intermediate of the two.

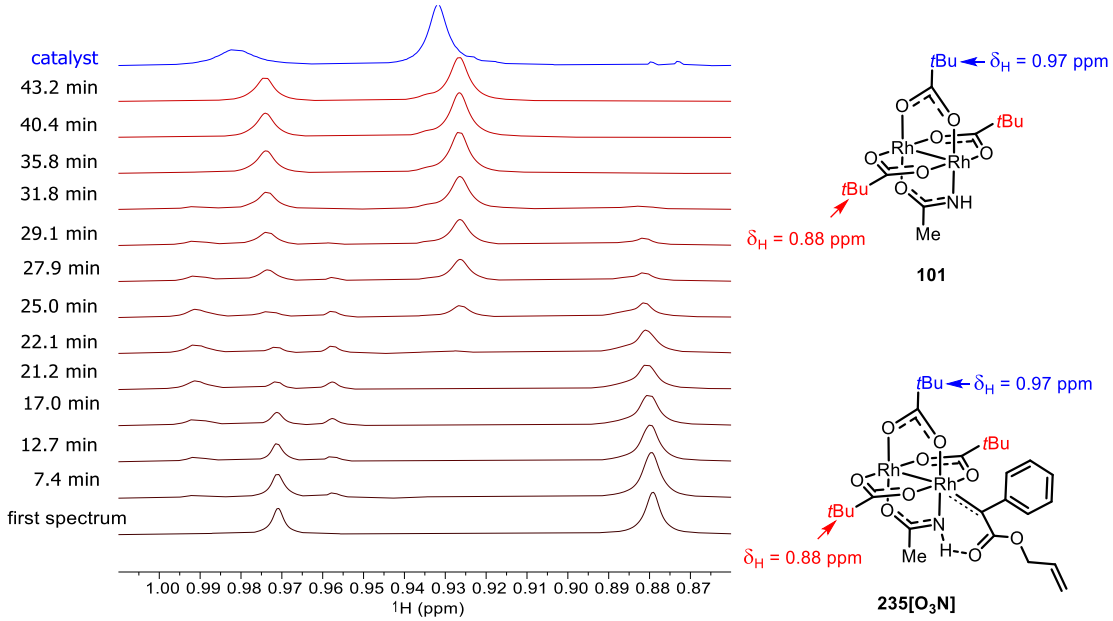

Figure 59-Aliphatic region of the ^{1}H NMR spectra (600 MHz, CD_2Cl_2, 233 K), showing the two signals corresponding to the *t*Bu-groups (trans and cis, 1:2) of the putative carbene intermediate **235** (red). For reference, the two signals of the *t*Bu-groups of the bare catalyst can be seen in blue colored ^{1}H NMR spectrum.

Although these results were certainly suggestive, less ambiguous data was needed. To enable the detection of such reactive intermediate by more characteristic spectral fingerprints such as ^{13}C NMR, attention was turned toward ^{13}C labeling studies. Doubly labeled diazoester $[^{13}C]_2$-**231** was readily prepared from commercially available $[^{13}C]_2$-phenylacetic acid by means of a Steglich esterification with allyl alcohol, followed by diazotation, in overall good yield (Scheme 64).

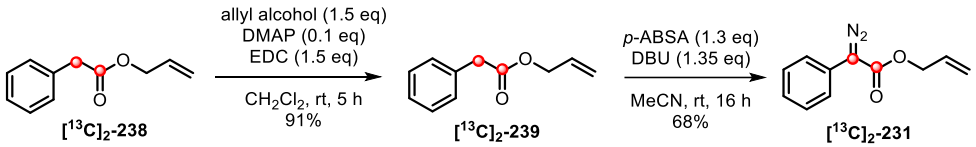

Scheme 64-Synthesis of the doubly ^{13}C-labeled diazoester **231** starting from $[^{13}C]_2$-phenylacetic (The red dots represent the ^{13}C labeled carbons).

With the ^{13}C labeled diazoester $[^{13}C]_2$-**231** at hand, initial attempts were made with $[Rh_2(OPiv)_4]$ (**102**) as the catalyst to detect the carbene intermediate via ^{13}C NMR spectroscopy. When 5 mol% of **102** was employed in CD_2Cl_2 at –90 °C, a distinct signal was observed at $\delta = 232.0$ ppm (Figure 60). Owing to the vicinal ^{13}C-labeled carbonyl group, the carbene resonance appears as a doublet and is noticeably broadened. This broadening is attributed to the high reactivity of the intermediate, which, even at such low temperatures, undergoes intramolecular reaction with the tethered olefin on a timescale comparable to that required for acquiring a ^{13}C NMR spectrum of adequate signal-to-noise ratio.

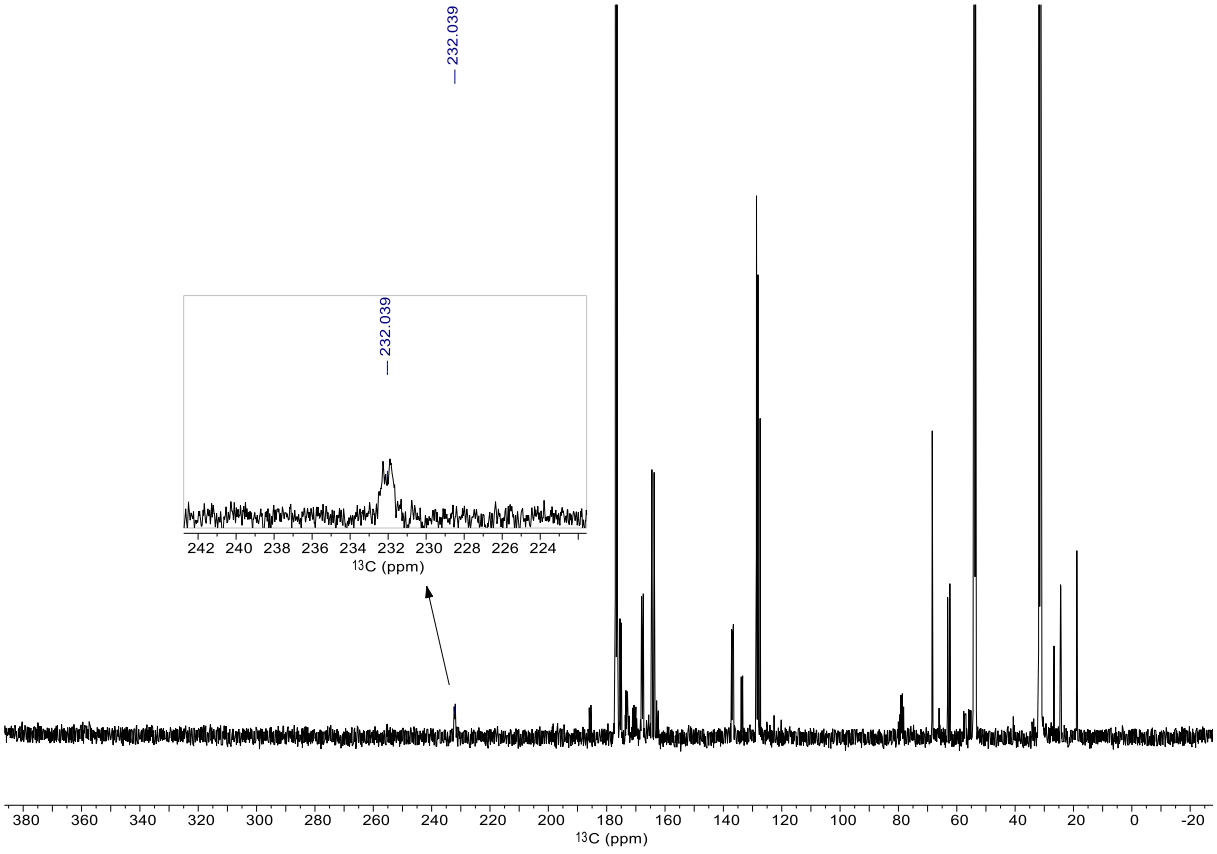

Figure 60-^{13}C NMR spectrum (126 MHz, CD_2Cl_2, 185 K) of $[^{13}C]_2$-**231** with 5 mol% of $[Rh_2(OPiv)_4]$.

Additional support for the assignment of the carbene species was provided by a 2D-HMBC experiment, which revealed a cross peak between the carbene carbon and the *ortho*-proton of the adjacent phenyl ring at δ_H= 8.9 ppm (Figure 61). Moreover, the observed chemical shift is consistent with values reported for other characterized dirhodium carbenes located at [O_4]-faces (Scheme 65), further supporting the structural assignment.

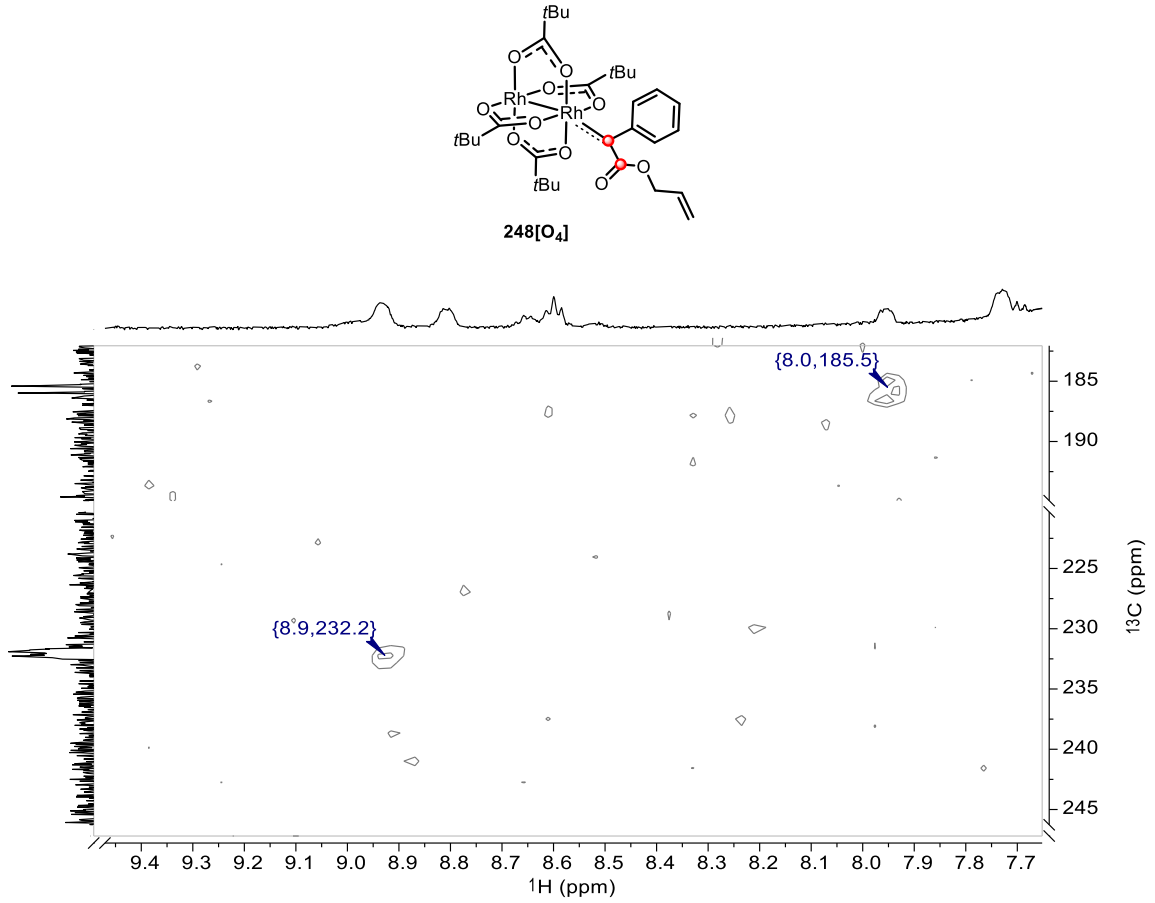

Figure 61- ^{1}H-^{13}C HMBC acquired at 183 K with [Rh_2(OPiv)$_4$] showing the cross peak to the carbene **XX** at δ_H= 8.9 ppm.

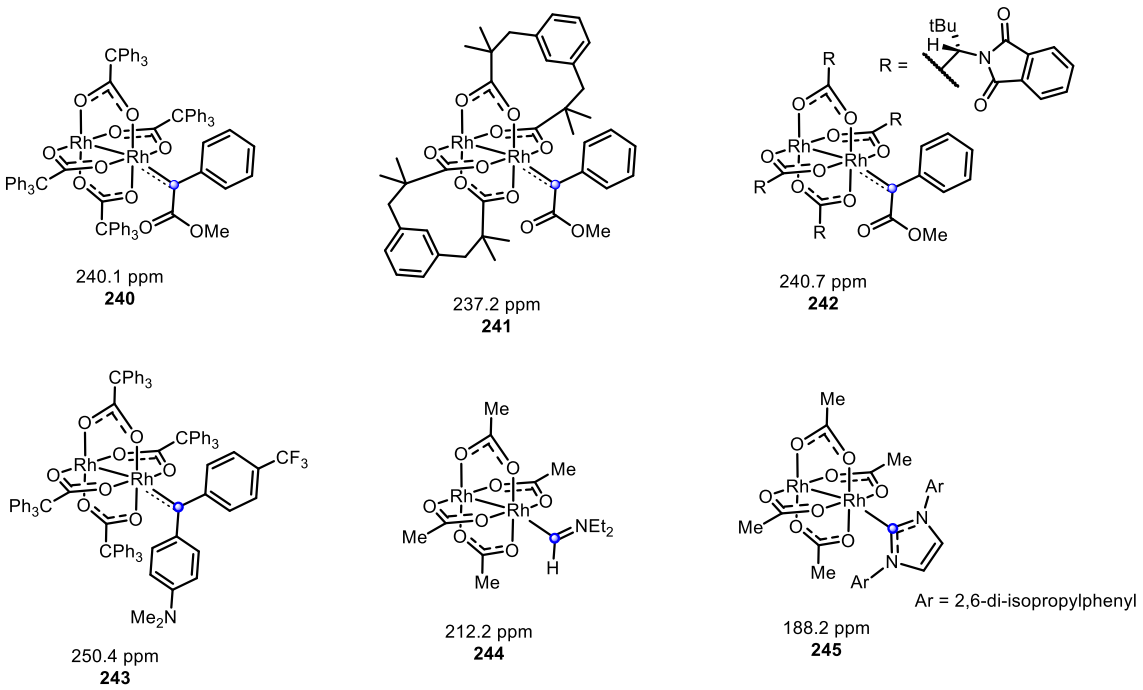

Scheme 65-Examples of ^{13}C NMR shifts of the carbene carbon (blue dot) of dirhodium carbene complexes **240**[65], **241**[25], **242**[26], **243**[25], **244**[205], and **245**[160].

Analogously, attempts were made to obtain the carbene ^{13}C chemical shift with amidate complex **101**. At –80 °C in CD_2Cl_2 a broad peak at δ_C = 215.2 ppm was recorded, which also disappeared after complete conversion of the substrate (Figure 62). Since the recorded carbene signal resonates 16.8 ppm upfield of to the carbene signal obtained with complex **102**, it was postulated that the observed chemical shift belongs to the carbene bound at the [O_3N]-face of complex **101**. This observation would be in agreement with the observed computational findings stating the increased thermodynamic stability of the [O_3N]-**235** carbene intermediate.

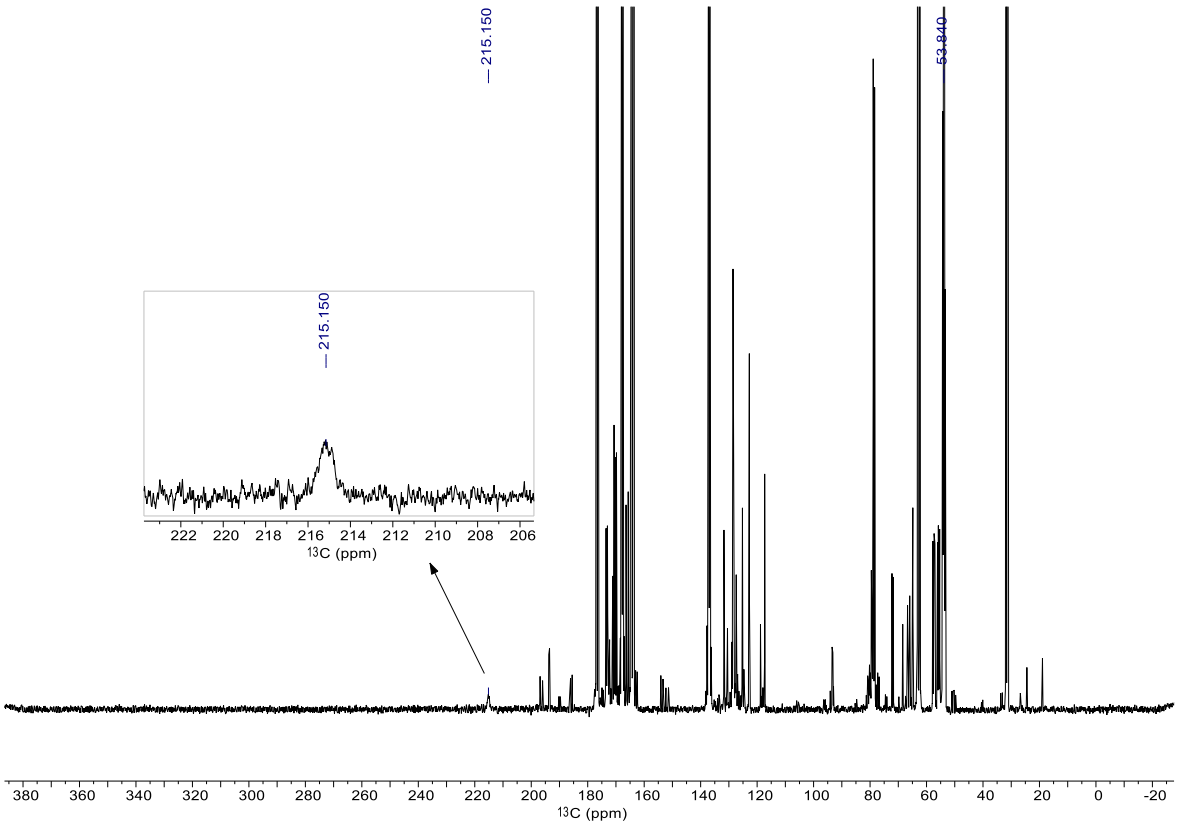

Figure 62-^{13}C NMR spectrum (126 MHz, CD_2Cl_2, 195 K) of [^{13}C]$_2$-**231** with 5 mol% of complex **101**.

Due to the low solubility of complex **101**— and consequently, the reduced concentration of the carbene intermediate under low-temperature conditions — no cross-peaks were observed in the 2D-HMBC spectrum. To further support the assignment of the ^{13}C chemical shift at 215.2 ppm to the carbene carbon, it was hypothesized that removal of the allylic double bond in diazo compound [^{13}C]$_2$-**231** would increase the lifetime of the resulting carbene intermediate. This, in turn, was expected to enhance the likelihood of obtaining a more detailed spectroscopic characterization.

Similarly to [^{13}C]$_2$-**231**, [^{13}C]$_2$-**246** was prepared and exposed to complex **101** at –90 °C in CD_2Cl_2. A distinctive signal at δ_C = 217.3 ppm was observed, which is in close proximity to the chemical shift observed with allyl ester [^{13}C]$_2$-**231**. Furthermore, cross-peaks in the ^{1}H-^{13}C HMBC between the carbene carbon and two magnetically inequivalent *ortho*-protons of the adjacent phenyl ring were observed (δ_H= 9.1, 8.8 ppm) (Figure 63).

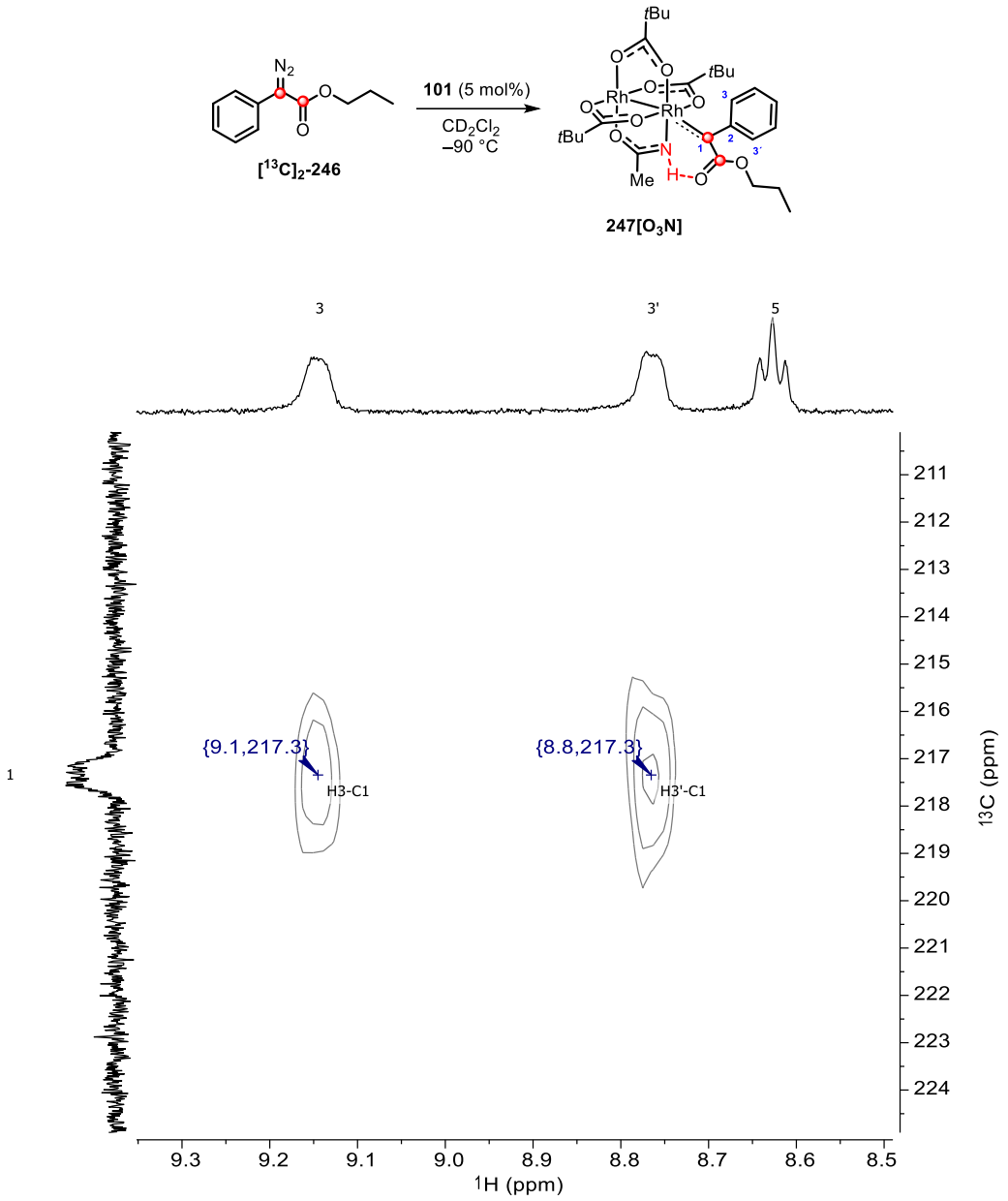

Figure 63-^{1}H-^{13}C HMBC (500 MHz, CD_2Cl_2, 183 K) showing the cross peak between the signal of the ^{13}C-labeled carbene C1 atom of carbene **247[O$_3$N]** and the two *ortho*-H atoms H3 and H3′ on the flanking phenyl ring.

The fact that the *ortho*-protons are magnetically inequivalent indicates hindered rotation around the Ar-C=M bond at –80 °C. This conformational feature is a hallmark of donor/acceptor dirhodium carbenes; prior crystallographic studies by Fürstner and co-workers demonstrated that these highly reactive intermediates typically adopt a geometry in which the aryl ring is oriented coplanar to the carbene center, facilitating effective overlap between the aromatic π-system and the vacant p-orbital of the carbene carbon.[25-26] This structural feature was further investigated by VT-NMR, in which the signals average out at elevated temperatures (Figure 64). From the acquired VT-NMR data, the coalescence temperature (T_c = 213 K) and the difference in the resonance frequency of the two inequivalent

ortho-H signals (Δν = 194 Hz) were derived. With this data, the rate of exchange (k) and the corresponding rotational barrier was calculated, which was found to be approximately 9.8 ± 0.2 kcal.

$$k_{ex} = \frac{\pi * \Delta\nu}{\sqrt{2}} = 431 \text{ Hz}$$

$$\Delta G^{\ddagger}_{Tc} = -\ln\left(\frac{k_{ex} * h}{k_B * T_c}\right) * RT = 40.8 \frac{kJ}{mol} = 9.8 \frac{kcal}{mol}$$

Physical constants: $R = 8.31446 \frac{J}{K * mol}, h = 6.63 * 10^{-34}\ J * s, k_B = 1.4 * 10^{-23} \frac{J}{K}$

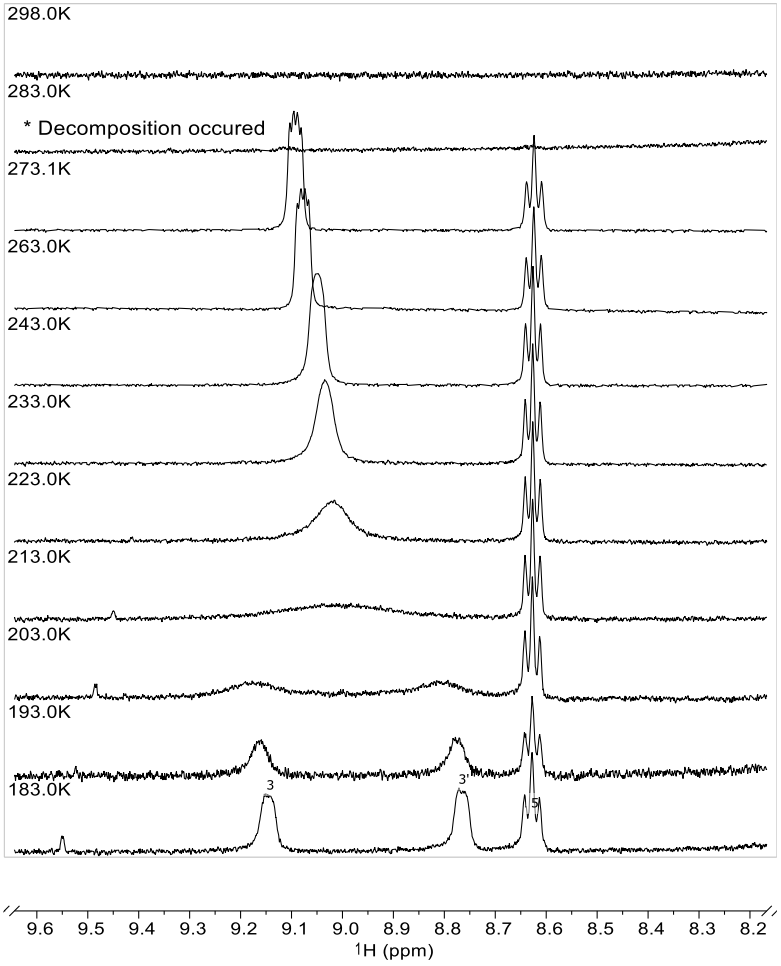

Figure 64- VT ^{1}H NMR data of carbene **247**[O_3N] showing the characteristic region of signals H3, H3' and H5.

In addition to the strong spectroscopic evidence, it was attempted to compute the ^{13}C NMR chemical shifts for carbenes **235[O_3N]**, **235[O_4]** and **248[O_4]**, to further validate the assignments. Computing such shifts of the carbene center is non-trivial, as it is strongly

influenced by the C-Rh bond for which an accurate description by DFT is challenging. Therefore, multiple computational methods were tested to compute the desired chemical shift of the target carbene intermediates (Table 13).

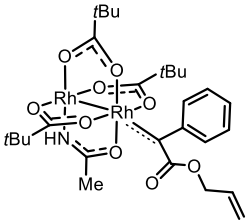

235[O$_4$]

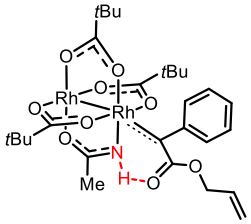

235[O$_3$N]

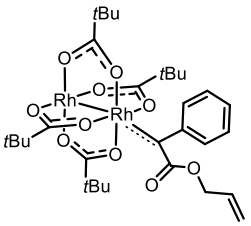

248[O$_4$]

#	Functional/basis set	ZORA/SOC	$\Delta_{248[O4]}$ [ppm]	$\Delta_{235[O3N]}$ [ppm]	$\Delta_{235[O4]}$ [ppm]
1	B3LYP/TZVPP	No/No	306.7	295.6	304.4
2	PBE0/ TZVPP	No/No	317.2	306.2	315.3
3	TPSSh/TZVPP	Yes/No	317.6	306.3	315.8
4	TPSSh/TZVPP	Yes/No	261.9	251.7	260.1
5	TPSSh/TZVPP/ decontracted basis	Yes/No	265.3	255.6	263.6
6	TPSSh/TZVPP	Yes/Yes*	237.6	227.0	235.1

Table 13- NMR shifts of the carbenic carbon for the intermediates **235**[O_3N] and **235**[O_4] and **248**[O_4] using different computational setups. (ZORA= 0th order regular approximation, SOC= spin-orbit couplings). * calculated with ADF 2017.

The computed chemical shifts were referenced to tetramethylsilane (TMS) in all calculations. Independent of the computations protocols, it can be observed that the calculated carbene carbon ^{13}C chemical shift of **235[O$_3$N]** resonates invariably at lower frequencies than the chemical shift for **235[O$_4$]**. Eventually, the best quantitative agreement with the experimental data was found by employing a composite computational protocol. This method integrates scalar relativistic single-point NMR calculations performed at the TPSSh/ZORA-def2-TZVPP + CPCM level using ORCA 5.0.3,[206-210] supplemented by spin–orbit coupling (SOC) corrections[211] computed at the PBE0 level with the Amsterdam Density Functional (ADF) 2017 software package.[212-213] Using this protocol, the calculated ^{13}C chemical shifts for complexes **235[O$_4$]** and **235[O$_3$N]** were 235.1 ppm and 227.0 ppm, respectively. These values are in excellent agreement with the experimentally observed resonances at 232.0 ppm and 215.2 ppm. Additionally, the predicted shift for the ester carbonyl carbon in **235[O$_3$N]**

(174.7 ppm) closely matched the experimental value (177.7 ppm), further validating the accuracy and reliability of the composite method employed.

7.3. Conclusion

In this chapter, the innate role of amidate ligands on the reactivity and selectivity of dirhodium paddlewheel complexes in catalysis was investigated. Notably, the effect of the amidate ligand differs strongly depending on the nature of the catalytic transformation in which it is involved.

In the case of the *intermolecular* cyclopropanation shown in Figure 49, the incorporation of a primary amidate ligand into the catalyst — further assisted by the steric bulk of the triphenylcyclopropyl ligands of **25** — not only enhances reactivity but also dictates the selectivity when compared to its carboxylate-counterpart. The protic equatorial ligand promotes preferential carbene formation at the [O_3N]-face through interligand hydrogen bonding with the carbonyl functionality of the donor/acceptor carbene. Detailed computational analysis (Figure 52) revealed that the **230[O_3N]** intermediate is thermodynamically more stable and features a lower TS energy compared to the carbene residing at the [O4]-face, hence making it more reactive. This hydrogen bonding interaction persists throughout the reaction coordinate, providing a consistent enthalpic advantage that accounts for the high reactivity and excellent enantioselectivity observed in the transformations catalyzed by complex **25**.

In contrast, in an *intramolecular* setting, the scenario becomes more complicated—particularly when smaller equatorial ligands are used, which allow the incoming diazoester to reach both faces of a heteroleptic catalyst such as complex **101** with similar ease. Interestingly, kinetic studies of complexes **100-101** and **233-234** revealed that the amidate-containing catalysts exhibit significantly lower reactivity than their carboxylate analogues. Computational analysis of the full reaction coordinate of the cyclopropanation with complex **101** showed that the carbene intermediate at the [O_3N]-face is again more stable. However, during the cyclopropanation event the hydrogen bond becomes distorted as the tethered olefin approaches the reactive center, resulting in a higher TS energy. In contrast, ring formation at the [O_4]-face does not suffer from such a distortion and proceeds via a lower-energy transition state. As a result of these opposing factors, the reaction likely proceeds at both rhodium sites to some extent.

Remarkably, the computed reaction profile indicated that cyclopropanation, rather than carbene formation, constitutes the turnover-limiting step, in contrast to what had been assumed in the literature so far**.** To experimentally verify these computational observations, *in*

situ ^{13}C NMR spectroscopy was employed to detect the carbene intermediates. For the first time ever, such reactive intermediates were observed under truly catalytic conditions with both $[Rh_2(OPiv)_4]$ and complex **101**. In the latter case, the carbene bound to the $[O_3N]$-face was uniquely observed at a chemical shift of 215.2 ppm, as confirmed by the ^{13}C NMR predictions calculated by DFT. These findings align well with the computational prediction that the $[O_3N]$-bound carbene is more stable yet less reactive, explaining why only this species was detected.

Together, the computational, kinetic, and spectroscopic data presented in this chapter clearly demonstrate that the rate-determining step in the intramolecular cyclopropanation with complex **101** is the formation of the cyclopropane ring itself. This finding stands in contrast to the widely accepted view that carbene formation constitutes the turnover-limiting step as originally postulated by Davies and Autschbach. Therefore, it is important to emphasize that one has to be aware about such generalizations, as the equatorial ligands of dirhodium complexes have far more subtle effects on reactivity and selectivity in a catalytic transformation.

8. Summary

Cyclopropanes are the smallest carbocyclic motifs and are prevalent building blocks in medicines, agrochemicals and natural products. Due to their unique structural and electronic characteristics and the widespread applications in which these molecules are used, the construction of cyclopropanes has remained a key focus point in organic synthesis, particularly in asymmetric fashion. One of the most powerful ways of obtaining cyclopropane motifs with high optical purity is via dirhodium(II)-catalyzed cyclopropanations. Dirhodium(II) paddlewheel complexes are highly reactive species due to the "superelectrophilic" nature of the corresponding carbenes and are typically air and moisture stable, making them easy to handle. Many different versions have been developed over the last decades; the majority of these catalysts typically consist of four identical chiral ligands that envelope the reactive rhodium metal center. Due to the proximity of the chiral environment near the reactive center, high levels of stereoinduction can be obtained in the desired [2+1]-cycloaddition reactions. However, there are certain limitations; specific cyclopropane motifs are particularly challenging to obtain with high levels of optical purity.

Over the last decade, our group has sought to address those limitations, and has been actively engaged in the development of novel types of rhodium(II) complexes. One notable outcome of this work was the development of a new class of chiral bismuth–rhodium catalysts, whose performance is driven by London dispersion interactions. These catalysts outperformed established chiral dirhodium complexes in terms of enantioinduction, achieving superior results in both the cyclopropanation and C–H insertion reactions of aryl diazoesters. Additionally, a heteroleptic complex **29** was developed that proved uniquely effective in the cyclopropanation of α-metallated diazoesters, delivering high levels of enantioinduction. Building on this success, a second generation of such heteroleptic complex was designed (**31**) to overcome the poor diastereoselectivity observed with the prototype. This improved catalyst achieved both high enantioselectivity and pronounced *trans*-diastereoselectivity.

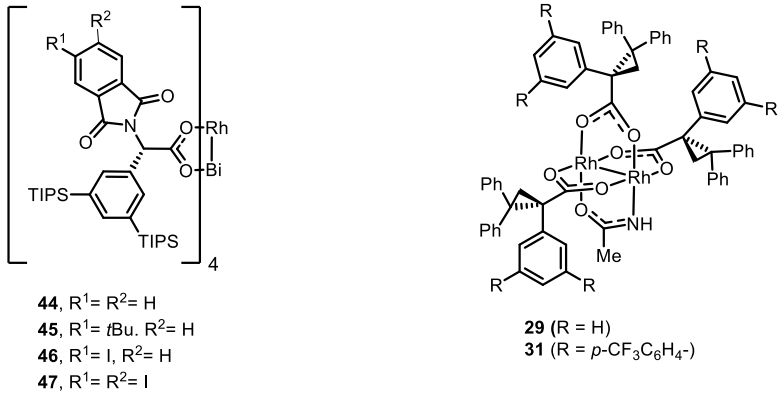

Figure 65- Overview of Bi-Rh(II) and Rh_2(II)-complexes previously developed in the Fürstner group.

Building on this prior knowledge, the primary objective of this thesis was twofold: first, to broaden the applicability of the catalysts previously developed in our group towards challenging asymmetric cyclopropane motifs, and second, to advance the design of heteroleptic amidate-containing complexes.

One such challenging motif is 2-furyl substituted cyclopropanes, of which no asymmetric variant is known to date. The main reason for this synthetic challenge is that the corresponding 2-furyl diazo derivatives are highly unstable as they can readily undergo electrocyclic ring opening. Therefore, a protocol was developed in this work, in which the desired 2-furyl cyclopropanes could be formed in a highly enantioenriched manner. A hydrazone relay approach, utilizing *N*-triftosylhydrazone **58** as a stable, crystalline diazo surrogate successfully provided access to 2-(1-(trifluoromethyl)cyclopropyl)furan derivatives. Key to obtaining a high level of asymmetry in this transformation was the use of chiral bismuth-rhodium(II) catalyst **47**. This new methodology led to a diverse range of 2-furylcyclopropanes or cyclopropenes with excellent diastereo- and enantioselectivity.

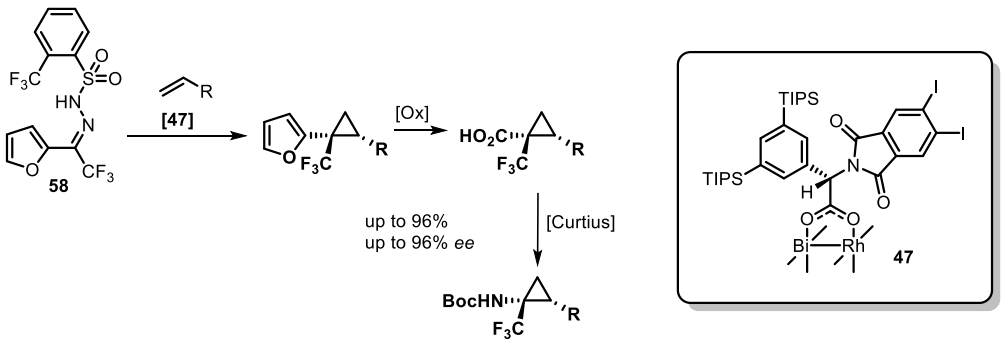

Scheme 66-Asymmetric cyclopropanation of 2-furyl hydrazone **58** via a hydrazone relay approach with **47**.

Furthermore, oxidative cleavage of the furan moiety gave access to 1-(trifluoromethyl)cyclopropane-1-carboxylic acid derivatives in a highly asymmetric fashion, which could not be made by any other method with high optical purity so far. Moreover, it was shown that such carboxylic acids serve as valuable building blocks for further downstream functionalization such as peptide-couplings and Curtius rearrangement, giving access to the corresponding cyclopropanes in a stereoretentive manner.

A novel chiral dirhodium catalyst was developed, which conceptually stands out from the traditional dirhodium complexes in the sense that it bears its chirality on the metal centers itself and not on the ligand sphere. Only a single type of (homo)chiral-at-metal dirhodium complexes has previously been reported in the literature. This type of complexes existed of two *ortho*-metalated phosphine ligands in a head-to-tail arrangement and two trifluoroacetate ligands, which had shown its (limited) potential in the intramolecular cyclopropanation and C–H insertion reactions of diazoketones. For our design, we envisioned to use an amidate ligand and a sterically encumbered *cisoid* chelating diacid, resulting in a heterochiral-at-metal dirhodium complex. This approach was inspired by the promising performance of the amidate ligand in [Rh_2(acam)(*R*-TPCP)$_3$], which has been successfully applied to the cyclopropanation of α-stannylated diazoesters. In this context, a prototype complex **134** was synthesized in just two steps from [Rh_2(acam)$_4$] by selective ligand replacement methods, that have been further improved and developed in this work. The enantiopure complexes ***P*-134** and ***M*-134** were obtained through HPLC separation on a chiral stationary phase, which proved essential for accessing the enantiomerically pure materials.

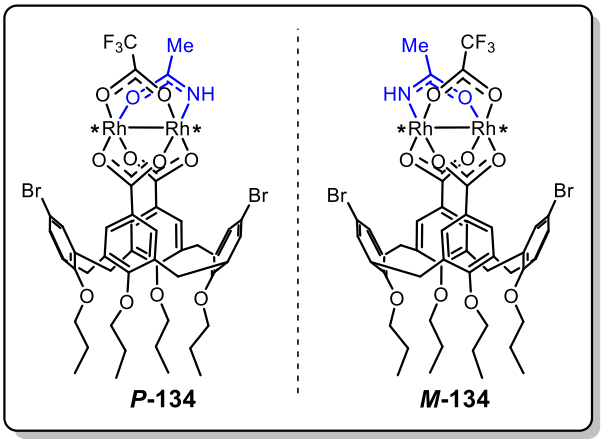

Figure 66-Novel heterochiral-at-metal dirhodium paddlewheel complex **134** (both enantiomers depicted).

Catalyst **134** could be successfully employed in the cyclopropanation reaction of α-stannylated diazoesters, leading to exceptionally high levels of enantioselectivity and moreover *cis*-diastereoselectivity. This outcome is complementary to the *trans*-diastereoselectivity

obtained in such transformations with **31**, as previously described in our group. Similar to catalyst **31**, extensive DFT studies into the mode of action of prototype complex **134** showed that a hydrogen-bonding interaction between the amidate ligand and the carbonyl moiety of the carbene is key to the success as it restricts the conformational freedom of the carbene intermediate.

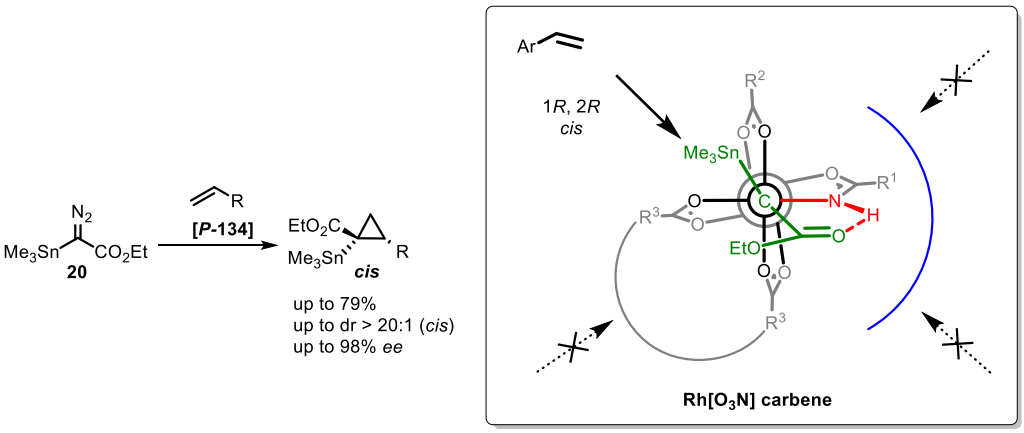

Scheme 67-Asymmetric cyclopropanation of α-stannylated diazoester **20** with ***P*-134** and a graphical representation showcasing the favored olefin trajectory towards the corresponding carbene intermediate.

The applicability of complex **134** is not only limited to α-stannylated diazoesters, but also showed its superiority in the cyclopropanation of α-trifluoromethyl diazoesters, leading to the corresponding cyclopropanes in high enantioselectivity and good *trans*-diastereoselectivity. No other catalyst to date is capable of achieving such high levels of enantioselectivity, as the highest levels of enantiomeric induction previously reported reached a mere 50% *ee* with $[Rh_2(S\text{-DOSP})_4]$; thus, the level of stereoinduction obtained with ***P*-134** is truly remarkable. The *trans*-diastereoselectivity can be explained by extensive DFT studies which have shown that in addition to the hydrogen-bonding interactions, the catalytic system also picks up dispersive fluorine-bromine interactions between the CF_3- group of the diazo compound and the bromo-substituents of the calix[4]arene unit. Therefore, the carbene retains the initial conformation when the olefin approaches, leading to the corresponding isomer.

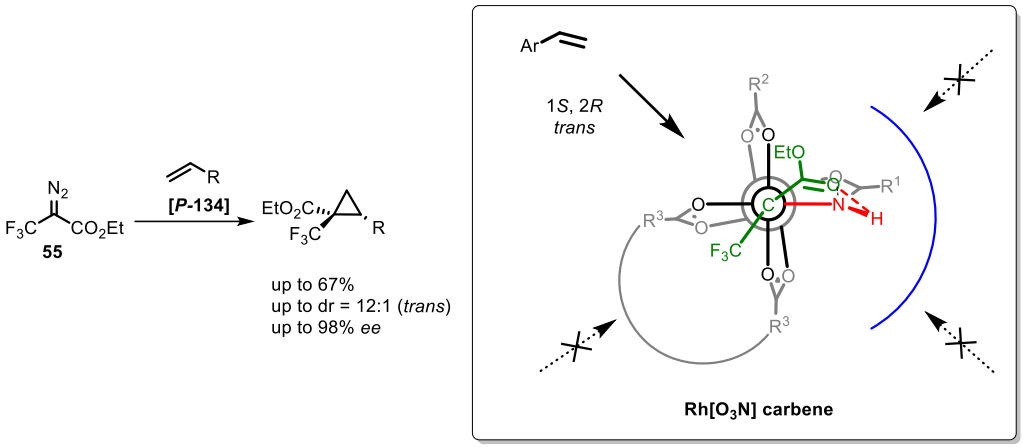

Scheme 68-Asymmetric cyclopropanation of α-trifluoromethylated diazoester **55** with ***P*-134** and a graphical representation showcasing the favored olefin trajectory towards the corresponding carbene intermediate.

Furthermore, the prototype catalyst showed potential in the cyclopropanation reactions of the more traditional aryl diazo esters. Attempts to further improve the prototype catalyst by replacement of the bromo-substituents of the calix[4]arene unit by a variety of other substituents proved less rewarding. The level of asymmetric induction reached (~70% *ee*) is acceptable, however does not surpass the levels of enantioinduction obtained with the current state-of-the-art catalysts. Incorporation of fluorine-atoms on the aryl ring of such diazo compounds might improve the level of enantioselectivity reached with ***M*-134** as it potentially can benefit from the dispersive fluorine-bromine interactions, leading to a more energetically favored carbene conformer, and thus higher levels of enantioselectivity. These prospects will be of further interest in our laboratory.

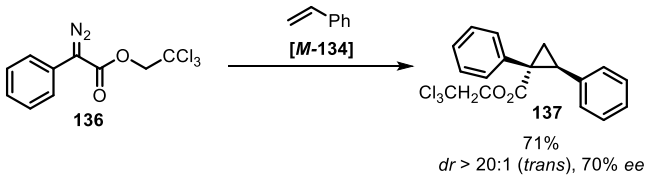

Scheme 69-Best result of initial studies in the asymmetric cyclopropanation of aryl diazoester **136** with ***M*-134**.

Attempts to obtain chiral-at-metal bismuth–rhodium(II) complexes were unsuccessful, particularly with respect to the isolation of these complexes in enantiopure form. The main challenges lie within finding suitable conditions for the HPLC separation on a chiral stationary phase and the inherent instability during workup. These observations suggest that the bismuth-rhodium complexes possess significantly lower stability compared to their dirhodium counterparts.

Furthermore, the innate role of amidate ligands on the reactivity and selectivity of a variety of heteroleptic dirhodium paddlewheel complexes was examined in catalysis. An intramolecular cyclopropanation reaction of diazo compound **231** was performed in which a series of simple dirhodium(II) complexes (**100-101** and **233-234**) and more bulky TPCP-containing complexes (**25** and **229**) were tested. Notably, the effect of the amidate ligand on the reactivity differed strongly depending on the complex employed in the transformation. A comprehensive computational analysis of the full reaction coordinate with complex **101** showed that the carbene intermediate formed at the [O_3N]-face is thermodynamically more stable due to the favorable H-bonding interactions between the carbene and the –NH moiety of the amidate ligand. Even more remarkable was the finding that the cyclopropanation event rather than carbene formation constitutes the turnover-limiting step. This finding stands in contrast with the widely accepted view that carbene formation constitutes the turnover-limiting step as originally described by Davies and Autschbach. Therefore, it is important to emphasize that one has to be aware about such generalizations, as the equatorial ligands of dirhodium complexes have far more subtle effects on reactivity and selectivity in a catalytic transformation. This observation was further verified by detection of the carbene intermediate under truly catalytic settings via *in situ* ^{13}C NMR spectroscopy. The observation of such reactive intermediates under catalytic conditions was unprecedented. With complex **101**, only one resonance at 215.2 ppm was observed, corresponding to the [O_3N]-bound carbene, as it is the more thermodynamically stable one of the two.

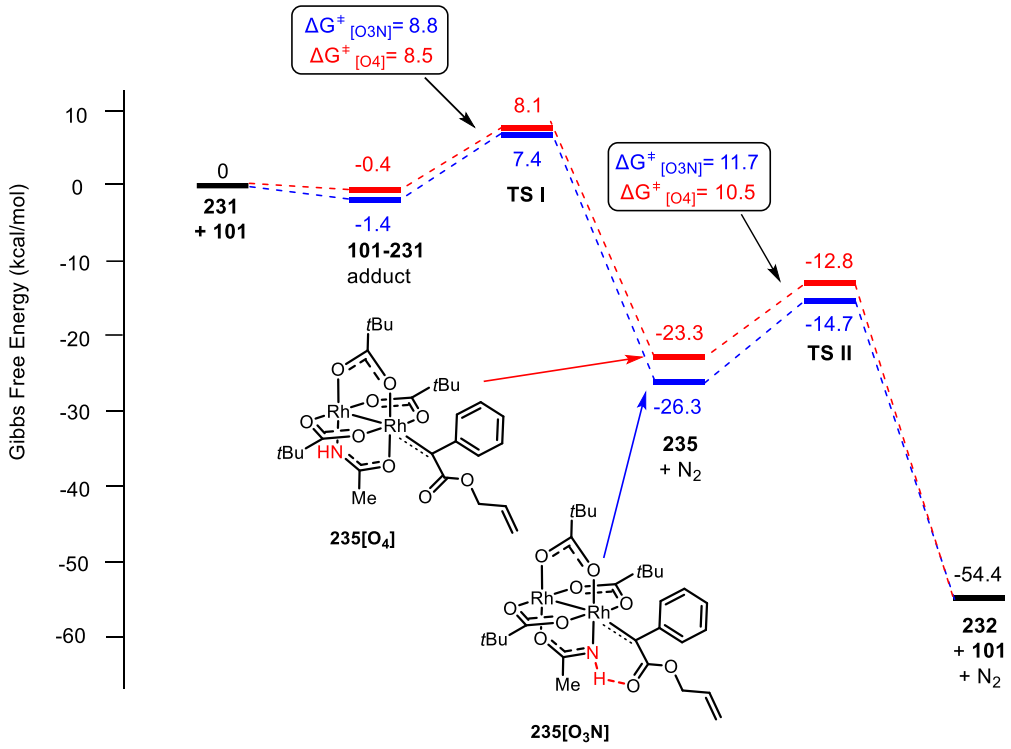

Figure 67-Gibbs free energy profile of the intramolecular cyclopropanation of **231** into **232** catalyzed by complex **101**.

Lastly, ^{103}Rh NMR studies were performed on axially ligated adducts of dirhodium paddlewheel complexes. The aim of these studies was to gain more insight in the electronics of these adducts. Adducts with NHCs or phosphines had been previously investigated by ^{103}Rh triple resonance NMR spectroscopy, however only one of the two ^{103}Rh chemical shifts could be obtained. Now, we report two alternative ways that overcome this hurdle; by either using a ^{103}Rh–^{31}P{^{1}H} HMBC experiment in the case of phosphine adducts; or by usage of a ^{1}H–^{103}Rh HMBC experiment for Rh(II) phosphine/NHC-adducts in the cases were [Rh_2(formate)$_4$] is used. Importantly, this methodology was extended to a reactive donor/donor carbene intermediate (**224**), for which the ^{103}Rh chemical shifts could be obtained. The resulting data revealed that the chemical environment at rhodium in **224** resembles the most of that of NHC adduct; however, the distal rhodium nucleus is more shielded than in the NHC adduct.

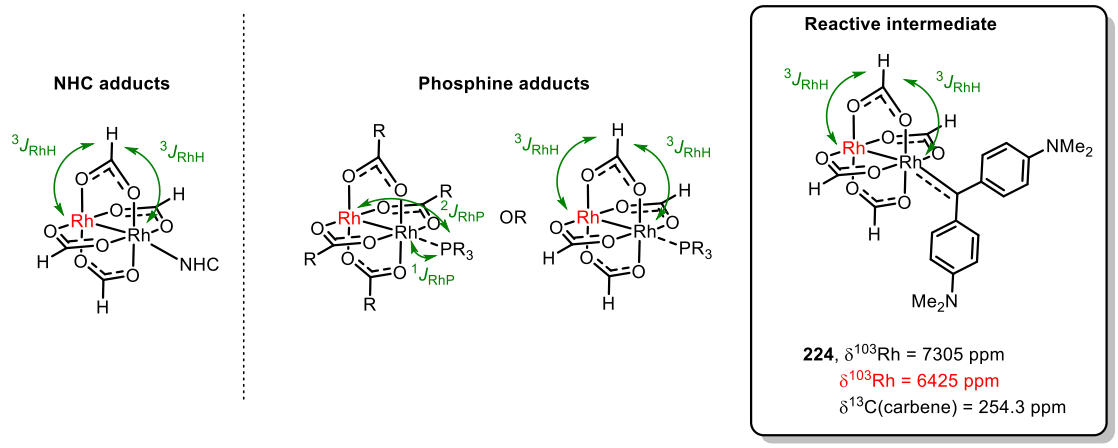

Figure 68-^{103}Rh NMR techniques to measure both ^{103}Rh chemical shifts of the Rh(II) nuclei of phosphine adducts, NHC adducts and reactive carbene intermediate **224**.

To rationalize the influence of different axial ligands on the electronic environment at rhodium, particularly in terms of donor strength, a more in-depth understanding is required. Therefore, ongoing DFT calculations will be crucial to gain insights on how the observed chemical shifts can be correlated to the ligand donor properties.

9. Experimental Section

9.1. General Information

Unless stated otherwise, all reactions were carried out under argon atmosphere in flame-dried Schlenk glassware, ensuring inert conditions. The solvents were purified by distillation over the indicated drying agents and were transferred under argon: THF, Et_2O (Mg/anthracene); pentane, toluene (Na/K); CH_2Cl_2 (CaH_2). MeCN was dried by an absorption solvent purification system based on molecular sieves. Flash chromatography: Merck Geduran silica gel 60 (40 – 63 µm). Thin layer chromatography (TLC): Macherey-Nagel precoated plates (POLYGRAM®SIL/UV254); visualization by UV light (254 nm) and by staining with solutions of phosphomolybdic acid (PMA), $KMnO_4$ or cerium ammonium nitrate (CAN).

NMR spectra were recorded on a Bruker Avance III HD nanobay 300, Avance III HD 400, Avance III 500 or Avance Neo 600 MHz NMR spectrometer. ^{1}H and ^{13}C NMR chemical shifts are given in ppm relative to Me_4Si (δ = 0 ppm), coupling constants (*J*) in Hz. ^{1}H and ^{13}C NMR chemical shifts were referenced using the solvent signals internal reference;[214] For ^{1}H NMR the following residual proton peaks of the deuterated solvents were used: $CDCl_3$, δ H($CHCl_3$) 7.26 ppm; CD_2Cl_2, δ H ($CHDCl_2$) 5.32 ppm; [D_8]-THF, δ H($(CD_2)_3CHDO$) 3.58 ppm; CD_3CN, δ H(CHD_2CN) 1.94 ppm. For ^{13}C NMR: $CDCl_3$, δ 77.16 ppm; CD_2Cl_2, δ 54.0 ppm; [D_8]-THF, δ 67.57 ppm; CD_3CN, δ 1.32 ppm. Signal assignments were established using ^{1}H–^{13}C-edited-HSQC and ^{1}H–^{13}C-HMBC experiments. ^{19}F and ^{103}Rh NMR shifts were referenced indirectly to the ^{1}H NMR frequency of the sample with the 'xiref'-macro in Bruker TOPSPIN3.6.2 (for ^{103}Rh)/TOPSPIN 4.0.6.2 ^{19}F shifts are reported relative to $\delta(CFCl_3)$ = 0 ppm ($\Xi(^{19}F)$= 94.094011%). ^{103}Rh NMR shifts are referenced to $\Xi(^{103}Rh)$ = 3.16% unless indicated otherwise. ^{119}Sn NMR spectra were recorded using Me_4Sn as an external standard. Unless stated otherwise, all ^{13}C, ^{19}F and ^{119}Sn spectra were recorded in {1H}-decoupled manner. For simple ^{1}H–^{103}Rh experiments, a 5 mm BBFO probe (^{1}H, ^{19}F & ^{31}P-^{109}Ag) with z-gradient was used which could be tuned on the X-channel to ^{103}Rh beyond the specifications. For the triple-resonance H, C, Rh experiments a 5 mm TBI probe (^{1}H, ^{31}P-^{109}Ag, ^{13}C) with z-gradient coil which could be tuned on the broadband X-channel to ^{103}Rh beyond the specifications. For the P, Rh experiments a QUAD systems 5 mm Probe (^{1}H/^{19}F, ^{31}P, 89Y-^{103}Rh/187Os) equipped with a z-gradient was used. For the 2D X-Rh HMBC measurements standard sequences from the Bruker library were used (hmbcgpqfnd). For the $^{31}P\{^{1}H\}$-^{103}Rh HMBC measurements, a low-power proton ^{1}H decoupling of the aromatic signals was additionally applied during the pulse sequence.

MS (EI): Finnigan MAT 8200 (70 eV), ESI-MS: ESQ 3000 (Bruker) or Thermo Scientific LTQ-FT or Thermo Scientific Exactive Spectrometer. HRMS: Bruker APEX III FT-MS (7T magnet), MAT 95 (Finnigan), Thermo Scientific LTQ-FT or Thermo Scientific Exactive Spectrometer.

Optical rotations were measured with an A-Krüss Otronic Model P8000-t polarimeter at a wavelength of 589 nm. The values are given as specific optical rotation with exact temperature, concentration (c in g/100 mL) and solvent.

HPLC: analytical LC analyses were conducted on a Shimadzu LC 2020 instrument equipped with a Shimadzu SPD-M20A UV/VIS detector or Agilent system equipped with a G4212A 1290 DAD. Preparative separations were performed on a Shimadzu Prominence prep HPLC system equipped with two LC-20 AP preparative pumps, a SIL-20 AC HT sample injector, CTO-20AC oven, SPD-20A UV-detector with variable flow cell, a FRC-10 A fraction collector and a CBM 20A controller module. The specific column employed and respective solvent mixtures are indicated for each experiment.

UV-VIS measurements have been performed from 1200 nm to 200 nm at room temperature on an Agilent Cary6000i double beam spectrometer. The circular dichroism spectra were measured on a J-1100 CD UV-Visible/NIR spectrometer, High precision cells made of quartz Suprasil Hellma Analytics cuvettes were used for the measurements.

Unless stated otherwise, all commercially available compounds (Alfa Aesar, Sigma Aldrich, TCI, BLD Pharm, ABCR and SCBT) were used as received.

9.2. Preparation of Carbene Precursors

9.2.1. Synthesis of Starting Materials

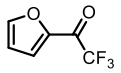

2,2,2-Trifluoro-1-(furan-2-yl)ethan-1-one (56). n-BuLi (1.6 M solution in hexanes, 27.5 mL, 44 mmol) was added dropwise over 20 min to a stirred solution of furan (2.90 mL, 40 mmol) in THF (80.0 mL) at 0 °C (ice bath). Once the addition was complete, stirring was continued for 30 min before the solution was cooled to −78 °C. Ethyl trifluoroacetate (7 mL, 58 mmol) was added dropwise at this temperature to the reaction mixture. The solution was then allowed to warm to ambient temperature and stirring was continued overnight. The reaction was quenched with sat. aq. NH_4Cl and the aqueous layer was extracted with diethyl ether. The combined organic phases were dried over $MgSO_4$, filtered and concentrated. The residue was purified by flash chromatography (hexanes/EtOAc 95:5) to afford the title compound as a yellow oil (53 %, 3.5 g). The spectral data were consistent with those previously reported in the literature.[215]

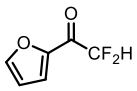

2,2-Difluoro -1-(furan-2-yl)ethan-1-one (249). Prepared analogously to **56** from difluoroacetic acid as a yellow oil (2.7 g, 54%). The spectral data were consistent with those previously reported in the literature. [216]

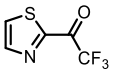

2,2,2-Trifluoro-1-(thiazol-2-yl)ethan-1-one (250). A solution of 2-bromothiazole was added dropwise over 30 min to a stirred solution of *n*-BuLi (8.4 mL, 0.8 M in hexanes, 6.7 mmol) at –78 °C. After stirring for 30 min at –78 °C, a solution of ethyltrifluoracetate (1.31 mL, 11 mmol) in Et_2O (2.5 mL) was added dropwise. The reaction mixture was stirred for 1 h 30 min at –78 °C, then warmed to room temperature and quenched with aq. $NaHCO_3$ solution (50 mL). The two liquid layers were separated and the aqueous phase was extracted with Et_2O (3 x 25 mL). The combined organic phases were washed with brine (50 mL), dried with $MgSO_4$, filtered and concentrated under reduced pressure. The crude material was purified by flash chromatography (silica, hexane/EtOAc 2:1 + 1% TEA to 100% EtOAc) afforded the title compound as a white solid in hydrated form (532 mg, 48%). ^{1}H NMR (400 MHz, CD_3CN) δ 7.86 (d, *J* = 3.2 Hz, 1H), 7.67 (d, *J* = 3.2 Hz, 1H), 5.93 (s, 2H, hydrate). ^{13}C NMR (101 MHz, CD_3CN) δ 167.0, 143.8, 124.8 (q, *J* = 286.4 Hz), 124.1, 93.1 (d, *J* = 33.2 Hz). IR (ATR): $\tilde{\nu}$ = 1208, 1166, 1115, 1074, 1050, 913, 743, 609 cm^{-1}. HRMS (EI) m/z calcd. for $C_5H_2ONSF_3$ $[M]^+$: 180.98037; found: 180.98068.

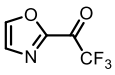

2,2,2-Trifluoro-1-(oxazol-2-yl)ethan-1-one (251). Oxazole (200 mg, 0.19 mmol) in THF (20 mL) was added dropwise *n*-BuLi (2 mL, 1.6 M in hexanes, 3.19 mmol) at –78 °C. The yellow colored solution was stirred for 1h30 at this temperature, followed by dropwise addition of ethyltrifluoroacetate (0.52 mL, 4.34 mmol). The mixture was allowed to warm to room temperature and stirred overnight. The reaction mixture was diluted with EtOAc (20 mL) and washed with water (80 mL). The organic layer was dried with $MgSO_4$, filtered and concentrated under reduced pressure. The crude material was purified by flash chromatography (silica, hexane/EtOAc 3:1 to 1:1) to afford the title compound as an off-white solid in hydrated form (260 mg, 54%). ^{1}H NMR (400 MHz, CD_3CN) δ 7.92 (d, *J* = 0.9 Hz, 1H), 7.23 (d, *J* = 0.9 Hz, 1H), 5.95 (s, 2H, hydrate). ^{13}C NMR (101 MHz, CD_3CN) δ 159.5, 142.5, 128.4, 124.4 (q, *J* = 285.9 Hz), 90.8 (d, *J* = 34.5 Hz). ^{19}F NMR (282 MHz, CD_3CN) δ -74.83. IR (ATR): $\tilde{\nu}$ = 1208, 1185, 1143, 1113, 1079, 1061, 985, 913, 788, 510 cm^{-1}. HRMS (EI) m/z calcd. for $C_5H_2O_2NF_3$ $[M]^+$: 165.00321; found: 165.00349.

Allyl 2-phenylacetate (252). Phenyl acetic acid (0.5 g, 12.2 mmol) was dissolved in CH_2Cl_2 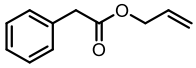 (0.1 M), followed by addition of allylalcohol (0.3 mL, 4.4 mmol) and DMAP (45 mg, 0.37 mmol). The reaction mixture was cooled to 0 °C and stirred for 15 min prior to portionwise addition of EDC·HCl (0.84 g, 4.4 mmol). After full consumption of the starting material, the reaction was diluted with water (30 mL) and extracted with CH_2Cl_2 (3 x 20 mL). The organic phase was washed with brine (30 mL), dried over $MgSO_4$ and concentrated under reduced pressure. The residue was purified by flash chromatography (silica, pentane/MTBE 19:1) which afforded the title compound as a colorless oil (587 mg, 91%). The spectral data were consistent with those previously reported in the literature.[217]

Allyl 2-phenylacetate-α,β-$^{13}C_2$ ([^{13}C]$_2$-252). Prepared analogously to **252** from phenylacetic 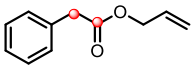 acid-α,β-$^{13}C_2$ and allylalcohol as a colorless oil (470 mg, 91%). ^{1}H NMR (400 MHz, $CDCl_3$) δ 7.36 – 7.27 (m, 5H), 5.91 (ddt, *J* = 17.2, 10.4, 5.7 Hz, 1H), 5.27 (dq, *J* = 17.2, 1.5 Hz, 1H), 5.22 (dq, *J* = 10.4, 1.3 Hz, 1H), 4.64 – 4.56 (m, 2H), 3.66 (dd, *J* = 129.6, 7.9 Hz, 2H).^{13}C NMR (101 MHz, $CDCl_3$) 171.4 (d, *J* = 57.5 Hz), 134.1 (dd, *J* = 43.9, 3.0 Hz), 132.2 (d, *J* = 2.2 Hz), 129.7 – 129.2 (m), 128.7 (d, *J* = 3.7 Hz), 127.3, 118.4, 65.6 (dd, *J* = 2.5, 1.2 Hz), 41.5 (d, *J* = 57.7 Hz). IR (ATR): $\tilde{\nu}$ = 1690, 1496, 1454, 1272, 1222, 1123, 986, 928, 758, 696 cm^{-1}. HRMS (EI): [M]$^+$: 178.08989; found: 178.08979.

Propyl 2-phenylacetate- α,β-$^{13}C_2$ ([^{13}C]$_2$-253). Prepared analogously to **252** from 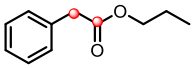 phenylacetic acid-α,β-$^{13}C_2$ and 1-propanol as a colorless oil (287 mg, 89%). ^{1}H NMR (400 MHz, $CDCl_3$) δ 7.37 – 7.21 (m, 5H), 4.06 (td, *J* = 6.7, 3.0 Hz, 2H), 3.62 (dd, *J* = 129.5, 7.9 Hz, 2H), 1.71 – 1.58 (m, 2H), 0.91 (t, *J* = 7.4 Hz, 3H). ^{13}C NMR (101 MHz, $CDCl_3$) δ 171.82 (d, *J* = 57.6 Hz), 134.34 (dd, *J* = 43.8, 2.9 Hz), 129.42 – 129.31 (m), 128.67 (d, *J* = 3.8 Hz), 127.15, 66.58 (dd, *J* = 2.7, 1.1 Hz), 41.60 (d, *J* = 57.6 Hz), 22.08 (d, *J* = 2.2 Hz), 10.46. IR (ATR): $\tilde{\nu}$ = 2968, 1689, 1496, 1455, 1227, 1131, 969, 703 cm^{-1}. HRMS (EI): [M]$^+$: 180.10554; found: 180.10539.

2,2,2-Trichloroethyl 3,3,3-trifluoropropanoate (174). Prepared analogously to **252** from 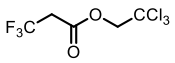 3,3,3-trifluorpropionic acid and trichloroethanol as a colorless oil (1.04 g, 79%).^{1}H NMR (400 MHz, $CDCl_3$) δ 4.83 (s, 2H), 3.35 (q, *J* = 9.8 Hz, 2H). ^{13}C NMR (101 MHz, $CDCl_3$) δ 162.8 (d, *J* = 4.4 Hz), 123.1 (q, *J* = 275.7 Hz), 94.2, 74.7, 39.5 (q, *J* = 31.7 Hz). ^{19}F NMR (282 MHz, $CDCl_3$) δ –63.4. IR (ATR): $\tilde{\nu}$ = 1768, 1393, 1266, 1201, 1108, 1023, 747, 717, 594, 569 cm^{-1}. HRMS was not successful.

9.2.2. Diazo/ Hydrazone Synthesis

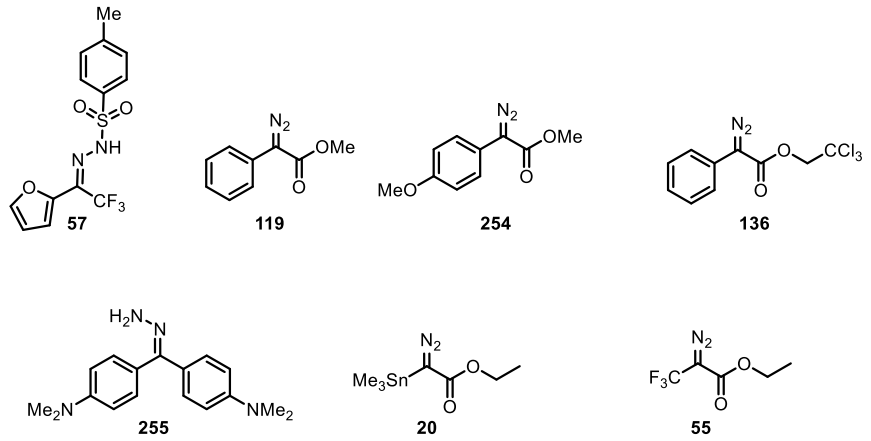

Figure 69- Overview of diazo compounds and hydrazone precursors that were synthesized according to the literature.

Compounds **57**[218], **119**[81], **254**[219], **255**[220], **55**[150], **20**[80] and **136**[221] were prepared according to the literature. The characterization data matched the reported data.

Allyl 2-diazo-2-phenylacetate (231). A solution of allyl ester **252** (801 mg, 4.54 mmol) and

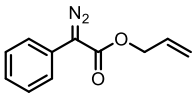

4-acetamidobenzenesulfonyl azide (*p*-ABSA) (1.4 g, 5.9 mmol) in acetonitrile (10 mL) was cooled in an ice bath to 0 °C, then DBU (0.94 mL, 6.27 mmol) was added. The mixture was warmed to room temperature and stirred overnight before being diluted with water (30 mL). The mixture was extracted with CH_2Cl_2 (2 x 25 mL) and the combined organic layers were washed with water (50 mL), dried over $MgSO_4$ and concentrated under reduced pressure in the presence of Celite. The crude product was purified by flash chromatography (silica, pentane/EtOAc 50:1 to 30:1) which afforded the title compound as a yellow oil (715 mg, 78%). The spectral data were consistent with those previously reported in the literature.[216]

Allyl 2-diazo-2-phenylacetate-α,β-$^{13}C_2$ ([^{13}C]$_2$-231). Prepared analogously to **231** from the

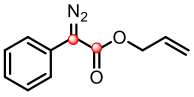

[^{13}C]$_2$-252 to afford the title compound as a red oil (250 mg, 68%). ^{1}H NMR (400 MHz, $CDCl_3$) δ 7.54 – 7.45 (m, 2H), 7.44 – 7.34 (m, 2H), 7.23 – 7.14 (m, 1H), 5.99 (ddt, J = 17.2, 10.5, 5.6 Hz, 1H), 5.37 (dq, J = 17.2, 1.5 Hz, 1H), 5.28 (dq, J = 10.4, 1.3 Hz, 1H), 4.82 – 4.74 (m, 2H).^{13}C NMR (101 MHz, $CDCl_3$) δ 164.98 (d, *J* = 95.9 Hz), 132.24 (d, *J* = 2.1 Hz), 129.09 (d, *J* = 4.6 Hz), 126.01 (d, *J* = 1.2 Hz), 125.58 (dd, *J* = 69.2, 3.7 Hz), 124.15 (dd, *J* = 2.9,1.4 Hz), 118.52, 65.81 – 65.34 (m), 63.42 (d, *J* = 95.9 Hz). IR (ATR): $\tilde{\nu}$ = 2079, 1659, 1497, 1308, 1210, 1130, 1041, 1014, 993, 932, 750, 690, 667 cm^{-1}. HRMS (ESI$^+$): $[M+Na]^+$: 227.07017; found: 227.07013.

Propyl 2-diazo-2-phenylacetate-α,β-$^{13}C_2$ ([^{13}C]$_2$-246). Prepared analogously to **231** from the **[^{13}C]$_2$-253** to afford the title compound as a red oil (96 mg, 42 %). ^{1}H NMR (400 MHz, CDCl3) δ 7.53 – 7.44 (m, 2H), 7.43 – 7.33 (m, 2H), 7.23 – 7.14 (m, 1H), 4.24 (td, *J* = 6.6, 3.1 Hz, 2H), 1.80 – 1.67 (m, 2H), 0.99 (t, *J* = 7.4 Hz, 3H). ^{13}C NMR (101 MHz, $CDCl_3$) δ 165.4 (d, *J* = 95.3 Hz), 125.89 (d, *J* = 1.2 Hz), 125.79 (dd, *J* = 65.3, 3.8 Hz), 124.11 (dd, *J* = 2.9, 1.4 Hz), 66.92 – 66.38 (m), 63.44 (d, *J* = 95.3 Hz), 22.3 (d, *J* = 2.2 Hz), 10.5. IR (ATR): $\tilde{\nu}$ = 2969, 2080, 1661, 1497, 1310, 1213, 1136, 1062, 1007, 752, 691 cm^{-1}. HRMS (ESI$^+$): [M+Na]$^+$: 229.085806; found: 229.085680.

***N*'-(2,2,2-Trifluoro-1-(furan-2-yl)ethylidene)-2-(trifluoromethyl)benzenesulfono hydrazide (58).** A round bottom flask was charged with trifluoromethyl ketone **56** (5.4 g, 31.55 mmol) and trifluorotoluene (TFT):EtOAc (30:1, 62 mL). o-Trifluoromethylbenzenesulfonyl hydrazide[222] ($TfsNHNH_2$, 6.3 g, 26.3 mmol) and $Et_2O \cdot BF_3$ (3.9 mL, 31.55 mmol) were then added and the resulting mixture was stirred at room temperature until a clear solution had formed (~2 h). The mixture was then stirred at 40 °C (bath temperature) for 16 h. The mixture was concentrated under reduced pressure and the residue was purified by flash chromatography (hexane/EtOAc, 6:1) to give a brown solid. The solid was recrystallized from hexane/EtOAc to afford the title compound as a crystalline white solid material (5.77 g, 57 %). M.p. = 142-143°C. ^{1}H NMR (400 MHz, $CDCl_3$): δ 10.37 (s, 1H), 8.47 – 8.37 (m, 1H), 7.94 – 7.84 (m, 1H), 7.83 – 7.68 (m, 3H), 6.88 (ddt, J = 3.7, 1.8, 0.9 Hz, 1H), 6.62 (dd, J = 3.8, 1.8 Hz, 1H). ^{13}C NMR (101 MHz, $CDCl_3$) δ 145.5, 144.0, 136.3, 134.0, 133.7, 132.7, 128.8 (d, J = 35.7 Hz), 128.6 (q, J = 6.3 Hz), 128.1 (d, J = 33.1 Hz), 122.9 (q, J = 273.8 Hz), 120.0 (q, J = 275.0 Hz), 116.2 (q, J = 2.6 Hz), 112.4. ^{19}F NMR (282 MHz, $CDCl_3$) δ –68.3, –66.4; IR (ATR): $\tilde{\nu}$ = 3317, 1394, 1361, 1309, 1274, 1243, 1181, 1148, 1119, 1082, 1033, 997, 864, 759, 583, 562 cm^{-1}. HRMS (ESI$^+$) for [M+Na]$^+$: calcd: 409.00520, found: 409.00546.

Methyl-(*E*)-2-(furan-2-yl)-2-(2-((2-(trifluoromethyl)phenyl)sulfonyl)hydrazineylidene) acetate (61). Prepared analogously to **58** from the corresponding keto methylester[223]. The crude residue was purified by flash chromatography (hexane/EtOAc, 8:1 to 6:1) afforded the desired product as a yellow solid The solid was further purified by washing with MTBE (3 mL) to get an off-white solid (180 mg, 16%). ^{1}H NMR (400 MHz, $CDCl_3$) δ 12.04 (s, 1H), 8.50 – 8.41 (m, 1H), 7.89 – 7.85 (m, 1H), 7.79 – 7.69 (m, 2H), 7.44 (dd, *J* = 1.9, 0.8 Hz, 1H), 6.83 (dd, *J* = 3.5, 0.8 Hz, 1H), 6.40 (dd, *J* = 3.5, 1.8 Hz, 1H), 3.95 (s, 3H). ^{13}C NMR (101 MHz, $CDCl_3$) δ 161.3, 147.2, 144.4, 136.9, 133.5, 133.3, 132.5, 129.3, 128.4 (q, *J* = 6.4 Hz), 122.8 (q, *J* = 276.0 Hz), 114.3, 111.5, 53.1. ^{19}F NMR (282 MHz, $CDCl_3$) δ -58.2. IR (ATR):

$\tilde{\nu}$ = 1705, 1392, 1309, 1272, 1248, 1226, 1176, 1145, 1116, 1095, 1035, 584, 552 cm^{-1} HRMS (ESI +): m/z calcd. for $C_{14}H_{11}F_3N_2O_5SNa$ $[M+Na]^+$: 399.0233; found: 399.02317.

2,2,2-Trichloroethyl-(*E*)-2-(furan-2-yl)-2-(2-((2-(trifluoromethyl)phenyl)sulfonyl)hydrazineylidene) acetate (62). A flask was charged with the corresponding keto trichloroethylester[224] (560 mg, 2.1 mmol) and trichloroethanol:MTBE (3:1, 7 mL). Then $TfsNHNH_2$ (401 mg, 1.9 mmol) and $La(OTf)_3$ (55 mg, 0.09 mmol) were added respectively and the mixture was stirred at room temperature for 3 h. The solvent was distilled off under reduced pressure (60- 65 °C, $1 \cdot 10^{-3}$ mbar). The residue was washed with MTBE/pentane (1:1, 2 x 4mL) and dried under reduced pressure to give the title compound as an off-white solid (400 mg, 43%). ^{1}H NMR (400 MHz, $CDCl_3$) δ 11.98 (s, 1H), 8.50 – 8.44 (m, 1H), 7.89 (dd, *J* = 7.7, 1.6 Hz, 1H), 7.82 – 7.70 (m, 2H), 7.46 (dd, *J* = 1.8, 0.8 Hz, 1H), 7.08 (dd, *J* = 3.5, 0.8 Hz, 1H), 6.43 (dd, *J* = 3.5, 1.8 Hz, 1H), 4.97 (s, 2H). ^{13}C NMR (101 MHz, $CDCl_3$) δ 159.1, 146.5, 144.6, 136.6, 133.8, 133.4, 132.6, 128.5 (q, *J* = 6.3 Hz), 127.6, 122.8 (q, *J* = 275.2 Hz), 114.9, 111.8, 93.4, 75.2. ^{19}F NMR (282 MHz, $CDCl_3$) δ -58.21. IR (ATR): $\tilde{\nu}$ = 1722, 1502, 1434, 1265, 1315, 1221, 1170, 1154, 1014, 741, 696 cm^{-1}. IR (ATR): $\tilde{\nu}$ = 1715, 1394, 1308, 1272, 1212, 1176, 1144, 1115, 1036, 775, 715, 581, 554 cm^{-1}. HRMS (ESI +) m/z calcd. for $C_{15}H_{10}O_5N_2F_3SCl_3Na$ $[M]^+$: 514.92203; found: 514.92182.

***N*'-(1-(Benzofuran-2-yl)-2,2,2-trifluoroethylidene)-2-(trifluoromethyl)benzenesulfonohydrazide (256).** Prepared analogously to **58** from 1-(benzofuran-2-yl)-2,2,2-trifluoroethan-1-one.[225] The crude residue was purified by flash chromatography (hexane/EtOAc, 8:1 to 6:1) afforded the desired product as a yellow solid. The yellow impurity was removed by washing the product thrice with ice-cold pentane to leave the title compound as a white solid (133 mg, 41%). M.p. = 173-174 °C. ^{1}H NMR (400 MHz, $CDCl_3$) δ 10.74 (s, 1H), 8.49 – 8.39 (m, 1H), 7.94 – 7.86 (m, 1H), 7.83 – 7.74 (m, 2H), 7.69 (ddd, J = 7.8, 1.3, 0.7 Hz, 1H), 7.52 (ddd, J = 8.5, 7.2, 1.3 Hz, 1H), 7.38 (ddd, J = 8.1, 7.2, 1.0 Hz, ^{1}H), 7.22 (qd, J = 1.8, 0.9 Hz, 1H). ^{13}C NMR (101 MHz, $CDCl_3$) δ 154.8, 144.4, 136.3, 134.0, 133.6, 132.8, 128.7 (q, J = 6.3 Hz), 128.3, 126.0, 125.0, 123.0 (q, J = 274.4 Hz), 121.1 (q, J = 275.7 Hz), 112.4 (q, J = 2.6 Hz), 111.9. ^{19}F NMR (282 MHz, $CDCl_3$) δ –58.3, –66.0. IR (ATR): $\tilde{\nu}$ = 1387, 1341, 1308, 1271, 1251, 1177, 1160, 1141, 1086, 1037, 1007, 862, 751, 728, 584, 561 cm^{-1}. HRMS (ESI^+) for $[M+H]^+$: calcd: 437.03891, found: 437.03874.

(*E*)-*N*'-(2,2-Difluoro-1-(furan-2-yl)ethylidene)-2-(trifluoromethyl)benzenesulfono hydrazide (84). 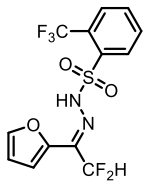 A flask was charged with difluoromethyl ketone **249** (608 mg, 4.16 mmol) and EtOAc (4 mL). Then $TfsNHNH_2$ (800 mg, 3.33 mmol) and $Et_2O{\cdot}BF_3$ (0.49 mL, 4.0 mmol) were added respectively. The reaction mixture was heated to 40 °C and stirred for 18 h. The reaction mixture was concentrated under reduced pressure and directly purified by flash chromatography (pentane/EtOAc 6:1 to 4:1) to give the title compound as a brown solid. The brown solid was further purified by recrystallization from hexane/EtOAc affording the title compound as a crystalline white solid (583 mg, 48%). ^{1}H NMR (400 MHz, $CDCl_3$) δ 10.36 (s, 1H), 8.43 – 8.33 (m, 1H), 7.93 – 7.85 (m, 1H), 7.81 – 7.73 (m, 2H), 7.71 (dd, *J* = 1.8, 0.7 Hz, 1H), 7.09 – 6.97 (m, 1H), 6.61 (dd, *J* = 3.7, 1.8 Hz, 1H), 6.12 (t, *J* = 53.9 Hz, 1H). ^{13}C NMR (101 MHz, $CDCl_3$) δ 145.2, 144.2 (t, *J* = 2.2 Hz), 136.6, 134.1 (t, *J* = 29.6 Hz), 133.8, 133.3, 132.6, 128.7 (q, *J* = 6.3 Hz), 128.0 (q, *J* = 33.1 Hz), 124.2 (q, *J* = 273.5 Hz), 116.3 (t, *J* = 3.2 Hz), 115.1 (t, *J* = 241.6 Hz), 112.3. ^{19}F NMR (282 MHz, $CDCl_3$) δ −58.4, −115.1. IR (ATR): $\tilde{\nu}$ = 1392, 1369, 1308, 1272, 1173, 1146, 1119, 1037, 1022, 881, 745, 588 cm^{-1}. HRMS (ESI +) m/z calcd. for $C_{13}H_9F_5O_3N_2SNa$ [M+Na]$^+$: 391.01462; found: 391.01453.

(*Z*)-*N*'-(2,2,2-Trifluoro-1-(thiazol-2-yl)ethylidene)-2-(trifluoromethyl)benzenesulfono hydrazide (88). 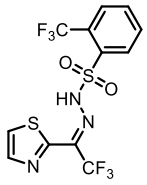 A flask was charged with trifluoromethyl ketone (hydrate) **250** (273 mg, 1.51 mmol) and EtOAc (3 mL). Then $TfsNHNH_2$ (302 mg, 1.26 mmol) and $Et_2O{\cdot}BF_3$ (0.20 mL, 1.63 mmol) were added respectively. The reaction mixture was heated to 45 °C and stirred for 20 h. The reaction mixture was concentrated under reduced pressure and directly purified by flash chromatography (hexane/EtOAc 4:1 to 2:1) to give the title compound as a white solid (210 mg, 41%). ^{1}H NMR (400 MHz, $CDCl_3$) δ 14.29 (s, 1H), 8.46 – 8.40 (m, 1H), 8.11 (d, *J* = 3.2 Hz, 1H), 7.93 – 7.83 (m, 1H), 7.81 – 7.72 (m, 2H), 7.65 (d, *J* = 3.3 Hz, 1H). ^{13}C NMR (101 MHz, $CDCl_3$) δ 155.0, 143.2, 136.8, 133.9, 133.3, 132.7, 128.6 (q, *J* = 6.2 Hz), 128.0 (q, *J* = 33.6 Hz), 124.2 (q, *J* = 273.8 Hz), 122.3, 121.7 (q, *J* = 275.4 Hz). ^{19}F NMR (282 MHz, $CDCl_3$) δ –58.1, –66.0. IR (ATR): $\tilde{\nu}$ = 1377, 1308, 1269, 1201, 1180, 1139, 1119, 1091, 1037, 1006, 777, 580, 556 cm^{-1}. HRMS (ESI +) m/z calcd. for $C_{12}H_7F_6O_2N_3S_2Na$ [M+Na]$^+$: 425.97761; found: 425.97756.

(*E*)-*N*'-(2,2,2-Trifluoro-1-(oxazol-2-yl)ethylidene)-2-(trifluoromethyl)benzenesulfono hydrazide (86). 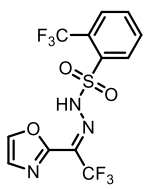 Prepared analogously to **88** from corresponding ketone **251**. The crude residue was purified by flash chromatography (hexane/EtOAc 5:1 to 4:1) afforded the title compound as a white solid (68 mg, 21%). ^{1}H NMR (600 MHz, $CDCl_3$) δ 13.30 (s, 1H), 8.43 (dd, *J* = 7.4, 1.9 Hz, 1H), 7.92 – 7.86 (m, 1H), 7.81 – 7.77 (m, 3H), 7.47 (d, *J* = 0.8 Hz, 1H). ^{13}C NMR (151 MHz, $CDCl_3$) δ 152.2, 141.1, 139.3, 136.5 (q, *J* = 1.3 Hz), 134.1, 133.4, 132.7, 128.6 (q, *J* = 6.2 Hz), 128.3 (q, *J* =

33.5 Hz), 122.9 (q, *J* = 37.8 Hz), 122.8 (q, *J* = 274.0 Hz), 119.5 (q, *J* = 274.2 Hz). IR (ATR): $\tilde{\nu}$ = 1384, 1309, 1269, 1177, 1134, 1116, 1093, 1026, 917, 775, 589, 556 cm^{-1}. HRMS (ESI +) m/z calcd. for $C_{12}H_7F_6O_3N_3SNa$ $[M+Na]^+$: 410.00045; found: 410.00049.

(*E*)-*N*'-(1-(Benzo[d]oxazol-2-yl)-2,2,2-trifluoroethylidene)-2-(trifluoromethyl)benzenesulfono hydrazide (87). Prepared analogously to **88** from the corresponding ketone [226]. The crude residue was purified by flash chromatography (pentane/EtOAc 8:1 to 4:1) to give the title compound as a yellow solid. The yellow solid was subsequently washed with ice-cold pentane (3 x 2mL) to give the desired product as a white solid (390 mg, 43%). ^{1}H NMR (400 MHz, $CDCl_3$) δ 13.65 (s, 1H), 8.54 – 8.39 (m, 1H), 7.91 (ddd, *J* = 7.6, 1.7, 0.7 Hz, 2H), 7.84 – 7.76 (m, 2H), 7.73 – 7.64 (m, 1H), 7.60 – 7.48 (m, 2H). ^{13}C NMR (101 MHz, $CDCl_3$) δ 152.5, 148.5, 139.2, 136.4, 134.2, 133.4, 132.8, 128.7 (q, *J* = 6.4 Hz), 128.6, 128.2, 126.5, 124.2 (q, *J* = 274.6 Hz), 122.9 (q, *J* = 38.3 Hz), 121.1, 118.3 (q, *J* = 273.3 Hz), 111.8. ^{19}F NMR (282 MHz, $CDCl_3$) δ −58.1, −66.5. IR (ATR): $\tilde{\nu}$ = 1387, 1310, 1271, 1178, 1126, 1030, 764, 748, 591, 554 cm^{-1}. HRMS (ESI +) m/z calcd. for $C_{16}H_9F_6O_3N_3SNa$ $[M+Na]^+$: 460.01610; found: 460.01622.

4,4'-(Diazomethylene)bis(*N*,*N*-dimethylaniline) (257). The diazoalkane was prepared according to a modified literature procedure.[227] A flame dried Schlenk flask, wrapped in aluminium foil, was charged with the corresponding hydrazone **255**[228] (250 mg, 0.89 mmol), followed by addition of THF (10 mL) in the dark. The solution was cooled to −78 °C and freshly prepared activated MnO_2 (770 mg, 8.8 mmol) was added to the cooled solution. The resulting mixture was warmed to 0 °C and stirred for an additional 20 min. The mixture was filtered over celite under inert atmosphere. The resulting filtrate was concentrated under reduced pressure, washed with pentane (5 mL) and dried under vacuo to afford the desired diazo compound as a green solid (198 mg, 80%). Note: sensitive compound. NMR sample was prepared under inert atmosphere and measured directly. Over time, the compound starts to decompose. ^{1}H NMR (400 MHz, $[D_6]$-DMSO) δ 7.08 – 7.00 (m, 4H), 6.86 – 6.71 (m, 4H), 2.90 (s, 12H). ^{13}C NMR (101 MHz, $[D_6]$-DMSO) δ 148.7, 125.9, 115.0, 113.5, 60.0 (determined via 2D ^{1}H-^{13}C-HMBC measurement) 40.1 (signal of methyl groups overlapping with $[D_6]$-DMSO peak). HRMS was not successful.

2,4-Dimethylpentan-3-yl 2-diazo-3,3,3-trifluoropropanoate (184). The title compound

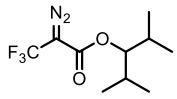

was synthesized according to a modified literature procedure.[150] A two-neck round bottom flask was charged with trifluoropyruvate ester[149] (4.0 g, 15.5 mmol) and the reactant was dissolved in CH_2Cl_2 (25 mL), followed by addition of tosylhydrazide (3.46 g, 18.6 mmol). After stirring the reaction mixture for 18 h at ambient temperature, pyridine (7.5 mL, 92.9 mmol) and $POCl_3$ (1.4 mL, 15.5 mmol) were dropwise added. The reaction mixture heated and refluxed for 30 min, then allowed to cooled to room temperature. TEA (2.6 mL, 18.6 mmol) was then added and the mixture was refluxed for 30 min. The reaction mixture was cooled to room temperature and carefully diluted with water (50 mL). The aqueous phase was extracted with CH_2Cl_2 (3 x 20 mL). The combined organic phases were washed with aq. HCl-solution (1M), $NaHCO_3$ and brine, dried over $MgSO_4$ and concentrated under reduced pressure. The crude material was purified by Kugelrohr distillation (150 °C, 20 mbar) to afford a pale yellow oil (1.68 g, 43%, 95% purity). ^{1}H NMR (400 MHz, $CDCl_3$) δ 4.72 (t, *J* = 6.1 Hz, 1H), 1.95 (pd, *J* = 6.8, 6.1 Hz, 2H), 0.90 (dd, *J* = 12.1, 6.8 Hz, 12H). ^{13}C NMR (101 MHz, $CDCl_3$) δ 161.5, 124.3 (q, *J* = 270.1 Hz), 85.6, 29.6, 19.6, 17.2, carbene carbon not detected. ^{19}F NMR (282 MHz, $CDCl_3$) δ −57.2. IR (ATR): $\tilde{\nu}$ = 2968, 2938, 2881, 2128, 1728, 1711, 1466, 1373, 1346, 1314, 1300, 1210, 1135, 1040, 938, 898, 731, 721 cm^{-1}. HRMS (ESI +) m/z calcd. for $C_{10}H_{15}F_3O_2N_2Na$ $[M+Na]^+$: 275.09778; found: 275.0980.

9.3. Ligand Synthesis

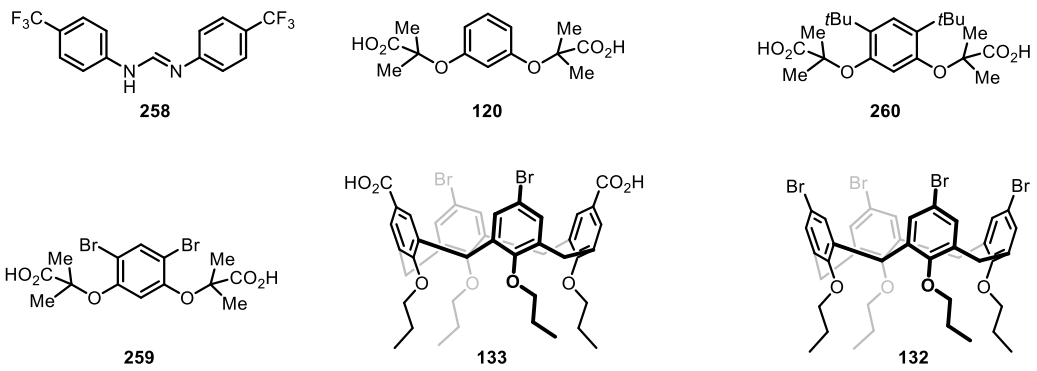

Figure 70-Overview of known ligands that have been synthesized according to their literature reference.

Compounds **258**[229], **(120, 259-260)**[136]and **(133, 132)**[138] were synthesized according to the literature. The characterization data matched the reported data.

9.3.1. Synthesis of O-Esp Ligands

Diethyl 2,2'-((4,6-dichloro-1,3-phenylene)bis(oxy))bis(2-methylpropanoate) (261).

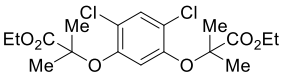

Diethyl 2,2'-(1,3-phenylenebis(oxy))bis(2-methylpropanoate)[136] (410 mg, 1.2 mmol) was dissolved in CH_2Cl_2 (2 mL) in a flame dried Schlenk flask and cooled to 0 °C in an ice bath. SO_2Cl_2 (0.25 mL, 2.5 mmol) was added dropwise to the cooled reaction solution and left stirring for 10 min at 0 °C, followed by stirring the reaction at room temperature for 1 h. The reaction mixture was quenched by addition of $NaHCO_3$ (5 mL) and was extracted with CH_2Cl_2 (2 x 15 mL). The combined organic phases were washed with brine (30 mL), dried with $MgSO_4$, filtered and concentrated under reduced pressure. The crude residue was purified by flash chromatography (silica, n-hexane/EtOAc 20:1 to 15:1) to afford the title compound as a clear oil (255 mg, 52%). ^{1}H NMR (400 MHz, $CDCl_3$) δ 7.36 (s, 1H), 6.64 (s, 1H), 4.26 (q, *J* = 7.1 Hz, 4H), 1.57 (s, 12H), 1.28 (t, *J* = 7.1 Hz, 6H). ^{13}C NMR (101 MHz, $CDCl_3$) δ 173.6, 150.4, 130.5, 120.9, 112.8, 81.5, 61.9, 25.2, 14.2. HRMS (ESI +): m/z calcd. for $C_{18}H_{24}O_6Cl_2Na$ $[M+Na]^+$: 429.08422; found: 429.08464.

2,2'-((4,6-Dichloro-1,3-phenylene)bis(oxy))bis(2-methylpropanoic acid) (262).

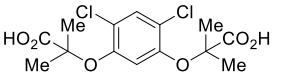

Aqueous NaOH (1 M, 3 ml) was added to a solution of diethyl ester **261** (239 mg, 0.59 mmol) in EtOH (6 ml) and stirred at 80 °C overnight. After completion of the reaction, the volatiles were removed under reduced pressure. The residue was acidified with aq. HCl (1 M, 20 mL) and extracted with EtOAc (3 x 20 mL). The combined organic phases were washed with brine (30 mL), dried with $MgSO_4$, filtered and concentrated under reduced pressure to afford the title compound as a white solid (179 mg, 89%). ^{1}H NMR (400 MHz, $[D_6]$-acetone) δ 7.46 (s, 1H), 6.89 (s, 1H), 1.60 (s, 12H). ^{13}C NMR (101 MHz, $[D_6]$-acetone) δ 174.6, 151.5, 130.1, 119.8, 112.3, 81.8, 25.5. IR (ATR): $\tilde{\nu}$ = 2933, 1718, 1477, 1384, 1293, 1191, 1156, 1095, 766, 753 cm^{-1}. HRMS (ESI +): m/z calcd. for $C_{14}H_{16}O_6Cl_2Na$ $[M+Na]^+$: 373.02162; found: 373.02188.

9.3.2. Synthesis of Calix[4]arene Ligands

Calix[4]arene (139). *n*-BuLi (0.77 mL, 1.24 mmol) was added dropwise to a cooled solution

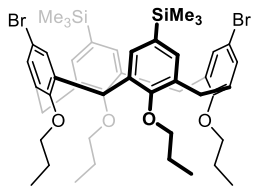

of **132** (450 mg, 0.50 mmol) in THF (20 mL) at –78 °C. The yellow solution was stirred for 20 min at –78 °C, followed by addition of TMSCl (0.63 mL, 5.0 mmol). The reaction was kept stirring at –78 °C for 2 h and quenched by addition of aq. saturated NH_4Cl solution. The aqueous phase was extracted with EtOAc (3 x 20 mL). The combined organic phases were washed with brine (50 mL), dried over $MgSO_4$ and concentrated under reduced pressure to afford the title compound as an off-white solid (400 mg, 90%). ^{1}H NMR (400 MHz, $CDCl_3$) δ 4.40 (d, *J* = 13.3 Hz, 4H), 4.11 – 3.93 (m, 4H), 3.65 (t, *J* = 6.7 Hz, 4H), 3.13 (d, *J* = 13.4 Hz, 4H), 2.01 – 1.80 (m, 8H), 1.09 (t, *J* = 7.4 Hz, 6H), 0.87 (t, *J* = 7.5 Hz, 6H), 0.32 (s, 18H). ^{13}C NMR (101 MHz, $CDCl_3$) δ 158.5, 154.5, 135.7, 135.6, 134.4, 134.0, 130.4, 115.3, 77.4, 76.6, 31.1, 23.6, 23.1, 11.0, 9.9, -0.7. IR (ATR): ṽ = 2957, 2933, 2874, 1454, 1246, 1196, 1109, 1004, 906, 832, 753 cm^{-1}. HRMS (ESI +): m/z calcd. for $C_{46}H_{62}O_4Si_2Br_2Na$ $[M+Na]^+$: 915.24456; found: 915.24511.

Calix[4]arene (142). *n*-BuLi (0.54 mL, 0.86 mmol) was added dropwise to a cooled solution

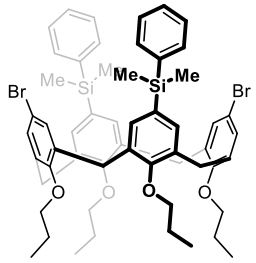

of **132** (300 mg, 0.33 mmol) in THF (15 mL) at –78 °C. The yellow solution was stirred for 20 min at –78 °C, followed by addition of a premixed mixture of $PhMe_2SiCl$ and Et_3N (1:1 v/v, 1.0 mL, 3 mmol of the chlorosilane). The reaction was slowly warmed to room temperature and stirred for an additional 2 h. The reaction mixture was quenched by addition of aq. saturated NH_4Cl solution. The aqueous phase was extracted with EtOAc (3 x 20 mL). The combined organic phases were washed with brine (50 mL), dried over $MgSO_4$ and concentrated under reduced pressure to afford the title compound as an off-white solid (400 mg, 90%). The crude product was recrystallized from hot MeOH/CH_2Cl_2. The crystals were washed with cold MeOH (2 x 3 mL) affording colorless crystals (243 mg, 72%). ^{1}H NMR (400 MHz, $CDCl_3$) δ 7.53 – 7.48 (m, 4H), 7.46 – 7.41 (m, 4H), 7.39 – 7.34 (m, 2H), 7.29 (s, 4H), 6.30 (s, 4H), 4.41 (d, *J* = 13.2 Hz, 4H), 4.09 – 4.00 (m, 4H), 3.63 (t, *J* = 6.8 Hz, 4H), 3.12 (d, *J* = 13.3 Hz, 4H), 2.05 – 1.79 (m, 8H), 1.09 (t, *J* = 7.4 Hz, 6H), 0.88 (t, *J* = 7.5 Hz, 6H), 0.61 (s, 12H). ^{13}C NMR (101 MHz, $CDCl_3$) δ 159.0, 154.3, 139.6, 136.1, 135.6, 135.4, 134.3, 131.2, 130.5, 129.1, 128.2, 115.4, 77.4, 76.7, 31.0, 23.6, 23.2, 11.0, 9.9, -2.0. IR (ATR): ṽ = 2960, 2934, 1875, 1454, 1428, 1385, 1294, 1275, 1248, 1219, 1197, 1165, 1111, 1005, 964, 907, 865, 830, 808, 775, 729, 700 cm^{-1}. HRMS (ESI +): m/z calcd. for $C_{56}H_{66}O_4Si_2Br_2Na$ $[M+Na]^+$: 1039.275887; found: 1039.275940.

Calix[4]arene (143). *n*-BuLi (0.73 mL, 1.16 mmol) was added dropwise to a cooled solution of **139** (400 mg, 0.45 mmol) in THF (16 mL) at –78°C. The solution was stirred for 20 min at –78°C, followed by bubbling CO_2 (g) through the solution for 30 min at –78°C. The reacted was kept stirring at –78 °C for 2 h and poured into ice cold aq. HCl-solution (2 M), followed by extraction with $CHCl_3$ (3 x 50 mL). The combined organic phases were washed with water (50 mL), dried over $MgSO_4$ and concentrated under reduced pressure. The crude product was washed with cold MeOH (2 x 5 mL) affording the desired product as a white solid (238 mg, 65%) ^{1}H NMR (400 MHz, $CDCl_3$) δ 12.44 (s, broad, 2H), 7.31 (s, 4H), 6.74 (s, 4H), 4.42 (d, *J* = 13.4 Hz, 4H), 4.11 – 3.90 (m, 4H), 3.67 (t, *J* = 6.6 Hz, 4H), 3.16 (d, *J* = 13.6 Hz, 4H), 1.89 (ddq, *J* = 28.1, 14.1, 7.5 Hz, 8H), 1.11 (t, *J* = 7.4 Hz, 6H), 0.88 (t, *J* = 7.4 Hz, 6H), 0.33 (s, 18H). ^{13}C NMR (101 MHz, $CDCl_3$) δ 171.1, 159.6, 158.5, 136.2, 134.8, 134.3, 133.6, 129.9, 123.5, 77.0, 76.6, 30.9, 23.6, 23.2, 11.0, 9.9, -0.7. IR (ATR): ṽ = 2959, 2935, 2876, 1700, 1423, 1288, 1247, 1218, 1199, 1119, 1007, 916, 836 cm^{-1}. HRMS (ESI +): m/z calcd. for $C_{48}H_{64}O_8Si_2Na$ $[M+Na]^+$: 847.40320; found: 847.40353.

Calix[4]arene (144). Prepared analogously to **143** with calix[4]arene **142**. The crude product was recrystallized from hot MeOH/THF. The crystals were washed with cold MeOH (2 x 3 mL) affording colorless crystals (56 mg, 40 %). ^{1}H NMR (400 MHz, $CDCl_3$) δ 12.57 (s, broad, 2H), 7.60 – 7.51 (m, 4H), 7.42 – 7.28 (m, 10H), 6.80 (s, 4H), 4.42 (d, *J* = 13.5 Hz, 4H), 4.08 – 3.95 (m, 4H), 3.66 (t, *J* = 6.6 Hz, 4H), 3.15 (d, *J* = 13.5 Hz, 4H), 1.99 – 1.79 (m, 8H), 1.10 (t, *J* = 7.3 Hz, 6H), 0.87 (t, *J* = 7.6 Hz, 6H), 0.54 (s, 12H). ^{13}C NMR (101 MHz, $CDCl_3$) δ 171.0, 159.7, 158.9, 139.0, 136.3, 135.8, 134.4 (d, *J* = 5.4 Hz), 133.6, 131.8, 129.9, 129.0, 128.0, 123.6, 77.0, 76.6, 31.0, 23.6, 23.2, 11.0, 9.9, -2.0. IR (ATR): ṽ = 2960, 2933, 2875, 1697, 1464, 1425, 1286, 1247, 1218, 1199, 1112, 1006, 966, 913, 830, 808, 714, 731, 700 cm^{-1}. HRMS (ESI +): m/z calcd. for $C_{58}H_{68}O_8Si_2Na$ $[M+Na]^+$: 971.43449; found: 971.43425.

Calix[4]arene (147). To a solution of calix[4]arene **133** (600 mg, 0.72 mmol) in DMF/ CH_2Cl_2 (1:2 v/v, x mL) was added DMAP (17.5 mg, 0.14 mmol) and MeOH (87 µL, 2.15 mmol). The reaction mixture was cooled to 0 °C and stirred for 15 min prior to the portionwise addition of EDC (412 mg, 2.15 mmol). After stirring for 4 h, the reaction mixture was diluted with water extracted with CH_2Cl_2 (3x 40 mL). The organic phase was washed with brine (2 x 40 mL), dried with $MgSO_4$, filtered and concentrated under reduced pressure. The crude material was purified by flash chromatography (silica, Hexane/EtOAc 10:1 to 7:1) to give the title compound as a white solid (542 mg, 87 %). ^{1}H NMR (400 MHz, $CDCl_3$) δ 7.70 (s, 4H),

6.45 (s, 4H), 4.40 (d, *J* = 13.5 Hz, 4H), 4.08 – 4.00 (m, 4H), 3.69 (t, *J* = 7.0 Hz, 4H), 3.20 (d, *J* = 13.5 Hz, 4H), 1.98 – 1.80 (m, 8H), 1.06 (t, *J* = 7.4 Hz, 6H), 0.90 (t, *J* = 7.5 Hz, 6H). ^{13}C NMR (101 MHz, $CDCl_3$) δ 167.1, 161.7, 154.8, 136.0, 135.4, 130.8, 130.7, 124.4, 115.5, 77.5 (overlap $CDCl_3$), 77.0, 52.1, 31.0, 23.5, 23.2, 10.7, 10.0. IR (ATR): ṽ = 2961, 2934, 2876, 1720, 1456, 1433, 1316, 1294, 1199, 1003, 963 cm^{-1}. HRMS (ESI +): m/z calcd. for $C_{44}H_{50}O_8Na$ $[M+Na]^+$: 887.17646; found: 887.17588.

Calix[4]arene (149). A two-neck round bottom flask was charged with **147** (100 mg, 0.12 mmol), K_2CO_3 (96 mg, 0.7 mmol), *p*-tolueneboronic acid (63 mg, 0.46 mmol) and dissolved in MeOH (2 mL) and toluene (3 mL). After stirring the reaction mixture for 15 min at room temperature, $PdCl_2$(dppf) (12 mg, 0.017 mmol, 15 mol%) was added and the mixture was heated to 80 °C for 24 h. The reaction mixture was cooled to room temperature, diluted with water and was extracted with CH_2Cl_2 (3 × 15 mL). The combined organic phases were washed with water (20 mL), brine (20 mL), dried over $MgSO_4$ and concentrated under reduced pressure. The crude material was purified by flash chromatography (silica, Hexane/EtOAc 12:1 to 7:1) to give the title compound as a white solid. (65 mg, 63 %). ^{1}H NMR (400 MHz, $CDCl_3$) δ 7.57 (s, 4H), 6.83 (s, 8H), 6.67 (s, 4H), 4.50 (d, *J* = 13.3 Hz, 4H), 4.10 – 4.01 (m, 4H), 3.83 (s, 6H), 3.81 (t, *J* = 7.3 Hz, 4H), 3.28 (d, *J* = 13.4 Hz, 4H), 2.27 (s, 6H), 2.04 – 1.86 (m, 8H), 1.05 (t, *J* = 7.4 Hz, 6H), 0.99 (t, *J* = 7.4 Hz, 6H). ^{13}C NMR (101 MHz, $CDCl_3$) δ 167.2, 161.5, 155.4, 138.0, 135.9, 135.6 (d, *J* = 1.8 Hz), 133.8, 130.2, 129.0, 126.9, 126.6, 123.9, 77.3, 77.0, 51.9, 31.3, 23.5, 23.3, 21.2, 10.6, 10.3. IR (ATR): ṽ = 2960, 2933, 2875, 1719, 1464, 1434, 1311, 1230, 1197, 1183, 1005, 964, 814, 769 cm^{-1}. HRMS (ESI +): m/z calcd. for $C_{58}H_{64}O_8Na$ $[M+Na]^+$: 911.44934; found: 911.44875.

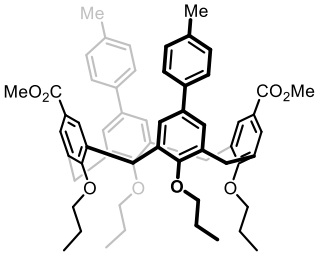

Calix[4]arene (148). Prepared analogously to **149** with 3,5-dimethylphenyl boronic acid to afford the title compound as a white solid (94 mg, 44%). ^{1}H NMR (400 MHz, $CDCl_3$) δ 7.31 (s, 4H), 6.94 (s, 4H), 6.81 (s, 6H), 4.50 (d, *J* = 13.4 Hz, 4H), 3.95 – 3.85 (m, 8H), 3.75 (s, 6H), 3.27 (d, *J* = 13.4 Hz, 4H), 2.21 (s, 12H), 1.95 (hd, *J* = 7.3, 1.4 Hz, 8H), 1.05 (t, *J* = 7.5 Hz, 6H), 1.00 (t, *J* = 7.5 Hz, 6H). ^{13}C NMR (101 MHz, $CDCl_3$) δ 166.9, 160.7, 156.2, 141.2, 137.9, 135.9, 135.0, 134.9, 129.9, 128.2, 127.6, 125.0, 124.0, 77.1 (d, *J* = 2.0 Hz) (overlap $CDCl_3$), 51.8, 31.3, 23.4, 23.3, 21.5, 10.5, 10.4. IR (ATR): ṽ = 2960, 2922, 2875, 1601, 1461, 1433, 1312, 1285, 1221, 1196, 1004, 964, 910, 846, 769, 732 cm^{-1}. HRMS (ESI +): m/z calcd. for $C_{60}H_{68}O_8Na$ $[M+Na]^+$: 939.48064; found: 939.48008.

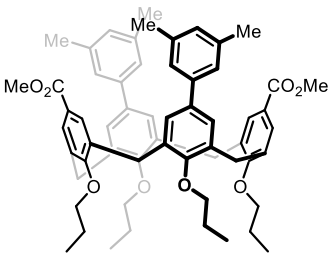

Calix[4]arene (152). A flame dried pressure Schlenk flask was charged with CuI (7 mg, 0.035 mmol, 10 mol %), Calix[4]arene **147** (300 mg, 0.35 mmol), NaI (208 mg, 1.4 mmol), Racemic trans-N,N'-dimethyl-1,2-cyclohexanediamine (11 µL, 0.07 mmol, 20 mol%) and the reactants were dissolved in 1,4-dioxane (1.5 mL). The reaction mixture was stirred at 110 °C for 22 h. The resulting suspension was cooled to room temperature and diluted with a 30% aqueous ammonia solution (5 mL). The mixture was poured into water (20 mL), and extracted with dichloromethane (3 × 15 mL). The combined organic phases were dried with $MgSO_4$, filtered and concentrated under reduced pressure. The residue was purified by flash chromatography (silica, cyclohexane/EtOAc 14:1) to give the title compound as a white solid (304 mg, 91 %). ^{1}H NMR (400 MHz, $CDCl_3$) δ 7.61 (s, 4H), 6.75 (s, 4H), 4.37 (d, *J* = 13.4 Hz, 4H), 4.07 – 3.97 (m, 4H), 3.91 (s, 4H), 3.72 (t, *J* = 7.1 Hz, 4H), 3.18 (d, *J* = 13.5 Hz, 4H), 1.98 – 1.80 (m, 8H), 1.04 (t, *J* = 7.4 Hz, 6H), 0.92 (t, *J* = 7.5 Hz, 6H). ^{13}C NMR (101 MHz, $CDCl_3$) δ 167.0, 161.4, 155.9, 137.0, 136.1, 135.6, 130.5, 124.4, 86.3, 77.5 (overlap $CDCl_3$), 77.0, 52.1, 30.8, 23.4, 23.2, 10.6, 10.1. IR (ATR): ṽ = 2961, 2933, 2875, 1719, 1456, 1433, 1316, 1290, 1231, 1198, 1163, 1003, 962, 769 cm^{-1}. HRMS (ESI +): m/z calcd. for $C_{44}H_{50}O_8I_2Na$ $[M+Na]^+$: 983.14874; found: 983.15002.

Calix[4]arene (153). Calix[4]arene **152** (200 mg, 0.21 mmol) was dissolved in THF (7 mL), followed by addition of KOTMS (267 mg, 2.1 mmol). The reaction mixture was stirred at room temperature for 3 days. An aq. solution of citric acid (3 M, 1 mL) was carefully added to the reaction mixture and left stirring for 1 h at room temperature. The mixture was diluted with water and extracted with CH_2Cl_2 (3 x 20 mL). The combined organic phases were washed with brine (50 mL), dried with $MgSO_4$, filtered and concentrated under reduced pressure.The crude product was washed with cold pentane (2 x 3mL) to afford the title compound as a white solid (158 mg, 83 %). ^{1}H NMR (400 MHz, $CDCl_3$) δ 12.82 (s, broad, 2H), 7.50 (s, 4H), 6.83 (s, 4H), 4.35 (d, *J* = 13.8 Hz, 4H), 4.01 – 3.92 (m, 4H), 3.64 (t, *J* = 6.7 Hz, 4H), 3.10 (d, *J* = 13.9 Hz, 4H), 1.93 – 1.75 (m, 8H), 1.08 (t, *J* = 7.4 Hz, 6H), 0.83 (t, *J* = 7.5 Hz, 6H). ^{13}C NMR (101 MHz, $CDCl_3$) δ 171.8, 159.9, 157.9, 139.1, 138.0, 133.3, 129.9, 123.8, 86.2, 77.4 (overlap $CDCl_3$), 76.7, 30.8, 23.6, 22.8, 10.9, 9.8. IR (ATR): ṽ = 2963, 2932, 2876, 1700, 1461, 1423, 1385, 1305, 1284, 1202, 1110, 1001, 964 cm^{-1}. HRMS (ESI -): m/z calcd. for $C_{42}H_{45}O_8I_2$ $[M-H]^-$: 931.120940; found: 931.121530.

Calix[4]arene (150). Prepared analogously to **153** with calix[4]arene ester **148** to afford the title compound as a white solid (59 mg, 85%). ^{1}H NMR (400 MHz, $CDCl_3$) δ 7.40 (s, 4H), 7.31 (s, 4H), 6.95 (s, 2H), 6.85 (s, 4H), 4.47 (d, *J* = 13.6 Hz, 4H), 4.07 – 3.95 (m, 4H), 3.69 (t, *J* = 6.6 Hz, 4H), 3.22 (d, *J* = 13.7 Hz, 4H), 2.40 (s, 12H), 1.89 (tq, *J* = 14.2, 7.5 Hz, 8H), 1.12 (t, *J* = 7.4 Hz, 6H), 0.86 (t, *J* = 7.5 Hz, 6H). ^{13}C NMR (101 MHz, $CDCl_3$) δ 171.6, 159.9, 157.3, 140.9, 138.0, 136.7, 135.5, 133.7, 129.9, 128.4, 127.9, 125.2, 123.7, 77.0 (overlap $CDCl_3$), 76.6, 31.3, 23.6, 22.9, 21.6, 11.0, 9.9. IR (ATR): ṽ = 2961, 2921, 2874, 1697, 1602, 1463, 1422, 1307, 1281, 1223, 1199, 1106, 1036, 1003, 965, 908, 846, 733 cm^{-1}. HRMS (ESI +): m/z calcd. for $C_{58}H_{64}O_8Na$ $[M+Na]^+$: 911.44934; found: 911.44906.

Calix[4]arene (151). Prepared analogously to **153** with calix[4]arene ester **149** to afford the title compound as a white solid (28 mg, 98 %). ^{1}H NMR (400 MHz, $CDCl_3$) δ 7.58 (d, *J* = 7.7 Hz, 4H), 7.38 (s, 4H), 7.25 (d, *J* = 6.4 Hz, 4H), 6.82 (s, 4H), 4.46 (d, *J* = 13.6 Hz, 4H), 4.07 – 3.97 (m, 4H), 3.67 (q, *J* = 6.9 Hz, 4H), 3.21 (d, *J* = 13.7 Hz, 4H), 2.44 (s, 6H), 1.90 (dq, *J* = 20.9, 7.5 Hz, 8H), 1.11 (t, *J* = 7.4 Hz, 6H), 0.86 (t, *J* = 7.4 Hz, 6H). ^{13}C NMR (101 MHz, $CDCl_3$) δ 171.3, 159.9, 157.3, 138.3, 136.8, 136.2, 135.3, 133.7, 129.9, 129.4, 127.8, 127.2, 123.7, 77.0 (overlap $CDCl_3$), 76.7, 31.4, 23.6, 23.0, 21.3, 11.0, 9.9. IR (ATR): ṽ = 2959, 2917, 2871, 2851, 1696, 1679, 1470, 1421, 1307, 1278, 1237, 1204, 1194, 1104, 1034, 997, 962, 905, 817 cm^{-1}. HRMS (ESI +): m/z calcd. for $C_{56}H_{60}O_8Na$ $[M+Na]^+$: 883.4180; found: 883.41759.

9.4. Preparation of Dirhodium Complexes

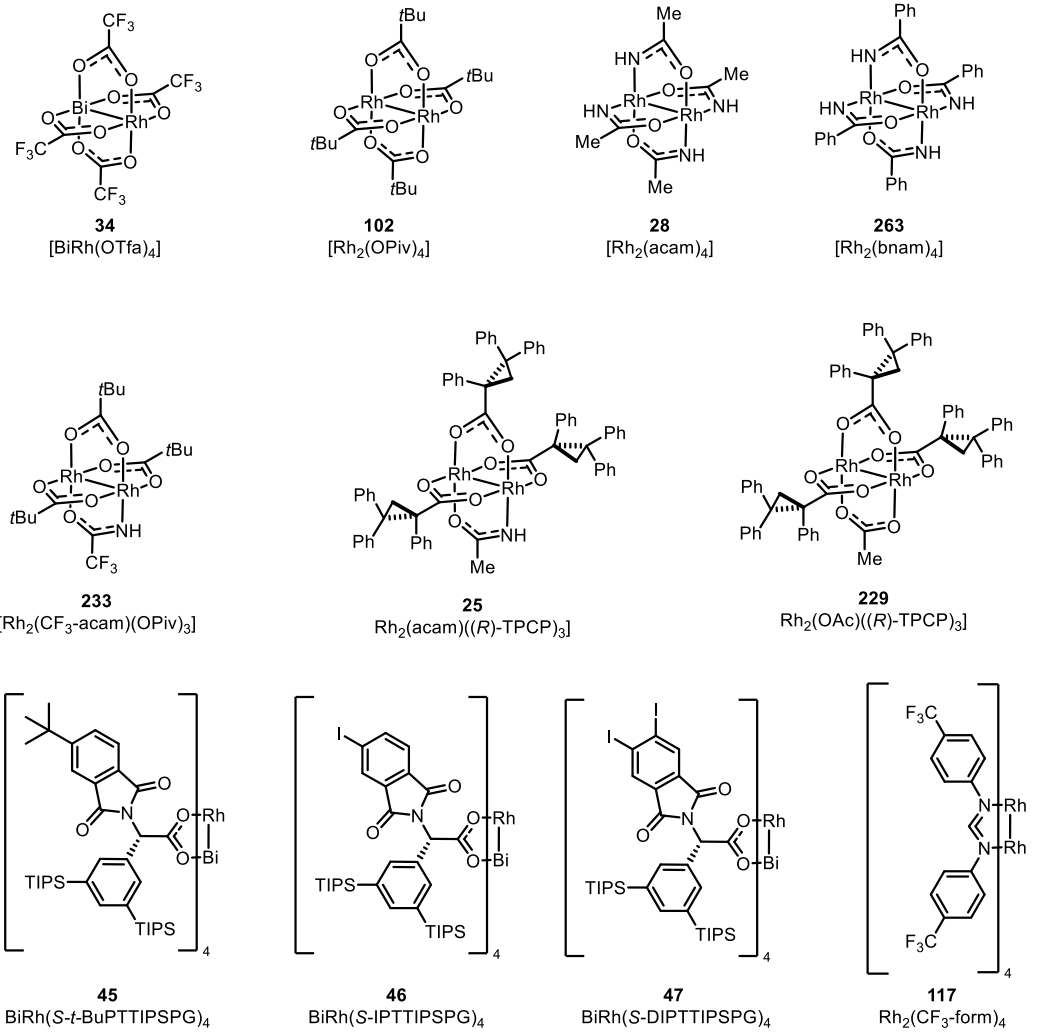

Figure 71-Overview of known complexes that have been prepared according to the literature.

[BiRh(OTfa)$_4$] (**34**),[98] [Rh$_2$(OPiv)$_4$] (**102**),[230] [Rh$_2$(acam)$_4$] (**28**),[81] [Rh$_2$(bnam)$_4$] (**263**) ,[114] [Rh$_2$(CF$_3$-acam)(OPiv)$_3$](**233**),[80] [Rh$_2$(acam)(TPCP)$_3$](**25**),[80] [Rh$_2$(OAc)(TPCP)$_3$](**229**),[80] [BiRh(L$_4$*)](**45-47**)[99] and [Rh$_2$(CF$_3$-form)$_4$] (**117**)[240] were prepared according to the literature. The characterization data matched the reported data.

[Rh_2(*N*-Me-acam)$_4$] (160). A 50 mL two-neck flask was equipped with a returning-arm frit (or

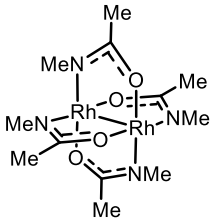

Soxhlet extractor) topped by a reflux condenser. The Soxhlet extractor was filled with an oven-dried mixture of K_2CO_3 and sand (1:1, ca. 3 g). The flask was charged with [$Rh_2(OAc)_4{\cdot}2H_2O$] (250 mg, 1.05 mmol), *N*-methylacetamide (2.30 g, 31.4 mmol) and chlorobenzene (40 mL). Argon was bubbled through the reaction mixture for 15 min, before the flask was immersed into a pre-heated oil bath (165 °C bath temp). The mixture was stirred at reflux temperature such that a gentle flow of condensing solvent passed through the Soxhlet extractor. After stirring for 48 h, the mixture was cooled to room temperature and chlorobenzene was removed by distillation under reduced pressure (30-40°C, $1{\cdot}10^{-3}$ mbar). The residual brown solid was purified by sublimation under reduced pressure (65-70°C, $1{\cdot}10^{-3}$ mbar) to remove any remaining *N*-methylacetamide; this purification afforded the title complex as blue solid, which is essentially insoluble in deuterated DMSO, acetonitrile, water and chloroform; therefore, no NMR spectra could be recorded. IR (ATR): $\tilde{\nu}$ = 2920, 1433, 1373, 1350, 1112, 1021, 849, 658, 636, 618, 595 cm^{-1}. HRMS (ESI +): m/z calcd. for C12H24O4N4Rh2Na $[M+Na]^+$: 516.97998; found: 516.98001.

[Rh_2(acam)(OTfa)$_3$] (103). [$Rh_2(acam)_4{\cdot}2H_2O$] (400 mg, 0.84 mmol) was filled into a flame

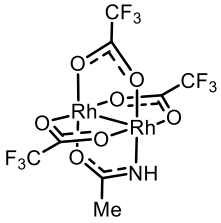

dried two neck round bottom flask with an attached reflux condenser. TFA (16 mL, 210 mmol) was added and the resulting suspension was stirred at 60 °C for 22 min. Then the mixture was quickly cooled to 0 °C in an ice bath. All volatile materials were distilled off under reduced pressure. The remaining crude material was purified by flash chromatography (silica, toluene/MeCN 9:1) to give the title compound as a green solid (424 mg, 79%). ^{1}H NMR (600 MHz, CD_3CN): δ 5.40 (s, 1H), 1.90 (s, 3H) ppm. ^{13}C NMR (151 MHz, CD_3CN): δ 191.3, 175.7 (q, J = 39.1 Hz), 173.8 (q, J = 38.9 Hz), 112.8 (q, J = 285.1 Hz), 111.6 (q, J = 284.7 Hz), 24.1 ppm. ^{19}F NMR (565 MHz, CD_3CN): δ −75.77, −75.84 ppm. HRMS (ESI $^-$): m/z calcd. for $C_8H_3F_9NO_7Rh_2$ $[M-H]^-$: 601.7881; found: 601.7885.

[Rh_2(bnam)(OTfa)$_3$] (106). [$Rh_2(bnam)_4{\cdot}2H_2O$] (150 mg, 0.22 mmol) was filled into a flame

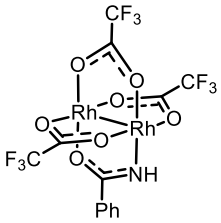

dried two neck round bottom flask with an attached reflux condenser. TFA (6 mL, 78 mmol) was added and the resulting suspension was stirred at 60 °C for 30 min. Then the mixture was quickly cooled to 0 °C in an ice bath and all volatile materials were distilled off under reduced pressure (0 °C, $1{\cdot}10^{-3}$ mbar). The remaining crude material was purified by flash chromatography (silica, toluene/MeCN 99:1 to 9:1) to give the title compound as a purple solid (109 mg, 75%). The spectral data matched those reported in the literature.[114]

[Rh$_2$(acam)(OTfa)$_2$(OPiv)] (107). Pivalic acid (22.4 mg, 0.22 mmol) was filled into a flame dried Schlenk flask and dissolved in MeCN (4 mL). DBU (33 µL, 0.21 mmol) was added and the reaction mixture was stirred for 10 min. [Rh$_2$(acam)(OTfa)$_3$] (120 mg, 0.20 mmol) in MeCN (6 mL) was added dropwise and the reaction mixture was stirred at room temperature for 4 h. The reaction mixture was concentrated and the residue was purified by preparative HPLC (150 mm YMC triart C-18, Ø 30 mm i.D., acetonitrile / water = 55:45) to give the title compound as a green solid (64.2 mg, 55%). ^{1}H NMR (600 MHz, CD_3CN) δ 5.28 (s, 1H), 1.88 (d, J = 0.4 Hz, 3H), 0.97 (s, 9H). ^{13}C NMR (151 MHz, CD_3CN) δ 199.6, 189.8, 174.6 (q, J = 38.5 Hz), 111.7 (q, J = 284.7 Hz), 41.2, 27.9, 24.2. ^{19}F NMR (282 MHz, CD_3CN) δ –75.8. ^{103}Rh NMR (H(C)Rh, 15.9 MHz, CD_3CN) δ 7502, 6499. IR (ATR): $\tilde{\nu}$ = 1653, 1418, 1219, 1193, 1170, 857, 783, 737 cm^{-1}. HRMS (ESI -): m/z calcd. for $C_{11}H_{12}F_6NO_7Rh_2$ [M-H]$^-$: 589.86335; found: 589.86374.

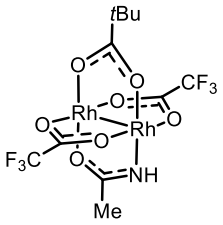

[Rh$_2$(acam)(OTfa)$_2$(OOCPh$_3$)] (108). Triphenylacetic acid (36.7 mg, 0.13 mmol) was filled into a flame dried Schlenk flask and dissolved in THF (2 mL). DBU (33 µL, 0.21 mmol) was added and the reaction mixture was stirred for 10 min. [Rh$_2$(acam)(OTfa)$_3$] (73 mg, 0.12 mmol) in THF (4 mL) was added dropwise and the reaction mixture was stirred at room temperature for 5 h. The reaction mixture was concentrated and the residue was purified by preparative HPLC (150 mm YMC triart C-18, Ø 30 mm i.D., methanol / water = 85:15) to give the title compound as a green solid (46 mg, 49%). ^{1}H NMR (600 MHz, CD_3CN) δ 7.26 – 7.18 (m, 9H), 6.89 – 6.85 (m, 6H), 5.32 (s, 1H), 1.90 (d, *J* = 0.4 Hz, 3H). ^{13}C NMR (151 MHz, CD_3CN) δ 192.8, 190.2, 175.0 (q, *J* = 38.6 Hz), 144.9, 131.0, 128.4, 127.7, 111.7 (q, *J* = 285.1 Hz), 70.0, 24.2. ^{19}F NMR (565 MHz, CD_3CN) δ –75.5. IR (ATR): $\tilde{\nu}$ = 1654, 1373, 1192, 1162, 857, 736, 700 cm^{-1}. HRMS (ESI +): m/z calcd. for $C_{26}H_{19}F_6NO_7Rh_2Na$ [M+Na]$^+$: 799.90680; found: 799.90625.

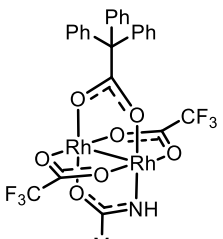

[Rh$_2$(bnam)(OTfa)$_2$(OPiv)] (110). Pivalic acid (3.4 mg, 0.033 mmol) was filled into a flame dried pressure Schlenk flask and dissolved in MeCN (0.5 mL). DBU (5 µL, 0.033 mmol) was added and the reaction mixture was stirred for 10 min. [Rh$_2$(bnam)(OTfa)$_3$] (20 mg, 0.03 mmol) in MeCN (1 mL) was added dropwise and the reaction mixture was stirred at 60 °C for 6 h. The reaction mixture was concentrated and the residue was purified by preparative HPLC (150 mm YMC triart C-18, Ø 30 mm i.D., methanol / water = 75:25) to give the title compound as a green solid (8.5 mg, 43%). ^{1}H NMR (600 MHz, CD_3CN) δ 7.73 – 7.69 (m, 2H), 7.48 – 7.43 (m, 1H), 7.40 – 7.36 (m, 2H), 6.03 (s, 1H), 1.01 (s, 9H). ^{13}C NMR (151 MHz, CD_3CN)

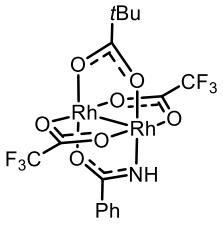

δ 200.0, 185.7, 174.81 (q, *J* = 38.7 Hz), 134.6, 131.8, 129.1, 127.1, 118.3, 111.7 (q, *J* = 284.4 Hz), 41.3, 27.9. ^{19}F NMR (565 MHz, CD_3CN) δ -75.8. IR (ATR): ṽ = 1649, 1549, 1418, 1326, 1217, 1194, 1165, 857, 737 cm^{-1}. HRMS (ESI +): m/z calcd. for $C_{16}H_{15}F_6NO_7Rh_2Na$ $[M+Na]^+$: 675.8755; found: 675.87499.

[Rh$_2$(OMe-bnam)(OTfa)$_2$(OPiv)] (111). Triphenylacetic acid (4.8 mg, 0.048 mmol) was filled into a flame dried Schlenk flask and dissolved in MeCN (0.8 mL). DBU (7.1 µL, 0.048 mmol) was added and the reaction mixture was stirred for 10 min. [Rh$_2$(OMe-bnam)(OTfa)$_3$][114] (30 mg, 0.043 mmol) in MeCN (1.2 mL) was added dropwise and the reaction mixture was stirred at 60 °C for 5 h. The reaction mixture was concentrated and the residue was purified by preparative HPLC (150 mm YMC triart C-18, Ø 30 mm i.D., acetonitrile / water = 75:25, v= 35 mL/min) to give the title compound as a green solid (11 mg, 37%). ^{1}H NMR (600 MHz, CD_3CN) δ 7.83 – 7.39 (m, 2H), 6.97 – 6.71 (m, 2H), 5.83 (s, 1H), 3.80 (s, 3H), 1.00 (s, 9H). ^{13}C NMR (151 MHz, CD_3CN) δ 199.8, 185.1, 174.7 (q, *J* = 38.5 Hz), 162.7, 128.8, 127.2, 114.2, 111.6 (q, *J* = 284.5 Hz), 56.1, 41.3, 27.9. ^{19}F NMR (565 MHz, CD_3CN) δ −75.8. ^{103}Rh NMR (H(C)Rh, 15.9 MHz, CD_3CN) δ 7510, 6506. IR (ATR): ṽ = 1651, 1609, 1440, 1417, 1218, 1194, 1163, 857, 737,637 cm^{-1}. HRMS (ESI -): m/z calcd. for $C_{17}H_{16}F_6NO_8Rh_2$ $[M-H]^-$: 681.88957; found: 681.88946.

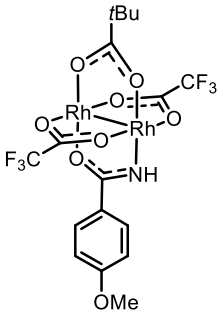

[Rh$_2$(acam) (OTfa)$_2$(*S*-TPCP)] (109). *S*-TPCP acid (23 mg, 0.07 mmol) was filled into a flame dried pressure Schlenk flask and dissolved in MeCN (1 mL). DBU (10.4 µL, 0.07 mmol) was added and the reaction mixture was stirred for 10 min. [Rh$_2$(acam)(OTfa)$_3$] (40 mg, 0.066 mmol) in MeCN (1.8 mL) was added dropwise and the reaction mixture was stirred at 60 °C for 3 h. The reaction mixture was concentrated and the residue was purified by flash chromatography (silica, toluene/MeCN 10:1) to give the title compound as a green solid (29.5 mg, 55%). ^{1}H NMR (400 MHz, CD_3CN) δ 7.48 – 6.81 (m, 15H), 5.17 (s, 1H), 2.39 (d, *J* = 5.3 Hz, 1H), 2.28 (d, *J* = 5.2 Hz, 1H), 1.80 (s, 3H). HRMS (ESI +): m/z calcd. for $C_{28}H_{21}F_6NO_7Rh_2Na$ $[M+Na]^+$: 825.92245; found: 825.92202.

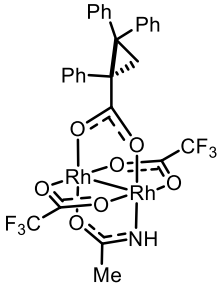

[Rh$_2$(acam)(OPiv)$_3$] (101). Pivalic acid (29.4 mg, 0.29 mmol) was filled into a flame dried pressure Schlenk and dissolved in MeCN (0.8 mL). *N*-Ethyldiisopropylamine (48 µL, 0.27 mmol) was added and the reaction mixture was stirred for 10 min. [Rh$_2$(acam)(OTfa)$_3$] (55 mg, 0.09 mmol) in MeCN (2.4 mL) was added dropwise and the reaction mixture was heated to 60 °C for 18 hours. The mixture was cooled to room temperature and

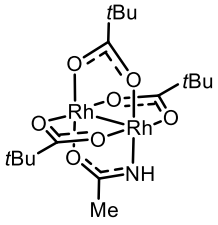

concentrated. The residue was purified by flash chromatography (silica, toluene/acetonitrile 5:1) to give the title compound as a green solid (19.8 mg, 38%). The spectral data were consistent with the literature.[157]

[Rh_2(OTfa)(OPiv)$_3$] (234). [Rh_2(OTfa)$_4$] (69 mg, 0.10 mmol) was filled into a flame dried pressure Schlenk. Pivalic acid (32 mg, 0.31 mmol), acetonitrile (4 mL) and *N*-ethyldiisopropylamine (55 µL, 0.31 mmol) were added. The reaction mixture was heated to 60°C and left stirring overnight. The mixture was cooled to room temperature and concentrated. The residue was purified by flash chromatography (silica, toluene/acetonitrile 20:1 to 10:1) to give the title compound as a green solid (26 mg, 40%). ^{1}H NMR (600 MHz, CD_3CN) δ 0.93 (s, 18H), 0.92 (s, 9H). ^{13}C NMR (151 MHz, CD_3CN) δ 201.8, 201.2, 173.9 (q, J = 38.5 Hz), 111.9 (q, J = 285.1 Hz), 41.3, 41.2, 27.9 (2 C). ^{19}F NMR (565 MHz, CD_3CN) δ –76.0. ^{103}Rh NMR (H(C)Rh, 15.9 MHz, CD3CN) δ 7386. HRMS (ESI$^+$): m/z calcd. for $C_{17}H_{27}F_3NaO_8Rh_2$ $[M+Na]^+$: 644.96603; found: 644.96643.

[Rh_2(OAc)(OPiv)$_3$] (100). To a flame dried Schlenk flask was added *n*-tetrabutylammonium acetate (11 mg, 0.04 mmol) and MeCN (0.5 mL). [Rh_2(OTfa)(OPiv)$_3$] (16 mg, 0.03 mmol) in MeCN (1 mL) was added dropwise to the reaction mixture. The mixture was stirred for 3 h at room temperature. The reaction mixture was concentrated and the residue was purified via flash chromatography (silica, toluene/acetonitrile 8:1) to afford the title compound as a green solid (10 mg, 68%). ^{1}H NMR (600 MHz, CD_3CN) δ 1.76 (s, 3H), 0.92 (s, 18H), 0.90 (s, 9H). ^{13}C NMR (151 MHz, CD_3CN) δ 199.8, 199.7, 41.0, 40.8, 28.0, 28.0, 23.6. ^{103}Rh NMR (H(C)Rh, 15.9 MHz, CD_3CN) δ 7304. HRMS (ESI$^+$): m/z calcd. for $C_{17}H_{30}NaO_8Rh_2$ $[M+Na]^+$: 590.99430; found: 590.99409.

Rh_2(*N*-Me-acam)(OTfa)$_3$ (161). Rh_2(*N*-Me-acam)$_4$ (**160**) (159 mg, 0.32 mmol) was filled into a flame dried two neck round bottom flask with an attached reflux condenser. TFA (6.2 mL, 80.4 mmol) was added and the resulting suspension was submerged in a preheated oil bath at 60°C and stirred for 42 min. Then the mixture was quickly cooled below ambient temperature in an ice bath. All volatile materials were distilled off under reduced pressure. The remaining crude material was purified by flash chromatography (silica, toluene/MeCN 99:1 to 1:1) to give the title compound as a purple solid (88 mg, 44 %). ^{1}H NMR (400 MHz, [D_8]-THF) δ 3.02 (s, 1H), 1.96 (s, 1H). ^{13}C NMR (101 MHz, [D_8]-THF) δ 186.4, 174.7, 38.6, 20.7. ^{19}F NMR (282 MHz, [D_8]-THF) δ –76.1 (6F), –76.2 (3F). IR (solid, ATR) $\tilde{\nu}$ = 1660,

1392, 1192, 1156, 858, 784, 738, 530 cm^{-1}. HRMS (ESI +): m/z calcd. for $C_9H_6F_9NO_7Rh_2$ $[M+H]^+$: 617.81834; found: 617.81823.

$[Rh_2(formate)_4]$ (264). Formic acid (0.15 mL, 4.1 mmol) was filled into a flame dried Schlenk and dissolved in MeCN (12 mL). *N*-Ethyldiisopropylamine (0.71 mL, 4.1 mmol) was added and the reaction mixture was stirred for 10 min. $[Rh_2(OTfa)_4]$ (450 mg, 0.68 mmol) in MeCN (8 mL) was added and the reaction mixture was stirred at room temperature for 22 h. The mixture was concentrated and the residue was purified by flash chromatography (silica, toluene/acetonitrile 5:1) to afford the desired complex as a green solid (237 mg, 90%). ^{1}H NMR (400 MHz, CD_3CN) δ 6.88 (t, *J* = 4.7 Hz, 4H). ^{13}C NMR (101 MHz, CD_3CN) δ 183.7. IR (ATR): $\tilde{\nu}$ = 1601, 1369, 1335, 788, 445 cm^{-1}. HRMS (ESI +): m/z calcd. for $C_4H_4O_8Rh_2$ $[M]^+$: 385.80108; found: 385.80125.

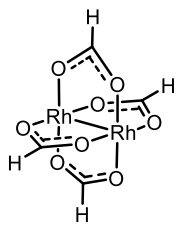

$[Rh_2(CF_3\text{-form})_2(OTfa)_2]$ (118). $[Rh_2(CF_3\text{-form})_4]$ (**117**) (151 mg, 0.1 mmol) was filled into a flame dried two neck round bottom flask with an attached reflux condenser. TFA (7.5 mL, 98 mmol) was added and the resulting suspension was stirred at room temperature for 1 h 20 min. The mixture was quickly cooled to 0 °C in an ice bath and all volatile materials were distilled off under reduced pressure (0 °C, $1\cdot10^{-3}$ mbar). The remaining crude material was purified by flash chromatography (silica, toluene/MeCN 99:1 to 9:1) to give the title compound as a dark green solid (85 mg, 79%). ^{1}H NMR (600 MHz, CD_3CN) δ 7.60 – 7.48 (m, 8H), 7.45 (t, *J* = 3.8 Hz, 2H), 7.23 – 7.18 (m, 8H). ^{13}C NMR (151 MHz, CD_3CN) δ 172.6 (q, *J* = 36.9 Hz), 172.3, 155.1 (q, *J* = 1.4 Hz), 128.0, 126.7 (q, *J* = 32.3 Hz), 126.4 (q, *J* = 3.8 Hz), 124.8 (d, *J* = 270.9 Hz), 114.8 (q, *J* = 285.1 Hz). ^{19}F NMR (565 MHz, CD_3CN) δ −62.6, −75.6. IR (ATR): $\tilde{\nu}$ = 1654, 1614, 1565, 1511, 1321, 1201, 1162, 1111, 1067, 864, 738 cm^{-1}. HRMS (ESI +): m/z calcd. for $C_{34}H_{19}F_{18}N_4O_4Rh_2$ $[M+H]^+$: 1094.92235; found: 1094.92287.

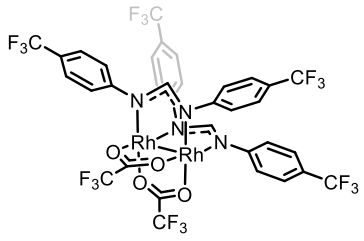

$[Rh_2(acam)(OPiv)_2(OTfa)]$ (113). Pivalic acid (3.3 mg, 0.032 mmol) was filled into a flame dried Schlenk flask and dissolved in MeCN (0.5 mL). DBU (5 µL, 0.032 mmol) was added and the reaction mixture was stirred for 10 min. $[Rh_2(acam)(OPiv)(OTfa)_2]$ (20 mg, 0.034 mmol) in MeCN (1 mL) was added dropwise and the reaction mixture was stirred at room temperature for 24 h. The reaction mixture was concentrated and the residue was purified by flash chromatography (silica, toluene/MeCN 10:1 to 2:1) to afford the title compound as a green solid (6 mg, 30%). ^{1}H NMR (600 MHz, CD_3CN) δ 5.08 (s, 1H), 1.83 (d, *J* = 0.4 Hz, 3H), 0.95 (s, 9H), 0.90 (s, 9H). ^{13}C NMR (151 MHz, CD_3CN) δ 200.6, 198.2, 188.4, 173.0

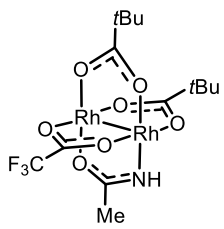

(q, *J* = 37.9 Hz), 112.2 (q, *J* = 285.2 Hz), 41.1, 40.8, 28.1, 27.9, 24.2. ^{19}F NMR (565 MHz, CD_3CN) δ –75.9. ^{103}Rh NMR (H(C)Rh, 15.9 MHz, CD_3CN) δ 7404, 6481. HRMS (ESI -): m/z calcd. for $C_{14}H_{22}F_3NO_7Rh_2$ $[M-H]^-$: 577.93857; found: 577.93882. Note: The complex is unstable in CD_3CN solution over time and decomposed to an unknown species

[Rh$_2$(acam)(esp)(OTfa)] (121). α,α,α′,α′-Tetramethyl-1,3-benzenedipropionic acid

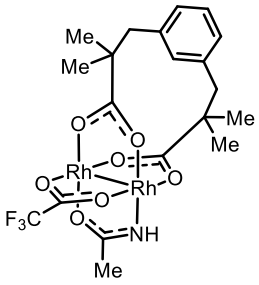

(12.1 mg, 0.044 mmol) was filled into a flame dried Schlenk flask and dissolved in THF (0.6 mL). DBU (13 µL, 0.087 mmol) was added and the reaction mixture was stirred for 10 min. [Rh_2(acam)$(OTfa)_3$] (25 mg, 0.041 mmol) in THF (1.4 mL) was added dropwise and the reaction mixture was stirred at room temperature for 5 h. The reaction mixture was concentrated and the residue was purified by flash chromatography (silica, toluene/MeCN 6:1 to 1:1) to afford the desired complex as a green solid (15 mg, 55%). IR (ATR): $\tilde{\nu}$ = 2925, 1641, 1578, 1475, 1459, 1409, 1376, 1199, 1157, 740, 710 cm^{-1}. ^{1}H NMR (400 MHz, CD_3CN) δ 7.08 (t, *J* = 7.5 Hz, 1H), 6.92 – 6.81 (m, 3H), 5.06 (s, 1H), 2.61 (d, *J* = 2.5 Hz, 2H), 2.55 (s, 2H), 1.83 (s, 3H), 0.95 (d, *J* = 5.0 Hz, 6H), 0.90 (d, *J* = 4.1 Hz, 6H). ^{13}C NMR (101 MHz, CD_3CN) δ 198.4, 196.0, 188.3, 172.7, 139.4, 139.1, 132.1, 128.8, 128.8, 127.8, 47.6, 47.4, 46.8, 46.5, 26.1, 26.0, 25.9, 25.8, 24.1 (CF_3 not detected). ^{19}F NMR (282 MHz, CD_3CN) δ -75.9. HRMS (ESI +): m/z calcd. for $C_{20}H_{24}F_3NO_7Rh_2Na$ $[M+Na]^+$: 675.95072; found: 675.95061. The enantiomers were not separable by chiral HPLC.

[Rh$_2$(acam)(O-esp)(OTfa)] (122). 2,2'-(1,3-Phenylenebis(oxy))bis(2-methylpropanoic

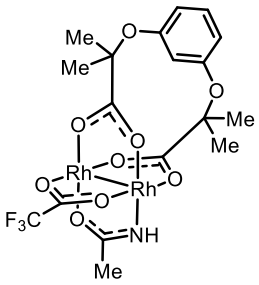

acid)[136] (19.5 mg, 0.07 mmol) was filled into a flame dried Schlenk flask and dissolved in THF (1.2 mL). DBU (20.6 µL, 0.14 mmol) was added and the reaction mixture was stirred for 10 min. [Rh_2(acam)$(OTfa)_3$] (40 mg, 0.066 mmol) in THF (2.2 mL) was added dropwise and the reaction mixture was stirred at room temperature for 4 h. The reaction mixture was concentrated and the residue was purified by flash chromatography (silica, toluene/MeCN 10:1 to 5:1) to afford the desired complex as a green solid (11 mg, 25%). ^{1}H NMR (400 MHz, CD_3CN) δ 7.10 (t, *J* = 8.1 Hz, 1H), 6.50 (dddd, *J* = 11.6, 8.1, 2.3, 0.9 Hz, 2H), 6.10 (t, *J* = 2.3 Hz, 1H), 5.15 (s, 1H), 1.86 (s, 3H), 1.31 (d, *J* = 3.7 Hz, 6H), 1.27 (s, 3H), 1.23 (s, 3H). ^{13}C NMR (101 MHz, CD_3CN) δ 194.9, 192.5, 189.2, 173.9, 157.1, 156.9, 130.2, 116.5, 116.4, 110.7, 81.6, 81.3, 25.3, 25.2, 25.1, 25.0, 24.1 (CF_3 not detected). ^{19}F NMR (282 MHz, CD_3CN) δ –75.8. HRMS (ESI +): m/z calcd. for $C_{18}H_{21}F_3NO_9Rh_2$ $[M+H]^+$: 657.9273; found: 657.92707. IR (ATR): $\tilde{\nu}$ = 1640, 1594, 1469, 1407, 1367, 1199, 1150 cm^{-1}. HPLC analysis: 150 mm Chiralpak IG-3, Ø 4.6 mm i.D., *n*-heptane/2-propanol = 97:3, v= 1.0 mL / min, λ = 220 nm, t(enantiomer 1) = 4.01 min, t(enantiomer 2) = 6.41 min.

The enantiomers were separated by preparative HPLC using the following conditions: 250 mm Chiralpak IG-5, 5µm, 30.0 mm i.D., *i*-hexane/2-propanol = 97:3, v= 20.0 mL / min, λ = 220 nm. Note: the complex decomposes in alcoholic solvents, therefore acetonitrile was added before concentration of the separated enantiomers.

[Rh_2(acam)(Bromo-O-esp)(OTfa)] (124). 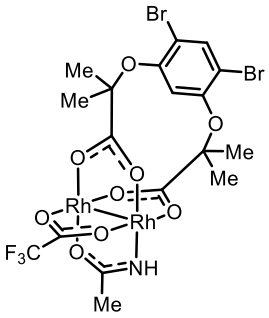

2,2'-((4,6-Dibromo-1,3-phenylene)bis(oxy))bis(2-methylpropanoic acid)[136] (24.1 mg, 0.055 mmol) was filled into a flame dried Schlenk flask and dissolved in THF (1 mL). DBU (16.4 µL, 0.11 mmol) was added and the reaction mixture was stirred for 10 min. [Rh_2(acam)$(OTfa)_3$] (30 mg, 0.05 mmol) in THF (2mL) was added dropwise and the reaction mixture was stirred at room temperature for 6 h. The reaction mixture was concentrated and the residue was purified by flash chromatography (silica, toluene/MeCN 10:1 to 5:1) to afford the desired complex as a green solid (22 mg, 54%).^{1}H NMR (400 MHz, CD_3CN) δ 7.69 (s, 1H), 6.13 (s, 1H), 5.19 (s, 1H), 1.87 (s, 3H), 1.37 (d, *J* = 1.1 Hz, 6H), 1.32 (s, 3H), 1.30 (s, 3H). ^{13}C NMR (101 MHz, CD_3CN) δ 194.4, 192.0, 189.5, 173.8 (q, *J* = 39.3 Hz), 153.1, 152.9, 136.6, 111.6, 108.6, 108.5, 83.6, 83.3, 25.3, 25.0, 24.1, (CF_3 not detected). ^{19}F NMR (282 MHz, CD_3CN) δ -75.7. IR (ATR): $\tilde{\nu}$ = 2927, 1631, 1580, 1470, 1406, 1367, 1198, 1157, 1061, 740 cm^{-1}. HRMS (ESI +): m/z calcd. for $C_{18}H_{18}F_3NO_9Br_2Rh_2$ $[M+Na]^+$: 835.73027; found: 835.72958. HPLC analysis: 150 mm Chiralpak IG-3, Ø 4.6 mm i.D., *n*-heptane/2-propanol = 98:2, v= 1.0 mL / min, λ = 220 nm, t(enantiomer 1) = 3.53 min, t(enantiomer 2) = 5.23 min. The enantiomers were separated by preparative HPLC using the following conditions: 250 mm Chiralpak IG-5, 5µm, 30.0 mm i.D., *i*-hexane/2-propanol = 98:2, v= 20.0 mL / min, λ = 220 nm. Note: the complex decomposes in alcoholic solvents, therefore acetonitrile was added before concentration of the separated enantiomers.

Rh_2(acam)(Chloro-O-esp)(OTfa) (123). 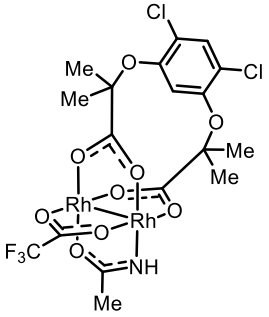

2,2'-((4,6-dichloro-1,3-phenylene)bis(oxy))bis(2-methylpropanoic acid) **262** (19.2 mg, 0.055 mmol) was filled into a flame dried Schlenk flask and dissolved in THF (1 mL). DBU (16.4 µL, 0.11 mmol) was added and the reaction mixture was stirred for 10 min. [Rh_2(acam)$(OTfa)_3$] (30 mg, 0.05 mmol) in THF (2mL) was added dropwise and the reaction mixture was stirred at room temperature for 6 h. The reaction mixture was concentrated and the residue was purified by flash chromatography (silica, toluene/MeCN 10:1 to 2:1) to afford the desired complex as a green solid (15.3 mg, 42%). ^{1}H NMR (400 MHz, CD_3CN) δ 7.32 (s, 1H), 6.13 (s, 1H), 5.11 (s, 1H), 1.79 (s, 3H), 1.29 (s, 6H), 1.24 (s, 3H), 1.21 (s, 3H). ^{13}C NMR (101 MHz, CD_3CN) δ 194.3, 191.9, 189.4, 174.0 (q, *J* = 38.5 Hz), 151.2, 151.0, 131.1, 119.8, 119.7,

112.26, 83.7, 83.4, 25.2, 24.9 (d, *J* = 4.2 Hz), 24.8, 24.1, (CF_3 not detected). IR (ATR): $\tilde{\nu}$ = 1627, 1578, 1542, 1481, 1469, 1405, 1377, 1196, 1154, 1092, 842, 741, 673 cm^{-1}. HRMS (ESI +): m/z calcd. for $C_{18}H_{18}F_3NO_9Cl_2Rh_2$ $[M+Na]^+$: 747.83130; found: 747.83097. HPLC analysis: 150 mm Chiralpak IG-3, Ø 4.6 mm i.D., *n*-heptane/ethanol = 98:2, v= 1.0 mL / min, λ = 220 nm, t(enantiomer 1) = 3.40 min, t(enantiomer 2) = 4.54 min. The enantiomers were separated by preparative HPLC using the following conditions: 250 mm Chiralpak IG-5, 5µm, 30.0 mm i.D., *i*-hexane/ethanol = 98:2, v= 20.0 mL / min, λ = 220 nm. Note: the complex decomposes in alcoholic solvents, therefore acetonitrile was added before concentration of the separated enantiomers.

[Rh_2(acam)(*t*Bu-O-esp)(OTfa)] (125). 2,2'-((4,6-Di-tert-butyl-1,3-phenylene)bis(oxy))bis(2-methylpropanoic acid)[136] (27.5 mg, 0.07 mmol) was filled into a flame dried Schlenk flask and dissolved in THF (1.2 mL). DBU (20.3 µL, 0.14 mmol) was added and the reaction mixture was stirred for 10 min. [Rh_2(acam)$(OTfa)_3$] (40 mg, 0.066 mmol) in THF (2.5 mL) was added dropwise and the reaction mixture was stirred at room temperature for 4 h. The reaction mixture was concentrated and the residue was purified by flash chromatography (silica, toluene/MeCN 10:1 to 5:1) to afford the desired complex as a green solid (33 mg, 65%). ^{1}H NMR (600 MHz, CD_3CN) δ 7.13 (s, 1H), 5.36 (s, 1H), 5.18 (s, 1H), 1.88 (d, *J* = 0.6 Hz, 3H), 1.39 (s, 3H), 1.37 (s, 3H), 1.32 (s, 9H), 1.32 (s, 3H), 1.31 (s, 3H), 1.30 (s, 9H). ^{13}C NMR (151 MHz, CD_3CN) δ 196.0, 193.9, 189.2, 173.8 (q, *J* = 38.3 Hz), 152.7, 152.5, 131.3, 131.2, 125.9, 111.9 (q, *J* = 285.9 Hz), 107.5, 80.2, 79.8, 35.1, 35.0, 30.7, 26.2, 25.9, 25.7, 25.6, 24.1. ^{19}F NMR (565 MHz, CD_3CN) δ -75.76. IR (ATR): $\tilde{\nu}$ = 1641, 1580, 1505, 1468, 1398, 1374, 1361, 1285, 1195, 1156, 1112, 1069, 840, 739, 616 cm^{-1}. HRMS (ESI -): m/z calcd. for $C_{26}H_{35}F_3NO_9Rh_2$ $[M-H]^-$: 768.03795; found: 768.03806. The enantiomers were not separable by chiral HPLC.

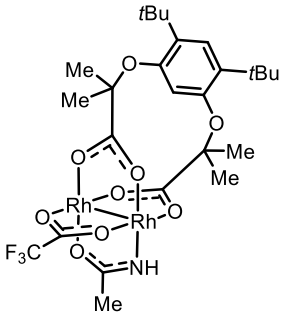

[Rh_2(acam)(*t*Bu-O-esp)(OAc)] (128). [Rh_2(Acam)(*t*Bu-O-Esp)(OTfa)] (**125**) and nBu_4NOAc (13.7 mg, 0.046 mmol) were filled into a Schlenk flask and dissolved in MeCN (2 mL). The reaction was stirred for 3 h at room temperature. The reaction mixture was concentrated and the residue was purified by flash chromatography (silica, toluene/MeCN 4:1 to 1:1) to afford the title compound as a green solid (15 mg, 65%). ^{1}H NMR (400 MHz, CD_3CN) δ 7.11 (s, 1H), 5.44 (s, 1H), 5.00 (s, 1H), 1.84 (s, 3H), 1.75 (s, 3H), 1.37 (s, 3H), 1.35 (s, 3H), 1.32 (s, 9H), 1.30 (s, 12H), 1.29 (s, 3H).

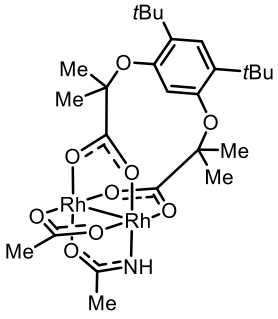

^{13}C NMR (101 MHz, CD_3CN) δ 194.1, 192.6, 191.5, 188.1, 152.8, 152.69, 131.2, 131.2, 125.7, 108.0, 80.1, 79.9, 35.0 (d, *J* = 3.4 Hz), 30.7 (d, *J* = 2.4 Hz), 26.2, 25.9, 25.6 (d, *J* = 4.9 Hz), 24.0, 23.5. IR (ATR): ṽ = 2952, 1599, 1504, 1467, 1432, 1398, 1360, 1284, 1199, 1165, 1112, 1068, 842, 711, 616 cm^{-1}. HRMS (ESI +): m/z calcd. for $C_{26}H_{39}NO_9Rh_2Na$ [M+Na]$^+$: 738.06271; found: 738.06214.

Complex (126). (*R*)-Mosher acid (8.5 mg, 0.036 mmol) was filled into a flame dried Schlenk flask and dissolved in MeCN (0.5 mL). DBU (5.2 µL, 0.035 mmol) was added and the reaction mixture was stirred for 10 min. Rh_2(acam)(*t*Bu-O-esp)(OTfa) (**125**) (20 mg, 0.026 mmol) in THF (0.8 mL) was added dropwise and the reaction mixture was stirred at room temperature for 22 h. The reaction mixture was concentrated and the residue was purified by flash chromatography (silica, toluene/MeCN 5:1) to afford a diastereomeric mixture of the title complex as a green solid (17.5 mg, 76%, 1:1 dr). Attempts to separate the diastereomers via preparatory HPLC were not successful. HRMS (ESI +): m/z calcd. for $C_{34}H_{44}F_3NO_{10}Rh_2Na$ [M+Na]$^+$: 912.09196; found: 912.09207. ^{1}H NMR (600 MHz, CD_3CN) δ 7.40 – 7.36 (m, 2H), 7.35 – 7.31 (m, 4H), 7.23 (~d, 2H), 7.22 (~d, *J* = 9.5, 1.1 Hz, 2H), 7.13 (s, 2H), 5.35 (~s, 1H), 5.34 (~s, 1H), 5.25 (s, 1H), 5.15 (s, 1H), 3.29 (~q(br), *J* = 1.2 Hz, 3H), 3.26 (~q(br), *J* = 1.1 Hz, 3H), 1.89 (s, 3H), 1.86 (s, 3H), 1.43 (s, 3H), 1.41 (s, 3H), 1.40 (s, 3H), 1.39 (s, 3H), 1.36 (d, *J* = 3.4 Hz, 12H), 1.34 (s, 18H), 1.31 (s, 18H). ^{13}C NMR (151 MHz, CD_3CN) δ 195.1, 193.3 (d, *J* = 2.8 Hz), 188.8 (d, *J* = 5.2 Hz), 152.6 (d, *J* = 1.9 Hz), 152.5 (d, *J* = 2.1 Hz), 134.9 (d, *J* = 11.0 Hz), 130.7 (dd, *J* = 18.2, 4.5 Hz), 130.4 (d, *J* = 1.7 Hz), 129.2 (d, *J* = 2.6 Hz), 128.1, 128.0, 125.8, 124.4 (q, *J* = 287.8 Hz), 107.3 (d, *J* = 2.3 Hz), 84.7 (q, *J* = 26.9 Hz), 84.6 (q, *J* = 26.7 Hz), 80.0, 79.7, 55.5 (d, *J* = 13.1 Hz), 35.1 (d, *J* = 5.3 Hz), 30.6, 26.3 (d, *J* = 4.6 Hz), 26.2, 26.0, 25.8, 25.7, 25.6, 23.9 (d, *J* = 5.4 Hz). ^{19}F NMR (565 MHz, CD_3CN) δ –72.0, –71.9. HRMS (ESI +): m/z calcd. for $C_{34}H_{44}F_3NO_{10}Rh_2Na$ [M+Na]$^+$: 912.09196; found: 912.09207.

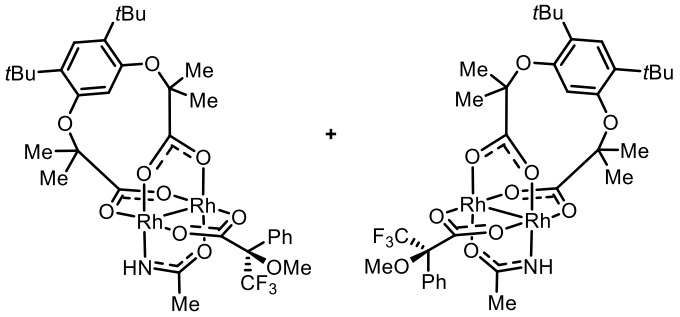

Complex (127). *N*-Tosyl-(*L*)-proline (8.1 mg, 0.03 mmol) was filled into a flame dried Schlenk flask and dissolved in MeCN (0.5 mL). DBU (4.7 µL, 0.031 mmol) was added and the reaction mixture was left stirring for 10 min. [Rh_2(acam)(*t*Bu-O-esp)(OTfa)] (**125**) (20 mg, 0.026 mmol) in THF (0.8 mL) was added dropwise and the

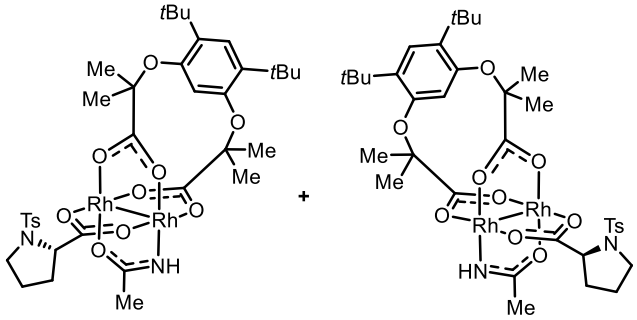

reaction mixture was stirred at room temperature for 22 h. The reaction mixture was concentrated and the residue was purified by flash chromatography (silica, toluene/MeCN 5:1) to afford a diastereomeric mixture of the title complex as a green solid (17.5 mg, 73%, 1:1 *dr*). The diastereomers were separated via preparatory HPLC using the following conditions: 250 mm Multo-Krom 100-Si, 5µm, 20.0 mm i.D., *i*-hexane/ethanol = 95:5, v= 10.0 mL / min, λ = 220 nm. Diastereomer 1: ^{1}H NMR (600 MHz, CD_3CN) δ 7.65 (AA'(m), 2H), 7.39 (XX'(m), 2H), 7.12 (s, 1H), 5.42 (s, 1H), 5.01 (~s, 1H), 3.89 (dd, *J* = 8.1, 4.5 Hz, 1H), 3.25 (ddd, *J* = 9.8, 6.7, 5.3 Hz, 1H), 3.16 – 3.10 (m, 1H), 2.42 (s, 3H), 1.83 (s, 3H), 1.76 – 1.68 (m, 2H), 1.53 – 1.45 (m, 1H), 1.42 – 1.36 (m, 2H), 1.35 (s, 3H), 1.33 (s, 3H), 1.32 (s(overlapped), 3H), 1.32 (s, 9H), 1.31 (s, 3H), 1.31 (s, 9H). ^{13}C NMR (151 MHz, CD_3CN) δ 194.4, 192.7 (d, *J* = 4.9 Hz), 188.1, 152.8, 152.6, 144.7, 136.3, 131.1 (d, *J* = 23.5 Hz), 130.6, 107.8, 79.9 (d, *J* = 44.4 Hz), 62.4, 49.4, 35.0 (d, *J* = 5.8 Hz), 32.3, 30.6 (d, *J* = 3.2 Hz), 26.1, 25.9, 25.6 (d, *J* = 10.4 Hz), 25.3, 24.0, 21.5. HRMS (ESI +): m/z calcd. for $C_{36}H_{50}N_2SO_{11}Rh_2Na$ $[M+Na]^+$: 947.11376; found: 947.11349. IR (ATR): ṽ = 2952, 1604, 1468, 1406, 1360, 1200, 1158, 1112, 670, 667 cm^{-1}. Diastereomer 2: ^{1}H NMR (600 MHz, CD_3CN) δ 7.65 (AA'(m), 2H), 7.39 (XX'(m), 2H), 7.12 (s, 1H), 5.43 (s, 1H), 5.02 (~s, 1H), 3.94 (dd, *J* = 8.0, 4.2 Hz, 1H), 3.29 – 3.21 (m, 1H), 3.13 (~dt, *J* = 9.6, 7.2 Hz, 1H), 2.42 (s, 3H), 1.84 (~d, 3H), 1.76 – 1.67 (m, 2H), 1.56 – 1.48 (m, 1H), 1.39 – 1.36 (m, 2H), 1.35 (s, 3H), 1.34 (s, 3H), 1.32 (s, 12H), 1.31 (s, 9H), 1.31 (s, 3H). ^{13}C NMR (151 MHz, CD_3CN) δ 194.4, 192.7 (d, *J* = 5.2 Hz), 188.1, 152.8, 152.6, 144.6, 136.4, 131.1 (d, *J* = 23.4 Hz), 130.6, 128.5, 125.7, 107.8, 79.9 (d, *J* = 42.3 Hz), 62.4, 35.0 (d, *J* = 5.7 Hz), 32.3, 26.1 (d, *J* = 34.9 Hz), 25.6, 25.5, 25.2, 24.0, 21.5. HRMS (ESI +): m/z calcd. for $C_{36}H_{51}N_2SO_{11}Rh_2$ $[M+H]^+$: 925.13182; found: 925.1319. IR (ATR): ṽ = 2956, 1602, 1468, 1407, 1361, 1200, 1158, 1112, 669 cm^{-1}.

[Rh_2(acam)(Bromo-calix[4]arene)(OTfa)] (134). A two-neck flask was equipped with a

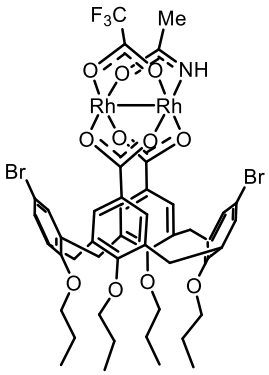

Soxhlet extractor (returning-arm frit) topped by a reflux condenser. The Soxhlet extractor was filled with an ovendried mixture of K_2CO_3 and sand (1:1, ca. 5 g). The flask was charged with the calix[4]arene derivative **133** (334 mg, 0.40 mmol) and Rh_2(acam)$(OTfa)_3$ (200 mg, 0.33 mmol), followed by addition of *tert*-butyl acetate (40 mL) and toluene (12 mL). Argon was bubbled through the mixture for 15 min, before the flask was immersed into a pre-heated oil bath (130 °C bath temperature). The mixture was stirred at reflux temperature such that a gentle flow of condensing solvent passed through the Soxhlet extractor. (Note: initially the reaction mixture is a suspension, but as the reaction progresses, the suspension slowly becomes a transparent green solution). After 5 h, the mixture was cooled to room temperature

and concentrated under reduced pressure. The green residue was purified by flash chromatography (silica, toluene/acetonitrile 12:1 to 7:1) to afford the title compound as a green solid (147 mg, 37%). ^{1}H NMR (600 MHz, [D$_8$]-THF) δ 7.39 (d, *J* = 2.5 Hz, 1H), 7.37 (d, *J* = 2.7 Hz, 2H), 7.35 (d, *J* = 2.5 Hz, 1H), 6.74 – 6.71 (m, 2H), 6.66 (d, *J* = 2.2 Hz, 1H), 6.59 (d, *J* = 2.2 Hz, 1H), 5.27 (s, 1H), 4.41 – 4.34 (m, 4H), 4.00 – 3.95 (m, 4H), 3.68 – 3.63 (m, 4H), 3.19 – 3.11 (m, 4H), 1.88 – 1.81 (m, 8H), 1.80 (s, 3H), 1.08 (t, *J* = 7.4 Hz, 3H), 1.08 (t, *J* = 7.4 Hz, 3H), 0.82 (t, *J* = 7.5 Hz, 3H), 0.82 (t, *J* = 7.5 Hz, 3H). ^{13}C NMR (151 MHz, [D$_8$]-THF) δ 186.46, 185.71, 184.26, 171.99 (q, *J* = 37.9 Hz), 159.43, 159.28, 158.23, 158.19, 140.34, 140.23, 140.18, 140.09, 132.97, 132.90, 132.88, 132.73, 132.57 (d, *J* = 3.5 Hz), 130.30, 129.97, 129.80, 129.40, 127.92, 127.03, 115.19, 115.05, 111.87 (q, *J* = 286.3 Hz), 77.76, 77.46, 77.38, 31.58 (t, *J* = 5.6 Hz), 24.33, 23.68, 23.62, 23.35, 11.14, 11.12, 9.95, 9.93. ^{19}F NMR (565 MHz, [D$_8$]-THF) δ –75.8. IR (ATR): $\tilde{\nu}$ = 2964, 2934, 2877, 1637, 1570, 1403, 1384, 1200, 1159, 959, 740 cm^{-1}. HRMS (ESI +): m/z calcd. for $C_{46}H_{48}Br_2F_3NO_{11}Rh_2Na$ [M+Na]$^+$: 1233.95485; found: 1233.95486.

HPLC analysis: 150 mm Chiralcel IB-N3, 4.6 mm Ø, acetonitrile/water = 70:30, v = 1.0 mL / min, λ = 220 nm, t(enantiomer 1) = 12.79 min, t(enantiomer 2) = 14.06 min. The enantiomers were separated by preparative HPLC using the following conditions: 250 mm YMC Chiral Art Cellulose-SB, 5µm, 20.0 mm ∅, acetonitrile / water= 70:30 , v = 15.0 mL / min, λ = 220 nm. The overall yield of each enantiomer ranged between 9-13%.

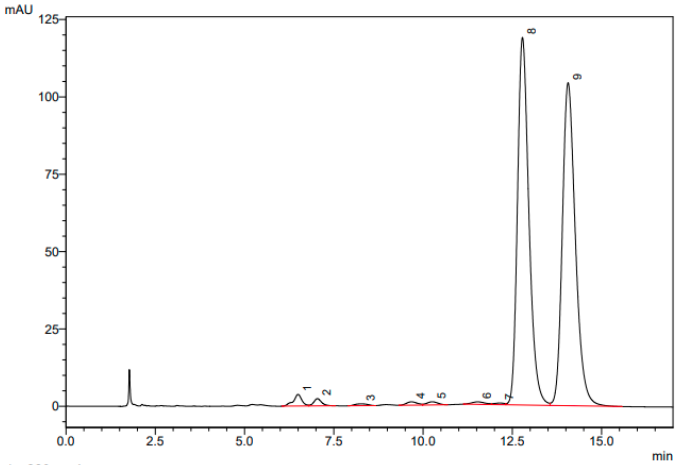

1 220nm,4nm

PDA Ch1 220nm

Peak #	Ret. Time	Area %	Name
1	6.50	1.13	
2	7.04	0.65	
3	8.28	0.26	
4	9.68	0.41	
5	10.26	0.39	
6	11.53	0.38	
7	12.17	0.19	
8	12.79	48.21	1. enantiomer
9	14.06	48.38	2. enantiomer
Total		100.00	

Separation of the enantiomers of complex **134** by HPLC under the conditions described above.

CD spectra of complex **134** were measured in 10 mm Quartz cuvettes with a concentration of 1 mg/mL in *tert*-butyl methyl ether. The UV-VIS spectrum of complex **134** was measured in a 2 mm Suprasil Quartz cuvette at a concentration of 1.8 mM in *tert*-butyl methyl ether (see Appendix). A cuvette with pure solvent (*tert*-butyl methyl ether) was placed in the reference beam. The measured absorption was subsequently converted to molar absorption coefficient using the Lambert-Beer law. Two relatively weak bands at 624 nm and 425 nm are present with molar absorption coefficients of 115 $M^{-1}cm^{-1}$ and 120 $M^{-1}cm^{-1}$, respectively.

During flash chromatography, a second fraction was isolated. Subsequent trituration of the remaining solid with *tert*-butyl methyl ether afforded complex **[Rh_2(Bromo-calix[4]arene)(OTfa)$_2$] (265)** as a green solid (70 mg, 16%). ^{1}H NMR (600 MHz, [D_8]-THF) δ 7.41 (s, 4H), 6.68 (s, 4H), 4.37 (d, J = 13.9 Hz, 4H), 4.01 – 3.95 (m, 4H), 3.68 (t, J = 6.7 Hz, 4H), 3.17 (d, J = 13.7 Hz, 4H), 1.89 – 1.79 (m, 8H), 1.08 (t, J = 7.4 Hz, 6H), 0.82 (t, J = 7.5 Hz, 6H). ^{13}C NMR (151 MHz, [D_8]-THF) δ 188.21, 174.30, 174.05, 173.79, 173.53, 160.20, 158.09, 140.10, 133.44, 132.75, 130.03, 126.14, 115.26, 114,25, 112.36, 110.47, 108.58, 77.89, 77.47, 31.47, 24.31, 23.69, 11.09, 9.92. ^{19}F NMR (565 MHz, [D_8]-THF) δ –75.9. IR (ATR): $\tilde{\nu}$ = 2963, 2926, 1647, 1462, 1403, 1383, 1196, 1159, 1111, 1001, 958, 866, 740 cm^{-1}. HRMS (ESI +): m/z calcd. for $C_{46}H_{44}Br_2F_6O_{12}Rh_2Na$ $[M+Na]^+$: 1288.91060; found: 1288.91081.

[Rh_2(acam)(Iodo-calix[4]arene)(OTfa)] (154). Prepared analogously to **134** from calix[4]arene **153**. The green residue was purified by flash chromatography (silica, toluene/acetonitrile 12:1 to 7:1) affording the title compound as a green solid (35 mg, 54%). ^{1}H NMR (600 MHz, [D_8]-THF) δ 7.57 (d, *J* = 2.3 Hz, 1H), 7.55 (d, *J* = 2.3 Hz, 1H), 7.54 (d, *J* = 2.3 Hz, 1H), 7.53 (d, *J* = 2.3 Hz, 1H), 6.72 (d, *J* = 2.3 Hz, 1H), 6.71 (d, *J* = 2.1 Hz, 1H), 6.65 (d, *J* = 2.1 Hz, 1H), 6.58 (d, *J* = 1.9 Hz, 1H), 5.28 (s, 1H), 4.35 (d, *J* = 13.8 Hz, 2H), 4.34 (d, *J* = 13.3 Hz, 2H), 3.99 – 3.96 (m, 4H), 3.67 – 3.63 (m, 4H), 3.15 (d, *J* = 14.0 Hz, 1H), 3.14 (d, *J* = 14.0 Hz, 1H), 3.13 (d, *J* = 14.0 Hz, 1H), 3.11 (d, *J* = 14.0 Hz, 1H), 1.87 – 1.81 (m, 8H), 1.80 (s, 3H), 1.08 (t, *J* = 7.4 Hz, 3H), 1.07 (t, *J* = 7.4 Hz, 3H), 0.81 (t, *J* = 7.5 Hz, 3H), 0.80 (t, *J* = 7.5 Hz, 3H). ^{13}C NMR (151 MHz, [D_8]-THF) δ 186.63, 185.93, 184.50, 172.15 (q, *J* = 37.7 Hz), 159.60, 159.46, 159.26, 159.22, 140.93, 140.79, 140.76, 140.67, 138.99, 138.87, 138.82, 138.76, 133.20, 133.14, 133.11, 132.96, 130.47, 130.16, 129.95, 129.54, 128.09, 127.21, 112.04 (q, *J* = 286.0 Hz), 86.37, 86.25, 77.92, 77.64, 77.53, 31.61 (t, *J* = 6.5 Hz), 24.50, 23.83, 23.76, 23.53, 11.31 (d, *J* = 3.1 Hz), 10.08 (d, *J* = 3.5 Hz). ^{19}F NMR (282 MHz, [D_8]-THF) δ –75.8. IR (ATR): $\tilde{\nu}$ = 2965, 2933, 2876, 1639, 1462,

1403, 1384, 1294, 1200, 1158, 1113, 1002, 959, 840, 740 cm^{-1}. HRMS (ESI +): m/z calcd. for $C_{46}H_{48}I_2F_3NO_{11}Rh_2Na$ $[M+Na]^+$: 1329.92712; found: 1329.92715. HPLC analysis: 150 mm Chiralcel IB-N3, Ø 4.6 mm i.D., acetonitrile / water = 75:25, v = 1.0 mL / min, λ = 220 nm, t(enantiomer 1) = 8.69 min, t(enantiomer 2) = 9.75 min. The enantiomers were separated by preparative HPLC using the following conditions: 250 mm YMC Chiral Art Cellulose-SB, 5µm, 20.0 mm i.D., acetonitrile / water = 70:30, v = 15.0 mL / min, λ = 220 nm. The overall yield of each enantiomer ranged between 14-16%.

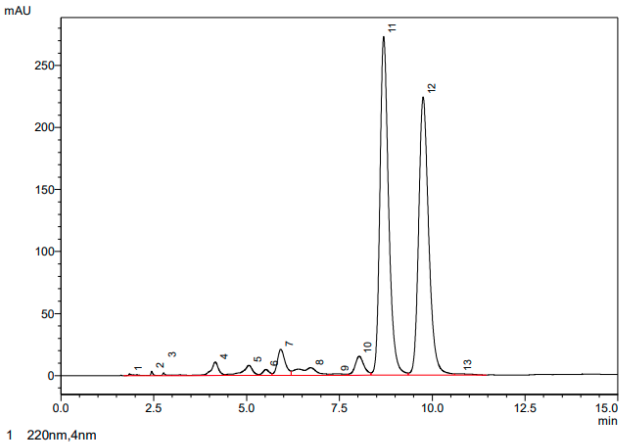

1 220nm,4nm

PDA Ch1 220nm

Peak #	Ret. Time	Area %	Name
1	1.85	0.15	
2	2.44	0.15	
3	2.76	0.25	
4	4.16	1.56	
5	5.06	1.60	
6	5.52	0.59	
7	5.92	3.13	
8	6.73	2.23	
9	7.42	0.32	
10	8.03	2.57	
11	8.69	44.83	1. Enantiomer
12	9.75	42.31	2. Enantiomer
13	10.72	0.30	
Total		100.00	

Separation of the enantiomers of complex **154** by HPLC under the conditions described above.

[Rh_2(*N*-Me-acam)(Bromo-calix[4]arene)(OTfa)] (162). Prepared analogously to **134** from

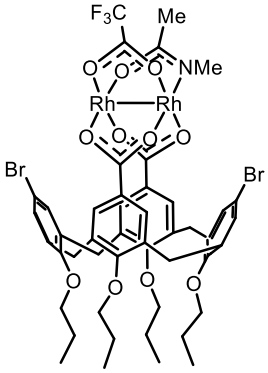

[Rh_2(*N*-Me-acam)(OTfa)$_3$] (**161**) and calix[4]arene **133** (note: 4 h reaction time instead of 6 h). The green residue was purified by flash chromatography (silica, toluene/acetonitrile 10:1 to 7:1) affording the title compound as a green solid (29 mg, 48%). ^{1}H NMR (600 MHz, [D_8]-THF) δ 7.39 – 7.35 (m, 4H), 6.75 (d, *J* = 2.1 Hz, 1H), 6.70 (d, *J* = 2.1 Hz, 1H), 6.65 (d, *J* = 2.1 Hz, 1H), 6.60 (d, *J* = 2.2 Hz, 1H), 4.39 – 4.35 (m, 4H), 4.04 – 3.94 (m, 4H), 3.70 – 3.63 (m, 4H), 3.21 – 3.08 (m, 4H), 3.02 (s, 3H), 1.88 – 1.81 (m, 11H), 1.08 (t, *J* = 7.4 Hz, 3H), 1.08 (t, *J* = 7.4 Hz, 3H), 0.82 (t, *J* = 7.8 Hz, 3H), 0.81 (t, *J* = 7.5 Hz, 3H). ^{13}C NMR (151 MHz, [D_8]-THF) δ 185.79, 184.29, 183.07, 171.95 (q, *J* = 38.0 Hz), 159.51, 159.34, 158.23 (d, *J* = 3.0 Hz), 140.32, 140.24, 140.21, 140.07, 133.01, 132.99, 132.95, 132.82, 132.78, 132.75, 132.58, 132.50, 130.45,

130.00, 129.62, 129.35, 128.00, 126.95, 115.20, 114.99, 111.88 (q, *J* = 285.7 Hz), 77.77 (d, *J* = 2.3 Hz), 77.54, 77.32, 38.59, 31.59 (dd, *J* = 16.9, 7.1 Hz), 24.33, 23.70, 23.55, 19.97, 11.13 (d, *J* = 2.9 Hz), 9.95, 9.89. ^{19}F NMR (565 MHz, [D$_8$]-THF) δ –75.9. IR (ATR): $\tilde{\nu}$ = 2962, 2930, 2876, 1633, 1590, 1519, 1462, 1404, 1383, 1200, 1159, 1113, 1003, 960, 864 cm^{-1}. HRMS (ESI +): m/z calcd. for $C_{47}H_{50}Br_2F_3NO_{11}Rh_2Na$ [M+Na]$^+$: 1247.9705; found: 1247.97017. HPLC analysis: 150 mm Chiralpak IE-3, Ø 4.6 mm i.D., acetonitrile / water = 82:18, v = 1.0 mL / min, λ = 220 nm, t(enantiomer 1) = 6.54 min, t(enantiomer 2) = 9.69 min. The enantiomers were separated by preparative HPLC using the following conditions: 250 mm Chiralpak IE, 5µm, 20.0 mm i.D., acetonitrile / water = 80:20, v = 15.0 mL / min, λ = 220 nm. The overall yield of each enantiomer ranged between 14-16%.

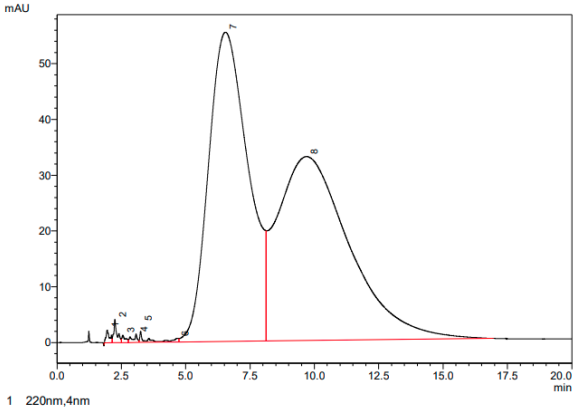

1 220nm,4nm

PDA Ch1 220nm

Peak #	Ret. Time	Area %	Name
1	1.95	0.17	
2	2.25	0.29	
3	2.56	0.10	
4	3.07	0.14	
5	3.25	0.17	
6	4.67	0.11	
7	6.54	47.53	1. Enantiomer
8	9.69	51.49	2. Enantiomer
Total		100.00	

Analytical chiral HPLC trace of complex **162** under the HPLC conditions described above.

[Rh$_2$(Acam)(*p*-tolyl-calix[4]arene)(OTfa)] (156). Prepared analogous to **134** from

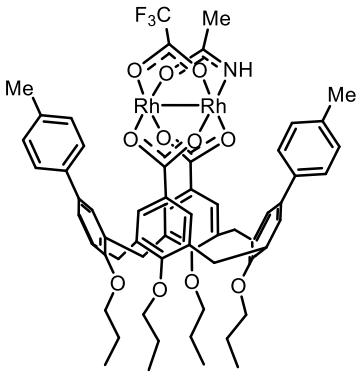

[Rh$_2$(acam)(OTfa)$_3$] (26 mg, 0.043 mmol) and calix[4]arene **151** (44 mg, 0.51 mmol) as a green solid (23.4 mg, 44%). ^{1}H NMR (600 MHz, [D$_8$]-THF) δ 7.78 (d, *J* = 8.0 Hz, 2H), 7.76 (d, *J* = 8.0 Hz, 2H), 7.59 – 7.54 (m, 4H), 7.33 (d, *J* = 10.2 Hz, 2H), 7.32 (d, *J* = 10.3 Hz, 2H), 6.79 (d, *J* = 2.3 Hz, 1H), 6.78 (d, *J* = 2.3 Hz, 1H), 6.72 (d, *J* = 2.2 Hz, 1H), 6.65 (d, *J* = 2.2 Hz, 1H), 5.15 (s, 1H), 4.50 – 4.43 (m, 4H), 4.07 – 4.01 (m, 4H), 3.75 – 3.68 (m, 4H), 3.31 – 3.17 (m, 4H), 2.44 (s, 3H), 2.43 (s, 3H), 1.93 – 1.86 (m, 8H), 1.74 (s, 3H), 1.12 (td, *J* = 7.4, 0.8 Hz, 3H), 1.12 (td, *J* = 7.4, 0.8 Hz, 3H), 0.85 (t, *J* = 7.3 Hz, 2H), 0.84 (t, *J* = 7.5 Hz, 3H). ^{13}C NMR (151 MHz, [D$_8$]-THF) δ 186.20, 185.96, 184.56, 171.75 (d, *J* = 37.8 Hz), 159.48, 159.33, 158.45, 158.39, 138.65, 138.53, 138.36, 138.17, 138.09, 137.07 (d,

J = 4.3 Hz), 134.80, 134.48, 133.42, 133.38, 133.32, 133.15, 130.36, 130.22, 130.07, 129.88, 129.44, 127.89, 127.84, 127.79 (d, *J* = 3.7 Hz), 127.53, 127.24, 127.07, 126.96, 111.83 (q, *J* = 287.0 Hz), 77.65 (d, *J* = 2.1 Hz), 77.36, 77.26, 32.11 (dd, *J* = 7.3, 4.4 Hz), 24.42 (d, *J* = 1.6 Hz), 23.80, 23.74, 23.31, 21.16 (d, *J* = 2.3 Hz), 11.24 (d, *J* = 3.5 Hz), 10.06 (d, *J* = 3.3 Hz). ^{19}F NMR (565 MHz, [D$_8$]-THF) δ –75.9. IR (ATR): $\tilde{\nu}$ = 2960, 2925, 2874, 2854, 1641, 1468, 1402, 1384, 1201, 1158, 1109, 1005, 817 cm^{-1}. HRMS (ESI +): m/z calcd. for $C_{60}H_{62}F_3NO_{11}Rh_2Na$ [M+Na]$^+$: 1258.22773; found: 1258.22737. HPLC analysis: 150 mm Chiralcel IB-N3, Ø 4.6 mm i.D., acetonitrile / water = 80:20, v = 1.0 mL / min, λ = 220 nm, t(enantiomer 1) = 7.75 min, t(enantiomer 2) = 8.16 min. The enantiomers were separated by preparative HPLC using following conditions: 250 mm YMC Chiral Art Cellulose-SB, 5µm, Ø 20.0 mm i.D., acetonitrile / water= 80:20, v= 15.0 mL / min, λ = 220 nm with recycling loop (5 cycles).

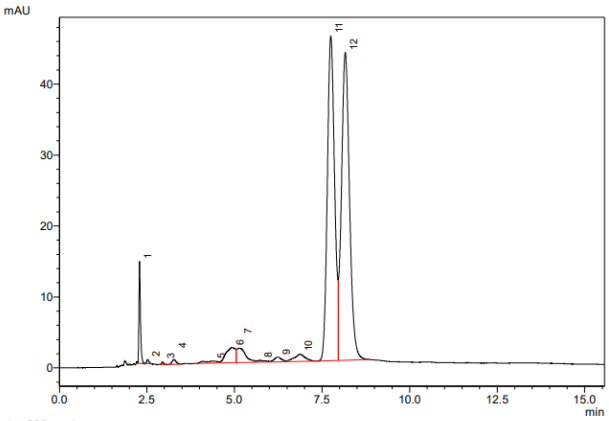

1 220nm,4nm

PDA Ch1 220nm

Peak #	Ret. Time	Area %	Name
1	2.29	2.83	
2	2.53	0.17	
3	2.94	0.09	
4	3.28	0.35	
5	4.38	0.55	
6	4.92	2.67	
7	5.15	2.32	
8	5.72	0.30	
9	6.24	0.67	
10	6.87	1.43	
11	7.75	42.94	
12	8.16	45.68	
Total		100.00	

Analytical chiral HPLC trace of complex **156** under the HPLC conditions described above.

[Rh$_2$(acam)(3,5-dimethylphenyl-calix[4]arene)(OTfa)] (157). Prepared analogously to **134** from [Rh$_2$(acam)(OTfa)$_3$] and calix[4]arene **150** as a green solid (27.9 mg, 44%). ^{1}H NMR (600 MHz, [D$_8$]-THF) δ 7.58 (d, *J* = 2.4 Hz, 1H), 7.56 – 7.54 (m, 3H), 7.51 – 7.50 (m, 2H), 7.48 – 7.47 (m, 2H), 7.03 – 7.02 (m, 1H), 7.02 – 7.01 (m, 1H), 6.80 (d, *J* = 2.2 Hz, 1H), 6.78 (d, *J* = 2.2 Hz, 1H), 6.72 (d, *J* = 2.0 Hz, 1H), 6.66 (d, *J* = 2.2 Hz, 1H), 5.16 (s, 1H), 4.52 – 4.44 (m, 4H), 4.09 – 4.02 (m, 4H), 3.75 – 3.68 (m, 4H), 3.31 – 3.17 (m, 4H), 2.46 (d, *J* = 0.7 Hz, 6H), 2.45

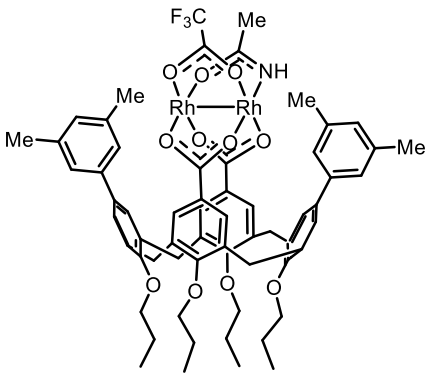

(d, *J* = 0.7 Hz, 6H), 1.94 – 1.86 (m, 8H), 1.75 (s, 3H), 1.13 (t, *J* = 7.4 Hz, 3H), 1.13 (t, *J* = 7.4 Hz, 3H), 0.85 (t, *J* = 7.5 Hz, 3H), 0.85 (t, *J* = 7.5 Hz, 3H). ^{13}C NMR (151 MHz, [D$_8$]-THF) δ 186.20, 185.97, 184.56, 171.77 (q, *J* = 37.7 Hz), 159.49, 159.33, 158.55, 158.49, 141.39, 141.34, 138.80 (d, *J* = 2.9 Hz), 138.28, 138.10, 138.02 (d, *J* = 1.3 Hz), 135.12, 134.88, 133.45, 133.38, 133.35, 133.16, 130.36, 130.07, 129.89, 129.47, 129.07 (d, *J* = 3.1 Hz), 128.15 (d, *J* = 3.1 Hz), 128.09, 127.85, 126.96, 125.35, 125.27, 111.84 (q, *J* = 285.9 Hz), 77.65 (d, *J* = 1.4 Hz), 77.33, 77.27, 32.10 (t, *J* = 4.4 Hz), 24.43 (d, *J* = 1.6 Hz), 23.77 (d, *J* = 6.7 Hz), 23.32, 21.65, 11.26 (d, *J* = 3.5 Hz), 10.08 (d, *J* = 1.9 Hz). ^{19}F NMR (565 MHz, [D$_8$]-THF) δ –75.8. IR (ATR): $\tilde{\nu}$ = 2963, 2924, 2876, 1641, 1602, 1464, 1403, 1384, 1200, 1158, 1108, 1005, 960, 846, 740 cm^{-1}. HRMS (ESI +): m/z calcd. for $C_{62}H_{66}F_3NO_{11}Rh_2Na$ [M+Na]$^+$: 1286.25903; found: 1286.26015. HPLC analysis: 150 mm Chiralcel IB-N3, Ø 4.6 mm i.D., acetonitrile / water = 70:30, v = 1.0 mL / min, λ = 220 nm, t(enantiomer 1) = 35.21 min, t(enantiomer 2) = 37.57 min. The enantiomers were separated by preparative HPLC using following conditions: 250 mm YMC Chiral Art Cellulose-SB, 5µm, Ø 20.0 mm i.D., acetonitrile / water= 70:30, v = 15.0 mL / min, λ = 220 nm. The overall yield of each enantiomer ranged between 15-19%.

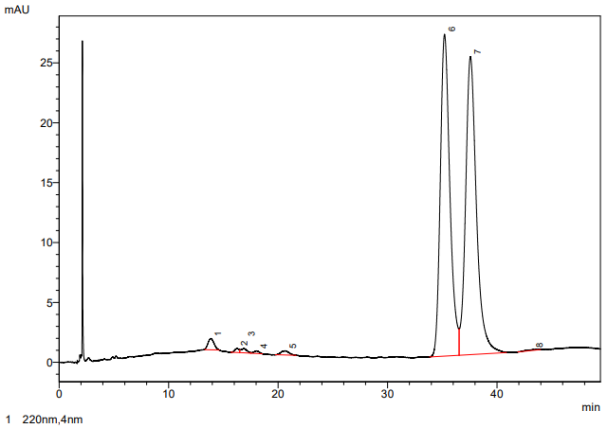

PDA Ch1 220nm

Peak #	Ret. Time	Area %	Name
1	13.86	1.06	
2	16.25	0.26	
3	16.92	0.39	
4	18.03	0.20	
5	20.68	0.51	
6	35.21	47.51	1st enantiomer
7	37.57	49.92	2nd enantiomer
8	43.23	0.14	
Total		100.00	

Analytical chiral HPLC trace of complex **157** under the HPLC conditions described above.

[Rh$_2$(bnam)(Bromo-calix[4]arene)(OTfa)] (158). Prepared analogously to **134** from

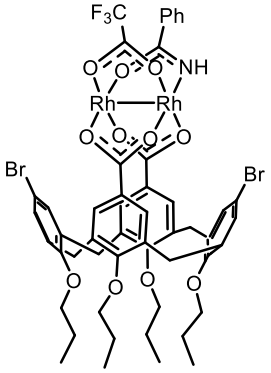

[Rh$_2$(bnam)(OTfa)$_3$] (30 mg, 0.045 mmol) and calix[4]arene **133** (45.4 mg, 0.54 mmol) as a green solid (28 mg, 49%). ^{1}H NMR (600 MHz, [D$_8$]-THF) δ 7.69 – 7.66 (m, 2H), 7.41 (d, *J* = 2.5 Hz, 1H), 7.39 – 7.38 (m, 2H), 7.36 (d, *J* = 2.5 Hz, 1H), 7.30 – 7.26 (m, 1H), 7.25 – 7.22 (m, 2H), 6.77 (d, *J* = 2.2 Hz, 1H), 6.76 (d, *J* = 2.2 Hz, 1H), 6.67 (d, *J* = 2.2 Hz, 1H), 6.60 (d, *J* = 2.2 Hz, 1H), 6.04 (s, 1H), 4.43 – 4.29 (m, 4H), 4.02 – 3.96 (m, 4H), 3.68 (td, *J* = 6.7, 2.2 Hz, 2H), 3.64 (t, *J* = 6.6 Hz, 2H), 3.19 (d, *J* = 14.0 Hz, 1H), 3.18 (d, *J* = 13.9 Hz, 1H), 3.14 (d, *J* = 14.0 Hz, 1H), 3.13 (d, *J* = 14.0 Hz, 1H), 1.90 – 1.80 (m, 8H), 1.09 (t, *J* = 7.4 Hz, 3H), 1.07 (t, *J* = 7.4 Hz, 3H), 0.83 (t, *J* = 7.5 Hz, 3H), 0.82 (t, *J* = 7.5 Hz, 3H). ^{13}C NMR (151 MHz, [D$_8$]-THF) δ 185.95, 184.62, 183.29, 172.20 (q, *J* = 38.2 Hz), 159.50, 159.40, 158.21 (d, *J* = 4.5 Hz), 140.34, 140.22 (d, *J* = 2.2 Hz), 140.11, 135.04, 133.02, 132.97 (d, *J* = 1.5 Hz), 132.81, 132.77, 132.62 (d, *J* = 1.6 Hz), 132.56, 115.22, 115.07, 111.85 (q, *J* = 285.6 Hz), 77.79, 77.75, 77.48, 77.38, 31.57 (t, *J* = 7.3 Hz), 24.33 (d, *J* = 3.2 Hz), 23.70, 23.63, 11.13 (d, *J* = 5.1 Hz), 9.94 (d, *J* = 3.2 Hz). ^{19}F NMR (565 MHz, [D$_8$]-THF) δ –75.8. IR (ATR): $\tilde{\nu}$ = 2962, 2925, 1639, 1552, 1454, 1403, 1384, 1200, 1158, 1111, 1003, 959, 694 cm^{-1}. HRMS (ESI +): m/z calcd. for $C_{51}H_{50}Br_2F_3NO_{11}Rh_2Na$ [M+Na]$^+$: 1295.9705; found: 1295.97155. HPLC analysis: 150 mm Chiralcel IB-N3, Ø 4.6 mm i.D., acetonitrile / water = 80:20, v= 1.0 mL / min, λ = 220 nm, t(enantiomer 1) = 7.20 min, t(enantiomer 2) = 7.44 min]. The enantiomers were separated by preparative HPLC using following conditions: 250 mm YMC Chiral Art Cellulose-SB, 5µm, Ø 20.0 mm i.D., acetonitrile / water= 80:20, v = 15.0 mL / min, λ = 220 nm with recycling loop (5 cycles).

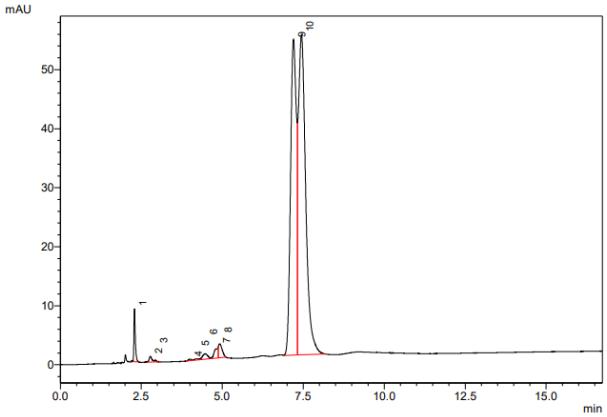

1 220nm,4nm

PDA Ch1 220nm

Peak #	Ret. Time	Area %	Name
1	2.29	1.67	
2	2.78	0.36	
3	2.94	0.09	
4	4.00	0.12	
5	4.22	0.12	
6	4.47	0.67	
7	4.87	0.85	
8	4.92	1.16	
9	7.20	41.39	
10	7.44	53.57	
Total		100.00	

Analytical chiral HPLC trace of complex **158** under the HPLC conditions described above.

[Rh_2(acam)$_2$(Bromo-calix[4]arene) (163). A two-neck flask was charged with calix[4]arene

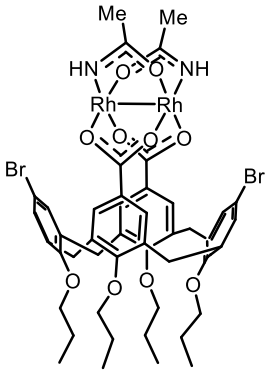

133 (111 mg, 0.13 mmol) and [Rh_2(acam)$_4$] (50 mg, 0.11 mmol) followed by addition of chlorobenzene (20 mL). The reaction mixture was submerged in an oil bath (135 °C bath temp) and heated to reflux for 1 h 30 min. The reaction mixture was cooled to room temperature and concentrated under reduced pressure. The green residue was purified by flash chromatography (silica, toluene/acetonitrile 10:1 to 100% acetonitrile) followed by preparatory HPLC (150 mm Eclipse Phenyl-hexyl, 5µm, Ø 21.1 mm i.D., methanol / water = 90:10, v= 15 mL/min) to afford the title complex as a green solid (9 mg, 7%). ^{1}H NMR (600 MHz, [D_8]-THF) δ 7.33 (s, 4H), 6.72 (d, *J* = 2.1 Hz, 2H), 6.65 (d, *J* = 2.1 Hz, 2H), 4.86 (s, 2H), 4.37 (d, *J* = 13.8 Hz, 4H), 4.01 – 3.95 (m, 4H), 3.65 (t, *J* = 6.7 Hz, 4H), 3.14 (t, *J* = 14.5 Hz, 4H), 1.89 – 1.81 (m, 8H), 1.71 (s, 6H), 1.08 (t, *J* = 7.4 Hz, 6H), 0.81 (t, *J* = 7.5 Hz, 6H). ^{13}C NMR (151 MHz, [D_8]-THF) δ 183.20, 181.09, 157.65, 157.32, 139.32, 139.28, 131.58, 131.42, 131.41, 131.34, 128.78, 128.74, 127.75, 113.98, 76.64, 76.37, 30.67, 23.34, 22.82, 22.60, 10.16, 8.93. HRMS (ESI +): m/z calcd. for $C_{46}H_{52}N_2O_{10}Rh_2Na$ $[M+Na]^+$: 1178.9991; found: 1178.99929.

HPLC analysis: 150 mm Chiralcel IB-N3, Ø 4.6 mm i.D., acetonitrile / water = 60:40, v= 1.0 mL / min, λ = 220 nm, t(enantiomer 1) = 10.07 min, t(enantiomer 2) = 11.87 min. The enantiomers were separated by preparative HPLC using the following conditions: 250 mm YMC Chiral Art Cellulose-SB, 5µm, Ø 20.0 mm i.D., acetonitrile / water = 60:40, v = 15.0 mL / min, λ = 220 nm.

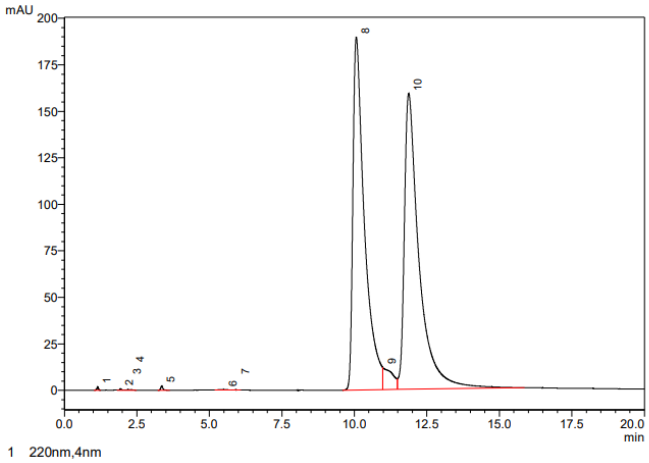

1 220nm,4nm

PDA Ch1 220nm

Peak #	Ret. Time	Area %	Name
1	1.15	0.07	
2	1.93	0.03	
3	2.20	0.02	
4	2.30	0.01	
5	3.36	0.11	
6	5.50	0.05	
7	5.93	0.01	
8	10.07	46.92	1. Enantiomer
9	10.98	2.46	
10	11.87	50.33	2. Enantiomer
Total		100.00	

Analytical chiral HPLC trace of complex **163** under the HPLC conditions described above.

Adduct-(219). A flame dried Schlenk flask was charged with [$Rh_2(OAc)_4$] (17 mg, 0.039 mmol), 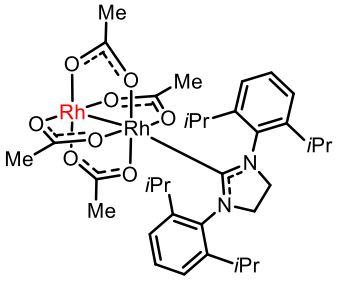

1,3-bis(2,6-diisopropylphenyl) imidazolinium chloride (49.3 mg, 0.12 mmol) and KO*t*Bu (13 mg, 0.12 mmol). DME (2 mL) was added and the suspension was stirred at 60 °C. The green suspension changed slowly over time to orange-brown. After 1 h at this temperature, the mixture was concentrated under vacuo. The solid residue was dissolved in toluene (2 x 2 mL) and cannula filtered. The purple filtrate was concentrated under vacuo and purified via prep TLC (silica, *n*-hexane/EtOAc 70:30) to afford the desired adduct as a purple solid (13 mg, 41%). ^{1}H NMR (600 MHz, C_6D_6) δ 7.10 – 7.05 (m, 2H), 7.04 – 7.01 (m, 4H), 3.80 (s, 4H), 3.74 (hept, *J* = 6.8 Hz, 4H), 1.32 (d, *J* = 6.9 Hz, 12H), 1.11 (d, *J* = 6.7 Hz, 12H), ($\underline{CH_3}$COO not detected). ^{13}C NMR (151 MHz, C_6D_6) δ 188.8, 182.5 (d, *J* = 37.4 Hz), 146.4, 139.4, 128.4, 123.9, 54.8, 28.4, 25.7, 24.0, 23.2. ^{103}Rh NMR (H(C)Rh, 45 MHz, C_6D_6) δ 7285. IR (ATR): $\tilde{\nu}$ = 2961, 2929, 2868, 1594, 1421, 1268, 1240, 805, 760, 697 cm^{-1}. HRMS (ESI +): m/z calcd. for $C_{35}H_{50}N_2O_8Rh_2Na$ [M+Na]$^+$: 855.15695; found: 855.15685.

Adduct-(220). A flame dried Schlenk flask was charged with KO*t*Bu (14 mg, 0.12 mmol) and 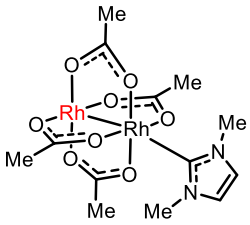

suspended in THF (2 mL). 1,3-Dimethylimidazolinium chloride (16.4 mg, 0.12 mmol) was added to this mixture at room temperature and the suspension was stirred for 45 min. Then [$Rh_2(OAc)_4$] (18 mg, 0.04 mmol) was added in one portion to the reaction mixture. The green suspension changed over time slowly to red-brown. After stirring the reaction mixture for 18h at room temperature, it was concentrated under vacuo. The brown residue was dissolved with toluene (2 x 2 mL) and cannula filtered. The red/pink filtrate was concentrated under vacuo to afford the desired adduct as a dark pink solid (10.8 mg, 49%). ^{1}H NMR (600 MHz, C_6D_6) δ 6.23 (s, 2H), 3.75 (s, 6H), 1.70 (s, 12H). ^{13}C NMR (151 MHz, C_6D_6) δ 189.6, 155.7 (d, *J* = 42.5 Hz), 121.1, 36.3, 23.7. ^{103}Rh NMR (H(C)Rh, 45 MHz, C_6D_6) δ 7213. IR (ATR): $\tilde{\nu}$ = 2928, 1590, 1413, 1346, 1260, 1226, 1089, 1020, 795, 696 cm^{-1}. HRMS (ESI +): m/z calcd. for $C_{13}H_{20}N_2O_8Rh_2Na$ [M+Na]$^+$: 560.92219; found: 560.92242.

Adduct-(222). Prepared analogously to **220** with [$Rh_2(formate)_4$]. Dark pink solid (7 mg, 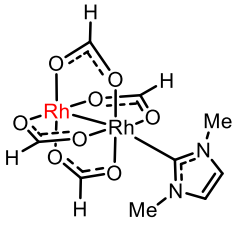

42%). ^{1}H NMR (600 MHz, C_6D_6) δ 6.79 – 6.75 (m, 4H), 6.13 (s, 2H), 3.55 (s, 6H). ^{13}C NMR (151 MHz, C_6D_6) δ 180.8, 152.6 (d, *J* = 40.7 Hz), 121.3, 36.3. ^{103}Rh NMR (^{1}H-^{103}Rh-HMBC, C_6D_6) δ 7285, 6670. HRMS (ESI +): m/z calcd. for $C_9H_{12}N_2O_8Rh_2Na$ [M+Na]$^+$: 504.85959; found: 504.85969.

Adduct-218. $[Rh_2(OAc)_4]$ (10 mg, 0.021 mmol) was suspended in CD_2Cl_2 (0.6 mL) in a flame dried Schlenk flask. Triphenylphosphine (5.5 mg, 0.021 mmol) was added to this green suspension and the mixture was stirred for 20 min. The resulting orange-brown mixture was filtered with a PTFE-filter and the filtrate was directly transferred to a flame dried NMR tube under argon atmosphere. ^{1}H NMR (600 MHz, CD_2Cl_2) δ 7.68 – 7.60 (m, 6H), 7.55 – 7.47 (m, 3H), 7.44 – 7.38 (m, 6H), 1.77 (s, 12H). ^{13}C NMR (151 MHz, CD_2Cl_2) δ 191.3, 134.7 (d, *J* = 10.7 Hz), 131.7 (d, *J* = 29.6 Hz), 130.3 (d, *J* = 2.3 Hz), 128.5(d, *J* = 9.2 Hz), 24.0. ^{31}P NMR (243 MHz, CD_2Cl_2) δ -37.81 (dd, *J* = 95.1, 31.3 Hz). ^{103}Rh NMR (^{103}Rh—^{31}P{ ^{1}H} HMBC, JRhP (30Hz, 92Hz), CD_2Cl_2) δ 6596, 7001.

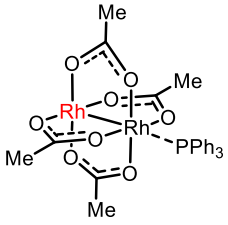

Adduct-221. $[Rh_2(OAc)_4]$ (10 mg, 0.021 mmol) was suspended in CH_2Cl_2 (0.6 mL) in a flame dried Schlenk flask. Dimethylphenylphosphine (3.6 µL, 0.025 mmol) was added to this green suspension and the mixture was stirred for 20 min. The resulting orange-brown mixture was washed with pentane and the brown residual solid was dried under vacuo. The residual solid was dissolved in CD_2Cl_2 and directly transferred to a flame dried NMR tube under argon atmosphere. ^{1}H NMR (600 MHz, CD_2Cl_2) δ 7.93 – 7.89 (m, 2H), 7.55 – 7.51 (m, 1H), 7.51 – 7.47 (m, 2H), 1.81 (d, *J* = 10.7 Hz, 6H), 1.80 (s, 12H). ^{13}C NMR (151 MHz, CD_2Cl_2) δ 190.9, 134.2 (d, *J* = 27.4 Hz), 131.5 (d, *J* = 9.8 Hz), 130.2 (d, *J* = 2.6 Hz), 128.8 (d, *J* = 9.2 Hz), 23.9, 10.3 (d, *J* = 18.0 Hz). ^{31}P NMR (243 MHz, CD_2Cl_2) δ -54.22 (dd, *J* = 103.2, 26.8 Hz). ^{103}Rh NMR (^{103}Rh—^{31}P{ ^{1}H} HMBC, *J*RhP (30Hz, 102Hz), CD_2Cl_2) δ 6454, 6847.

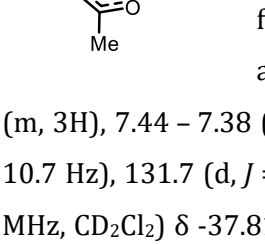

Adduct-223. Prepared analogously to **221** with $[Rh_2(formate)_4]$. ^{1}H NMR (500 MHz, CD_2Cl_2) δ 7.95 – 7.87 (m, 2H), 7.58 – 7.53 (m, 1H), 7.53 – 7.48 (m, 2H), 6.88 (t, *J* = 4.4 Hz, 4H), 1.87 (d, *J* = 11.5 Hz, 6H). ^{13}C NMR (126 MHz, CD_2Cl_2) δ 181.8, 133.4 (d, *J* = 30.5 Hz), 131.2 (d, *J* = 9.4 Hz), 130.4 (d, *J* = 2.8 Hz), 129.1 (d, *J* = 9.6 Hz), 10.2 (d, *J* = 19.4 Hz). ^{31}P NMR (202 MHz, CD_2Cl_2) δ -53.05 (dd, *J* = 101.8, 21.2 Hz). ^{103}Rh NMR (^{1}H-^{103}Rh-HMBC, CD_2Cl_2) δ 6529, 6963.

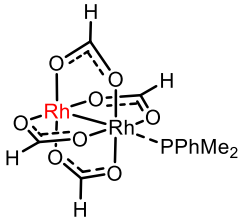

Adduct-224. A solution of the corresponding diazoalkane **257** (7.3 mg, 0.026 mmol) in C_6D_6 (0.5 mL) was added dropwise to a cold (8 °C) solution of Rh_2(formate)$_4$ (10 mg, 0.026 mmol) in C_6D_6 (0.5 mL) under rigorously inert conditions. A vigorous effervescence and concomitant color change were observed. The solution was stirred at 5 °C for 5 min before being transferred into an NMR tube under inert conditions. The NMR tube was kept at this temperature until inserted in the NMR probe head that was precooled to 10 °C. ^{1}H NMR (600 MHz, C_6D_6) δ 8.38 – 8.33 (m, 4H), 6.98 (bs, 4H), 6.42 – 6.38 (m, 4H), 2.22 (s, 12H). ^{13}C NMR (151 MHz, C_6D_6) δ 254.3 (d, *J* = 23.8 Hz), 179.9, 154.3, 142.7, 137.8, 111.0, 39.3. ^{103}Rh NMR (^{1}H-^{103}Rh-HMBC, C_6D_6) δ 7305, 6425. Note: Besides the desired carbene adduct, the corresponding azine[231] and ketone[232] products were also detected in the mixture.

9.5. Preparation of Bismuth-Rhodium Complexes

[RhBi(O-Esp)(OTfa)$_2$] (197). 2,2'-(1,3-Phenylenebis(oxy))bis(2-methylpropanoic acid)[136] (12 mg, 0.042 mmol) was filled into a flame dried Schlenk flask and dissolved in THF (2 mL). DBU (12.5 µL, 0.083 mmol) was added and the reaction mixture was stirred for 10 min. [RhBi(OTfa)$_4$] (30 mg, 0.039 mmol) in THF (4 mL) was added dropwise and the reaction mixture was stirred at room temperature for 30 min. The reaction mixture was concentrated and the residue was purified by flash chromatography (silica, toluene/MeCN 5:1 to 3:1). The isolated product was dissolved in MTBE and the solution was washed with water (2 x 10 mL) and brine (2 x 10 mL). The organic phase was dried with $MgSO_4$, filtered and concentrated under reduced pressure to afford the desired complex as a yellow solid (17 mg, 53%). ^{1}H NMR (400 MHz, [D$_8$]-THF) δ 6.95 (t, *J* = 8.2 Hz, 1H), 6.38 (dd, *J* = 8.1, 2.3 Hz, 2H), 5.59 (t, *J* = 2.3 Hz, 1H), 1.37 (s, 6H), 1.32 (s, 6H). ^{13}C NMR (101 MHz, [D$_8$]-THF) δ 188.8, 169.3 (q, *J* = 38.8 Hz), 156.1, 128.9, 128.4, 114.4, 108.2, 81.8, 24.7 (overlap with [D$_8$]-THF). IR (ATR): $\tilde{\nu}$ = 1643, 1594, 1485, 1402, 1193, 1155, 1014, 831, 789, 735 cm^{-1}. HRMS (ESI +): m/z calcd. for $C_{18}H_{17}F_6O_{10}RhBi$ [M+H]$^+$: 818.95795; found: 818.95787.

[RhBi(Bromo-O-Esp)(OTfa)$_2$] (198). 2,2'-((4,6-Dibromo-1,3-phenylene)bis(oxy))bis(2-methylpropanoic acid)[136] (18.6 mg, 0.042 mmol) was filled into a flame dried Schlenk flask and dissolved in THF (1 mL). DBU (12.5 µL, 0.083 mmol) was added and the reaction mixture was stirred for 10 min. [RhBi(OTfa)$_4$] (30 mg, 0.039 mmol) in THF (2 mL) was added dropwise and the mixture was stirred at room temperature for 30 min. The reaction mixture was concentrated and the residue was purified by flash chromatography (silica, toluene/MeCN 5:1 to 3:1). The isolated product was dissolved in MTBE and the solution was washed with water (2 x 10 mL) and brine (2 x 10 mL). The organic phase was dried with $MgSO_4$, filtered and concentrated under reduced pressure, to afford the desired complex as a yellow solid (20.6 mg, 54%). ^{1}H NMR (600 MHz, [D$_8$]-THF) δ 7.68 (s, 1H), 5.60 (s, 1H), 1.53 (s, 6H), 1.51 (s, 6H). ^{13}C NMR (151 MHz, [D$_8$]-THF) δ 189.2, 171.0, 170.6 (q, *J* = 38.5 Hz), 152.8, 136.7, 115.8 (q, *J* = 287.3 Hz), 109.3, 106.9, 84.5, 25.7, 25.6. ^{19}F NMR (565 MHz, [D$_8$]-THF) δ −74.4. IR (ATR): $\tilde{\nu}$ = 1643, 1470, 1403, 1366, 1197, 1158, 1062, 736 cm^{-1}. HRMS (ESI +): m/z calcd. for $C_{18}H_{14}F_6O_{10}Br_2RhBiNa$ [M+Na]$^+$: 996.76091; found: 996.76139.

[RhBi(Chloro-O-Esp)(OTfa)$_2$] (199). 2,2'-((4,6-Dichloro-1,3-phenylene)bis(oxy))bis(2-methylpropanoic acid) **262** (14.8 mg, 0.042 mmol) was filled into a flame dried Schlenk flask and dissolved in THF (2 mL). DBU (12.5 µL, 0.083 mmol) was added and the reaction mixture was stirred for 10 min. RhBi(OTfa)$_4$ (30 mg, 0.039 mmol) in THF (2 mL) was added dropwise and the mixture was stirred at room temperature for 30 min. The reaction mixture was concentrated and the residue was purified by flash chromatography (silica, toluene/MeCN 5:1 to 3:1). The isolated product was dissolved in MTBE and the solution was washed with water (2 x 10 mL) and brine (2 x 10 mL). The organic phase was dried with $MgSO_4$, filtered and concentrated under reduced pressure, to afford the desired complex as a yellow solid (14 mg, 40%). ^{1}H NMR (400 MHz, [D$_8$]-THF) δ 7.39 (s, 1H), 5.74 (s, 1H), 1.53 (s, 6H), 1.50 (s, 6H). ^{13}C NMR (101 MHz, [D$_8$]-THF) δ 189.3, 170.5 (q, *J* = 38.2 Hz), 151.3, 131.3, 119.0, 110.6, 84.9, 25.8, 25.6, (CF_3 not detected). ^{19}F NMR (282 MHz, [D$_8$]-THF) δ −74.4. IR (ATR): $\tilde{\nu}$ = 2924, 2853, 1641, 1479, 1377, 1196, 1158, 1093, 750, 736 cm^{-1}. HRMS (ESI +): m/z calcd. for $C_{18}H_{14}F_6O_{10}Cl_2RhBi$ [M]$^+$: 885.87218; found: 885.87217.

[RhBi(O-Esp)(OTfa)(OPiv)] (200). Pivalic acid (1.6 mg, 0.016 mmol) was filled in a Schlenk flask and dissolved in THF (0.5 mL). DBU (2.4 µL, 0.016 mmol) was added and the reaction mixture was stirred for 10 min. [RhBi(O-Esp)(OTfa)$_2$] **197** (13.9 mg, 0.015 mmol) in THF (0.6 mL) was added dropwise and the mixture was stirred at room temperature for 5 h. The reaction mixture was concentrated and purified by preparatory HPLC (150 mm YMC triart C8, Ø 20 mm i.D., acetonitrile / water = 70:30 for 20 min then gradient in 10 min to 95:5, v = 15 mL/min) to afford the title complex as a yellow solid (3.2 mg, 26%). ^{1}H NMR (400 MHz, [D$_8$]-THF) δ 7.03 (t, *J* = 8.1 Hz, 1H), 6.46 (dddt, *J* = 7.7, 3.2, 2.3, 1.0 Hz, 2H), 5.71 (t, *J* = 2.3 Hz, 1H), 1.47 (s, 3H), 1.45 (s, 3H), 1.43 (s, 3H), 1.41 (s, 3H), 1.07 (s, 9H). ^{19}F NMR (282 MHz, [D$_8$]-THF) δ –74.4. HRMS (ESI +): m/z calcd. for $C_{21}H_{25}F_3O_{10}RhBiNa$ [M+Na]$^+$: 829.01511; found: 829.01545.

[RhBi(Bromo-O-Esp)(OTfa)(OPiv)] (201). Pivalic acid (2.6 mg, 0.026 mmol) was filled in a Schlenk flask and dissolved in THF (1 mL). DBU (3.9 µL, 0.026 mmol) was added to this solution and the reaction mixture was stirred for 10 min. [RhBi(Bromo-O-Esp)(OTfa)$_2$] **198** (30.0 mg, 0.025 mmol) in THF (1.2 mL) was added dropwise and the mixture was stirred at room temperature for 6 h. The reaction mixture was concentrated and purified by preparatory HPLC (150 mm YMC triart C8, Ø 20 mm i.D., acetonitrile / water = 65:35 for 20 min then gradient in 10 min to 95:5, v = 15 mL/min) to afford the title complex as a yellow solid (4.4 mg, 19%).^{1}H NMR (400 MHz, [D$_8$]-THF) δ 7.66 (s, 1H), 5.65 (s, 1H), 1.53 (s, 3H), 1.51 (s, 3H), 1.50 (s, 3H), 1.49 (s, 3H), 1.08 (s, 9H). ^{19}F NMR (282 MHz, [D$_8$]-THF) δ -74.34. ^{13}C NMR (101 MHz, [D$_8$]-THF) δ 189.0, 187.6, 153.1, 152.8, 136.5, 109.5, 107.0, 106.7, 83.9 (d, *J* = 24.0 Hz), 28.3 (overlap [D$_8$]-THF) (CF_3 not detected). IR (ATR): ṽ = 1632, 1559, 1470, 1410, 1372, 1198, 1158, 1061, 735 cm^{-1}. HRMS (ESI +): m/z calcd. for $C_{21}H_{23}F_3O_{10}Br_2RhBiNa$ [M+Na]$^+$: 984.83613; found: 984.83682. No separation of the corresponding enantiomers on any of the tested chiral HPLC columns.

[RhBi(Chloro-O-Esp)(OPiv)$_2$] (202). Pivalic acid (1.7 mg, 0.017 mmol) was filled in a Schlenk flask and dissolved in THF (0.5 mL). DBU (2.5 µL, 0.017 mmol) was added to this solution and the reaction mixture was stirred for 10 min. [RhBi(Chloro-O-Esp)(OTfa)$_2$] **199** (13.9 mg, 0.016 mmol) in THF (0.6 mL) was added dropwise and the mixture was stirred at room temperature for 6 h. The reaction mixture was concentrated and purified by preparatory HPLC (150 mm YMC triart C8, Ø 20 mm i.D., Acetonitrile / Water = 75:25, v = 15 mL/min) to afford the title complex as a

yellow solid (3.9 mg, 28%). ^{1}H NMR (400 MHz, [D$_8$]-THF) δ 7.33 (s, 1H), 5.81 (s, 1H), 1.48 (s, 6H), 1.46 (s, 6H), 1.06 (s, 18H). IR (ATR): ṽ = 1580, 1481, 1410, 1374, 1224, 1204, 1092, 750 cm^{-1}. HRMS (ESI +): m/z calcd. for $C_{24}H_{32}O_{10}Cl_2RhBiNa$ [M+Na]$^+$: 885.01238; found: 885.01195.

[RhBi(Bromo-calix[4]arene)(OTfa)$_2$] (203). Calix[4]arene **133** (60.4 mg, 0.072 mmol) and

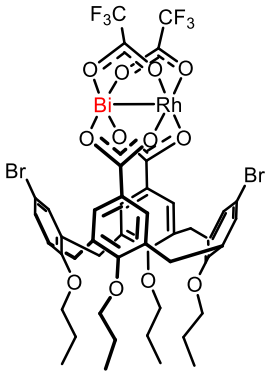

[RhBi(OTfa)$_4$] (50 mg, 0.065 mmol) were filled into a two-neck flask and dissolved in chlorobenzene (20 mL). The reaction mixture was degassed by bubbling argon through it for 15 min, followed by heating the mixture to reflux temperature for 2 h (135 °C bath temperature). The reaction mixture was cooled to room temperature and the chlorobenzene was distilled off (40 °C, 3·10^{-3} mbar). The residue was purified by flash chromatography (silica, toluene/MeCN 80:1) to afford the desired complex as a yellow solid (62.5 mg, 69%). ^{1}H NMR (400 MHz, [D$_8$-THF) δ 7.42 (d, *J* = 1.0 Hz, 4H), 6.82 (dd, *J* = 17.3, 2.2 Hz, 4H), 4.41 (d, *J* = 13.9 Hz, 4H), 4.10 – 3.91 (m, 4H), 3.71 (tt, *J* = 6.7, 3.0 Hz, 4H), 3.21 (dd, *J* = 14.0, 5.7 Hz, 4H), 1.87 (h, *J* = 7.4 Hz, 8H), 1.10 (t, *J* = 7.4 Hz, 6H), 0.85 (t, *J* = 7.4 Hz, 6H). ^{13}C NMR (101 MHz, [D$_8$]-THF) δ 185.1, 170.6 (q, *J* = 38.1 Hz), 160.6, 158.2 (d, *J* = 6.2 Hz), 140.4, 140.1, 134.5, 133.5, 133.0, 131.3, 130.9, 127.5, 117.4 (q, *J* = 288.1 Hz), 115.6, 115.5, 78.1, 78.0, 77.4, 31.8, 31.5, 24.5, 24.1, 23.7, 11.3, 10.2, 10.1. ^{19}F NMR (282 MHz, [D$_8$]-THF) δ -74.5. IR (ATR): ṽ = 1649, 1397, 1382, 1193, 1155, 1110, 1033, 1000, 957, 859, 734 cm^{-1}. HRMS (ESI +): m/z calcd. for $C_{46}H_{44}O_{12}Br_2F_6RhBiNa$ [M+Na]$^+$: 1394.98549; found: 1394.98499.

[RhBi(Bromo-calix[4]arene)(OPiv)(OTfa)] (204). Pivalic acid (1.7 mg, 0.017 mmol) was

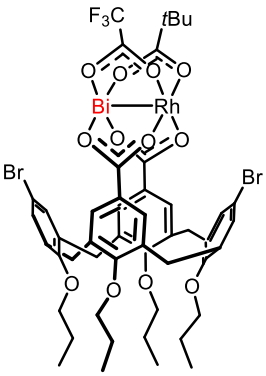

filled in a Schlenk flask and dissolved in THF (1 mL). DBU (2.5 µL, 0.017 mmol) was added to this solution and the reaction mixture was stirred for 10 min. [RhBi(Calix[4]arene)(OTfa)$_2$] **203** (34 mg, 0.025 mmol) in THF (1.2 mL) was added dropwise and the mixture was stirred at room temperature for 6 h. The reaction mixture was concentrated and purified by preparatory HPLC (150 mm YMC triart C18, Ø 20 mm i.D., acetonitrile / water = 97:3, v = 15 mL/min) to afford the title complex as a yellow solid (6.3 mg, 19%). ^{1}H NMR (600 MHz, [D$_8$]-THF) δ 7.42 – 7.40 (m, 2H), 7.40 – 7.39 (m, 2H), 6.84 (d, *J* = 1.9 Hz, 1H), 6.82 (dd, *J* = 1.9, 1.1 Hz, 1H), 6.80 (d, *J* = 2.1 Hz, 1H), 6.77 – 6.75 (m, 1H), 4.42 – 4.38 (m, 4H), 4.03 – 3.98 (m, 4H), 3.73 – 3.64 (m, 4H), 3.22 – 3.15 (m, 4H), 1.91 – 1.83 (m, 8H), 1.09 (t, *J* = 7.4 Hz, 6H), 1.04 (s, 9H), 0.87 (t, *J* = 7.5 Hz, 3H), 0.83 (t, *J* = 7.5 Hz, 3H). ^{13}C NMR (151 MHz, [D$_8$]-THF) δ 194.01, 184.65, 183.57, 170.65 (q, *J* = 37.8 Hz), 160.30, 160.00, 158.20, 140.54, 140.30, 140.17, 140.05, 134.35, 134.00, 133.31, 133.14, 133.06, 132.96, 132.93, 132.89, 131.23, 131.12 (d, *J* = 2.3 Hz), 130.90,

127.49, 127.43, 115.87 (q, *J* = 287.7 Hz), 115.60, 115.46, 78.06, 78.02, 77.94, 77.35, 41.42, 31.81 (d, *J* = 6.9 Hz), 31.53 (d, *J* = 8.6 Hz), 28.40, 24.50 (d, *J* = 3.5 Hz), 24.08, 23.72, 11.30 (d, *J* = 1.5 Hz), 10.25, 10.09. ^{19}F NMR (565 MHz, [D$_8$]-THF) δ –74.6. HRMS (ESI +): m/z calcd. for $C_{49}H_{53}O_{12}Br_2F_3RhBiNa$ $[M+Na]^+$: 1383.06071; found: 1383.06065.

As a byproduct, the following complex could be identified and characterized by NMR and HRMS: **RhBi(Bromo-calix[4]arene)(OPiv)$_2$ (205)** (yellow solid, 6.6 mg, 20%). ^{1}H NMR (600 MHz, [D$_8$]-THF) δ 7.38 (s, 4H), 6.83 (d, *J* = 1.9 Hz, 2H), 6.77 (d, *J* = 1.9 Hz, 2H), 4.40 (d, *J* = 14.1 Hz, 2H), 4.39 (d, *J* = 13.6 Hz, 2H), 4.03 – 3.95 (m, 4H), 3.68 (qt, *J* = 9.4, 6.7 Hz, 4H), 3.18 (d, *J* = 12.5 Hz, 2H), 3.16 (d, *J* = 11.2 Hz, 2H), 1.92 – 1.81 (m, 8H), 1.09 (t, *J* = 7.4 Hz, 6H), 1.03 (s, 18H), 0.87 (t, *J* = 7.5 Hz, 3H), 0.83 (t, *J* = 7.5 Hz, 3H). ^{13}C NMR (151 MHz, [D$_8$]-THF) δ 193.44, 182.82, 159.51, 158.04 (d, *J* = 12.8 Hz), 140.28, 139.92, 133.58, 133.17 – 132.31 (m), 130.87 (d, *J* = 8.6 Hz), 127.43, 115.29 (d, *J* = 28.0 Hz), 77.81, 77.72, 77.17, 40.92, 31.66, 31.38, 28.39, 24.32, 23.91, 23.58, 11.14, 10.09, 9.93. HRMS (ESI +): m/z calcd. for $C_{52}H_{62}O_{12}Br_2RhBiNa$ $[M+Na]^+$: 1371.13593; found: 1371.13626.

9.6. Preparation of Cyclopropanes

2,2,2-Trichloroethyl (1*R*,2*S*)-1,2-diphenylcyclopropane-1-carboxylate (137). An oven dried cooling Schlenk flask equipped with a magnetic stir bar was charged with catalyst ***M*-134** (1.0 mol%). Styrene (0.06 mL, 0.51 mmol) and pentane (1 mL) were added and the mixture was cooled to –40 °C. At this temperature, a solution of 2,2,2-trichloroethyl 2-diazo-2-phenylacetate **136** (30 mg, 0.1 mmol) in pentane (2 mL) was added dropwise over 5 min and the reaction mixture was kept stirring at –40 °C for 5 h. The reaction mixture was concentrated under reduced pressure and the residue was purified by flash chromatography (silica, *n*-pentane/MTBE 40:1) which afforded the desired product as a white oil (27 mg, 71%, d.r. > 20:1 (*trans*), 70% *ee*). $[\alpha]_D^{20}$ = –8.1 (c = 1.2, $CHCl_3$). The optical purity was determined by HPLC (Chiralcel OJ-3R, 4.6 mm ∅, acetonitrile/water= 60:40, v= 1.0 mL/min, λ =220 nm): 10.24 min (major) and 13.34 min (minor). ^{1}H NMR (600 MHz, $CDCl_3$) δ 7.14 – 7.12 (m, 3H), 7.09 – 7.06 (m, 5H), 6.82 – 6.79 (m, 2H), 4.84 (d, *J* = 12.0 Hz, 1H), 4.65 (d, *J* = 11.9 Hz, 1H), 3.22 (dd, *J* = 9.4, 7.4 Hz, 1H), 2.29 (dd, *J* = 9.4, 5.1 Hz, 1H), 2.02 (dd, *J* = 7.4, 5.1 Hz, 1H). ^{13}C NMR (151 MHz, $CDCl_3$) δ 172.3, 135.9, 133.8, 132.2, 128.3, 127.9, 127.8, 127.4, 126.7, 95.2, 74.5, 37.4, 34.0, 20.4. The spectral data matched those previously reported in the literature.[98]

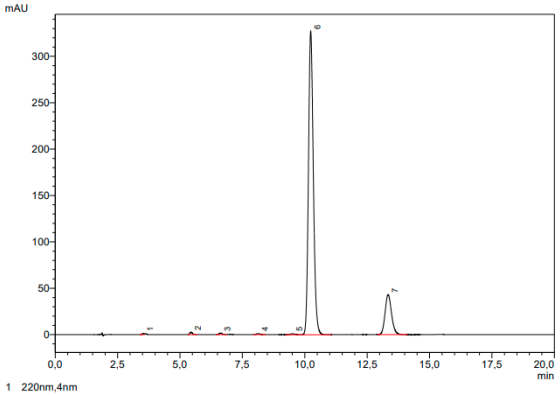

PDA Ch1 220nm

Peak #	Ret. Time	Area %	Name
1	3,53	0,13	
2	5,44	0,37	
3	6,63	0,29	
4	8,13	0,22	
5	9,52	0,23	
6	10,24	84,04	1. Enantiomer 70.2 % ee
7	13,34	14,73	2. Enantiomer
Total		100,00	

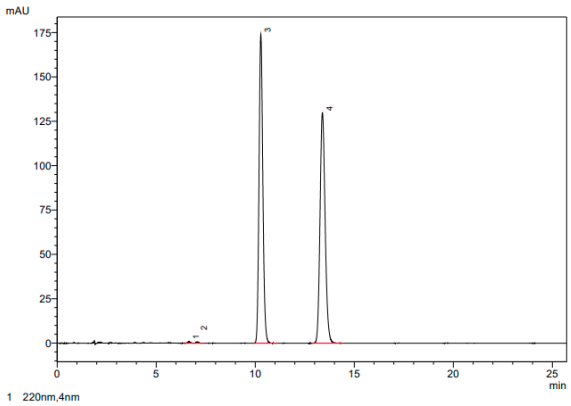

PDA Ch1 220nm

Peak #	Ret. Time	Area %	Name
1	6,65	0,16	
2	7,07	0,16	
3	10,28	49,84	1. Enantiomer
4	13,39	49,84	2. Enantiomer
Total		100,00	

HPLC traces of **133** (left) and corresponding racemate (right).

9.6.1. Preparation of 2-Furyl Cyclopropanes

General procedure A

An oven dried Schlenk flask equipped with a magnetic stir bar was charged with [BiRh] **47** (0.5 mol%) under argon. Alkene or alkyne (0.45-0.9 mmol), hydrazone (0.09 mmol) and CH_2Cl_2 (1 mL) was added and the reaction mixture was stirred at rt. A solution of DIPEA (0.18 mmol) in CH_2Cl_2 (3 mL) was added dropwise over 0.5 h. The resulting mixture was monitored by TLC analysis and stirred for 16-20 h. The mixture was concentrated and the residue was directly purified by either flash chromatography or preparative thin layer chromatography, which afforded the desired cyclopropane or cyclopropene product.

The corresponding racemates were prepared accordingly with 2 mol% $Rh_2(esp)_2$.

Methyl (1*S*,2*R*)-1-(furan-2-yl)-2-phenylcyclopropane-1-carboxylate (63). Prepared

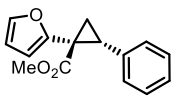

according to general procedure **A** with 0.45 mmol of alkene. The crude residue was purified by flash chromatography (pentane/Et_2O 15:1) afforded the title compound as a colorless liquid (14 mg, 62%, 64% *ee*). [The *ee* was determined by HPLC analysis: 150 mm Chiralcel OJ-3R, Ø 4.6 mm, acetonitrile/water = 70:30, v = 0.5 mL/min, λ = 220 nm, t(minor) = 5.69 min, t(major) = 6.14 min]. ^{1}H NMR (400 MHz, $CDCl_3$) δ 7.19 – 7.05 (m, 4H), 7.05 – 6.91 (m, 2H), 6.15 (dd, *J* = 3.2, 1.9 Hz, 1H), 6.00 (dd, *J* = 3.2, 0.9 Hz, 1H), 3.73 (s, 3H), 3.16 (dd, *J* = 9.2, 7.6 Hz, 1H), 2.09 (dd, *J* = 9.2, 4.9 Hz, 1H), 2.01 (dd, *J* = 7.6, 4.9 Hz, 1H). ^{13}C NMR (101 MHz, $CDCl_3$) δ 173.1, 149.4, 142.2, 135.9, 128.2, 128.0, 126.9, 110.9, 110.1, 52.9, 34.0, 30.6, 20.7. IR (ATR): $\tilde{\nu}$ = 1722, 1502, 1434, 1265, 1315, 1221, 1170, 1154, 1014, 741, 696 cm^{-1}. HRMS (EI) m/z calcd. for $C_{15}H_{14}O_3$ [M]$^+$: 242.09375; found: 242.09371.

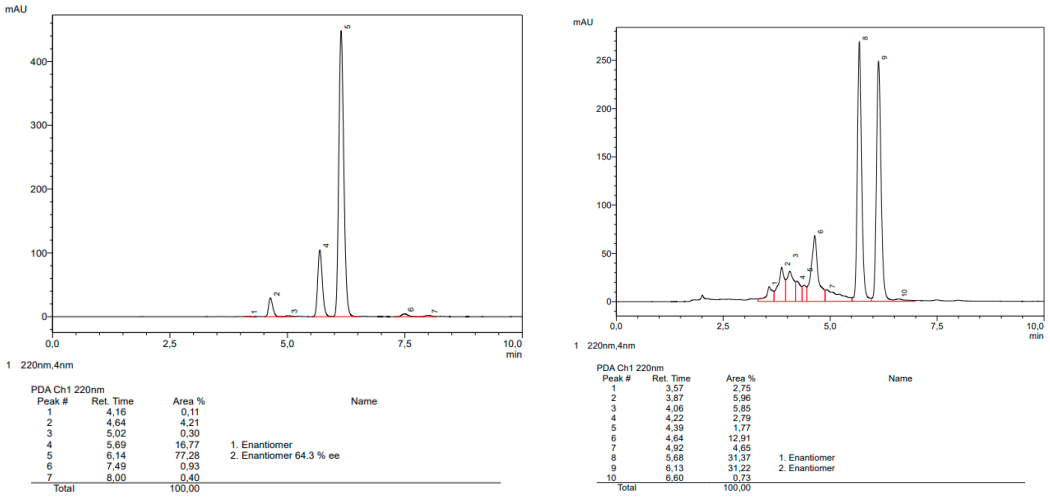

HPLC traces of **63** (left) and corresponding racemate (right).

2,2,2-Trichloroethyl (1*S*,2*R*)-1-(furan-2-yl)-2-phenylcyclopropane-1-carboxylate (64).

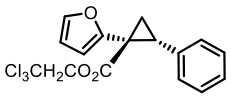

Prepared according to general procedure **A** with 0.45 mmol of alkene. The crude residue was purified by flash chromatography (pentane/Et_2O 20:1) which afforded the title compound as a colorless liquid (22 mg, 60%, 75% *ee*). [The *ee* was determined by HPLC analysis: 150 mm Chiralcel OJ-3R, Ø 4.6 mm, acetonitrile/water = 70:30, v = 0.5 mL/min, λ = 220 nm, t(minor) = 5.69 min, t(major) = 6.14 min]. ^{1}H NMR (400 MHz, $CDCl_3$) δ 7.21 – 7.11 (m, 2H), 7.03 – 6.96 (m, 2H), 6.15 (dd, *J* = 3.3, 1.9 Hz, 1H), 4.83 (d, *J* = 11.9 Hz, 1H), 4.74 (d, *J* = 11.9 Hz, 1H), 3.27 (dd, *J* = 9.3, 7.7 Hz, 1H), 2.23 (dd, *J* = 9.3, 5.1 Hz, 1H), 2.16 (dd, *J* = 7.8, 5.1 Hz, 1H). ^{13}C NMR (101 MHz, $CDCl_3$) δ 170.9, 148.2, 142.3, 135.4, 128.3, 128.1, 127.2, 111.4, 110.2, 95.0, 74.7, 34.8, 30.6, 20.7. IR (ATR): $\tilde{\nu}$ = 1736, 1250, 1217, 1169, 1149, 1013, 812, 740, 713, 695, 574 cm^{-1}. HRMS (EI) m/z calcd. for $C_{16}H_{13}O_3Cl_3$ $[M]^+$: 357.99248; found: 357.99267.

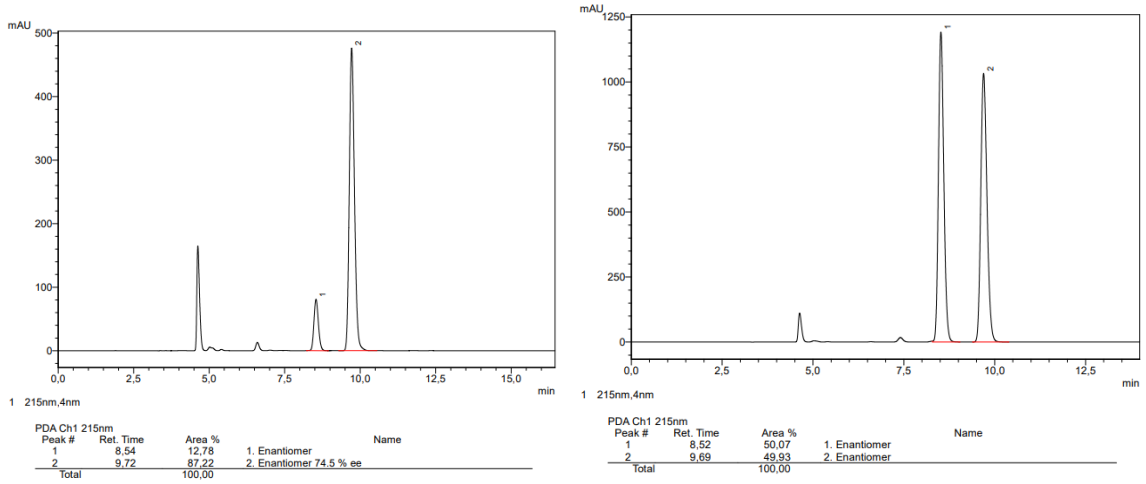

HPLC traces of **64** (left) and corresponding racemate (right).

2-((1*S*,2*R*)-2-Phenyl-1-(trifluoromethyl)cyclopropyl)furan (60). Prepared according to general procedure **A** with 0.45 mmol of alkene. The crude residue was purified by flash chromatography (hexanes/MTBE 98:2) which afforded the title compound as a colorless liquid (19.5 mg, 85%, 92% *ee*). [The *ee* was determined by HPLC analysis: Daicel 150 mm Chiralcel OJ-3R, Ø 4.6 mm, acetonitrile/water = 60/40, v = 0.5 mL/min, λ = 220 nm, t(minor) = 9.81 min, t(major) = 10.75 min]. $[\alpha]_D^{20}$ = –23.1 (c = 0.43, $CHCl_3$); ^{1}H NMR (400 MHz, $CDCl_3$): δ = 7.21 (dd, J = 1.9, 0.8 Hz, 1H), 7.20 – 7.08 (m, 3H), 7.04 – 6.88 (m, 2H), 6.17 (dd, J = 3.3, 1.9 Hz, 1H), 6.10 (dd, J = 3.3, 0.8 Hz, 1H), 2.86 (dd, J = 9.5, 7.3 Hz, 1H), 1.96 – 1.89 (m, 1H), 1.85 (dd, J = 9.5, 6.0 Hz, 1H). ^{13}C NMR (101 MHz, $CDCl_3$): δ = 142.8, 135.2, 128.1 (2C), 127.0, 125.23 (q, *J* = 274.0 Hz), 112.2, 110.6, 29.7 (d, *J* = 34.8 Hz), 27.2 (d, *J* = 2.0 Hz), 14.0 (d, *J* = 2.3 Hz). ^{19}F NMR (282 MHz, $CDCl_3$) δ –69.4. IR (ATR): $\tilde{\nu}$ = 3033, 2865, 1501, 1334, 1288, 1138, 1054, 1014, 740, 695 cm^{-1}. HRMS (ESI$^+$) m/z calcd. for $C_{14}H_{12}F_3O$ $[M+H]^+$: calcd: 252.07565, found: 252.07605.

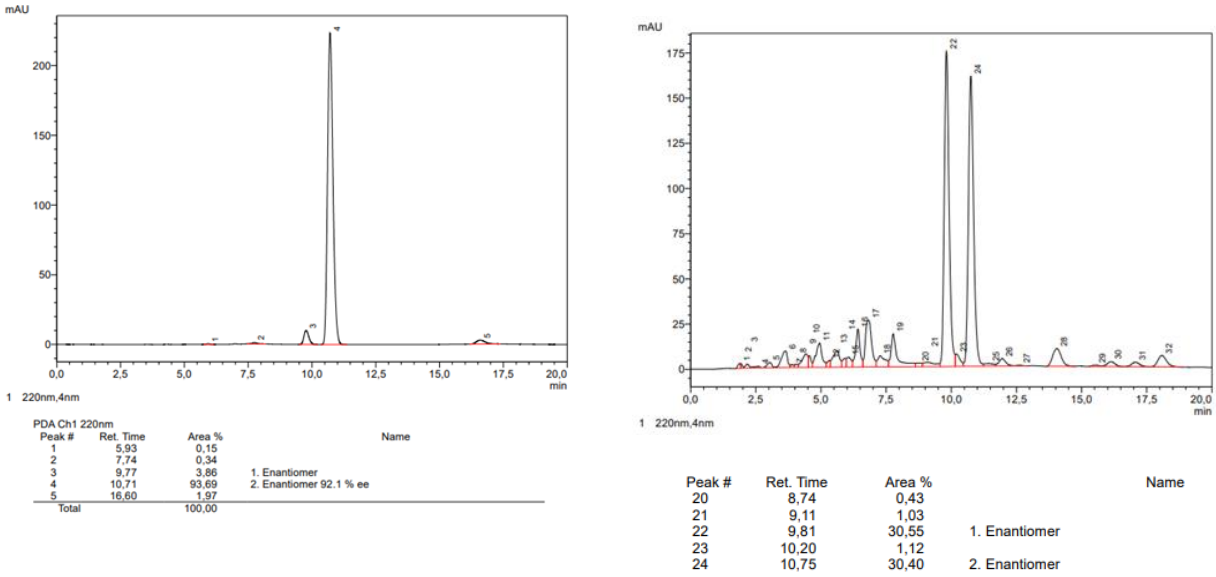

HPLC traces of **60** (left) and corresponding racemate (right).

2-((1*S*,2*R*)-2-(4-Methoxyphenyl)-1-(trifluoromethyl)cyclopropyl)furan (65). Prepared according to general procedure **A** with 0.45 mmol of alkene. The crude residue was purified by preparative TLC (pentane:EtOAc 90:10) affording the title compound as a pale yellow oil (20.1 mg, 80%, 91% *ee*). [The *ee* was determined by HPLC analysis: 150 mm YMC Cellulose SJ-3, Ø 4.6 mm, acetonitrile/water = 50:50 v = 1.0 mL/min, λ = 220 nm, t(minor) = 9.46 min, t(major) = 10.38 min]. $[\alpha]_D^{20}$ = –63.7 (c

= 1.0, $CHCl_3$). ^1H NMR (400 MHz, $CDCl_3$) δ 7.22 (dd, J = 1.9, 0.8 Hz, 1H), 6.93 – 6.83 (m, 2H), 6.74 – 6.66 (m, 2H), 6.18 (dd, J = 3.3, 1.9 Hz, 1H), 6.10 (dd, J = 3.3, 0.8 Hz, 1H), 3.74 (s, 4H), 2.81 (dd, J = 9.5, 7.4 Hz, 1H), 1.89 – 1.77 (m, 2H). ^{13}C NMR (101 MHz, $CDCl_3$) δ 158.7, 146.4, 142.7, 129.2, 127.2, 125.3 (q, *J* = 273.8 Hz), 113.6, 112.1, 110.6, 55.3, 29.4 (q, *J* = 34.6 Hz), 26.6 (q, *J* = 2.1 Hz), 14.0 (q, *J* = 2.3 Hz). ^{19}F NMR (282 MHz, $CDCl_3$) δ –69.3. IR (ATR): $\tilde{\nu}$ = 1517, 1333, 1287, 1249, 1223, 1178, 1134, 1058, 1034, 1014, 848, 807, 740 cm^{-1}. HRMS (EI) m/z calcd. for $C_{15}H_{13}F_3O_2$ $[M]^+$: calcd: 282.08622, found: 282.08657.

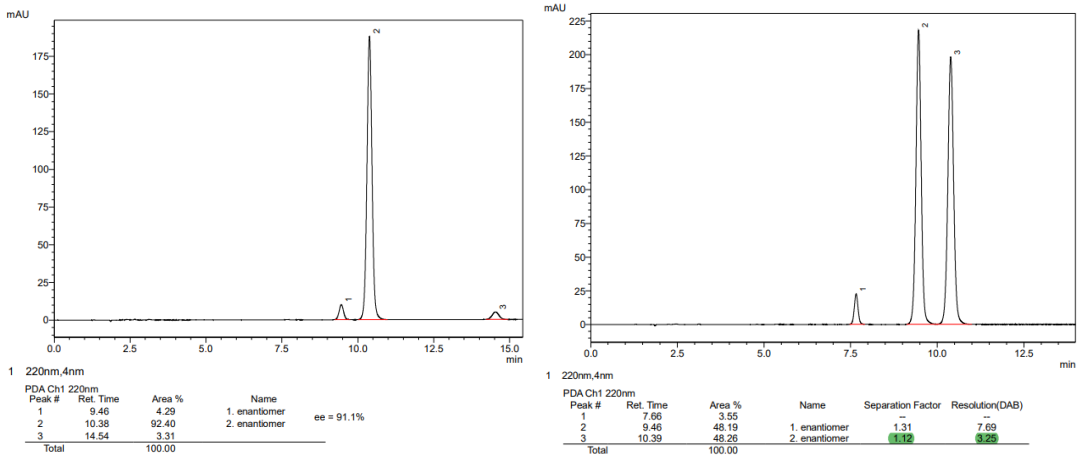

HPLC traces of **65** (left) and corresponding racemate (right).

2-((1*S*,2*R*)-2-(Naphthalen-2-yl)-1-(trifluoromethyl)cyclopropyl)furan (66). Prepared

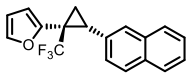

according to the general procedure **A** with 0.45 mmol of alkene. The crude residue was purified by flash chromatography (75:1 pentane:EtOAc) which afforded the title compound as a pale yellow oil (22.8 mg 83%, 87% *ee*). [The *ee* was determined by HPLC analysis: 150 mm YMC Cellulose SJ-3, Ø 4.6 mm i.D. acetonitrile/water = 60:40 v = 1.0 mL/min, λ = 220 nm, t(minor) = 7.76 min, t(major) = 9.47 min]. $[\alpha]_D^{20}$ = –33.3 (c = 1.0, $CHCl_3$). ^1H NMR (400 MHz, $CDCl_3$) δ 7.78 – 7.67 (m, 2H), 7.65 (d, J = 8.5 Hz, 1H), 7.49 – 7.37 (m, 3H), 7.17 (dd, J = 1.7, 0.9 Hz, 1H), 7.10 (dd, J = 8.5, 1.8 Hz, 1H), 6.11 (qd, J = 3.3, 1.3 Hz, 2H), 3.03 (dd, J = 9.5, 7.3 Hz, 1H), 2.06 (ddq, J = 7.6, 6.0, 1.6 Hz, 1H), 1.94 (dd, J = 9.5, 6.1 Hz, 1H). ^{13}C NMR (101 MHz, $CDCl_3$) δ 146.5, 143.1, 133.5, 133.2, 132.9, 128.0 (d, J = 5.1 Hz), 127.3, 126.6, 126.5, 126.2, 125.6 (q, *J* = 273.9 Hz), 112.6, 110.9, 77.7, 30.1 (q, J = 34.3 Hz) 27.7 (q, J = 2.1 Hz), 14.5 (q, J = 2.2 Hz). ^{19}F NMR (282 MHz, $CDCl_3$) δ –69.3. IR (ATR): $\tilde{\nu}$ = 1346, 1332, 1293, 1224, 1185, 1137, 1063, 1014, 859, 813, 742, 476 cm^{-1}. HRMS (ESI^+) m/z calcd. for $C_{18}H_{13}F_3ONa$ $[M+Na]^+$: calcd: 325.08107, found: 325.08074.

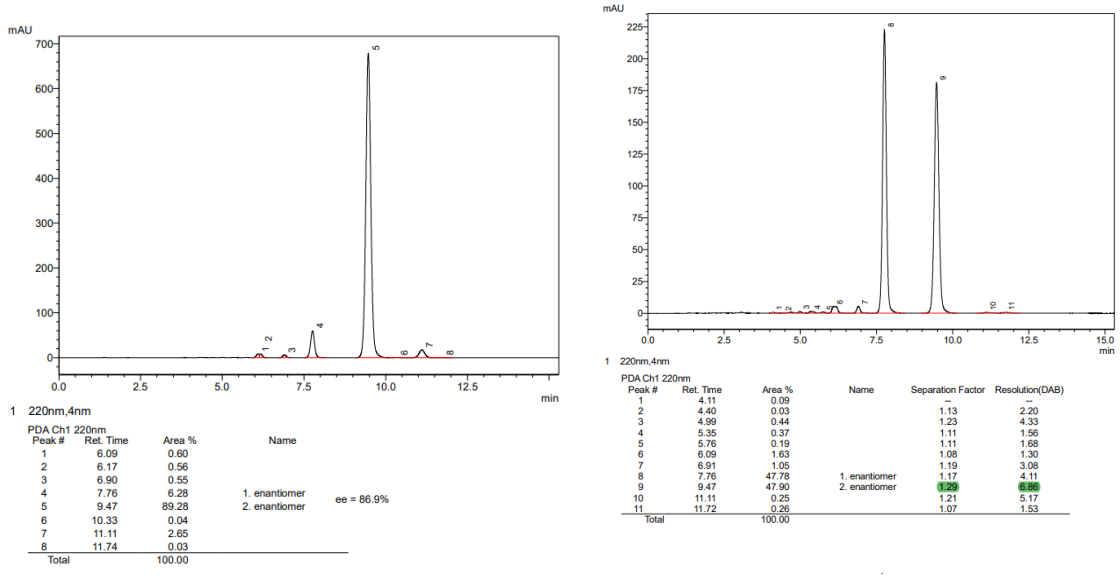

HPLC traces of **66** (left) and corresponding racemate (right).

2-((1*S*,2*S*)-2-(Thiophen-2-yl)-1-(trifluoromethyl)cyclopropyl)furan (68). Prepared

according to the general procedure **A** with 0.45 mmol of alkene. The crude residue was purified by flash chromatography (75:1 pentane:EtOAc) which afforded the title compound as a pale yellow oil (17.6 mg 75 %, 95 % *ee*). [The *ee* was determined by HPLC analysis: 150 mm Chiralpak OJ-3R, Ø 4.6 mm i.D. *n*-heptane/2-propanol = 98:2, v= 1.0 mL/min, λ = 220 nm, t(minor) = 3.45 min, t(major) = 3.98 min]. $[\alpha]_D^{20}$ = –51.7(c = 0.7, $CHCl_3$). ^{1}H NMR (400 MHz, $CDCl_3$) δ 7.28 (dd, *J* = 1.8, 0.9 Hz, 1H), 7.05 (dd, *J* = 5.1, 1.2 Hz, 1H), 6.81 (dd, *J* = 5.1, 3.5 Hz, 1H), 6.65 (dt, *J* = 3.6, 1.1 Hz, 1H), 6.25 (qd, *J* = 3.3, 1.3 Hz, 2H), 3.00 (dd, *J* = 9.5, 7.0 Hz, 1H), 1.95 (dd, *J* = 9.6, 6.0 Hz, 1H), 1.85 (tdd, *J* = 6.1, 3.2, 1.6 Hz, 1H). ^{13}C NMR (101 MHz, $CDCl_3$) δ 145.9, 143.0, 139.0, 126.7, 125.8, 125.0 (q, *J* = 274.6 Hz), 124.5, 112.5, 110.7,30.2 (q, *J* = 34.7 Hz), 22.5 (q, *J* = 2.5 Hz), 16.4 (q, *J* = 2.2 Hz). ^{19}F NMR (282 MHz, $CDCl_3$) δ –69.4. IR (ATR): $\tilde{\nu}$ = 1344, 1295, 1224, 1150, 1063, 1014, 742, 698 cm^{-1}. HRMS (EI) m/z calcd. for $C_{12}H_9F_3OS$ $[M]^+$: calcd: 258.03258, found: 258.03207.

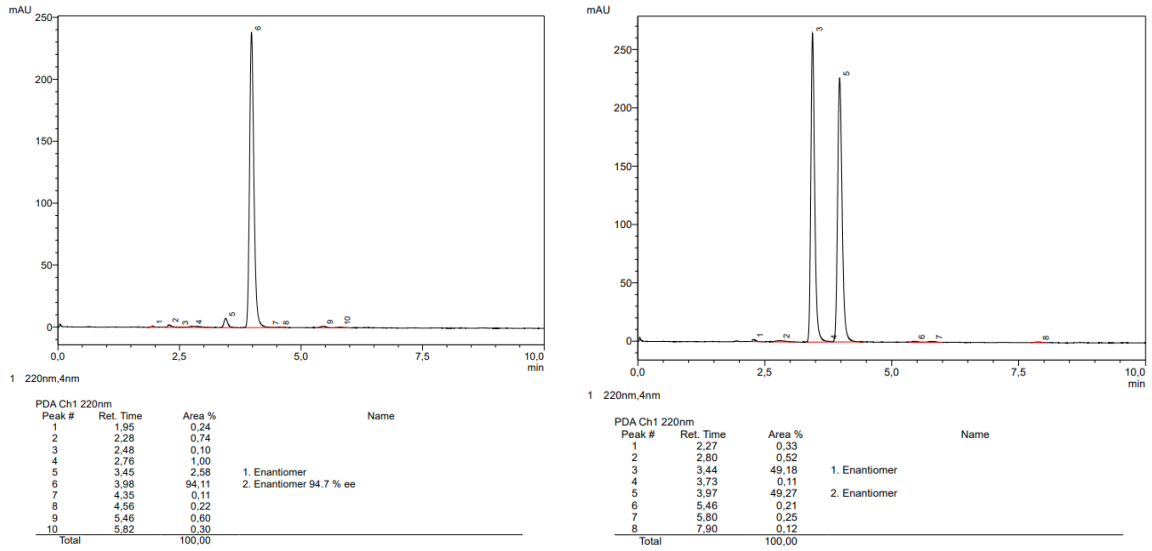

HPLC traces of **68** (left) and corresponding racemate (right).

2-((1*S*,2*R*)-2-(4-bromophenyl)-1-(trifluoromethyl)cyclopropyl)furan (69). Prepared

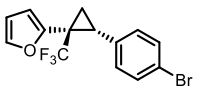

according to the general procedure **A** with 0.9 mmol of alkene. The crude residue was purified by flash chromatography (75:1 pentane:EtOAc) which afforded the title compound as a pale yellow oil (22 mg, 73%, 94% *ee*) which contained a small amount of an unknown impurity. An analytically pure sample for characterization was obtained via preparatory HPLC. [The *ee* was determined by HPLC analysis: 150 mm Chiralpak OJ-3R, Ø 4.6 mm i.D. acetonitrile/water = 60:40, v= 1.0 mL/min, λ = 220 nm, t(minor) = 6.98 min, t(major) = 7.65 min]. $[\alpha]_D^{20}$ = –42.5 (c =1.4, $CHCl_3$). ^{1}H NMR (600 MHz, $CDCl_3$) δ 7.30 – 7.27 (m, 2H), 7.22 (dd, *J* = 1.8, 0.8 Hz, 1H), 6.85 – 6.81 (m, 2H), 6.19 (dd, *J* = 3.3, 1.8 Hz, 1H), 6.13 (dd, *J* = 3.3, 0.8 Hz, 1H), 2.80 (dd, *J* = 9.3, 7.4 Hz, 1H), 1.87 (ddq, *J* = 7.4, 6.2, 1.4 Hz, 1H), 1.86 (dd, *J* = 9.4, 6.2 Hz, 1H). ^{13}C NMR (151 MHz, $CDCl_3$) δ 125.10 (q, *J* = 274.2 Hz), 29.74 (q, *J* = 34.8 Hz), 26.62 (q, *J* = 2.2 Hz), 14.14 (q, *J* = 2.3 Hz). ^{19}F NMR (565 MHz, $CDCl_3$) δ -69.50 (d, *J* = 1.4 Hz). IR (ATR): ṽ =1493, 1381, 1333, 1294, 1224, 1213, 1152, 1115, 1076, 1056, 1012, 843, 813, 742 cm^{-1}. HRMS (EI) m/z calcd. for $C_{14}H_{10}BrF_3O$ $[M]^+$: calcd: 329.98618, found: 329.98622.

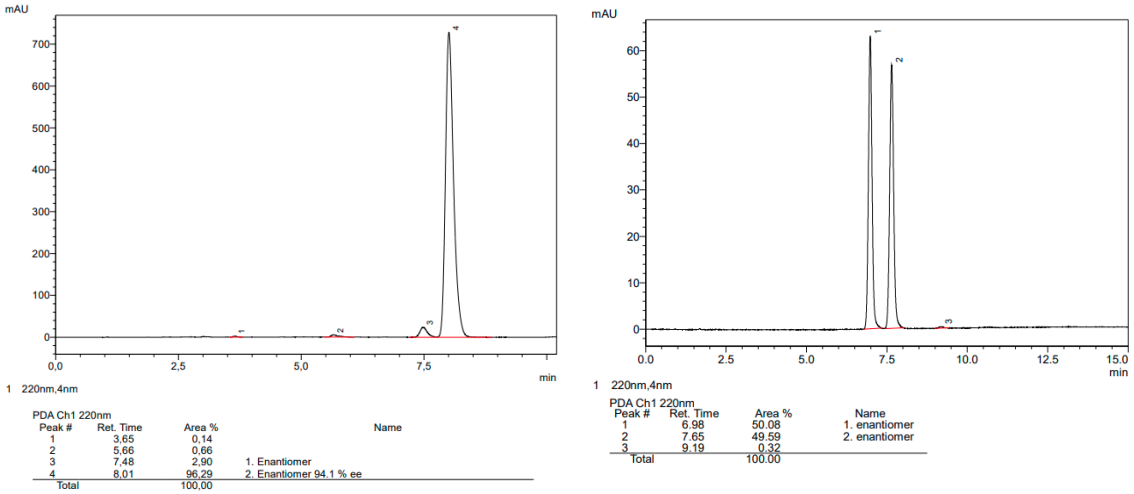

HPLC traces of **69** (left) and corresponding racemate (right).

2-((1*S*,2*R*)-2-(*p*-Tolyl)-1-(trifluoromethyl)cyclopropyl)furan (70). Prepared according to

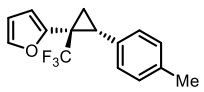

the general procedure **A** with 0.9 mmol of alkene. The crude residue was purified by flash chromatography (75:1 pentane:EtOAc) which afforded the title compound as a colorless oil (19.9 mg, 83%, 94% *ee*). [The *ee* was determined by HPLC analysis: 150 mm Chiralpak OJ-3R, Ø 4.6 mm i.D., acetonitrile / water = 50:50, v = 1.0 mL / min, λ = 220 nm, t(minor) = 16.04 min, t(major) = 17.63 min]. $[\alpha]_D^{20}$ = –58.1 (c = 1.2, $CHCl_3$). ^{1}H NMR (400 MHz, $CDCl_3$) δ 7.23 (dd, *J* = 1.9, 0.9 Hz, 1H), 7.01 – 6.94 (m, 2H), 6.89 – 6.81 (m, 2H), 6.18 (dd, *J* = 3.3, 1.9 Hz, 1H), 6.11 (dd, *J* = 3.3, 0.8 Hz, 1H), 2.83 (dd, *J* = 9.6, 7.3 Hz, 1H), 2.26 (s, 3H), 1.88 (ddq, *J* = 7.5, 6.0, 1.6 Hz, 1H), 1.83 (dd, *J* = 9.5, 6.0 Hz, 1H). ^{13}C NMR (101 MHz, $CDCl_3$) δ 146.4, 142.7, 136.6, 128.8 (2C), 128.0 (2C), 125.4 (q, *J* = 274.6 Hz), 112.2, 110.6, 29.5 (q, *J* = 34.6 Hz), 26.9 (q, *J* = 2.0 Hz), 21.15, 14.0 (q, *J* = 2.3 Hz). ^{19}F NMR (282 MHz, $CDCl_3$) δ –69.4. IR (ATR): $\tilde{\nu}$ = 1333, 1291, 1223, 1140, 1059, 1014, 840, 809, 740 cm^{-1}. HRMS (EI) m/z calcd. for $C_{15}H_{13}F_3O$ $[M]^+$: calcd: 266.09130, found: 266.09153.

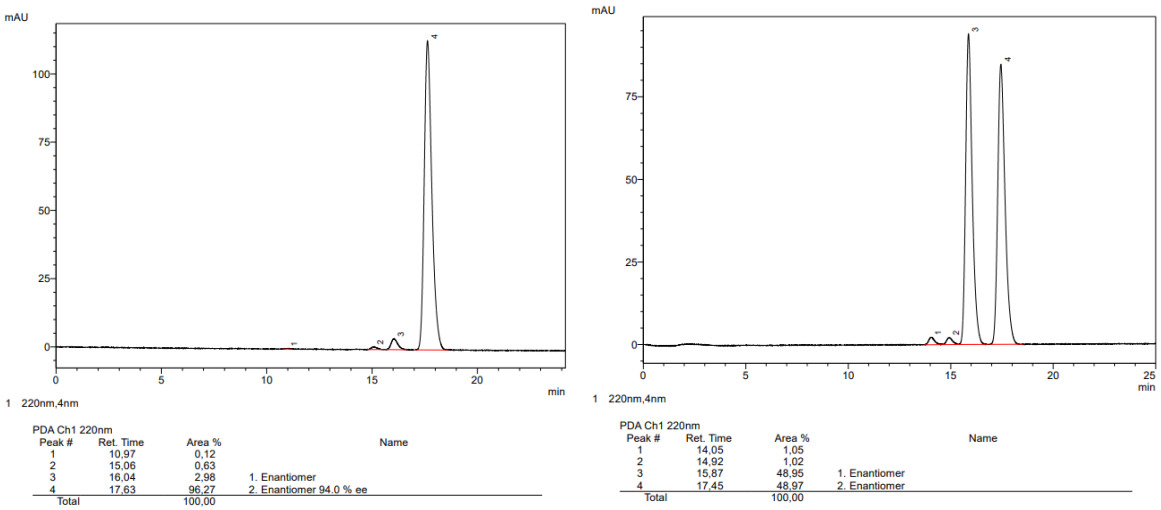

HPLC traces of **70** (left) and corresponding racemate (right).

2-((1*S*,2*R*)-1-(Trifluoromethyl)-2-(4-(trifluoromethyl)phenyl)cyclopropyl)furan (71).

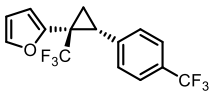

Prepared according to the general procedure **A** with 0.9 mmol of alkene. The crude residue was purified by flash chromatography (75:1 pentane:EtOAc) afforded the title compound as a colorless oil (18 mg, 62%, 95% *ee*). [The *ee* was determined by HPLC analysis: 150 mm Chiralpak OJ-3R, Ø 4.6 mm i.D., acetonitrile / water gradient: 50 % to 70 % in 10 min, v = 1.0 mL / min, λ = 220 nm, t(minor) = 6.97 min, t(major) = 7.23 min]. $[\alpha]_D^{20}$ = −48.5 (c = 0.4, $CHCl_3$). ^{1}H NMR (400 MHz, $CDCl_3$) δ 7.41 (d, *J* = 7.9 Hz, 2H), 7.21 (dd, *J* = 1.9, 0.8 Hz, 1H), 7.06 (d, *J* = 7.2 Hz, 2H), 6.19 (dd, *J* = 3.3, 1.9 Hz, 1H), 6.15 (dd, *J* = 3.3, 0.8 Hz, 1H), 2.89 (dd, *J* = 9.4, 7.3 Hz, 1H), 2.00 – 1.86 (m, 2H). ^{13}C NMR (101 MHz, $CDCl_3$) δ 145.6, 143.1, 139.5, 129.3 (q, *J* = 32.6 Hz) 128.4 (2C), 125.0 (q, *J* = 3.6 Hz, 2C), 124.6 (q, *J* = 274.2 Hz), 124.3 (q, *J* = 271.8 Hz), 112.6, 110.7, 30.1 (q, *J* = 35.1 Hz), 26.8 (q, *J* = 2.1 Hz), 14.4 (q, *J* = 2.3 Hz). ^{19}F NMR (282 MHz, $CDCl_3$) δ −62.5, −69.6. IR (ATR): $\tilde{\nu}$ = 1324, 1289, 1219, 116, 1070, 1058, 1017, 851, 742 cm^{-1}. HRMS (EI) m/z calcd. for $C_{15}H_{10}F_6O$ $[M]^+$: calcd: 320.06304, found: 320.06360.

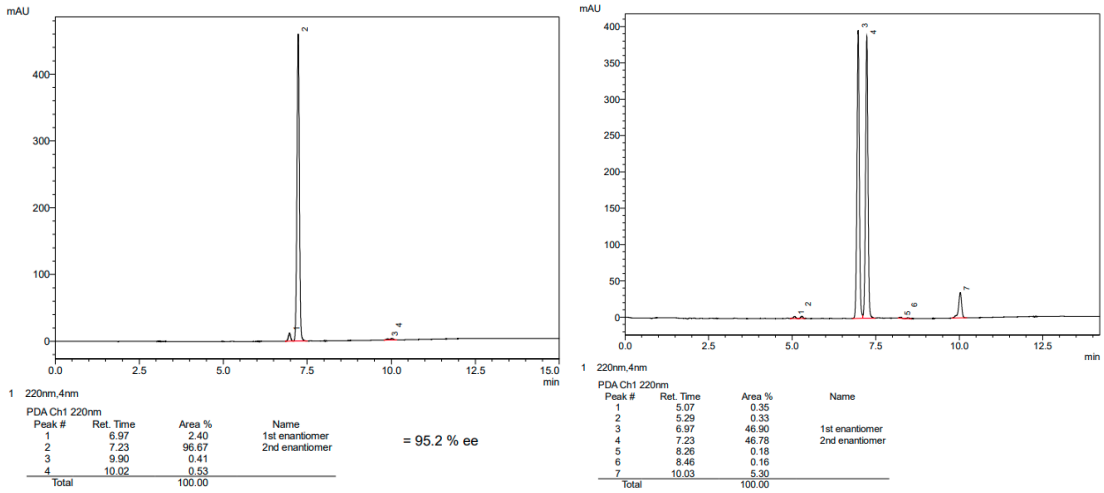

HPLC traces of **71** (left) and corresponding racemate (right).

Methyl 4-((1*R*,2*S*)-2-(furan-2-yl)-2-(trifluoromethyl)cyclopropyl)benzoate (72).

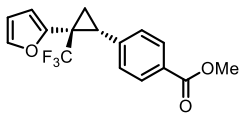

Prepared according to the general procedure **A** with 0.9 mmol of alkene. The crude residue was purified by flash chromatography (40:1 to 30:1 pentane:EtOAc) which afforded the title compound as a pale yellow oil (19.6 mg, 70%, 95% *ee*). [The *ee* was determined by HPLC analysis: 150 mm Chiralcel IB-N3, Ø 4.6 mm i.D., acetonitrile / water = 50:50, v = 1.0 mL / min, λ = 240 nm, t(minor) = 26.35 min, t(major) = 27.33 min]. $[\alpha]_D^{20}$ = –72.3 (c = 0.2, $CHCl_3$). ^{1}H NMR (400 MHz, $CDCl_3$) δ 7.87 – 7.79 (m, 2H), 7.19 (dd, *J* = 1.8, 0.8 Hz, 1H), 7.06 – 6.97 (m, 2H), 6.16 (dd, *J* = 3.3, 1.8 Hz, 1H), 6.12 (dd, *J* = 3.3, 0.8 Hz, 1H), 3.87 (s, 3H), 2.89 (dd, *J* = 9.4, 7.3 Hz, 1H), 1.97 (ddq, *J* = 7.6, 6.2, 1.6 Hz, 1H), 1.90 (dd, *J* = 9.4, 6.2 Hz, 1H). ^{13}C NMR (101 MHz, $CDCl_3$) δ 167.0, 145.7, 143.0, 140.7, 129.4 (2C), 128.9, 128.1 (2C), 125.1 (q, *J* = 274.2 Hz), 112.47, 110.67, 52.18, 30.16 (q, *J* = 35.1 Hz), 27.04 (q, *J* = 2.3 Hz), 14.34 (q, *J* = 2.3 Hz). ^{19}F NMR (282 MHz, $CDCl_3$) δ –69.6. IR (ATR): $\tilde{\nu}$ = 1718, 1332, 1277, 1217, 1183, 1139, 1111, 1058, 1016, 743, 716 cm^{-1}. HRMS (EI) m/z calcd. for $C_{16}H_{13}F_3O_3$ $[M]^+$: calcd: 310.08113, found: 310.08133.

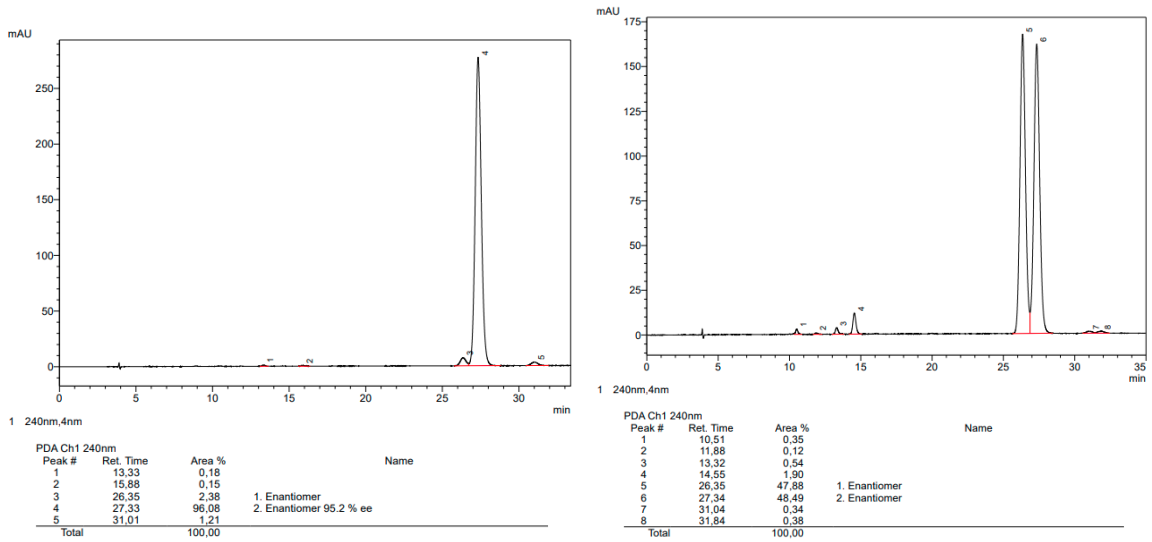

HPLC traces of **72** (left) and corresponding racemate (right).

2-((1*S*,2*R*)-2-(3-Chlorophenyl)-1-(trifluoromethyl)cyclopropyl)furan (73). Prepared

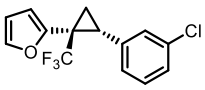

according to the general procedure **A** with 0.9 mmol of alkene. The crude residue was purified by flash chromatography (75:1 pentane:EtOAc) which afforded the title compound as a yellow oil (18.4 mg, 71%, 81% *ee*). [The *ee* was determined by HPLC analysis: 150 mm Chiralpak OJ-3R, Ø 4.6 mm i.D., acetonitrile / water = 40:60 v = 1.0 mL / min, λ = 220 nm, t(minor) = 56.87 min, t(major) = 65.45 min]. $[\alpha]_D^{20}$ = –45.4 (c =0.9, $CHCl_3$). ^{1}H NMR (400 MHz, $CDCl_3$) δ 7.22 (dd, *J* = 1.8, 0.8 Hz, 1H), 7.16 – 7.04 (m, 2H), 6.96 (t, *J* = 1.9 Hz, 1H), 6.88 – 6.81 (m, 1H), 6.20 (dd, *J* = 3.3, 1.9 Hz, 1H), 6.15 (dd, *J* = 3.4, 0.8 Hz, 1H), 2.82 (dd, *J* = 9.4, 7.3 Hz, 1H), 1.95 – 1.82 (m, 2H). ^{13}C NMR (101 MHz, $CDCl_3$) δ 145.7, 143.0, 137.4, 134.0, 129.3, 128.4, 127.3, 126.3, 125.0 (q, *J* = 273.8 Hz), 112.4, 110.7, 29.9 (q, *J* = 35.5 Hz), 26.7 (q, *J* = 2.3 Hz), 14.1 (q, *J* = 2.3 Hz).^{19}F NMR (282 MHz, $CDCl_3$) δ -69.5. IR (ATR): $\tilde{\nu}$ = 1391, 1332, 1300, 1223, 1152, 1082, 1062, 1015, 814, 784, 742, 690 cm^{-1}. HRMS (EI) m/z calcd. for $C_{14}H_{10}ClF_3O$ $[M]^+$: calcd: 286.03668, found: 286.03656.

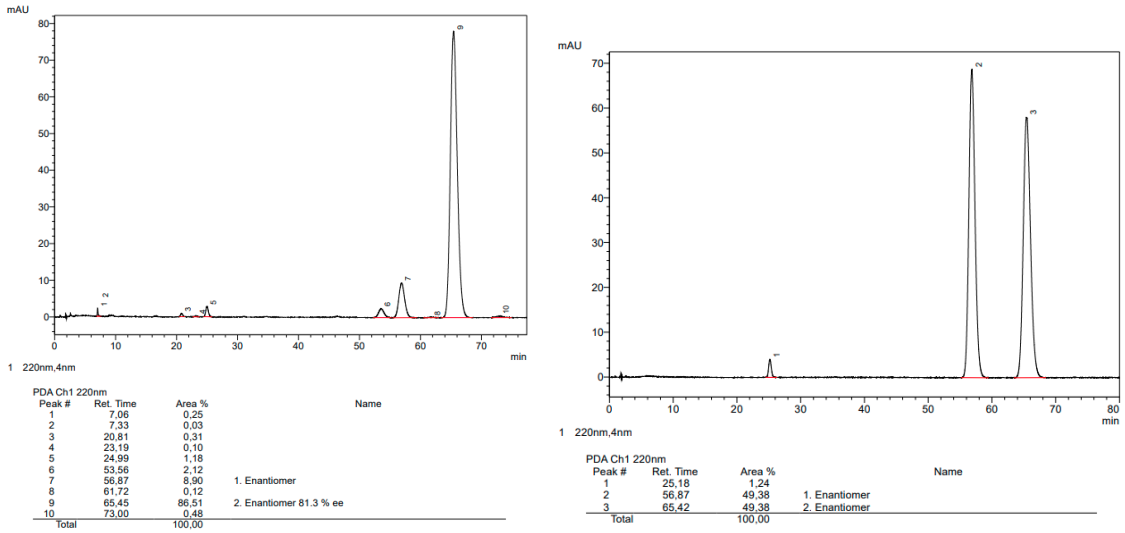

HPLC traces of **73** (left) and corresponding racemate (right).

2-((1*S*,2*S*)-2-(2-Chlorophenyl)-1-(trifluoromethyl)cyclopropyl)furan (74). Prepared

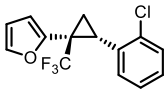

according to the general procedure **A** with 0.9 mmol of alkene. The crude residue was purified by flash chromatography (75:1 pentane:EtOAc) which afforded the title compound as a pale yellow oil (20 mg, 77%, 89% *ee*). [The *ee* was determined by HPLC analysis: 150 mm Chiralpak OJ-3R, Ø 4.6 mm i.D., acetonitrile / water = 60:40 v = 1.0 mL / min, λ = 220 nm, t(minor) = 5.38 min, t(major) = 5.86 min]. $[\alpha]_D^{20}$ = –118.5 (c = 0.8, $CHCl_3$). ^{1}H NMR (400 MHz, $CDCl_3$) δ 7.33 (dd, *J* = 7.9, 1.3 Hz, 1H), 7.14 (dd, *J* = 0.9, 0.8 Hz, 1H), 7.10 (td, *J* = 7.7, 6.1 Hz, 1H), 7.03 (td, *J* = 7.5, 1.3 Hz, 1H), 6.18 (d, *J* = 3.1 Hz, 1H), 6.11 (dd, *J* = 3.3, 1.9 Hz, 1H), 3.06 (dd, *J* = 9.4, 7.4 Hz, 1H), 2.04 (ddd, *J* = 7.5, 6.1, 1.4 Hz, 1H), 1.86 (dd, *J* = 9.4, 6.2 Hz, 1H). ^{13}C NMR (101 MHz, $CDCl_3$) δ 145.8, 142.5, 136.2, 133.2, 129.3, 128.5, 128.4, 126.4, 125.2 (q, *J* = 274.4 Hz), 111.6, 110.7, 29.5 (q, *J* = 35.1 Hz), 26.1 (q, *J* = 2.2 Hz), 12.8 (q, *J* = 2.1 Hz). ^{19}F NMR (282 MHz, $CDCl_3$) δ –69.4. IR (ATR): $\tilde{\nu}$ = 1390, 1333, 1298, 1212, 1149, 1063, 1053, 1014, 754, 740 cm^{-1}. HRMS (EI) m/z calcd. for $C_{14}H_{10}ClF_3O$ $[M]^+$: calcd: 286.03668, found: 286.03672.

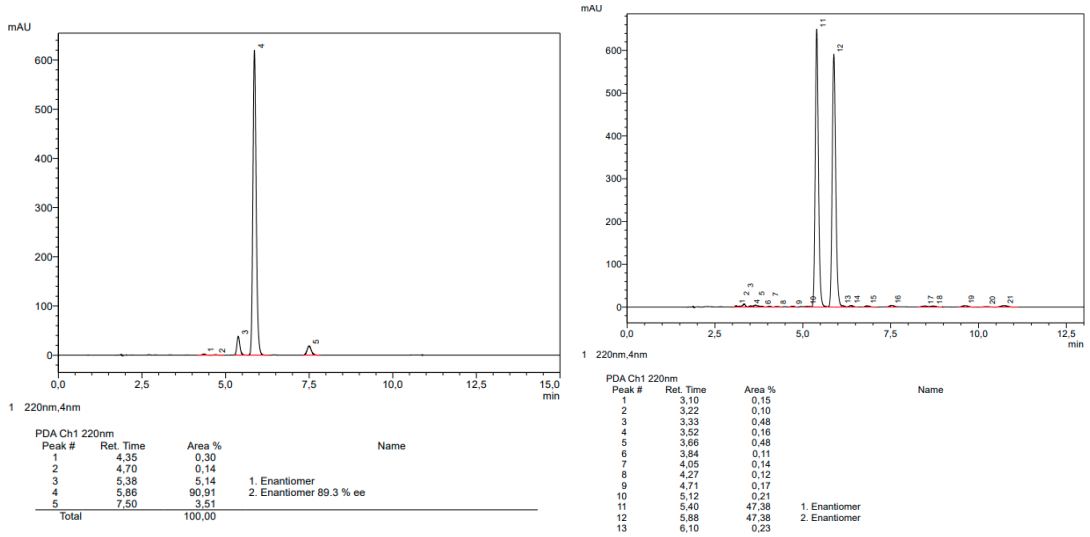

HPLC traces of **74** (left) and corresponding racemate (right).

2-((1*S*,1a*R*,6a*R*)-1-(Trifluoromethyl)-1,1a,6,6a-tetrahydrocyclopropa[a]inden-1-yl)furan (75). Prepared according to the general procedure **A** with 0.9 mmol of alkene. The crude residue was purified by flash chromatography (50:1 pentane:EtOAc) which afforded the title compound as a pale yellow oil (17.5 mg, 73%, 91% *ee*). [The *ee* was determined by HPLC analysis: 150 mm Chiralcel OJ-3R, Ø 4.6 mm i.D., acetonitrile/water = 60:40, v = 0.5 mL/min, λ = 220 nm, t(minor) = 12.28 min, t(major) = 13.70 min]. $[\alpha]_D^{20}$ = −24.0 (c = 0.9, $CHCl_3$). ^{1}H NMR (600 MHz, $CDCl_3$) δ 7.39 (d, *J* = 7.5 Hz, 1H), 7.16 (dd, *J* = 1.9, 0.8 Hz, 1H), 7.11 (tq, *J* = 7.4, 0.9 Hz, 1H), 7.02 (td, *J* = 7.5, 1.2 Hz, 1H), 6.88 (d, *J* = 6.8 Hz, 1H), 6.05 (dd, *J* = 3.3, 1.8 Hz, 1H), 5.86 (dd, *J* = 3.3, 0.8 Hz, 1H), 3.30 (dd, *J* = 6.9, 1.3 Hz, 1H), 3.22 (ddq, *J* = 17.6, 6.9, 1.3 Hz, 1H), 2.96 (d, *J* = 17.6 Hz, 1H), 2.66 (td, *J* = 6.9, 0.8 Hz, 1H). ^{13}C NMR (151 MHz, $CDCl_3$) δ 144.8 (q, *J* = 1.0 Hz), 143.1, 142.9, 139.9, 126.9, 126.5, 125.1 (q, *J* = 274.9 Hz), 125.0, 124.3, 113.3, 110.0, 34.4 (q, *J* = 2.4 Hz), 33.0, 31.3 (q, *J* = 33.5 Hz), 26.2 (q, *J* = 2.2 Hz). ^{19}F NMR (565 MHz, $CDCl_3$) δ −68.6. IR (ATR): $\tilde{\nu}$ = 1330, 1278, 1265, 1224, 1136, 1026, 1011, 760, 739, 725, 598, 457 cm^{-1}. HRMS (EI) m/z calcd. for $C_{15}H_{11}F_3O$ $[M]^+$: calcd: 264.075650, found: 264.076120.

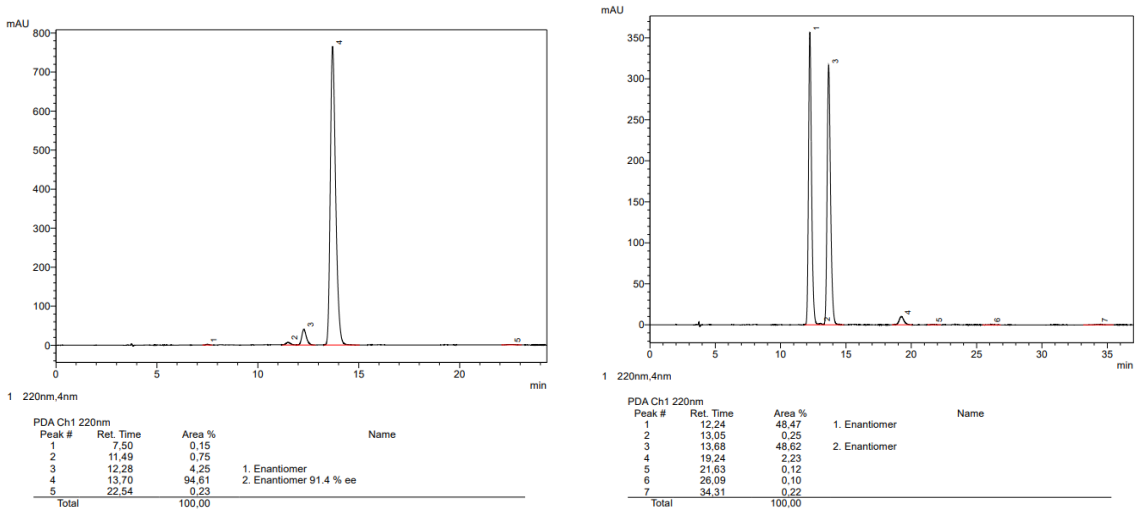

HPLC traces of **75** (left) and corresponding racemate (right).

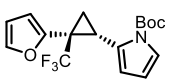

***tert*-Butyl 2-((1*S*,2*S*)-2-(furan-2-yl)-2-(trifluoromethyl)cyclopropyl)-1H-pyrrole-1-carboxylate (76).** Prepared according to the general procedure **A** with 0.9 mmol of alkene. The crude residue was purified by preparative TLC (20:1 n-hexane: EtOAc) which afforded the title compound as a pale yellow oil (22.1 mg, 71%, 89% *ee*). [The *ee* was determined by HPLC analysis: 150 mm Chiralpak IB-N3, Ø 4.6 mm i.D., *n*-heptane/2-propanol = 99.99:0.01, v= 1.0 mL / min, λ = 220 nm, t(minor) = 4.29 min, t(major) = 4.79 min]. $[\alpha]_D^{20}$ = −180.8 (c =1.3, $CHCl_3$). ^{1}H NMR (400 MHz, CD_2Cl_2) δ 7.22 (dd, *J* = 1.9, 0.9 Hz, 1H), 7.11 (ddd, *J* = 3.3, 1.8, 0.6 Hz, 1H), 6.20 (dd, *J* = 3.3, 1.9 Hz, 1H), 6.12 (dd, *J* = 3.3, 0.8 Hz, 1H), 5.88 (t, *J* = 3.4 Hz, 1H), 5.72 (ddd, *J* = 3.2, 1.8, 1.1 Hz, 1H), 3.30 (dd, *J* = 9.0, 7.6 Hz, 1H), 1.85 – 1.74 (m, 2H), 1.64 (s, 9H). ^{13}C NMR (101 MHz, CD_2Cl_2) δ 149.6, 147.3, 143.0, 130.0, 125.6 (q, *J* = 274.3 Hz), 122.4, 112.8, 111.8, 110.7, 109.7, 84.3, 29.4 (q, *J* = 34.1 Hz), 28.1 (3C), 22.3 (q, *J* = 2.5 Hz), 14.1z (q, *J* = 2.1 Hz). ^{19}F NMR (282 MHz, $CDCl_3$) δ –69.0. IR (ATR): ṽ = 1744, 1417, 1371, 1327, 1307, 1288, 1126, 1102, 1059, 1013, 729, 717 cm^{-1}. HRMS (EI) m/z calcd. for $C_{17}H_{18}F_3NO_3$ $[M]^+$: calcd: 341.12333, found: 341.12314.

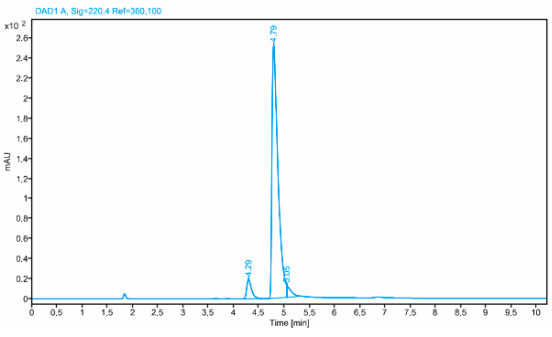

Signal: DAD1 A, Sig=220,4 Ref=360,100

RT [min]	Area%	Name
4,29	5,58	1st enantiomer
4,79	91,42	2nd enantiomer
5,05	3,00	

= 88.5 % ee

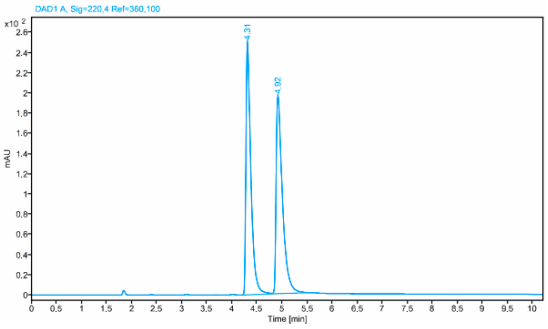

Signal: DAD1 A, Sig=220,4 Ref=360,100

RT [min]	Area%	Name
4,31	49,98	1st enantiomer
4,92	50,02	2nd enantiomer

HPLC traces of **76** (left) and corresponding racemate (right).

2-((1*S*,2*S*)-2-Butoxy-1-(trifluoromethyl)cyclopropyl)furan (77). Prepared according to

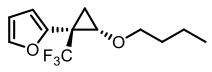

the general procedure **A** with 0.9 mmol of alkene. The crude residue was purified by flash chromatography (75:1 pentane:EtOAc) which afforded the title compound as a pale yellow oil (19.8 mg, 88%, 15:1 *dr*, 69% *ee*). [The *ee* was determined by HPLC analysis: 150 mm Chiralpak IB N-3, Ø 4.6 mm i.D., 100 % *n*-heptane, v = 1.0 mL/min, λ = 220 nm, t(minor) = 2.97 min, t(major) = 3.26 min]. $[\alpha]_D^{20}$ = –42.5 (c = 0.2, $CHCl_3$). ^{1}H NMR (400 MHz, $CDCl_3$) δ 7.40 (dd, *J* = 1.9, 0.9 Hz, 1H), 6.42 (dd, *J* = 3.3, 0.8 Hz, 1H), 6.38 (dd, *J* = 3.3, 1.8 Hz, 1H), 3.73 (dd, *J* = 7.4, 4.7 Hz, 1H), 3.56 – 3.43 (m, 2H), 1.71 (ddq, *J* = 7.6, 4.6, 1.5 Hz, 1H), 1.55 (t, *J* = 7.2 Hz, 1H), 1.45 – 1.30 (m, 2H), 1.24 – 1.07 (m, 2H), 0.81 (t, *J* = 7.4 Hz, 3H). ^{13}C NMR (101 MHz, $CDCl_3$) δ 146.1, 142.7, 124.9 (q, *J* = 272.8 Hz), 111.5, 110.8, 71.2, 59.6 (q, *J* = 2.6 Hz), 31.5, 29.0 – 26.7 (m), 19.2, 15.6 (q, *J* = 2.3 Hz), 13.9. ^{19}F NMR (282 MHz, $CDCl_3$) δ –62.5 (minor dia), –67.9 (major dia). IR (ATR): $\tilde{\nu}$ = 1361, 1337, 1299, 1225, 1136, 1087, 1011, 738 cm^{-1}. HRMS (EI) m/z calcd. for $C_{12}H_{15}F_3O_2$ $[M]^+$: calcd: 248.101865, found: 248.101740.

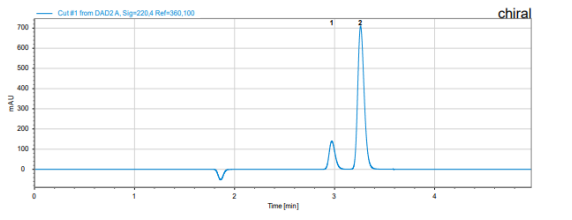

Signal: DAD2 A, Sig=220,4 Ref=360,100

Compound	Cut	Ret.Time	Area	Width	Height	Symmetry	
1	1	2.972	588.173 **588.173**	0.070	139.943	0.773	1st enantiomer
2	1	3.260	3178.451 **3178.451**	0.075	710.262	0.802	2nd enantiomer

ee = 68.8 %

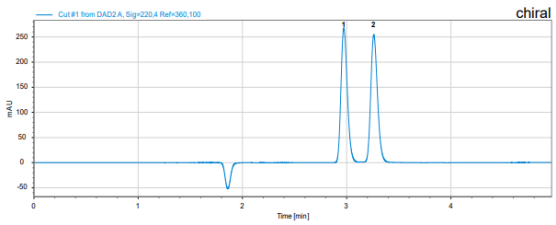

Signal: DAD2 A, Sig=220,4 Ref=360,100

Compound	Cut	Ret.Time	Area	Width	Height	Symmetry	
1	1	2.973	1123.390 **1123.390**	0.070	266.904	0.790	1st enantiomer
2	1	3.261	1123.058 **1123.058**	0.074	253.506	0.809	2nd enantiomer

HPLC traces of **77** (left) and corresponding racemate (right).

2-((1*S*,2*S*)-2-(*tert*-Butoxy)-1-(trifluoromethyl)cyclopropyl)furan (78). Prepared

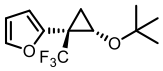

according to the general procedure **A** with 0.9 mmol of alkene. The crude residue was purified by flash chromatography (75:1 pentane:EtOAc) which afforded the title compound as a colorless oil (20 mg, 89%, 17:1 *dr*, 88% *ee*). [The *ee* was determined by HPLC analysis: 150 mm Chiralpak IG-3, Ø 4.6 mm i.D., methanol / water = 55:45, v = 1.0 mL / min, λ = 220 nm, t(minor) = 22.74 min, t(major) = 25.49 min]. $[\alpha]_D^{20}$ = –62.7 (c = 0.4, $CHCl_3$). ^{1}H NMR (400 MHz, $CDCl_3$) δ 7.40 (t, *J* = 1.3 Hz, 1H), 6.37 (d, *J* = 1.4 Hz, 2H), 3.78 (dd, *J* = 7.7, 5.0 Hz, 1H), 1.64 (ddq, *J* = 6.3, 5.0, 1.4 Hz, 1H), 1.55 (dd, *J* = 7.7, 6.9 Hz, 1H), 1.15 (s, 9H). ^{13}C NMR (101 MHz, $CDCl_3$) δ 146.5, 142.3, 125.1 (q, *J* = 272.7 Hz), 110.7, 75.9, 54.1 (q, *J* = 2.8 Hz), 27.8 (3C), 27.8 (signal overlap quadruplet), 15.5 (q, *J* = 2.3 Hz).^{19}F NMR (282 MHz, $CDCl_3$) δ –62.5 (minor dia), –67.6. (major dia). IR (ATR): $\tilde{\nu}$ = 1719, 1578, 1468, 1383, 1366, 1291, 1271, 1191, 1183, 1083, 755, 746 cm^{-1}. HRMS (EI) m/z calcd. for $C_{12}H_{15}F_3O_2$ $[M]^+$: calcd: 248.101865, found: 248.101840.

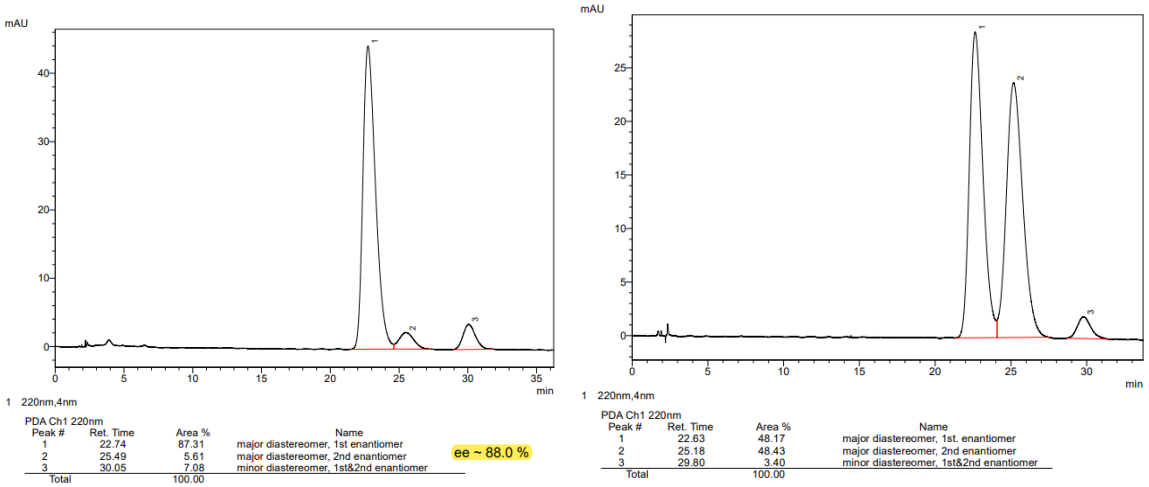

HPLC traces of **78** (left) and corresponding racemate (right).

2-((1*S*,2*R*)-2-Methyl-2-phenyl-1-(trifluoromethyl)cyclopropyl)furan (79). Prepared

major dia + minor dia

according to the general procedure **A** with 0.9 mmol of alkene. The crude residue was purified by flash chromatography (75:1 to 50:1 pentane: EtOAc) which afforded a diastereomeric mixture of the title compound as a pale yellow oil (19.6 mg, 81%, 1:1.6 *dr*, minor dia: >99% *ee*, major dia: 83% *ee*). [The *ee* was determined by HPLC analysis: 150 mm Chiralcel OD-3, Ø 4.6 mm i.D., *n*-heptan = 100%, v = 1.0 mL / min, λ = 220 nm, $t_{minor\ dia}$(minor) = 4.53 min, $t_{major\ dia}$ (major) = 4.66 min; $t_{major\ dia}$(minor) = 10.47 min, $t_{major\ dia}$ (major) = 26.44 min]. $[\alpha]_D^{20}$ = –45.8 (c = 1.0), $CHCl_3$). IR (ATR): $\tilde{\nu}$ = 1339, 1274, 1214, 1134, 1113, 1096, 1084, 1071, 1043, 1028, 1011, 927, 766, 736, 698 cm^{-1}. HRMS (EI) m/z calcd.

for $C_{15}H_{13}F_3O$ $[M]^+$: calcd: 266.09130, found: 266.09140. NMR characterization of major diastereoisomer: ^{1}H NMR (600 MHz, $CDCl_3$) δ 7.18 – 7.12 (m, 4H), 7.10 – 7.08 (m, 1H), 7.07 (m, 1H), 6.02 (dd, *J* = 3.3, 1.8 Hz, 1H), 5.92 (dd, *J* = 3.3, 0.8 Hz, 1H), 2.10 (dq, *J* = 6.0, 1.9 Hz, 1H), 1.73 (d, *J* = 6.0 Hz, 1H), 1.69 (q, *J* = 1.3 Hz, 3H). ^{13}C NMR (151 MHz, $CDCl_3$) δ 148.70 (q, *J* = 1.8 Hz), 142.13 (q, *J* = 0.9 Hz), 141.98, 128.35, 127.99, 126.65, 126.00 (q, *J* = 275.2 Hz), 110.17, 109.71 (q, *J* = 0.9 Hz), 34.57, 32.73 (q, *J* = 33.8 Hz), 22.22 (q, *J* = 2.7 Hz), 20.70 (q, *J* = 2.3 Hz). ^{19}F NMR (565 MHz, $CDCl_3$) δ –60.3. NMR characterization of minor diastereoisomer: ^{1}H NMR (600 MHz, $CDCl_3$) δ 7.47 – 7.43 (m, 1H), 7.41 (d, *J* = 7.4 Hz, 2H), 7.34 (t, *J* = 7.4 Hz, 2H), 7.26 (tt, *J* = 7.4, 1.1 Hz, 1H), 6.48 (d, *J* = 3.2 Hz, 1H), 6.43 (dd, *J* = 3.2, 1.9 Hz, 1H), 2.02 (d, *J* = 5.7 Hz, 1H), 1.59 (dq, *J* = 5.7, 1.7 Hz, 1H), 1.17 (s, 3H). ^{13}C NMR (151 MHz, $CDCl_3$) δ 149.07 (q, *J* = 1.5 Hz), 142.74, 141.15 (q, *J* = 0.8 Hz), 128.75, 128.47, 127.11, 125.29 (q, *J* = 275.2 Hz), 111.29 (q, *J* = 0.7 Hz), 110.76, 34.08, 32.33 (q, *J* = 33.2 Hz), 25.77 (q, *J* = 0.8 Hz), 20.53 (q, *J* = 2.2 Hz). ^{19}F NMR (565 MHz, $CDCl_3$) δ –63.2.

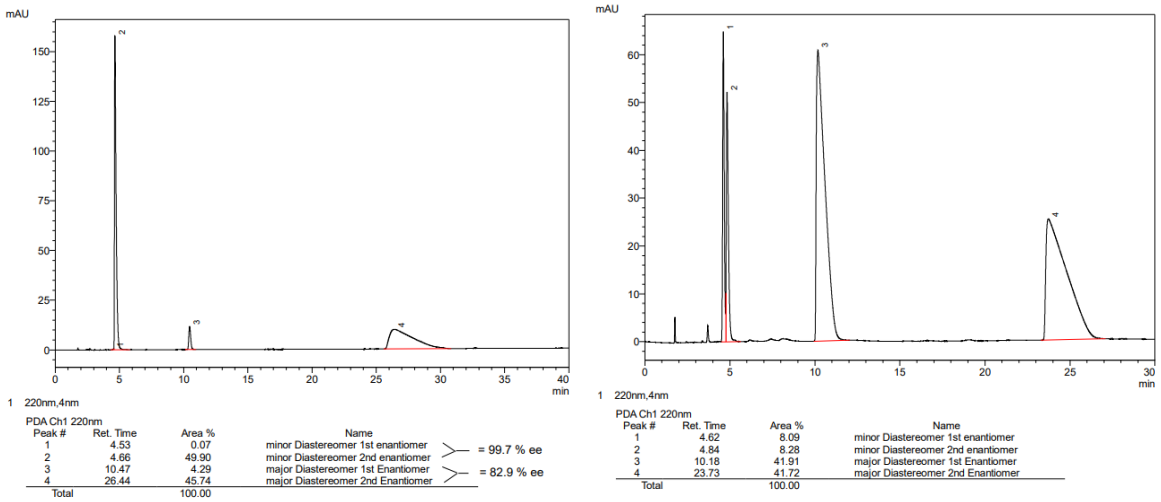

HPLC traces of **79** (left) and corresponding racemate (right).

2-((1*S*,2*R*)-2-(*p*-Tolyl)-1-(trifluoromethyl)cyclopropyl)benzofuran (80). Prepared

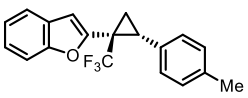

according to the general procedure **A** with 0.9 mmol of alkene and benzofuran hydrazone **256** (0.0917 mmol, 40 mg). The crude residue was purified by flash chromatography (75:1 to 50:1 pentane:EtOAc) which afforded the title compound as a yellow oil that solidified after prolonged standing at rt. (27.8 mg, 96%, 96% *ee*). [The *ee* was determined by HPLC analysis: 150 mm Chiralpak IJ-3, Ø 4.6 mm i.D., methanol / water = 85:15, v= 1.0 mL / min, λ = 220 nm, t(minor) = 10.56 min, t(major) = 13.39 min]. $[\alpha]_D^{20}$ = –112.0 (c =1.6, $CHCl_3$). ^{1}H NMR (400 MHz, $CDCl_3$) δ 7.40 (ddq, *J* = 20.2, 8.3, 0.8 Hz, 1H), 7.23 (ddd, *J* = 8.3, 7.2, 1.4 Hz, 1H), 7.15 (td, *J* = 7.5, 1.1 Hz, 1H), 6.99 – 6.88 (m, 4H), 6.51 (d, *J* = 1.0 Hz, 1H), 2.96 (dd, *J* = 9.6, 7.5 Hz, 1H), 2.21 (s, 3H), 2.07 (ddq, *J* = 7.6, 6.1, 1.6 Hz, 1H), 1.94 (dd, *J* = 9.6, 6.1 Hz, 1H). ^{13}C NMR (101 MHz, $CDCl_3$) δ 154.8, 149.2, 136.8, 131.6, 129.0 (2C),

128.1 (2C), 128.1, 125.3 (q, *J* = 272.7 Hz), 124.4, 122.7, 121.1, 111.3, 108.9, 30.1 (q, *J* = 34.5 Hz), 27.5 (q, *J* = 2.0 Hz), 21.1, 14.1 (q, *J* = 2.2 Hz). ^{19}F NMR (282 MHz, $CDCl_3$) δ –68.84. IR (ATR): ṽ = 1453, 1384, 1319, 1282, 1257, 1235, 1209, 1132, 1095, 1053, 850, 816, 780, 750, 741, 730, 707 cm^{-1}. HRMS (EI) m/z calcd. for $C_{19}H_{15}F_3O$ [M]$^+$: calcd: 316.10695, found: 316.10710.

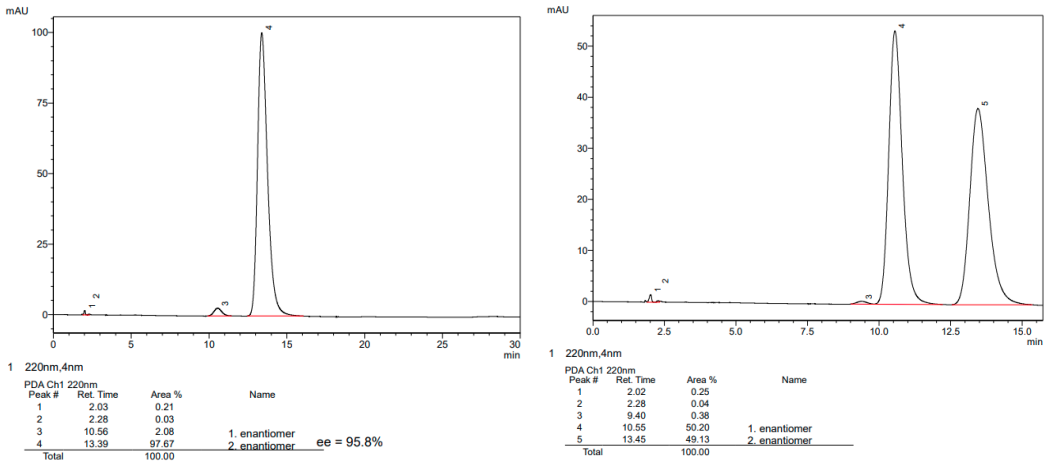

HPLC traces of **80** (left) and corresponding racemate (right).

2-((1*S*,2*S*)-2-(Furan-2-yl)-2-(trifluoromethyl)cyclopropyl)benzofuran (81). Prepared according to the general procedure **A** with 0.9 mmol of alkene. The crude residue was purified by flash chromatography (75:1 pentane:EtOAc) which afforded the title compound as a pale yellow oil (23.4 mg, 88%, 52% *ee*). [The *ee* was determined by HPLC analysis: 150 mm Chiralpak IJ-3, Ø 4.6 mm i.D., methanol / water = 85:15, v= 1.0 mL / min, λ = 220 nm, t(minor) = 7.22 min, t(major) = 9.57 min]. $[\alpha]_D^{20}$ = –31.5 (c = 1.5, $CHCl_3$). ^{1}H NMR (400 MHz, $CDCl_3$) δ 7.41 (ddd, *J* = 7.4, 1.5, 0.7 Hz, 1H), 7.37 – 7.29 (m, 1H), 7.27 – 7.24 (m, 1H), 7.23 – 7.10 (m, 2H), 6.29 – 6.23 (m, 2H), 6.19 (dd, *J* = 3.3, 1.9 Hz, 1H), 2.96 (dd, *J* = 9.6, 7.0 Hz, 1H), 2.06 – 1.91 (m, 2H). ^{13}C NMR (101 MHz, $CDCl_3$) δ 154.9, 153.0, 145.8, 143.1, 128.4, 126.2 (q, *J* = 274.4 Hz), 124.0, 122.8, 120.7, 112.2, 110.9, 110.8, 104.1, 29.5 (q, *J* = 35.1 Hz), 20.8 (q, *J* = 2.5 Hz), 14.2 (q, *J* = 2.2 Hz). ^{19}F NMR (282 MHz, $CDCl_3$) δ -69.8. IR (ATR): ṽ = 1454, 1334, 1289, 1139, 1108, 1061, 1013, 804, 738, 723, 426 cm^{-1}. HRMS (EI) m/z calcd. for $C_{16}H_{11}F_3O_2$ [M]$^+$: calcd: 292.07057, found: 292.07075.

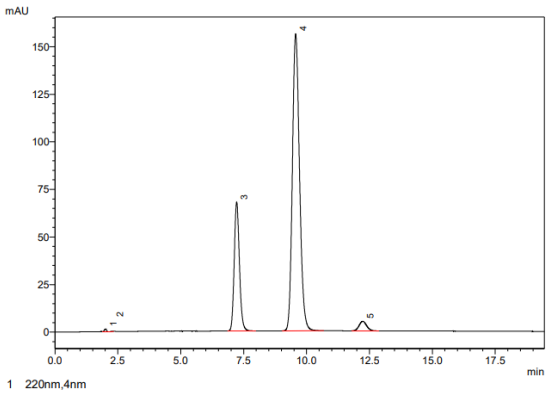

1 220nm,4nm

PDA Ch1 220nm

Peak #	Ret. Time	Area %	Name
1	2.02	0.21	
2	2.28	0.04	
3	7.22	23.34	1. enantiomer
4	9.57	73.88	2. enantiomer
5	12.23	2.52	
Total		100.00	

ee = 52.0 %

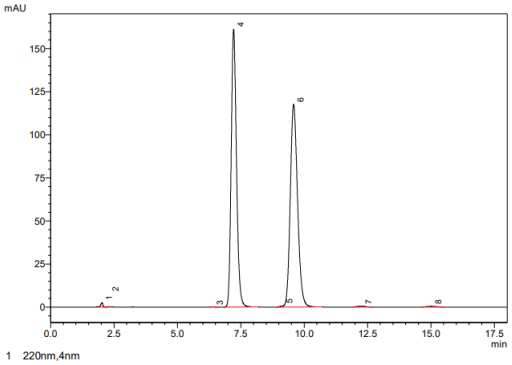

1 220nm,4nm

PDA Ch1 220nm

Peak #	Ret. Time	Area %	Name
1	2.03	0.31	
2	2.28	0.03	
3	6.40	0.04	
4	7.22	49.44	1. enantiomer
5	9.15	0.10	
6	9.58	49.58	2. enantiomer
7	12.25	0.26	
8	15.01	0.24	
Total		100.00	

HPLC traces of **81** (left) and corresponding racemate (right).

(*S*)-2-(2-(4-Methoxyphenyl)-1-(trifluoromethyl)cycloprop-2-en-1-yl)furan (82).

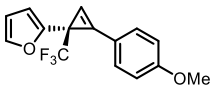

Prepared according to the general procedure **A** with 0.9 mmol of alkyne. The crude residue was purified by flash chromatography (50:1 to 40:1 hexane:EtOAc) which afforded the title compound as a fluorescent yellow oil (22.7 mg, 90%, 92% *ee*). [The *ee* was determined by HPLC analysis: 150 mm Chiralpak OJ-3R, Ø 4.6 mm i.D. acetonitrile/water = 60:40, v = 0.5 mL/min, λ = 220 nm, t(minor) = 15.80 min, t(major) = 22.49 min]. $[\alpha]_D^{20}$ = –198.8 (c = 1.4, $CHCl_3$). ^{1}H NMR (400 MHz, $CDCl_3$) δ 7.64 – 7.54 (m, 2H), 7.28 (dd, J = 1.8, 0.9 Hz, 1H), 7.01 – 6.93 (m, 2H), 6.89 (q, J = 1.5 Hz, 1H), 6.39 – 6.30 (m, 2H), 3.85 (s, 3H). ^{13}C NMR (101 MHz, $CDCl_3$) δ 161.6, 152.0, 141.6, 131.9 (2C), 125.9 (q, *J* = 276.0 Hz), 117.3, 114.7 (2C), 110.7, 107.5, 94.0 (q, J = 2.5 Hz), 55.6, 27.3 (q, *J*= 37.2Hz). ^{19}F NMR (282 MHz, $CDCl_3$) δ –66.6. IR (ATR): $\tilde{\nu}$ = 1605, 1505, 1302, 1251, 1171, 1149, 1129, 1030, 953, 834, 731cm^{-1}. HRMS (ESI$^+$) m/z calcd. for $C_{15}H_{12}F_3O_2$ $[M+H]^+$: calcd: 281.07839, found: 281.07848.

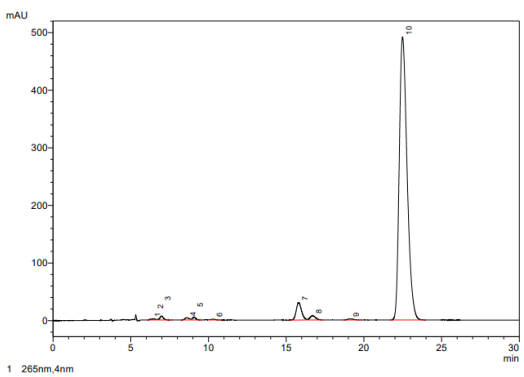

PDA Ch1 265nm

Peak #	Ret. Time	Area %	Name
1	6,30	0,10	
2	6,50	0,11	
3	6,98	0,63	
4	8,61	0,42	
5	9,07	0,39	
6	10,31	0,17	
7	15,80	3,93	1. Enantiomer
8	16,70	1,01	
9	19,11	0,30	
10	22,49	92,94	2. Enantiomer 91.9 % ee
Total		100,00	

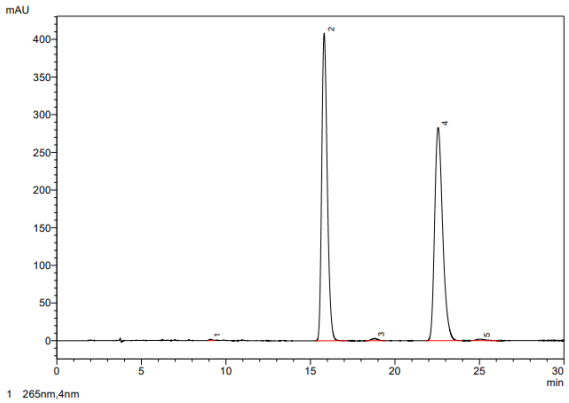

PDA Ch1 265nm

Peak #	Ret. Time	Area %	Name
1	9,09	0,10	
2	15,82	49,53	1. Enantiomer
3	18,77	0,40	
4	22,56	49,58	2. Enantiomer
5	25,04	0,37	
Total		100,00	

HPLC traces of **82** (left) and corresponding racemate (right).

(*S*)-2-(2-(4-Chlorophenyl)-1-(trifluoromethyl)cycloprop-2-en-1-yl)furan (83).

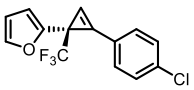

Prepared according to the general procedure **A** with 0.9 mmol of alkyne. The crude residue was purified by flash chromatography (50:1 hexane:EtOAc) affording the title compound as a fluorescent yellow oil (20.7 mg, 80%, 95% *ee*). [The *ee* was determined by HPLC analysis: 150 mm Chiralpak OJ-3R, Ø 4.6 mm i.D. methanol/water = 85:15, v = 0.5 mL/min, λ = 220 nm, t(minor) = 15.18 min, t(major) = 17.99 min]. $[\alpha]_D^{20}$ = –226.4 (c = 1.3, $CHCl_3$). ^{1}H NMR (400 MHz, $CDCl_3$) δ 7.58 (d, *J* = 57.2 Hz, 2H), 7.43 (d, *J* = 53.2 Hz, 2H), 7.28 (dd, *J* = 1.8, 0.8 Hz, 1H), 7.09 (q, *J* = 1.4 Hz, 1H), 6.38 (dt, *J* = 3.3, 0.9 Hz, 1H), 6.35 (dd, *J* = 3.3, 1.8 Hz, 1H). ^{13}C NMR (101 MHz, $CDCl_3$) δ 151.5, 142.1, 137.2, 131.7, 129.8, 125.9 (q, *J* = 276.2 Hz), 123.6, 114.9 (d, *J* = 2.0 Hz), 111.2, 108.1, 98.1 (q, *J* = 2.4 Hz), 27.9 (q, *J* = 38.1 Hz). ^{19}F NMR (282 MHz, $CDCl_3$) δ –66.6. IR (ATR): $\tilde{\nu}$ = 1486, 1308, 1175, 1131, 1094, 1014, 953, 869, 831, 767, 725, 686, 452 cm^{-1}. HRMS (EI) m/z calcd. for $C_{14}H_8ClF_3O$ $[M]^+$: calcd: 284.02103, found: 284.02124.

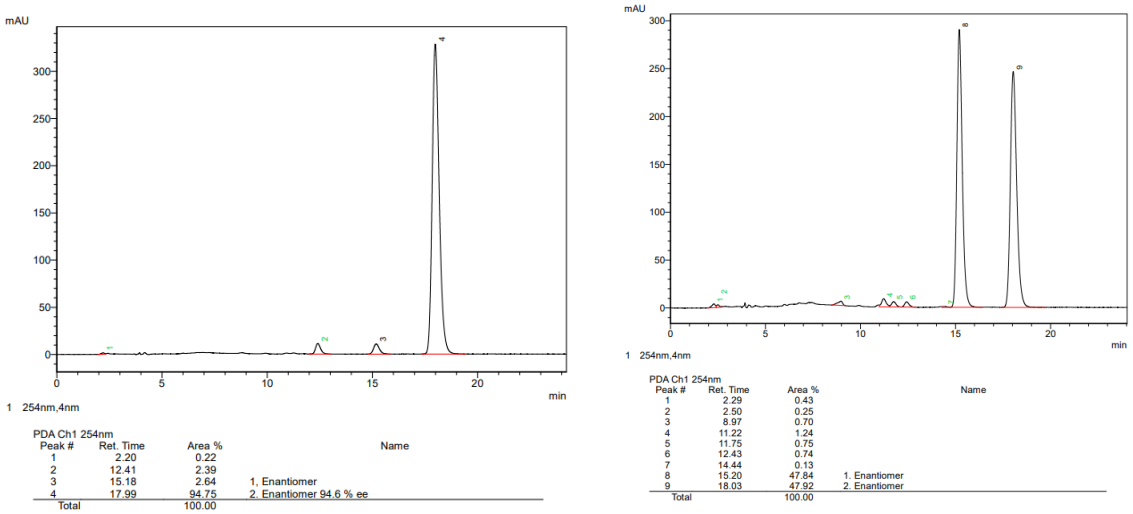

HPLC traces of **83** (left) and corresponding racemate (right).

(1*S*,2*R*)-1-(Furan-2-yl)-2-(p-tolyl)cyclopropane-1-carbaldehyde (85). Prepared

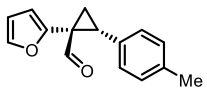

according to general procedure **A** with 0.9 mmol of alkene and hydrazone **84**. The crude residue was purified by flash chromatography (silica, pentane/EtOAc 50:1) which afforded the title compound as a colorless oil (9.7 mg, 41%, 78% *ee*). [The *ee* was determined by HPLC analysis: 150 mm Chiralpak IA-3, Ø 4.6 mm i.D. *n*-heptane/water = 99:1, v = 1.0 mL/min, λ = 220 nm, t(major) = 4.27 min, t(minor) = 6.00 min]. ^{1}H NMR (400 MHz, $CDCl_3$) δ 9.73 (s, 1H), 7.25 (dd, *J* = 1.9, 0.8 Hz, 1H), 6.96 (d, *J* = 7.8 Hz, 2H), 6.91 – 6.83 (m, 2H), 6.22 (dd, *J* = 3.3, 1.9 Hz, 1H), 6.06 (dd, *J* = 3.2, 0.9 Hz, 1H), 3.05 (t, *J* = 8.5 Hz, 1H), 2.25 (s, 3H), 2.15 (d, *J* = 8.5 Hz, 2H). ^{13}C NMR (101 MHz, $CDCl_3$) δ 199.2, 149.3, 142.6, 136.9, 132.2, 128.8, 128.1, 110.6, 110.5, 39.6, 37.1, 21.2, 20.9. IR (ATR): ṽ =1705, 1519, 1506, 1194, 1159, 1012, 983, 818, 737, 599 cm^{-1}. HRMS (ESI +) m/z calcd. for $C_{15}H_{14}O_2Na$ $[M+H]^+$: 249.0886; found: 249.08862.

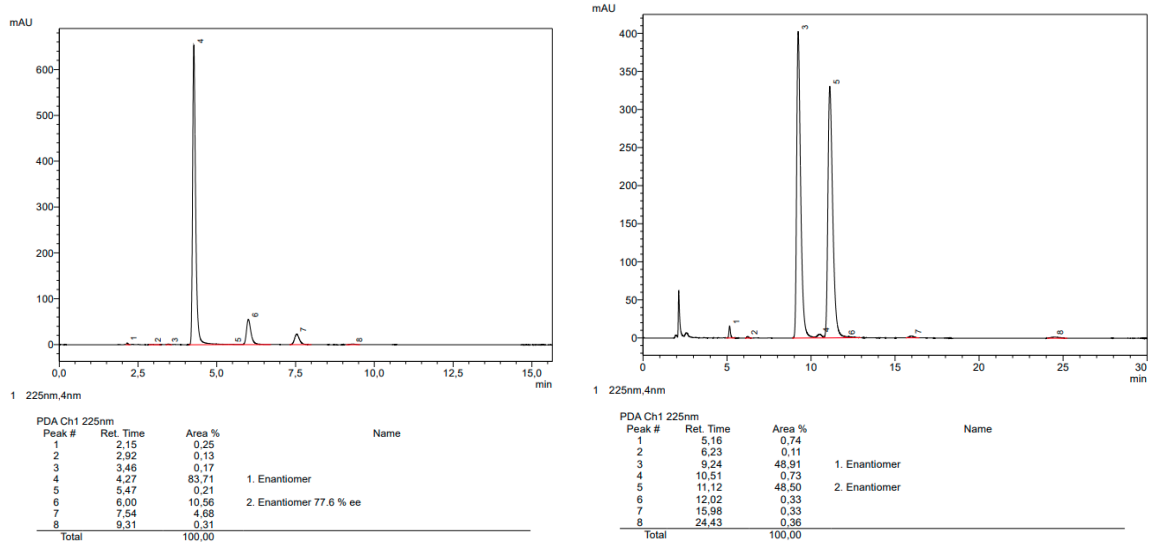

HPLC traces of **85** (left) and corresponding racemate (right).

2-((1*S*,2*R*)-2-(*p*-Tolyl)-1-(trifluoromethyl)cyclopropyl)oxazole (89). Prepared according

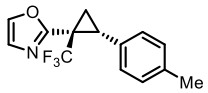

to general procedure **A** with 0.9 mmol of alkene. The crude residue was purified by flash chromatography (silica, pentane/EtOAc 20:1 to 18:1) which afforded the title compound as a colorless oil (9 mg, dr = 1.5:1, 54% *ee* (major diastereomer)). [The *ee* was determined by HPLC analysis: 150 mm Chiralcel IC-3, Ø 4.6 mm, *n*-heptane/2-propanol = 98:2, v = 1.0 mL/min, λ = 215 nm, t(minor) = 2.99 min, t(major) = 3.33 min]. $[\alpha]_D^{20}$ = +9.7 (c = 0.35, $CHCl_3$). ^{1}H NMR (600 MHz, CD_2Cl_2) δ 7.50 – 7.44 (m, 1H), 6.98 (d, *J* = 7.8 Hz, 2H), 6.96 – 6.90 (m, 3H), 2.94 (dd, *J* = 9.8, 7.6 Hz, 1H), 2.29 (ddq, *J* = 7.9, 6.1, 1.7 Hz, 1H), 2.24 (s, 3H), 1.94 (dd, *J* = 9.7, 6.2 Hz, 1H). ^{13}C NMR (151 MHz, CD_2Cl_2) δ 156.9, 140.4, 137.5, 131.2, 129.2, 128.4, 127.5, 125.1 (q, *J* = 273.9 Hz), 30.6 (q, *J* = 35.3 Hz), 28.3 (q, *J* = 1.7 Hz), 21.1, 14.6 (q, *J* = 2.1 Hz). ^{19}F NMR (565 MHz, CD_2Cl_2) δ –68.1 (d, *J* = 1.8 Hz). IR (ATR): ṽ =1576, 1520, 1380, 1320, 1288, 1149, 1120, 1063, 815, 762, 693 cm^{-1}. HRMS (EI) m/z calcd. for $C_{14}H_{12}F_3ON$ $[M]^+$: 267.08655; found: 267.08704.

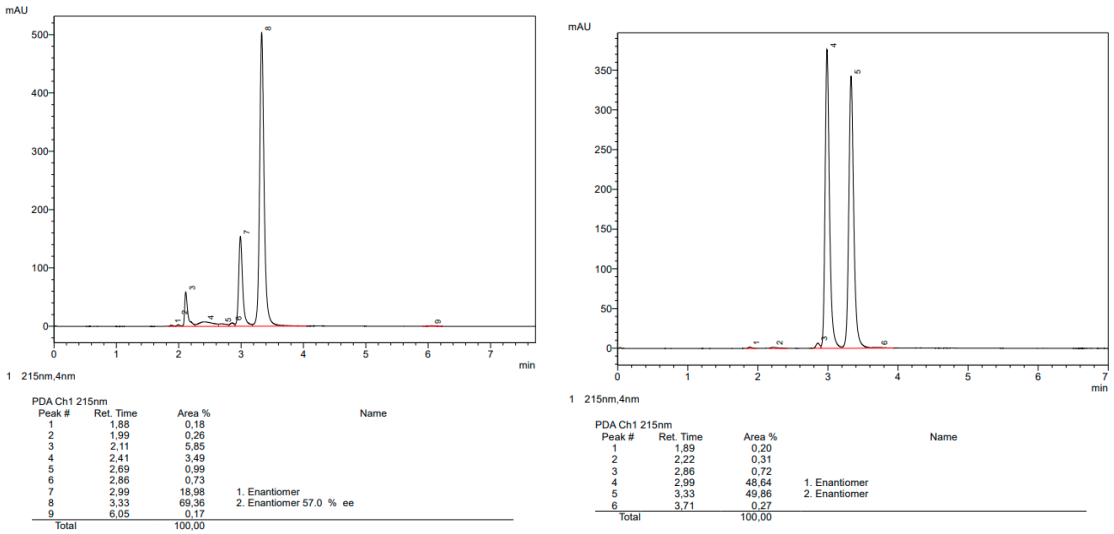

HPLC traces of **89** (left) and corresponding racemate (right).

2-(2-(*p*-Tolyl)-1-(trifluoromethyl)cyclopropyl)benzo[d]oxazole (90). Prepared

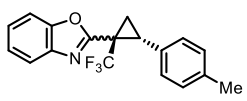

according to general procedure **A** with 0.9 mmol of alkene. The crude residue was purified by flash chromatography (silica, pentane/EtOAc 50:1 to 30:1) which afforded the title compound as mix of both diastereomers as a colorless oil (42 mg, dr = 1.1:1, 67% *ee*, 68% *ee*). [The *ee* was determined by HPLC analysis: 150 mm Chiralcel OJ-3R, Ø 4.6 mm, acetonitrile/water = 60:40, v = 1.0 mL/min, λ = 220 nm, t(diastereomer 1, minor) = 5.39 min, t(diastereomer 1, major) = 5.90 min, t(diastereomer 2, minor) = 13.39 min, t(diastereomer 2, major) = 15.36 min]. ^{1}H NMR (400 MHz, $CDCl_3$) δ 7.79 –

7.70 (m, 1H), 7.68 – 7.59 (m, 1H), 7.59 – 7.53 (m, 1H), 7.40 – 7.33 (m, 3H), 7.28 – 7.22 (m, 4H), 7.20 – 7.13 (m, 2H), 7.04 (d, *J* = 8.1 Hz, 2H), 6.97 – 6.83 (m, 2H), 3.19 (t, *J* = 8.9 Hz, 1H), 3.07 (dd, *J* = 9.6, 7.9 Hz, 1H), 2.49 (ddq, *J* = 8.0, 6.2, 1.7 Hz, 1H), 2.35 (s, 4H), 2.29 (ddt, *J* = 9.5, 5.7, 1.8 Hz, 1H), 2.22 (dd, *J* = 8.3, 5.9 Hz, 1H), 2.16 (s, 3H), 2.05 (dd, *J* = 9.6, 6.2 Hz, 1H). ^{13}C NMR (101 MHz, $CDCl_3$) δ 162.3, 158.7, 151.1, 150.9, 141.0, 140.6, 137.7, 137.3, 130.23, 129.4, 129.2, 129.1, 128.4, 125.4, 125.3, 124.9, 124.5, 120.2, 120.2, 110.8, 110.7, 32.9, 29.0, 21.3, 21.1, 16.3, 14.9. ^{19}F NMR (282 MHz, $CDCl_3$) δ –61.6, –67.2. IR (ATR): ṽ =1569, 1455, 1362, 1307, 1243, 1150, 1118, 1076, 7059, 749, 738 cm^{-1}. HRMS (EI) m/z calcd. for $C_{18}H_{14}F_3ON$ [M]$^+$: 317.10220; found: 317.10248.

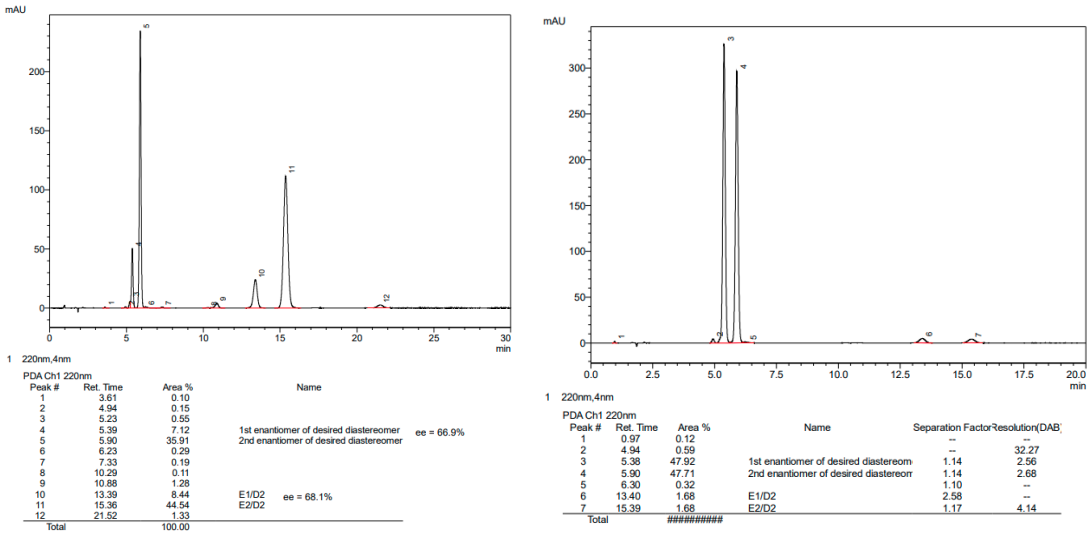

HPLC traces of **90** (left) and corresponding racemate (right).

9.6.2. Preparation of α-Stannylated Cyclopropanes

General procedure B

A flame dried Schlenk flask equipped with a magnetic stir bar was charged with catalyst ***P*-134** catalyst (0.5 mol%). The respective olefin (5 equiv.) and CH_2Cl_2 (3 mL) were added, followed by the addition of a solution of α-stannyl-α-diazoacetate **20** (55mg, 0.2 mmol, 1 equiv.) in CH_2Cl_2 (1 mL). The resulting mixture was stirred at room temperature for an arbitrary time of 4 h. The reaction mixture was concentrated under reduced pressure and the dr of the crude material was determined by ^{1}H-NMR. The crude residue was purified by flash chromatography. If the diastereomers were separable under these conditions, only the major diastereomer was isolated.

The corresponding racemic compounds were prepared accordingly with 1 mol% $Rh_2(esp)_2$.

Ethyl (1*R*,2*R*)-2-(4-methoxyphenyl)-1-(trimethylstannyl)cyclopropane-1-carboxylate (27). Prepared according to general procedure **B.** The crude residue was purified by flash chromatography (silica, *n*-pentane/MTBE 30:1) which afforded the desired product as a colorless oil (43.5 mg, 58%, dr = 10:1 (*cis*), 98% *ee*). $[\alpha]_D^{20}$ = +46.9 (c = 1.9, $CHCl_3$). The optical purity was determined by HPLC (Chiralpak IG-3, 4.6 mm i.D., *n*-heptan/2-propanol = 98:2, v = 1.0 mL/min, λ =230 nm): 3.48 min (major) and 3.90 min (minor). The spectral data matched those previously reported in the literature.[80]

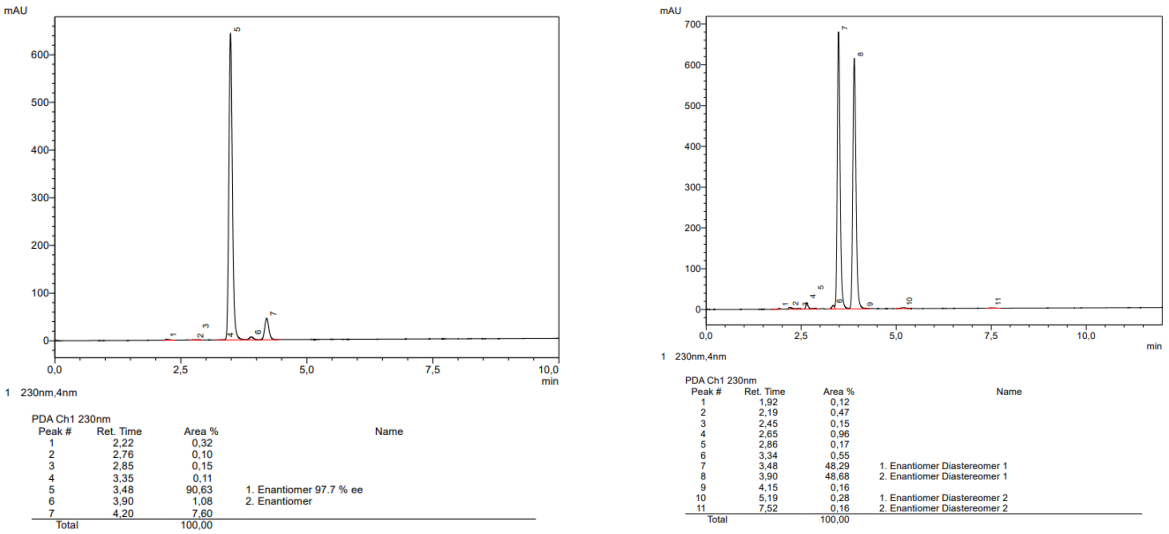

HPLC traces of **27**(left) and corresponding racemate (right).

Ethyl (1*R*,2*R*)-2-(4-(trifluoromethyl)phenyl)-1-(trimethylstannyl)cyclopropane-1-carboxylate (164). Prepared according to general procedure **B.** The crude residue was purified by flash chromatography (silica, *n*-pentane/MTBE 30:1) which afforded the desired product as a colorless oil (54.4 mg, 64%, d.r. = 7:1 (*cis*), 98% *ee*). $[\alpha]_D^{20}$ = +32.1 (c = 1.3, $CHCl_3$). The optical purity was determined by HPLC (Chiralpak IM-3, 4.6 mm i.D., methanol/water = 80:20, v = 1.0 mL/min, λ =220 nm): 7.09 min (minor) and 7.85 min (major). ^{1}H NMR (600 MHz, $CDCl_3$) δ 7.55 – 7.51 (m, 2H), 7.37 – 7.33 (m, 2H), 4.18 – 4.12 (m, 2H), 2.77 (dd, *J* = 8.8, 6.4 Hz, 1H), 1.78 (dd, *J* = 8.8, 4.3 Hz, 1H), 1.35 (dd, *J* = 6.4, 4.3 Hz, 1H), 1.28 (t, *J* = 7.1 Hz, 3H), -0.18 (s, 9H). ^{13}C NMR (151 MHz, $CDCl_3$) δ 176.9, 144.2 (q, *J* = 1.4 Hz), 129.9, 129.3 (q, *J* = 32.4 Hz), 125.3 (q, *J* = 3.8 Hz), 124.3 (q, *J* = 271.9 Hz), 61.2, 30.3, 21.2, 16.5, 14.4, –8.4. ^{119}Sn NMR (224 MHz, $CDCl_3$) δ 5.94. ^{19}F NMR (565 MHz, $CDCl_3$) δ -62.4. IR (ATR): $\tilde{\nu}$ = 1709, 1323, 1226, 1163, 1122, 1110, 1066, 1017, 843,

768, 529 cm^{-1}. HRMS (ESI+) m/z calcd. for $C_{16}H_{21}F_3O_2SnNa$ $[M+Na]^+$: calcd: 445.04078; found: 445.04121.

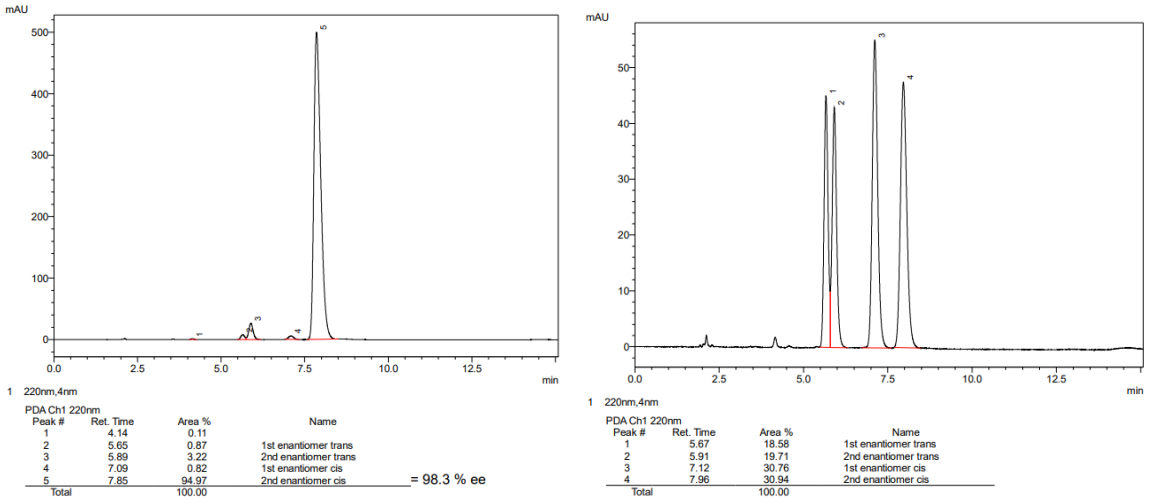

HPLC traces of **164** (left) and corresponding racemate (right).

Ethyl (1*R*,2*S*)-2-(*tert*-butoxy)-1-(trimethylstannyl)cyclopropane-1-carboxylate (165).

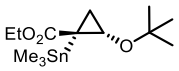

Prepared according to general procedure **B.** The crude residue was purified by flash chromatography (silica, *n*-pentane/MTBE 30:1) which afforded the desired product as a colorless oil (55 mg, 79%, d.r. > 20:1 (*cis*), 96% *ee*). $[\alpha]_D^{20}$ = +37.3 (c = 1.3, $CHCl_3$). The optical purity was determined by HPLC (Chiralpak OJ-3R, 4.6 mm i.D., methanol/water = 80:20, v = 1.0 mL/min, λ =210 nm): 3.63 min (major) and 4.19 min (minor). The spectral data matched those previously reported in the literature.[80]

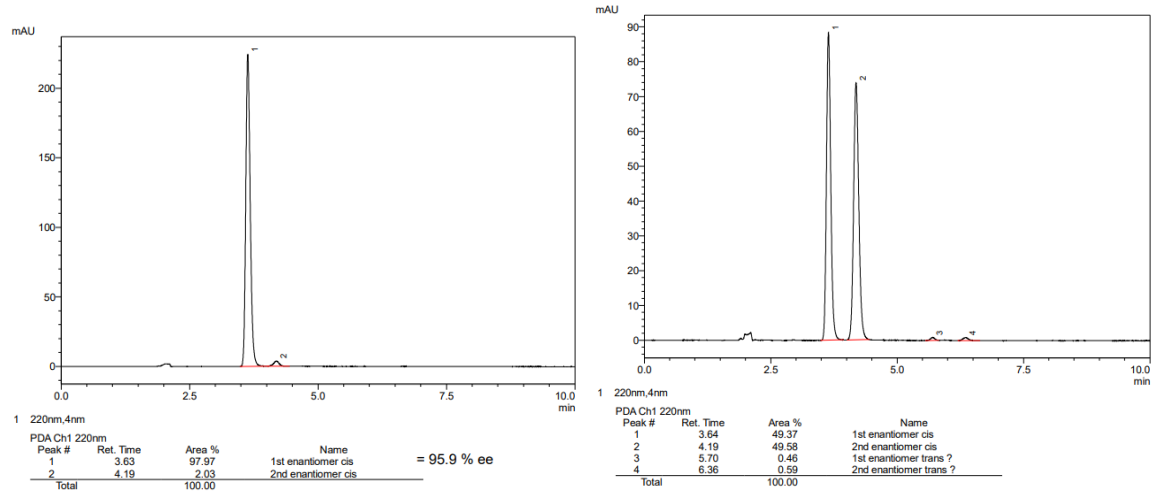

HPLC traces of **165** (left) and corresponding racemate (right).

Ethyl (1*R*,2*R*)-2-(3-chlorophenyl)-1-(trimethylstannyl)cyclopropane-1-carboxylate

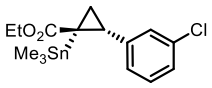

(166). Prepared according to general procedure **B.** The crude residue was purified by flash chromatography (silica, *n*-pentane/MTBE 30:1) which afforded the desired product as a colorless oil (57 mg, 71% (contains *trans*-diastereomer), d.r. = 7:1 (*cis*), 96% *ee*). $[\alpha]_D^{20}$= +40.3 (c = 1.5, $CHCl_3$). The optical purity was determined by 2D-HPLC: 1st dimension: (50 mm Eclipse Plus C18, 4.6 mm i.D., methanol/water 80:20, 1.0 mL/min, 308 K, λ =220 nm): 4.63-4.67 min; 2nd dimension: (Chiralpak OJ-3R, 4.6 mm i.D., methanol/water gradient = 70:30 to 95:5 in 10 min, v = 1.0 mL/min, λ =220 nm): 8.82 min (major) and 9.12 min (minor). The spectral data matched those previously reported in the literature.[81]

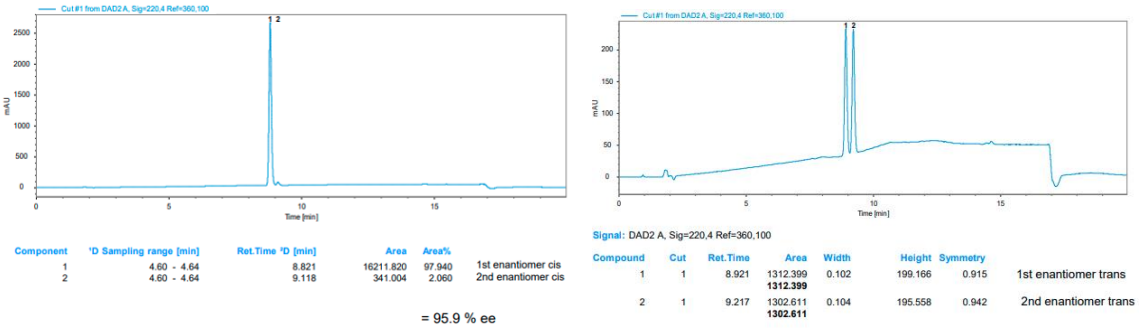

HPLC traces of **166** (left) and corresponding racemate (right).

Ethyl (1*R*,2*R*)-2-(2-chlorophenyl)-1-(trimethylstannyl)cyclopropane-1-carboxylate

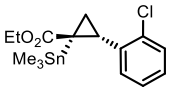

(167). Prepared according to general procedure **B.** The crude residue was purified by flash chromatography (silica, *n*-pentane/MTBE 30:1) which afforded the desired product as a colorless oil (50 mg, 66%, d.r. = 9:1 (*cis*), 98% *ee*). The optical purity was determined by HPLC (Chiralpak OJ-3R, 4.6 mm i.D., methanol/water gradient = 70:30 to 95:5 in 10 min, v = 1.0 mL/min, λ =220 nm): 9.16 min (major) and 10.45 min (minor). $[\alpha]_D^{20}$ = –43.7 (c = 1.0, $CHCl_3$). ^{1}H NMR (400 MHz, $CDCl_3$) δ 7.41 – 7.31 (m, 1H), 7.24 – 7.12 (m, 2H), 7.11 – 7.08 (m, 1H), 4.25 – 4.08 (m, 2H), 2.73 (ddd, *J* = 8.6, 6.6, 0.8 Hz, 1H), 1.79 (dd, *J* = 8.6, 4.3 Hz, 1H), 1.41 (dd, *J* = 6.6, 4.3 Hz, 1H), 1.28 (t, *J* = 7.1 Hz, 3H), -0.17 (s, 9H). ^{13}C NMR (101 MHz, $CDCl_3$) δ 176.9, 137.8, 136.9, 129.6, 129.4, 128.3, 126.5, 61.0, 29.7, 21.3, 16.4, 14.5, -8.4. ^{119}Sn NMR (149 MHz, $CDCl_3$) δ 6.59. IR (ATR): $\tilde{\nu}$ = 1708, 1442, 1372, 1240, 1222, 1123, 1052, 758, 741, 528 cm^{-1}. HRMS (ESI$^+$) m/z calcd. for $C_{15}H_{21}O_2ClSnNa$ $[M+Na]^+$: calcd: 411.01442; found: 411.01419.

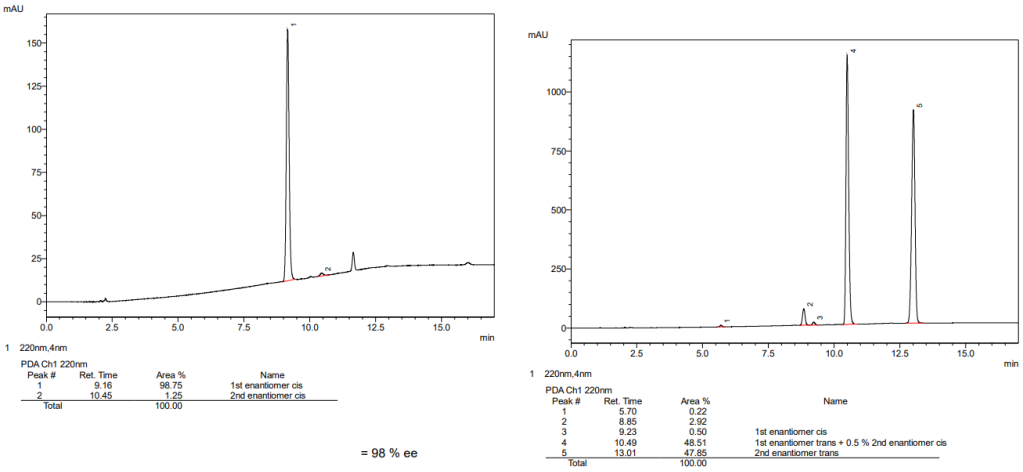

HPLC traces of **167** (left) and corresponding racemate (right).

Ethyl (1*R*,1a*R*,6a*R*)-1-(trimethylstannyl)-1,1a,6,6a-tetrahydrocyclopropa[a]indene-1-carboxylate (168). Prepared according to general procedure **B.** The crude residue was purified by flash chromatography (silica, *n*-pentane/MTBE 30:1) which afforded the desired product as a colorless oil (51.2 mg, 71%, d.r. = 15:1 (cis), 97% *ee*). $[\alpha]_D^{20}$ = +127.3 (c = 1.1, $CHCl_3$). The optical purity was determined by HPLC (Chiralpak OJ-3R, 4.6 mm i.D., methanol/water gradient = 60:40 to 80:20 in 10 min, v = 1.0 mL/min, λ =220 nm): 8.82 min (major) and 9.12 min (minor). The spectral data matched those previously reported in the literature.[80]

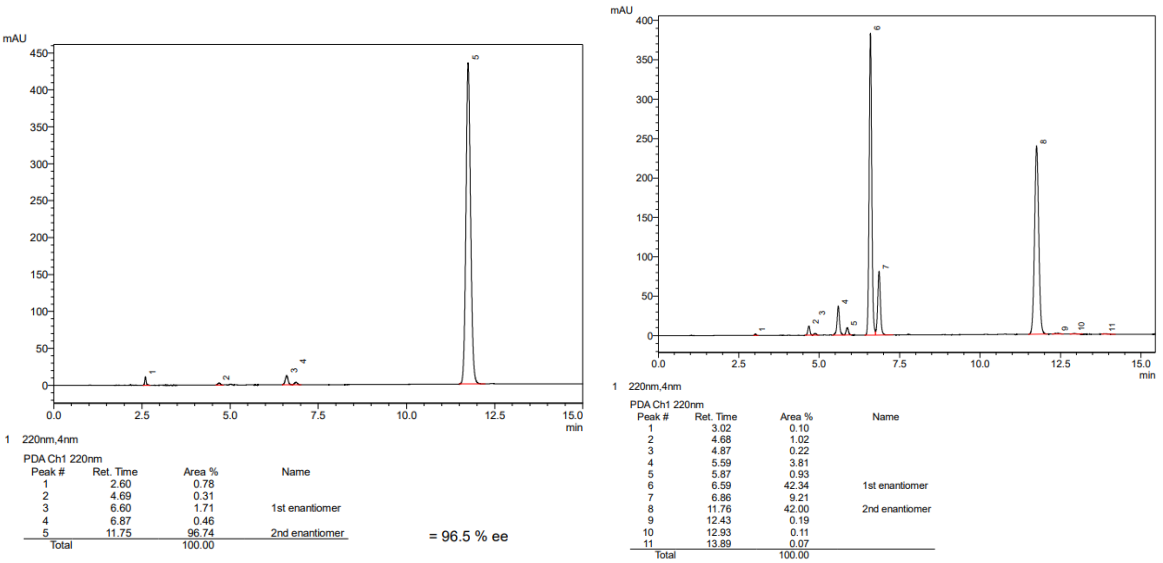

HPLC traces of **168** (left) and corresponding racemate (right).

Ethyl (1*R*,2*R*)-2-(thiophen-2-yl)-1-(trimethylstannyl)cyclopropane-1-carboxylate (169). Prepared according to general procedure **B.** The crude residue was purified by flash chromatography (silica, *n*-pentane/MTBE 30:1) which afforded the desired product as a dark yellow oil (28 mg, 40%, d.r. = 10:1 (*cis*), 96% *ee*). The optical purity was determined by HPLC (Chiralpak OJ-3R, 4.6 mm i.D., acetonitrile/water = 55:45, v = 1.0 mL/min, λ = 220 nm): 9.11 min (major) and 10.00 min (minor). $[\alpha]_D^{20}$ = +6.9 (c = 0.8, $CHCl_3$). ^{1}H NMR (400 MHz, $CDCl_3$) δ 7.12 (ddd, *J* = 5.2, 1.2, 0.6 Hz, 1H), 6.88 (dd, *J* = 5.1, 3.5 Hz, 1H), 6.80 (dt, *J* = 3.5, 1.2 Hz, 1H), 4.22 – 4.05 (m, 2H), 2.71 (ddd, *J* = 8.8, 5.8, 1.0 Hz, 1H), 1.81 (dd, *J* = 8.8, 3.9 Hz, 1H), 1.32 (dd, *J* = 6.1, 4.0 Hz, 1H), 1.28 (t, *J* = 7.1 Hz, 3H), -0.09 (s, 9H). ^{13}C NMR (101 MHz, $CDCl_3$) δ 176.7, 144.4, 126.7, 126.3, 124.6, 61.2, 24.7, 22.2, 18.7, 14.4, –8.5. ^{119}Sn NMR (149 MHz, $CDCl_3$) δ 4.26. IR (ATR): $\tilde{\nu}$ = 1707, 1367, 1236, 1209, 1125, 1082, 767, 695, 528, 512 cm^{-1}. HRMS (ESI$^+$) m/z calcd. for $C_{13}H_{20}O_2SSnNa$ $[M+Na]^+$: calcd: 383.00982; found: 383.0097.

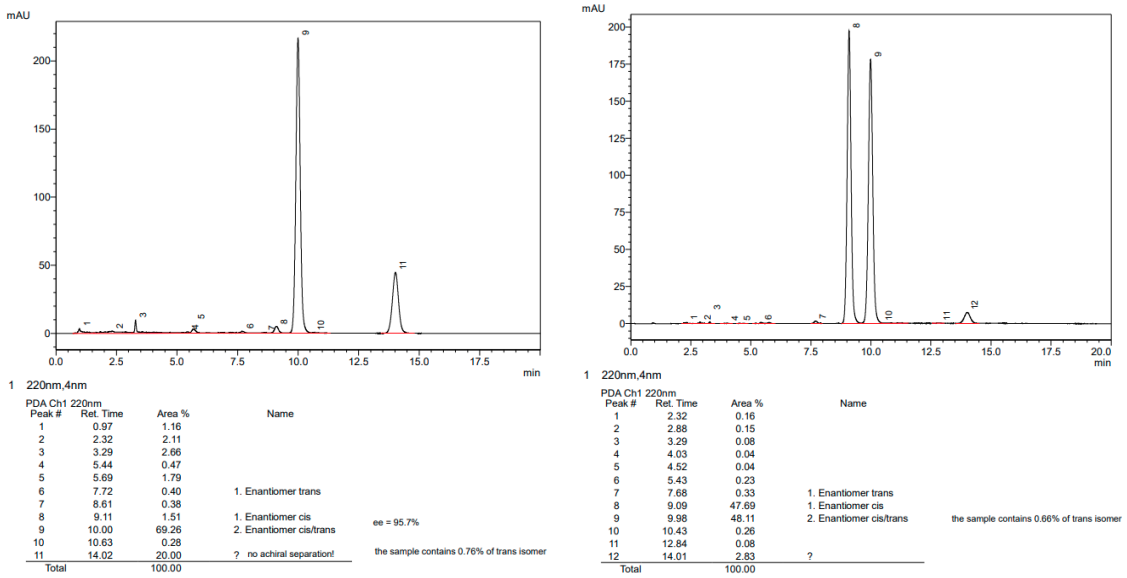

HPLC traces of **169** (left) and corresponding racemate (right).

Ethyl (1*R*,2*S*)-2-(1,3-dioxoisoindolin-2-yl)-1-(trimethylstannyl)cyclopropane-1-carboxylate (170). Prepared according to general procedure **B.** The crude residue was purified by flash chromatography (silica, *n*-pentane/EtOAc 12:1 to 10:1) which afforded the desired product as a colorless oil (60 mg, 70%, d.r. > 20:1 (*cis*), 97% *ee*). $[\alpha]_D^{20}$ = +8.4 (c = 1.2, $CHCl_3$). The optical purity was determined by HPLC (Chiralpak OJ-3R, 4.6 mm i.D., methanol/water = 85:15, v = 1.0 mL/min, λ = 220 nm): 4.73 min (major) and 6.29 min (minor). The spectral data matched those previously reported in the literature.[80]

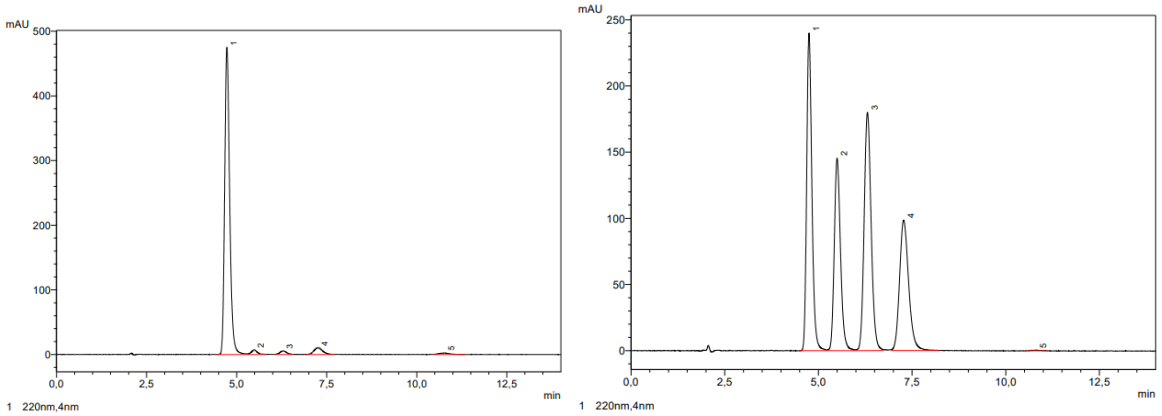

HPLC traces of **170** (left) and corresponding racemate (right).

Ethyl (1*R*,2*R*)-2-((trimethylsilyl)methyl)-1-(trimethylstannyl)cyclopropane-1-carboxylate (171). Prepared according to general procedure **B.** The crude residue was purified by flash chromatography (silica, *n*-pentane/MTBE 30:1) which afforded the desired product as a colorless oil (58.8 mg, 80% (contains *trans*-diastereomer), d.r. = 3:1 (*cis*), 93% *ee*). $[\alpha]_D^{20}$ = +29.2 (c = 1.3, $CHCl_3$). The optical purity was determined by HPLC (Chiralpak IG-3, 4.6 mm i.D., methanol/water = 70:30, v = 1.0 mL/min, λ = 220 nm): 23.32 min (minor) and 24.85 min (major). ^{1}H NMR (400 MHz, $CDCl_3$) δ 4.18 – 3.96 (m, 2H), 1.56 – 1.43 (m, 1H), 1.33 (dddd, *J* = 11.8, 9.1, 6.2, 3.1 Hz, 1H), 1.23 (t, *J* = 7.1 Hz, 3H), 1.16 – 1.05 (m, 1H), 0.57 (dt, *J* = 6.2, 3.0 Hz, 1H), 0.15 (s, 9H), 0.03 (s, 9H). ^{13}C NMR (101 MHz, $CDCl_3$) δ 177.7, 60.7, 24.3, 21.6, 20.3, 19.9, 14.4, -1.4, -7.6. ^{119}Sn NMR (149 MHz, $CDCl_3$) δ 19.67 (minor diastereomer), –0.45 (major diastereomer). IR (ATR): $\tilde{\nu}$ = 1710, 1248, 4219, 1175, 1130, 856, 837, 765, 695, 527, 512 cm^{-1}. HRMS (ESI$^+$) m/z calcd. for $C_{13}H_{28}O_2SiSnNa$ $[M+Na]^+$: calcd: 387.07727; found: 387.07709.

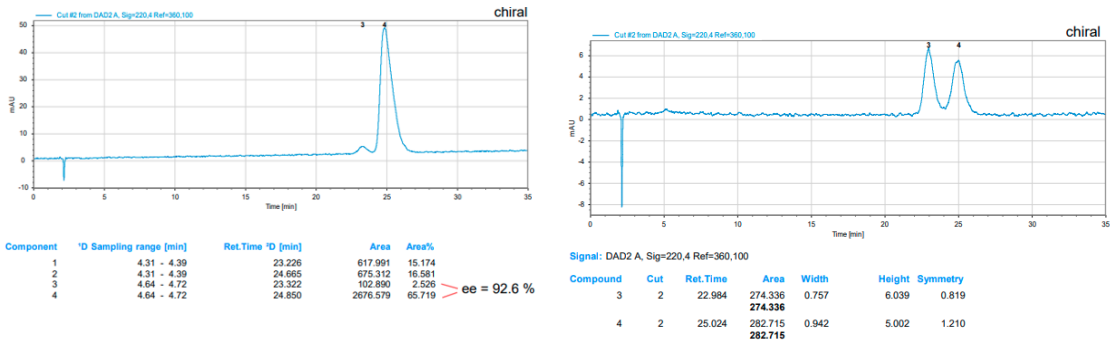

HPLC traces of **171** (left) and corresponding racemate (right).

9.6.3. Preparation of α-Trifluoromethyl Cyclopropanes

General procedure C

An oven dried cooling Schlenk flask equipped with a magnetic stir bar was charged with catalyst ***P*-134** (0.5 mol%). The respective olefin (5 equiv.) and *n*-pentane (1 mL) were added and the mixture was cooled to –40 °C. At this temperature, a solution of ethyl 3,3,3-trifluoro-2-diazopropionate **55** (36.4 mg, 0.2 mmol, 1 equiv.) in *n*-pentane (2 mL) was added dropwise over 5 min and the mixture was stirred at –40°C for 20-22 h (arbitrary time). The reaction mixture was concentrated under reduced pressure and the d.r. of the crude material was determined by ^{19}F-NMR. The crude residue was purified by flash chromatography (silica, *n*-pentane/MTBE). If the diastereomers were separable under these conditions, only the major diastereomer was isolated.

The corresponding racemic compounds were prepared accordingly with 1 mol% $Rh_2(esp)_2$.

Ethyl (1*S*,2*R*)-2-phenyl-1-(trifluoromethyl)cyclopropane-1-carboxylate (172). Prepared

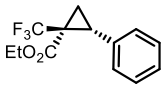

according to the general procedure **C**. The crude residue was purified by flash chromatography (silica, *n*-pentane/MTBE 40:1) which afforded the desired product as a colorless oil (33 mg, 63%, d.r. = 12:1 (*trans*), 95% *ee*). $[\alpha]_D^{20}$ = –2.6 (c = 1.0, $CHCl_3$). The optical purity was determined by HPLC (Chiralcel OJ-3R, 4.6 mm ∅, methanol/water = 80:20, v = 1.0 mL/min, λ =220 nm): 5.32 min (minor) and 7.45 min (major). ^{1}H NMR (600 MHz, $CDCl_3$) δ 7.33 – 7.21 (m, 5H), 3.92 – 3.82 (m, 2H), 2.95 (t, *J* = 9.0 Hz, 1H), 2.19 – 2.13 (m, 1H), 1.78 (dd, *J* = 9.7, 5.7 Hz, 1H), 0.88 (t, *J* = 7.1 Hz, 3H). ^{13}C NMR (151 MHz, $CDCl_3$) δ 165.2 (q, *J* = 1.1 Hz), 133.9, 129.3, 128.4, 127.7, 125.5 (q, *J* = 272.6 Hz), 61.6, 34.5 (q, *J* = 33.4 Hz), 29.3 (q, *J* = 1.9 Hz), 15.1 (q, *J* = 2.0 Hz), 13.7. ^{19}F NMR (565 MHz, $CDCl_3$) δ –66.9. IR (ATR): $\tilde{\nu}$ = 1737, 1395, 1372, 1334, 1315, 1224, 1198, 1146, 1121, 1079, 1026, 732, 697 cm^{-1}. HRMS (EI) m/z calcd. for $C_{13}H_{13}O_2F_3$ $[M]^+$: calcd: 258.08622; found: 258.08632.

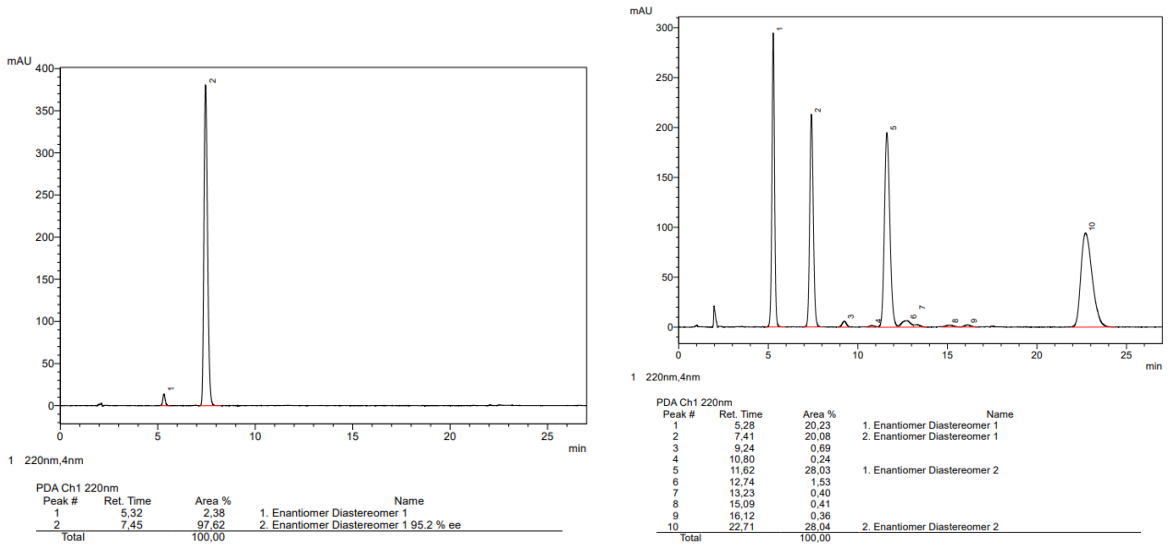

HPLC traces of **172** (left) and corresponding racemate (right).

Ethyl (1*S*,2*R*)-2-(4-methoxyphenyl)-1-(trifluoromethyl)cyclopropane-1-carboxylate (186). 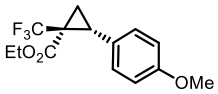

Prepared according to the general procedure **C**. The crude residue was purified by flash chromatography (silica, *n*-pentane/MTBE 25:1 to 12:1) which afforded the desired product as a colorless oil (40.5 mg, 71% (contains *cis*-diastereomer), d.r. = 6:1 (*trans*), 92% *ee*). $[\alpha]_D^{20}$ = +8.7 (c = 1.1, $CHCl_3$). The optical purity was determined by HPLC (Chiralcel OJ-3, 4.6 mm ∅, *n*-heptane/ethanol= 98:2, v = 1.0 mL/min, λ =230 nm): 4.49 min (minor) and 5.21 min (major). ^{1}H NMR (400 MHz, $CDCl_3$) δ 7.20 – 7.13 (m, 2H), 6.85 – 6.78 (m, 2H), 3.91 (qd, *J* = 7.1, 1.7 Hz, 2H), 3.78 (s, 3H), 2.89 (t, *J* = 8.9 Hz, 1H), 2.12 (ddq, *J* = 9.5, 5.7, 1.9 Hz, 1H), 1.75 (dd, *J* = 9.7, 5.7 Hz, 1H), 0.94 (t, *J* = 7.1 Hz, 3H). ^{13}C NMR (101 MHz, $CDCl_3$) δ 165.3, 159.2, 130.3, 125.8, 124.5 (q, *J* = 274.0 Hz), 113.7, 61.6, 55.4, 34.5 (q, *J* = 33.3 Hz), 28.7 (q, *J* = 1.9 Hz), 15.2 (q, *J* = 2.2 Hz), 13.8. ^{19}F NMR (282 MHz, $CDCl_3$) δ –61.1 (minor diastereomer), –66.7 (major diastereomer). IR (ATR): $\tilde{\nu}$ =1733, 1614, 1517, 1391, 1372, 1332, 1316, 1295, 1248, 1225, 1197, 1142, 1113, 1077, 1032, 837, 809 cm^{-1}. HRMS (EI) m/z calcd. for $C_{14}H_{15}O_3F_3$ $[M]^+$: calcd: 288.09678; found: 288.09710.

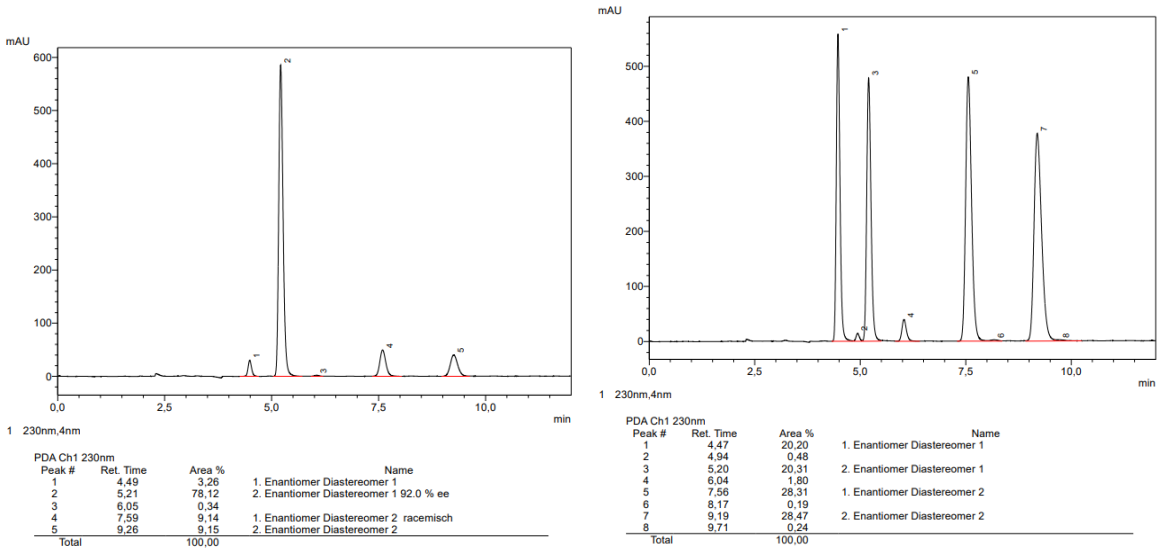

HPLC traces of **186** (left) and corresponding racemate (right).

Ethyl (1*S*,2*R*)-2-(3-chlorophenyl)-1-(trifluoromethyl)cyclopropane-1-carboxylate (187). 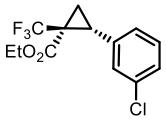 Prepared according to the general procedure **C**. The crude residue was purified by flash chromatography (silica, *n*-pentane/MTBE 40:1) which afforded the desired product as a colorless oil (40.4 mg, 67%, d.r. = 10:1 (*trans*), 96% *ee*). $[\alpha]_D^{20}$ = +7.5 (c = 1.2, $CHCl_3$). The optical purity was determined by HPLC (Chiralcel OJ-3R, 4.6 mm ∅, acetonitrile/water= 50:50, v = 1.0 mL/min, λ =220 nm): 9.83 min (minor) and 11.13 min (major). ^{1}H NMR (400 MHz, $CDCl_3$) δ 7.28 – 7.19 (m, 3H), 7.17 – 7.11 (m, 1H), 3.93 (qd, *J* = 7.1, 2.2 Hz, 2H), 2.91 (t, *J* = 8.9 Hz, 1H), 2.13 (ddq, *J* = 7.7, 5.7, 1.9 Hz, 1H), 1.79 (dd, *J* = 9.7, 5.8 Hz, 1H), 0.95 (t, *J* = 7.1 Hz, 3H). ^{13}C NMR (101 MHz, $CDCl_3$) δ 164.9, 136.0, 134.3, 129.6, 128.0, 127.5, 124.4 (q, *J* = 274.9 Hz), 61.8, 34.48 (q, *J* = 33.7 Hz), 28.7 (q, *J* = 2.2 Hz), 15.1 (q, *J* = 2.1 Hz), 13.8. ^{19}F NMR (282 MHz, $CDCl_3$) δ –67.0. IR (ATR): $\tilde{\nu}$ = 1735, 1390, 1372, 1334, 1314, 1223, 1196, 1145, 1120, 1076, 1027, 788, 692, 678 cm^{-1}. HRMS (EI) m/z calcd. for $C_{13}H_{12}O_2F_3Cl$ $[M]^+$: calcd: 292.04724; found: 292.04721.

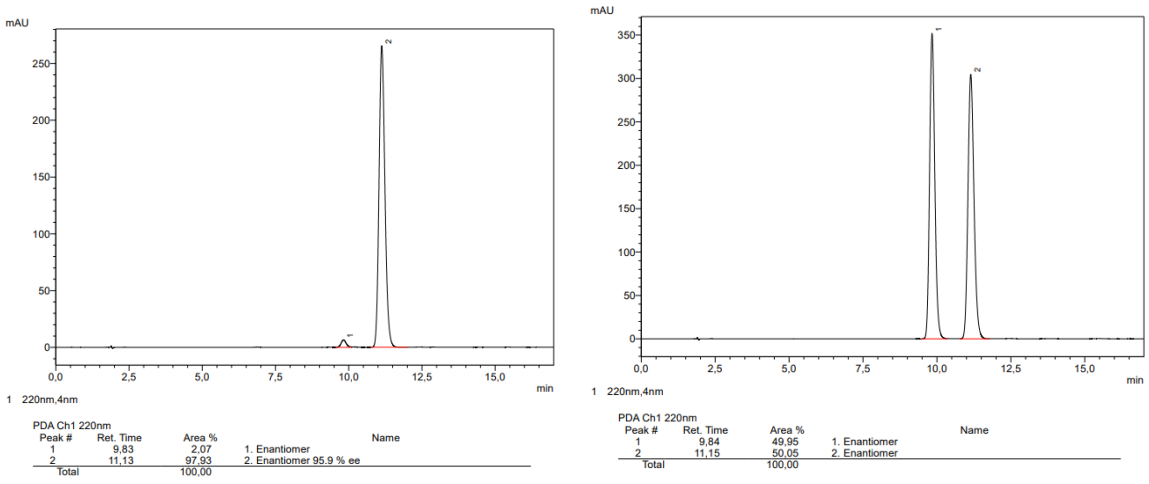

HPLC traces of **187** (left) and corresponding racemate (right).

Ethyl (1*S*,2*R*)-1-(trifluoromethyl)-2-(4-(trifluoromethyl)phenyl)cyclopropane-1-carboxylate (188). Prepared according to the general procedure **C**. The crude residue was purified by flash chromatography (silica, *n*-pentane/MTBE 40:1) which afforded the desired product as a colorless oil (33 mg, 51%, d.r. = 10:1 (*trans*), 96% *ee*). $[\alpha]_D^{20}$ = +1.7 (c = 1.0, $CHCl_3$). The optical purity was determined by HPLC (Chiralcel OJ-3R, 4.6 mm ∅, acetonitrile/water= 40:60, v = 1.0 mL/min, λ = 220 nm): 34.32 min (minor) and 36.34 min (major). ^{1}H NMR (600 MHz, $CDCl_3$) δ 7.58 – 7.51 (m, 2H), 7.41 – 7.34 (m, 2H), 3.93 (dd, *J* = 7.1, 0.4 Hz, 1H), 3.90 (d, *J* = 7.1 Hz, 1H), 2.97 (t, *J* = 9.0 Hz, 1H), 2.18 (ddq, *J* = 7.7, 5.7, 1.9 Hz, 1H), 1.84 (dd, *J* = 9.7, 5.8 Hz, 1H), 0.91 (t, *J* = 7.1 Hz, 3H). ^{13}C NMR (151 MHz, $CDCl_3$) δ 164.9, 138.1 (q, *J* = 1.3 Hz), 130.1 (q, *J* = 32.6 Hz), 125.3 (q, *J* = 3.8 Hz), 124.3 (q, *J* = 273.5 Hz), 124.1 (q, *J* = 272.0 Hz), 61.9, 34.6 (q, *J* = 33.9 Hz), 28.8 (q, *J* = 1.9 Hz), 15.3 (q, *J* = 2.1 Hz), 13.7. ^{19}F NMR (565 MHz, $CDCl_3$) δ −62.7, −67.0. IR (ATR): $\tilde{\nu}$ = 1736, 1393, 1373, 1323, 1225, 1152, 1109, 1063, 1019, 848, 603 cm^{-1}. HRMS (EI) m/z calcd. for $C_{14}H_{12}O_2F_6$ $[M]^+$: calcd: 326.07360; found: 326.07352.

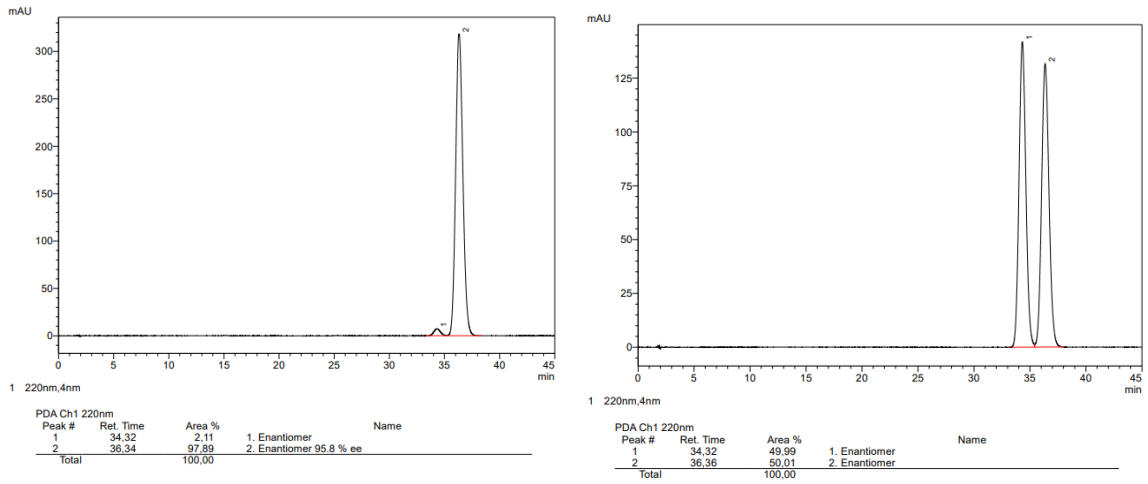

HPLC traces of **188** (left) and corresponding racemate (right).

Ethyl (1*S*,2*S*)-2-(2-chlorophenyl)-1-(trifluoromethyl)cyclopropane-1-carboxylate (189). Prepared according to the general procedure **C**. The crude residue was purified by flash chromatography (silica, *n*-pentane/MTBE 40:1 to 30:1) which afforded the desired product as a colorless oil (37 mg, 63%, d.r. = 7:1 (*trans*), 93% *ee*). $[\alpha]_D^{20}$ = −61.5 (c = 1.1, $CHCl_3$). The optical purity was determined by 2D-HPLC: 1st dimension: (50 mm Eclipse Plus C18, 4.6 mm ∅, acetonitrile/water gradient 60:40 to 90:10 in 5min, 1.0 mL/min, 308 K, λ =220 nm): 2.71-2.73 min; 2nd dimension: (Chiralpak OJ-3R, 4.6 mm ∅, methanol/water = 80:20, v= 1.0 mL/min, λ =220 nm): 4.65 min (minor) and 6.83 min (major). ^{1}H NMR (400 MHz, $CDCl_3$) δ 7.38 – 7.32 (m, 1H), 7.28 – 7.20 (m, 3H), 3.95 (q, *J* = 7.1 Hz, 2H), 2.99 (t, *J* = 9.0 Hz, 1H), 2.13 (ddq, *J* = 8.6, 5.6, 1.5 Hz, 1H), 1.84 (dd, *J* = 9.6, 5.7 Hz, 1H), 0.94 (t, *J* = 7.1 Hz, 3H). ^{13}C NMR (101 MHz, $CDCl_3$) δ 165.4, 135.9, 132.3, 130.9, 129.3, 129.1, 126.5, 124.4 (q, *J* = 273.7 Hz), 61.7, 34.1 (q, *J* = 33.5 Hz), 28.4 (q, *J* = 2.3 Hz), 15.8 (q, *J* = 2.1 Hz), 13.7. ^{19}F NMR (282 MHz, $CDCl_3$) δ −66.8. IR (ATR): $\tilde{\nu}$ = 1734, 1390, 1372, 1335, 1314, 1221, 1142, 1116, 1053, 1025, 769, 747, 686 cm^{-1}. HRMS (EI) m/z calcd. for $C_{13}H_{12}O_2F_3Cl$ $[M]^+$: calcd: 292.04724; found: 292.04721.

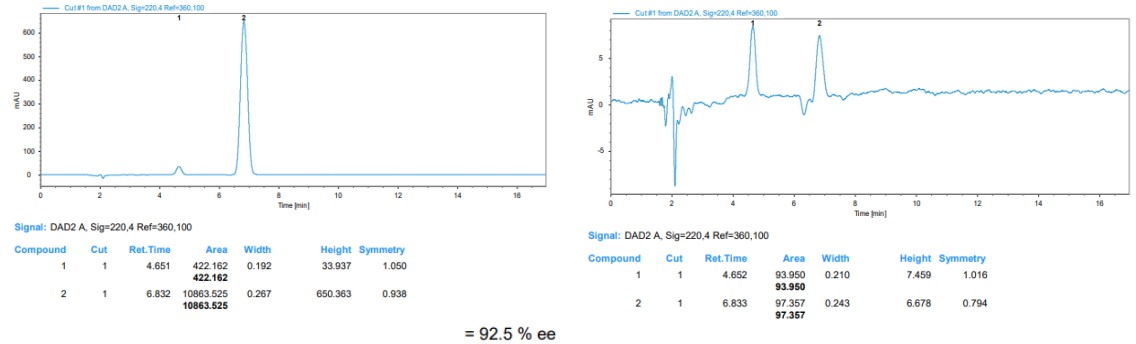

= 92.5 % ee

HPLC traces of **189** (left) and corresponding racemate (right).

Ethyl (1*S*,2*S*)-2-phenoxy-1-(trifluoromethyl)cyclopropane-1-carboxylate (190).

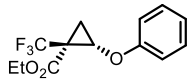

Prepared according to the general procedure **C**. The crude residue was purified by flash chromatography (silica, *n*-pentane/MTBE 40:1) which afforded the desired product as a colorless oil (32 mg, 59%, d.r. = 5:1 (*trans*), 92% *ee*). $[\alpha]_D^{20}$ = −150.3 (c = 1.1, $CHCl_3$). The optical purity was determined by HPLC (Chiralcel OJ-3R, 4.6 mm ∅, acetonitrile/water = 50:50, v = 1.0 mL/min, λ = 220 nm): 7.41 min (minor) and 8.64 min (major). ^{1}H NMR (400 MHz, $CDCl_3$) δ 7.33 – 7.27 (m, 2H), 7.07 – 6.97 (m, 3H), 4.25 (dd, *J* = 7.4, 5.3 Hz, 1H), 4.09 (q, *J* = 7.1 Hz, 2H), 2.27 (tt, *J* = 5.4, 1.7 Hz, 1H), 1.80 (t, *J* = 7.3 Hz, 1H), 1.04 (t, *J* = 7.1 Hz, 3H). ^{13}C NMR (101 MHz, $CDCl_3$) δ 163.6, 157.3, 129.7, 123.8 (q, *J* = 272.3 Hz), 122.5, 115.0, 62.2, 57.7 (q, *J* = 2.5 Hz), 34.0 (q, *J* = 33.2 Hz), 17.2 (q, *J* = 2.2 Hz), 13.9. ^{19}F NMR (282 MHz, $CDCl_3$) δ −65.3. IR (ATR): $\tilde{\nu}$ = 1739, 1591, 1494, 1383, 1372, 1319, 1249, 1202, 1140, 1100, 1080, 1026, 753, 691 cm^{-1}. HRMS (EI) m/z calcd. for $C_{13}H_{13}O_3F_3$ $[M]^+$: calcd: 274.08113; found: 274.08121.

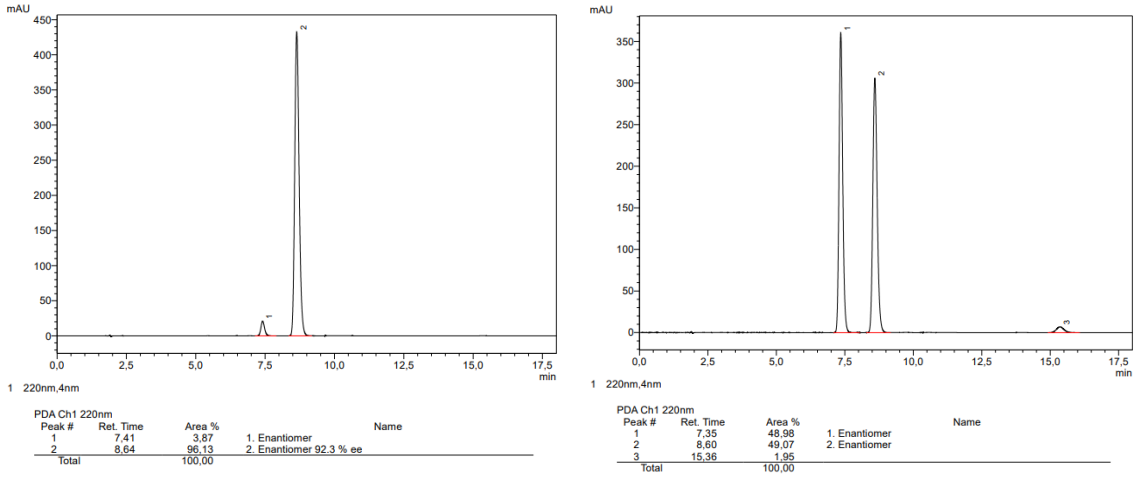

HPLC traces of **190** (left) and corresponding racemate (right).

Ethyl (1*S*,1a*R*,6a*R*)-1-(trifluoromethyl)-1,1a,6,6a-tetrahydrocyclopropa[a]indene-1-carboxylate (191).

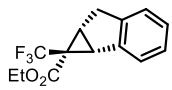

Prepared according to the general procedure **C**. The crude residue was purified by flash chromatography (silica, *n*-pentane/MTBE 40:1) which afforded the desired product as a colorless oil (43 mg, 80% (contains unknown impurity), d.r. > 50:1 (*trans*), 97% *ee*). $[\alpha]_D^{20}$ = 36.8 (c = 0.4, $CHCl_3$). The optical purity was determined by HPLC (Chiralcel OJ-3R, 4.6 mm ∅, methanol/water= 80:20, v= 1.0 mL/min, λ =220 nm): 6.16 min (minor) and 7.38 min (major). An analytically pure sample was obtained after preparatory HPLC separation. ^{1}H NMR (600 MHz, $CDCl_3$) δ 7.41 – 7.36 (m, 1H), 7.20 – 7.12 (m, 3H), 3.84 – 3.72 (m, 2H), 3.39 (d, *J* = 17.5 Hz, 1H), 3.29 (dd, *J* = 17.5, 6.7 Hz, 1H), 3.15 (dd, *J* = 6.8, 1.3 Hz, 1H), 2.54 (td, *J* = 6.8, 0.9 Hz, 1H), 0.77 (t, *J* = 7.1 Hz, 3H). ^{13}C NMR (151 MHz, $CDCl_3$)

δ 163.6, 142.2, 139.4, 127.5, 126.9, 125.7, 125.0, 124.0 (q, *J* = 275.6 Hz), 61.6, 38.0 (q, *J* = 32.7 Hz), 33.6 (q, *J* = 2.3 Hz), 33.1, 25.4 (q, *J* = 2.6 Hz), 13.6. ^{19}F NMR (565 MHz, $CDCl_3$) δ –66.4. IR (ATR): ṽ = 1735, 1372, 1327, 1314, 1287, 1229, 1215, 1155, 1077, 1042, 1024, 750, 725 cm^{-1}. HRMS (EI) m/z calcd. for $C_{14}H_{13}O_2F_3$ $[M]^+$: calcd: 270.08622; found: 270.08621.

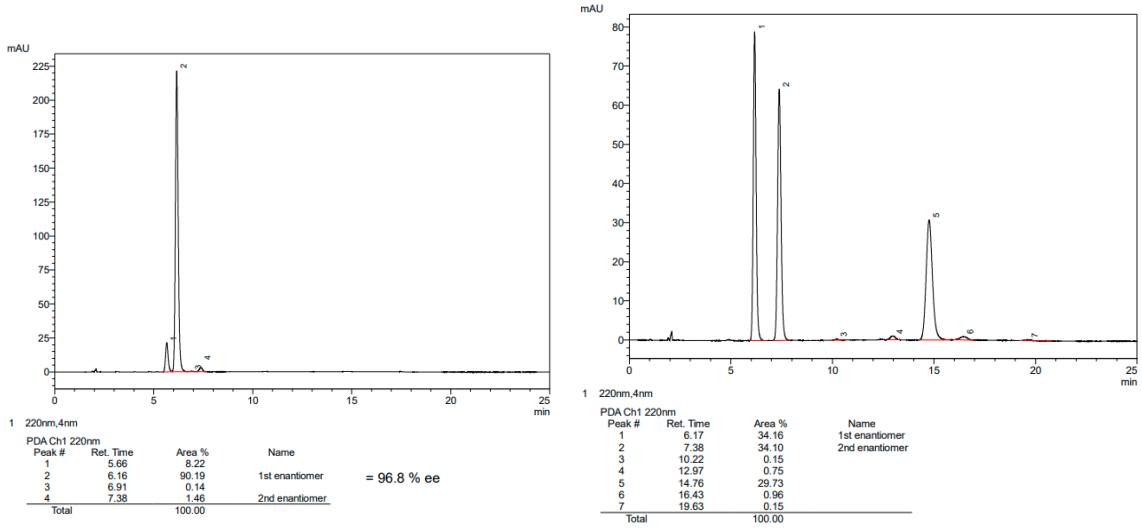

HPLC traces of **191** (left) and corresponding racemate (right).

Ethyl (1*S*,2*R*)-1-(trifluoromethyl)-2-((*E*)-2-((triisopropylsilyl)oxy)vinyl)cyclopropane-1-carboxylate (192). Prepared according to the general procedure **C**. The crude residue was purified by flash chromatography (silica, *n*-pentane/MTBE 100:1 to 40:1) which afforded the desired product as a colorless oil (52 mg, 68%, d.r. = 4:1 (contains *cis*-diastereomer) (*trans*), 80% *ee*). $[\alpha]_D^{20}$ = -38.1 (c = 1.3, $CHCl_3$). The optical purity was determined by HPLC (Chiralcel OJ-3R, 4.6 mm ∅, acetonitrile/water = 50:50, v = 1.0 mL/min, λ = 220 nm): 32.28 min (minor) and 34.71 min (major). ^{1}H NMR (600 MHz, $CDCl_3$) δ 6.55 (dd, *J* = 11.9, 0.6 Hz, 1H), 4.89 (dd, *J* = 12.0, 8.8 Hz, 1H), 4.24 – 4.16 (m, 2H), 2.18 (qd, *J* = 9.3, 0.6 Hz, 1H), 1.61 (ddq, *J* = 7.5, 5.5, 1.8 Hz, 1H), 1.55 (dd, *J* = 9.7, 5.5 Hz, 1H), 1.28 (t, *J* = 7.1 Hz, 3H), 1.20 – 1.08 (m, 3H), 1.06 (d, *J* = 6.9 Hz, 18H). ^{13}C NMR (151 MHz, $CDCl_3$) δ 166.3, 145.2, 124.6 (q, *J* = 272.2 Hz), 104.8, 61.8, 33.3 (q, *J* = 33.4 Hz), 24.7 (q, *J* = 2.0 Hz), 17.8, 17.3 (q, *J* = 2.1 Hz), 14.2, 12.1 (q, *J* = 1.5 Hz). ^{19}F NMR (565 MHz, $CDCl_3$) δ –61.0 (minor *cis*-diastereomer), –66.6. IR (ATR): ṽ = 2946, 2869, 1735, 1659, 1371, 1328, 1309, 1206, 1181, 1153, 1112, 1098, 925, 881, 787, 686, 664 cm^{-1}. HRMS (ESI+) m/z calcd. for $C_{18}H_{31}O_3F_3SiNa$ $[M+Na]^+$: calcd: 403.18868; found: 403.18887.

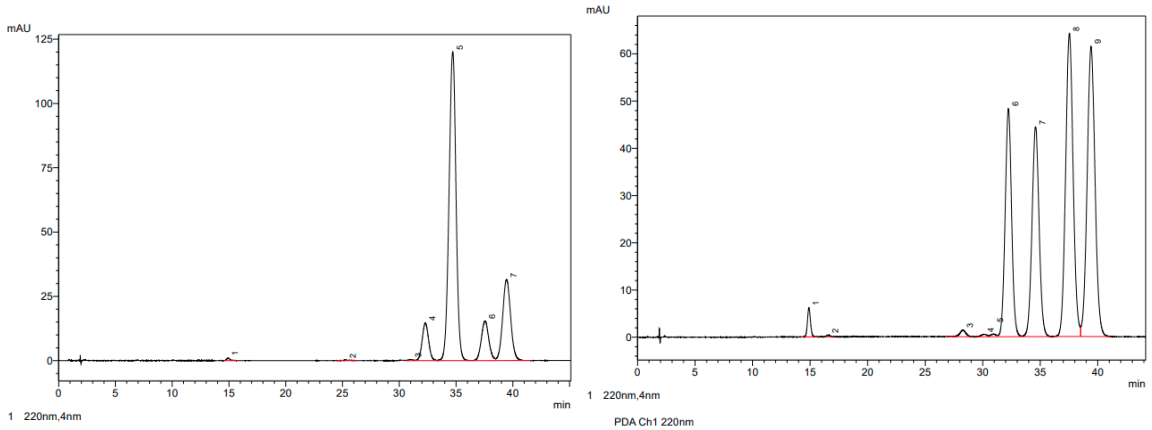

HPLC traces of **192** (left) and corresponding racemate (right).

Ethyl (1*S*,2*R*)-2-((*E*)-styryl)-1-(trifluoromethyl)cyclopropane-1-carboxylate (193).

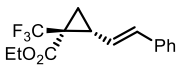

Prepared according to the general procedure **C**. The crude residue was purified by flash chromatography (silica, *n*-pentane/MTBE 40:1) which afforded the desired product as a colorless oil (34 mg, 59%, d.r. = 5:1 (*trans*), 88% *ee*). $[\alpha]_D^{20}$ = 29.5 (c = 2.2, $CHCl_3$). The optical purity was determined by HPLC (Chiralcel OJ-3R, 4.6 mm ∅, acetonitrile/water = 55:45, v = 1.0 mL/min, λ = 220 nm): 11.52 min (minor) and 13.69 min (major).^{1}H NMR (400 MHz, $CDCl_3$) δ 7.36 – 7.28 (m, 4H), 7.26 – 7.20 (m, 1H), 6.68 (d, *J* = 15.9 Hz, 1H), 6.07 (dd, *J* = 15.9, 8.8 Hz, 1H), 4.54 – 4.09 (m, 2H), 2.47 (q, *J* = 8.7 Hz, 1H), 1.84 (tt, *J* = 5.7, 1.9 Hz, 1H), 1.72 (dd, *J* = 9.5, 5.6 Hz, 1H), 1.29 (t, *J* = 7.1 Hz, 3H). ^{13}C NMR (101 MHz, $CDCl_3$) δ 166.3, 136.7, 134.6, 128.8, 127.9, 126.3, 125.7, 123.5, 62.1, 34.1 (q, *J* = 33.7 Hz), 28.4 (q, *J* = 2.1 Hz), 18.0 (q, *J* = 2.3 Hz), 14.3. ^{19}F NMR (282 MHz, $CDCl_3$) δ –66.7. IR (ATR): $\tilde{\nu}$ = 1731, 1394, 1372, 1323, 1313, 1218, 1203, 1152, 1137, 1111, 1048, 1022, 964, 761, 740, 692 cm^{-1}. HRMS (EI) m/z calcd. for $C_{15}H_{15}O_2F_3$ $[M]^+$: calcd: 284.10187; found: 284.10205.

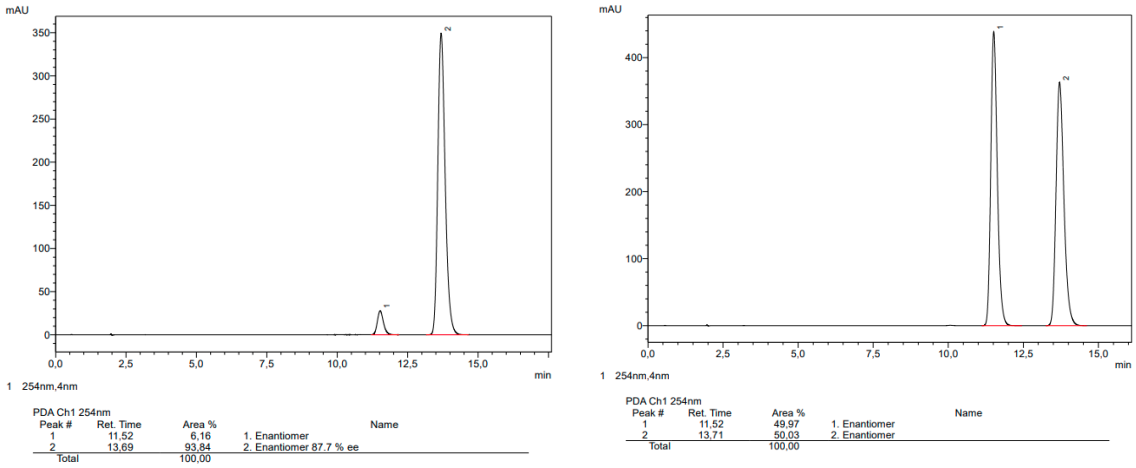

HPLC traces of **193** (left) and corresponding racemate (right).

Ethyl (1*S*,2*R*)-2-(2,4-dimethylphenyl)-1-(trifluoromethyl)cyclopropane-1-carboxylate

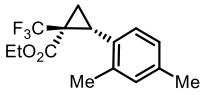

(194). Prepared according to the general procedure **C**. The crude residue was purified by flash chromatography (silica, *n*-pentane/MTBE 40:1) which afforded the desired product as a colorless oil (34 mg, 59%, d.r. = 9:1 (*trans*), 96% *ee*). $[\alpha]_D^{20}$ = −28.1 (c = 0.9, $CHCl_3$). The optical purity was determined by HPLC (Chiralcel OJ-3R, 4.6 mm ∅, acetonitrile/water = 80:20, v= 1.0 mL/min, λ = 220 nm): 8.75 min (minor) and 13.04 min (major). ^{1}H NMR (400 MHz, $CDCl_3$) δ 7.07 – 7.00 (m, 1H), 6.97– 6.93 (m, 2H), 3.90 (q, *J* = 7.1 Hz, 2H), 2.82 (t, *J* = 8.9 Hz, 1H), 2.32 (s, 3H), 2.29 (s, 3H), 2.18 (ddt, *J* = 7.3, 3.7, 1.7 Hz, 1H), 1.78 (dd, *J* = 9.6, 5.6 Hz, 1H), 0.90 (t, *J* = 7.1 Hz, 3H). ^{13}C NMR (101 MHz, $CDCl_3$) δ 165.4, 138.3, 137.5, 130.9, 129.0, 126.3, 124.7 (q, *J* = 273.4 Hz), 61.5, 34.3 (q, *J* = 33.2 Hz), 28.2 (q, *J* = 2.2 Hz), 21.1, 19.2, 15.1 (q, *J* = 2.3 Hz), 13.7. ^{19}F NMR (282 MHz, $CDCl_3$) δ −66.4. IR (ATR): $\tilde{\nu}$ = 1736, 1389, 1372, 1334, 13114, 1252, 1218, 1198, 1149, 1111, 1076, 1028, 829 cm^{-1}. HRMS (EI) m/z calcd. for $C_{15}H_{17}O_2F_3$ $[M]^+$: calcd: 286.11752; found: 286.11773.

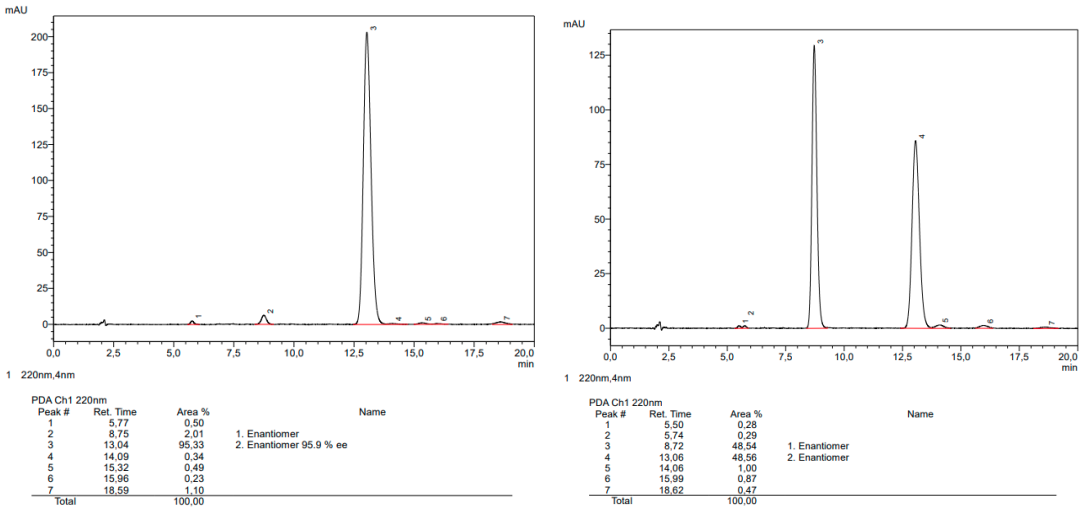

HPLC traces of **194** (left) and corresponding racemate (right).

Ethyl (1*S*,2*S*)-2-((dimethyl(phenyl)silyl)methyl)-1-(trifluoromethyl)cyclopropane-1-carboxylate (195). Prepared according to the general procedure **C**. The crude residue was purified by flash chromatography (silica, *n*-pentane/MTBE 40:1) which afforded the desired product as a colorless oil (34 mg, 51%, d.r. = 2:1 (*trans*), 68% *ee*). $[\alpha]_D^{20}$ = 7.0 (c = 0.3, $CHCl_3$). The optical purity was determined by HPLC (Chiralcel OJ-3R, 4.6 mm ∅, methanol/water = 80:20, v = 1.0 mL/min, λ = 220 nm): 16.23 min (major) and 18.60 min (minor). ^{1}H NMR (400 MHz, $CDCl_3$) δ 7.53 – 7.48 (m, 2H), 7.41 – 7.34 (m, 3H), 4.33 – 4.12 (m, 2H), 1.62 (tdd, *J* = 9.2, 8.1, 5.7 Hz, 1H), 1.42 (dd, *J* = 9.5, 5.2 Hz, 1H), 1.30 (t, *J* = 7.2 Hz, 4H), 1.09 (dd, *J* = 14.8, 5.7 Hz, 1H), 1.00 – 0.90 (m, 1H), 0.33 (d, *J* = 2.0 Hz, 6H). ^{13}C NMR (101 MHz, $CDCl_3$) δ 167.0, 138.1, 133.7, 129.4, 128.0, 124.8 (q, *J* = 272.4 Hz), 61.8, 32.5 (q, *J* = 33.4 Hz), 22.5 (d, *J* = 1.8 Hz), 18.7 (q, *J* = 2.1 Hz), 14.3, 13.0, -3.1 (d, *J* = 6.5 Hz). ^{19}F NMR (282 MHz, $CDCl_3$) δ –66.2. IR (ATR): ṽ = 1731, 1371, 1321, 1213, 1146, 1126, 1114, 1094, 832, 806, 732, 698 cm^{-1}. HRMS (ESI +) m/z calcd. for $C_{16}H_{21}O_2F_3SiNa$ $[M+Na]^+$: calcd: 353.11551; found: 353.11553.

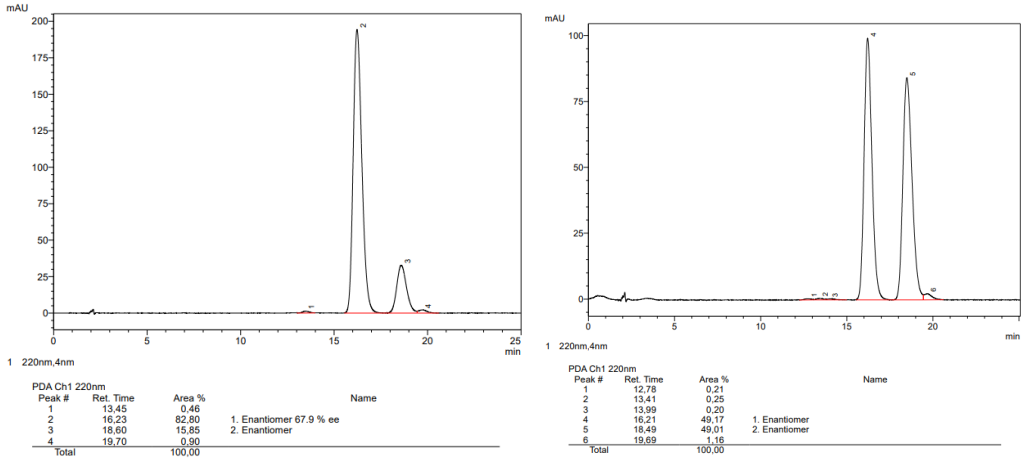

HPLC traces of **195** (left) and corresponding racemate (right).

2,4-Dimethylpentan-3-yl (1*S*,2*R*)-2-phenyl-1-(trifluoromethyl)cyclopropane-1-carboxylate (185). Prepared according to the general procedure **C**. The crude residue was purified by flash chromatography (silica, *n*-pentane/MTBE 40:1) which afforded the desired product as a colorless oil (34 mg, 51%, d.r. = 3:1 (*trans*) contains *cis*-diastereomer, 46% *ee*). The optical purity was determined by HPLC (Chiralcel OJ-3R, 4.6 mm ∅, methanol/water = 80:20, v = 1.0 mL/min, λ = 220 nm): 11.36 min (major) and 20.52 min (minor). ^{1}H NMR (600 MHz, $CDCl_3$) δ 7.27 – 7.26 (m, 3H), 7.25 – 7.20 (m, 2H), 4.41 (t, *J* = 6.0 Hz, 1H), 2.97 (dd, *J* = 9.9, 8.4 Hz, 1H), 2.21 (ddt, *J* = 8.5, 5.5, 1.8 Hz, 1H), 1.79 (dd, *J* = 9.8, 5.7 Hz, 1H), 1.77 (pd, *J* = 6.8, 6.0 Hz, 1H), 1.74 (pd, *J* = 6.8, 6.1 Hz, 1H), 0.77 (d, *J* = 6.9 Hz, 3H), 0.75 (d, *J* = 6.7 Hz, 3H), 0.57 (d, *J* = 6.9 Hz, 3H), 0.57 (d, *J* = 6.7 Hz, 3H). ^{13}C NMR (151 MHz, $CDCl_3$) δ 165.1, 133.3, 129.5, 128.3, 127.7, 124.7 (q, *J* = 273.4 Hz), 85.2, 35.1 (q, *J* = 33.5 Hz),

29.9 (q, J = 2.0 Hz), 29.5, 29.2, 19.5, 19.3, 17.1, 16.9, 15.2 (q, J = 2.0 Hz). ^{19}F NMR (565 MHz, $CDCl_3$) δ −66.2. HRMS (ESI +) m/z calcd. for $C_{18}H_{23}O_2F_3Na$ $[M+Na]^+$: calcd: 351.15423; found: 351.15411.

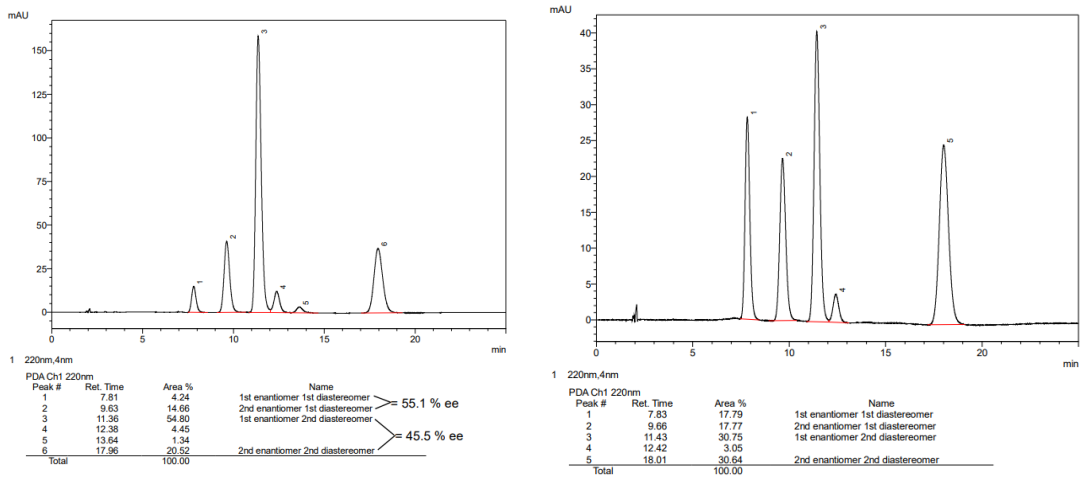

HPLC traces of **185** (left) and corresponding racemate (right).

9.7. Derivatization of Cyclopropanes

9.7.1. Derivatization of 2-Furyl Cyclopropanes

(1*S*,2*R*)-2-(*p*-Tolyl)-1-(trifluoromethyl)cyclopropane-1-carboxylic acid (92). $NaIO_4$ (602 mg, 2.82 mmol) was added to a solution of cyclopropane **70** (150 mg, 0.56 mmol) in heptane/EtOAc/H_2O (1:1:2 12 mL). The reaction mixture was stirred for 5 min and $RuCl_3$ (3 mg, 2.5 mol%) was added. The reaction mixture was stirred for 18 h at 25 °C. A second portion of $NaIO_4$ (3 eq) was added to the reaction mixture and was left stirring for an additional 4 h. Water (10 mL) was added followed by EtOAc (10 mL) and the layers were separated. The aqueous layer was extracted with EtOAc (3 × 20 mL). The organic layers were combined, dried over $MgSO_4$ and concentrated under reduced pressure. The residue was purified by flash chromatography (10:1 pentane: EtOAc + 1 % formic acid) to afford the title compound as a white crystalline solid (90 mg, 65%, 94% *ee*). [The *ee* was determined by HPLC analysis: 150 mm Chiralpak OJ-3R, Ø 4.6 mm i.D. methanol / 0.1 % TFA in water = 70:30, v = 0.5 mL/min, λ = 220 nm, t(minor) = 17.6 min, t(major) = 19.2 min]. $[\alpha]_D^{20}$ = 0.6 (c = 1.2, $CHCl_3$). ^{1}H NMR (400 MHz, $CDCl_3$) δ 7.09 (s, 4H), 2.98 (t, J = 9.1 Hz, 1H), 2.33 (s, 3H), 2.08 (ddq, J = 9.2, 5.6, 1.8 Hz, 1H), 1.80 (dd, J = 9.8, 5.7 Hz, 1H). ^{13}C NMR (101 MHz, $CDCl_3$) δ 170.7, 137.6, 129.9, 129.2, 129.0, 124.2 (q, J = 273 Hz), 34.1 (q, J = 33.9 Hz), 30.4, 21.3, 16.1. ^{19}F NMR (282 MHz, $CDCl_3$) δ −66.9. IR (ATR): ṽ = 1708, 1433, 1387, 1321, 1234, 1147,

1129, 1084, 823 cm^{-1}. HRMS (EI) m/z calcd. for $C_{12}H_{11}F_3O_2$ $[M]^+$: calcd: 244.07057, found: 244.07060.

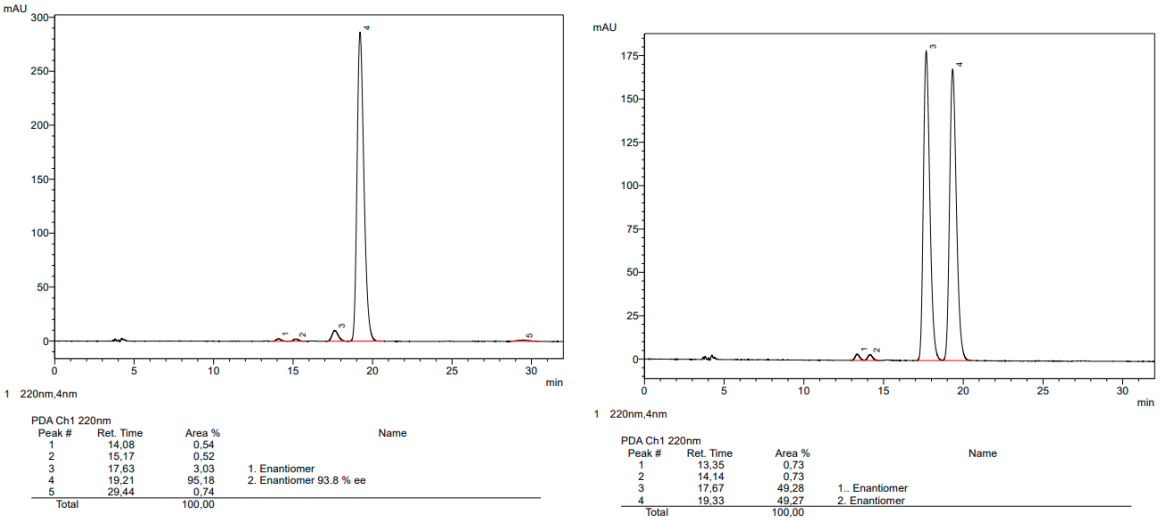

HPLC traces of **92** (left) and corresponding racemate (right).

(1*S*,2*R*)-2-Phenyl-1-(trifluoromethyl)cyclopropane-1-carboxylic acid (196). Prepared

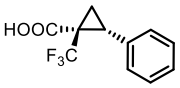

analogously from 2-furyl cyclopropane **67** (100 mg, 0.40 mmol). The residue was purified by flash chromatography (pentane/EtOAc 10:1 + 1 % formic acid) to afford the title compound as a colorless solid (72 mg, 79%). $[\alpha]_D^{20}$ = –12.4 (c = 0.75, $CHCl_3$). ^{1}H NMR (400 MHz, $CDCl_3$) δ 7.33 – 7.24 (m, 3H), 7.23 – 7.15 (m, 2H), 3.01 (t, *J* = 9.1 Hz, 1H), 2.10 (ddq, *J* = 9.3, 5.6, 1.8 Hz, 1H), 1.81 (dd, *J* = 9.7, 5.7 Hz, 1H). ^{13}C NMR (101 MHz, $CDCl_3$) δ 170.4, 133.1, 129.2 (2C), 128.5 (2C), 127.8 124.2 (q, *J* = 274.0 Hz), 34.1 (q, *J* = 33.9 Hz), 30.5 (q, *J* = 2.0 Hz), 16.0 (q, *J* = 2.0 Hz). ^{19}F NMR (282 MHz, $CDCl_3$) δ –67.0. IR (ATR): $\tilde{\nu}$ = 1710, 1433, 1393, 1322, 1233, 1147, 1128, 1086, 783, 728, 697, 684 cm^{-1}. HRMS (EI) m/z calcd. for $C_{11}H_9F_3O_2$ $[M]^+$: calcd: 230.05492, found: 230.05496.

(1*S*,2*R*)-1-(Trifluoromethyl)-2-(4-(trifluoromethyl)phenyl)cyclopropane-1-carboxylic

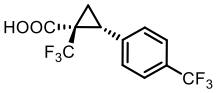

acid (268). Prepared analogously from 2-furyl cyclopropane **71** (51 mg, 0.16 mmol). The residue was purified by flash chromatography (pentane/EtOAc 9:1 + 1 % formic acid) to afford the title compound as a colorless oil (34.3 mg, 72%). $[\alpha]_D^{20}$ = –4.2 (c = 0.74, $CHCl_3$). ^{1}H NMR (400 MHz, $CDCl_3$) 7.54 (d, *J* = 8.1 Hz, 2H), 7.31 (d, *J* = 8.0 Hz, 2H), 3.04 (t, *J* = 9.1 Hz, 1H), 2.12 (dddd, *J* = 7.6, 6.1, 3.6, 1.7 Hz, 1H), 1.88 (dd, *J* = 9.7, 5.9 Hz, 1H) ^{13}C NMR (101 MHz, $CDCl_3$) δ 170.7, 137.2, 130.2 (q, *J* = 33.0 Hz), 129.7 (2C), 125.4 (2C, q, *J* = 3.8 Hz), 124.2 (q, *J* = 274.1 Hz), 124.0 (q, *J* = 272.5 Hz), 34.2 (q, *J* = 34.3 Hz), 30.1 (d, *J* = 2.0 Hz), 16.1 (d, *J* = 2.1 Hz). ^{19}F NMR (282 MHz, $CDCl_3$) δ –62.7, –67.2. IR (ATR): $\tilde{\nu}$ = 1712,

1434, 1392, 1323, 1233, 1152, 1124, 1113, 1065, 1020, 846 cm^{-1}.HRMS (EI) m/z calcd. for $C_{12}H_8F_6O_2$ $[M]^+$: calcd: 298.04230, found: 298.04246.

Methyl ((1*S*,2*R*)-2-(*p*-tolyl)-1-(trifluoromethyl)cyclopropane-1-carbonyl)glycinate (93). A flame dried Schlenk flask was charged with acid **92** (40 mg, 0.164 mmol) and dissolved in DMF (1 mL). The solution was cooled to 0 °C followed by addition of HATU (62.3 mg, 0.164 mmol), DIPEA (0.11 mL, 0.655 mmol) and glycine methyl ester hydrochloride (30.8 mg, 0.246 mmol). The reaction mixture was stirred at room temperature for 16 h. The mixture was diluted with water and was extracted with EtOAc (3x 15 mL). The organic layer was washed with sat. aq. $NaHCO_3$ and brine, dried over $MgSO_4$, and concentrated under reduced pressure. The crude product was purified by flash chromatography (60:40 pentane/MTBE) to afford the title compound as transparent oil that solidified upon standing to an off-white solid (37.4 mg, 72%, 94% *ee*).). [The *ee* was determined by HPLC analysis: 150 mm Chiralpak IC-3, Ø 4.6 mm i.D. *n*-heptane / 2-propanol = 95:5, v= 1.0 mL/min, λ = 220 nm, t(minor) = 17.84 min, t(major) = 13.78 min]. $[\alpha]_D^{20}$ = 39.3 (c = 1.5, $CHCl_3$). M.p. = 86-87 °C. ^{1}H NMR (400 MHz, $CDCl_3$) δ 7.08 (s, 4H), 6.40 (s, 1H), 3.90 (dd, *J* = 18.4, 5.0 Hz, 1H), 3.73 (dd, *J* = 18.5, 4.7 Hz, 1H), 2.81 (t, *J* = 9.1 Hz, 1H), 2.19 (ddq, *J* = 7.8, 5.8, 1.8 Hz, 1H), 1.67 (dd, *J* = 9.7, 5.9 Hz, 1H). ^{13}C NMR (101 MHz, $CDCl_3$) δ 169.7, 162.8, 137.3, 130.5, 129.2, 128.5, 125.3 (q, *J* = 274.0 Hz), 52.5, 41.9, 36.2 (q, *J* = 32.9 Hz), 28.0 (q, *J* = 2.1 Hz), 21.2, 13.5 (d, *J* = 2.5 Hz). ^{19}F NMR (282 MHz, $CDCl_3$) δ -65.46. IR (ATR): $\tilde{\nu}$ = 1746, 1688, 1521, 1439, 1376, 1323, 1305, 1208, 1182, 1132, 1087, 828 cm^{-1}. HRMS (EI) m/z calcd. for $C_{15}H_{16}F_3NO_3$ $[M]^+$: calcd: 315.10768, found: 315.10750.

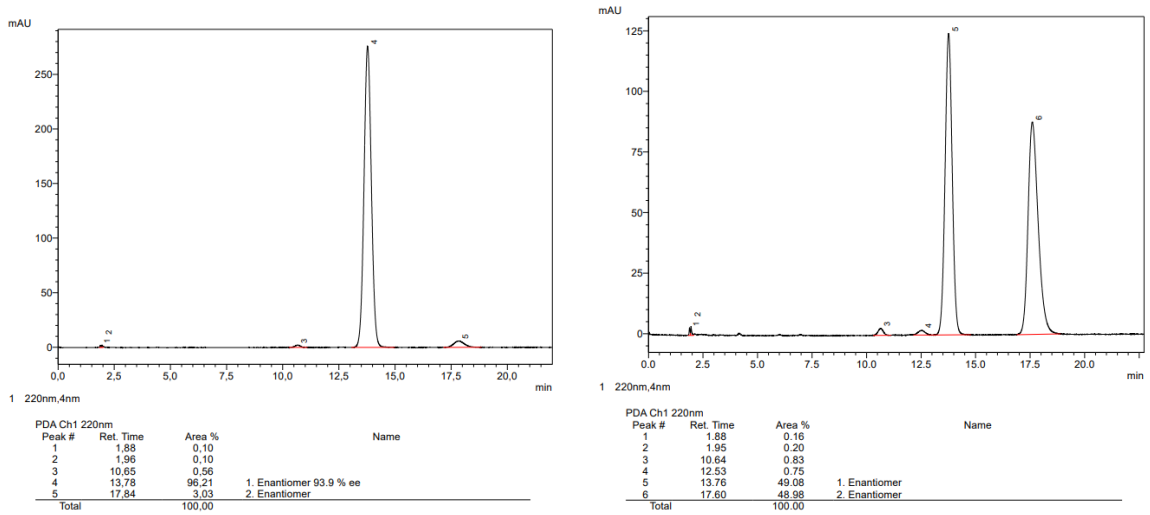

HPLC traces of **93** (left) and corresponding racemate (right).

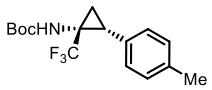

***tert*-Butyl ((1*R*,2*R*)-2-(*p*-tolyl)-1-(trifluoromethyl)cyclopropyl)carbamate (94).** A flame dried two-neck round bottom flask was charged with acid **92** (35 mg, 0.14 mmol) in toluene (1.5 mL). TEA (30 µL, 0.22 mmol) was added to the reaction mixture followed by dropwise addition of diphenylphosphoryl azide (37 µL, 0.17 mmol). The mixture was heated to 90 °C and left stirred for 30 min. Dry *t*-BuOH (0.3 mL) was added reaction and was left stirring for 18 h. The reaction mixture was diluted with EtOAc and water. The organic phase was washed with water (2 x 20 mL) and brine (20 mL), dried over $MgSO_4$ and concentrated under reduced pressure. The crude residue was purified by flash chromatography (pentane/MTBE 16:1) to afford the title compound as an off-white solid (39.7 mg, 89%, 93% *ee*). [The *ee* was determined by HPLC analysis: 150 mm Chiralpak OJ-3R, Ø 4.6 mm i.D. Acetonitrile / water = 40:60, v= 0.5 mL/min, λ = 225nm, t(minor) = 43.91 min, t(major) = 45.98 min]. $[\alpha]_D^{20}$ = −109.9 (c = 1.4, $CHCl_3$). Characterization at elevated temperature (80 °C). At lower temperature signal broadening was observed due to Boc rotamers. ^{1}H NMR (600 MHz, CD_3CN) δ 7.19 – 7.14 (m, 2H), 7.12 – 7.07 (m, 2H), 5.18 (s, 1H), 2.72 (dd, *J* = 10.0, 8.1 Hz, 1H), 2.34 (s, 3H), 1.77 (ddd, *J* = 10.0, 7.0, 0.7 Hz, 1H), 1.73 (t, *J* = 7.8 Hz, 1H), 1.32 (s, 9H). ^{13}C NMR (151 MHz, CD_3CN) δ 156.2, 138.3, 132.5, 130.2, 129.9, 126.8 (q, *J* = 275.5 Hz), 80.9, 40.2 (q, *J* = 37.0 Hz), 28.7, 27.7, 21.3, 16.8. ^{19}F NMR (565 MHz, CD_3CN) δ –74.24. IR (ATR): $\tilde{\nu}$ = 1708, 1495, 1392, 1367, 1299, 1245, 1136, 1091, 1067, 1047, 827 cm^{-1}. HRMS (ESI+) m/z calcd. for $C_{16}H_{20}F_3NO_2Na$ $[M+Na]^+$: calcd: 338.133833, found: 338.134190.

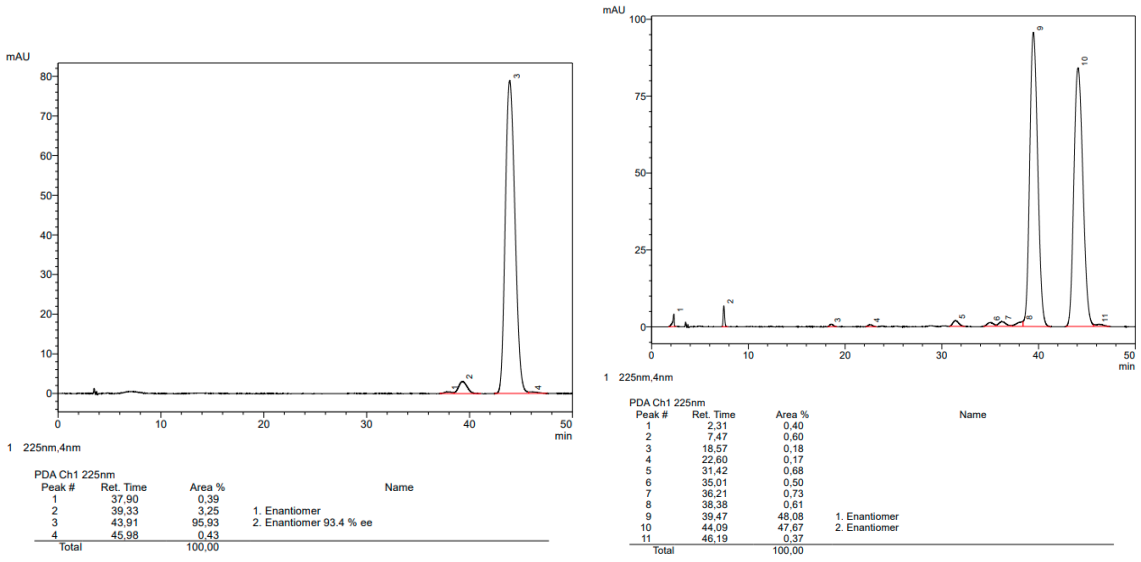

HPLC traces of **94** (left) and corresponding racemate (right).

5-((1*S*,2*R*)-2-(*p*-Tolyl)-1-(trifluoromethyl)cyclopropyl)furan-2-carbaldehyde (95). A

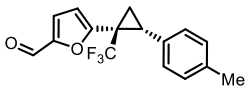

flame dried Schlenk flask was charged with *n*-BuLi (1.6 M in hexane, 0.18 mL, 0.28 mmol) in THF (0.5 mL) and cooled to –78 °C. A solution of cyclopropane **70** (50 mg, 0.19 mmol) in THF (0.2 mL) was added dropwise to the cooled solution. The reaction mixture was stirred for 3 h at –78 °C before DMF (0.15 mL, 1.8 mmol) was added dropwise. The mixture was left stirring for an additional 4 h at –78 °C before being quenched with sat. aq. NH_4Cl (10 mL). The mixture was warmed to room temperature and the layers were separated. The aqueous layer was extracted with EtOAc (3 x 10 mL). The combined organic layers were dried over anhydrous $MgSO_4$ and concentrated under reduced pressure. The residue was purified by flash chromatography (10:1 pentane:EtOAc) to afford the title compound as a pale yellow oil (47.4 mg, 86%, 94% *ee*). $[\alpha]_D^{20}$ = –350.9 (c = 0.9, $CHCl_3$). [The ee was determined by HPLC analysis: 150 mm Chiralpak OJ-3R, Ø 4.6 mm i.D. *n*-heptane / 2-propanol = 98:2, v= 1.0 mL/min, λ = 276 nm, t(minor) = 9.86 min, t(major) = 13.31 min]. ^{1}H NMR (400 MHz, $CDCl_3$) δ 9.46 (s, 1H), 6.99 (d, J = 3.6 Hz, 1H), 6.97 (d, J = 7.9 Hz, 2H), 6.89 (d, J = 8.1 Hz, 2H), 6.28 (d, J = 3.7 Hz, 1H), 2.95 (dd, J = 9.6, 7.5 Hz, 1H), 2.24 (s, 3H), 2.14 (ddd, J = 7.8, 6.2, 1.6 Hz, 1H), 1.91 (dd, J = 9.6, 6.4 Hz, 1H). ^{13}C NMR (101 MHz, $CDCl_3$) δ 177.5, 152.7, 152.3, 137.2, 130.9, 129.1 (2C), 128.0 (2C), 124.9 (q, *J* = 274.1 Hz), 121.7, 114.3, 30.1 (q, J = 34.8 Hz), 28.0 (d, J = 2.1 Hz), 21.1, 13.7 (q, J = 2.2 Hz). ^{19}F NMR (282 MHz, $CDCl_3$) δ –68.62. IR (ATR): $\tilde{\nu}$ = 1680, 1520, 1330, 1289, 1270, 1137, 1069, 1024, 806, 765, 755 cm^{-1}. HRMS (EI) m/z calcd. for $C_{16}H_{13}F_3O_2$ $[M]^+$: calcd: 294.08622, found: 294.08641.

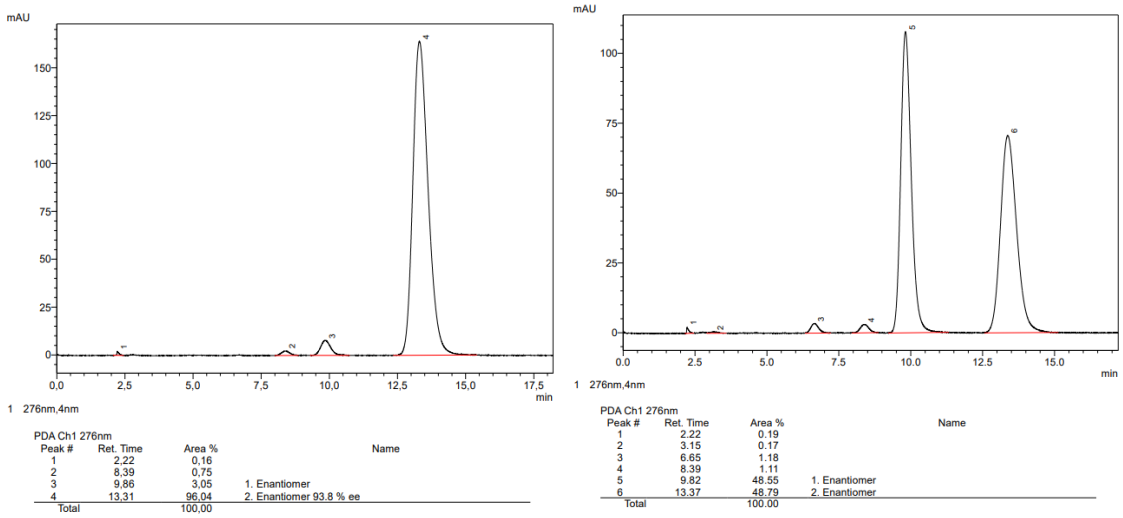

HPLC traces of **95** (left) and corresponding racemate (right).

((1*S*,2*R*)-2-(*p*-Tolyl)-1-(trifluoromethyl)cyclopropyl)methanol (266). Carboxylic acid **95**

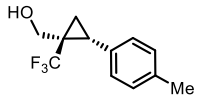

(17 mg, 0.06 mmol) was dissolved in THF (1 mL) and cooled to 0 °C in an ice bath. A suspension of $LiAlH_4$ (3.3 mg, 0.09 mmol) in THF (0.33 mL) was added to the reaction solution. The reaction was warmed to room temperature and stirred for 2 h. The reaction was cooled to 0 °C and carefully quenched with aq. Rochelle salt solution (2 mL, 1 M). The biphasic mixture was stirred for an additional 1 h at room temperature, followed by an extraction of the aqueous phase with EtOAc (3 x 10 mL). The combined organic phases were washed with brine (15 mL), dried over $MgSO_4$, filtered and concentrated under reduced pressure to afford the title compound as a clear oil (17 mg, 99%). ^{1}H NMR (400 MHz, $CDCl_3$) δ 6.98 (d, *J* = 7.9 Hz, 2H), 6.93 – 6.81 (m, 2H), 6.12 – 6.02 (m, 2H), 4.38 (d, *J* = 1.8 Hz, 2H), 2.84 (dd, *J* = 9.5, 7.3 Hz, 1H), 1.89 (ddq, *J* = 7.5, 6.0, 1.6 Hz, 1H), 1.82 (dd, *J* = 9.6, 6.0 Hz, 1H). IR (ATR): ṽ = 12923, 2854, 1385, 1336, 1293, 1210, 1138, 1065, 1015, 795, 730, 708 cm^{-1}. HRMS (EI) m/z calcd. for $C_{12}H_{13}F_3O$ $[M]^+$: calcd: 296.10187, found: 296.10172.

9.7.2. Derivatization of α-Trifluoromethyl Cyclopropanes

(1*S*,2*R*)-2-Phenyl-1-(trifluoromethyl)cyclopropane-1-carboxylic acid (196). A

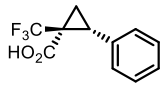

microwave vial (10 mL) equipped with a magnetic stirring bar was charged with cyclopropane ester **172** (100 mg, 0.35 mmol) which was dissolved in ethanol/THF/water (1:1:1, 6 mL). The vial was sealed and heated at 100 °C for 12 h in the microwave reactor. The solvent was evaporated under reduced pressure and the remaining aqueous residue was acidified with aq. HCl (1 M). The residue was extracted with CH_2Cl_2 (3 x 10 mL), washed with brine (20 mL), dried over anhydrous $MgSO_4$ and concentrated under reduced pressure. The residue was purified by flash chromatography (silica, *n*-pentane/EtOAc 10:1 + 1% formic acid) to afford the desired product as a colorless oil that solidified upon standing at 4 °C (78.2 mg, 97%). $[\alpha]_D^{20}$ = –11.6 (c = 1.0, $CHCl_3$). The optical purity was determined by HPLC (Chiralcel OJ-3R, 4.6 mm ∅, methanol/water = 70:30 + 0.1% TFA, v= 0.5 mL/min, λ =220 nm): 12.24 min (minor) and 13.20 min (major). ^{1}H NMR (400 MHz, $CDCl_3$) δ 7.33 – 7.22 (m, 3H), 7.23 – 7.16 (m, 2H), 3.02 (t, *J* = 9.1 Hz, 1H), 2.09 (dtd, *J* = 9.3, 3.8, 1.8 Hz, 1H), 1.82 (dd, *J* = 9.7, 5.7 Hz, 1H). ^{13}C NMR (101 MHz, $CDCl_3$) δ 170.7, 133.0, 129.2, 128.5, 127.9, 124.1 (q, *J* = 274.3 Hz), 34.1 (q, *J* = 34.1 Hz), 30.6 (q, *J* = 1.8 Hz), 16.1 (q, *J* = 2.0 Hz). The spectral data matched those previously reported in the literature.[233]

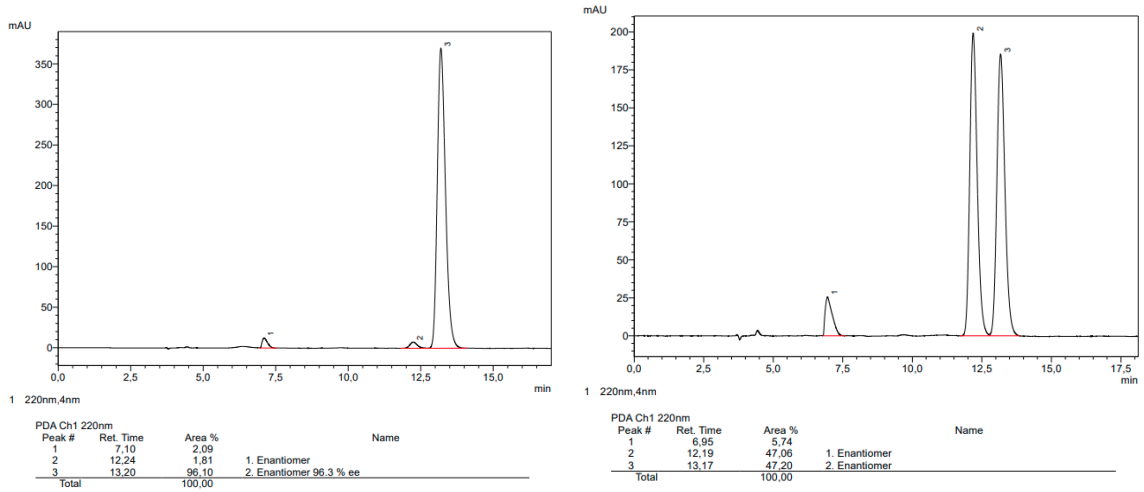

HPLC traces of **196** (left) and corresponding racemate (right).

9.8. Gram-scale Experiments

9.8.1. Cyclopropanation of 58

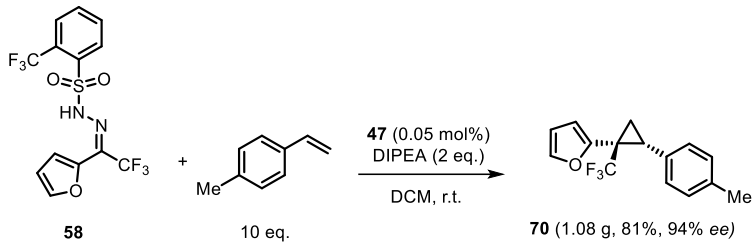

A flame dried three-neck flask equipped with a magnetic stirring bar was charged with **47** (9.2 mg, 0.05 mol%), hydrazone **58** (1.93 g, 5.0 mmol) and *p*-methylstyrene (6.6 mL, 50 mmol) in CH_2Cl_2 (50 mL). A solution of DIPEA (1.74 mL, 10 mmol) in CH_2Cl_2 (150 mL) was added dropwise to the reaction mixture over a period of 1 h. Once the addition was complete, the reaction mixture was stirred further for 16 h. The mixture was concentrated and purified by flash chromatography (pentane/EtOAc 75:1 to 50:1) to afford cyclopropane **70** as a pale yellow oil (1.08 g, 81%, 94% *ee*).

9.8.2. Cyclopropanation of 55

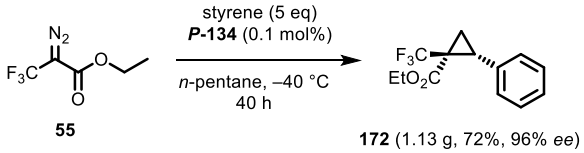

An oven dried cooling Schlenk flask equipped with a magnetic stir bar was charged with catalyst ***P*-134** (8 mg, 0.1 mol%). Styrene (3.5 mL, 30.2 mmol) and *n*-pentane (10 mL) were added and the mixture was cooled to –40 °C. At this temperature, a solution of ethyl 3,3,3-trifluoro-2-diazopropionate **55** (1.11 g, 6.1 mmol, 1 equiv.) in *n*-pentane (20 mL) was added dropwise over 20 min and the mixture was stirred at –40 °C for 40 h. The reaction mixture was concentrated under reduced pressure and purified by flash chromatography (silica, *n*-pentane/MTBE 40:1) to afford product **172** as a colorless oil (1.13 g, 72%, 96% *ee*).

9.9. Specialized Experiments

9.9.1. Kinetic Measurements

Kinetic Studies with Complexes 100-101 and 233-234

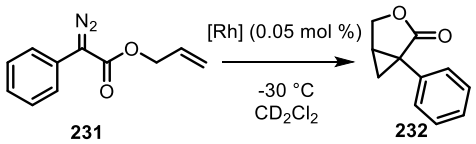

Stock solution catalyst: (c= 1 mg/mL in acetonitrile)

Stock solution diazo: (c**=** 100 mg/mL in CD_2Cl_2)

A flame-dried NMR tube under Argon was charged with a stock solution of catalyst (0.05 mol%). The solvent was evaporated under vacuo and the NMR tube gently heated to dry the catalyst. Then the dried catalyst was dissolved in CD_2CL_2 (0.1 mL). The NMR tube was cooled to –78 °C in a dry ice/ethanol mixture. The solution was overlaid with CD_2CL_2 (0.3 mL), then a stock solution of the diazo (50 µL) was added carefully. The solution was mixed by turning it upside down and vortexing and then immediately transferred to the NMR probe head precooled to –30 °C. After fast shimming single scan ^1H NMR spectra were acquired every 60 s until full conversion of the starting material was observed.

The NMR data was afterwards imported imported into MNOVA 15.0.1 with the Reaction monitoring plugin and processed therein (baseline correction, phasing, integration). The data from the first spectrum was used as concentration reference (100 mol%) for the following spectra. An overview of the obtained reaction profiles is shown in Figure 72A.

In order to extract the relative reaction rates of the different catalyst a variable time normalization approach inspired by the work Burés[187] was used. Instead of normalizing it to a concentration of the catalyst, we multiplied the time scale with a factors k_x/k_{ref} in order to obtain a rate relative to a reference reaction. In the current dataset all of the rates are given relative to the reaction with catalyst **101**, which was the slowest reaction. All the time-normalized data with the relative rates used is shown in Figure 72B.

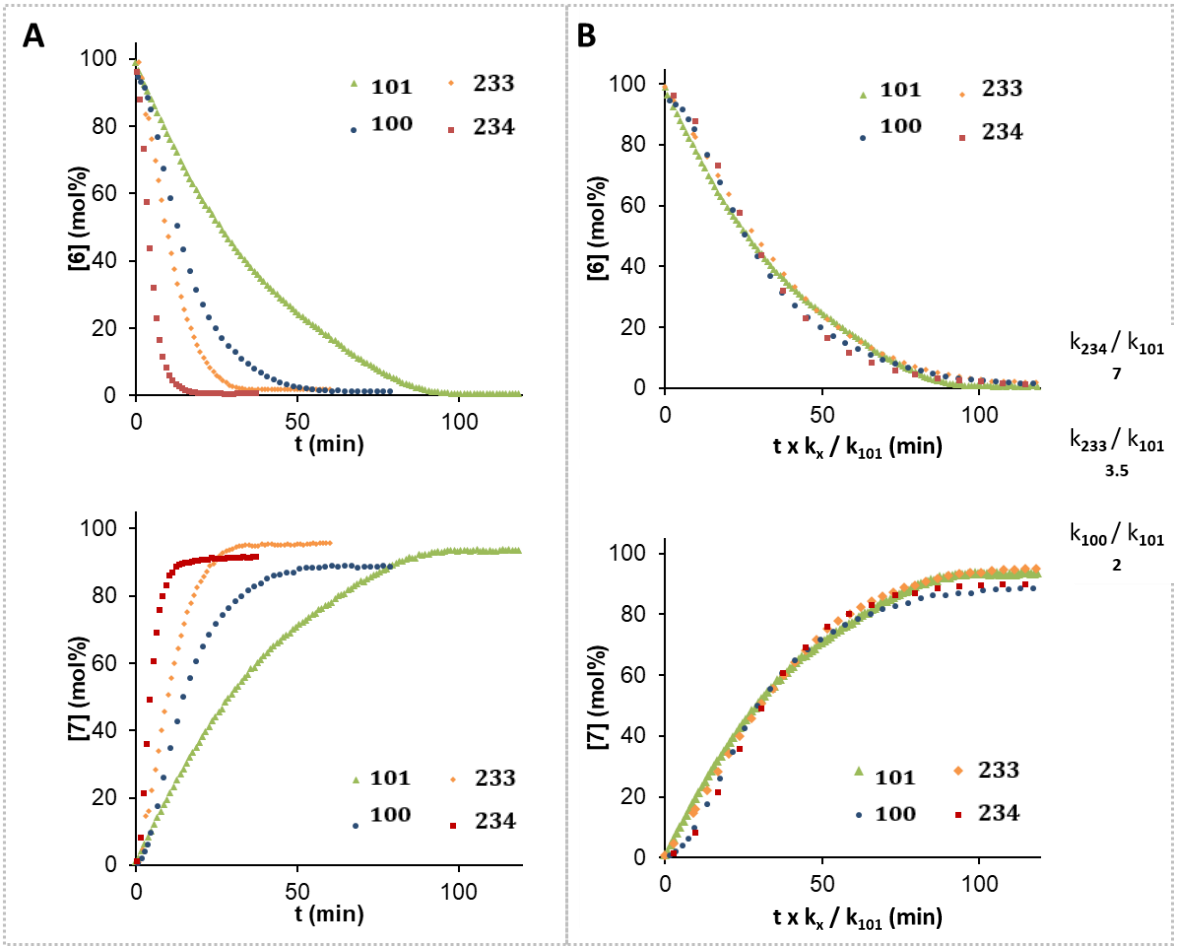

Figure 72: A: Reaction profiles of the consumption of **231** and formation of **232** using catalysts **100, 101, 233, 234**. B: Reaction profiles with time-normalized scales. The relative rates on the right are values used in these graphs.

Kinetic Studies with ´Bulky´ Complexes 25 and 229

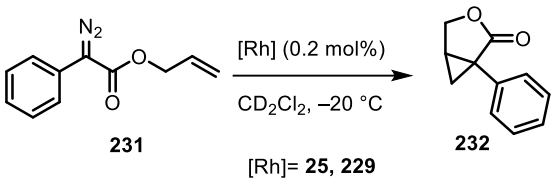

Stock solution catalyst: (c= 1mg/mL in acetonitrile)

Stock solution diazo: (c= 100mg/mL in CD_2Cl_2)

A flame-dried NMR tube under Argon was charged with a stock solution of catalyst (0.2 mol%). The solvent was evaporated under vacuo and the NMR tube heated to dry the catalyst. Then the dried catalyst was dissolved in CD_2CL_2 (0.1 mL). The NMR tube was cooled to −78 °C in a dry ice/ethanol mixture. The solution was overlaid with CD_2CL_2 (0.3 mL), then a stock solution of diazo (50 µL) was added carefully. The solution was mixed by turning it upside down and vortexing and then immediately transferred to the NMR probe head precooled to –20 °C. After fast shimming single scan ^{1}H NMR spectra were acquired every 60 s until full conversion of the starting material was observed.

The NMR data was afterwards imported imported into MNOVA 15.0.1 with the Reaction monitoring plugin and processed therein (baseline correction, phasing, integration). The data from the first spectrum was used as concentration reference (100 mol%) for the following spectra. An overview of the obtained reaction profiles and the time-normalized data is shown in Figure 73.

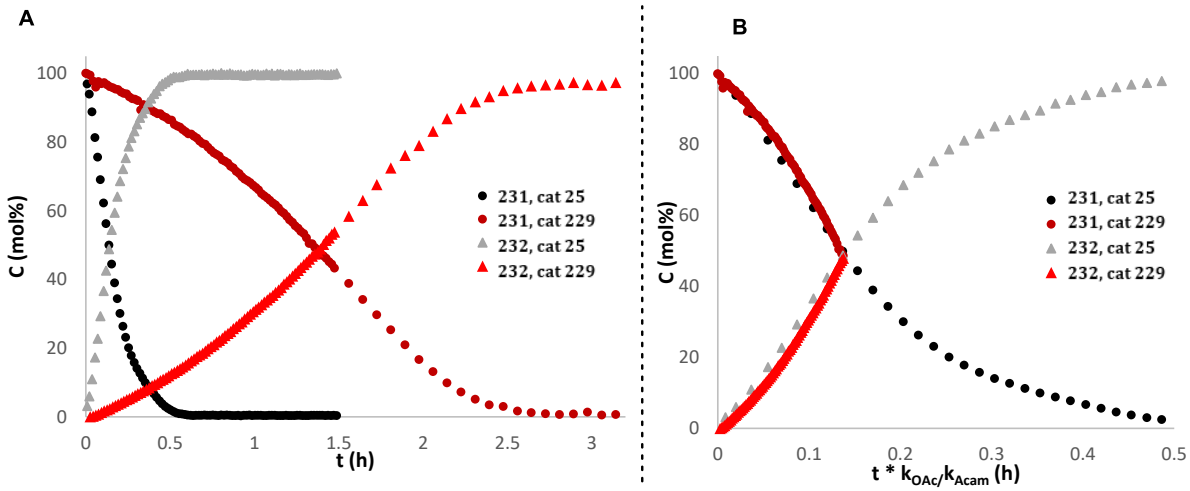

Figure 73: A: Reaction profiles of the consumption of **231** and formation of **232** using catalysts **25** and **229**. B: Reaction profiles with time-normalized scales. The relative rate is shown as insert in the graph.

9.9.2. ^{13}C Labeling Studies

^{13}C Labeling Studies with Diazo $[^{13}C]_2$-231

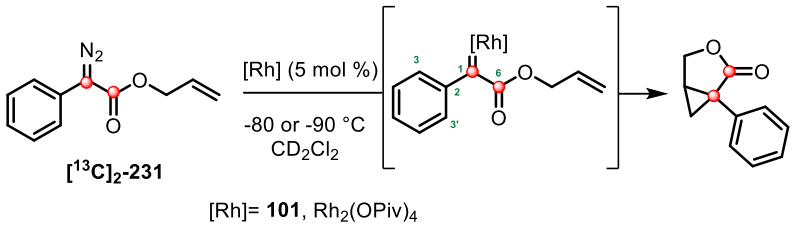

Stock solution catalyst: (c= 1mg/mL in acetonitrile)

Stock solution diazo: (c= 100mg/mL in CD_2Cl_2)

A flame-dried NMR tube under Argon was charged with a stock solution of catalyst (5 mol %). The solvent was evaporated under vacuo and the NMR tube heated to dry the catalyst. The dried catalyst was dissolved in CD_2CL_2 (0.1 mL). The NMR tube was cooled to −78°C in a dry ice/ethanol mixture. The solution was overlaid with CD_2CL_2 (0.35 mL), then a stock solution of diazo (50 µL) was added carefully. The solution was mixed immediately before the tube was inserted into the NMR probe precooled to -80°C in case of $Rh_2(acam)(OPiv)_3$ **(101)** and –90°C in case of $Rh_2(OPiv)_4$. After quick shimming the NMR data was immediately acquired.

^{13}C Labeling Studies with Diazo $[^{13}C]_2$-246

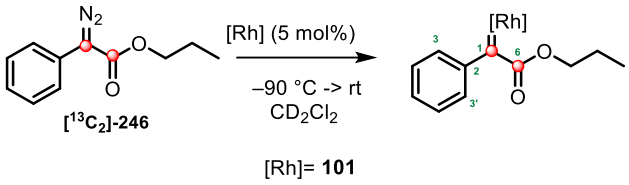

Stock solution catalyst: (c = 1mg/mL in acetonitrile)

Stock solution diazo: (c = 100mg/mL in CD_2Cl_2)

A flame-dried NMR tube under Argon was charged with a stock solution of catalyst (5 mol%). The solvent was evaporated under vacuo and the NMR tube heated to dry the catalyst. The dried catalyst was dissolved in CD_2CL_2 (0.1 mL). The NMR tube was cooled to −78 °C in a dry ice/ethanol mixture. The solution was overlaid with CD_2CL_2 (0.35 mL), then a stock solution of diazo (50 µL) was added carefully. The solution was mixed immediately before the tube was

inserted into the NMR probe precooled to –80 °C in case of $Rh_2(acam)(OPiv)_3$ (**101**). After quick shimming the NMR data was immediately acquired.

9.9.3. UV-VIS and CD Measurements of Complex 134

CD spectra of complex **134** was measured in 10 mm Quartz cuvettes with a concentration of 1mg/mL in MTBE.

The UV-VIS spectrum of complex **134** was measured in a 2 mm Suprasil Quartz cuvette at a concentration of 1.8mM in MTBE. A cuvette with pure solvent (MTBE) was placed in the reference beam. The measured absorption has subsequently been converted to molar absorption coefficient using the Lambert-Beer law. Two relatively weak bands at 624nm and 425nm are present with molar absorption coefficients of 115 $M^{-1}cm^{-1}$ and 120 $M^{-1}cm^{-1}$, respectively.

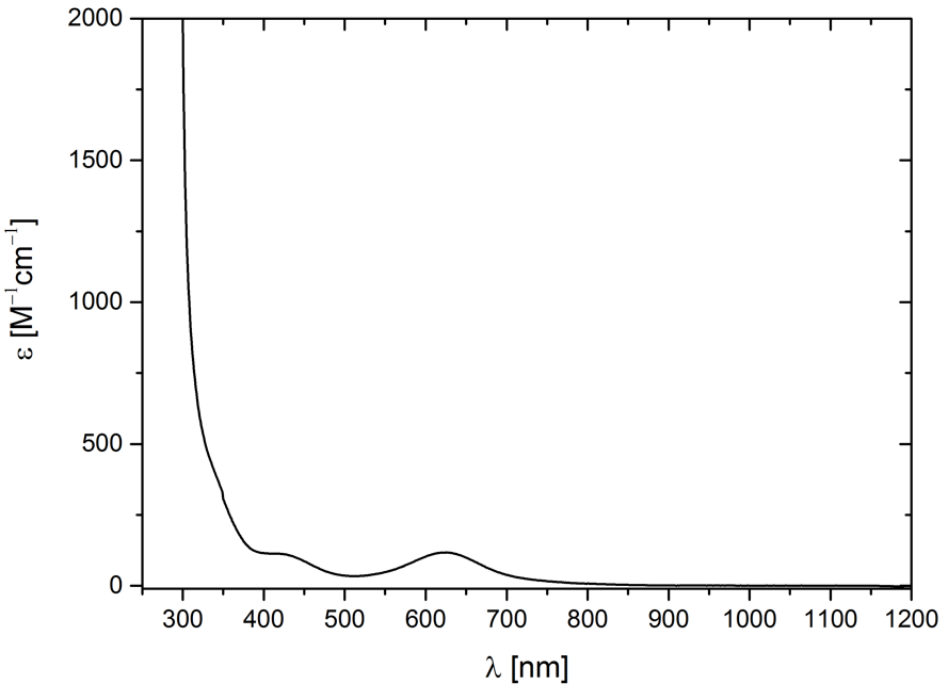

Figure 74-UV-VIS spectrum plotted as molar absorption coefficient to wavelength of complex **134** measured in MTBE (c = 1.8 mM).

10. Appendix

10.1. Overview of Tools

In this thesis, ChatGPT was used by the author to assist with language proofreading, grammar corrections, and occasional rephrasing, resulting in minor textual revisions.

10.2. Appendix 1

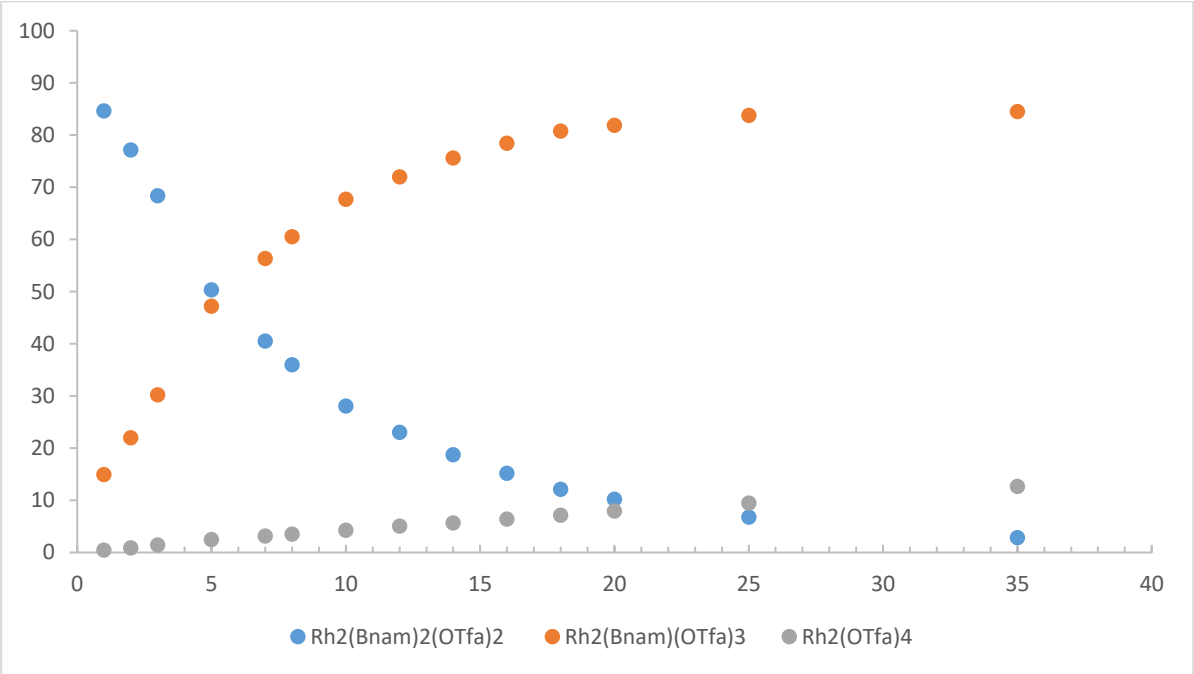

Figure 75-Reaction profile of the ligand exchange reaction of [$Rh_2(Bnam)_4 \cdot 2H_2O$] with TFA at 60°C monitored via HPLC.

10.3. Appendix 2

Conformational sampling was performed using CREST program.[190] The simulations employed the GFN2-xTB//GFN-FF composite methodology[234] sampling and optimizations were performed at the GFN-FF level, complemented by a GFN2-xTB single-point calculation. Two distinct families of conformers were found, as illustrated in Figure 73. The primary difference between these conformer families lies in the relative orientations of the propoxy substituents of the cyclic ligand. In Family 2, all propoxy substituents are oriented at the same side, whereas in Family 1, their orientation is alternated.

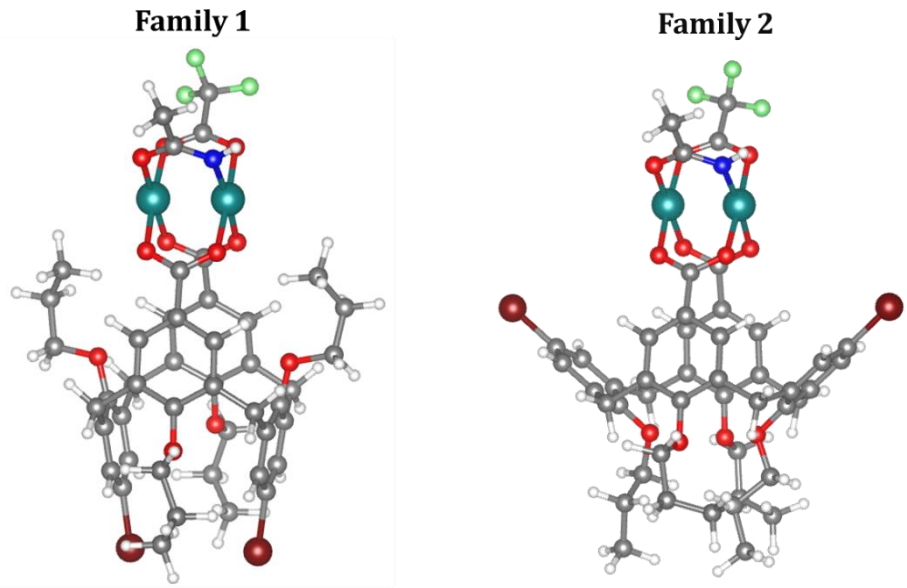

Figure 76-Representative conformers from the two main families identified with unconstrained metadynamics simulations. Family 1 features a 1,3-alternating orientation of the propoxy substituents, while Family 2 displays a uniform cone conformer.

The exploration of conformational space yielded a substantial number of distinct conformers (on the order of ~10^3). To enable a focused and representative investigation of the optical properties of the catalyst while accounting for conformational diversity, in the initial structural ensemble only a subset of structures were selected, using an in-house code that performs iterative screening of conformers by comparing RMSD values between each conformer and a reference conformer. In each iteration, the code selects the conformer with the lowest energy and a high RMSD compared to the previous reference conformer. This approach ensures a diverse and representative subset of conformers. All the selected conformers in our initial structural ensamble were reoptimized at the DFT level. These calculations were carried out with a development version of the ORCA quantum package based on v. 5.0.3.[206] Specifically, the geometries of the selected conformers were reoptimized using the using B3LYP-D3(BJ) functional[235-237] and Ahlrichs def2-SVP basis set.[195] Implicit solvation effects were incorporated at the CPCM level using the parameters for MTBE.[196-197] The resolution of identity (RI) approximation was used in the RIJCOSX variant together with the corresponding auxiliary basis set.[198-199, 238] Subsequently, the electronic energies were further refined at the wB97X/def2-TZVP(-f) level, again incorporating RIJCOSX and CPCM.[239] This refinement of both geometry and electronic energy for all conformers in the structural ensemble was essential for accurately modeling the optical properties of the catalyst (all computed at the wB97X/def2-TZVP(-f) + RIJCOSX + CPCM level for consistency). Notably, circular dichroism (CD) spectra are particularly sensitive to geometric changes. Therefore, to address this delicate aspect, the refined electronic energies based on accurate geometries were used to calculate

both UV-Vis and CD spectra. These spectra were obtained as a convolution of the individual spectra of each selected conformer, where the contributions are weighted according to the Boltzmann distribution.

To validate the established computational protocol, the UV-visible absorption spectra of the catalyst was calculated using our chosen level of theory and compared to the experimental data. Comparison of the data shows excellent agreement using a normalized intensity scale, as all the significant spectral features were reproduced.

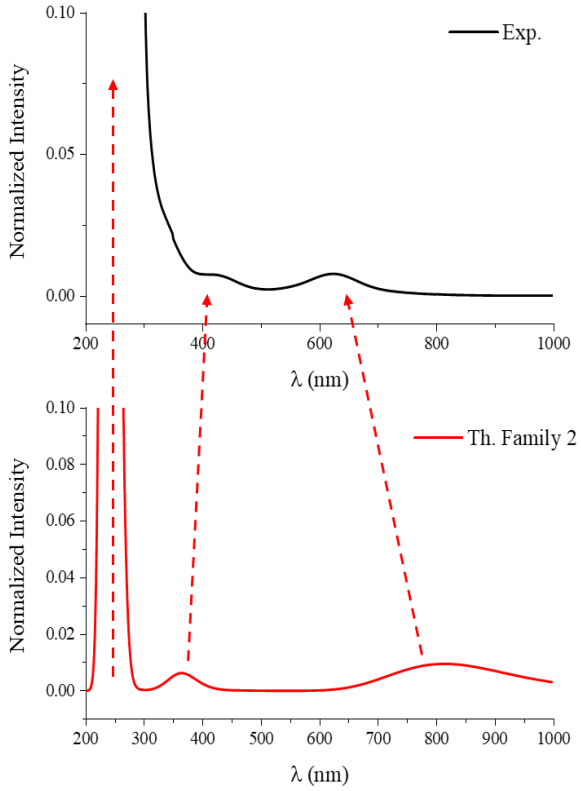

Figure 77- Comparison of experimental and calculated UV-visible absorption spectra.

With the validated computational protocol at hand the corresponding CD spectra were calculated (see Chapter 4).

10.5. Crystallographic Data

Cyclopropane (93):

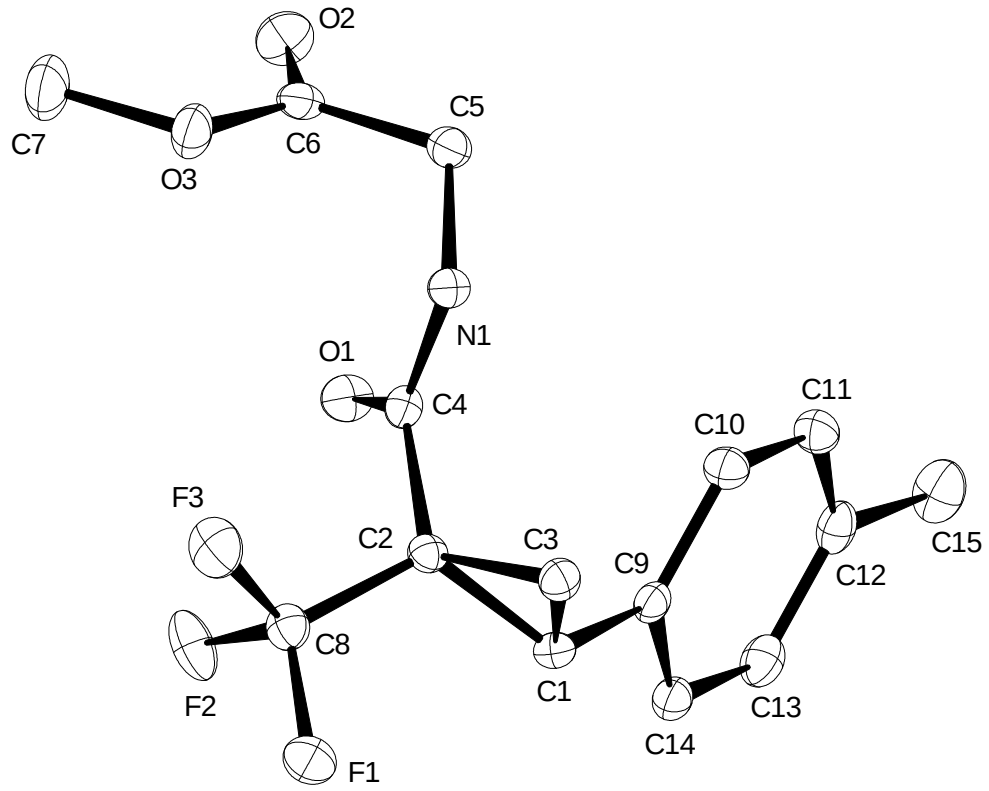

Figure 78-Structure of cyclopropane **93** in the solid state. Hydrogen atoms were removed for clarity.

X-ray Crystal Structure Analysis of 93: $C_{15}\ H_{16}\ F_3\ N\ O_3$, M_r = 315.29 g mol^{-1} , colourless needle, crystal size 0.113 x 0.046 x 0.032 mm^3 , orthorhombic, space group $P2_12_12_1$ [19], a = 5.0016(2) Å, b = 14.7658(8) Å, c = 19.8117(10) Å, V = 1463.15(12) Å^3 , T = 100(2) K, Z = 4, Dcalc = 1.431 g·cm^3 , λ = 0.71073 Å, μ(Mo-Kα) = 0.124 mm^{-1}, analytical absorption correction (Tmin =0.99, Tmax =1.00), Bruker-AXS Kappa Mach3 with APEX-II detector and IμS microfocus source, 1.720 < θ < 31.024°, 49169 measured reflections, 4666 independent reflections, 3892 reflections with I > 2σ(I), R_{int} = 0.0528, absolute structure parameter = 0.1(2). The structure was solved by SHELXT and refined by full-matrix least-squares (SHELXL) against F^2 to R_1 = 0.0353 [I > 2σ(I)], *w*R^2 = 0.077, 209 parameters. **CCDC 2287213**

Dirhodium complex (107):

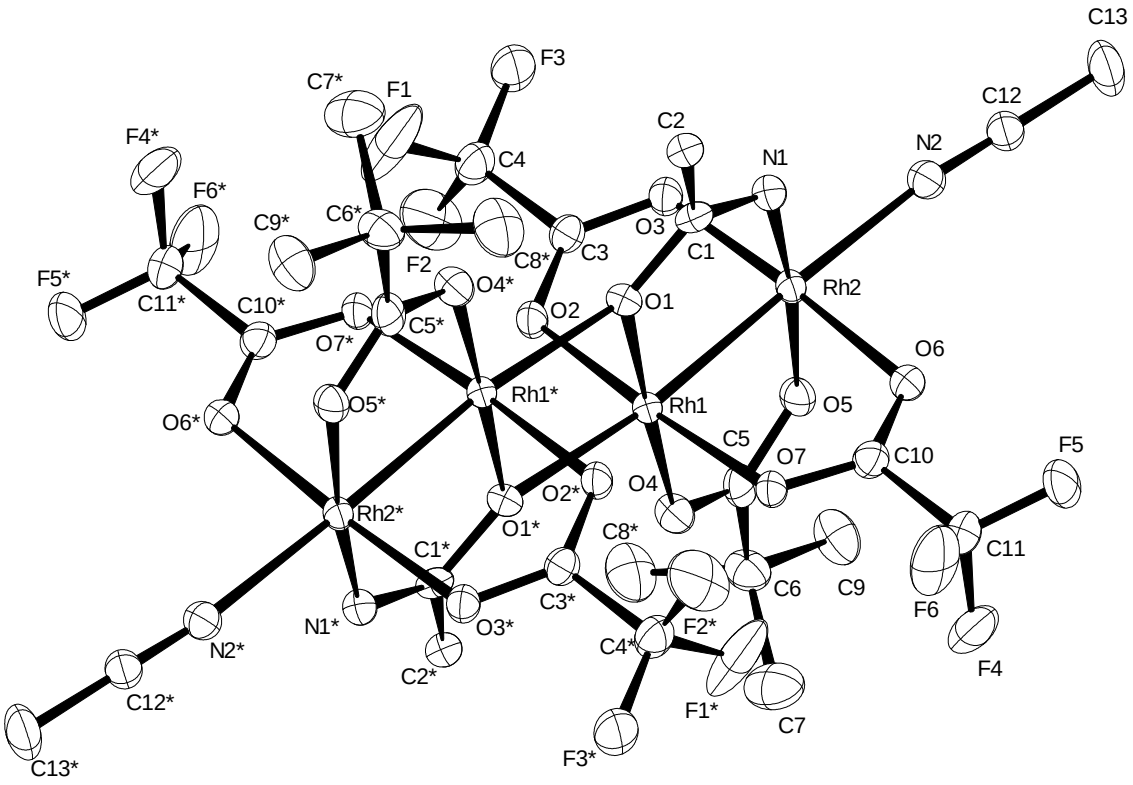

Figure 79-Structure of Complex **107** in the solid state as a dimeric species. Hydrogen atoms were omitted for clarity.

X-ray Crystal Structure Analysis of 107: C_{26} H_{32} F_{12} N_4 O_{14} Rh_4, M_r = 1264.19 g mol^{-1} , blue crystal, crystal size 0.1 x 0.024 x 0.01 mm^3 , triclinic, space group $P\bar{1}$ [2], a = 9.599(4) Å, b = 9.803(5) Å, c = 12.520(18) Å, V = 1088.3(18) $Å^3$, T = 100(2) K, Z = 1, Dcalc = 1.929 g·cm^3 , λ = 0.71073 Å, μ(Mo-Kα) = 0.124 mm^{-1}, analytical absorption correction (Tmin = 0.90, Tmax = 0.98), Bruker-AXS Kappa Mach3 with APEX-II detector and IμS microfocus source, 2.808 < θ < 33.233°, 34800 measured reflections, 8327 independent reflections, 5300 reflections with I > 2σ(I), R_{int} = 0.0993, The structure was solved by SHELXT and refined by full-matrix least-squares (SHELXL) against F^2 to R_1 = 0.0563 [I > 2σ(I)], wR^2, *w*R^2 = 0.0714, 276 parameters.

11. Abbreviation List

Å	Ångstrom, 1 Å = 10^{-10} m
acam	Acetamidate
ATR	Attenuated Total Reflectance
bnam	Benzamidate
Boc	*tert*-butoxycarbonyl
Bu	Butyl
COSY	Correlation Spectroscopy
DBU	Diazabicycloundecene
DIPEA	*N*,*N*-Diisopropylethylamine (Hünig base)
DFT	Density Functional Theory
DCE	1,2-dichloroethane
DME	Dimethoxyethane
DMF	Dimethylformamide
DMAP	4-Dimethylaminopyridine
DOSP	*N*-(*p*-Dodecylphenylsulfonyl)prolinate
DPPA	Diphenylphosphoroylazide
DPTI	*R*,*R*-diphenyl-N-triflylimidazolidinone
dr	diastereomeric ratio
ee	enantiomeric excess
EDA	Ethyldiazoacetate
EDC	1-Ethyl-3-(3-dimethylaminopropyl)carbodiimide

EDG	Electron Donating Group
EI	Electron Ionization
ESI	Electronspray Ionization
esp	α,α,α',α'-Tetramethyl-1,3-benzendipropionate
Et	Ethyl
EtOAc	Ethyl acetate
EWG	Electron Withdrawing Group
form	Formamidinate
g	gram(s)
G	Gibbs Energy
h	hour(s)
HATU	Hexafluorophosphate Azabenzotriazole Tetramethyl Uronium
HOMO	Highest Occupied Molecular Orbital
HPLC	High-Pressure Liquid Chromatography
HMBC	Heteronuclear Multiple Bond Coherence
HMQC	Heteronuclear Multiple Quantum Correlation
HRMS	High-Resolution Mass Spectroscopy
HSQC	Heteronuclear Single Quantum Correlation
i.e.	that is
i.D.	inner Diameter
IR	Infrared
*i*Pr	isopropyl

kcal	kilocalories
L	Ligand
LUMO	Lowest Unoccupied Molecular Orbital
M	Molar (mol/L)
MeCN	Acetonitrile
MeOH	Methanol
MEPY	Methylpyroglutamate
mg	milligram(s)
MHz	Megahertz, 1Hz = $1s^{-1}$
MTBE	Methyl *tert*-Butyl Ether
MW	Microwave
NBS	*N*-bromosuccinimide
n.d.	Not determined
NHC	*N*-heterocyclic carbene
NMR	Nuclear Magnetic Resonance
NOESY	Nuclear Overhauser Effect Spectroscopy
NTTL	*N*-1,8-Naphthoyl-*tert*-leucinate
o-NBSA	*o*-Nitrobenzenesulfonyl azide
OAc	Acetate
OTfa	Trifluoroacetate
p-ABSA	*p*-acetamidobenzoylsulfonyl azide
Ph	Phenyl

PMP	*p*-methoxyphenyl
ppm	parts per million
PTAD	1-adamantyl-(*N*-phthalimide)acetate
PTFE	Polytetrafluoroethylene
PTTL	N-Phthaloyl-(S)-tert-leucinate
rt	Room temperature
RMSD	Root Mean Square Deviation
T	Temperature
*t*Bu	*tert*-Butyl
TBSP	*N*-(*p*-*tert*-butylphenylsulfonyl)prolinate
TCPTTL	*N*-tetrachlorphthaloyl-*tert*-leucinate
TEA	Triethylamine
TFA	Trifluoroacetic acid
Tfs	2-Trifluoromethyltosyl
TFT	Trifluorotoluene
THF	Tetrahydrofuran
TIPS	Triisopropylsilyl
TLC	Thin-Layer Chromatography
TMS	Trimethylsilyl
TPCP	1,2,2-Triphenylcyclopropane carboxylate
TS	Transition State

12. Bibliography

[1] L. Falivene, Z. Cao, A. Petta, L. Serra, A. Poater, R. Oliva, V. Scarano, L. Cavallo, *Nat. Chem.* **2019**, *11*, 872-879.

[2] R. Noyori, *Adv. Synth. Catal.* **2003**, *345*, 15-32.

[3] T. D. Stephens, C. J. W. Bunde, B. J. Fillmore, *Biochem. Pharmacol.* **2000**, *59*, 1489-1499.

[4] W. Lenz, K. Knapp, *Dtsch Med Wochenschr* **1962**, *87*, 1232-1242.

[5] *Chemical & Engineering News Archive* **1990**, *68*, 9-14.

[6] *Chemical & Engineering News Archive* **1992**, *70*, 46-79.

[7] S. Hanessian, *Pure Appl. Chem.* **1993**, *65*, 1189-1204.

[8] G. Snatzke, *Berichte der Bunsengesellschaft für physikalische Chemie* **1982**, *86*, 1087-1087.

[9] H. Pellissier, *Tetrahedron* **2003**, *59*, 8291-8327.

[10] H. U. Blaser, *Chem. Rev.* **1992**, *92*, 935-952.

[11] A.N. Collins, J. Crosby, *Chirality in industry: the commercial manufacture and applications of optically active compounds*, Wiley, **1995**.

[12] E. L. Eliel, H. S. Mosher, *Science* **1975**, *190*, 772-774.

[13] D. Adam, *Nature* **2001,** https://doi.org/10.1038/news011011-17.

[14] A. Fürstner, *Nachrichten aus der Chemie* **2021**, *69*, 8-11.

[15] R. R. Schrock, *J. Am. Chem. Soc.* **1974**, *96*, 6796-6797.

[16] R. R. Schrock, *Science* **1983**, *219*, 13-18.

[17] E. O. Fischer, K. H. Dötz, *Chem. Ber.* **1972**, *105*, 3966-3973.

[18] J. F. Hartwig, *Organotransition metal chemistry: from bonding to catalysis*, University Science Books, **2010**.

[19] R. H. Crabtree, *The Organometallic Chemistry of the Transition Metals*, Wiley, **2005**.

[20] I. C. L. Nazarova , A. S. Morozova *Russ. J. Inorg. Chem.* **1965**, *10*, 539.

[21] R. Paulissen, H. Reimlinger, E. Hayez, A. J. Hubert, P. Teyssié, *Tetrahedron Lett.* **1973**, *14*, 2233-2236.

[22] J. F. Berry, *Dalton Trans.* **2012**, *41*, 700.

[23] H. M. L. Davies, R. E. J. Beckwith, *Chem. Rev.* **2003**, *103*, 2861.

[24] C. Werlé, R. Goddard, A. Fürstner, *Angew. Chem., Int. Ed.* **2015**, *54*, 15452.

[25] C. Werlé, R. Goddard, P. Philipps, C. Farès, A. Fürstner, *J. Am. Chem. Soc.* **2016**, *138*, 3797.

[26] C. Werlé, R. Goddard, P. Philipps, C. Farès, A. Fürstner, *Angew. Chem., Int. Ed.* **2016**, *55*, 10760.

[27] O. G. Kulinkovich, *Cyclopropanes in Organic Synthesis*, John Wiley and Sons, Hoboken, New Jersey, **2015**.

[28] J. D. Dill, A. Greenberg, J. F. Liebman, *J. Am. Chem. Soc.* **1979**, *101*, 6814-6826.

[29] A. D. Walsh, *Trans. Faraday Soc.* **1949**, *45*, 179-190.

[30] A. de Meijere, *Angew. Chem., Int. Ed.* **1979**, *18*, 809-826.

[31] N. A. Meanwell, *J. Med. Chem.* **2011**, *54*, 2529-2591.

[32] T. T. Talele, *J. Med. Chem.* **2016**, *59*, 8712-8756.

[33] Z. Časar, *Synthesis* **2020**, *52*, 1315-1345.

[34] P. Paggiaro, E. Bacci, *Ther. Adv. Chron. Dis.* **2010**, *2*, 47-58.

[35] H. Kuhl, *Climacteric* **2005**, *8 Suppl 1*, 3-63.

[36] J. C. Adkins, S. Noble, *Drugs* **1998**, *56*, 1055-1064.

[37] D. J. Augeri, J. A. Robl, D. A. Betebenner, D. R. Magnin, A. Khanna, J. G. Robertson, A. Wang, L. M. Simpkins, P. Taunk, Q. Huang, S.-P. Han, B. Abboa-Offei, M. Cap, L. Xin, L. Tao, E. Tozzo, G. E. Welzel, D. M. Egan, J. Marcinkeviciene, S. Y. Chang, S. A. Biller, M. S. Kirby, R. A. Parker, L. G. Hamann, *J. Med. Chem.* **2005**, *48*, 5025-5037.

[38] M. Elliott, N. Janes, C. Potter, *Annu. Rev. Entomol.* **1978**, *23*, 443-469.

[39] T. Yang, L. Gao, H. Hu, G. Stoopen, C. Wang, M. A. Jongsma, *J. Biol. Chem.* **2014**, *289*, 36325-36335.

[40] X. Huang, X. Tang, A. Liao, W. Sun, L. Lei, J. Wu, *J. Mol. Struct.* **2025**, *1326*, 141171.

[41] N. Wang, J.-X. Zhao, J.-M. Yue, *Org. Chem. Front.* **2025**, *12*, 2439-2456.

[42] C. Ebner, E. M. Carreira, *Chem. Rev.* **2017**, *117*, 11651-11679.

[43] S. Jin, J. Gong, Y. Qin, *Angew. Chem., Int. Ed.* **2015**, *54*, 2228-2231.

[44] S. Levin, R. R. Nani, S. E. Reisman, *J. Am. Chem. Soc.* **2011**, *133*, 774-776.

[45] A. Homs, M. E. Muratore, A. M. Echavarren, *Org. Lett.* **2015**, *17*, 461-463.

[46] A. Zimmer, A. Fürstner, *Chem. Eur. J.* **2024**, *2*, e202400064.

[47] R. D. Little, J. R. Dawson, *Tetrahedron Lett.* **1980**, *21*, 2609-2612.

[48] H. Nozaki, S. Moriuti, H. Takaya, R. Noyori, *Tetrahedron Lett.* **1966**, *7*, 5239-5244.

[49] L. Garve, D. B. Werz, in *Metal-Catalyzed Cyclization Reactions 2, Vol. 2016/4b*, 1st edition ed., Georg Thieme Verlag, Stuttgart, **2016**.

[50] X. Zhao, Y. Zhang, J. Wang, *Chem. Comm.* **2012**, *48*, 10162-10173.

[51] D. Qiu, J. Wang, *Recent Developments of Diazo Compounds in Organic Synthesis*, **2021**.

[52] H. Pellissier, *Tetrahedron* **2008**, *64*, 7041-7095.

[53] G. Maas, *Chem. Soc. Rev.* **2004**, *33*, 183-190.

[54] Y. Zhang, J. Wang, *Eur. J. Org. Chem.* **2011**, *2011*, 1015-1026.

[55] J. Hansen, H. M. L. Davies, *Coord. Chem. Rev.* **2008**, *252*, 545.

[56] M. P. Doyle, *J. Org. Chem.* **2006**, *71*, 9253-9260.

[57] D. Yongming, Q. Huang, D. S. Harathi, P. D. Michael, *Curr. Org. Chem.* **2016**, *20*, 61-81.

[58] B. Wei, J. C. Sharland, P. Lin, S. M. Wilkerson-Hill, F. A. Fullilove, S. McKinnon, D. G. Blackmond, H. M. L. Davies, *ACS Catal.* **2020**, *10*, 1161-1170.

[59] A. J. Anciaux, A. J. Hubert, A. F. Noels, N. Petiniot, P. Teyssie, *J. Org. Chem.* **1980**, *45*, 695-702.

[60] D. T. Nowlan, T. M. Gregg, H. M. Davies, D. A. Singleton, *J. Am. Chem. Soc.* **2003**, *125*, 15902-15911.

[61] M. C. Pirrung, A. T. Morehead, *J. Am. Chem. Soc.* **1996**, *118*, 8162-8163.

[62] F. M. Wong, J. Wang, A. C. Hengge, W. Wu, *Org. Lett.* **2007**, *9*, 1663-1665.

[63] J. Hansen, J. Autschbach, H. M. Davies, *J. Org. Chem.* **2009**, *74*, 6555-6563.

[64] S. M. Sheehan, A. Padwa, J. P. Snyder, *Tetrahedron Lett.* **1998**, *39*, 949-952.

[65] K. P. Kornecki, J. F. Briones, V. Boyarskikh, F. Fullilove, J. Autschbach, K. E. Schrote, K. M. Lancaster, H. M. L. Davies, J. F. Berry, *Science* **2013**, *342*, 351.

[66] C. J. Laconsay, A. Pla-Quintana, D. J. Tantillo, *Organometallics* **2021**, *40*, 4120-4132.

[67] F. G. Adly, *Catalysts,* **2017**, *7*, 347.

[68] H. M. L. Davies, P. R. Bruzinski, D. H. Lake, N. Kong, M. J. Fall, *J. Am. Chem. Soc.* **1996**, *118*, 6897-6907.

[69] N. Watanabe, Y. Ohtake, S.-i. Hashimoto, M. Shiro, S. Ikegami, *Tetrahedron Lett.* **1995**, *36*, 1491-1494.

[70] A. DeAngelis, O. Dmitrenko, G. P. Yap, J. M. Fox, *J. Am. Chem. Soc.* **2009**, *131*, 7230-7231.

[71] A. DeAngelis, D. T. Boruta, J.-B. Lubin, J. N. Plampin III, G. P. Yap, J. M. Fox, *Chem. Comm.* **2010**, *46*, 4541-4543.

[72] H. T. Chifotides, K. R. Dunbar, (Eds.: F. A. Cotton, C. A. Murillo, R. A. Walton), *Multiple Bonds between Metal Atoms*. Springer US, Boston, MA, **2005**, pp. 591-632.

[73] A. Abshire, D. Moore, J. Courtney, A. Darko, *Org. Biomol. Chem.* **2021**, *19*, 8886-8905.

[74] N. R. Candeias, C. A. M. Afonso, P. M. P. Gois, *Org. Biomol. Chem.* **2012**, *10*, 3357-3378.

[75] V. N. G. Lindsay, A. B. Charette, *ACS Catal.* **2012**, *2*, 1221.

[76] D. T. Boruta, O. Dmitrenko, G. P. A. Yap, J. M. Fox, *Chem. Sci.* **2012**, *3*, 1589.

[77] A. DeAngelis, R. Panish, J. M. Fox, *Acc. Chem. Res.* **2016**, *49*, 115-127.

[78] Y. Lou, T. P. Remarchuk, E. J. Corey, *J. Am. Chem. Soc.* **2005**, *127*, 14223-14230.

[79] Y. Lou, M. Horikawa, R. A. Kloster, N. A. Hawryluk, E. J. Corey, *J. Am. Chem. Soc.* **2004**, *126*, 8916-8918.

[80] F. Caló, A. Fürstner, *Angew. Chem., Int. Ed.* **2020**, *59*, 13900.

[81] F. P. Caló, A. Zimmer, G. Bistoni, A. Fürstner, *J. Am. Chem. Soc.* **2022**, *144*, 7465.

[82] L. Li, C.-Y. Wang, R. Huang, M. R. Biscoe, *Nat. Chem.* **2013**, *5*, 607-612.

[83] M. Bihani, J. C. G. Zhao, *Adv. Synth. Catal.* **2017**, *359*, 534-575.

[84] B. Wang, F. Wu, Y. Wang, X. Liu, L. Deng, *J. Am. Chem. Soc.* **2007**, *129*, 768-769.

[85] X.-X. Yan, Q. Peng, Q. Li, K. Zhang, J. Yao, X.-L. Hou, Y.-D. Wu, *J. Am. Chem. Soc.* **2008**, *130*, 14362-14363.

[86] X. Huo, R. He, X. Zhang, W. Zhang, *J. Am. Chem. Soc.* **2016**, *138*, 11093-11096.

[87] S. Singha, E. Serrano, S. Mondal, C. G. Daniliuc, F. Glorius, *Nat. Catal.* **2020**, *3*, 48-54.

[88] W. Wen, M.-J. Luo, Y. Yuan, J.-H. Liu, Z.-L. Wu, T. Cai, Z.-W. Wu, Q. Ouyang, Q.-X. Guo, *Nat. Comm.* **2020**, *11*, 5372.

[89] J. Zhang, X. Huo, J. Xiao, L. Zhao, S. Ma, W. Zhang, *J. Am. Chem. Soc.* **2021**, *143*, 12622-12632.

[90] E. V. Dikarev, T. G. Gray, B. Li, *Angew. Chem., Int. Ed.* **2005**, *44*, 1721-1724.

[91] A. S. Filatov, M. Napier, V. D. Vreshch, N. J. Sumner, E. V. Dikarev, M. A. Petrukhina, *Inorg. Chem.* **2012**, *51*, 566-571.

[92] J. Hansen, B. Li, E. Dikarev, J. Autschbach, H. M. L. Davies, *J. Org. Chem.* **2009**, *74*, 6564.

[93] L. R. Collins, M. van Gastel, F. Neese, A. Fürstner, *J. Am. Chem. Soc.* **2018**, *140*, 13042.

[94] Z. Ren, T. L. Sunderland, C. Tortoreto, T. Yang, J. F. Berry, D. G. Musaev, H. M. L. Davies, *ACS Catal.* **2018**, *8*, 10676-10682.

[95] L. R. Collins, S. Auris, R. Goddard, A. Fürstner, *Angew. Chem., Int. Ed.* **2019**, *58*, 3557.

[96] S.-i. Hashimoto, N. Watanabe, S. Ikegami, *Tetrahedron Lett.* **1990**, *31*, 5173-5174.

[97] N. Watanabe, T. Ogawa, Y. Ohtake, S. Ikegami, S.-i. Hashimoto, *Synlett* **1996**, *1996*, 85-86.

[98] S. Singha, M. Buchsteiner, G. Bistoni, R. Goddard, A. Fürstner, *J. Am. Chem. Soc.* **2021**, *143*, 5666-5673.

[99] M. Buchsteiner, S. Singha, J. Decaens, A. Fürstner, *Angew. Chem., Int. Ed.* **2022**, *61*, e202212546.

[100] P. Müller, S. Grass, S. P. Shahi, G. Bernardinelli, *Tetrahedron* **2004**, *60*, 4755-4763.

[101] B. V. Hoffman, H. Shechter, *J. Org. Chem.* **1974**, *39*, 2939-2940.

[102] R. V. Hoffman, H. Shechter, *J. Am. Chem. Soc.* **1971**, *93*, 5940-5941.

[103] K. Miki, F. Nishino, K. Ohe, S. Uemura, *J. Am. Chem. Soc.* **2002**, *124*, 5260-5261.

[104] B. Seiller, C. Bruneau, P. H. Dixneuf, *J. Chem. Soc., Chem. Comm.* **1994**, 493-494.

[105] K. Hong, J. Shu, S. Dong, Z. Zhang, Y. He, M. Liu, J. Huang, W. Hu, X. Xu, *ACS Catal.* **2022**, *12*, 14185-14193.

[106] Z. Liu, K. Raveendra Babu, F. Wang, Y. Yang, X. Bi, *Org. Chem. Front.* **2019**, *6*, 121-124.

[107] Z.-X. Niu, Y.-T. Wang, S.-N. Zhang, Y. Li, X.-B. Chen, S.-Q. Wang, H.-M. Liu, *Eur. J. Med. Chem.* **2023**, 115172.

[108] E. A. Hussain, A. Ghani, Z. Sadiq, in *Oxazole, Isoxazole, Benzoxazole-Based Drug Discovery* (Eds.: E. A. Hussain, A. Ghani, Z. Sadiq), Elsevier, **2025**, pp. 21-37.

[109] D. Patel, K. Patel, S. Patel, B. Patel, A. Patel, *ChemistrySelect* **2024**, *9*, e202403179.

[110] A. Abdullahi, K. Y. Yeong, *Med. Chem. Res.* **2024**, *33*, 406-438.

[111] M. F. Arshad, A. Alam, A. A. Alshammari, M. B. Alhazza, I. M. Alzimam, M. A. Alam, G. Mustafa, M. S. Ansari, A. M. Alotaibi, A. A. Alotaibi, S. Kumar, S. M. B. Asdaq, M. Imran, P. K. Deb, K. N. Venugopala, S. Jomah, *Molecules* **2022**, *27*.

[112] A. Dondoni, *Synthesis* **1998**, *1998*, 1681-1706.

[113] F. P. Caló, PhD thesis, Technische Universität Dortmund **2022**.

[114] X. Gui, D. Sorbelli, F. P. Caló, M. Leutzsch, M. Patzer, A. Fürstner, G. Bistoni, A. A. Auer, *Chem. Eur. J.* **2024**, *30*, e202301846.

[115] H. M. L. Davies, K. Liao, *Nat. Rev. Chem.* **2019**, *3*, 347-360.

[116] R. Wu, D. Zhu, S. Zhu, *Org. Chem. Front.* **2023**, *10*, 2849-2878.

[117] H. M. L. Davies, Y. Lian, *Acc. Chem. Res.* **2012**, *45*, 923-935.

[118] H. Lebel, J.-F. Marcoux, C. Molinaro, A. B. Charette, *Chem. Rev.* **2003**, *103*, 977-1050.

[119] A. R. Chakravarty, F. A. Cotton, D. A. Tocher, *J. Chem. Soc., Chem. Commun.* **1984**, 501.

[120] A. R. Chakravarty, F. A. Cotton, D. A. Tocher, J. H. Tocher, *Organometallics* **1985**, *4*, 8.

[121] D. F. Taber, S. C. Malcolm, K. Bieger, P. Lahuerta, M. Sanaú, S.-E. Stiriba, J. Pérez-Prieto, M. A. Monge, *J. Am. Chem. Soc.* **1999**, *121*, 860-861.

[122] M. Barberis, J. Pérez-Prieto, K. Herbst, P. Lahuerta, *Organometallics* **2002**, *21*, 1667-1673.

[123] F. Estevan, K. Herbst, P. Lahuerta, M. Barberis, J. Pérez-Prieto, *Organometallics* **2001**, *20*, 950-957.

[124] K. Bieger, F. Estevan, P. Lahuerta, J. Lloret, J. Pérez-Prieto, M. Sanaú, N. Siguero, S. E. Stiriba, *Organometallics* **2003**, *22*, 1799.

[125] F. Estevan, P. Lahuerta, J. Lloret, M. Sanaú, M. A. Ubeda, J. Vila, *Chem. Commun.* **2004**, 2408.

[126] F. Estevan, J. Lloret, M. Sanaú, M. A. Úbeda, *Organometallics* **2006**, *25*, 4977.

[127] D. F. Taber, P. V. Joshi, *J. Org. Chem.* **2004**, *69*, 4276.

[128] Z. Li, N. A. Leed, N. M. Dickson-Karn, K. R. Dunbar, C. Turro, *Chem. Sci.* **2014**, *5*, 727-737.

[129] T. A. White, K. R. Dunbar, R. P. Thummel, C. Turro, *Polyhedron* **2016**, *103*, 172-177.

[130] S. E. Witt, T. A. White, Z. Li, K. R. Dunbar, C. Turro, *Chem. Comm.* **2016**, *52*, 12175-12178.

[131] T. J. Whittemore, A. Millet, H. J. Sayre, C. Xue, B. S. Dolinar, E. G. White, K. R. Dunbar, C. Turro, *J. Am. Chem. Soc.* **2018**, *140*, 5161-5170.

[132] P. Piraino, G. Bruno, G. Tresoldi, S. Lo Schiavo, P. Zanello, *Inorg. Chem.* **1987**, *26*, 91-96.

[133] M. P. Doyle, D. C. Forbes, *Chem. Rev.* **1998**, *98*, 911.

[134] C. G. Espino, K. W. Fiori, M. Kim, J. Du Bois, *J. Am. Chem. Soc.* **2004**, *126*, 15378-15379.

[135] K. Williams Fiori, J. J. Fleming, J. Du Bois, *Angew. Chem., Int. Ed.* **2004**, *43*, 4349-4352.

[136] J. Bickley, R. Bonar-Law, T. McGrath, N. Singh, A. Steiner, *Nouv. J. Chem.* **2004**, *28*, 425-433.

[137] J. Seitz, G. Maas, *Chem. Comm.* **2002**, 338-339.

[138] M. Larsen, M. Jørgensen, *J. Org. Chem.* **1996**, *61*, 6651.

[139] L. H. Gade, *Koordinationschemie*, **1998**.

[140] N. G. Connelly, T. Damhus, *IUPAC Red Book, Nomenclature of Inorganic Chemistry*, RSC Publishing, **2005**.

[141] D. M. Guptill, H. M. L. Davies, *J. Am. Chem. Soc.* **2014**, *136*, 17718-17721.

[142] X. Tang, H. Noda, M. Shibasaki, *Angew. Chem., Int. Ed.* **2023**, *62*, e202311027.

[143] K. Liao, S. Negretti, D. G. Musaev, J. Bacsa, H. M. L. Davies, *Nature* **2016**, *533*, 230-234.

[144] P. F. Hudrlik, W. D. Arasho, R. J. Butcher, *Synthesis* **2008**, *18*, 2968-2976.

[145] S. Sameni, C. Jeunesse, M. Awada, D. Matt, R. Welter, *Eur. J. Inorg. Chem.* **2010**, *2010*, 4917-4923.

[146] A. Klapars, S. L. Buchwald, *J. Am. Chem. Soc.* **2002**, *124*, 14844-14845.

[147] N. A. Meanwell, *J. Med. Chem.* **2018**, *61*, 5822-5880.

[148] J. Decaens, S. Couve-Bonnaire, A. B. Charette, T. Poisson, P. Jubault, *Chem. Eur. J.* **2021**, *27*, 2935-2962.

[149] K. Aikawa, K. Yabuuchi, K. Torii, K. Mikami, *Beilstein J. Org. Chem.* **2018**, *14*, 576-582.

[150] G. Shi, Y. Xu, *J. Chem. Soc., Chem. Comm.* **1989**, 607-608.

[151] E. V. Dikarev, B. Li, H. Zhang, *J. Am. Chem. Soc.* **2006**, *128*, 2814-2815.

[152] J. M. Ernsting, S. Gaemers, C. J. Elsevier, *Magn. Reson. Chem.* **2004**, *42*, 721.

[153] B. E. Mann, *Annu. Rep. NMR Spectrosc.* **1991**, *23*, 141.

[154] R. Benn, A. Rufińska, *Angew. Chem., Int. Ed. Engl.* **1986**, *25*, 861.

[155] R. Benn, H. Brenneke, R. D. Reinhardt, *Z. Naturforsch., B: J. Chem. Sci.* **1985**, *40*, 1763.

[156] D. S. Gill, O. A. Gansow, F. J. Bennis, K. C. Ott, *J. Magn. Reson.* **1979**, *35*, 459.

[157] F. P. Caló, G. Bistoni, A. A. Auer, M. Leutzsch, A. Fürstner, *J. Am. Chem. Soc.* **2021**, *143*, 12473-12479.

[158] A. Fürstner, H. Krause, *Adv. Synth. Catal.* **2001**, *343*, 343-350.

[159] P. M. P. Gois, A. F. Trindade, L. F. Veiros, V. André, M. T. Duarte, C. A. M. Afonso, S. Caddick, F. G. N. Cloke, *Angew. Chem., Int. Ed.* **2007**, *46*, 5750-5753.

[160] A. F. Trindade, P. M. P. Gois, L. F. Veiros, V. André, M. T. Duarte, C. A. M. Afonso, S. Caddick, F. G. N. Cloke, *J. Org. Chem.* **2008**, *73*, 4076-4086.

[161] A. F. Trindade, V. André, M. T. Duarte, L. F. Veiros, P. M. P. Gois, C. A. M. Afonso, *Tetrahedron* **2010**, *66*, 8494-8502.

[162] A. F. Trindade, J. A. S. Coelho, C. A. M. Afonso, L. F. Veiros, P. M. P. Gois, *ACS Catal.* **2012**, *2*, 370-383.

[163] J. Tan, Y. Kuang, Y. Wang, Q. Huang, J. Zhu, Y. Wang, *Organometallics* **2016**, *35*, 3139-3147.

[164] J. Lee, H. Hahm, J. Kwak, M. Kim, *Adv. Synth. Catal.* **2019**, *361*, 1479-1499.

[165] B. Hong, L. Shi, L. Li, S. Zhan, Z. Gu, *Green Synth. Catal.* **2022**, *3*, 137-149.

[166] Q. Ma, Y. Ma, X. Liu, W. Duan, B. Qu, C. Song, *Tetrahedron: Asymmetry* **2010**, *21*, 292-298.

[167] H. Jacobsen, A. Correa, A. Poater, C. Costabile, L. Cavallo, *Coord. Chem. Rev.* **2009**, *253*, 687-703.

[168] M. N. Hopkinson, C. Richter, M. Schedler, F. Glorius, *Nature* **2014**, *510*, 485-496.

[169] D. Enders, T. Balensiefer, *Acc. Chem. Res.* **2004**, *37*, 534-541.

[170] J. G. J. Raj, *Rev. Inorg. Chem.* **2015**, *35*, 25-56.

[171] O. Kühl, *Coord. Chem. Rev.* **2005**, *249*, 693-704.

[172] A. Padwa, M. D. Weingarten, *Chem. Rev.* **1996**, *96*, 223.

[173] M. P. Doyle, R. Duffy, M. Ratnikov, L. Zhou, *Chem. Rev.* **2010**, *110*, 704.

[174] H. M. L. Davies, D. Morton, *Chem. Soc. Rev.* **2011**, *40*, 1857.

[175] A. Ford, H. Miel, A. Ring, C. N. Slattery, A. R. Maguire, M. A. McKervey, *Chem. Rev.* **2015**, *115*, 9981.

[176] S. Jana, Y. Guo, R. M. Koenigs, *Chem. - Eur. J.* **2021**, *27*, 1270.

[177] M. P. Doyle, V. Bagheri, T. J. Wandless, N. K. Harn, D. A. Brinker, C. T. Eagle, K. L. Loh, *J. Am. Chem. Soc.* **1990**, *112*, 1906.

[178] M. P. Doyle, R. J. Pieters, S. F. Martin, R. E. Austin, C. J. Oalmann, P. Mueller, *J. Am. Chem. Soc.* **1991**, *113*, 1423.

[179] M. P. Doyle, R. E. Austin, A. S. Bailey, M. P. Dwyer, A. B. Dyatkin, A. V. Kalinin, M. M. Y. Kwan, S. Liras, C. J. Oalmann, *J. Am. Chem. Soc.* **1995**, *117*, 5763.

[180] A. Padwa, D. J. Austin, A. T. Price, M. A. Semones, M. P. Doyle, M. N. Protopopova, W. R. Winchester, A. Tran, *J. Am. Chem. Soc.* **1993**, *115*, 8669.

[181] C. A. Merlic, A. L. Zechman, *Synthesis* **2003**, *2003*, 1137.

[182] J. Lloret, J. J. Carbó, C. Bo, A. Lledós, J. Pérez-Prieto, *Organometallics* **2008**, *27*, 2873.

[183] M. Q. Ahsan, I. Bernal, J. L. Bear, *Inorg. Chem.* **1986**, *25*, 260.

[184] S. Harada, M. Kono, T. Nozaki, Y. Menjo, T. Nemoto, Y. Hamada, *J. Org. Chem.* **2015**, *80*, 10317-10333.

[185] S. U. Dunham, T. S. Remaley, B. S. Moore, D. L. Evans, S. U. Dunham, *Inorg. Chem.* **2011**, *50*, 3458-3463.

[186] X. Xu, M. P. Doyle, *Inorg. Chem.* **2011**, *50*, 7610-7617.

[187] J. Burés, *Angew. Chem., Int. Ed.* **2016**, *55*, 16084-16087.

[188] P. P. Chen, P. Wipf, K. N. Houk, *Nat. Commun.* **2022**, *13*, 7292.

[189] P. Pracht, F. Bohle, S. Grimme, *Phys. Chem. Chem. Phys.* **2020**, *22*, 7169.

[190] C. Bannwarth, S. Ehlert, S. Grimme, *J. Chem. Theory Comput.* **2019**, *15*, 1652.

[191] A. D. Becke, *J. Chem. Phys.* **1992**, *96*, 2155.

[192] C. Lee, W. Yang, R. G. Parr, *Phys. Rev. B* **1988**, *37*, 785.

[193] S. H. Vosko, L. Wilk, M. Nusair, *Can. J. Phys.* **1980**, *58*, 1200.

[194] P. J. Stephens, F. J. Devlin, C. F. Chabalowski, M. J. Frisch, *J. Phys. Chem.* **1994**, *98*, 11623.

[195] F. Weigend, R. Ahlrichs, *Phys. Chem. Chem. Phys.* **2005**, *7*, 3297.

[196] V. Barone, M. Cossi, *J. Phys. Chem. A* **1998**, *102*, 1995.

[197] M. Cossi, N. Rega, G. Scalmani, V. Barone, *J. Comput. Chem.* **2003**, *24*, 669.

[198] K. Eichkorn, O. Treutler, H. Öhm, M. Häser, R. Ahlrichs, *Chem. Phys. Lett.* **1995**, *240*, 283.

[199] F. Neese, *J. Comput. Chem.* **2003**, *24*, 1740.

[200] G. Henkelman, H. Jónsson, *J. Chem. Phys.* **2000**, *113*, 9978.

[201] G. Henkelman, B. P. Uberuaga, H. Jónsson, *J. Chem. Phys.* **2000**, *113*, 9901.

[202] B. Wei, J. C. Sharland, D. G. Blackmond, D. G. Musaev, H. M. L. Davies, *ACS Catal.* **2022**, *12*, 13400.

[203] M. C. Pirrung, H. Liu, A. T. Morehead, *J. Am. Chem. Soc.* **2002**, *124*, 1014.

[204] D. J. Tindall, C. Werlé, R. Goddard, P. Philipps, C. Farès, A. Fürstner, *J. Am. Chem. Soc.* **2018**, *140*, 1884.

[205] M. Álvarez, F. Villalba, M. Casciotti, F. Molina, G. Sciortino, A. Lledós, A. C. Albéniz, T. R. Belderrain, P. J. Pérez, *Chem.* **2024**, *10*, 1576.

[206] F. Neese, *Wiley Interdiscip. Rev.: Comput. Mol. Sci.* **2022**, *12*, e1606.

[207] J. Tao, J. P. Perdew, V. N. Staroverov, G. E. Scuseria, *Phys. Rev. Lett.* **2003**, *91*, 146401.

[208] V. N. Staroverov, G. E. Scuseria, J. Tao, J. P. Perdew, *J. Chem. Phys.* **2003**, *119*, 12129.

[209] E. v. Lenthe, E. J. Baerends, J. G. Snijders, *J. Chem. Phys.* **1993**, *99*, 4597.

[210] C. van Wüllen, *J. Chem. Phys.* **1998**, *109*, 392.

[211] S. K. Wolff, T. Ziegler, *J. Chem. Phys.* **1998**, *109*, 895.

[212] C. Fonseca Guerra, J. G. Snijders, G. Te Velde, E. J. Baerends, *Theor. Chem. Acc.* **1998**, *99*, 391.

[213] G. te Velde, F. M. Bickelhaupt, E. J. Baerends, C. Fonseca Guerra, S. J. A. van Gisbergen, J. G. Snijders, T. Ziegler, *J. Comput. Chem.* **2001**, *22*, 931.

[214] G. R. Fulmer, A. J. M. Miller, N. H. Sherden, H. E. Gottlieb, A. Nudelman, B. M. Stoltz, J. E. Bercaw, K. I. Goldberg, *Organometallics* **2010**, *29*, 2176-2179.

[215] M. M. Kremlev, A. I. Mushta, W. Tyrra, D. Naumann, H. T. M. Fischer, Y. L. Yagupolskii, *J. Fluor. Chem.* **2007**, *128*, 1385-1389.

[216] X. Zhang, X. Zhang, Q. Song, P. Sivaguru, Z. Wang, G. Zanoni, X. Bi, *Angew. Chem., Int. Ed.* **2022**, *61*, e202116190.

[217] M. P. Doyle, W. Hu, *Adv. Synth. Catal.* **2001**, *343*, 299-302.

[218] Z. Zhang, Q. Zhou, W. Yu, T. Li, Y. Zhang, J. Wang, *Chin. J. Chem.* **2017**, *35*, 387-391.

[219] H. M. L. Davies, T. Hansen, M. R. Churchill, *J. Am. Chem. Soc.* **2000**, *122*, 3063-3070.

[220] C. L. Bagwell, D. M. L. Leonard, J.-P. Griffiths, M. G. Moloney, N. J. Stratton, D. P. Travers, *Macromol. React. Eng.* **2014**, *8*, 170-180.

[221] C. Tortoreto, D. Rackl, H. M. L. Davies, *Org. Lett.* **2017**, *19*, 770-773.

[222] X. Ning, Y. Chen, F. Hu, Y. Xia, *Org. Lett.* **2021**, *23*, 8348-8352.

[223] D. Fokas, J. E. Patterson, G. Slobodkin, C. M. Baldino, *Tetrahedron Lett.* **2003**, *44*, 5137-5140.

[224] J. M. Domagala, *Tetrahedron Lett.* **1980**, *21*, 4997-5000.

[225] B. M. Trost, L. Debien, *J. Am. Chem. Soc.* **2015**, *137*, 11606-11609.

[226] P. V. Khodakovskiy, D. M. Volochnyuk, D. M. Panov, I. I. Pervak, E. V. Zarudnitskii, O. V. Shishkin, A. A. Yurchenko, A. Shivanyuk, A. A. Tolmachev, *Synthesis* **2008**, *2008*, 948-956.

[227] A. G. Tskhovrebov, R. Goddard, A. Fürstner, *Angew. Chem., Int. Ed.* **2018**, *57*, 8089-8094.

[228] K. Orłowska, K. Łuczak, P. Krajewski, J. V. Santiago, K. Rybicka-Jasińska, D. Gryko, *Chem. Comm.* **2023**, *59*, 14649-14652.

[229] W. Bury, A. M. Walczak, M. K. Leszczyński, J. A. R. Navarro, *J. Am. Chem. Soc.* **2018**, *140*, 15031-15037.

[230] D. M. Upp, R. Huang, Y. Li, M. J. Bultman, B. Roux, J. C. Lewis, *Angew. Chem., Int. Ed.* **2021**, *60*, 23672-23677.

[231] S. Hünig, M. Kemmer, H. Wenner, F. Barbosa, G. Gescheidt, I. F. Perepichka, P. Bäuerle, A. Emge, K. Peters, *Chem. Eur. J.* **2000**, *6*, 2618-2632.

[232] B. K. Lee, M. R. Biscoe, S. L. Buchwald, *Tetrahedron Lett.* **2009**, *50*, 3672-3674.

[233] M. Peeters, J. Decaens, A. Fürstner, *Angew. Chem., Int. Ed.* **2023**, *62*, e202311598.

[234] S. Spicher, S. Grimme, *Angew. Chem., Int. Ed.* **2020**, *59*, 15665.

[235] A. D. Becke, *J. Chem. Phys.* **1993**, *98*, 1372-1377.

[236] S. Grimme, J. Antony, S. Ehrlich, H. Krieg, *J. Chem. Phys.* **2010**, *132*, 154104.

[237] S. Grimme, S. Ehrlich, L. Goerigk, *J. Comp. Chem.* **2011**, *32*, 1456-1465.

[238] F. Weigend, *Phys. Chem. Chem. Phys.* **2006**, *8*, 1057.

[239] J. D. Chai, M. Head-Gordon, *Phys. Chem. Chem. Phys.* **2008**, *10*, 6615.

[240] T. Ren, C. Lin, E. J. Valente, J. D. Zubkowski, *Inorg. Chim. Acta* **2000**, *297*, 283-290.